PROCEEDINGS
Vol. II

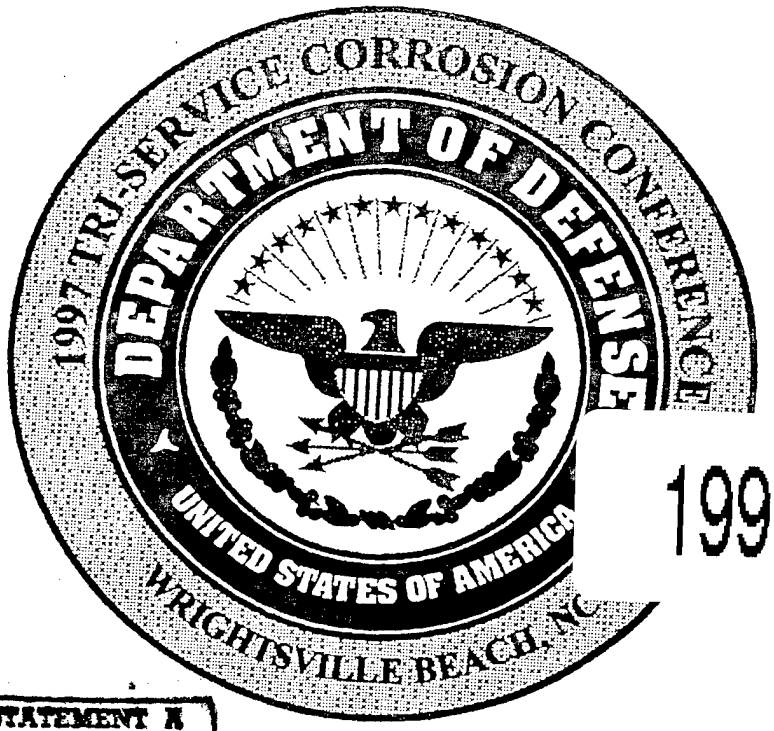

19971210 008

DISTRIBUTION STATEMENT A
Approved for public release
Distribution Unlimited

DTIC QUALITY INSPECTED 2

1997 TRI-SERVICE CONFERENCE ON CORROSION

NOVEMBER 17-21, 1997

BLOCKADE RUNNER HOTEL
WRIGHTSVILLE BEACH, NC

Organized by
Naval Surface Warfare Center - Carderock Division

Sponsored by
Office of Naval Research

Thermal-Spray Coatings for Coastal Infrastructure

Gordon R. Holcomb, Bernard S. Covino, Jr., Stephen D. Cramer, Sophie J. Bullard
Albany Research Center, U.S. Department of Energy
1450 Queen Avenue SW, Albany, OR 97321

Galen E. McGill
Oregon Department of Transportation
2950 State Street, Salem, OR 97310

ABSTRACT

Several protection strategies for coastal infrastructure using thermal-spray technology are presented from research at the Albany Research Center. Thermal-sprayed zinc coatings for anodes in impressed current cathodic protection systems are used to extend the service lives of reinforced concrete bridges along the Oregon coast. Thermal-sprayed Ti is examined as an alternative to the consumable zinc anode. Sealed thermal-sprayed Al is examined as an alternative coating to zinc dust filled polyurethane paint for steel structures.

INTRODUCTION

The use of thermal-spray metallic coatings is increasing for infrastructure applications. Currently, there are three reinforced concrete bridges (Yaquina Bay, Cape Creek, and Depoe Bay for at total of 428,000 ft^2 (39,763 m^2) covered area) along the Oregon coast that were rehabilitated using thermal-sprayed zinc as anodes in impressed current cathodic protection (ICCP) systems. More bridge restoration projects are in the bidding and planning stages. A 3015 ft^2 (280 m^2) section of the Depoe Bay bridge has thermal-sprayed Ti as a field-test of a nonconsumable anode in an ICCP system. The Albany Research Center and the Oregon Department of Transportation (ODOT) are involved in the characterization of these ICCP systems, in the development of improved installation procedures, and in the development of alternative systems. The results of electrochemical aging thermal-sprayed zinc and Ti anodes are presented.

EXPERIMENTAL PROCEDURES

Zinc Anode ICCP Experiments

Sample Preparation--Concrete samples ("slabs" measuring 9 × 13 × 2 inches (23 × 33 × 5 cm)) were cast to physically, mechanically, and electrochemically approximate a section of bridge substructure in a thermal-sprayed zinc anode ICCP system. More complete descriptions of the experimental procedures are presented elsewhere.[1-4] The concrete mix design included 5 lb/yd^3 (3 kg/m^3) of NaCl. A steel mesh was embedded in the slab, with 1.25 inches (3.2 cm) of concrete cover, to simulate rebar and to act as the cathode. After curing, the top surfaces of the slabs were sandblasted and prepared to receive a thermal-sprayed zinc coating. Immediately prior to thermal-spraying, the top surfaces of half of the slabs were heated with a propane torch to between 250 and 320°F (120-160°C). The remaining slabs were not heated prior to spraying. These are the "preheated" and "unheated" conditions.

A twin-wire arc-spray process was used to apply zinc to the concrete surface. The spray parameters for zinc were a current of 300-350 A_{dc}, a voltage of 25 V_{dc}, a spray distance of 6-9 inches (15-23 cm), and a wire diameter of 1/8 inch (3.2 mm). A custom designed and constructed programmable X-Y traversing system was used to control the movement of the spray head to obtain a nominal zinc coating thickness of 20 mils (0.5 mm).

Electrochemical Aging--Electrochemical aging of the slabs was conducted in a warm, high humidity room. The temperature was about 75°F (24°C) and the relative humidity (RH) was 80 to 85%. The slabs were wired in series, the zinc as the anode and the steel mesh as the cathode. The slabs were polarized at a current density of 3 mA/ft^2 (32 mA/m^2) using constant current power supplies. The total voltage, the impressed current, and the laboratory temperature were recorded hourly to provide long-term performance data for the system.

Even in the high humidity room, the slabs would tend to dry out and the voltage needed to maintain the current density of 3 mA/ft^2 (32 mA/m^2) would rise. Therefore, the slabs were sprayed as needed with deionized water; midway in the experiment they were being sprayed every day or every other day.

Adhesion Strength Measurements--Preheated and unheated slabs were removed from the experiment at regular time intervals following the passage of a given total charge through the zinc coating. The slabs were equilibrated with dry air for one day, then prepared for adhesion strength measurements by attaching aluminum dollies (1.9 inches (50 mm) in diameter) to the zinc coating at six predetermined locations using epoxy. A high viscosity, high strength, short cure time (300 sec) epoxy was used to eliminate failures at the epoxy-dolly interface and to prevent epoxy penetration through the coating to the concrete. Zinc adhesion strength measurements were made using a universal tensile testing machine. Initial zinc adhesion strengths were determined by measurements on two preheated and two unheated slabs, for a total of 12 measurements for each condition. All subsequent adhesion strengths were the result of six measurements each time a slab was pulled from the experiment.

Comparison to Coastal Bridges--Conditions within the experimental slabs differ from those expected to exist within coastal bridges in two important ways. First, the chloride was uniformly distributed throughout the slab (obtained by dissolving NaCl in the mix water prior to mixing), rather than diffused into the concrete from the outer surface with the associated concentration gradient. The salt distribution obtained by mixing may also put chloride in locations not readily accessible by diffusion, *i.e.*, in isolated pores and blind channels. Second, the current density in the accelerated test is a factor of 15 higher than the approximately 0.2 mA/ft^2 (2.2 mA/m^2) used by ODOT on coastal bridges. This could have the effect of altering transport processes and reactions so as to give results that vary, at least in fine detail, from those being approximated by the experiment and that may occur over much longer times on cathodically protected bridges. However, the California Department of Transportation (CalTrans) reports[5] obtaining higher current densities (up to 1.7 mA/ft^2 (18.3 mA/m^2)), which would be much closer to the experimental current densities.

Richmond-San Rafael Bridge (CA)--The south column of pier 4 of the Richmond-San Rafael Bridge has five thermal-sprayed zinc anode zones, applied in 1983 as part of a cathodic protection study conducted by CalTrans.[5] Each anode is 4 ft (1.2 m) in vertical height, surrounds the column, and is separated from the one above and below it by a 6 inch (15 cm) gap. The lowest anode was operated as a galvanic cathodic protection (GCP) system. The four above it, bands 1 through 4, were operated as an ICCP system. The low edge of band 1 is within 10 ft (3 m) of the water surface and fully exposed to the action of waves and precipitation. Band 4 is higher on the column, roughly 22 ft (6.7 m) above the water, partially sheltered from precipitation by the roadbed immediately above it, while fully exposed to

the drying effects of the wind. The driving (or operating) voltage and system current for each anode was monitored continuously for 12 years from 1983 through 1994.

Titanium Anode ICCP Experiments

Sample Preparation--Laboratory procedures using Ti anodes instead of zinc are described elsewhere,[6-8] and follow much the same procedures as for zinc. The spray parameters were a current of 300 A_{dc}, a voltage of 36-40 V_{dc}, a spray distance of 6-9 inches (15-23 cm), and annealed wire with a diameter of 1/8 inch (3.2 mm). Only 2-4 mils (0.051-0.13 mm) of Ti was applied instead of 20 mils (0.51 mm) in the case of zinc. A lower impressed current was used than that for zinc--2 mA/ft^2 (21 mA/m^2) instead of 3 mA/ft^2 (32 mA/m^2). A major difference with Ti was the use of a cobalt nitrate catalyst that was applied onto thermal-sprayed Ti surface. A catalyst is used because the passive films that form on Ti would block or reduce current flow. For characterization purposes, some Ti coatings were applied to pyrex glass instead of concrete, and one on concrete was electrochemically aged without catalyst.

Depoe Bay Bridge (OR)--The Depoe Bay Bridge consists of the original structure built in 1926 and another bridge built adjacent to the west face in 1939 to widen the bridge. Installation of an ICCP system began in 1993. A Ti anode was thermal-sprayed to the underdeck and beam areas of the southern-most approach span of the bridge built in 1939. The remainder of the bridge was cathodically protected using a thermal-sprayed zinc anode system. Considerable experience was gained from this and the details of that installation have been published.[6-7]

The thermal-sprayed Ti anode was catalyzed with cobalt nitrate. The catalyst was sprayed onto the Ti anode surface at an application rate of 0.355 L/m^2 (0.0087 gal/ft^2) with 5.4 mA/m^2 (0.5 mA/ft^2) cathodic protection current density flowing between the Ti and the rebar. This zone measured 280 m^2 (3015 ft^2) and was operated at a current density of 2.8 to 3.8 A/m^2 (0.26 to 0.35 mA/ft^2) and a voltage of 1.4 -1.7 V. The anode was operated approximately 1.4 years after the system was energized when two 5.1 cm (2 in) diameter core samples were taken for purposes of characterizing the Ti-concrete interface. At the time of coring the anode electrochemical age was about 146 kC/m^2 (3.8 $A\text{-}h/ft^2$).

Surface Resistance Measurements--The resistance of the Ti anode was measured with a multi-pin resistance probe before and after electrochemical aging. No surface preparation was required for these measurements which, for the laboratory concrete slabs, were made prior to and at the conclusion of the electrochemical aging experiment. Measurements from the Depoe Bay Bridge were taken under field conditions. The initial measurements were made immediately after the anode was applied to the concrete and prior to catalyzing the anode. Measurements were then made on the catalyzed anodes after electrochemical aging.

Interfacial Chemical Analysis

X-Ray Diffraction (XRD)--XRD analysis was used to identify crystalline phases in the reaction products formed by electrochemical dissolution of the zinc anode and by secondary mineralization. The samples examined were reaction products taken from the zinc concrete interface and from the surface of the zinc coating, and included samples taken from laboratory slabs and from the Cape Creek Bridge. XRD analysis was also used to characterize the phases formed during the thermal-spraying of Ti coatings.

Analytical Scanning Electron Microscope (ASEM) and Electron Microprobe (EMP)--Cross-sections of electrochemically aged slabs were examined using ASEM to determine physical, chemical, and

mineralogical characteristics of the coating-concrete interface and changes that may be associated with electrochemical aging and that affect adhesion strength and operation of ICCP systems. To keep the concrete from crumbling during grinding and polishing, the samples were embedded in ring forms using a 5:1 ratio epoxy, infiltrated under vacuum, and then cured overnight.

The cross-sectioned samples were carbon coated prior to imaging. Chemical analysis was performed using a wave-length dispersive (WDS) x-ray analyzer with 4 crystals, and an energy-dispersive x-ray analyzer (EDS) with atmospheric thin window for low atomic number elements.

Interfacial pH Measurements--Electrochemically-aged thermal-sprayed zinc and Ti coatings were carefully pealed from the concrete substrate. Some of the zinc minerals formed during the aging process were retained on the peeled zinc. A drop of high purity water was placed on the metal surface that had been in contact with the concrete and mixed, using a glass rod, with minerals adhering to the surface. The pH of the droplet was measured using a micro-combination pH electrode and required as little as 0.1 mL of solution. A similar measurement using powder scraped from the exposed concrete surface generally resulted in pH values somewhat higher than that measured on the exposed metallic surface because of the larger amount of cementatious material included in the measurement.

RESULTS AND DISCUSSION

Thermal-sprayed Zinc ICCP Anodes

Zinc Pull-Off Failure Mechanism--A backscattered electron (BSE) ASEM photomicrograph of a cross-section of the zinc concrete interface from a preheated slab aged an equivalent of 13.2 years (1100 kC/m^2 or 28.4 $A\text{-}h/ft^2$) is shown in Fig. 1. The white and light gray zones are areas with high atomic number elements (primarily zinc). The brightest zone is the zinc coating. Voids and delaminations between the zinc splats typical of thermal-sprayed zinc are evident within the coating. Figure 1 shows the zinc coating followed the topography of the concrete surface. There was no obvious difference between the interfaces for the preheated and unheated slabs. The reaction zones identified in Fig. 1 are discussed later.

The primary failure mode when the coating is pulled from the concrete substrate was cohesive fracture within a thin layer of the zinc minerals and zinc-rich concrete immediately adjacent to the zinc. As failure occurs, cracks propagate through the hardened cement paste and around sand particles, causing some pull-out of the particles. The layer of concrete where failure occurs is roughly 0.05-0.20 mm (2-8 mils) thick. This failure zone coincides, as will be shown later, with zones affected by the zinc reaction products. In contrast, tensile failure of the underlying concrete, using the same test technique, produced massive pullout of the concrete matrix.

Adhesion Strength--Adhesion strength as a function of charge passed during electrochemical aging is shown in Fig. 2 for the preheated (a) and unheated (b) zinc-coated slabs. The six individual measurements from each test slab are given for the purposes of illustrating the scatter in the data. The lines through the data arise from an empirical model developed to describe the adhesion behavior.[4] The scatter in adhesion strength values is typical of measurements on these types of samples. In spite of the scatter, it is evident that there are several trends associated with the data. To aid interpretation, note that 200 kC/m^2 (5.2 $A\text{-}h/ft^2$) is roughly equivalent to 3 years of service for the zinc anode ICCP systems used by ODOT.

The average initial adhesion strength was 2.06 MPa (299 psi) for the preheated slabs and 1.15 MPa (167 psi) for the unheated slabs. These strength values show the benefits gained from preheating the

concrete, at least in terms of initial adhesion strengths. Values for the preheated slabs are 80% higher than for the unheated slabs. This benefit is consistent with the results of Brousseau *et al.*[9]

With charge transfer across the zinc-concrete interface, Fig. 2 shows the adhesion strength decreases during the early stages of aging for both the preheated and unheated slabs. This decrease is more pronounced for the preheated slabs. The adhesion strength reaches a minimum for both types of slabs at about 50 kC/m^2 (1.3 A-h/ft^2) and then begins to increase for larger values of charge. The minimum corresponds to roughly nine months for the ICCP systems used by ODOT.

For charge values of about 200 kC/m^2 (5.2 A-h/ft^2), adhesion strengths for the preheated and unheated slabs are nearly identical. The adhesion strength then continues to increase for larger values of charge. This increase concludes at strengths greater than the initial adhesion strengths--strengths of about 2.5 MPa (363 psi) at 400 to 600 kC/m^2 (10.3 to 15.5 A-h/ft^2).

With further charge transfer, the adhesion strengths of both preheated and unheated slabs decrease. This is in contrast to Brousseau *et al.*[10] where adhesion strengths decreased rapidly after much smaller values of charge were passed. Adhesion strengths near zero, observed in the later stages of aging for both preheated and unheated slabs, occur when there is significant delamination of the coating from the concrete. When the zinc coating is removed, the exposed concrete has a mottled appearance produced by a mosaic of white corrosion products and gray concrete (representing remaining points of attachment for the coating). Many of the remaining points of attachment were characterized by "fingers" of the zinc coating projecting deeply into the concrete at locations of deep narrow surface hollows. The nonhomogeneous distribution of the coating dissolution products undoubtedly contributes to much of the scatter found in the adhesion strength measurements.

Voltage Response--The electrochemical performance of the zinc anodes was examined by the voltage required to maintain a constant anodic current density. Even though laboratory tests were conducted in an environment where the RH was controlled between 80 to 85%, the concrete continually lost water during electrochemical aging due to evaporation or consumption. To avoid exceeding the operating range of the current sources used in the aging experiment, it was necessary to periodically wet the zinc anodes with deionized water. The potential-charge record for one group of slabs is shown in Fig. 3. The saw-tooth pattern is a result of the wetting and drying periods. Potentials rapidly dropped after wetting and gradually climbed during drying. As electrochemical aging preceded, the minimum voltage reached upon wetting gradually increased. The rate of voltage increase during drying also increased with electrochemical aging.

Operating results for the Richmond San Rafael Bridge are shown in Fig. 4 for bands 1 and 4, expressed in terms of a circuit resistance (voltage divided by current) to normalize variations in voltage and current over the 12 year period. The circuit resistance of band 1 (dashed curve) increased slowly over this period, reaching 1 kΩ within 7 years, and 2 kΩ in an additional 4 years. The periodic rise and fall of the circuit resistance reflects seasonal variations of moisture within the concrete delivered by fog, precipitation, and humidity. The resistance of band 4 (solid curve) increased much more rapidly, reaching 2 kΩ within 4 years. Furthermore, the circuit resistance of band 4 exceeded 7 kΩ at the end of the 12 year period, more than three times the resistance of band 1. The seasonal fluctuations in circuit resistance for band 4 are greatly exaggerated compared to those for band 1, presumably reflecting drier conditions during part of the annual cycle for the concrete in contact with band 4. This interpretation is reinforced by the fact that the annual minimum resistance, when conditions are wettest, are often the same for both bands. Laboratory research has shown that the rise in the minimum circuit resistance is associated with mineral formation from zinc dissolution products at the zinc-concrete interface.[3] The

effect of this mineral formation is a requirement for increasing system voltage with increasing electrochemical age of the ICCP system.

Zinc-Concrete Interfacial Chemistry--The zinc-cement interface in Fig. 1 was characterized by WDS and EDS analyses. Two reaction zones, "zone 1" and "zone 2", are observed in Fig. 1 between the zinc and cement paste. Zone 1 is primarily Zn and O in roughly equal amounts of each. Zone 1 was also found to be enriched in Cl and S. Silica particles in zone 2 (the roundish dark areas) serve as markers for the original location of the cement paste in contact with the zinc. The presence of these silica particles shows that zone 1 formed from the original zinc coating and zone 2 formed from the original cement paste. Zone 2 is cement paste enriched in Zn and depleted in Ca. The presence of Zn within this zone indicates reactions where Zn has modified the mineralogy of the original cement paste during repeated wetting and drying cycles. This modification of the original cement paste with Zn is termed "secondary mineralization".

The thickness of these zones show significant variation within aged samples. Nevertheless, observations of several samples[2-4] indicate that the zones develop over time and that zone 1 forms prior to zone 2. Cape Creek core samples show evidence of zones similar to those found in the laboratory samples (zone 1 and one case of zone 2). However, in the laboratory, accelerated aging takes place without accelerated diffusion (from concentration gradients). So the mass transport mechanisms associated with Zn enrichment and Ca depletion that define zone 2 may bear a somewhat different relationship to the electrochemical processes at the Cape Creek Bridge.

The white corrosion products found underneath the zinc coatings after the later stages of aging were examined with XRD. The corrosion products were primarily zincite (ZnO). Also present as minor constituents were wulfingite ($Zn(OH)_2$), simonkolleite ($Zn_5(OH)_8Cl_2 \cdot H_2O$), and hydrated zinc hydroxide sulfates ($Zn_4SO_4(OH)_6 \cdot xH_2O$). The presence of the zincite phase supports the WDS and EDS results where the corrosion product in zone 1 has a one-to-one Zn-to-O ratio.

White corrosion products were also formed on the surface of the zinc coatings on both the laboratory slabs and on the Cape Creek Bridge (after 3.7 years of ICCP). Simonkolleite ($Zn_5(OH)_8Cl_2 \cdot H_2O$) was found in the Cape Creek Bridge samples. Simonkolleite was also the primary constituent from the surfaces of laboratory samples, along with hydrozincite ($Zn_5(CO_3)_2(OH)_6$) and $Zn_4SO_4(OH)_6 \cdot xH_2O$. The presence of simonkolleite as the major surface corrosion products from both the Cape Creek Bridge and the laboratory samples suggests a good correspondence between the conditions in the natural and accelerated aging processes.

Interfacial pH--The pH measured under the zinc coating dropped rapidly from about 10 to 7.5 after aging 500 kC/m^2 (12.9 A-h/ft^2) in laboratory studies where the concrete was periodically wetted. With further aging, the pH approached 7.[11] Similar measurements on samples removed from the Cape Creek Bridge (OR) after 250 kC/m^2 (6.4 A-h/ft^2) gave pH values in the range 8.6 to 10.[11] A sample from the East Camino Undercrossing (CA) aged 1670 kC/m^2 (42.9 A-h/ft^2) gave a value of 9.5.[11] Many samples taken from the south column of pier 4 of the Richmond-San Rafael Bridge (CA) aged 2170 kC/m^2 (55.8 A-h/ft^2) gave values in the range 7 to 8. Clearly, the pH at the interface decreases with aging for structures in service, with the values depending upon wetting, sheltering, and the amount of reaction product at the interface. For anodes that are exposed to significant wetting and drying, such as those on Pier 4 of the Richmond-San Rafael Bridge, the pH decreases to values similar to those observed in the laboratory for periodically wetted anodes.

Strengthening and Weakening Mechanisms--The initial bonding of the zinc to the concrete is purely mechanical. The "tooth" given to the concrete by sand blasting and by surface porosity allows the zinc to mechanically adhere. Preheating the concrete prior to spraying increases this initial adhesion strength.

The early decline in adhesion strength is from the degradation of some of the initial mechanical bonding. The current passing through the concrete follows paths of least resistance. Other things being equal, these paths would be where the zinc is closest to the rebar--at the recesses of surface roughness. These places would tend to be the first places to react to form zone 1. The tendency of the concrete to channel current (another example would be around aggregate) would lead to "hot spots" where current densities are higher and more zinc is reacted. The reaction is Zn oxidizing to ZnO. Since ZnO has a volume a factor of 1.6 larger than Zn, this expansion loosens the mechanical grip and reduces the adhesion strength.

Since both preheated and unheated slabs decline to the same strength levels (preheated strengths decline more), the advantages of preheating are lost. It may be that the extra strength provided by preheating is from the same locations that are degraded by the first reactions to form ZnO.

The subsequent increase in adhesion strength results from secondary mineralization.. Secondary mineralization (the dissolution and reprecipitation of zinc reaction products) allows cracks and pores within the cement paste to fill. This filling of cracks and pores eliminates stress-risers within the cement paste, as well as increasing the effective cross-sectional area under stress. No significant differences between preheated and unheated samples were observed.

Later declines in adhesion strength are due to the volume expansion in forming ZnO, combined with the nonhomogeneity in the thickness of the ZnO layer (from "hot spots") that result in local stresses at the coating-concrete interface. The stresses increase with increasing electrochemical aging. Cracking within zone 1 and between zone 1 and zone 2 (Fig. 1) results from these stresses and leads to a reduction in adhesion strength. Eventually, the cracks lead to widespread delamination of the coating. No significant differences between the preheated and unheated samples were observed.

The presence of cracks at the coating-concrete interface would presumably cause delamination much sooner in applications where freeze-thaw cycles exist. Water, when present in the cracks, would freeze and expand, adding further stresses to the coating-concrete interface.

Lifetime Predictions--Based on adhesion strength (Fig. 2), the lifetime of the zinc coatings, for both preheated and unheated concrete, was approximately 1800 kC/m^2 (46.4 $A\text{-}h/ft^2$). Based on ODOT ICCP currents of 0.2 mA/ft^2 (2.2 mA/m^2), this represents a lifetime of 27 years. Figure 2 was for experiments that experienced frequent wetting and drying cycles. When the concrete slabs were not wetted,[12] the adhesion strengths continually declined. The life estimate for slabs that were not wetted was 10 years rather than 27 years for the periodically wetted slabs.

Thermal-Sprayed Titanium ICCP Systems

The primary advantage to using Ti anodes for ICCP rather than zinc is that Ti anodes are non-consumable. Titanium is also very corrosion resistant due to passivation. However, passivation means that Ti alone would not work as an effective anode material since the passive layer would prevent significant current flow. Hence, a cobalt nitrate catalyst is used and Ti simply acts as a conductor for the cathodic protection current and as a support structure for the catalyst. Neither the catalyst nor the Ti is consumed in the anodic reaction, which is reported[13] to be:

$$4OH^- \rightarrow O_2 + 2H_2O + 4e^- \quad (1)$$

The catalyst may need to be reapplied due to migration, leaching, or reaction with other compounds, but this could be done without requiring replacement of the Ti.

Coating Characterization Prior to Aging--The major phases identified by XRD were α-Ti having a close-packed hexagonal structure, and a phase similar to TiN and/or TiO having a face-centered cubic (fcc) structure. The fcc phase appeared to have a slightly contracted lattice structure (relative to the lattice dimensions for the TiN standard)--not unusual considering the nonequilibrium nature of the thermal-spray coating. TiO and TiN have the same fcc crystal structure and similar lattice parameters, which, in this case, made them indistinguishable by XRD. No TiO_2 was detected by XRD nor was there any body-centered cubic β-Ti.

A cross-section of Ti applied on pyrex glass using air atomization is shown in Fig. 5. The BSE image (b) shows banding in the Ti coating related to composition differences which are not evident in the SE image (a). The banding is produced by gradients in composition of the coating. The brighter bands contain higher concentrations of metallic Ti, and the darker bands higher concentrations of TiO and/or TiN. Thus, there are alternating layers first rich in α-Ti and then poor in α-Ti (but rich in TiO and/or TiN). EMP depth profiling indicates the presence of gradient bands corresponding to the banding in Fig. 5(b). The brighter bands are 70 to 80 at% Ti; the darker bands are 60 to 70 at% Ti.

Electrochemical Performance--Five Ti-coated concrete slabs were aged electrochemically for 1.8 years at a current density that was a factor of 6 to 8 higher than that used by ODOT at the Depoe Bay Bridge. The actual electrochemical age was 1520 kC/m^2 (39.2 A-h/ft^2), which is equivalent to 10 to 14 years at 2.8 to 3.8 mA/m^2 (0.26 to 0.35 mA/ft^2) as used by ODOT. The current was controlled in this experiment and thus the voltage varied due to changes in the environment and at the Ti-concrete interface. The minimum voltage after wetting remained low throughout the experiment for the catalyzed slabs, but increased for the uncatalyzed slab (similar to zinc anodes).

Figure 6 shows the response of the voltage of the five slabs to different levels of humidity at a current density of 21.5 mA/m^2 (2 mA/ft^2). The behavior of the four catalyzed slabs is similar and shows only a slight increase in voltage at lower levels of humidity. The uncatalyzed slab, however, shows a strong dependence on humidity, with lower levels of humidity causing greater voltage demands for the system. This is not unexpected because Ti oxide films have been considered for use as humidity sensors because they show increased levels of ionic conduction when water is adsorbed to the surface.[14] The increased levels of humidity may also reduce the voltage requirement for the system by reducing the resistance of the cement paste near the Ti-concrete interface.

Voltage decay following the application of water to the anode-concrete interface was reported to indicate the formation of a barrier layer of reaction products.[12] The voltage decay behavior of thermal-sprayed zinc anodes was exponential with the slope of that decay decreasing with greater levels of electrochemical aging. The decreasing slope was interpreted as an indication that a barrier layer was formed and that the layer retarded the inward transport of moisture to the interface. This was not the case for thermal-sprayed Ti anodes. Wetting of the Ti anode caused the voltage to drop to stable low levels within 60 s of wetting, even after 1520 kC/m^2 (39.2 A-h/ft^2) of electrochemical aging. This indicates that no barrier layer was formed at the Ti-concrete interface.

Physical and Mechanical Properties--Electrochemical aging of the thermal-sprayed Ti anode resulted in changes in physical and mechanical properties of the anode. There was no apparent change in thick-

ness due to electrochemical aging. This means that, as suspected, the Ti anode does not dissolve significantly nor is the coating lost in other ways during the electrochemical aging process. Anode resistivity was observed to increase due to aging. The resistivity increased from an average of 1470 to 4177 μΩ-cm for the catalyzed slabs and from 1178 to 3192 μΩ-cm for the uncatalyzed slab--both after 1520 kC/m^2 (39.2 A-h/ft^2) of aging. For the Depoe Bay Bridge, the increase was from 1934 to 2070 μΩ-cm after 146 kC/m^2 (3.8 A-h/ft^2) of aging. These resistivity measurements were taken using a surface probe that sampled only the thermal-sprayed anode and not the cement paste beneath the anode. The increase in resistivity was, therefore, due to physical or chemical changes within the Ti coating that retard the conduction of electrons. Increased cracking of the coating to lengthen the conduction path or further oxidation of the Ti anode are possible causes of this increase.

Anode bond strengths were observed to decrease markedly with aging. This decrease was more severe for the uncatalyzed sample where the bond strength dropped from an average of 1.17 MPa (171 psi) to 0.01 MPa (0.92 psi). For all of the catalyzed slabs, the bond strength decreased from an average of 1.17 MPa (171 psi) to an average of 0.29 MPa (43 psi). Most of this decrease in bond strength appeared to be due to a weakening of the cement paste beneath the thermal-sprayed Ti.

Interfacial Chemistry after Aging--Polished cross-sections of the anode-concrete interfaces of an aged (1520 kC/m^2 or 39.2 A-h/ft^2) catalyzed slab show two altered layers beneath the Ti coating.[7] The two layers are a "reaction zone" just beneath the Ti coating and a "dense zone" between the reaction zone and unaltered cement. The reaction zone is more porous than the unaltered cement and the dense zone is less porous than the unaltered cement. The formation of a dense zone has been reported previously for Ti mesh anodes embedded in concrete.[15]

The chemical composition of the reaction zone, the dense zone and the interface were studied using EDS x-ray maps. Maps for Ti, Ca, and Co along with a BSE ASEM photo for a cross-section of an aged (1520 kC/m^2 or 39.2 A-h/ft^2) catalyzed slab are shown in Fig. 7. Matching the BSE photo to the x-ray maps makes it possible to see the distribution of the elements of interest at the interface and within the reaction zone. Figure 7(b) shows that the thermal-spray Ti anode is not consumed because there are no Ti reaction products evident within the concrete. Figure 7(c) shows that the reaction zone contains essentially no calcium in what was originally a calcium-rich cement paste. The region below the reaction zone is the dense zone and it contains calcium (it is not possible, using this analytical technique, to see if the calcium from the reaction zone is now part of the dense zone). The final x-ray map, Fig. 7(d), shows that cobalt that was added to catalyze the anodic reaction is still present, but has moved into the reaction zone. Note that it does not appear to have moved into the densified cement paste.

pH measurements of the cement paste at the Ti-concrete interface gave values as low as 6.2 for the uncatalyzed slabs and 7.2 for the catalyzed slabs. These values are acidic enough to favor the dissolution of calcium minerals. Beyond the reaction zone, the Ca and Si levels (20 and 25 at%, respectively) are similar to those reported previously for zinc-concrete interfaces subjected to accelerated electrochemical aging.[12] Previous research[15] on Ti mesh anodes showed that calcium carbonate is removed from the region near the Ti anode and reprecipitated in voids further from the anode as calcite and vaterite, both being mineral forms of calcium carbonate ($CaCO_3$).

A cross-section of the Ti-concrete interface from the Depoe bay bridge after 146 kC/m^2 (3.8 A-h/ft^2) of aging appears similar to cross-sections of the laboratory slabs with the exception of the numerous cracks in the Depoe Bay sample.[7] The Depoe Bay cross-section, like Fig. 7(b), revealed that the Ti anode does not dissolve into the cement paste. This contrasts with the results of cross-sections from the Cape Creek Bridge and East Camino Undercrossing (CA) where zinc from the thermal-sprayed zinc anode migrated into the cement paste.[15] After 146 kC/m^2 (3.8 A-h/ft^2), the calcium has not been

leached from the cement paste adjacent to the Ti coating. It is possible that the leaching of the calcium is not yet detectable after only 146 kC/m^2 (3.8 A-h/ft^2) of aging. Alternatively, there may be a critical current density for Ti anodes below which the cement paste does not deteriorate by leaching of calcium minerals.[7]

ONGOING AND FUTURE RESEARCH

Rocky Creek Viaduct

The Rocky Point Viaduct is located on the south central Oregon Coast. It was constructed in 1955 and observed to have corrosion problems as soon as 1967. It was replaced in 1995, after approximately 40 years of use. One beam from the substructure is being studied to determine the causes of the early failure of this bridge. Measurements being done include potential mapping, corrosion rate determination, delamination survey, chloride distribution, compressive strength of the concrete, and aggregate characterization. Slices from the beam were cut and thermal-sprayed with zinc for electrochemical aging and chloride migration experiments.

Alternative ICCP Anode Materials

Thermal-spray zinc anodes have been used to cathodically protect reinforced concrete structures. Research has shown some of the limitations of the zinc material when used in an ICCP system.[1-4] A new zinc hydrogel anode,[16-17] which combines rolled zinc sheet with a hydrogel adhesive, is easy to apply to structures of simple geometry and may eliminate some of the problems of the thermal-spray zinc anode. The use of thermal-spray zinc for GCP systems has had mixed results.[18-19] A new Al-Zn-In thermal-spray anode has been reported[18] to provide adequate protection current for longer periods of time than thermal-spray zinc when used in GCP systems. Both of these novel anode materials and thermal-spray Zn-15Al are part of a new accelerated electrochemical aging study aimed at determining changes in the power requirements for the cathodic protection system, adhesion of the anode to the concrete, chemistry at the anode-concrete interface, and other anode-concrete interactions.

Humectant Use with Zinc Anodes

The presence of moisture is critical at the zinc-concrete interface of thermal-spray zinc cathodic protection systems.[12] This moisture facilitates current flow and aides in secondary mineralization reactions which cause an initial strengthening of the zinc-concrete bond. Estimated service life decreases from 27 to 10 years when the interface is kept dry.[12] A new research effort is underway to determine the usefulness of humectants in maintaining moisture at the zinc-concrete interface. Humectants are chemicals that absorb water easily and can be applied to the thermal-spray zinc anode after installation. Studies will determine the effectiveness of the humectants in extending the useful service life of newly-installed thermal-spray zinc anode cathodic protection systems and in rejuvenating older previously-installed thermal-spray zinc anode cathodic protection systems.

Atmospheric Corrosion of Thermal-Sprayed Aluminum Coatings

Coated panels of 1010 mild steel were boldly exposed (with horizontal and vertical orientations) on seven coastal Oregon bridges[20] along U.S. 101 for 3 years (Fig 8). The panels were sandblasted before coating. One set of panels (T) were thermal-sprayed with Al to a thickness of 8-10 mil (0.20-0.25 mm), which was then immediately sealed with a 1 mil (0.025 mm) thick epoxy coating, followed with a 2 mil (0.051 mm) thick pigmented urethane coating. A second set of panels (P) were coated using a three-coat paint system. This coating system consisted of a 3 mil (0.076 mm) zinc-dust filled urethane primer, a 3

mil (0.076 mm) moisture-cured urethane intermediate coat, and a 3 mil (0.076 mm) pigmented moisture-cured urethane topcoat. All paint coating thicknesses were wet thicknesses. Prior to exposure, the coating on each panel was cut with a tungsten carbide scribe in an X-pattern through to the mild steel substrate to exposed the steel along the scribe lines.

Panels thermal-sprayed with Al (T) showed little evidence of corrosion along the scribe lines or elsewhere at any of the bridge locations and at all orientations, Fig. 8. Panels using the three-coat paint system (P) showed varying degrees of corrosion, blistering, and undercutting depending upon bridge location and orientation, Fig. 8. In all cases, the paint system panels experienced corrosion of the steel along the scribe. In some cases, the panel damage was severe, as at the Spencer Creek Bridge on the central Oregon coast. In others, such as at the Rogue River Bridge on the southern Oregon coast, the damage was much less severe. The damage was more extensive for horizontal exposures, where moisture could pool on the surface for long periods, than for vertical exposures. For highly corrosive environments, such as at the Spencer Creek Bridge, the corrosion was severe regardless of orientation.

CONCLUSIONS

Electrochemical aging of thermal-sprayed zinc anodes results in the formation of reaction zones at the zinc-concrete interface. Zone 1 forms due to the oxidation of the thermal-sprayed zinc anode. Zone 2 forms when the zinc dissolution products replace Ca in the cement paste (secondary mineralization). Anode dissolution and secondary mineralization result in a lowering in pH and an increase in the voltage required to maintain a protective current. With wetting and drying cycles, adhesion strengths initially decreased due to zinc reactions degrading the mechanical bond and then increased due to the filling of voids and cracks by secondary mineralization. Eventually, the adhesion strength drops towards due to cracks arising from volume expansion in zone 1. Laboratory predictions of service lives until detachment are 27 years with wetting and drying cycles and 10 years without wetting. Preheating the surface prior to spraying made no difference in long term adhesion strengths of wetted anodes. Accelerated laboratory electrochemical aging of zinc is similar to field experience in terms of voltage response and interfacial chemistry (similar zone formation, mineral formation, and pH).

Thermal-sprayed Ti in air results in a layered TiO/TiN/α-Ti structure with sufficient conductivity to carry cathodic protection currents. After electrochemical aging, two zones are formed from the cement paste--a reaction zone just beneath the Ti and a dense zone below that. The reaction zone is depleted in Ca and has a low pH. No Ti products were found in the reaction zone. The Co in the catalyst was found in the reaction zone. The catalyst was found to keep operating voltages low, even under low humidity conditions. The catalyst also resulted in better long term adhesion strengths than without catalyst.

Thermal-sprayed Al coatings on mild steel performed well after 3 years of coastal atmospheric exposure, especially in comparison with a zinc-filled three-coat paint system.

REFERENCES

1 B. S. Covino, Jr., S. J. Bullard, G. R. Holcomb, S. D. Cramer, G. E. McGill, and C. B. Cryer, Corrosion, 53 (1997) 399-411.

2 B. S. Covino, Jr., S. D. Cramer, S. J. Bullard, G. R. Holcomb, G. E. McGill, and C. B. Cryer, "Factors Affecting Thermal-Sprayed Zinc Anodes on Concrete," Proceedings of 13th International Corrosion Congress, Volume II, Melbourne, Australia, Australasian Corrosion Association, Inc., paper 173 (1996) 7 pp.

3 B. S. Covino, Jr., S. D. Cramer, G. R. Holcomb, S. J. Bullard, G. E. McGill, and C. B. Cryer, "Thermal-Sprayed Zinc Anodes for Cathodic Protection of Reinforced Concrete Structures," in Materials for the New Millennium, Proceedings of the of 4th Materials Conference, ed. by K. P. Chong, American Society of Civil Engineers (1996) 1512-1521.
4 G. R. Holcomb, S. J. Bullard, B. S. Covino, Jr., S. D. Cramer, C. B. Cryer, and G. E. McGill, "Electrochemical Aging of Thermal-Sprayed Zinc Anodes on Concrete," in Thermal Spray: Practical Solutions for Engineering Problems, Proceedings of the 9th National Thermal Spray Conference, ed. by C. C. Berndt, ASM Thermal Spray Society (1996) 185-192.
5 J. A. Apostolos, D. M. Parks, and R. A. Carello, Materials Performance, 26, 12 (1987) 22-28.
6 G. E. McGill, S. D. Cramer, S. J. Bullard, B. S. Covino, Jr., and G. R. Holcomb, "Field Application of an Arc-Sprayed Titanium Anode for Cathodic Protection of Reinforcing Steel in Concrete," ODOT Interim Report, FHWA-OR-RD-97-01, Oregon Department of Transportation (1996).
7 B. S. Covino, Jr., S. D. Cramer, G. R. Holcomb, S. J. Bullard, W. K. Collins, R. D. Govier and G. E. McGill, "Characterization of Electrochemically-Aged Thermal-Spray Titanium Coatings on Concrete," Proceedings of the 1st United Thermal Spray Conference, (Indianapolis, IN, September, 1997), ASM International, (1997).
8 G. R. Holcomb, S. D. Cramer, S. J. Bullard, B. S. Covino, Jr., W. K. Collins, R. D. Govier, and G. E. McGill, "Characterization of Thermal-Sprayed Titanium Anodes for Cathodic Protection," Proceedings of the 1st United Thermal Spray Conference, (Indianapolis, IN, September, 1997), ASM International, (1997).
9 R. Brousseau, M. Arnott, and B. Baldock, Materials Performance, 33, 1 (1994) 40-42.
10 R. Brousseau, M. Arnott, and B. Baldock, "Arc Sprayed Zinc on Reinforced Concrete," ILZRO Project Report ZE-390, National Research Council of Canada (1994).
11 B. S. Covino, Jr., S. J. Bullard, S. D. Cramer, G. R. Holcomb, G. E. McGill, C. B. Cryer, A. Stoneman, and R. R. Carter, "Interfacial Chemistry of Zinc Anodes for Reinforced Concrete Structures," Corrosion/97, paper 97233, NACE International, Houston, TX (1997).
12 S. J. Bullard, B. S. Covino, Jr., G. R. Holcomb, S. D. Cramer, and G. E. McGill, "Bond Strength of Thermal-Sprayed Zinc on Concrete During Early Electrochemical Aging," Corrosion/97, paper 97232, NACE International, Houston, TX (1997).
13 Bennett, J.E., T.J. Schue, and G. McGill, Materials Performance, 34, 11 (1995) 23-26.
14 Gusmano, G.A., A. Bianco, G. Montesperelli, and E. Traversa, Electrochimica Acta, 41 (1996) 1359-1368.
15 Weale, C.J., "Cathodic Protection of Reinforced Concrete: Anodic Processes in Cements and Related Electrolytes," Thesis No. DX185652, The British Library, West Yorkshire, United Kingdom LS23 7BQ (1992) 415 pp.
16 R. J. Kessler, R. G. Powers, and I. R. Lasa, "Cathodic Protection Using Zinc Sheet Anodes and an Ion Conductive Gel Adhesive," Corrosion/97, paper 97234, NACE International, Houston, TX (1997).
17 R. Hartman and B. Hillier, "The Use of a Sacrificial Zinc Anode for Cathodic Protection of Steel in Reinforced Concrete," Corrosion/97, paper 97250, NACE International, Houston, TX (1997).
18 M. Funahashi and S. F. Daily, "New Sacrificial Anode for Cathodic Protection of Reinforced Concrete Structures," in Materials for the New Millennium, Proceedings of the of 4th Materials Conference, ed. by K. P. Chong, American Society of Civil Engineers (1996) 1257-1265.
19 R. Brousseau, "Sacrificial Cathodic Protection of a Concrete Overpass Using Metallized Zinc: Latest Update," Corrosion/97, paper 97239, NACE International, Houston, TX (1997).
20 S. D. Cramer, B. S. Covino, Jr., S. J. Bullard, and G. R. Holcomb, "Atmospheric Corrosion in Coastal Environments," in Innovative Ideas for Controlling the Decaying Infrastructure, ed. V. Chaker, NACE International, Houston, TX (1995) 151-164.

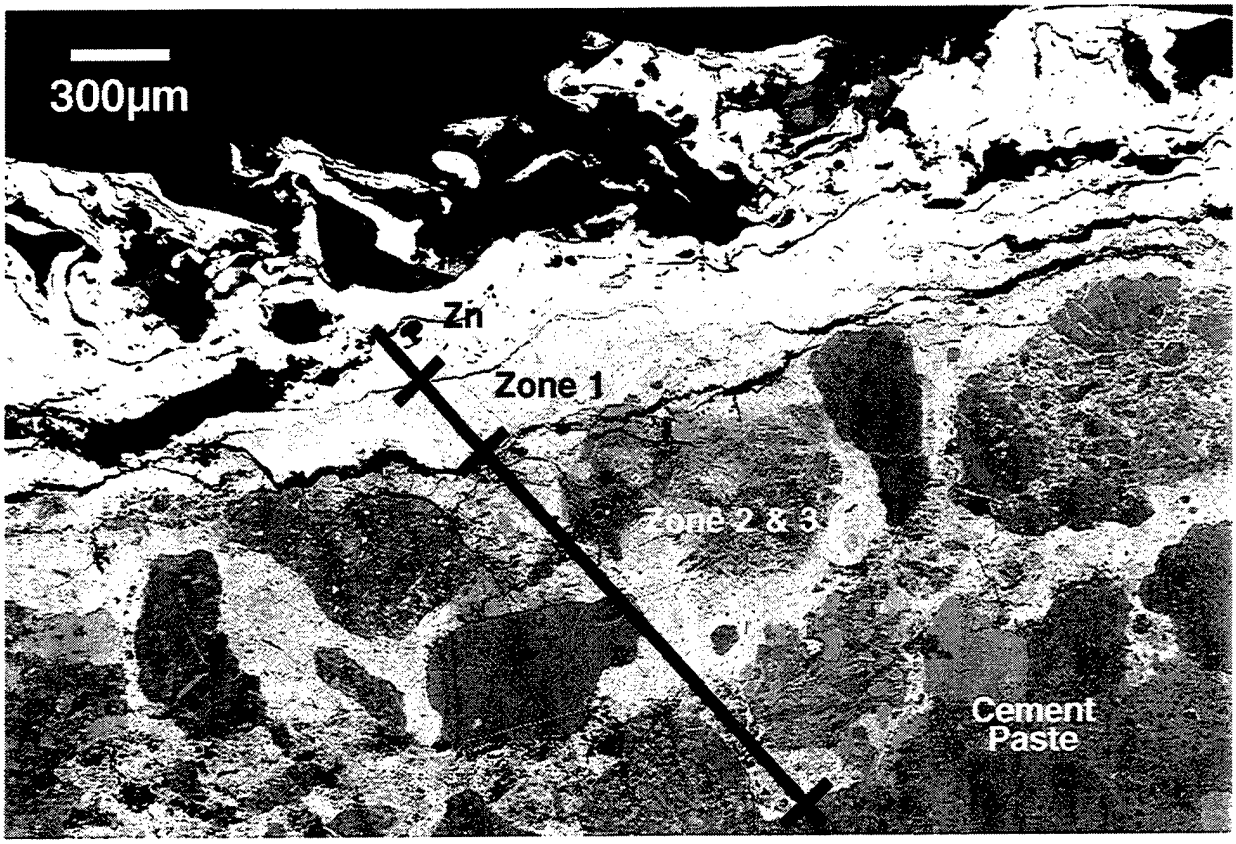

Fig. 1. Back-scattered ASEM micrograph of an electrochemically-aged zinc-concrete interface showing voids in the coating and failures along the interface. Reaction zones 1 and 2 are shown. Preheated with an effective aging time of 13.2 years.

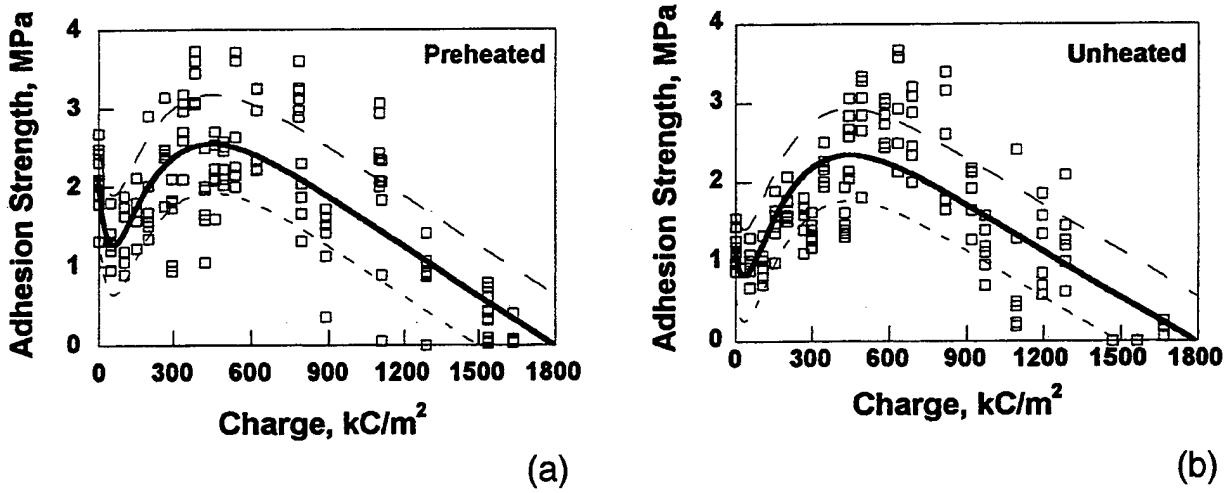

Fig. 2. Adhesion strength of electrochemically-aged arc-sprayed zinc on preheated (a) and unheated (b) concrete slabs as a function of aging charge. A multiplying factor of 0.0257 converts kC/m^2 to $A\text{-}h/ft^2$.

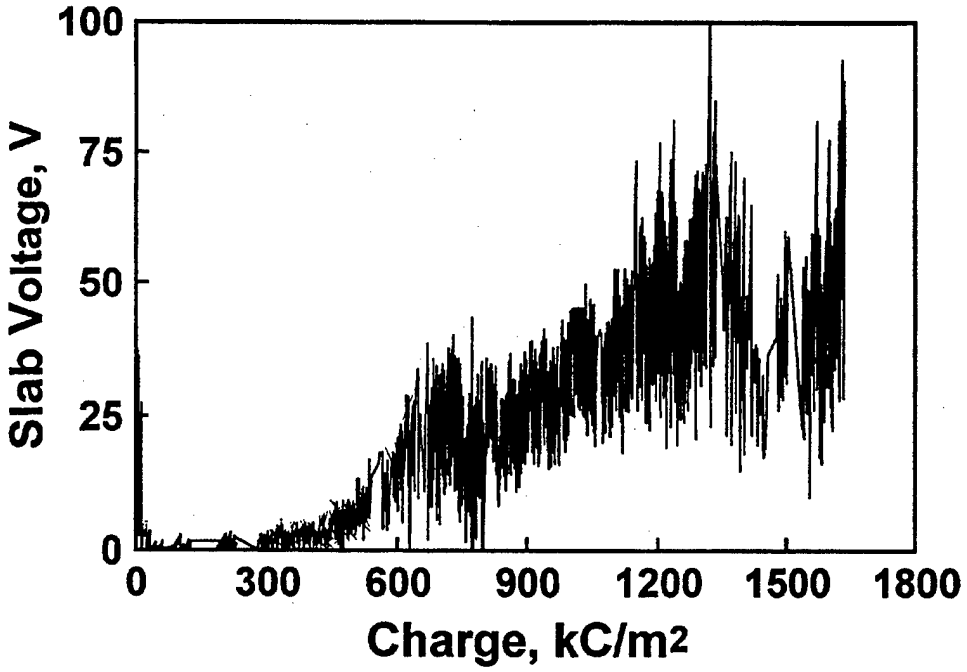

Fig. 3. Variation in voltage of a laboratory thermal-sprayed zinc ICCP system as a function of charge passed. A multiplying factor of 0.0257 converts kC/m^2 to $A\text{-}h/ft^2$.

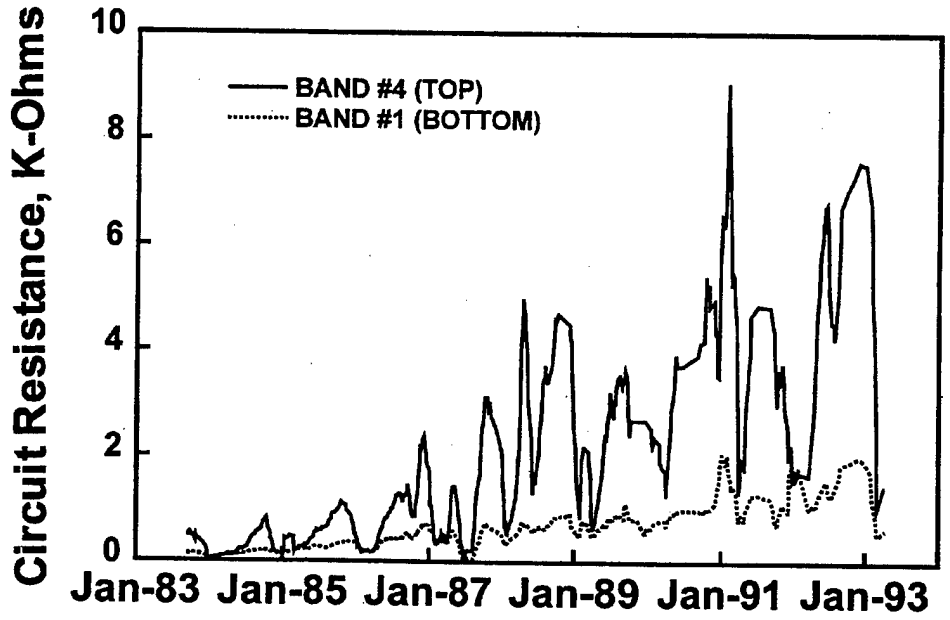

Fig. 4. Circuit resistance over 12 years of operation of the zinc ICCP system on pier 4 of the Richmond-San Rafael Bridge (CA). Band 4 is more sheltered to precipitation and wave action than band 1.

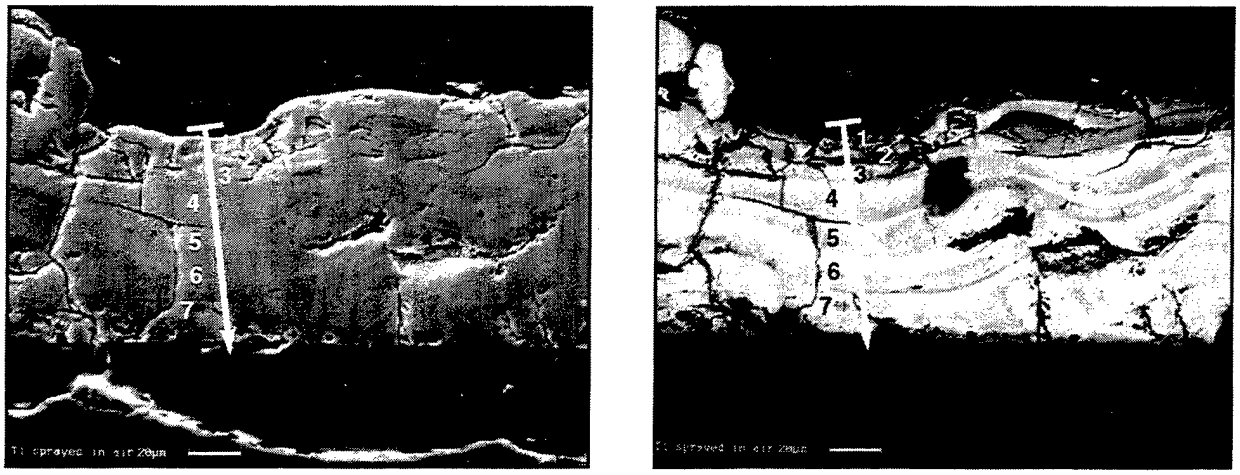

Fig. 5. Cross-section of thermal-sprayed Ti on pyrex glass: (a) SE image; (b) BE image. Arrow shows path of EMP traverse and the location of seven Ti gradient bands in the coating.

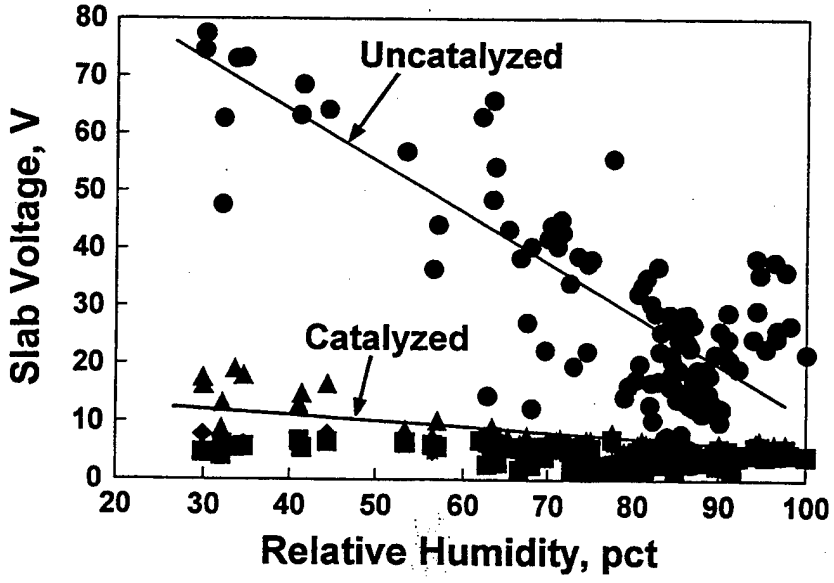

Fig. 6. Effect of humidity on voltage requirements during electrochemical aging of thermal-sprayed Ti in a laboratory ICCP system.

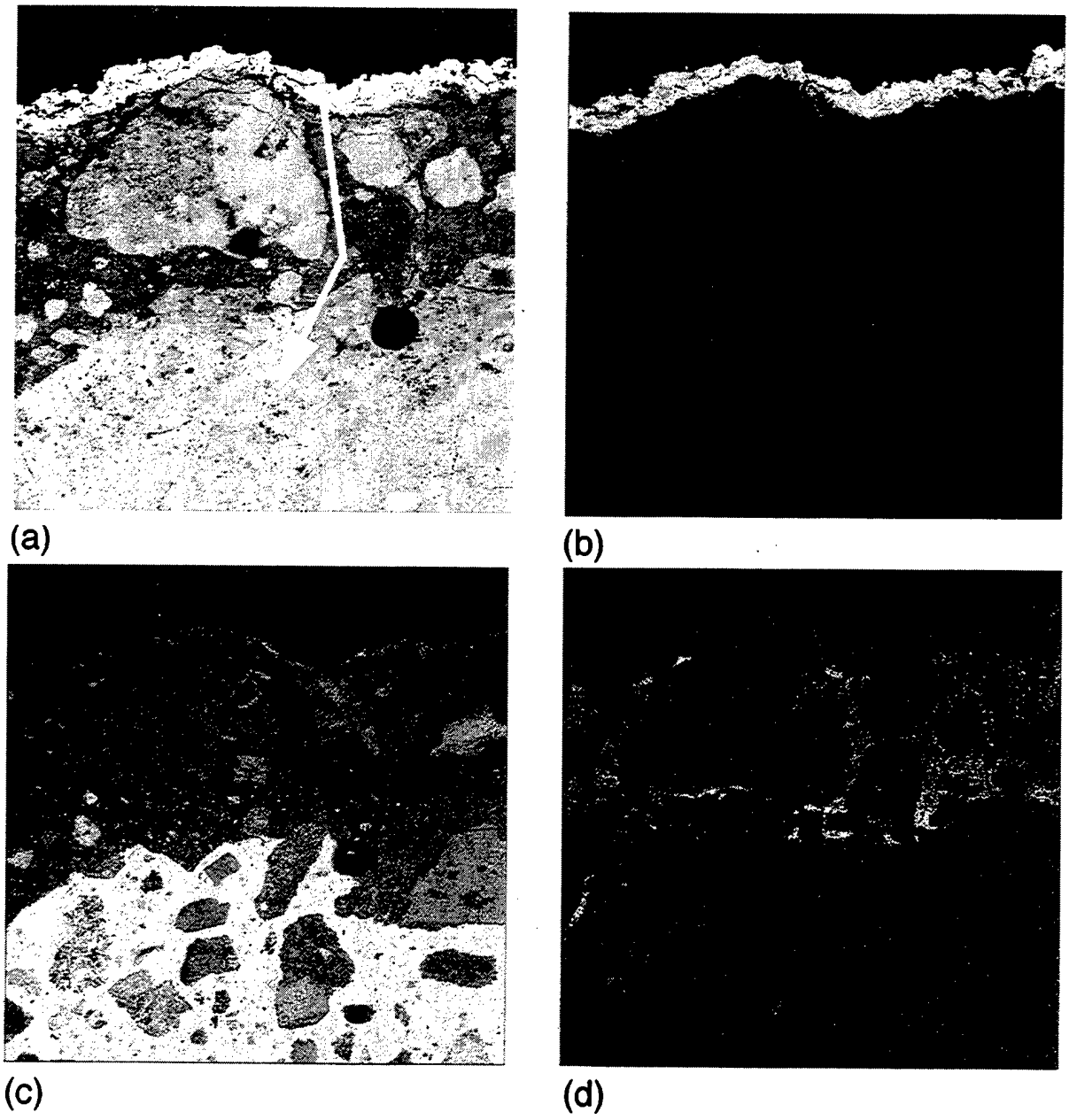

Fig. 7. Catalyzed thermal-sprayed Ti anode cross-section after electrochemical aging: (a) backscattere electron ASEM image; (b) Ti K_α x-ray map; (c) Ca K_α x-ray map; (d) Co K_α x-ray map.

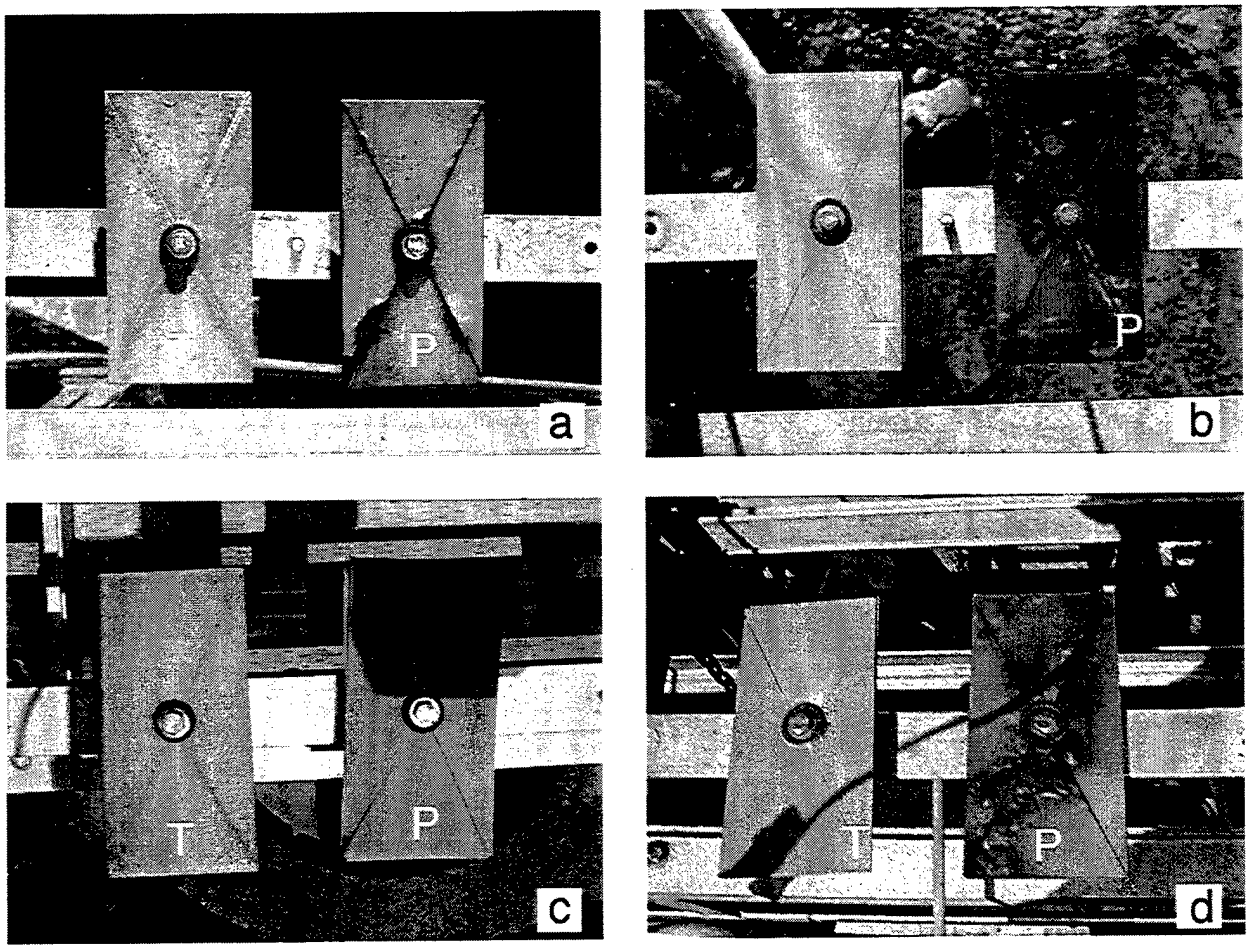

Fig. 8. Comparison of sealed thermal-sprayed Al coatings on mild steel (T) and three-coat moisture-cured urethane paint coatings on mild steel (P) in bold exposures. Photographs (a) and (c) are horizontal and vertical exposures from the Rogue River Bridge (OR). Photographs (b) and (d) are horizontal and vertical exposures from the Spencer Creek Bridge (OR).

EXTENDING USE OF ION VAPOR DEPOSITED (IVD) ALUMINUM AS A REPLACEMENT FOR ELECTROPLATED CADMIUM

Brian E. Placzankis, John H. Beatty
US Army Research Laboratory, Weapons and Materials Research Directorate
Aberdeen Proving Grounds, Maryland 21005

ABSTRACT

Continued environmental pressures have caused the Army and the rest of DoD to reduce their use of hazardous materials and processes. The process of electroplating cadmium usually produces considerable hazardous waste. Further, these electroplated items can release cadmium (a heavy metal toxin) back into the environment. As part of a program funded through the SERDP office (the Strategic Environmental Research and Development Program) sacrificial coatings of chromated ion vapor deposited (IVD) Al and electroplated Cd were applied to fasteners and components used in aerospace applications. Aerospace grade fasteners of 4340, Aermet 100, and Inconel 718 alloys were examined, along with the drag beam from a UH-60 Blackhawk helicopter. Fasteners were tested in several loading fixtures. Performance was compared using immersion tests in 3.5% NaCl, the GM9540P accelerated cyclic environmental test, and fatigue testing in accordance with MIL-STD-1312. Additionally, break-away torques were measured at the conclusion of all corrosion testing. The implications for expanding the use of IVD Al as a replacement for Cd in Army aircraft is discussed.

Keywords: Cadmium, IVD Al, fasteners, armor, fatigue, cyclic salt spray

INTRODUCTION

Corrosion of metallic components has always been a serious problem for military equipment. The harsh nature of the battlefield and varied climates found around the world compound the problem even further. To avoid destructive corrosion, countless protective schemes have been devised. One of the most common and successful strategies has been cathodic protection through the use of cadmium (Cd) as sacrificial anodic material on steel components. This coating is a proven lifecycle extender in many Army applications.

Unfortunately, cadmium poses a significant health risk. It is considered one of the toxic heavy metals which include lead (Pb), antimony (Sb), and mercury (Hg). The Environmental Protection Agency has continued to press for reductions in the use of Cd and improved processing techniques to eliminate Cd from the waste stream to reduce the threat to personnel and the environment. Although there has been a transition to Zn plated components, the U.S. Army continues to use Cd in its protection schemes for a wide variety of applications, especially in aircraft and in high strength fasteners. Due to these hazards and tougher environmental regulations, the Army is striving to reduce its dependency on the use of Cd.

Sacrificial cadmium coatings are used on steel to enhance corrosion resistance. The coating is anodic with respect to the substrate; therefore it corrodes first, supplying the protective cathodic polarization to the substrate. Although cleaner methods exist for applying Cd, most Cadmium is still electroplated. The electroplating methods can introduce significant hazardous material into their waste streams. Therefore, environmentally friendly alternatives to Cd need to be developed and exploited to further reduce the Army's use of Cd. To accomplish this, the US Army Research Laboratory (ARL)- Weapons and Materials Research Directorate, developed and executed a research program under the auspices of the Department of Defense Strategic Environmental Research and Development Program (SERDP) to examine commercially available alternatives for

electroplated cadmium. Ion Vapor Deposited(IVD) Aluminum was chosen as the most promising alternate to Cd and was the focus of our tests.

IVD Aluminum has been used as a sacrificial coating for steel substrates for a number of years. It is known for its environmentally clean application and a number of other properties which make it superior to Cd for a number of applications[1].
However, several barriers remain that prevent widespread substitution of IVD Al for electroplated cadmium. As an example, a flow chart developed by the Aviation & Troop Command (ATCOM) and Corpus Christi Army Depot (CCAD) to facilitate changes from Cd to IVD Al is shown in Figure 1. We see from this chart that the logical tests which lead to the decision "Not an IVD Al Candidate" are tight tolerances (such as fine threaded fasteners), and components that are flight critical and fatigue/SCC sensitive. Therefore, this study was aimed at providing baseline data that could be used to further define the logical tests used to make the IVD Al : Cd determination. A spectrum of tests was designed to examine fasteners and flight critical components. The tests included cyclic salt spray, salt water immersion, high cycle fatigue tests, and breakaway torque measurements. Fasteners, mock components, and actual components were tested.

EXPERIMENTAL PROCEDURE

Fasteners and Components

Three different high strength alloys were used for fastener testing: 4340 Steel (AMS 6415 @ R_c 51), Aermet 100 (AMS 6532 @ R_c 52) , and Inconel 718 (AMS 5662 @ R_c 45). Aerospace grade fasteners, 88.9 mm (3.5") long by 15.88 ±0.25 mm (5/8") diameter were machined with fine threads 0.6250-18 UNJF-3A per MIL-S-8879C. The hex head dimensions for the bolts were machined to 23.81 mm (15/16"). Mating nuts/washers were also machined from the test materials. Two mock assemblies were used to simulate real-world load conditions. These consisted of Joint A, two blocks of 4130 (R_c 32-34) steel with 17.46 mm (11/16") holes drilled through the centers of the faces, and Joint B, a 4130 block coupled to a threaded block of MIL-A-12560 (R_c 28-33) armor steel. The assemblies are discussed in detail in our earlier study[2]. Additionally, drag beams from the rear landing assembly of the UH-60 Blackhawk helicopter were also tested. These are made of 300M steel (AMS 6419), and are shown in Figure 2.

Cadmium & IVD Coatings

The fasteners were prepared in four different coating configurations: no coating, electroplated Cd - class III, IVD Al 1.0 mil, and IVD Al 1.5 mil. The thicknesses chosen for study were based on earlier work that suggested at least one mil of IVD Al was needed to give corrosion protection equivalent to a Cd Class III coating[3]. Both the Cd and IVD Al coatings were applied at Corpus Christi Army Depot, Corpus Christi, TX. Chromate conversion coatings were applied to both the IVD Al & Cd coatings, but not to the uncoated fasteners.

Corrosion Testing

The fasteners, fastener assemblies, and drag beams were placed into a cyclic salt spray chamber (Attotech Model CCTC-40) and tested with GM Standard Test 9540P, Method B[4] to provide a more realistic accelerated environmental test than conventional ASTM B117 salt fog[5]. The 9540P test consists of 18 separate stages which include the following: saltwater spray (1% NaCl, 0.1% $CaCl_2$), humidity, drying, ambient, and heated drying. The environmental conditions and duration of each stage for one complete 9540P cycle are given in Table 1. Specimens were all photographed prior to testing, upon significant observations, and at the suspension of the testing (100 cycles). Fastener assemblies were lubricated and torqued to 216 ft-pounds prior to testing. Breakaway torques were measured at the conclusion of the 9540P test.

Salt water immersion tests (3.5% NaCl solution) were performed on the fasteners in a circulating bath at 25 °C. Electrochemical potential measurements and visual observations were made at regular intervals. Each fastener was wired for immersion testing, and the electrical lead from each specimen was connected through a multiplexer to a digital multimeter that was monitored by a Mac based workstation. By recording the mixed corrosion potentials of the fasteners, it is possible to compare the relative performance of each coating on each alloy tested. To avoid fouling of the bath and prevent corrosion products from depositing on uncorroded specimens, specimens were removed from the immersion bath when approximately 25% of their surface area had corroded.

Fatigue Testing.

High cycle fatigue tests in accordance with MIL-STD-1312[6] were performed on the fasteners at the U.S. Navy Air Warfare Center (NAWC). Loading parameters for each alloy were scaled as a function of the ultimate tensile strength of each material, as given in Table 2.

RESULTS

Cyclic Salt Spray (GM 9540P)

Performance for each coating system on each fastener assembly is given in Table 3. The performance was rated on pass/fail basis, where the appearance of 3 or more rust spots at least one millimeter in diameter is considered a failure. Figure 3 shows an uncoated Aermet 100 fastener, which is representative in appearance of both the Aermet and 4340 fasteners after completion of the first cycle. All of the coatings provided good corrosion protection to the fasteners. The 1 mil IVD Al Joint A failed after 86 cycles, making it the only coated assembly to fail before the completion of the 100 cycles (Figure 4). The other assemblies showed varying signs of sacrificial coating degradation but no substrate corrosion.

The IVD Al coated drag beam displayed small scattered pits before the completion of the first cycle. Most of the pits stabilized for the remaining exposure, but continued build-up of corrosion products (Al_2O_3) suggested that some pits continued to grow at regions near the drag beam ends where sharp edges were present (Figure 5). The interior surfaces of the IVD Al coated beam (Figure 6) rusted within the first ten cycles. Very little rust was observed on the exterior of the IVD Al coated beam, even after 100 cycles (Figure 7). The Cd plated beam initially performed better than the IVD Al coating. Neither pitting nor rusting were observed until 65 cycles had been completed. After 65 cycles, however, rusting was observed in regions near the ends (Figure 8). Throughout the test the interior of the Cd plated drag beam showed very little rusting(Figure 6).

Breakaway Torques

As previously stated, fastener assemblies were initially torqued to 216 ft-lbs prior to cyclic saltspray testing. At the completion of the cyclic test, breaking torques were measured as the assemblies were disassembled. Table 4 shows the results for each alloy and each respective test assembly. With two exceptions, the breakaway torque measured for the IVD Al was significantly greater than the initial torque applied. The Cd assemblies produced mixed results. The specimens without a sacrificial coating exhibited breakaway torques equal to or lower than the initial torque.

It should be noted that in addition to the loaded assemblies, unloaded bolts with a washer and nut screwed onto the threads were also exposed for the full 100 cycles. At the end of the cycling, the unloaded Cd coated specimens turned easily on their threads. The IVD Al coated specimens were completely seized, and required wrenches to be loosened. Inspection by optical microscopy revealed galling on the IVD coated threads caused by the formation of hard Al_2O_3 deposits. The deposits grind in the threaded portions and damage the surface finish and may

degrade the performance of threaded components. (Figures 9a,b) Microscopic inspection of the Cd plated thread surfaces revealed little or no damage. (Figures 10a-b). Inconel bolts with no sacrificial coating also showed no galling.

High Cycle Fatigue Tests (MIL-STD-1312)

The high cycle fatigue test results are given in Figure 11a-c. It is evident that the useful fatigue life was not reduced by the addition of any of the sacrificial coatings.

Failures occurred in the threaded region for the Aermet 100 and Inconel bolts. The Aermet bolts performed exceptionally well, as the worst Aermet bolts outlasted many of the Inconel bolts and all of the 4340 bolts, despite the fact that the loads were scaled to the UTS of each material. The 4340 bolts, with one exception, all failed at the head/shank radius. This failure mode may have been caused by a manufacturing error. The addition of a Cd or IVD Al coating appears to slightly enhance the performance of the 4340 steel
bolts (Figure 11c).

Saltwater Immersion Testing

The potential vs. exposure time curves for the coated fasteners are given in Figures 12-14. The IVD Al coatings significantly outlasted the electroplated Cd coatings. Sacrificial coatings maintain cathodic protection for the substrate only if the mixed potential stays well negative with respect to the E_{corr} of the substrate (or uncoated bolt).

Differences between the fastener alloys studied were also observed. The 4340 bolts were the most difficult to protect. The uncoated 4340 bolt was removed from the bath after 6 days because of severe rusting. The Cd plated 4340 was next to fail , after 13 days of immersion (Figure 11). No rusting has been observed on either the 1.0 or 1.5 mil IVD Al coated 4340 bolts through nearly three months of immersion exposure. Aermet 100 bolts proved to be more resistant to corrosion than 4340 in this environment. The untreated Aermet lasted 38 days before termination, which surpasses the performance of the Cd plated 4340 bolt. Figure 12 shows a sharp rise in the E_{corr} value of Cd plated Aermet which coincides with the onset of rust. As was seen for the 4340 bolts, the IVD Al coated Aermet bolts have shown no rust after nearly three months of immersion.

As would be expected, the Inconel 718 bolts behaved quite differently from the steel bolts. Uncoated Inconel has proven to be impervious to attack in saltwater immersion; its lustrous surface finish has remained completely intact throughout our study. Figure 14 shows the Cd plating on the Inconel bolts was virtually depleted after just 4 days, after which its potential was equal to uncoated Inconel. As expected, no substrate corrosion was visible. As shown in Figure 13, the IVD Al was still cathodicly protecting the Inconel (whether it needs it or not) after 68 days.

DISCUSSION

Historically, cadmium plating has been an excellent sacrificial coating for steels due to a number of desirable properties; 1) it has good "throwing power" to cathodicly protect the steel even when partially disintegrated, 2) its corrosion products are not voluminous or very abrasive, 3) the cadmium itself is somewhat lubricious, which is very desirable for threaded components, and 4) the corrosion potential of Cd fully protects most steels, but it is not negative enough to cause hydrogen assisted stress corrosion cracking. Some Cd coating applications depend on all of these aspects, while others only depend on one or two. This study was aimed at extending the use of IVD Al into more applications by determining how important these properties are in specific situations, as outlined in the CCAD/ATCOM decision tree (Figure 1).

The general corrosion protection of the IVD Al coated fasteners, assemblies, and components was generally excellent. The 1.0 and 1.5 mil thicknesses of IVD Al equaled or exceeded the corrosion performance of the Class III Cd coating. Some localized pitting did occur, but the IVD Al adequately prevented severe rusting. The only drawback from a general corrosion

aspect is the ability to coat internal diameters. As was seen in the internal diameter of the IVD Al coated drag beam, the IVD process is not able to provide adequate coverage to these areas.

High cycle fatigue testing showed no degradation in performance from the uncoated samples for both the IVD Al and Cd coatings. The authors believe this should alleviate concerns about fatigue sensitive parts when other aspects indicate that a change from Cd to IVD Al is appropriate.

The effect of coating type on hydrogen assisted stress corrosion cracking was not directly studied, but can be inferred from the potential vs. exposure curves in Figures 12-14. Prior work on both Aermet 100 and 4340 has clearly shown the effect of polarization potential on hydrogen assisted SCC[7].As an example, the $K_{ISCC}$of Aermet 100 drops from approximately 25 $MPam^{-1/2}$ to about 17 $MPam^{-1/2}$ as the polarization potential changes from -0.63 V (open circuit) to -0.85V vs. SCE. Using a polarization potential of -0.700V vs SCE for cadmium from Figure 13, this would correlate to a drop in the K_{ISCC} of Aermet 100 of approximately 2.5 $MPam^{-1/2}$, or 10%. The worst case scenario for the IVD Al coating is a potential of -0.850 V vs SCE, which corresponds to a K_{ISCC} drop of 8$MPam^{-1/2}$, or 32%. However, it should be noted that this potential was reached after 4-5 days of immersion, and may not be representative of atmospheric exposure near marine environments. Also, the potential rebounds to values near -0.700V vs SCE, which would only produce changes equivalent to cadmium.

It should be restated that the Inconel 718 fasteners showed no signs of corrosion in any of the tests performed. Therefore, substitution of uncoated Inconel 718 fasteners for Cd plated steel fasteners can be made in instances where SCC of mating components is not a concern, and the increased cost of Inconel is warranted. If, however, the mating parts are susceptible to hydrogen assisted SCC, the hydrogen produced electrochemically by galvanic couples between the Inconel and the mating surfaces (steel, Cd, or IVD Al, etc.) can aggravate SCC in the mating component[7,8].

The galling and seizing of the bolts and nuts on the unloaded specimens clearly defines the biggest drawback of IVD Al coatings. Figure 15 shows the galling of the unloaded IVD Al fasteners after the cyclic corrosion tests. The production of Al_2O_3 on threaded regions creates problems for using IVD Al to coat fasteners that will routinely experience corrosive environments. Though the breakaway torques of the loaded assemblies remained fairly stable, the production of Al_2O_3 will create changes in the torque-tension relationships if the fasteners are re-used. In many instances this will preclude the substitution of IVD-Al for Cd on fine threaded, flight critical components without requalification of each part.

CONCLUSIONS

1. Ion Vapor Deposited Aluminum is an effective substitute for Cd coatings except where tight tolerances or internal diameters need protection.

2. High cycle fatigue tests of bolt assemblies showed no significant differences in fatigue life for either uncoated or Cd / IVD-Al coated fasteners. Aermet 100 showed exceptionally good fatigue lifetimes (loading as a % of UTS)

3. Both the 1.0 mil and 1.5 mil IVD coatings showed significant galling in the threaded regions of the fasteners. This is a significant barrier to extending its use on fine threaded aerospace grade fasteners.

4. The Cd plating showed no galling and provided good protection in the cyclic testing. Therefore, from a corrosion and reliability standpoint, it remains a superior sacrificial coating for

threaded aerospace grade fasteners.

5. Uncoated Inconel 718 may be used in place of Cd plated steel when the cost is warranted and SCC of mating parts is not a concern.

ACKNOWLEDGMENTS

The authors would like to thank several people who contributed to this study. Dr. Dr. W. Hughes and Messrs. M. Kauzlarich and D. Leadore (of the Survivability and Lethality Analysis Directorate of ARL) are also recognized for providing building space to operate our accelerated corrosion and immersion test equipment. Rick Eppright and Al Simkins of NAWC for High Cycle Fatigue Testing. Mr. Alonzo Gonzales of CCAD for applying the IVD Al and Cd plating. Finally, we thank the Strategic Environmental Research and Development Plan (SERDP) program office for funding this project.

REFERENCES

1. V.L. Holmes, D.E. Muehlenberger and J.J. Reilly, The Substitution of IVD Aluminum for Cadmium, McDonnell Douglas Corporation, Final Report for Period 1, February 1988 - 31 January 1989.

2. M. Levy, B. Placzankis, R. Brown, R. Huie, and M. Kane, The Effects of Co-mingling Dissimilar Fastener Coatings on the Corrosion Behavior of Steel Bolt Assemblies, MTL TR 92-40, (July 1992)

3. B. Placzankis, M. Levy, J. Beatty, S. Isserow, M. Kane, Evaluation of Environmentally Acceptable Protection Schemes for High Strength Steel Fasteners, 1994 Tri-Service Corrosion Conference.

4. General Motors Engineering Standards, Accelerated Corrosion Test, GM9540P, (July 1991) pp.1-5.

5. M. Petschel, Jr., "Statistical Evaluation of Accelerated Corrosion Test Results and Correlation with Two Year, On-Vehicle Field Results," SAE ACAP Division 3 Project, SAE Paper No. 912283, SAE 1991

6. MIL-STD-1312/11A, Fastener Test Methods-Method 11, Tension Fatigue, 19-OCT-84

7. P. F. Buckley, R. Brown, J. H. Graves, E.U. Lee, C.E. Neu, J. Kozol, "Corrosion Behavior of High Strength Steels for Aerospace Applications," Army Sagamore Conference Proceedings, August 1993, Plymouth, MA

8. M. Levy, P. Buckley, J. Beatty, R. Brown, R. Huie, K. Bhansali, " Failure Analysis of the Main Rotor Retention Nut from the AH-64 Helicopter," Proceedings of the Tri-Service Corrosion Conference, May 1992, Plymouth, MA

TABLE 1 INTERVAL STATISTICS PER CYCLE OF GM 9540P METHOD B[2]

Interval	Description	Time (min)	Temperature (+/-3C)
1	Ramp to Salt Mist	15	25
2	Salt Mist Interval	1	25
3	Dry Interval	15	30
4	Ramp to Salt Mist	70	25
5	Salt Mist Interval	1	25
6	Dry Interval	15	30
7	Ramp to Salt Mist	70	25
8	Salt Mist Interval	1	25
9	Dry Interval	15	30
10	Ramp to Salt Mist	70	25
11	Salt Mist Interval	1	25
12	Dry Interval	15	30
13	Ramp to Humidity	15	49
14	Humidity Interval	480	49
15	Ramp to Dry	15	60
16	Dry Interval	480	60
17	Ramp to Ambient	15	25
18	Ambient Interval	480	25

TABLE 2 HIGH CYCLE FATIGUE TEST PARAMETERS (MIL-STD-1312)

Bolt Alloy	Coating	High Load (lbs)	Low Load (lbs)	% High of UTS
Aermet 100	None	28900	2890	46
Aermet 100	Cd	28900	2890	46
Aermet 100	IVD Al	28900	2890	46
Inconel 718	None	27000	2700	46
Inconel 718	Cd	27000	2700	46
Inconel 718	IVD Al	27000	2700	46
*4340	None	32000	3200	46
4340	None	27800	2780	40
4340	Cd	27800	2780	40
4340	IVD Al	27800	2780	40

*% of UTS Load Decreased Due to Premature Failures (NAWC)

TABLE 3 FASTENER ASSEMBLY PERFORMANCE, GM 9540P

Bolt Alloy	Coating Type	Assembly Performance Pass/Fail - Cycles		
		Control	Joint A	Joint B
4340	None	Fail - 1	Fail - 1	Fail - 1
4340	Cd	Pass - 100	Pass - 100	Pass - 100
4340	IVD Al (1 mil)	Pass - 100	Fail - 86	Pass - 100
4340	IVD Al (1.5 mil)	Pass - 100	Pass - 100	Pass - 100
Aermet 100	None	Fail - 1	Fail - 1	Fail - 1
Aermet 100	Cd	Pass - 100	Pass - 100	Pass - 100
Aermet 100	IVD Al (1 mil)	Pass - 100	Pass - 100	Pass - 100
Aermet 100	IVD Al (1.5 mil)	Pass - 100	Pass - 100	Pass - 100
Inconel 718	None	Pass - 100	Pass - 100	Pass - 100
Inconel 718	Cd	Pass - 100	Pass - 100	Pass - 100
Inconel 718	IVD Al (1 mil)	Pass - 100	Pass - 100	Pass - 100
Inconel 718	IVD Al (1.5 mil)	Pass - 100	Pass - 100	Pass - 100

TABLE 4 BREAKAWAY TORQUES FOR CYCLIC EXPOSED FASTENER ASSEMBLIES

Coating/Bolt Assembly	Breakaway Torques (ft-lbs)		
	4340	Aermet 100	Inconel 718
Cd Joint A	208	200	246
IVD Al 1.0 mil Joint A	233	229	275
No Coating Joint B	217	192	192
Cd Joint B	258	263	275
IVD Al 1.0 mil Joint B	258	200	250
IVD Al 1.5 mil Joint B	250	283	200

FIGURE 1 IVD AL CANDIDATE FLOW CHART

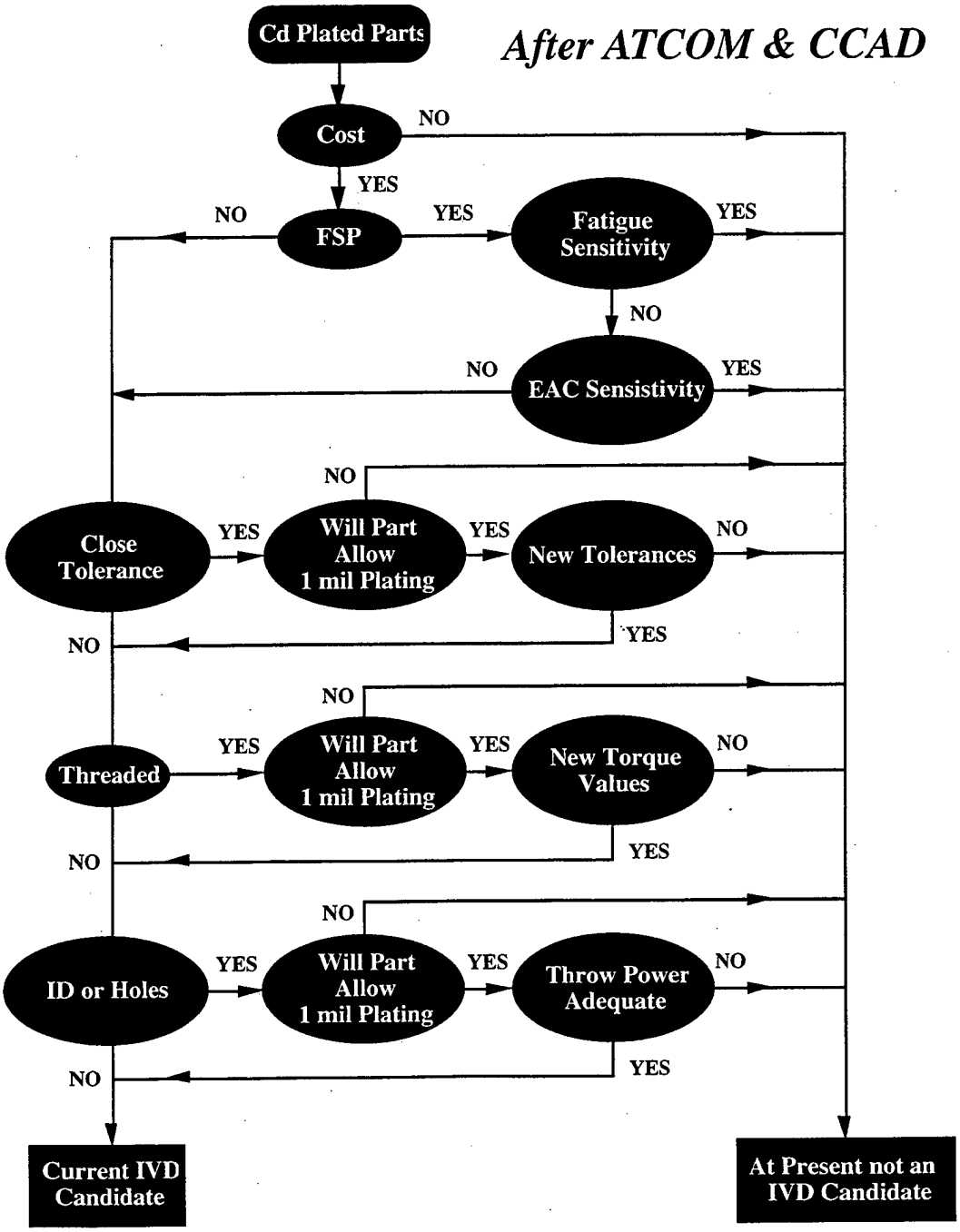

FIGURE 2 DRAG BEAM TEST SPECIMEN BEFORE CYCLIC SALTSPRAY EXPOSURE

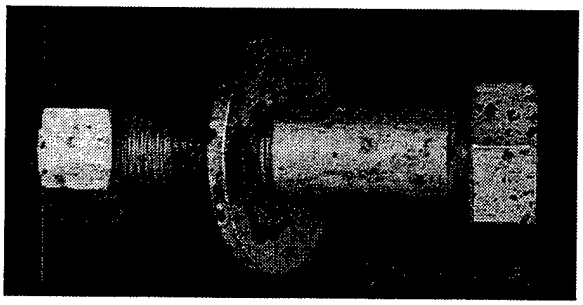

FIGURE 3 AERMET 100, 1 CYCLE 9540P
TYPICAL UNCOATED STEEL PERFORMANCE

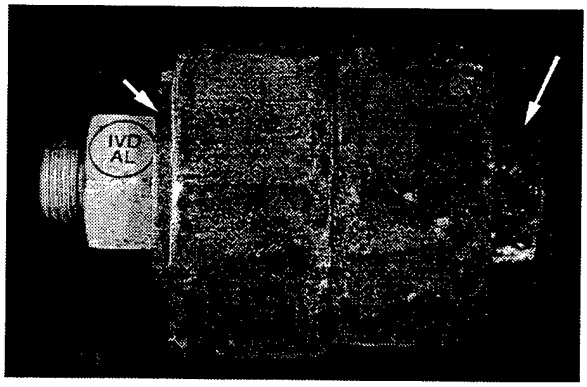

FIGURE 4 IVD AL, 1 MIL, JOINT A
RUST @86 CYCLES, 9540P

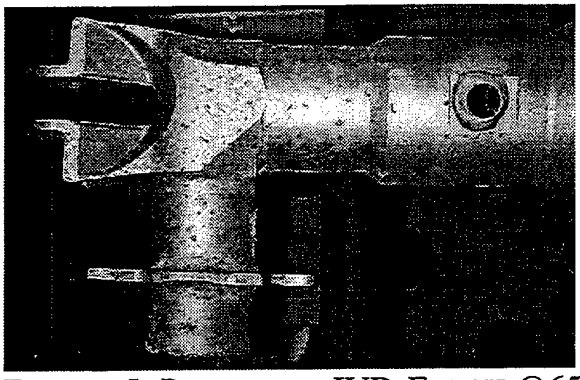

FIGURE 5 PITTING OF IVD FINISH @65 CYCLES 9540P (NO RUST)

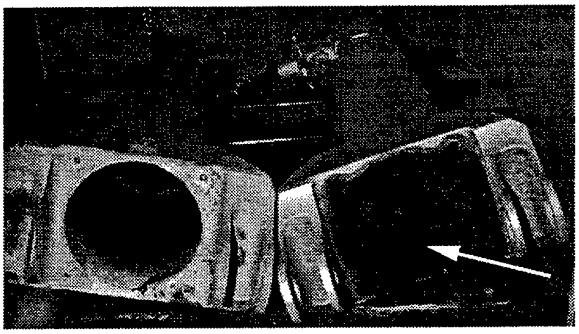

FIGURE 6 COMPARISON OF INTERIOR CORROSION OF Cd PLATED (LEFT) VS. IVD AL (RIGHT). NOTE THE HEAVY RUSTING ON THE IVD-AL DUE TO PROCESS LIMITATIONS.

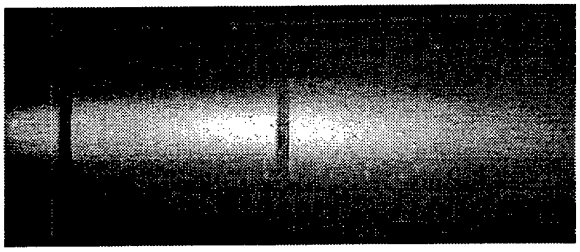

FIGURE 7 IVD DRAG BEAM MAIN BODY EXTERIOR @100 CYCLES, LIGHT PITTING, NO RUST.

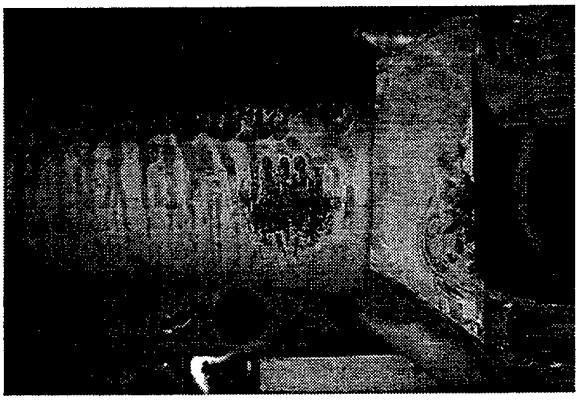

FIGURE 8 RUSTING OF Cd PLATED DRAG BEAM EXTERIOR NEAR END @65 CYCLES

a) 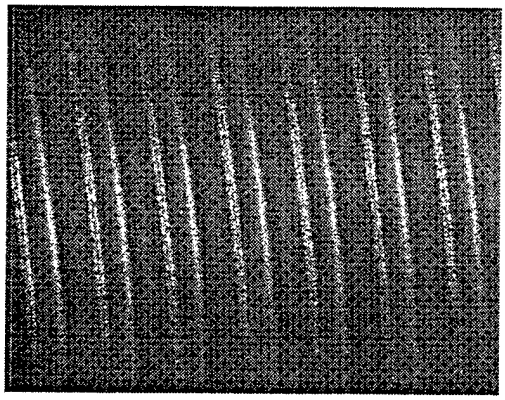 b) 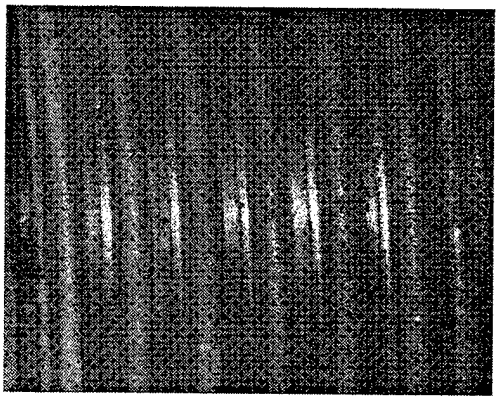

FIGURE 9 OPTICAL PHOTO MICROGRAPHS (5.7X) OF IVD Al 1.0 MIL THREADS ON AERMET 100, (a) INITIAL SURFACE, NO DAMAGE AND (b) AFTER 100 CYCLES OF 9540P CYCLIC SALTSPRAY SHOWING Al_2O_3 CORROSION PRODUCTS AND GALLING IN THE REFLECTIVE PORTIONS OF THE THREADS

a) 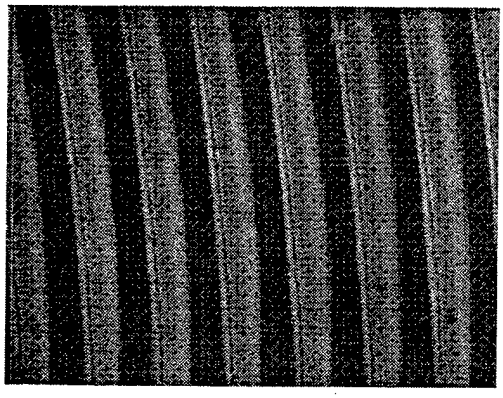 b) 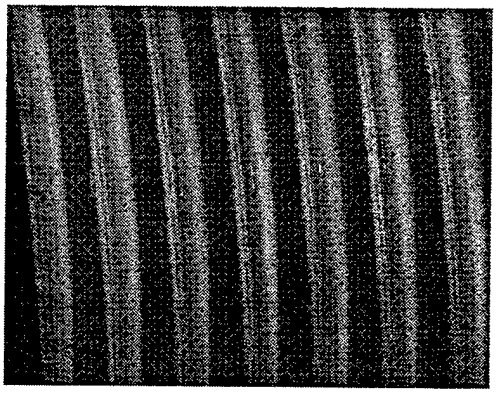

FIGURE 10 OPTICAL PHOTO MICROGRAPHS (5.7X) OF Cd PLATED THREADS ON AERMET 100, (a) INITIAL SURFACE, NO DAMAGE AND (b) AFTER 100 CYCLES OF 9540P CYCLIC SALTSPRAY WHERE NO DAMAGE CAN ALSO BE OBSERVED.

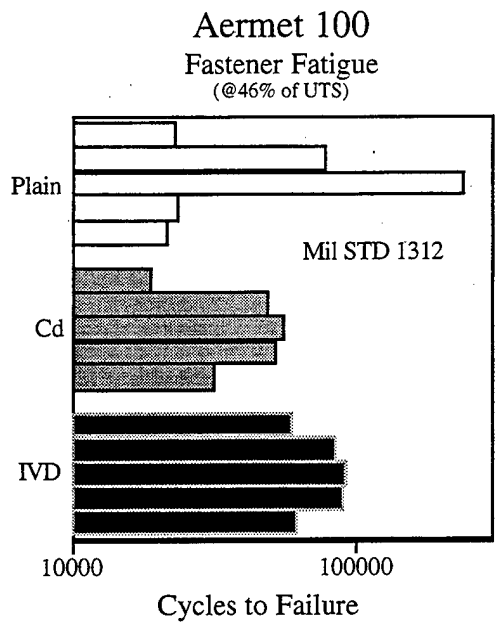

a)

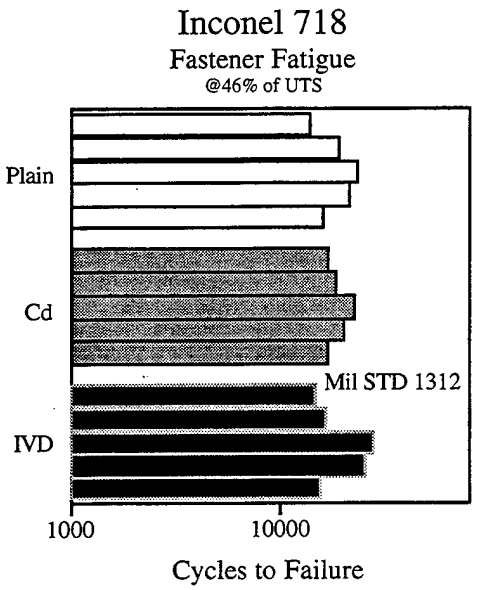

b)

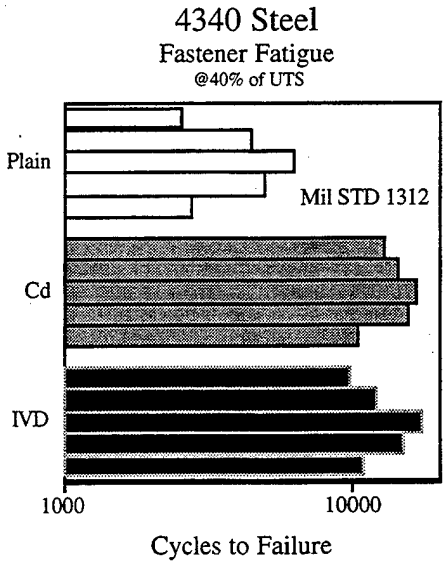

c)

FIGURE 11 HIGH CYCLE FATIGUE PERFORMANCE ON a) AERMET 100, b) INCONEL 718, c) 4340 STEEL. FATIGUE PERFORMANCE WAS NOT REDUCED BY THE ADDITION OF SACRIFICIAL PROTECTIVE COATINGS.

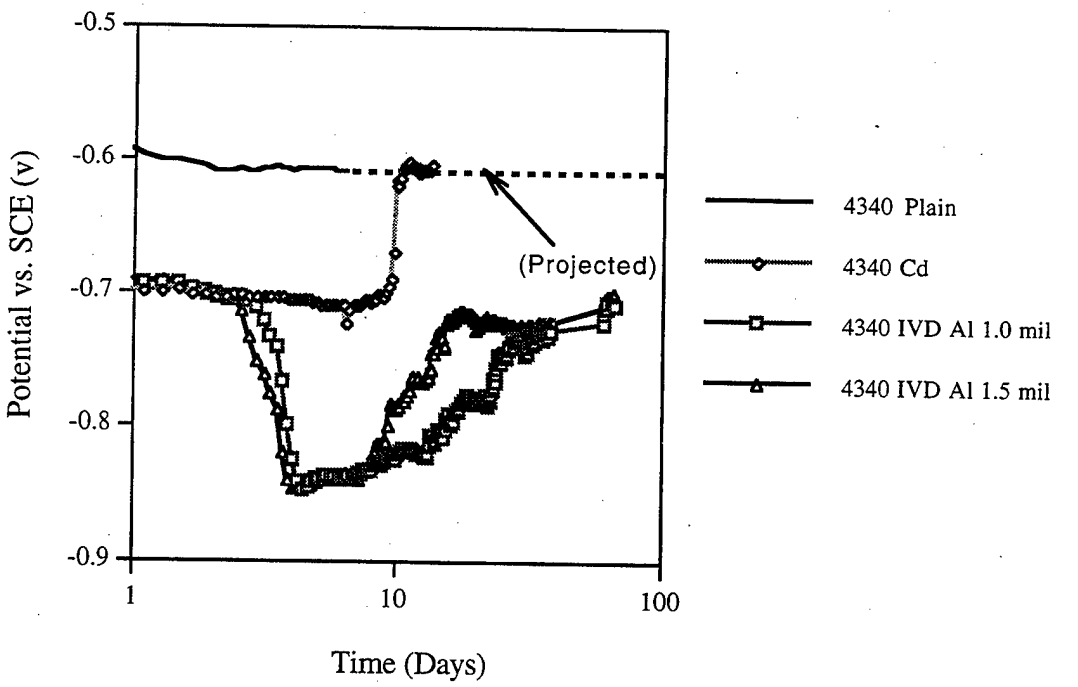

FIGURE 12 SALTWATER IMMERSION PERFORMANCE OF COATINGS ON 4340 STEEL BOLTS. Cd PLATED BOLTS WERE FIRST TO FAIL AT APPROXIAMATELY 10 DAYS.

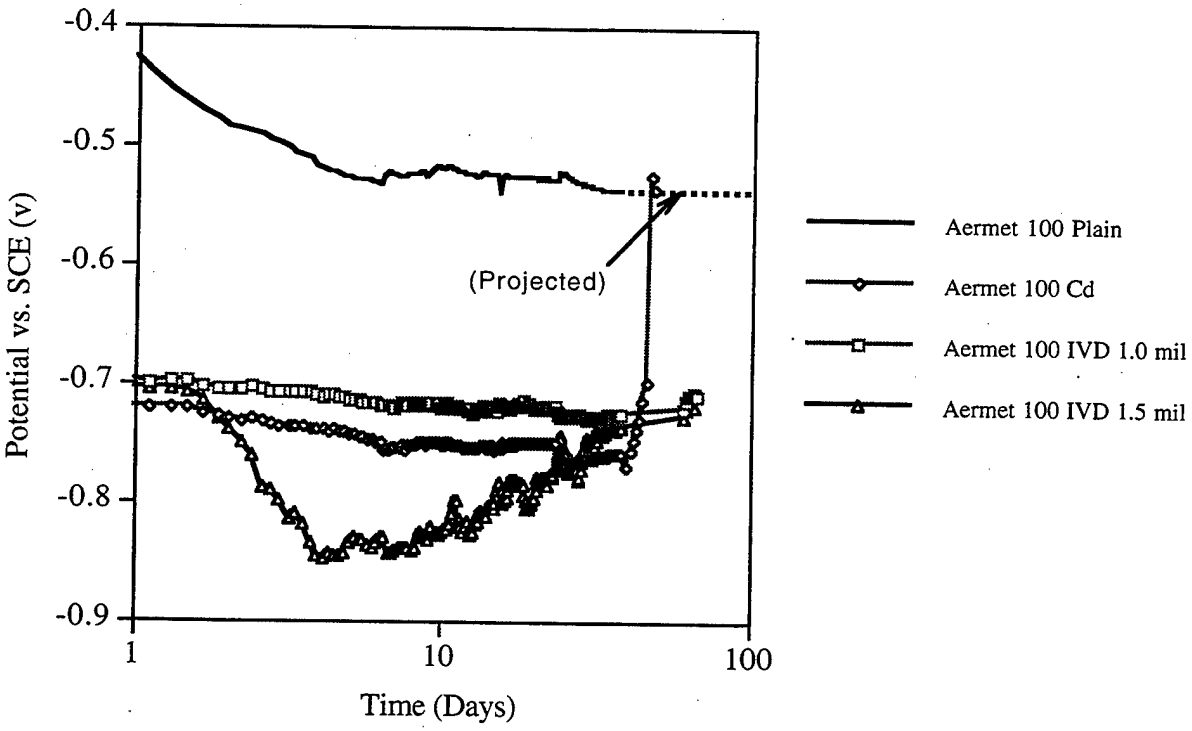

FIGURE 13 SALTWATER IMMERSION PERFORMANCE OF COATINGS ON AERMET 100 BOLTS. Cd PLATING, AS ON 4340 WAS FIRST TO FAIL BUT PROTECTED THE AERMET BOLT FOR A SIGNIFICANTLY LONGER DURATION.

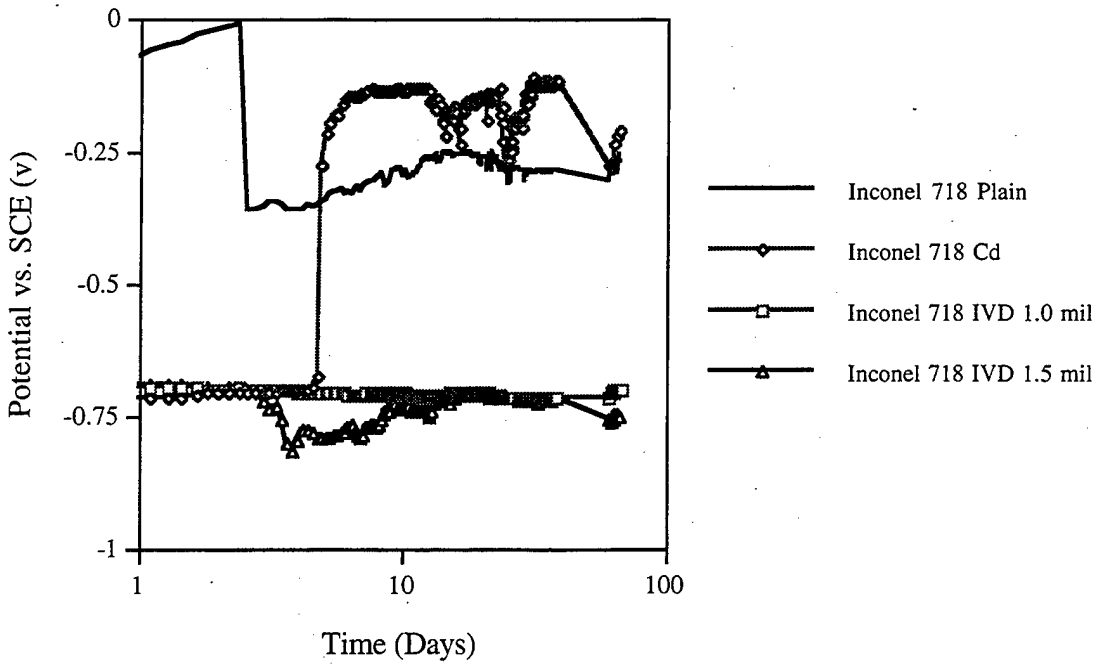

FIGURE 14 SALTWATER IMMERSION PERFORMANCE OF COATINGS ON INCONEL 718 BOLTS. NOTE THE FAST DEPLETION OF Cd AND THE LONG ENDURANCE OF IVD AL. THE INCONEL BOLTS SHOWED NO CORROSION UNTREATED OR ON Cd PLATE AFTER ITS SUBSEQUENT BREAKDOWN.

US Navy Coating Alternatives Utilizing Portable Systems

Mike Lincoln
COMNAVSURFPAC, NAB Coronado, CA 92155-54909

ABSTRACT

The U.S. Navy is dedicated to the concept of Engineering for Reduced Maintenance (ERM). This paper reviews the recent changes in coating systems and methods of application. Specifically the coatings of shipboard topside removable components, that for years have been a burden on manpower and budgets. Semi-portable corrosion control containers are being utilized to apply Triglycidyl Isocyanurate (TGIC) polyester and thermoplastic coatings. Further development and use of this technology will reduce the manpower requirements aboard ship and support reduced manning, while at the same time reduce equipment and hull failures.

INTRODUCTION

Facing ever declining budgets it has been necessary to identify and develop a method to correct expensive topside maintenance problems. Many of these problems have persisted for years despite numerous attempts at resolution. The fleet can no longer afford to fund the necessary maintenance actions at the present periodicity. To attack the problem a semi portable containerized corrosion control system has been developed.

REALIBILITY MAINTENANCE ASSESSMENT ON NAVAL SHIPS

In early 1996 Naval Sea Systems Command (NAVSEA) began a formal process to develop reliability engineering to combat high cost maintenance problems. One of the many items identified was topside corrosion. To improve topside preservation, reduce general house keeping workload i.e., painting water tight doors and hatches the U.S. Navy started using TGIC polyesters in the mid 1980's

The use of Thermoplastic coatings on U.S. Navy ships has been experimented with for some time. In 1995 Commander, Naval Surface Force, U.S. Pacific Fleet (COMNAVSURFPAC) utilized the USS Ingraham (FFG 61) as a test ship, and coated several items with thermoplastic coatings. The ship deployed to the Persian Gulf for six months. During this deployment, the thermoplastic-coated items were exposed to extreme weather and sea conditions and passed the performance evaluations. This provides another viable option to TGIC and standard Navy paint systems. Based on these results COMNAVSURFPAC, with the support of Commander in Chief, U.S. Pacific Fleet Maintenance officer, asked and received authorization from NAVSEA to use thermoplastic coatings on several items. One advantage of the thermoplastic powders over TGIC is that

ship's force can repair the chips and dings and maintain the thermoplastic coating intact. Conversely if TGIC is chipped or dinged it must be sanded, feathered and painted using the standard paint system.

In a recent inspection of Assault Craft Unit Five (ACU 5) at Camp Pendleton, CA.; the air conditioning units for the Landing Craft, Air Cushioned (LCAC) were discussed. One complaint of ACU 5 personnel was the high failure rate. Upon closer review of the units it was determined that part, if not all of the failures, were caused due to the high corrosion of component parts. These components are currently being coated with TGIC, thermoplastic powders and conventional paints. Once reinstalled and operated it is anticipated that the normal 3 to 4 month replacement schedules for these costly units can be extended. The man-hour savings for removal and reinstallation of these units alone will pay for the procurement of a portable corrosion facility.

This is just one of many challenges that face the maintenance community, not just the U.S. Navy, but nationwide. If in fact these processes continue to demonstrate exceptional performance, it would benefit all to require industry to coat new components with these processes.

To expand these two very important capabilities NAVSEA in conjunction with COMNAVSURFPAC procured a semi portable corrosion control facility and placed it at the Navy's new base in Everett, Washington. This portable unit allows for sand blasting, aluminum powder spray, TGIC and Thermoplastic powder coatings (see figure 1, page 6).

The increased capacity coupled with the benefit of having a facility that can be co-located with a ship greatly enhances the ability of the ship to become more self-sufficient and to reduce the long-term maintenance cost. An example of maintenance reduction can be illustrated by comparing powder coating with conventional coatings.

With the powder coat application process, the total production time for corrosion protection of a water tight door or hatch is dramatically cut in comparison with the standard shipboard preservation process (see figure's 2 and 3, page 7).

As you will see in figure 2. The service life of powder coatings is 8 years while the service life of conventional coating (see figure 3) is 1.5 years. In an eight year period an item conventionally coated would require re-preservation 4 times more than same item that has been powder coated. If the Navy continues to utilize conventional coatings there would be an unnecessary expenditure of 146 man-hours in comparison to an item, which is powder coated (see figure 4 on page 8).

A ship such as the CG-47 (class) has 268 watertight hatches. If all of these items were powder coated as opposed to conventionally coated a total of 47,012 man-hours would be realized over 8 years.

There are hundreds of applications for TGIC powder coatings besides watertight door and hatches, examples of which include:

Pyro lockers
Light shrouds
Lockers, bins and brackets
Ladders and stanchions
Speaker housings
Controllers
Line and cable reels
Scuppers and brackets
Hawse pipe covers
Handrails
Machine gun mounts
Handwheels and gageboards
Reach rods and cable hangers
Vent screens
Helo net frames
King posts and davits
Oil spill kits
Portable cleats
SRBOC launchers
Sea water strainers

Recently, NAVSEA released an interim fleet approval for Thermoplastic Powder coating to be used on the following items:

NOTE: Components will require an anchor tooth profile prior to TPC application

1MC speaker housing
Cable Hanger, detachable
First Aid boxes, flashlight holders
Oil spill containment kits
Hand rails, removable
Light shrouds
Stanchions
Electrical controller housing
Signal light housing
Gage boards
Handwheels (topside only)
Misc. covers

NAVSEA PROPOSES TWO OPTIONS FOR THIS PROJECT

Option 1:

One option utilizes ship's force personnel to accomplish the removal, coating and reinstallation tasking under the supervision of the lead CCCS technician. Implementation of this concept would mean that a certain number of ship's force personnel would actually work in the shop subsequent to indoctrination and initial on-the-job training. This method of operation will have a negative impact on the ship's ability to accomplish other maintenance efforts and training. Quality assurance will also be challenging when utilizing a rotating pool of Sailors. Further training in coating applications will only be of modest value to a ship without a deployable, onboard corrosion control facility. The drawback of this option is that Sailors will gain little professional benefit when assigned to a corrosion control facility. Few if any will ever see a second assignment doing similar work – therefore the professional enrichments are minimal. There are

also a very limited number of Pacific Fleet Battle Force Intermediate Maintenance Activity (BFIMA) billet requirements for Sailors with corrosion control systems application qualifications (9 billets total in the Pacific Fleet).

Option 2:

Option two proposes shipboard support for fitting removal, coating application, and re-installation. This option utilizes contractor personnel in place of shipboard Sailors. The San Diego afloat Commanding Officers and former Commanding Officers that were asked to comment on operating alternatives enthusiastically received this concept of operations. Deliberate under-manning, coupled with a large number of competing shipboard tasks has made it particularly difficult on the time demands that are made on afloat personnel. This option has the benefit of utilizing highly specialized, full and part-time contractor technicians to maximize productivity. A contractor work force would offer the flexibility to respond to the normal day to day workload surges associated with a ship's availability, without degrading readiness or quality of life for our Sailors. We would eliminate the demand on Sailor's time, which conflicts with training general equipment maintenance and repairs during in-port periods. A contractor work force would allow Sailors more time for greater productivity because the demand for constant retraining in corrosion control would end. It makes sense to pay market rate for technicians to handle these time consuming activities as opposed to the average cost of a Sailor. Most importantly it would conform to Fleet policy of dedicating time to those efforts that have the greatest positive impact on combat readiness and self-sufficiency at sea.

The Corrosion Control Containerized System is configured to rapidly and efficiently blast and apply high endurance coatings to removable fittings. The maximum fitting dimensions would normally be 4 feet by 4 feet by 8 feet. Candidate fittings are manufactured of carbon steel, sheet metal, stainless steel, aluminum alloys or ferrous castings. Weight of removable fittings that could be transported manually by one or two personnel would not be a limiting factor.

Additional benefits of the containerized corrosion control process are that this system greatly reduces environmental hazard. Powder coating produces zero volatile organic compounds (VOC's) or hazardous air pollutants (HAP's). Powder is unlike conventional paint that requires solvent for application and cleaning. Since powder is 100% solid material, no solvent-type vapors are released in the spray room and into the atmosphere. Spills are easily swept up or vacuumed. Cleaning clothes, skin and equipment is greatly simplified with powder. Powder is classified as a nuisance dust rather than a HAZMAT.

The Corrosion Control Containerized system minimizes the amount of paint stored on the ship. With a reduction in stored paint, there are reduced administrative efforts associated with hazardous flammable material storage. Reduced paint storage also means a benefit in weight reduction on the ship.

Bibliography

Jacobs, K. S. and J.P. McComas, "Maintenance Avoidance and Maintenance Reduction, *Naval Engineers Journal*, pp47-55, January 1997.

Powder Coating the Complete Finisher's Handbook, The Powder Coating Institute, (Alexandria, VA: 1994).

Extended Life, Maintenance Free Containerized Coating Process

GOAL: REDUCING / ELIMINATING CORROSION THROUGHOUT AN EXTENDED 8-YEAR LIFE CYCLE.

- **Requirements**
  - **Blast booth to properly prepare substrate (1-2 mil profile)**
  - **Aluminum powder spray booth for steel substrates**
  - **Powder spray booth to electrostatically apply coatings**
  - **Convection oven to preheat substrate and cure thermosetting resins**

Figure 1

Powder Coat Application Process

Maintenance Man Assigned
(Acquire Tools/Materials/Instructions) = .5 Hours

Substrate Preparation (Blasting to SSPC SP-5 white metal) = 1 Hour

Aluminum Application (7-10 Mils) = 1 Hour

TGIC Powder Coat Application = 1 Hour

Oven Curing Time = 2 Hours

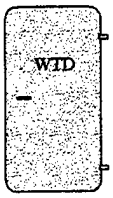

TOTAL = 5.5 HOURS (approx... 6)
(Production Time Only)

Figure 2

Standard Shipboard Preservation Process

Maintenance Man Assigned
(Acquire Tools/Materials/Instructions) = 2 Hours

Surface Preparation -Chipping and Sanding
(SSPC SP-2 or 3 Mechanically cleaned) = 16 Hours

First Prime Coat Application = 4 Hours (24 hrs to dry)

Barrier Coat Application = 4 Hours (24 hrs to dry)

Top Coat Application = 4 Hours (24 hrs to dry)
(7 days to cure)

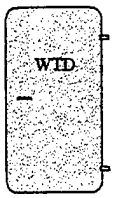

TOTAL = 30 HOURS
(Production Time Only)

Figure 3

MAN-HOUR EXPENDITURE COMPARISON

Standard Shipboard Process	**30 Hours**
Expected Service Life	**1.5 Years**
Anticipated Work Cycles	**x4 in 7.5 Years**
Preservation Hours Required	**150 Hours**
Remove/Re-hang 2 of 5 times @ 2 Hours	**4 Hours**
Total	**154 Hours**

Powder Application Process	**6 Hours**
Documented Service Life	**8 Years**
Anticipated Work Cycles	**x1 in 8 Years**
Preservation Hours Required	**6 Hours**
Remove/Re-hang 1 time @ 2 Hours	**2 Hours**
Total	**8 Hours**

Figure 4

Functionalized Sol-Gel Conversion Coatings

Dr. William E. Dorogy Jr.
Mr. Thomas Tiano
Ms. Mei-Ling Pan
Dr. K. Jayaraj
Foster-Miller, Inc.
195 Bear Hill Road, Waltham, MA 02154

ABSTRACT

Foster-Miller has developed an aqueous-based functionalized sol-gel coating for aircraft aluminum alloys that provides corrosion protection, generates a surface exhibiting good adhesive bonding and contains no hazardous or toxic chemicals. The coating is applied using a dip-coat process and is composed of two parts: a silica-like basecoat which provides most of the corrosion protection and a functionalized-silicate topcoat specifically designed to chemically interact with subsequently applied adhesives or paints. Specimens with an amine-functionalized topcoat/silicate basecoat exhibited good paint adhesion and cohesive failure in double lap shear, wedge crack, and floating roller peel tests.

INTRODUCTION

Much emphasis in recent years has been placed on modifying existing processes or developing new methods that are more environmentally acceptable than current practices. Treatment of aircraft grade aluminum alloys for corrosion protection and adhesive bonding currently involves the use of chemically grown hydrated oxides containing chromium corrosion inhibitors. There are currently two types of surface preparations commonly used for aircraft grade aluminum alloys, those used to impart corrosion resistance and those used for enhancing the bond strength to adhesives. When corrosion protection is the main goal, chromate conversion coatings such as ASTM B449, MIL-C5541 and MIL C-81706 are used. An understanding of the function of chromium in the formation of chromated chemical conversion coatings and its mechanisms for aluminum protection is critical to the development of alternative corrosion inhibition systems. The prevention of aluminum corrosion is achieved by creating a protective, hydrophobic, Cr(III and IV) oxide barrier over the surface of the substrate that prevents migration of oxygen or hydroxide ions to aluminum, electron transfer between cathodic/anodic corrosion sites, provides a "time release" source of Cr(IV) ions, and exhibits a capacity for "self-healing" small film defects[1-4]. However, chromium (VI) is a highly toxic material[5] and efforts are underway to eliminate its use from coating systems.

When adhesive bonding is the main goal, aluminum substrates are treated with phosphoric acid anodizing processes such as ASTM D3933 and the Boeing patented process. Both processes involve etching the substrate in a phosphoric acid bath while an electrical charge is placed on the substrate. The bonding area of the aluminum substrate becomes covered with a highly adherent alumina layer containing 400 nm deep pores[6]. Although phosphate is currently not considered to be a highly toxic material, the combination of phosphoric acid and the electric current creates a hazardous environment and a highly acidic waste stream containing phosphates. A significant

drawback of these processes is that the treated aluminum actually has a higher susceptibility to corrosion than untreated aluminum due the increased surface area. A chromate rinse can be applied to the treated aluminum surface to "seal" the pores and increase corrosion resistance. A primer coating is then applied to both types of surfaces within 16 hr of pretreatment to protect and prepare the surface for topcoating or adhesive bonding. The primer is normally a low viscosity form of the adhesive or topcoat whose function is to "wet out" the treated surface and fill any pores in the surface oxide. Bonding of the primer to the surface oxide occurs by a physical interlocking within surface pores combined with the wetting action and possibly some hydrogen bonding. Corrosion protection is afforded by the incorporation of chromate inhibitors into the primer[7] and they function as previously described for conversion coatings. Finally, the subsequently applied adhesive or topcoat interacts with the primer by a similar wetting action and some hydrogen bonding.

Foster-Miller has developed an environmentally acceptable functionalized sol-gel coating system to replace current systems employing phosphoric acid anodizing for increased adhesive bond strength and chromates for increased corrosion resistance. Coatings are applied by a multi-step dip-coat process with the corrosion resistance being a function of the number of applied coatings. Corrosion is prevented by the formation of an aluminosilicate/silica-like/silicate barrier layer (basecoat) that is chemically bound to the substrate, and prevents migration of corrosive agents to the substrate and corrosion products away from the substrate. Adhesive bonding is enhanced by the presence of organic functional groups at the coating surface (topcoat) which are ideally suited for chemically bonding to aerospace adhesives and primers. In this manner, our sol-gel coating will chemically tie the adhesive or primer layer to the substrate, allowing the formation of a coating system which is less prone to delamination, and thus more corrosion resistant.

EXPERIMENTAL PROCEDURE

The application of conversion coatings generally requires several steps to prepare the surface for coating application. We incorporated a degreasing and deoxidizing step prior to the application of our sol-gel coatings for corrosion resistance studies. Mr. Peter Gagne from Oakite Products, Inc. provided us with samples of the alkaline degreaser Oakite 61B and the acidic deoxidizer Oakite Deoxidizer LNC, all of which are aqueous based. Surface pretreatment baths were formulated according to manufacturer's specifications and used as shown in the procedure listed in Table 1. Functionalized sol-gel coatings were formed using an aqueous-based, multi-step, dip-coat process which utilizes an alkaline-catalyzed reactive coating system to grow the coating directly on the substrate by immersing the substrate into the coating solution at the time of its formation. Corrosion resistance was mainly determined by the number of basecoats while adhesive bonding properties were dependent on the type of functionalized topcoat. The performance properties of the coating system can be tailored to the end use by varying the number of basecoats and type of functionalized topcoat.

In order to establish coating parameters that influence the performance of the sol-gel coating, a research-scale coating apparatus was designed and built that could control the temperature of the system, prevent evaporation of the coating solution during substrate coating, and prevent the sol-gel precursors from being exposed to air before they are added to the coating system. The apparatus consisted of a Teflon-coated stainless steel vessel sealed with a glass cover having openings for a stirrer and addition funnels for sol-gel precursor delivery. Specimens to be coated were mounted on a plastic rack such that they were electrically isolated from one another and immersed beneath the coating solution. The alkoxysilanes were poured into the addition funnels in a glove bag to prevent exposure to air, preventing premature hydrolysis, and added to

the coating formulation at the appropriate time. This coating apparatus allowed us to closely control and monitor the coating parameters we felt were important and determine their influence on the resulting coating and its performance.

The above mentioned coating procedure and equipment were modified for adhesive bonding studies by enlarging the controlled coating apparatus and the substitution of surface roughening via grit blasting in place of the deoxidizing and water rinse steps. Grit blasting was carried out using a Cyclone model TF 1000 system with a tungsten carbide nozzle from MSC Industrial Supply Company, 50μ alumina grit purchased from A & B Deburring and clean, dry nitrogen at a pressure of approximately 60 psi. After grit blasting, the substrates were blown clean with nitrogen gas to dislodge any grit remaining on the surface of the specimen prior to sol-gel coating. Coated specimens for wedge crack and double lap shear testing were sent to Lockheed Martin Aeronautical Systems, Marietta, GA for preparation and assembly into test articles. The experimental, non-chromated aqueous primer XBR-6757, obtained from Cytec Engineering Materials Inc. through the assistance of Dr. Hermann Sitt, was applied to the coated substrates as per manufacturer's specification. Control specimens were bare aluminum substrates which were phosphoric acid anodized at Lockheed per the F-22 Specification 5PTPHL21. A FM-73 film adhesive, 0.06 LB/SF with a knit carrier, was used to form the adhesive bonds. Test articles for floating roller peel resistance testing were prepared at Wright Patterson Air Force Base (WPAFB) without the use of a primer. Sol-gel coated panels for paint adhesion testing were primed with a chromated water-based epoxy from Deft (qualified to MIL-P-85582), topcoated with a Deft high-solids urethane coating per MIL-C-85285 and cured at ambient temperature for 14 days at WPAFB.

RESULTS

Silicate-based sol-gel coatings are produced by the hydrolysis of alkoxysilanes and subsequent condensation to form polymeric species whose structure depends on the hydrolysis conditions. Figure 1 depicts the reactions and different polymeric species formed during the acid and base catalyzed hydrolysis of tetraethoxysilane. The relative rates of the hydrolysis and condensation reactions vary with type of catalysis. The hydrolysis reaction is fast compared to the condensation reaction with acid catalysis, releasing substantial quantities of ethanol into the reaction medium that assists in the alkoxysilane dissolution, generating water-soluble monomeric species which slowly condense into linear and branched polymers, becoming entangled and eventually cross-linking at the gel point. Condensation is faster than hydrolysis with base catalysis, so significant amounts of alkoxysilane are present throughout most of the sol-gel process, and the resulting polymeric species form into branched clusters which link together at the gel point[8]. Standard sol-gel coating procedures form a stable solution of the polymeric sol-gel species into which the specimen to be coated is dipped and subsequently dried. However, it has also been reported that functionally-gradient sol-gel coatings can be grown directly onto the substrate by immersing the substrate into the coating solution as soon as it is formulated, with the alkoxysilane being the last coating component to be added[9,10]. The barrier properties of films produced using different catalysts will depend on the packing density of the polymeric species on the substrate, the nature of their bonding to the substrate and how well they consolidate into a film.

Foster-Miller Coating System

The Foster-Miller approach utilizes an environmentally-friendly aqueous process that eliminates toxic chromates and hazardous acidic phosphate solutions. The process utilizes a reactive sol-gel coating which chemically and mechanically bonds to the substrate and is appropriately functionalized for chemical bonding to aerospace adhesives or primers. Reactive sol-gel coatings are produced by exposing the substrate to the alkoxysilanes as they are undergoing base hydrolysis and condensation into polymeric species. The base hydrolyzed alkoxysilanes can therefore react with either the surface of the substrate or themselves in solution, as in standard sol-gel preparations. The reactive sol-gel species can chemically bond to the substrate surface and then the bound species can consolidate into a layer. An aluminum oxide (alumina) surface layer is generally found on the substrate surface and our process generates an oxide layer whose composition gradually transitions from the alumina to aluminosilicate to silica-like to silicate at the coating surface. It appears that the surface portion of the alumina is either dissolved by the hydrolysis solution and is incorporated along with reactive sol-gel species into the coating or the reactive sol-gel species penetrates into the alumina pores forming the aluminosilicate region. Additional reactive sol-gel species can bond to this initial layer, filling in defects and increasing the layer thickness until the concentration of reactive species decreases to the point where the coating stops growing. The resulting coatings will be conformal and completely cover the substrate. Corrosion protection is attained by formation of a sol-gel barrier, the combined aluminosilicate and silica-like layers, that is chemically and mechanically bound to the substrate through a strongly adherent alumina layer.

The Foster-Miller coating system is applied in two-step to six-step processes utilizing alkoxysilane precursors depending upon the desired corrosion performance. Only the alkoxy groups of the precursors undergo hydrolysis and eventually result in formation of the Si-O-Si network, while the other groups remain attached to Si throughout the hydrolysis/condensation reactions and become incorporated into the coating. The 2024-T3 aluminum alloy substrate was first degreased and deoxidized according to manufacturer specifications before application of the initial sol-gel coating, with an optional surface roughening step being used in some instances. Each of our multi-step coating systems uses alkoxysilane to generate the initial coating and subsequent four coatings in the case of the six-step process, with the entire alkoxysilane layer being termed the "alkoxysilane basecoat." Epoxy- or amine-functionalized silane topcoats are then applied to the alkoxysilane basecoat under base hydrolysis conditions, forming epoxy- and amine-functionalized silicates respectively. These functional groups are the same as those contained in most aerospace adhesive and primer systems and therefore coatings containing these functional groups are suited for chemical bonding to these materials. The sol-gel coating in each step is dried in an air oven at 100°C prior to further processing. A summary of the multistep coating processes is presented in Table 1 and a schematic depicting the composition versus depth profile for coating is shown in Figure 2.

Our sol-gel coating solutions are reactive in nature and thus cannot be reused. Water is the major component in each coating formulation and the remaining constituents are fairly inexpensive. Coating formulations contain no hazardous or toxic chemicals and therefore the expended coating solutions can be disposed of with little or no post treatment. The water and basic component could easily be separated and recycled if deemed economically feasible. The pH's of the spent solutions are in the range of 9 to 10 and contain from less than 5 to about 10 weight percent solids which have a chemical structure similar to sand.

Development, Evaluation and Selection of Coating Formulations

Substrates measuring 1 in. x 4 in. were coated under a variety of conditions with numerous sol-gel basecoat and topcoat formulations. The appearance and corrosion resistance upon immersion in 4 wt. percent aqueous sodium chloride were used to select the basecoat formulation. Varying number of basecoats, basecoat with various amine-functionalized topcoats and basecoat with various epoxy-functionalized topcoats were applied to specimens and the resulting coated specimens were subjected to tests for coating thickness, corrosion resistance, coating composition, coating flexibility, and adhesive bond strength. The results of these tests were used to select an amine and epoxy topcoat formulation for adhesive bond and environmental resistance study.

Coating Thickness

Coating thicknesses on reflective polished substrates were determined using ellipsometry by Professor van Ooij at the University of Cincinnati. Reflective polished substrates are required in order to assure an accurate coating thickness is measured as the beam of light passes through the coating, is reflected by the substrate and again passes through the coating. Studies involved specimens which had undergone either 1, 3, 4, 5, 7 basecoat applications and five alkoxysilane basecoat applications with an epoxy-functionalized silane topcoat as well as specimens coated with a basecoat and either the amine- or epoxy-functionalized silane topcoat. Two specimens from each coating formulation were measured to determine coating thickness reproducibility. The refractive index of the sol-gel coatings was assumed to be 1.4 for the ellipsometry calculations based on previous experiences by Professor van Ooij.

For the multistep coatings, coating thicknesses were found to be virtually the same at 780 to 870Å for samples coated with one to five coating applications, with the seventh coating significantly increasing in thickness (Table 2). Since we found corrosion resistance increased with the number of applied coatings, we believe that this increase in corrosion resistance is due to a filling of pores or thin spots in the initial coating for up to and including five coating applications. Additional coating applications then build upon this filled surface, causing a significant increase in coating thickness. However, coatings of similar thickness are produced upon application of a functionalized topcoat to a single basecoat, suggesting topcoat formulations may be more effective than the basecoat at sealing porous underlayers. For both amine-functionalized silane topcoated samples, coating thicknesses were constant, measuring 1354 and 1337Å. For the epoxy-functionalized silane topcoated samples, coating thicknesses of the two specimens were found to be quite different, measuring 880 and 1613Å. This result tends to indicate some non-reproducibility exists with this latter topcoating process.

We also tried to measure coating thickness using a profilometer owned by Foster-Miller, but coating thicknesses were very small compared to the roughness of the specimen surface, and thus coating thicknesses could not be determined with this technique. Another problem with this type of measurement is that we are operating at the lower limits of the profilometer sensitivity.

Corrosion Resistance

In addition to the corrosion screening tests (immersion in 4 percent aqueous sodium chloride), specimens coated in the small-scale apparatus were tested for corrosion using DC

polarization, electrochemical impedance spectroscopy, filiform testing, salt spray (fog) testing and prohesion testing.

DC Polarization and Electrochemical Impedance Spectroscopy (EIS)-

The corrosion resistance of two-step coated specimens, single basecoat with either an epoxy- or amine-functionalized overcoat, was measured by Professor van Ooij using DC polarization and EIS techniques. These techniques determine the corrosion rate, the corrosion processes or mechanisms that are operating and the integrity of the various interfaces within the coating system. Aerated aqueous 3 percent NaCl solutions were used as the corrosion medium in both cases.

DC polarization measures the initial corrosion rate of the substrate in the corrosion electrolyte, with passivation and other longer-term effects not being considered. The experimental equipment consists of the specimen (working electrode), a reference electrode and an inert auxiliary electrode immersed in the corrosion electrolyte. The specimen and inert auxiliary electrode are connected so as to allow a variable current to be applied to the specimen. The potential of the specimen is measured against a reference electrode by means of a potentiometer-electrometer circuit. Experimental conditions were as follows: open-circuit delay time of 100 sec, voltage range $\pm$250 mV from the corrosion potential, and scan rate of 2 mV/s. This technique involves first measuring the corrosion potential or open circuit potential with respect to the reference electrode prior to the application of current and then varying the applied current such that the specimen potential changes $\pm$250 mV from the corrosion potential. A Tafel curve is constructed from the experimental data by plotting the logarithm of the applied current density (A/cm^2) versus the specimen potential (V). The two linear portions of the curves at a high applied current density are known as the Tafel regions and extrapolation of the slopes of the cathodic (lower) and anodic (upper) Tafel portions of the curves to the corrosion potential determines the corrosion current (I_{corr}). The corrosion current was then used to calculate the corrosion rate in mils of substrate lost per year (mpy) according to the equation (1):

$$\text{Corrosion Rate (mpy)} = (I_{corr} \bullet K \bullet EW) / d \bullet A \qquad (1)$$

where K = constant, EW = equivalent weight of the specimen in grams/equivalent, d = specimen density in $grams/cm^3$, and A = exposed specimen area (cm^2). Materials that function as anodic inhibitors have a smaller corrosion current and greater corrosion potential than the corresponding control, resulting in a decrease in the substrate dissolution rate. Cathodic inhibitors exhibit both a smaller corrosion current and corrosion potential than the control, resulting in a decrease in the rate of oxygen reduction. *Both coated specimens retard the cathodic and anodic reactions, resulting in a corrosion rate almost two orders of magnitude less than the bare aluminum specimen control, with the epoxy-functionalized topcoated specimen exhibiting the lower corrosion rate of the two coated specimens.* The epoxy-functionalized topcoat appears to reduce the cathodic reaction more than the anodic reaction, while the opposite is true for the amine-functionalized topcoat. DC polarization experiments were also performed on "yellow chromated" aluminum 2024-T3 specimens obtained from Q-Panel. The corrosion currents of these specimens were approximately one order of magnitude lower than those of either of the two-step coated specimens, indicating a lower corrosion rate. The Tafel curves were not smooth and not very reproducible, suggesting this film is non-porous and highly insulating. The "yellow chromated" coating exhibited a low

corrosion potential of about -700 mV, indicating the film is also a strong inhibitor of the oxygen reduction corrosion reaction.

EIS measurements were performed using the following experimental conditions: open circuit delay of 10 min, scan range of 10^5 to 10^2 Hz, five points per decade, AC voltage of 10 mV at the start of the experiment, immersion time of 1 hr, and sample area of 1 cm^2. The analysis of the EIS results was performed using Gamry software. Uncoated control, two-step epoxy- and amine-functionalized coatings exhibited initial total initial resistance values of 2 X 10^2, 10^5 and 4 X 10^5 ohms, respectively. These results indicate that the two-step coatings can almost withstand the complete EIS test range. The testing time was typically 45 min, and the two-step coatings did not show any visible damage after the test. Since the total initial resistance, the combination of the polarization (R_P) and pore (R_{po}) resistances, is inversely proportional to the corrosion rate, it can be concluded that *the initial corrosion resistance of the two-step coated samples are at least 1000 times that of the uncoated sample.* Also, the initial corrosion resistance of both two-step coatings was better than the "yellow chromated" Q-Panel specimens (10^4 ohms). However, the total resistance of the two-step coated specimens continually decreased with immersion time to values less than 10^3 ohms while the "yellow chromated" specimens decreased to 10^3 ohms but then remained constant after about 16 hr of immersion. The behavior of the "yellow chromated" specimens may be explained if one assumes the Al^{3+} cations present in solution from the dissolution of the substrate react with chromate ($CrO4^{2-}$) and cathodically generated hydroxyl (OH^-) anions to form a highly insoluble $(Al,Cr)_2(CrO_4^{2-})_3$ species which precipitates at anodic sites, effectively filling any pores or defects in the chromate film. This could be the reason for the "self-healing" nature of chromates.

Resistance to Filiform Corrosion-

A filiform corrosion test, similar to federal specification TT-P-2760 was performed to determine the ability of the coating to resist the propagation of corrosion at the coating metal. An uncoated control and alkoxysilane basecoated specimen were subjected to this test. Specimens were scribed to base metal, exposed to concentrated aqueous hydrochloric acid vapors for 1 hr, and were exposed to approximately 80 percent relative humidity at ambient temperature for an extended period. The appearance of the specimens with time was monitored. After only 18.5 hr, the control specimen showed white specs at the bottom of the specimen indicating corrosion. After 1193 hr, the basecoating specimen had developed a small amount of corrosion along the scribe, but had not sustained any corrosion outside of the scribed area. Another filiform corrosion test was attempted with specimens coated with the alkoxysilane basecoat, however the specimens changed color when subjected to the HCl vapor and the test was not continued.

Salt Spray (Fog) Testing-

Salt spray (fog) testing was performed by Mr. James Mazza at WPAFB in accordance with ASTM B-117 MIL-C-5541 and MIL-C-81706. Eleven coated specimens and three control specimens coated with chromate conversion coating were subjected to 5 percent aqueous NaCl spray for a maximum of 352 hr. *Specimens with five basecoat applications passed the salt fog test according to MIL-C-5541E by surviving 184 hr with no signs of corrosion, but failed according to MIL-C-81706 at 352 hr due to the observation of a small amount of pitting.* Specimens having a

single or three basecoat(s) failed the salt spray test after 184 hr because of the appearance of corrosion. Since only the coated specimens that passed the test underwent a five-step basecoating treatment, more work still needs to be performed to decrease the amount of time and materials needed to create this coating.

Prohesion Testing-

Prohesion testing was also performed by Mr. James Mazza at WPAFB. Testing was performed on seven different sol-gel coated specimens and three control specimens coated with chromate conversion coating in accordance with ASTM G-85, A5. Specimens having a single, three, or five basecoat applications as well as the chromated control exhibited excellent corrosion resistance after exposure for 354 hr, showing no visible signs of corrosion. *All sol-gel coated specimens passed the prohesion corrosion test according to ASTM G-85.*

Coating Composition

Samples coated using the multi-step process with either amine- and epoxy-functionalized silane topcoats were analyzed by Prof. van Ooij using reflectance/absorbance infrared spectroscopy. This analysis was performed to verify the presence of the functional groups in the topcoated specimens after application and drying processes. Spectra of coatings produced by five basecoat applications show a very strong Si-O absorption at approximately 1244 cm^{-1}, typical of a silica-like matrix. The basecoat is definitely not a silicate or siloxane due to the absence of residual alkoxy groups in the film, based on the lack of absorptions at 2900 to 3000 cm^{-1}. Application of a epoxy-functionalized silane topcoat to this basecoat adds organic functionality to the original coating. Siloxane structures (Si-O-Si) are now present due to absorptions at 1160 cm^{-1}. Absorptions at 2900 to 3000 cm^{-1} are due to alkyl vibrations while absorptions at 1000 to 1100 cm^{-1} can be attributed to Si-O-C structures, indicating the presence of alkoxy or epoxy groups in the coating. Time-of-Flight-Secondary-Ion-Mass-Spectrometry (TOF-SIMS) studies were carried out to identify these organic groups. TOF-SIMS provides a mass spectrum of the outermost 10Å of solid materials which can identify organic compounds by their parent peaks (organic groups essentially in tact) and fragmentation pattern (organic groups fragment in a known manner into smaller molecules). Samples were ultrasonically cleaned in n-hexane prior to analysis. Spectra were obtained of coatings composed of only one application of basecoat and the five-step basecoat with an epoxy-functionalized topcoat for comparison purposes. There is evidence for the presence of epoxy groups near the coating surface due to the appearance of absorptions typical for CH_3O^+ and $C_2H_3O^+$. This combined IR and TOF-SIMS data suggest epoxy groups are present at the coating surface upon application of an epoxy-functionalized topcoat. Similar results were obtained for the two-step epoxy- or amine-functionalized coatings, with absorptions observed at 2900 to 3000 cm^{-1} due to alkyl vibrations and at 1655 cm^{-1} for Si-alkoxy groups. *Epoxy or amine groups are therefore believed to be present in the topcoat depending upon whether epoxy- or amine-functionalized silane are used in the topcoat formulation based on the IR data.*

Coating Flexibility

Coating flexibility was evaluated using a mandrel bend test, ASTM D522-93a. A mandrel set conforming to this ASTM specification was purchased from BYK-Gardner. In this test, 0.032 in. thick specimens were bent around different sized mandrels which vary the coating elongation from 3.3 to 28 percent. *The alkoxysilane basecoat was bent around a 0.125 in. diameter mandrel, applying a 28 percent elongation to the coating, without showing any evidence of coating cracking.*

Adhesive and Environmental Resistance Performance

Wedge Crack Test-

Coated specimens for wedge crack testing were sent to Lockheed for preparation, assembly into test articles and testing according to ASTM D3764. Control specimens were bare aluminum substrates which were phosphoric acid anodized at Lockheed per the F-22 Specification 5PTPHL21. The specimens were solvent wiped and primed with Cytec XBR-6757 Water-Based Non-Chrome Primer using a Binks HVLP cup gun with tip 97S and cap 95AS. A primer coat thickness between 0.1 to 0.3 mils was achieved with one box coat. Primed specimens were air dried overnight and then cured at 250°F for 60 min. A FM-73 film adhesive, 0.06 LB/SF with a knit carrier, was used to form the adhesive bond. Since all specimens were pre-cut to their final width (1 in.) prior to surface preparation and bonding, precautions had to be taken during the bonding process to keep all specimens aligned and free from excess adhesive. The test articles were removed and both their edges polished to facilitate crack growth measurements during testing. The test was started by inserting a wedge into the test article end with the separation film (not bonded) using a lightweight rubber hammer with minimal force until the wedge was held in place. The wedge was then fully inserted by placing the specimen, with the wedge at one end, in a vice and slowly tightening the vice until the wedge was completely inserted. This minimized any dynamic force which may have induced plastic deformation in the adhesive. Tape was placed over the wedge end of the test article to keep the wedge from backing out. Crack lengths were measured using a 6 in. scale with 0.010-in. divisions under an optical microscope with variable magnification settings, with a 15X magnification being used to monitor crack length growth. A permanent marker was used to mark the crack extension at each reading with the average of the two crack lengths being reported. The initial crack length of each test article was measured before environmental conditioning, 140°F and 100 percent relative humidity. Readings were taken after environmental exposure for 1, 4, 8, 24 hr and 7 and 31 days. The final crack length was measured at the centerline of the test article after opening. A determination was also made whether the failure mode was adhesive, adhesive separated from coating, or cohesive, fracture occurred within the adhesive, in nature.

Test results are listed in Table 3 and displayed in Figure 3. Phosphoric acid anodized specimens performed the best overall of all the specimens, but the two-step amine-functionalized silane topcoated specimens gave very similar and promising results. The amine topcoated specimens were actually better up through the first day, however the anodized specimens exhibited shorter crack growth from 7 to 31 days. The two-step epoxy-functionalized silane topcoated specimens performed slightly worse that the amine topcoated specimens from the beginning of the test. All specimens had a curved final crack shape, longer in the center then at the edges. The control final average crack length was 2.75 in., while the crack length for the amine topcoated specimens was only 3.6 percent longer, and 8.4 percent longer for the epoxy topcoated specimens. The majority of the control and amine topcoated specimen failures were 100 percent cohesive,

with only a minor (about 2 percent) amount being adhesive. The epoxy topcoated specimens exhibited 85 percent cohesive and 15 percent adhesive failures. In conclusion, *we feel our two-step amine topcoated specimens performed similar to that of the phosphoric anodized control in this test designed to measure the environmental resistance of the adhesive bond.*

Double Lap Shear Test-

Coated specimens for double lap shear testing were also sent to Lockheed for preparation and assembly into test articles. These were prepared using the same primer and adhesive as the wedge test. Test specimens using phosphoric acid anodizing were also prepared by Lockheed according to their standard practices and used as control specimens. The prepared assemblies were sent to Mr. James Mazza at Wright-Patterson Air Force Base for testing. Double lap shear testing was performed under ambient conditions in accordance with ASTM D 3528. *The control and both the two-step epoxy and amine topcoated assemblies exhibited cohesive failure at 2200 psi, indicating the bonding surfaces generated by our sol-gel coatings were comparable to that of phosphoric acid anodizing.*

Floating Roller Peel Resistance Test-

Two-step amine topcoated specimens were sent to WPAFB for sample preparation and floating roller peel testing according to ASTM D3167. Test articles were constructed without application of a primer and from specimens coated from several days to weeks prior to assembly. *Assemblies cohesively failed at 50 psi, indicating a good bond had been formed directly between the sol-gel coating and adhesive.* This fact suggests that we may be able to eliminate the need for a primer with our functionalized sol-gel coatings, but additional testing is required for confirmation. Standard conversion coatings generally specify bonding surfaces must be protected by a primer within 18 hr of its formation to prevent severe decreases in bond strength. Therefore, *the amine functionalized bonding surface appears to be much more robust and resilient than conventional conversion coatings because of the elapsed time between coating formation and test article assembly.*

Paint Adhesion Test-

Two-step amine-functionalized coated specimens were sent to WPAFB for sample preparation and testing for paint adhesion according to a modified version of Federal Test Method Standard 141B (1 Feb. 79), Method 6301. Panels were primed with a chromated water-based epoxy from Deft (qualified to MIL-P-85582), topcoated with a Deft high-solids urethane coating per MIL-C-85285 and cured at ambient temperature for 14 days. The cured panels were "X" scribed and immersed in distilled water at 120°F for 4 days. After wiping off the excess water, a standard tape adhesion test was performed by the application of masking tape (3M Company No. 250) over the scribed area using a 2 kg roller followed by removal of the tape to see if any of the coating adhered to the tape. *All coated specimens passed the paint adhesion test, essentially no coating was removed from the edges of the scribed lines.* Coated specimens were then placed in an environment of condensing humidity at 120°F for 30 days to determine if any loss of coating adhesion, coating blistering, softening or other film defects occurred. *All coated specimens passed the humidity resistance test, exhibiting adequate coating adhesion and showing no coating defects.* Both of these tests indicate the amine-functionalized sol-gel topcoat provides a good adhesive surface that exhibits excellent water/humidity resistance.

CONCLUSIONS

The goal of this Air Force sponsored program was to develop an aqueous-based, environmentally friendly sol-gel coating for aircraft aluminum alloys that imparts corrosion protection to the substrate, creates a surface which increases the strength of adhesively bonded joints, and contains no hazardous or toxic chemicals. Foster-Miller has developed a sol-gel barrier conversion coating that is chemically and mechanically bonded to the substrate through their alumina surface layers, gradually changes its composition from an aluminosilicate to silica-like matrix to functionalized silicate, and is capable of forming chemical bonds to either aerospace-grade primers, adhesives or topcoats. The process is water-based, utilizes no hazardous or toxic chemicals, and generates corrosion resistant coatings without the use of hazardous and toxic chromates. This is a multi-step process that utilizes a reactive coating system to grow the coating directly on the substrate by immersing the substrate into the coating solution at the time of its formation. Our process is composed of essentially two types of coatings, basecoat(s) and functionalized topcoat, which were applied in a total of two to six steps depending upon the desired level of corrosion resistance. A single application of the basecoat produced a silica-like coating and additional applications appeared to fill in any pores or defects in the original coating. Once the appropriate number of basecoats had been applied, a functionalized overcoat was then applied to complete the conversion coating system. *Neither our sol-gel basecoat(s) or overcoat could be removed from the substrate by water rinsing prior to drying, unlike conventional sol-gel coatings, suggesting chemical bonding to the substrate or undercoats had occurred.* The surface of the overcoat was tailored to contain either epoxy ($-CH\overline{-}\underline{O}\overline{-}CH_2$) or amine ($-NH_2$) functional groups to chemically bond to subsequently applied adhesives or paints.

Coatings generated by the application of five basecoats passed the corrosion resistance specification of MIL-C-5541E, showing little indication of corrosion after exposure to 5 wt percent salt spray(fog) for 184 hr, but corrosion became apparent after 352 hr of exposure. Both the single and five basecoats showed little if any corrosion after exposure for 352 hr in the prohesion corrosion test (ASTM G-85). Reflectance/absorbance infrared spectroscopic and time-of-flight-secondary-ion-mass-spectroscopic data indicated functional groups were present at the surface for coatings composed of a basecoat with functionalized overcoat. DC polarization studies showed these coatings to retard both the cathodic (O_2 reduction) and anodic (aluminum dissolution) corrosion reactions, resulting in a decrease in the corrosion rate of two orders of magnitude compared to a bare substrate. Electrochemical impedance spectroscopy (EIS) indicated the initial corrosion resistance of these coated substrates to be slightly better than chromate controls, but their corrosion rate increased with time and surpassed that of the chromated control. Various assemblies were made using substrates having these two-step coatings for measurement of the interaction between our sol-gel conversion coating and the adhesive. Double lap shear test assemblies *failed cohesively*, within the adhesive rather than at the adhesive/primer/coating interface, at values (2200 psi) similar to the phosphoric acid anodized control. Wedge crack assemblies were made to test the environmental stability of the adhesive/primer/coating interface and the assemblies *cohesively failed* at values similar to the control. Floating roller peel test specimens (only amine-functionalized topcoat) were made without the use of a primer and assemblies *cohesively failed* at 50 psi. Two-step amine-functionalized coated specimens also passed paint adhesion and humidity resistance tests. These facts indicated *a strong, robust, resilient bonding surface had been produced using our environmentally-friendly sol-gel conversion coating process, a surface suitable for bonding adhesives or paints.*

ACKNOWLEDGMENTS

This work was performed under contract No. F33615-95-C-5621 for the Wright Laboratory Materials Directorate at Wright-Patterson Air Force Base located in Dayton, OH with funding provided by the Strategic Environmental Research and Development Program. We would like to thank our technical monitor Mr. Theodore J. Reinhart and Mr. James Mazza from Wright Laboratory for their technical support throughout this program. We would like to thank Mr. Peter Gagne from Oakite Products, Inc., Mr. David Klapprott from Hysol Aerospace Products and Mr. Hermann Sitt from Cytec Corporation for providing materials and information at no cost to the program. We would also like to thank Dr. Wim J. van Ooij of the University of Cincinnati, and Mr. Robert Stone and Ms. Sally Wu of Lockheed Martin Aeronautical Systems for their technical contributions to the program.

REFERENCES

1. Hinton, B.R.W., "Corrosion Inhibition with Rare Earth Metal Salts," *J. Alloys Compds ., 180*, 15-25, 1992.
2. Khedr, M.G.A. and Lashien, A.M.S., "The Role of Metal Cations in the Corrosion and Corrosion Inhibition of Aluminum in Aqueous Solutions," *Corrosion Science, 33*(1), 137-151, 1992.
3. Kendig, M.W.; Davenport, A.J.; Isacs, H.S., "The Mechanism of Corrosion Inhibition by Chromate Conversion Coatings from X-Ray Absorption Near Edge Spectroscopy (XANES)," *Corrosion Science, 34*(1), 41-49, 1993.
4. "Minutes of the Third Annual Workshop on Chromate Replacements in Light Metal Finishing," Albuquerque, NM, Sept. 15-16, 1993.
5. "1994-1995 Threshold Limit Values for Chemical Substances and Physical Agents and Biological Exposure Indices," American Conf. Govt. Industrial Hygienists, 1994.
6. Communications with Mr. David Klapprott, Dexter-Hysol Aerospace Products.
7. Discussions with Professor Wim J. van Ooij, The University of Cincinnati, OH.
8. Brinker, C.J. and Scherer, G.W., "Sol—>Gel—>Glass: I. Gelation and Gel Structure." *J. Non-Crystalline Solids*, 70, 301-322 (1985).
9. Holmes-Farley, S.R. and Yanyo, L.C., "Thin Anisotropic Coatings Based on Sol-Gel Technology." Mater. Res. Soc. Symp. Proc. 180. 439-444 (1990).
10. Holmes-Farley, S.R. and Yanyo, L.C., "Adhesion Promotion and Corrosion Prevention Using Thin Anisotropic Coatings." *J. Adhesion Sci. Technol.* 5(2), 131-151 (1991).

Table 1. Summary of Foster-Miller sol-gel multi-step coating process

Step	Description
1.	Optional surface roughening by sandblasting
2.	Rinse in deionized water
3.	Degrease using OAKITE 61B from Oakite Products, Inc., Berkeley Heights, NJ
4.	Rinse in deionized water
5.	Deoxidize using Oakite LNC
6.	Rinse in deionized water
7.	Apply alkoxysilane basecoat
8.	Dry at 100°C in air after each basecoat application
9.	Apply epoxy- or amine-functionalized topcoat
10.	Rinse in deionized water
11.	Dry at 100°C in air

Table 2. Thickness of various coatings by ellipsometry

Coating Type	Coating Thickness (Å)
One base coat	799 and 809
Three base coat applications	807 and 783
Four base coat applications	835 and 885
Five base coat applications	869 and 862
Seven base coat applications	946 and 963
Five base coat applications with epoxy-functionalized topcoat	1307 and 1165
Two-step formulation with epoxy-functionalized topcoat	1613 and 880
Two-step formulation with amine-functionalized topcoat	1354 and 1337

Table 3. Crack lengths versus exposure for the wedge crack test

Specimen ID		Final Length	Average Initial Length	Average 1 hr Length	Average 4 hr Length	Average 8 hr Length	Average 1 Day Length	Average 7 Day Length	Average 31 Day Length	Failure Mode
Control	1	2.77	2.02	2.20	2.22	2.22	2.24	2.29	2.31	98% CO/2% AD
	2	2.72	2.01	2.18	2.21	2.21	2.21	2.29	2.30	100% CO
	3	2.74	2.00	2.09	2.19	2.19	2.22	2.25	2.41	98% CO/2% AD
	4	2.78	1.94	2.06	2.10	2.12	2.16	2.21	2.31	98% CO/2% AD
	5	2.76	2.02	2.11	2.11	2.12	2.23	2.26	2.30	100% CO
	6	2.77	1.96	2.19	2.22	2.25	2.26	2.29	2.35	100% CO
	7	2.64	1.96	2.09	2.13	2.14	2.12	2.19	2.26	100% CO
	8	2.82	2.00	2.07	2.12	2.19	2.22	2.29	2.37	100% CO
Average		2.75	1.99	2.12	2.16	2.18	2.21	2.26	2.32	
Amine-Functionalized Topcoat	1	2.80	2.01	2.11	2.18	2.18	2.24	2.30	2.36	100% CO
	2	2.78	1.91	2.00	2.08	2.08	2.10	2.15	2.42	100% CO
	3	2.80	1.94	2.06	2.11	2.17	2.22	2.26	2.47	100% CO
	4	2.76	1.99	2.07	2.09	2.09	2.25	2.34	2.44	98% CO/2% AD
	5	2.97	2.11	2.15	2.22	2.22	2.23	2.43	2.60	98% CO/2% AD
	6	3.14	2.04	2.11	2.20	2.27	2.36	2.56	2.84	98% CO/2% AD
	7	2.73	2.00	2.08	2.10	2.11	2.15	2.28	2.38	98% CO/2% AD
Average		2.85	2.00	2.08	2.14	2.16	2.22	2.33	2.50	
Epoxy-Functionalized Topcoat	1	3.01	1.99	2.01	2.15	2.15	2.33	2.56	2.83	85% CO/15% AD
	2	2.86	2.05	2.19	2.25	2.28	2.34	2.51	2.64	85% CO/15% AD
	3	2.89	1.94	2.06	2.12	2.10	2.21	2.39	2.57	85% CO/15% AD
	4	2.96	2.15	2.17	2.22	2.23	2.26	2.46	2.71	85% CO/15% AD
	5	3.02	2.10	2.16	2.32	2.32	2.32	2.62	2.80	85% CO/15% AD
	6	3.03	2.12	2.16	2.24	2.24	2.26	2.57	2.65	85% CO/15% AD
	7	2.07	2.09	2.19	2.22	2.25	2.32	2.60	2.75	85% CO/15% AD
Average		2.98	2.06	2.13	2.21	2.22	2.29	2.53	2.71	

CO indicates cohesive failure and AD indicates adhesive failure

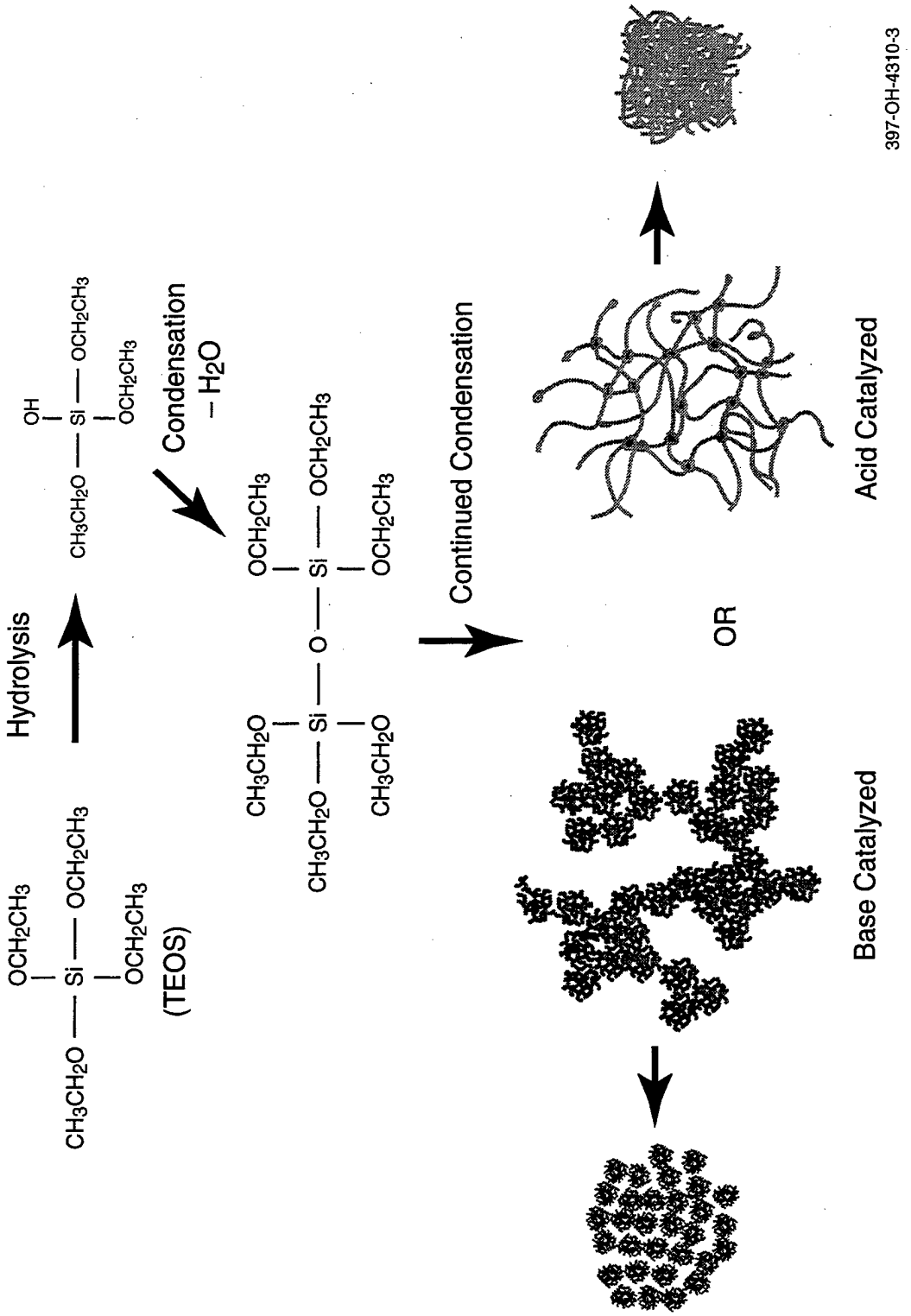

Figure 1. Nature of sol-gel polymeric species depends on hydrolysis conditions

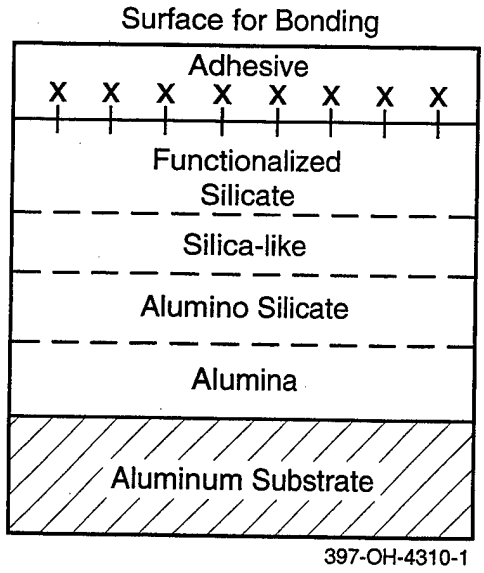

Figure 2. Schematic of aluminum substrate coated with Foster-Miller functionally-gradient sol-gel coating

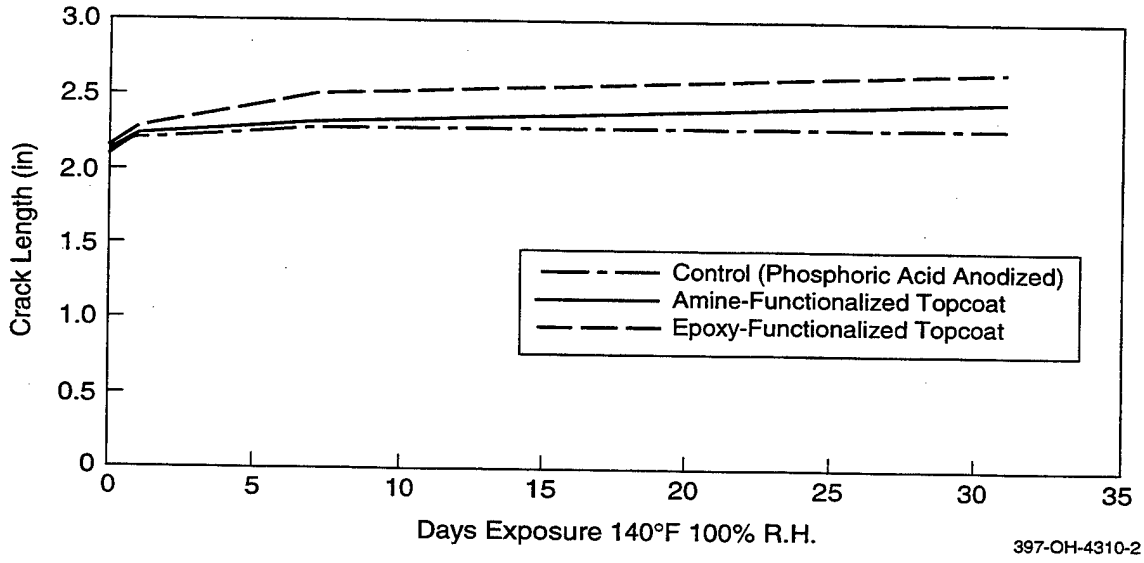

Figure 3. Wedge crack test results

Corrosion Resistance Evaluation of High Performance Aircraft Coatings Systems (HPACS)

L.B. Reynolds, M. Khobaib, N.N. Voevodin, R.L. Twite, C.S. Jeffcoate, and M.S. Donley
Wright laboratory, Materials Directorate, WL/MLBT, Wright-Patterson AFB, OH

The United States Air Force (USAF) requires improved aircraft coating systems. Corrosion prevention is an extremely important top-level requirement, due to the longevity of the USAF fleet, and these coating systems must meet requirements more stringent than the commercial sector. The High Performance Aircraft Coatings Systems (HPACS) Program addressed this need for improved coating systems by evaluating commercially available, off-the-shelf coating system. Accurately assessing the corrosion protection properties of coatings is an area of major concern in the test and evaluation of aircraft coatings. Although, salt spray was the test method of choice in the past, it has questionable correlation with field performance. Other test methods must be investigated. The corrosion resistant performance of eight different coating systems was evaluated by investigating the coating barrier properties to immersion using Electrochemical Impedance Spectroscopy (EIS). Application of this technique allows for discrimination between systems and enables the evaluation of the extent of degradation of the systems over extended periods of time when no visible signs of corrosion were present. Additional chemical analyses that relate to the degradation of the coated specimens will be reported. From the test results a recommendation is made on which coating systems would give the best corrosion prevention attributes for an aircraft coating system.

BACKGROUND

Aircraft coating systems are a major technological concern for the DoD, and one in which continual improvement is sought. Estimates indicate that aircraft painting/stripping/repainting and handling of the hazardous waste associated with these materials cost in excess of $150M per year for the USAF. The problems associated with corrosion are the number one maintenance cost for the USAF estimated at $700M per year, and 15% of this cost is associated with paint related corrosion.[2] A typical aircraft paint system consists of a surface treatment, primer, and topcoat. The surface treatment is applied to the substrate (typically an aluminum alloy, Al 2024-T3 or Al 7075-T6) to provide a surface morphology for optimum adhesion of the primer and typically contains inhibitors for corrosion protection.[1] The primer also contains corrosion inhibitors which help provide for its main function of corrosion prevention, but must be a compatible interface between the surface treatment and topcoat. Finally, the topcoat provides signature control, acceptable physical appearance, and a protective barrier to the outside

environment (i.e., sunlight, water, mechanical abrasion, etc.,). Each component plays an important role in protecting the underlying weapon system, whether it be from a hostile enemy or environmental factors, but components must be compatible with one another as a complete coating system package.

The corrosion protection requirements of coating systems are more demanding for aging aircraft. With shrinking budgets and the enormous cost of new weapon systems, fewer advanced aircraft are being developed. This directly results in the use of current aircraft systems far longer than they were ever intended. For example, certain systems such as the B-52 are projected to be in the air force fleet until the 2030's, giving it a service life of over 80 years. While structural integrity of the aircraft is crucial, the first line of defense to the outside environment is the coating system. As the service life of these weapon systems become longer, the demands of the coating system become greater, and there are large economic incentives to improve the coating systems. Escalating costs are driven by EPA, OSHA, and NESHAP regulations. Traditional coating systems were applied with formulations which relied heavily on hydrocarbon based solvents. These solvents are now classified as hazardous air pollutants (HAPs) and volatile organic compounds (VOCs) in the coatings which must be reduced or eliminated. The surface treatment and primer components relied solely on heavy metal hexavalent chromium (Cr^{6+}) as the corrosion inhibitor which must be eliminated to comply with legislation. These traditional chemistries with their established protocols, applications, and performance will no longer be available. New classes of corrosion inhibitors, polymer resin systems, and solvent application systems must be established. They must perform the multi-functional role of an air force aircraft coating system which consists of three main attributes: 1) corrosion protection, 2) survivability, and 3) cosmetic appearance.

Accurately assessing the corrosion protection properties of coatings is an area of major concern in the test and evaluation of aircraft coatings. In the past the USAF relied heavily on the use of salt spray cabinets (ASTM B117 test method) as a means of evaluating the corrosion protection potential of aircraft coating systems but it has been found that salt spray tests may not properly reflect how coating systems perform in the field.[5] Salt spray is still used by the air force but more as an acceptance test. An acceptable aircraft coating system sample should pass 2000 hours of salt spray with no visible signs of corrosion. The USAF realizes that salt spray is not an accurate predictor of real field use, but currently there is no other accepted accelerated test method. Other test methods are being considered. Prohesion™ is a cyclic test which allows the panels to be subjected to temperature cycling and alternate wet and dry cycles which is more representative of a dew cycle, but the ASTM standard calls for the use of dilute Harrison's solution as the electrolyte instead of 5% wt sodium chloride. Prohesion™ is a better discriminator between coating systems due to its cyclic nature, but it is still a qualitative test. Prohesion™ cabinets are now starting to take the place of salt spray testing. However, both Prohesion™ and salt spray testing are qualitative in nature. The interpretation of the data is reliant on the operator. Emerging electrochemical test methods such as using Electrochemical Impedance Spectroscopy (EIS) have

predominately been used evaluating steel substrates and there is not an extensive database evaluating aircraft coating systems, so a better understanding of electrochemical test data must be established.[7-9]

The USAF is aggressively pursuing the advancements of improved coating systems due to the aging of the current air force fleet. In an effort to utilize the best state-of-the-art coating systems, a program called the High Performance Aircraft Coatings Systems (HPACS) program was established to evaluate the best readily-available, off-the-shelf, commercial coating systems. Vendors supplied coated aluminum alloy specimens with a complete coating system: the surface treatment, primer, and topcoat system. A battery of 51 tests were performed on the systems evaluating the corrosion prevention, appearance, survivability, durability, cleanability, application methods, flow times, etc., based on an extensive performance requirements document. Wright Laboratory performed quantitative corrosion testing on these samples using Electrochemical Impedance Spectroscopy (EIS). EIS is an emerging electrochemical technique used to evaluate the rate and extent of corrosion for various substrates and coated systems.[4] Unlike salt spray and Prohesion™, EIS give quantitative results allowing for a better understanding of the corrosion prevention properties of the coating system.

Experimental

The HPACS program started with a qualitative screening evaluation of 23 coating systems. The focus of the program was a comparison of the corrosion protection properties of the complete aircraft coating systems, as delivered and described by the manufacturer's specifications. The program was not focused on application methods or an evaluation of the individual surface treatment, primer, or topcoat components. After the initial screening tests, these coating systems were down-selected to the 8 best systems which received a complete electrochemical evaluation, which included EIS testing. A listing of the 8 selected coatings and a make-up of their primer and topcoat components is presented in Table 1. The coated samples were 4 x 6 inch panels, all prepared from the same sheet of Al 2024-T3 to minimize the effects of substrate variations on corrosion prevention. Sample preparation followed the protocol as described by each manufacturer in preparing the samples to make a fair comparison of the aircraft coating systems' corrosion protection. As indicated in the table, these 8 aircraft coating systems tested included chromate-free primers, waterborne, solvent-based, and high solids systems. If the paint system met current environmental restrictions or exceeded these regulations, it was accepted for initial screening tests.

TABLE 1: Sample Identification.

System Number	Primer	Topcoat
3	epoxy polyamide	solvent-based urethane
4	waterborne epoxy	waterborne urethane
6	high solids epoxy	high solids polyurethane

14	high solids epoxy	high solids polyurethane
15	low density, chrome-free epoxy	high solids polyurethane
17		self-priming polyurethane
20	chrome-free epoxy	water-reducible polyurethane
23	high solids epoxy	high solids polyester primer surfacer high solids polyester urethane

Each coating system was evaluated using a Gamry Instruments Model 100 and 300 Electrochemical Measurement Systems. The Gamry system contains a PC3 potentiostat/galvanostat, CMS 300 software to perform the EIS measurements. All coating samples were exposed by immersion to dilute Harrison's solution, a mixture of 0.35 wt% ammonium sulfate and 0.05 wt% sodium chloride, throughout the entire testing period (approximately 11 months). This mixture of electrolytes closely simulate atmospheric conditions and thus was selected as a more representative environment air force aircraft are exposed to instead of standard sodium chloride solutions[6]. To contain the electrolyte, a 3 inch high piece of PVC tubing (ID = 1 5/8 inches) was attached to each 4X6 inch sample using Marine Goop™ (a propyl acetate and petroleum distillate). After 24 hours of drying time for the glue, the Harrison electrolyte was poured into the PVC tubing. The system was allowed to stabilize for 24 hours before the initial test was conducted. The EIS measurements were performed over a frequency range of 55,000 to .02 Hz using a 10 millivolt potential. The 11 month time frame was arbitrarily chosen in testing the samples to observe the coating systems degradation over a long time period.

Results/Discussion

The impedance measurements allow direct evaluation of the coating's capacitive and resistive nature while immersed in an electrolyte. From these impedance measurements other characteristics of the sample such as: passivity of the coating, water uptake within the coating, and diffusion within the coating system can be determined. All of these variables can be described using quantifiable results, thus most of the qualitative interpretation which salt spray and Prohesion™ rely heavily is eliminated. The Nyquist plot is a graphical representation of real impedance (in phase), Z', vs. imaginary impedance (out of phase), Z".

A Nyquist plot showing the impedance behavior of coating system 3 (an epoxy primer and polyurethane topcoat) is presented in Figure 1. As indicated by the data, the behavior of coating system 3 remained consistent throughout the 11 months of the evaluation. There were no signs of breakdown within the coating which are typically represented by a Warburg component or two or more time constants. Each test over the 11 month period for system 3 showed the start of a semi-circle with a high

Z' for the Nyquist plot representing a good coating system. No visible signs of corrosion were detectable on the sample. Systems 3 and 23 showed the best corrosion performance per EIS analysis, and the Nyquist plot showing the impedance behavior of coating systems 23 is similar to that shown in Figure 1.

To illustrate EIS data for a coating system which did not perform well, a Nyquist plot showing the impedance behavior of coating system 14 (a high solids epoxy primer and high solids polyurethane topcoat) is presented in Figure 2. As indicated in the plot, a breakdown of the coating occurred 2 weeks after initial exposure. The data also indicates that, after 7 months, the coating appeared to become diffusion controlled as the impedance measurements increase. This diffusion limiting process could be caused by corrosion products forming within the corrosion sites, thus reducing the observable corrosion rate. For months 9 and 11, the impedance measurements decreased with a noticeable second time constant forming. Diffusion within the coating system occurred and breakdown of the coating is taking place. Note that there is a 2 order of magnitude difference in the x-axis from Figures 1 and 2. Thus, the passivation of the coating at the 7 month experiment was related to the corrosion products filling the corrosion sites. Visual signs of coating breakdown were noticeable.

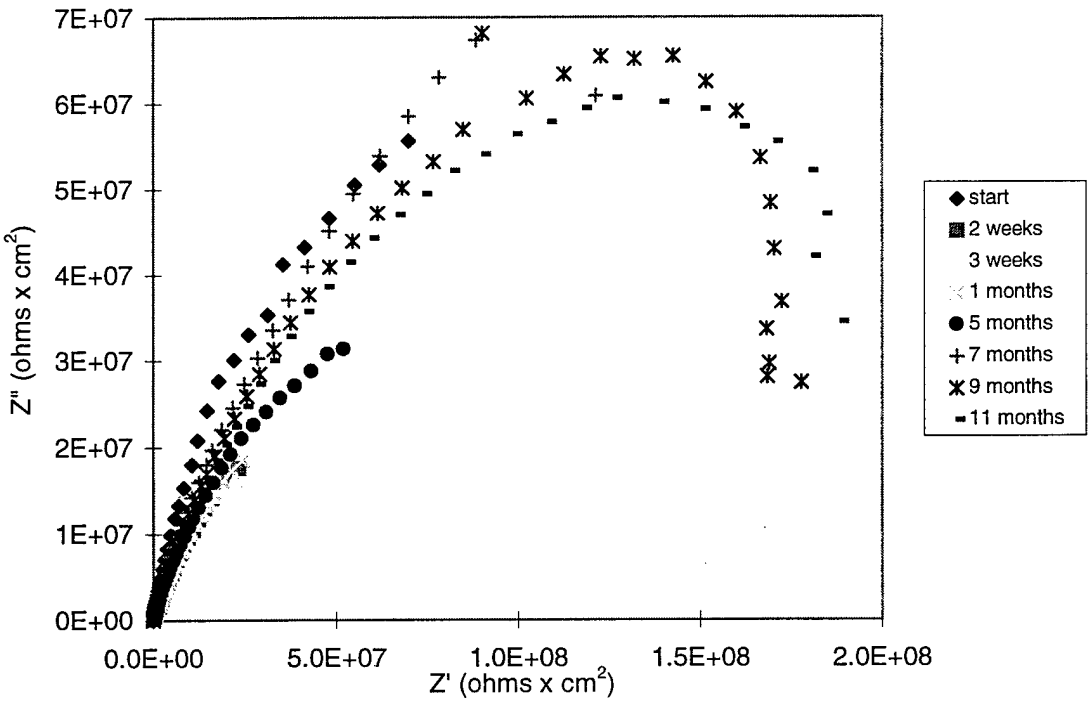

Figure 1. Nyquist Plot of coating system 3.

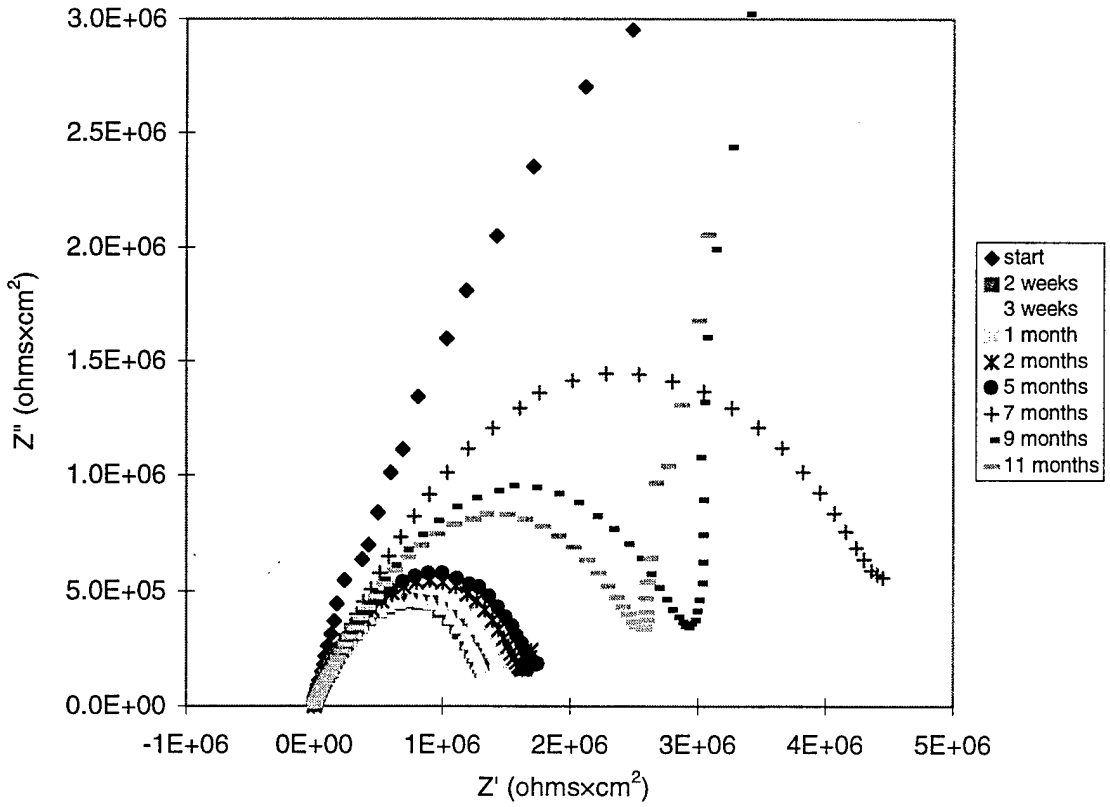

Figure 2. Nyquist Plot of coating system 14.

The Bode plot is a graphical representation of the impedance modulus, Zmodulus, vs. the log of the frequency, log f. If the data continues vertically, the coating system exhibits purely capacitive behavior. If the graph is horizontal, the coating system behaves resistive in nature. If the graph is diagonal the coating system is exhibiting a combination of capacitive and resistive behavior. The point on the graph where the line changes from vertical, horizontal, or diagonal is expressed as a breakpoint frequency. The impedance modulus represents the total impedance contribution whether it be capacitive, resistive or a combination. Generally, the higher the impedance modulus the better the coating system.

A Bode plot of the electrochemical impedance data for System 23 is presented in Figure 3. The coating showed a strong combination of capacitive and high resistive nature, there is no discernible breakpoint frequency, and the total Zmodulus is in the 10^8 ohms·cm^2 range. All of these features are indicative of good corrosion protection properties. Again, similar data was recorded for System 3. Based on the Bode plot data, systems 3 and 23 showed the most promising corrosion resistance behavior by electrochemical evaluation.

To illustrate EIS data for a coating system which did not perform well, a Bode plot for System 4 is presented in Figure 4. The initial experiment showed a strong coating system having both a capacitive and resistive nature. However, from 2 weeks to 2 month, a breakpoint frequency appeared and the coating

system began to show only resistive behavior in the lower frequencies with a decreasing Zmodulus. From experiments at 7, 9, and 11 months, the coating system began to show breakpoint frequencies in the higher frequencies as well. The coating system spectra began in the higher frequencies with a capacitive and resistive nature. The coating system experienced a breakpoint frequency and became purely resistive in nature. Then the coating system experienced another transition and once again, became capacitive and resistive in nature due to diffusion controlled processes. Note there is three orders of magnitude difference between Figure 3 and 4 after 2 months.

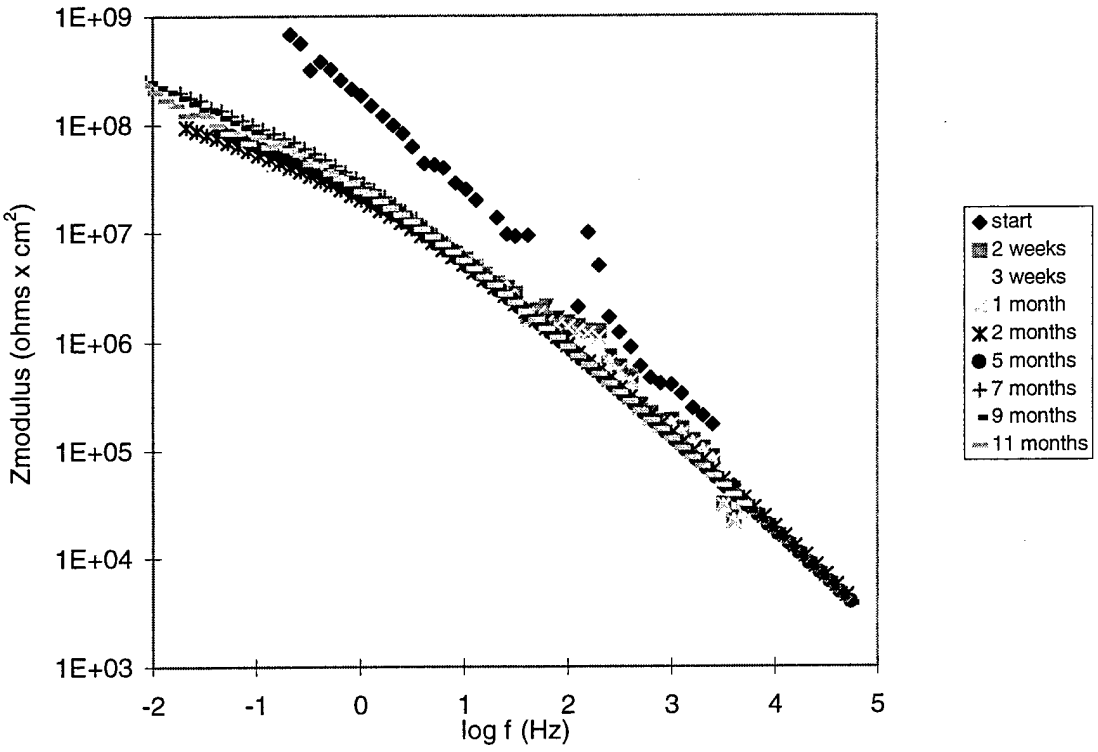

Figure 3. Bode Plot of coating system 23.

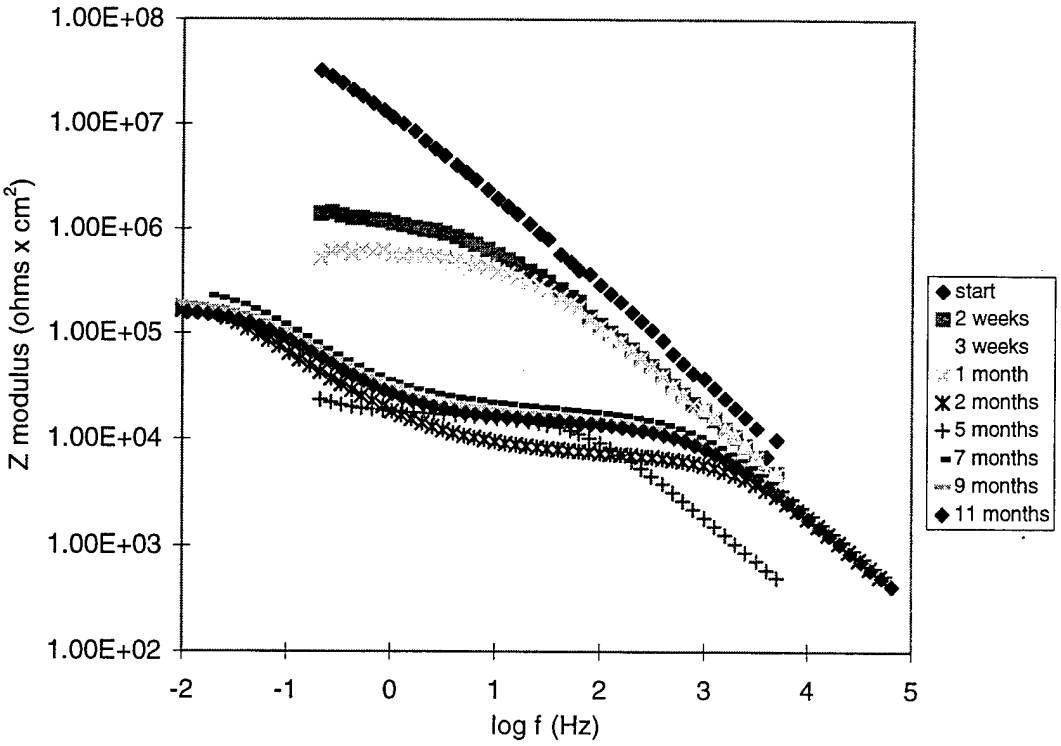

Figure 4. Bode Plot of coating system 4.

As seen from the Nyquist and Bode plots, valuable information can be obtained about the aircraft coating systems without even focusing on the quantifiable results. The graphs show relative orders of magnitude for the impedance values of each coating which helps explain the capacitive and resistive behavior or breakdown of the coating system. Salt spray and Prohesion™ show only visible signs of degradation, but from the above coatings, degradation is taking place even when no visible signs of corrosion are present. Even though the above mentioned charts provide valuable information just from their relative orders of magnitude and shapes, quantifiable results are still the key to establishing EIS as a predictive tool for aircraft coating systems. Impedance values, $|Z|$, were approximated as $|Z(\omega \rightarrow 0)|$, and for convenience, a low frequency of 0.84 Hertz was chosen for extrapolating $|Z|$ values from the impedance plots. Data for each coating system is presented in Figure 5, which includes measurements of each coating system after its initial experiment, at 5 months, and finally at 11 months. System 23 had the strongest impedance readings throughout the testing period (4.38×10^7 ohms·cm^2 initial experiment, 1.68×10^7 ohms·cm^2 after 5 months, and 1.71×10^7 ohms·cm^2 after 11 months). System 3 exhibited a similar trend (3.13 x ohms·cm^2 initial experiment, and 1.45 x ohms·cm^2 after 11 months), as well as system 14, but it was an order of magnitude lower (10^6 ohms·cm^2). Systems 4, 6, 15, and 20 exhibited coating breakdown from the impedance measurements after 11 months. Systems 4 and 20's impedance readings dropped 2 orders of magnitude (10^6 to 10^4 ohms·cm^2) while systems 6 and 15's impedance readings

dropped 3 orders of magnitude (10^7 to 10^4 ohms·cm^2). Coating system breakdown began on system 17 after 2 weeks of exposure, but a passivation of the sample took place due to the 11 months experiment having as strong an impedance reading as the initial experiment as seen by the Bode plot, Figure 6. It has not been determined if this passivation was caused by corrosion products filling the corrosion sites decreasing diffusion through the coating or whether the inhibitors are actually protecting the substrate.

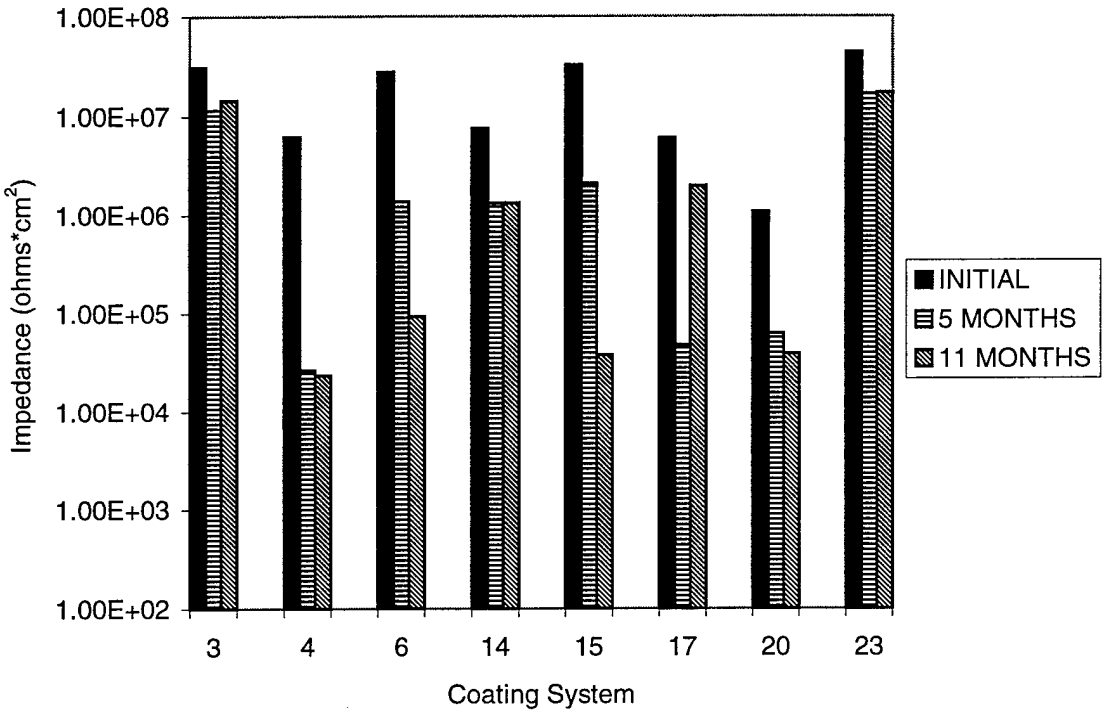

Figure 5. Impedance readings of all coating systems at 0.84 Hertz.

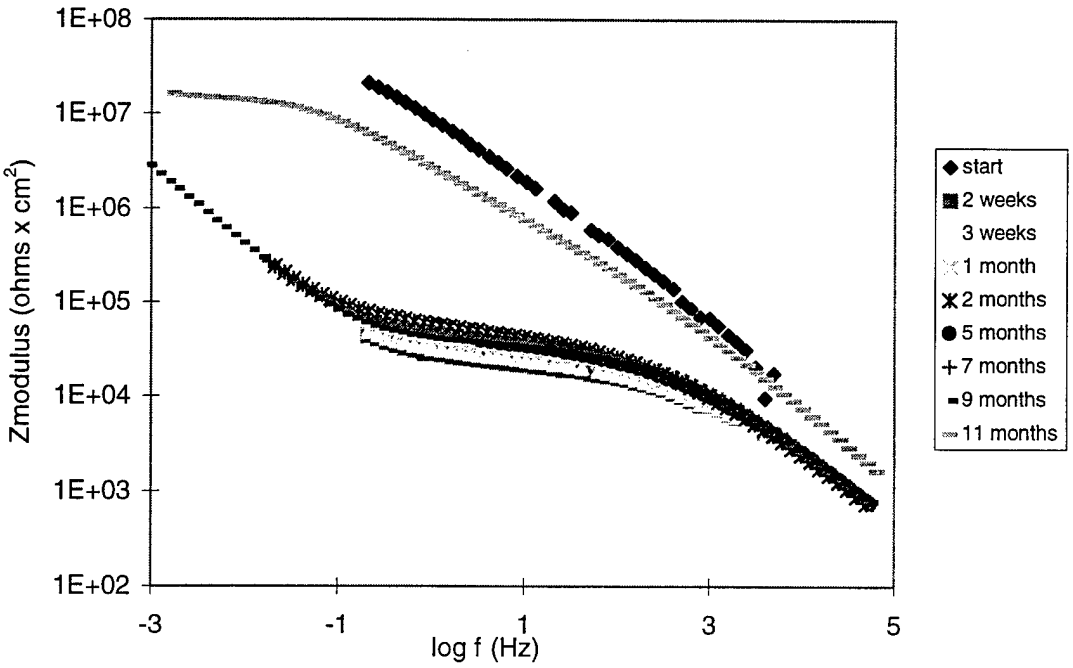

Figure 6. Bode Plot of System 17.

CONCLUSION

- Evaluating the systems using EIS, system 23 which was a high solids epoxy primer with a high solids polyester, primer surfacer, and high solids polyester urethane topcoat, and system 3 which was an epoxy polyamide primer with a solvent-based urethane topcoat were the 2 best performers.
- The other epoxy primer systems (4, 6, 14, 15, 17, 20) whether they were high solids, chromate-free, or waterborne with a waterborne or high solids polyurethane topcoat degraded significantly after 11 months, and all exhibited visible signs of corrosion.
- The current chromate free coatings are not as effective for corrosion protection as the existing chromate containing systems. System 15 (low density, chromate-free primer and a high solids polyurethane topcoat) exhibited good initial performance, signs of degradation after 5 months, but severe coating breakdown after 11 months (Figure 5).
- System 17 (self-priming polyurethane) was the only system which exhibited significant improvement in performance at 11 months after the coating showed severe degradation from only 2 weeks of exposure. A determination on this unusual behavior has yet to be determined.

BIBLIOGRAPHY

1 a. Mitani, M., "Process for Surface Treatment of Aluminum or Aluminum Alloy." US Patent No: US 5,132,003. 21 July 1992; b. Reghi, G.A., "Process for Corrosion resisting Treatments for Aluminum Surfaces." US Patent No: US 5089064. 18 Feb 1992; and c. Higgins, G.L., "Composition and Process for Treating Metal Surfaces." US Patent No: US 4,963,198. 16 Oct 1990.

2 Miller, R.N., R. Summitt, and F.H. Meyer, "Lifetime Prediction of Corrodible Structures", Vol. II, p1440, R.N. Parkins, ed. Houston TX, NACE, (1994).

3 Implementation Plan - Air Force Coatings System Strategy Department of the Air Force, United States of America, Washington D.C., 15 Mar 1995.

4 a. Skerry, B.S. and D.A. Eden, *Prog. Organic Coatings*, **15**, 269 (1987). And b. Chenm, C.T., and B.S. Skerry, *Corrosion*, **47**, 598 (1991). And c. Twite R.L.*, V. Balbyshev, G.P. Bierwagen and D.E. Tallman, "ENM Studies of Surface Treatments and Primers on Aircraft Alloys," the 188th Annual Meeting of the Electrochemical society, Chicago, IL October 9, 1995 to be published in Symposium volume by ECS.

5 Skerry B.S. and C.H. Simpson, "Combined Corrosion/Weathering Accelerated Testing of Coatings For Corrosion Control." NACE March 1991 National Meeting, Cincinnati, OH Paper 412.

6 Skerry B.S. and C.H. Simpson, *Corrosion,* **49(8)**, 663 (1993).

7 Reynolds, L.B., Twite, R.L., et. Al., "Preliminary Evaluation of Aircraft Coatings", *Progress in Organic Coatings,* to be published.

8 Jeffcoate, C.S., Wochen T., Bierwagen, G.P., *Journal Material Engineering and Performance*, 6-4, 1997.

9 Jeffcoate, C.S., Bierwagen, G.P., *Proceeding of ACS Symposium*, "Corrosion Protection by Organic Coatings" ACS Books, 1996.

The Air Force Coating Technology Integration Office: Operation and Objectives

Maj. W. Kevin Kuhn

Coating Technology Integration Office
AFRL - Materials and Manufacturing Technology Directorate
2179 Twelfth St, Suite 1
Wright-Patterson AFB, OH 45433

ABSTRACT

The objectives of the Coating Technology Integration Office (CTIO) are improved coating system performance and pollution prevention through the integration of improved environmentally acceptable materials and processes for aircraft finishing. The technical areas addressed by the CTIO include, but are not limited to, coating removal, surface preparation, coating application, and performance evaluation.

The CTIO is currently working projects on new product identification, integration and qualification; fielded coatings improvements and integration; and field support. In this paper, a discussion of the current concept of operation for CTIO, the capabilities of the facility, and current projects will be presented.

BACKGROUND AND OBJECTIVES

Prior to 1993, USAF aircraft coating systems were generally considered to be adequate. Their weaknesses were both masked and compensated for by an abundance of resources. Commanders treated frequent coating system failures by using organic resources to remove and apply more of the same paint, more frequently. Failures were generally attributed to inadequate coating materials performance, with little emphasis on process effectiveness. Parenthetically, the Air Force purchased aircraft coating products that cost three to twenty times less than the coating products used on quality automobiles. Commercial coating manufacturers dedicated their product development programs to their greatest market in the commercial aircraft coating arena. In contrast, coating systems requirements for DOD weapon systems rapidly became far more demanding because of the increased sophistication of the threats as well as materials and technologies used in DOD coating systems and service life extensions of many aircraft fleets far beyond original design. Further, increases in operational and aerospace environmentally-induced stresses accelerated coating failures because of the limited performance characteristics of these systems.

Early in 1994, the confluence of three events resulted in the current focus on USAF coating systems development and implementation through a single manager. First, the realization that the emerging National Emissions Standards for Hazardous Air Pollutants (NESHAP) rules and the concurrent Occupational Health and Safety Administration (OSHA) initiatives would have

dramatic impacts on core USAF depot and field level aircraft coating processes, inspired a search for alternative products. Paint and depaint activities accounted for 75 percent of the pollutants in Air Force Materiel Command (AFMC). These NESHAP rules impact the mission because they require the reduction of VOC/HAP emissions. Attention was refocused on the activities of the commercial aircraft coating manufacturers who were developing coatings with reduced volatile organic compounds (VOC). While these low VOC coatings satisfied the NESHAP requirements, they significantly complicated the USAF users' processes and decreased the performance of these products. This delayed the insertion of new, compliant products to the field. Second, increased dissatisfaction by field commanders with the performance of existing aircraft coating systems, focused HQ AFMC staff and development activities on improving the performance of existing products. Third, the new AFMC Commander expressed concern over the Command's dispersed development efforts for critical elements of the aircraft coating systems. Of particular concern was improving the timing and applicability of technology transition/insertion.

To meet these challenges HQ AFMC established a multi-command task force to bring all issues to the table. The first task was to create a prioritized list of customer requirements and a plan for addressing them. This task force provides-a standing capability/forum for the purpose of overseeing all policy and investment activities for aircraft coating systems and their removal throughout the USAF. It evolved into the current USAF Coating Technology Screening Committee (CTSC). The CTSC has produced and maintains three essential policy documents: the USAF Coating Systems Strategy, the USAF Coating Removal Strategy and the USAF Coating Technology Integration Office (CTIO) CONOPS. The USAF Coating Systems Strategy is the source document for meeting the Air Force's coating systems needs through changes in materials, processes, equipment, and application techniques. It specifies three key principles:

1. *Single manager for all coating systems.* This manager will be the single point of contact for the acquisition and sustainment of a comprehensive, integrated process that includes cleaning, stripping, surface preparation, coating application, upkeep, and waste disposal across the Air Force. This manager will identify the RDT&E needs and coordinate all technology activities. In addition, it will be the responsibility of this manager for ensuring adequate funding for coating systems.

2. *Establish a Science and Technology program.* Current commercial systems will not meet future Air Force requirements in the areas of performance and corrosion resistance. Therefore, new systems must be developed through an S&T program. A three-tier approach focuses on meeting the users' immediate needs while also anticipating the requirements of the future. It will include research, development, and testing appropriate to the Air Force near term, mid term, and long term coating needs.

3. *Establish a Coatings Technology Integration Office (CTIO).* This office will provide the core technical capabilities for making new coating systems ready for the depot and field environments. It will focus on understanding the user environment, testing the systems, deploying them, and supporting the users through sustainment. This office will have the responsibility for analyzing how the new coatings systems will impact the depot and field

processes and assisting the users in implementing new processes. In addition, the office will provide troubleshooting support for users of coatings systems.

COATING SYSTEM ISSUES

There are three main reasons the Air Force paints its air craft: survivability, corrosion protection, and appearance. Survivability includes things like the color of the paint, as well as its visual and IR signature. For corrosion protection, chromates are currently incorporated into the primer and are the inhibitor of choice since nothing else has been found to work as well. In addition, the whole coating system itself helps to inhibit corrosion since its acts as a barrier between the aluminum surface of the aircraft and the environment. Appearance deals with issues like finish, gloss, and color. More specifically, coating properties like abrasion, stain and chemical resistance as well as weatherability will contribute significantly to the appearance of the painted surface. For the person on the flight line, appearance is the first indicator of coating degradation and is therefore an important quality a paint must maintain over time.

As stated earlier, the application and removal of aircraft coatings generates approximately 75% of the air force's hazardous waste and costs the Air Force in excess of $150M per year. The total annual AF cost for corrosion control activities is in excess of $1 billion.[1] Stripping and re-coating an F-16 costs approximately $40,000, while for a C-5 the cost is over $1,000,000. Current practices have aircraft being repainted, primer as well as topcoat, well ahead of the planned depot maintenance cycle because of poor appearance. Based on a survey conducted by the CTIO in FY95, the Air Logistic Centers generate 438,000 lbs of VOCs, 489,000 lbs of HAPS, and 9,700 lbs of Cr^{6+} each year.[2] In addition, based on preliminary information, it is estimated that the field units generate 700,000 lbs of VOCs each year and use three times as much paint as the ALCs.

As we are being driven to new "greener" coatings, a common comment has been why aren't we using the coatings the commercial aircraft industry is using. There are three reasons why we aren't: they are the three reasons stated earlier as to why the AF does paint its planes. Commercial coatings don't meet the necessary survivability requirements, they don't have the proper appearance (wrong colors and too much gloss), and they don't meet Mil-Spec requirements for corrosion control. The corrosion control ability is critical for AF coating systems due to the age of the fleet and the necessity to extend aircraft lifetimes. An average commercial aircraft has approximately 3000 annual flight hours and is approximately 15 years old on average. An average Air Force equivalent aircraft (KC-135 for example), has about 375 annual flight hours and has an average age of 35 years. The fact that commercial aircraft are flying about 30% of the time means they are retired after about 20 years of service (fatigue lifetime). The KC-135 on the other hand, is only flying about 4% of the time giving it a fatigue lifetime of at least 80 years. Current plans expect to have KC-135s still flying even after the year 2025 (the original design life was 13 years). Corrosion, however is a function of environment and time, not flight hours. Therefore, superior corrosion protection is required to achieve the desired aircraft lifetime extension.

Thus, these requirements for superior corrosion control have to considered before any new environmentally acceptable coating is implemented. Indeed, performance is a driver in true pollution reductions. With regards to paint / de-paint operations, there are two ways to reduce the amount of pollution generated. The first, and most obvious way, is to reduce the amount of pollutants in the paint itself (make the paint "greener"). The second is to reduce the paint / de-paint frequency. Every time a plane need to be painted, pollution is generated. By increasing the required time between painting (improved coating performance) pollution generation will be reduced. In fact, if the performance of a new compliant coating is poor enough, then the successive re-paint cycles could generate enough pollutants to exceed what was being produced by the old high solvent, non-compliant coatings. It is of paramount importance for the Air Force to ensure that the new compliant coatings that are being implemented provide adequate corrosion prevention and have proper performance features to forestall the need for excessive touch-up / re-paint in the field. The costly cycle where planes are continually repainted due to poor coating performance has to be reduced if true pollution reductions are to be realized.

CTIO OPERATIONS

One of the three key principles of the Air Force Coatings System Strategy was to establish a Coatings Technology Integration Office (CTIO). This office will provide the core technical capabilities for making new coating systems ready for the depot and field environments. The CTIO will focus on understanding the user environment, testing the systems, deploying them, and supporting the users through sustainment. This office will have the responsibility for analyzing how the new coatings systems will impact the depot and field processes and assisting the users in implementing new processes. The mission of the CTIO is to transition new, emerging coating systems and technologies to the "user", and to improve the quality of and troubleshoot problems with existing fielded coating and related equipment.

The CTIO will provide the capability to accelerate the transition of new technology to the user, make it easier for them to use it, and maintain a troubleshooting role to enable the customer to debug existing coating system issues with minimum impact to the operational mission. This is accomplished by providing centralized influence into the aircraft coating development process. In this role the CTIO interprets user requirements into technical requirements to enable the commercial industry to focus their development programs for the USAF market. The CTIO has expertise in various facets of the coating process, to include: surface preparation, coating application, coating chemistry, material behavior, corrosion control, depaint technology, and environmental issues.

The CTIO is established as the integration and implementation agency for the S&T Coatings Program and functions as the role of the engineering arm of the Program. CTIO is organizationally aligned under the Systems Support Division in the Air Force Research Laboratory's Materials and Manufacturing Technology Directorate. The technical workload of the CTIO is performed primarily by contractors.

The CTIO's primary location at WPAFB has been sized for a core level of effort, but to accommodate peaks in workload, the CTIO will maintain several additional support locations.

Initially, the majority of the work will be performed at the Southwest Research Institute (SwRI) "home office" located in San Antonio, TX until the CTIO achieves Initial Operating Capability (IOC) in Feb 1998. Afterwards, the San Antonio SwRI facility can still be used to accommodate surge workloads, and to provide access to additional expertise that might be needed on an infrequent basis. The coating removal processes of the CTIO will be permanently located at WR-ALC to leverage that installation's existing depaint facilities and equipment. Other specialized testing and integration capabilities will be arranged through agreements with other organizations as required.

The CTIO facility at WPAFB currently occupies approximately 7500 sq ft with an additional 7000 sq ft planned to be gained in 2002. The facility is designed to replicate ALC equipment and processes and to provide the necessary test capability to determine coating properties and performance. At IOC, the facility will provide the capability to perform the following functions: coating application, environmental testing, dry film testing, and wet properties testing. The core capability of the facility will be the environmentally controlled paint booth. It will 10' x 14' x 10 ' high and will have temperature and humidity control to be able to replicate most real-world applications. It will provide the capability to paint from 40°F to 110°F with relative humidity ranging from 10% up to 90%. In addition, there will be an environmentally controlled wet process room where wet application processes can be tested under controlled environmental conditions.

As CTIO stands up, project work implementation will be accomplished in four phases: NESHAP compliance support, Near Term leverage, customer relations development, and core CTIO project initiation.

NESHAP Compliance Support

The first, and most critical, role of the CTIO is the technical capability it brings to the risk-reduction effort of the ALCs and MAJCOMs for 98 NESHAP compliance for coating systems. During this phase, the CTIO is evaluating each of the customer's NESHAP requirements in the aircraft coating program, support the identification of impact of these requirements on their mission and provide technical alternatives/options to abate non-compliance. This effort will take place primarily on-site at the customer operations and via discussions at CTSC meetings. The primary objective of this support is to ensure a sustained operation of the aircraft in the operational fleet by ensuring that acceptable compliant coatings are available.

Near Term Initiative

The CTIO has played a key role in the Near Term phase of the S&T Program, which was established to achieve immediate results by incorporating current technologies to address the critical requirements of the users today. Its goals are to achieve low VOCs, minimize chromates, and improve formulations. Its focus is to address key selected technologies for insertion into the Air Force environment and to begin efforts to replace chromates.

During the Near Term Program efforts to date, the CTIO has made great strides in baselining many of the customer processes and equipment and captured a significant amount of relevant information concerning the strengths and weaknesses of their organizational and depot coating systems programs. The Near Term Program approach was to first document the performance requirements, and then assess industry coatings for applicability to the Air Force needs. This was done to evaluate off-the-shelf commercial aircraft coating products not previously tested or used by the DoD to determine if NESHAP-compliant systems existed with improved performance characteristics. This was done by soliciting industry to "give us the best - material cost is not a constraint." The 23 coatings obtained from industry as well as three mil-spec controls were then subjected to over 100 different tests to assess performance. Of the coatings tested, some were found to be approximately equal in performance to the existing, compliant Mil-Spec coatings, but none were found to be decidedly superior.[3] An interesting side note to this is that of the three mil-spec coating systems tested, two ranked even with the new coatings submitted. The third mil-spec coating system, on the other hand, was the worst performing of the final 11 coatings (eight new products and three controls).[3] The cause for this discrepancy is uncertain right now, but we are looking into it.

Despite the less than spectacular performance of the new, state-of-the-art coatings, there were some direct benefits from this effort. A set of coating performance standards was established, as well as a baseline showing current coating performance.[3]

The Coatings Technology Integration Office (CTIO) will work with Near Term coating manufacturers to determine how the Near Term test results and feedback can be used to reformulate their products to increase performance. New products resulting from the effort will be screened by the CTIO, and if preliminary characteristics appear promising, they will be inserted into the formal CTIO integration program.

Customer Relations

The CTIO approach is based on a strong relationship with the user community (MAJCOM, SPO, field unit, and ALC personnel). It includes close contact with the customer, who defines the requirements and criticality of the projects. Periodic formal status assessments of projects are provided to customers, including a quarterly Program Management Review (PMR). In addition, weekly status assessments on the S&T side of the program are obtained at the ML Paint Team meetings detailing the most recent changes in the project status.

Projects

As CTIO has been ramping up, in addition to the work listed above, they have also been working on specific projects for customers. In the area of de-paint, they include determining that Polymedia Lite would be an acceptable stripping media, working on the medium pressure water stripping process, work to optimize the physical depaint process and assessing the quality and usability of current environmentally acceptable (EA) chemical strippers. In the paint area, they include assessing EA wipe solvent replacements, testing non-chromated primers for use as a tie coat, and trying to improve some of the properties of the currently available high solids and

waterborne primers. CTIO is also working on a project to determine if any of the airlines current processes or equipment is applicable to the AF and a project to get full baseline performance properties on the currently fielded compliant coatings. In total, CTIO has completed work on nine projects, has 19 on-going, and plans to begin another 10-12 next year.

SUMMARY AND CONCLUSIONS

The USAF identified a need to improve the performance of EA coating materials and developed a comprehensive plan do address this need in near, mid and long-term needs. The CTIO was established to address needs and integrate emerging technologies. Operations are transferring form SwRI - San Antonio to WPAFB and WR-ALC. Although not technically at IOC, CTIO has achieved functional IOC in that technical projects and quick-response are on-going in support of customer needs. The increased focus of effort in this are will hopefully produce coating that are environmentally acceptable and that have much higher performance characteristics. If the long term coating system strategy goals can be achieved, the coatings will be of such a quality that the aircraft will only have to be overcoated every 5-7 years. This alone will save the AF 10's of millions of dollars each year. In addition, preserving the aging AF aircraft fleet and extending its usable lifetime will spread the multi-billion dollar acquisition cost out over a much longer period of time helping the AF to continue operating within its total obligation authority in this time of reduced budgets.

ACKNOWLEDGEMENTS

This work is supported by Air Force Materiel Command's Civil Engineering Pollution Prevention Branch (AFMC/CEVV). The work was performed under contracts F41608-93-D-0651-0009, F33601-93-D-J029-5003, and F09603-95-D-0176-RZ01. Their financial support is gratefully acknowledged.

REFERENCES

1. Richard C. Kinzie, "Air Force Corrosion Program Overview," *Proceedings of the 1994 Tri-Service Conference on Corrosion*, pp 3-25.

2. Paint Stripping Equipment Reliability / Maintainability Problem Identification Study, Southwest Research Institute Report, 5 Apr 1996.

3. Reliability and Maintainability Improvement, High Performance Aerospace Coating System Program, Battelle Report, 30 Apr 1997.

Utilities Engineered Management Systems: Maximizing the Impact of Limited Maintenance and Repair Resources

Vicki Van Blaricum
U. S. Army Construction Engineering Research Laboratories (USACERL)
ATTN: CECER-FL-M
P. O. Box 9005
Champaign, IL 61826-9005

ABSTRACT

Declining maintenance budgets and reductions in force have made it increasingly difficult for Army installations to operate their aging utility distribution systems so that they perform safely and efficiently. This is particularly a concern for utilities in which corrosion is the chief mechanism of deterioration such as underground heat, water, and natural gas distribution systems. The Utilities Engineered Management System (EMS) Suite provides systematic procedures for identifying and prioritizing utility system maintenance and repair needs, as well as for quantifying the consequences of not performing the recommended actions. The EMSs contain utility system inventories, quantitative engineering-based condition assessments, condition prediction, and maintenance and repair planning tools. An overview of the Utilities EMS Suite will be given.

INTRODUCTION

Many of the Army's utility systems are rapidly deteriorating, are in fair to poor condition, and are constructed from outdated designs and materials. The average age of Army infrastructure is approximately 35 years, and approximately 70% is over 25 years old. The consequences of deteriorated, outdated utility systems include high rates of leaks and failures, high maintenance costs, high energy losses, safety hazards, and environmental violations.

These problems urgently need to be remedied, but Army funding levels are steadily declining and there is less money available for operating and maintaining infrastructure. It can be a challenging task for the facilities engineer to convince budget decision-makers that they need to allocate more money to utility systems. Priority is often given to highly visible projects, commander priorities, and projects that directly impact the installation's mission. Unfortunately, utility systems are mostly "out of sight--out of mind" until there is a problem. Furthermore, it is difficult to quantify the impact of performing (or not performing) maintenance and repair on utility systems as long as consumer demand is being met.

Another problem is that installations have lost a large number of their experienced facilities maintenance personnel due to reductions in force (RIF). This means a loss of "institutional knowledge" about the base infrastructure, as well as a loss of expertise concerning methods for dealing with problems. Many of the employees who have remained at the installations have been

forced to become "generalists" with a wide range of responsibilities that impede them from becoming experts in any particular area.

These budget and manpower cutbacks have forced installations to manage their utility systems "by crisis". Action is not taken until it becomes urgent, in other words, until a major failure or interruption of service occurs. This is usually not the most cost-effective strategy from the standpoint of life-cycle costs because it may mean completely replacing the system prematurely instead of simply repairing or rehabilitating it (Figure 1).

The Utilities Engineered Management System (EMS) Suite is being developed to help the Army facilities engineer combat these problems. Utilities EMSs provide a set of systematic procedures for identifying and prioritizing utility system maintenance and repair needs, as well as for quantifying the consequences of not performing the recommended actions.

ENGINEERED MANAGEMENT SYSTEM (EMS) CONCEPT

The U. S. Army Construction Engineering Research Laboratories (USACERL) is developing an entire family of EMSs that address the maintenance concerns of various facilities at Army installations including transportation systems, utility systems, and vertical structures. All of the EMSs follow a similar approach to facilities management and contain several common elements (Figure 2). These concepts will be explained in this section and an illustrative example will be given later in the paper.

One common EMS element is the inventory. The inventory is a physical description of the facility system that is being managed. A map is an important element of the inventory. The system is divided into a series of "management units", which are the smallest pieces for which maintenance & repair decisions will be made. For example, underground piping systems are divided into pipe sections. Pavement networks are divided into branches and sections. Physical attributes should be approximately uniform throughout the management unit. For example, each pipe section in a utility system would have the same diameter, material of construction, and date of installation along its entire length. Information about the attributes of each management unit is collected and stored in the inventory. This information typically does not change with time (unless the management unit is replaced) and may include attributes such as location, size, material of construction, and date of installation.

Another common EMS element is the inspection. The inspection is a procedure for gathering the data needed to determine the condition of each item in the inventory in a manner that is consistent from one inspection to the next and as independent as possible from the subjective judgements of the individual inspector. Inspection usually involves the documentation of "distresses" (defects or indicators of problems), the severity of the distress, and the quantity of the distress. For example, some common pavement distresses include potholes and alligator cracking. Inspection may involve in-situ non-destructive testing, visual inspections, and/ or laboratory testing. For example, inspection of a heat distribution system may involve visual inspection of the manhole internals and pressure testing of the underground lines.

EMSs also contain condition assessment procedures. Condition assessment is the process of interpreting the results of the inspection. In most EMSs, this is done by means of a condition index (CI). The CI is a quantifiable, repeatable measure of facility health that is calculated from the inspection data (Figure 3). The CI is expressed on a scale of 0 to 100, with 100 representing a facility in new, perfect condition and 0 representing a facility that is completely failed. The CI provides a common language for comparison of diverse facilities.

Another element of EMSs is condition prediction. This is a method for forecasting the future condition index of items in the inventory so that repair and replacement decisions may be timed correctly. Some EMSs may provide a set of prediction models that have been developed from a statistically significant number of data points, while others may provide users with the tools to build installation-specific models using their own data.

Each EMS includes procedures for identifying maintenance and repair requirements based on the findings of the previously described elements. Most EMSs can provide both annual and long range work plans that are constrained either by budget or by minimum acceptable condition.

The final element is called project formulation. This is the grouping of individual maintenance requirements together to form projects that can then be entered into an installation's work management system. For example, there may be several individual maintenance requirements involving replacement of building roofs. Those requirements would be grouped together in the project formulation phase so that it is only necessary to execute one large roofing project instead of a series of small ones.

EMS software development specifications have been developed to ensure that all EMSs have a similar "look and feel" to the user and are capable of sharing certain pieces of information. The specifications make use of object-oriented programming concepts and emphasize a modular software structure. The specifications also enable software developers to take advantage of "shared EMS tools". Each tool is a piece of reusable computer code that can simply be "plugged in" to an EMS that complies with the specification. The tools perform functions that are common to most EMSs, but that are not available in off-the-shelf software packages. The advantage of this approach is that the programming for these functions only has to be performed once, and does not need to be repeated for each EMS software package.

UTILITIES EMS SUITE CONCEPT

The facilities management concepts described above are being incorporated into the Utilities EMS Suite. The suite (Figure 4) will include: (1) "component" utility EMSs and (2) a set of shared utility analysis tools. Component EMSs are EMSs for specific utility systems such as water distribution and sewer collection systems. Each component EMS in the Utilities EMS Suite will include the standard EMS elements described above (as applicable), and will be designed and programmed in accordance with the EMS software development specifications.

Shared tools refer to analytic procedures that are applicable to more than one utility and can be used by more than one component utility EMS. For example, the method for cathodic protection (CP) evaluation is the same for all utilities, therefore it is much more efficient to develop one software tool for CP analysis that will interface with all component EMSs (instead of developing a separate CP analysis tool for each EMS).

To help readers understand the Utilities EMS Suite concept, the suite may be compared with an integrated applications suite such as Microsoft Office. Microsoft Office includes several component programs: a word processor (Word), a spreadsheet (Excel), presentation graphics (Powerpoint), and a database manager (Access). Each of these component programs can be purchased and used as a stand-alone application. They also may be used together. The user interfaces of the programs are so similar that if you know how to use one of them, you can learn to use any of the others very quickly. These individual, yet interoperable programs can be compared to the individual component Utilities EMSs such as HEATER and GPIPER. Microsoft Office also includes tools that may be used in several (or all) component programs--the Spell Checker, for example. These tools can be compared to the "shared tools" in the Utilities EMS Suite.

Development of the Utilities EMS Suite is being coordinated with the development of the Washington State University Energy Office's Utilities Map program. Utilities Map is used to design new distribution systems, model the operation of existing systems, and provide AutoCAD-based system maps. Utilities Map fits well with the EMSs since Utilities Map focuses on design and operation, and the EMSs focus on maintenance and repair. The Utilities EMSs and Utilities Map will share inventory data. Utilities Map will provide the EMSs with the capability to analyze the impact of repair/replace alternatives on the operational aspects of the distribution system. The program will also assist with the design of new distribution systems or system additions. The HeatMap module for steam and hot water distribution systems has been released, and modules are being planned for natural gas, water, sewers, and electrical distribution systems.

EXAMPLE OF A COMPONENT EMS: HEATER 1.0

The HEATER EMS is being developed to assist in managing heat distribution systems (HDS). It includes low-, medium-, and high-pressure steam distribution systems and condensate return, as well as low- and high-temperature hot water distribution systems. HEATER development is being given high priority because of the high payback on heat distribution system maintenance and modernization. HEATER is being developed in the Visual Basic programming language and utilizes Microsoft Access as the database manager.

In HEATER's inventory, the HDS is divided into pipe sections and manholes/branch takeoffs (nodes). These sections and nodes exactly match the inventory elements in the previously described HeatMap program (Figure 5). The HEATER inventory is more detailed than the HeatMap inventory.

The pipe section inventory data entry screen is shown in Figure 6. One record is entered for each pipe section. Each section may have one or more expansion joints, steam traps, valves, pipe supports, and/or pipe anchors associated with it. Users may enter data about these subcomponents associated with the currently selected pipe section by clicking on the appropriate tab on the screen. For example, Figure 7 shows the screen that appears when the user clicks on the steam trap tab. The user would then enter information about each steam trap that is associated with the pipe of interest.

The manhole inventory data entry screen is shown in Figure 8. One record is entered for each manhole. Each manhole typically has many subcomponents. These may include ladders, sump pumps, high water alarms, internal piping, pipe supports, pipe anchors, expansion joints, steam traps, valves, wall penetrations, and a cover. Users may enter data about the subcomponents associated with each manhole by clicking on the appropriate tab on the screen. For example, Figure 9 shows the screen that appears when the user clicks on the sump pump tab. Using tabbed screens to display data enables a large amount of information to be displayed on a single screen.

HEATER has a two-stage inspection process. The network-level inspection includes both visual and simple field testing procedures. It flags components where M&R is required, provides a rough estimate of the condition of the system components, and identifies components that require more extensive inspection before their condition can be determined. Condition indexes are assigned based on the results of the inspection. Table 1 shows an example of this. Project-level inspection includes more expensive and/or complicated techniques to establish the condition of components that cannot be readily evaluated with network level techniques. For example, conduit pressure testing is a project-level technique.

Very general condition prediction models have been developed for each type of HDS based upon case studies. The models predict the degradation of condition versus time. Further development on the models is planned so that the effects of soil chemistry, temperature, and other influencing factors can be incorporated. HEATER also includes the EMS shared tool for "family curve" prediction modeling, which allows users to build their own prediction curves from installation-specific data (Figure 10).

Based upon the findings of the condition assessment and prediction, the user will be able to generate maintenance and repair requirement lists. This part of HEATER is currently under development.

EXAMPLE OF A SHARED TOOL: CATHODIC PROTECTION (CP) ANALYSIS

Many buried utility distribution systems are cathodically protected, as well as the interiors of most water storage tanks. USACERL developed a stand-alone CP analysis program in the late 1980s called CP Diagnostic. The purpose of the program was to assist Army facilities engineers in organizing, storing, and evaluating CP system data. Unfortunately, there was no automated way to correlate the results of CP Diagnostic with the EMS inventories. Inventory

data had to be re-entered into CP Diagnostic.

The new shared tool for CP analysis is being developed to interface directly with the utility EMSs. This has the benefit of reducing the user's data entry requirements. Furthermore, the CP analysis tool only has to be programmed once instead of being programmed into each of the individual EMSs that deal with cathodically protected structures. Since the CP analysis procedure is the same no matter what type of utility is being protected, it is an ideal candidate for a Utilities EMS Suite shared tool.

The CP analysis tool will determine (1) whether existing sacrificial and impressed current CP systems are operating properly and (2) the cause of any problem detected and recommend a remedy for malfunctioning systems.

As in HEATER, the CP system is broken down into components to create the inventory. Figure 11 show how a sacrificial system is broken down and Figure 12 shows how an impressed current system is broken down. Once the components are identified, information about them may be input into the program. Figure 13 shows the inventory screen for impressed current CP systems. The inventory screen for sacrificial systems is similar, except it does not include rectifiers, rectifier circuits, or junction boxes. As in HEATER, the user may select a type of component by clicking on the appropriate tab on the screen. Figure 14 shows the test site tab.

After the inventory has been defined, the user may then input field test data. This includes rectifier outputs and settings, anode currents, and structure-to-soil potentials. The program will then generate a series of reports, including:

- Trouble readings report: Lists structure-to-soil (SSP) measurements (and their locations) that violate the user-specified NACE cathodic protection criterion.

- Anode current output drop report: Lists all anode current output sites where the anode current has dropped significantly over time—within a user specified range of dates. This includes drops of more than 10 percent over two consecutive readings, or a drop of any amount over 3 consecutive readings (i.e. 2 consecutive drops)

- Field data collection forms: Prints out data collection forms for the field inspector to use when testing rectifiers, structure to soil potentials, anode currents, and dielectric joints.

- Locations where testing is required: Lists all SSP test sites and/or rectifiers from which data has not been collected within a specified range of time, and gives the user the option to generated field data collection forms for them.

CONCLUSION

Concepts for the Utilities EMS Suite have been developed based upon the EMS principles

that have been developed for other Army installation facilities. The objective of the suite is to assist the facilities engineer in determining, prioritizing, and justifying current and future maintenance and repair requirements.

The EMS elements of inventory, inspection, condition assessment, condition prediction, M & R requirements identification, and project formulation are being applied to heat distribution systems through the HEATER program. Procedures for HEATER have been defined and a beta test software package has been completed.

The shared tools concept has been developed to address situations where the same type of analysis needs to be performed for different infrastructure systems. Cathodic protection analysis is a candidate for shared tool development. Procedures for analysis have been defined and software development is under way.

Table 1. Sample Condition Index Procedure

Manhole Inspection **Subcomponent: Endplate Assembly**	
Description	**Condition Index**
No signs of corrosion.	100
Thin, fine film of corrosion over metal surface	80
Some pitting, but pit depth is less than 25% of material thickness	60
Numerous pits on surface; pit depth is 25% of material thickness	40
Pit depth is 50% of material thickness; signs of scaling	30
Pit depth is 75% of material thickness; large amount of scaling	20
Holes in material	10
No end plate	0

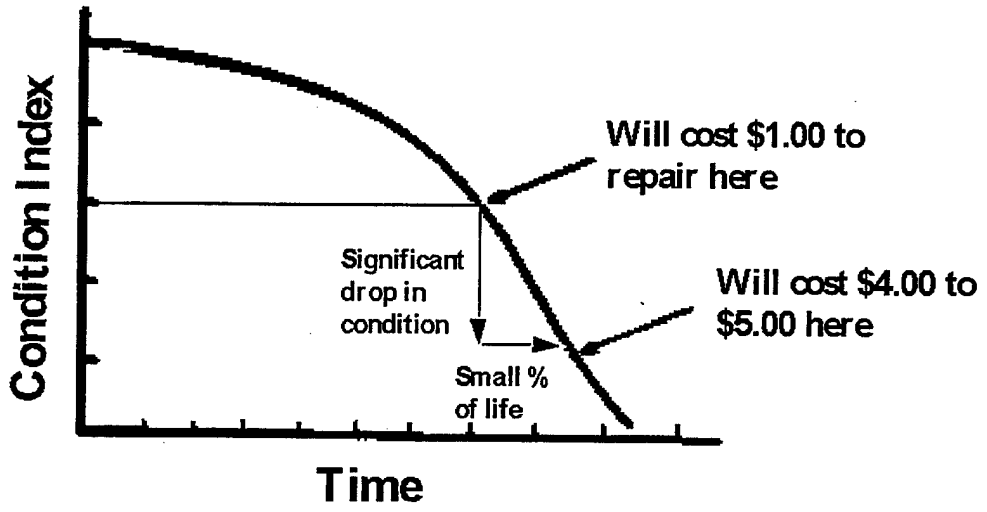

Figure 1: Sample facility life cycle.

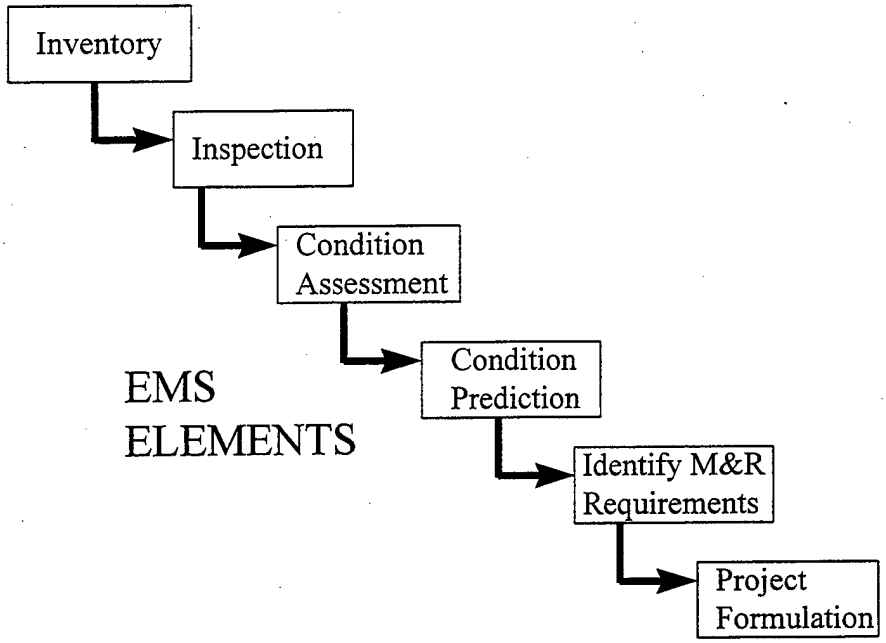

Figure 2: Common elements of EMSs

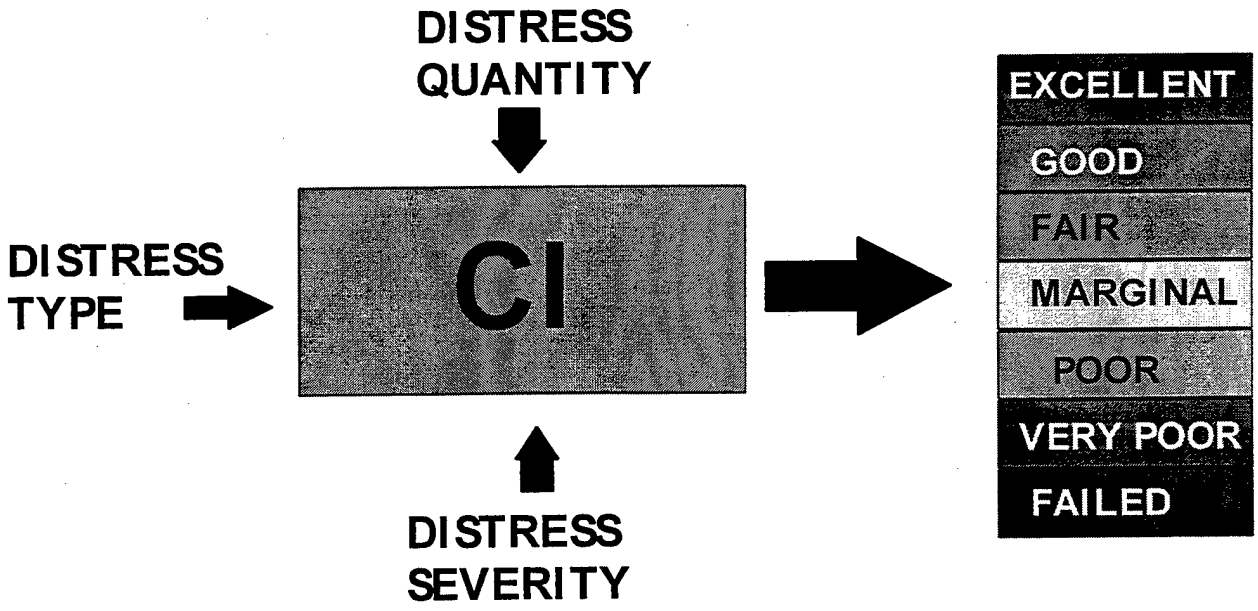

Figure 3: The EMS condition index.

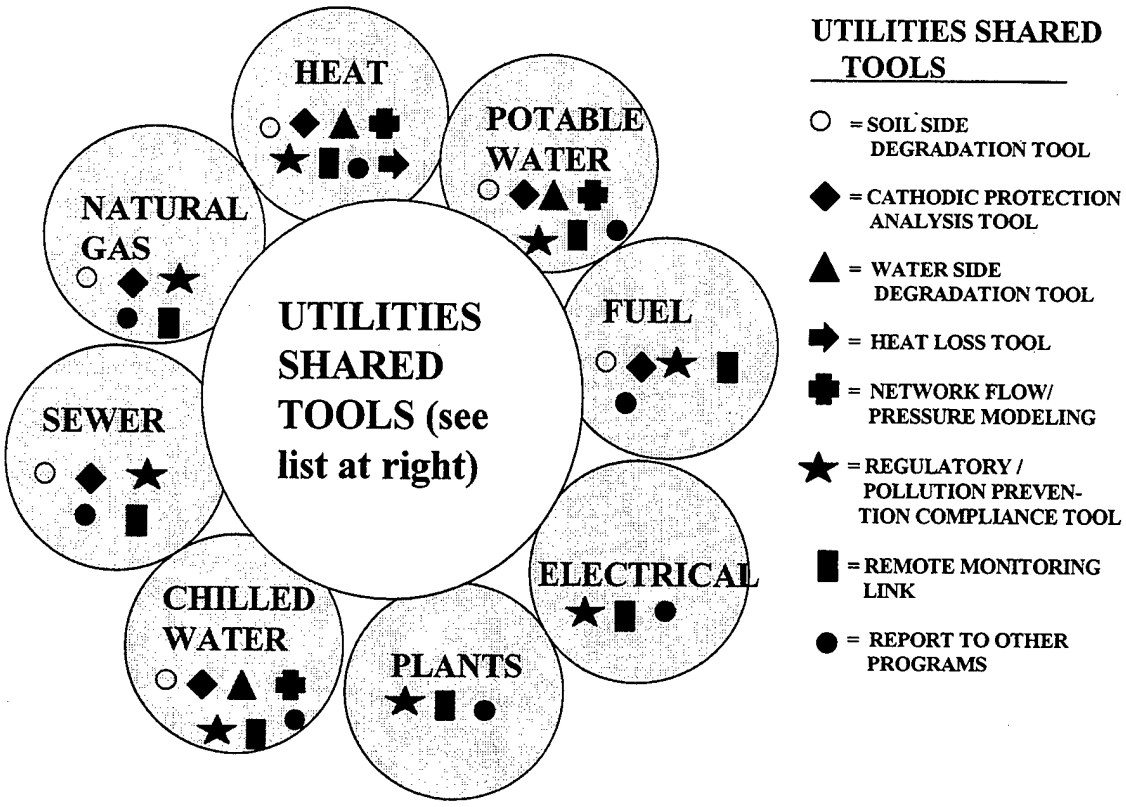

Figure 4: Utilities EMS Suite concept.

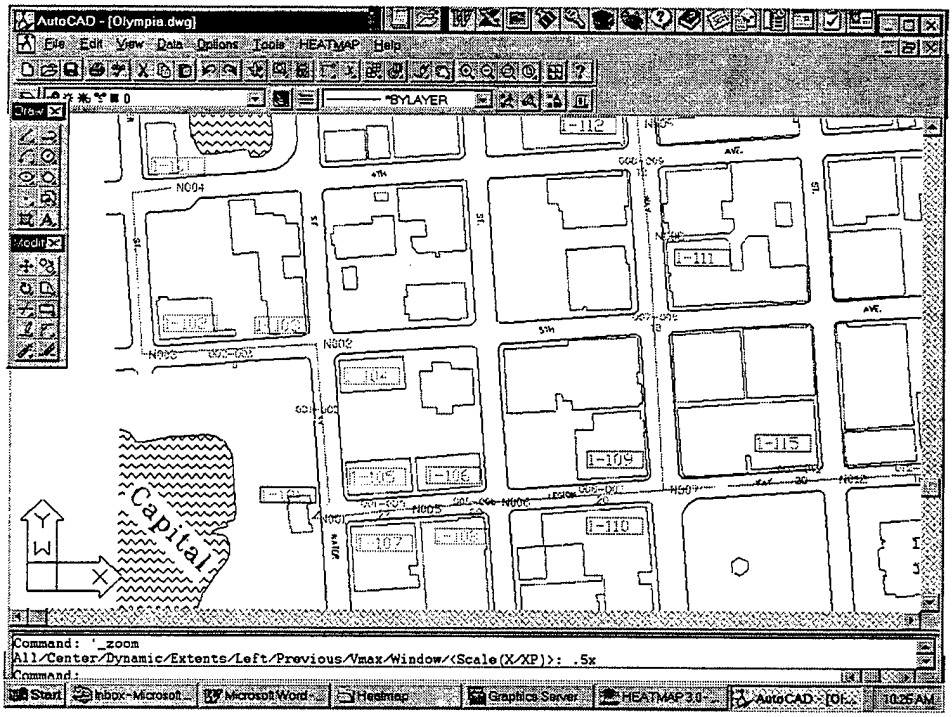

Figure 5: HeatMap representation of heat distribution system.

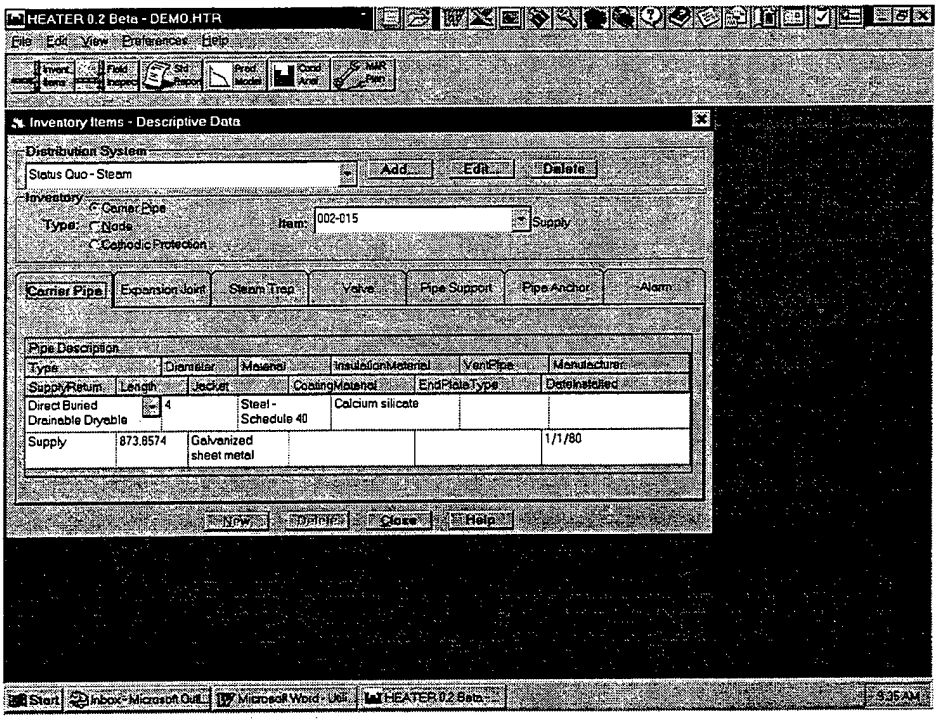

Figure 6: HEATER pipe section inventory screen.

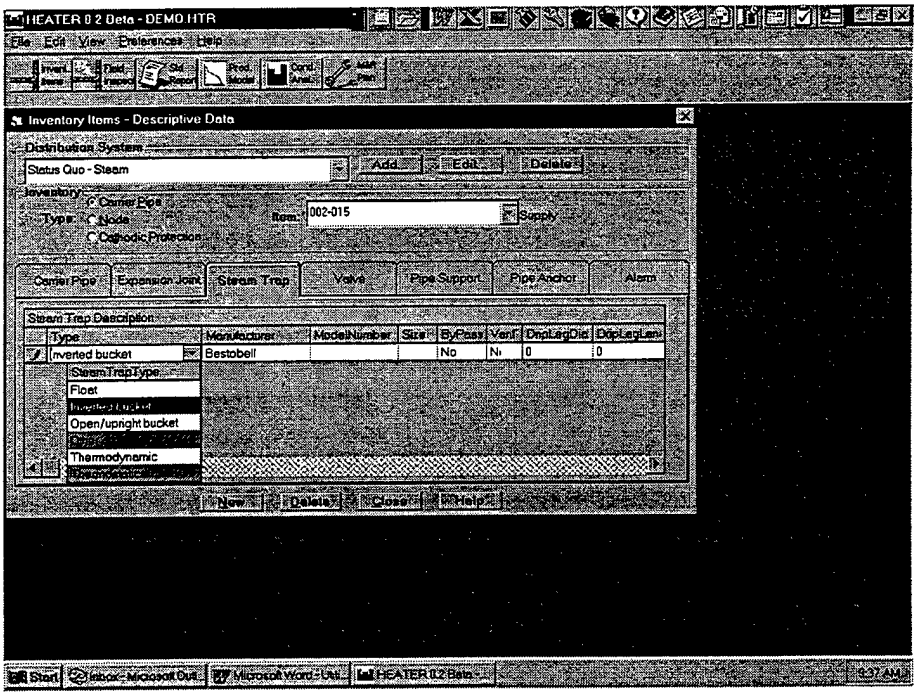

Figure 7: Steam trap tab on pipe section data entry screen.

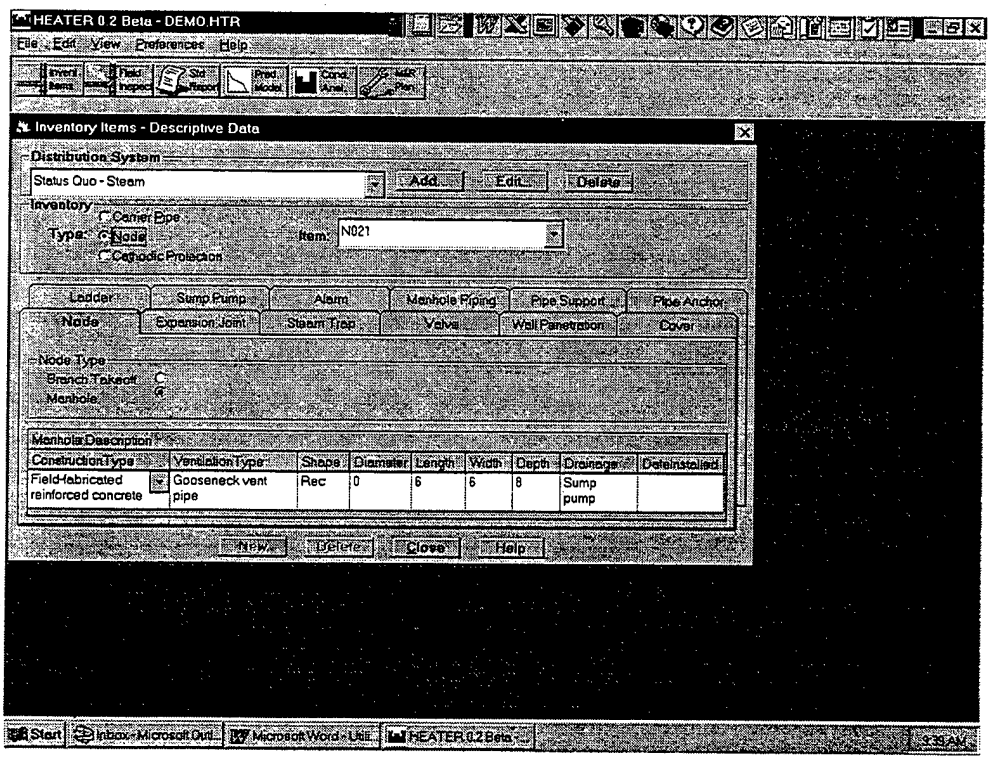

Figure 8: Manhole data entry screen.

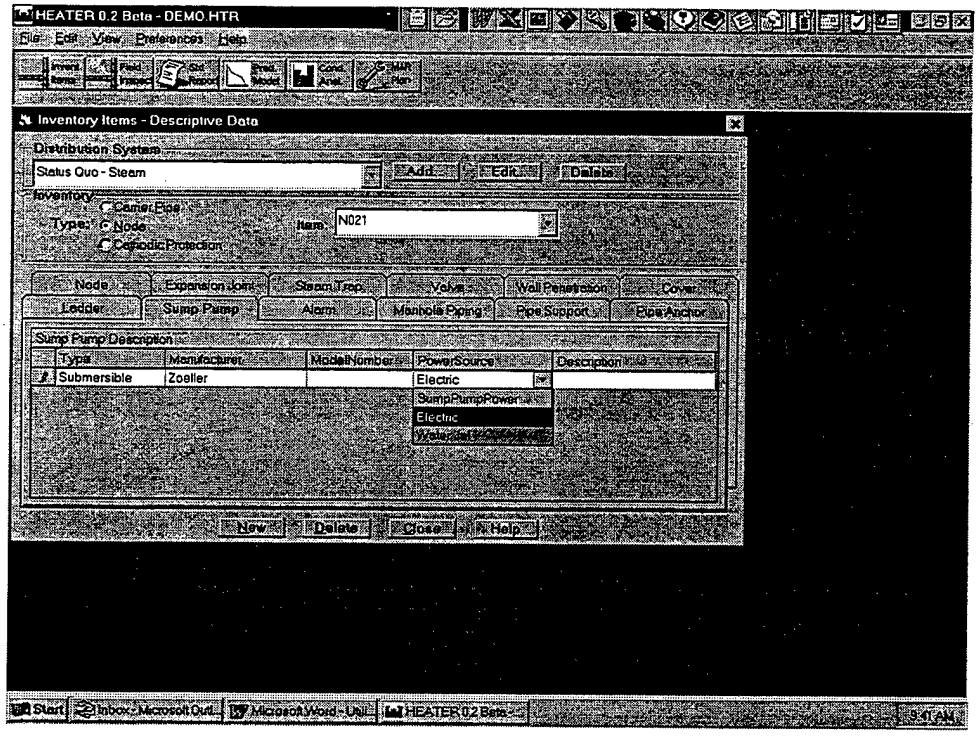

Figure 9: Sump pump tab of manhole data entry screen.

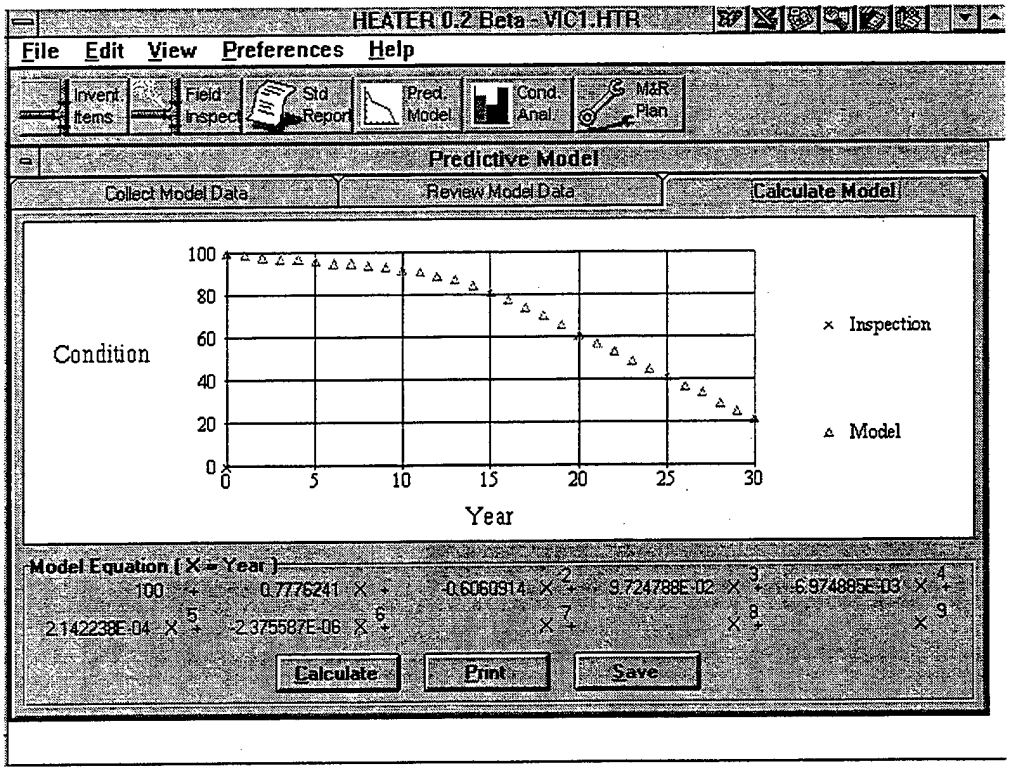

Figure 10: HEATER predictive modeling tool.

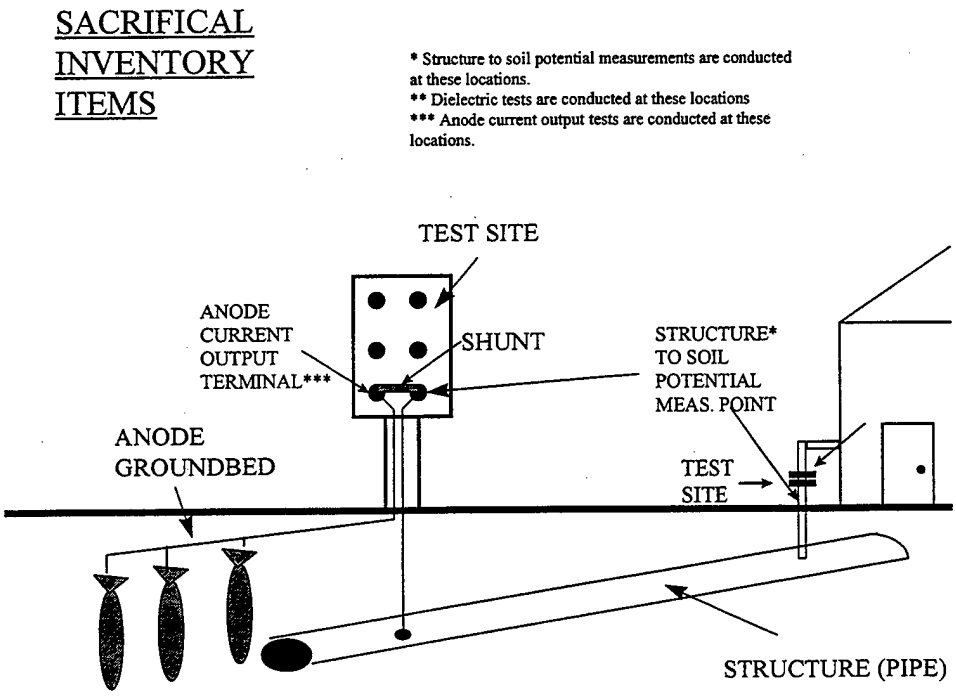

Figure 11: Inventory definition for sacrificial CP systems.

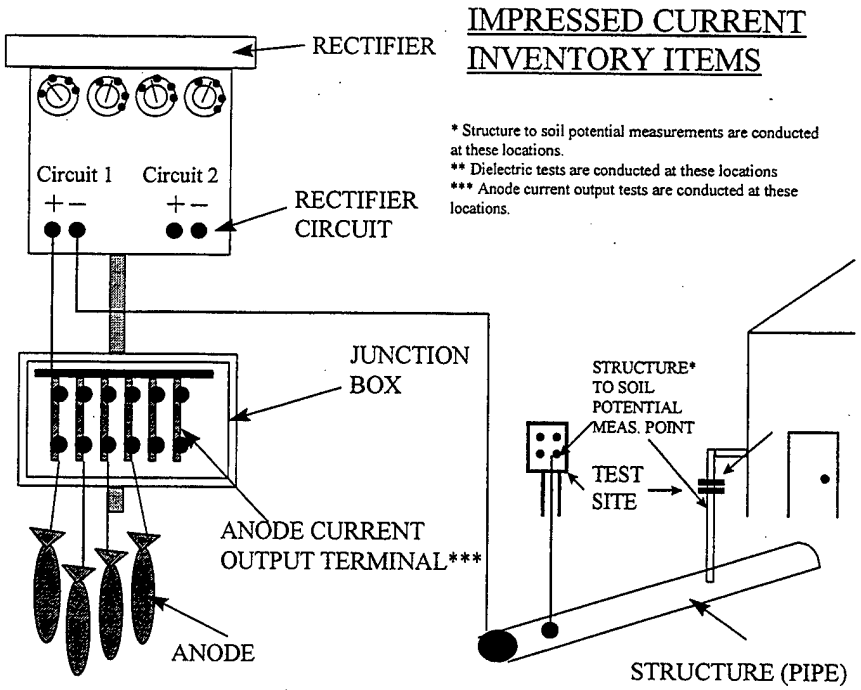

Figure 12: Inventory definition for impressed current CP systems.

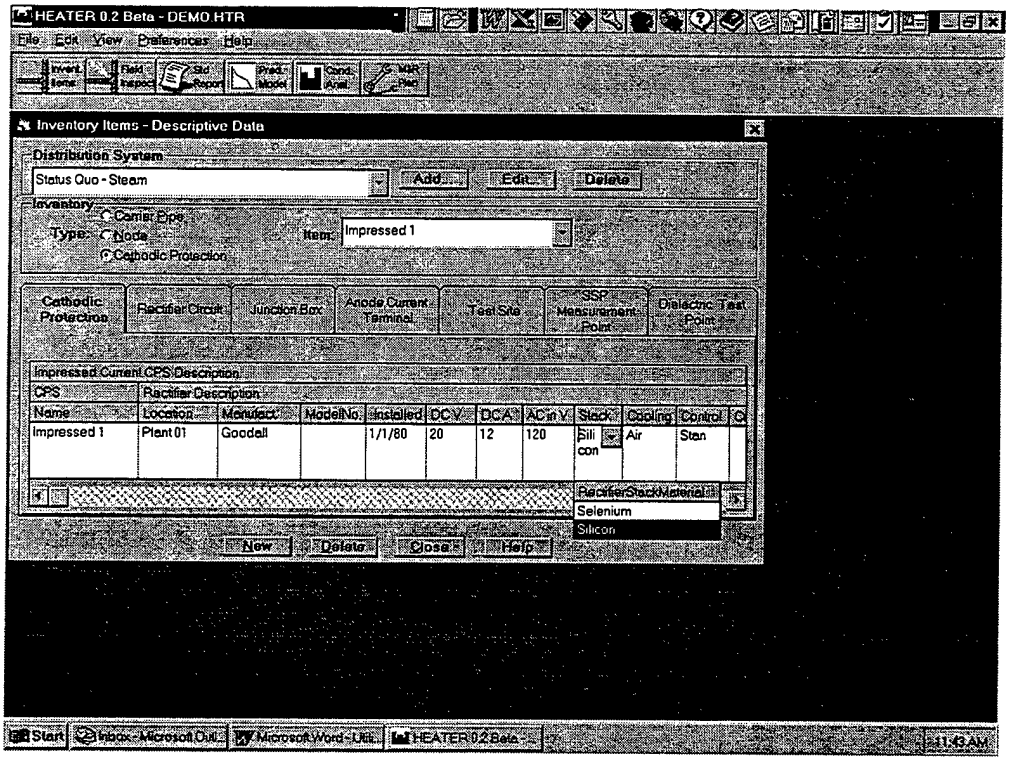

Figure 13: Impressed current CP inventory.

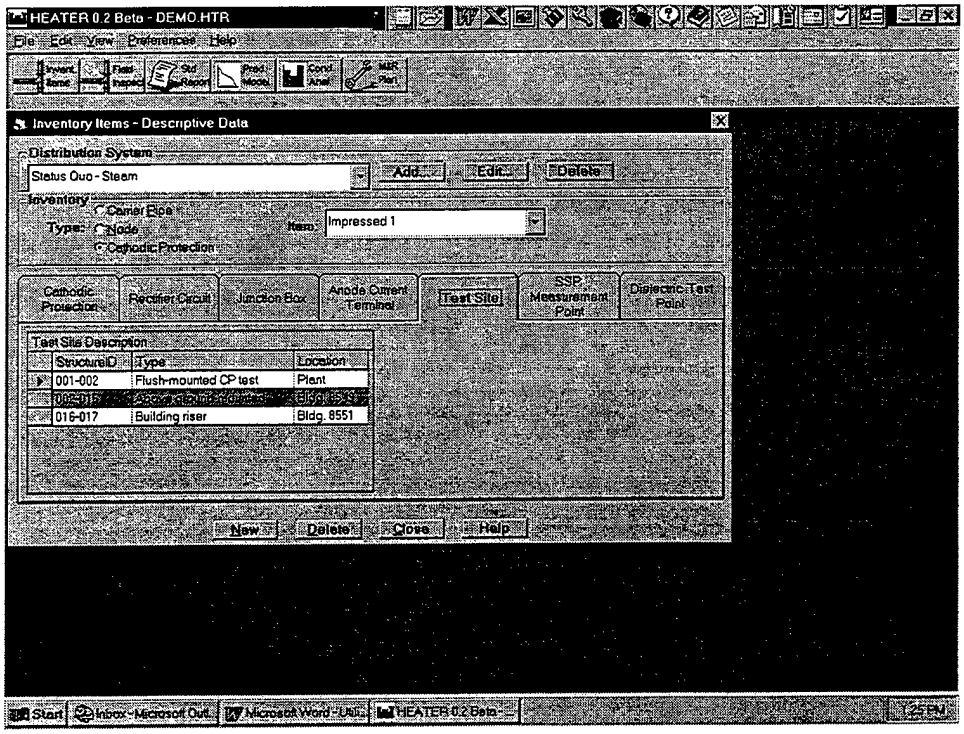

Figure 14: Test site tab of CP data entry screen.

Bonded Repairs for Corrosion Damage

Alan P. Kerr, Chief Design Engineer
Advanced Repair Technology International
6500 West Freeway, Fort Worth, TX 76116
Phone: (817) 737-1656
Email: kerra@ustx1.dyncorp.com

Introduction

The technology of bonded repairs has been discussed in many technical forums and there are currently thousands of bonded repairs applied to metallic aircraft structures in service throughout the world. Most of these examples and much of the discussion has focused on using the technology to overcome fatigue problems. This application is, however, only a small part of the overall potential which is available, and, even though bonded repairs have not yet been used as widely for corrosion applications the technology has some distinct advantages which make it a very useful resource. Lack of understanding, and the present need for individual repair approvals have been hurdles preventing a more popular use throughout the military and civilian aircraft industries.

The fundamental aspects of bonded repairs do not differ widely from those of the familiar conventional techniques, in that the strength of a damaged structure is restored by attaching reinforcements. The difference is that the reinforcement is attached using a high strength adhesive instead of mechanical fasteners. Some of the advantages which are attributed to bonded repairs are obtained by simply eliminating the use of fasteners. The adhesive does not present the same levels of stress concentration or provide a path for moisture and fuel leaks.

The key feature contributing to the success of the bonded repairs has been the development of suitable surface preparation processes. It is imperative to condition the metallic surface to provide a strong bond capable of remaining in service for the life of the aircraft. Many surface preparation processes are capable of providing a strong bond for a short period of time, but very few are resistant to environmental degradation and thus allow the bond strength to weaken after only short periods in service. Proper surface preparation provides a resilient surface which accepts the adhesive bond and remains impervious to the effects of moisture over very long periods.

This specialized surface preparation is the basis for one of the distinct advantages that bonded techniques bring to corrosion repairs. The cleaning, chemical treatment, and then sealing of the repair area with primer and adhesive is an enhanced form of the processes normally used to treat corrosion. Qualification of surface preparation processes for bonding is done using tests which validate the surface's resistance to breakdown caused by moisture. These are severe tests which are not used when corrosion prevention is the only consideration. When the surface preparation is for bonding purposes, very strict control is exercised on the manner in which the

preparation is performed and it is only performed by personnel who have been trained to do the task, and who submit process verification test pieces for destructive testing on a regular basis to verify their continuing capabilities. The validated processes, strict quality control, and use of specially skilled personnel assure that the repair will provide continued resistance to the onset of any further corrosion.

Bonded Repair Configurations

Bonding provides versatility in the configuration of the repair particularly when composite materials are used as the reinforcement. There are three different generic types of bonded repair configurations, the "filled repair", the "conformal repair" and the "insert repair". Choosing the most suitable repair depends on the geometry and design load conditions for the repair area.

In low load applications surface irregularities left behind after grinding away the corrosion are **filled with adhesive** (see Figure 1) to provide a surface for a flat external reinforcement. This is a simple single step application that does not require close machining tolerances. It is effective in returning the strength to thin, lightly loaded sheet metal components.

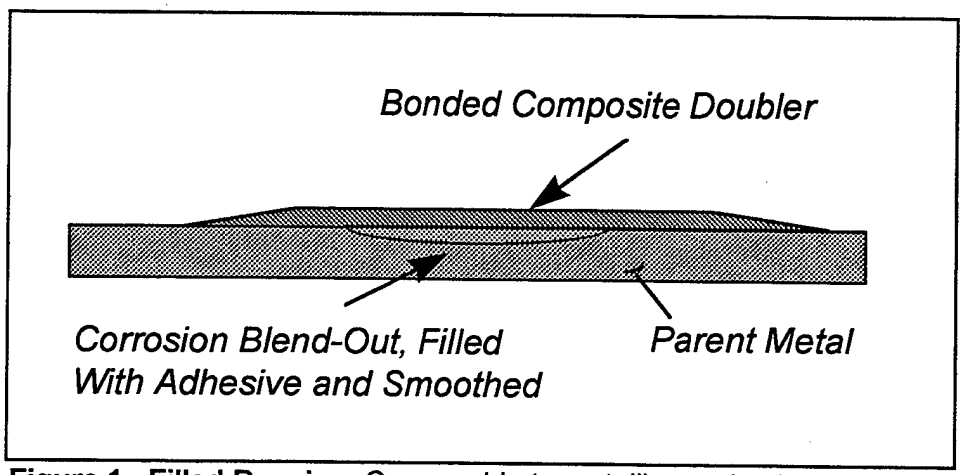

Figure 1. Filled Repairs. Comparable to metallic repairs, but without the added burden of holes, etc.

For thicker or more heavily loaded structures, or when crack growth is an important consideration, composite **reinforcements can be made to conform** (see Figure 2) to the irregular ground-away surface to provide a stiffer more efficient load transfer. The composite reinforcements can be cured in situ, or fabricated on splash molds taken from the irregular surface. Coupon tests have shown the conformal repair to be more effective at retarding crack growth than the filled repair as the thick adhesive fill allows more crack opening during cyclic loading. Conformal repairs are however quite simple to apply and offer the same benefits for corrosion prevention as the filled repair. Some extra detail is required to get an acceptable grind-out geometry.

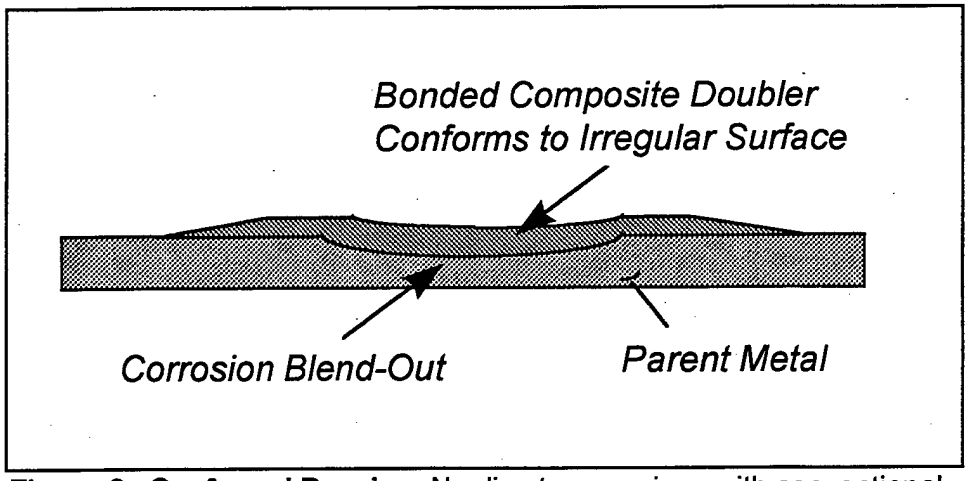

Figure 2. Conformal Repairs. No direct comparison with conventional repair techniques. Reinforcement molded to irregular shape of grind-out.

Repairs on sections which are greater than 0.25 inches thick or where extremely heavy loads are carried are best repaired using an **insert repair configuration** (see Figure 3). This is a more complicated repair requiring closer machining tolerances but is much more efficient and capable of high strength. In these repairs the grind-out configuration is sized to accept an insert piece. The insert is bonded into the structure using the same surface preparation, and high strength adhesives as the normal reinforcements. The insert is made to form part of the structural reinforcement. The insert joint is designed to allow the adhesive to transfer load into the insert in the same way as into an external reinforcement. Inserts can be single layer, laminated or stepped. Laminated or stepped inserts are most appropriate for the thicker section repairs.

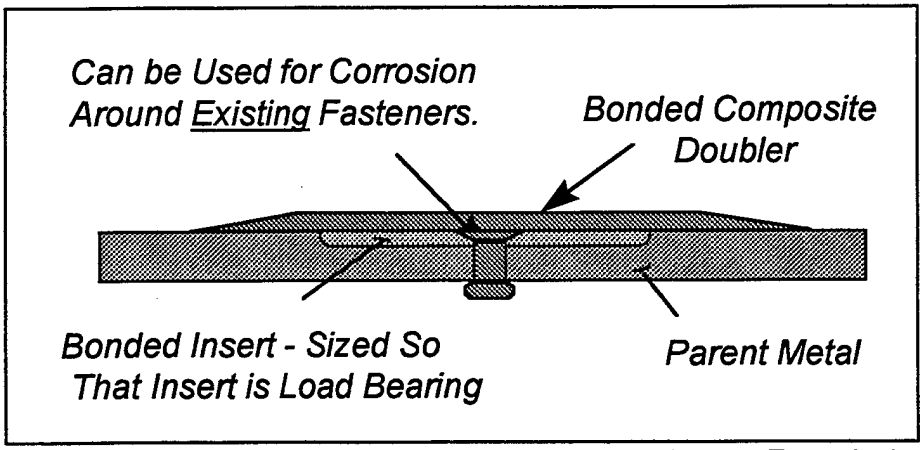

Figure 3. Insert Repairs. Structural load-bearing insert. Extends the capability of the bonded repair into thicker sections.

Approval Processes

Approval of a bonded repair is no different to any other approval operation. However, consideration has to be given to the specialty processes that are involved in obtaining a sound repair on the aircraft. Therefore, approval consideration must be given to both the design and application aspects.

Design Considerations

There are several stages required in the approval of the design of a bonded repair, namely that the repair has adequate static strength, and an adequate fatigue life.

Because corrosion damage is a material problem rather than a design fault or loads related problem, static strength and fatigue resistance are much more easily demonstrated than for a fatigue damage repair.

It is the preferred practice to design bonded repairs such that the adhesive joint is stronger than the ultimate strength of the materials being repaired. This fact together with the requirement to size the bond to resist adhesive creep, places the adhesive joint outside of the window where strength or fatigue resistance of the adhesive is a concern. If this strength reserve can be demonstrated, little else needs to be done to qualify the design of the repair. Moreover, using this approach of sizing repairs on material properties, generic configurations for bonded repairs can be sized for common sheet material thickness and approval can be obtained for these generic repairs prior to any actual repair application.

Adhesives being used in these repairs are all fully qualified to military and industry specifications. They have been proven capable of withstanding exposure to the kinds of environmental effects experienced by aircraft structures, provided the interface between the adhesive and the metal substrate remains intact.

Application Considerations

Approval considerations for the application of the repair must consider whether or not the repair is durable and will withstand the exposure to different environmental conditions. Consideration must also be given to ensure the techniques used to install the repair are reliable and repeatable.

As was mentioned previously, the joint strength is totally dependent on the type and resilience of the surface preparation used on the metal components. Bonded joints which are completely sound at manufacture can be degraded in time by exposure to environmental moistures. This degradation may not be totally obvious or predictable. It is not possible with current technology to non-destructively inspect the condition of the surface in a repair. Likewise, validation of the surface preparation for long term environmental exposure is not simply done with accelerated exposure tests which could be included with a normal repair approval process.

The only assurance for the quality of the surface preparation stems from the use of validated procedures, rigid process control, and the use of qualified applicators. There are currently two surface preparation techniques which are generally accepted for

repair application, the PAACS system, and the Grit-Blast-Silane treatment. Personnel wishing to use either of these processes must be qualified on type, in the same manner as an NDI technician or aircraft welder.

Special Application on Thin Sheet Materials

Wide spread surface corrosion on thin sheet material is a special case where bonded composite reinforcements can offer other advantages. Because of the thin sheet material it is often either impossible or impractical to grind out the corrosion. As a result the effected sections of the sheet have to be removed and replaced using traditional methods. The enhanced surface preparation, and sealing action of the repair allows a practical bonded repair solution without having to replace the thin sheet. A typical repair process would chemically treat the surface to remove the active corrosion material but leave the pitting and other irregularities in the material. A bonded repair with an appropriate reinforcement could be applied directly to this pitted surface to reduce the stress concentrating effects and effectively seal it from the ingress of further moisture. Thickness of the reinforcement would be sized to correspond with the skin thickness and would thus be capable of stopping any fatigue cracks which might originate from any of these pits.

Conclusion

The popularity of bonded repairs will increase as engineers and technicians obtain a better understanding of the approach, and more repairs are fielded in service. Once the repair concepts are understood, design of repairs which are typical of those required for corrosion damage is quite simple and relatively straight forward, as is certification of the repair designs. The manner in which the repairs are applied has the predominant impact on their long term durability. Particular attention needs to be paid in approving repairs to these application aspects and application needs to be restricted to personnel who have been trained and properly qualified for the processes being used. The skills necessary to install a bonded repair are not difficult, but at the same time they are more specialized than those currently used at facilities engaged in typical repairs of bonded structures.

Bonded repairs offer distinct advantages in the treatment of corrosion, and will become very much more popular in the foreseeable future.

ADVANCED ZINC PHOSPHATE CONVERSION COATINGS

By

I.Carl Handsy
U.S. Army Tank -automotive and Armaments Command
tank- Automotive research, Development and Engineering Center
ATTN: AMSTA-TR-E/MATL/267
Warren, MI 48397-5000

Toshi Sugama
Department of Applied Science
Brookhaven National Laboratory
Associated Universities, INC.
Upton, Long Island, NY 11973

ABSTRACT

A SERDP-sponsored program aimed at developing environmentally benign zinc phosphate conversion coatings and their process technologies for the electrogalvanized steel (EGS). we succeeded in formulating an environmentally acceptable phosphate solution without Co- and Ni-related additives, and also in replacing a hexavalent Cr acid sealant applied over the zinc phosphate (Zh×Ph) layers with a water-based polysiloxane sealers. The specific advantages of the newly developed Zn×Ph coatings were as follows: 1) there was rapid growth of uniform, dense embryonic Zn×Ph crystals on the EGS surfaces due to the creation of short-circuited cells with Mn acting as the cathode and the galvanized (zinc) coatings as the anode, 2) an excellent protection layer against corrosion was formed, extending the service life of zinc layers as galvanic sacrifice barriers, and 3) adhesion to the electro-deposited polymeric primer coating was improved because of the interaction between the siloxane sealer and primer. A full-scale demonstration to evaluate the reproducibility of this new coating technology on mini-sized automotive door panels made from EGS was carried out in collaboration with the Palnut Company (as industrial coating applicator) in New Jersey. All of the 150 mini-door panels were successfully coated with Zn×Ph.

Keywords: pretreatment, zinc phosphate, paint, acrylic acid, primer, galvanized, Co, Ni, Cr, environmental, corrosion, siloxane, electrodeposited.

1.0 Introduction

In the previous SERDP-sponsored program aimed at developing environmentally benign zinc phosphate conversion coatings and their process technologies for cold-rolled steel (CRS) substrates [1], we succeeded in formulating an environmentally acceptable phosphating solution without Co- and Ni-related additives. The basic formulation consisted of 5 wt% $Zn_3(PO_4)_2 \times 2H_2O$, 10 wt% (86 % H_3PO_4), 3 wt% poly(acrylic acid) [p(AA)] and 82 wt% water; appropriate amounts of the $Mn(NO_3)_2 \times 6H_2O$ and $FeSO_4 \times 7H_2O$ as additives were incorporated into this basic formulation. These additives had two important functions; one was to create a large number of nucleated sites of embryonic Zn×Ph crystals on the steel surfaces, and the other was to act as an inhibitor of corrosion. The p(AA)-modified Zn×Ph coatings not only displayed an excellent salt-spray resistance of > 1000 hrs, but also showed a strong electrochemical affinity with the electro-deposited polymeric primer coatings.

In the automotive industry, it is commonly known that electroplated coatings of pure zinc and various zinc alloys over steel surfaces are responsible for improving corrosion resistance by delaying the onset of "red rust" of body panels and various discrete parts, such as fasteners and brackets [2]. Pure zinc coatings currently have the major share of the automotive body-panel market. Although the art of making electroplated zinc coating for electrogalvanized coatings is well developed, two problem areas still remain. One problem is the poor adherent property of galvanized (Zn) coating surfaces to the polymeric topcoats, and the other is the necessity of post-treatment to inhibit the onset of "white rust", which represents deterioration of the zinc layer. The former problem relating to the paint's adhesion properties is due primarily to the chemically inert, smooth texture of coating surfaces. One method to solve this problem is to increase the roughness of the surface either by etching or by sandblasting [3]. Such roughening procedures, which increase the actual surface area, provide more mechanical interlocking bonds at interfaces between the paint and the Zn coating. However, there is no resolution to inhibiting the onset of "white rust" of Zn coatings. Thus, modifying the zinc coating surfaces is essential to improve their chemical and physical affinities for the primers, and to retard the corrosion themselves.

Based upon the information described above, our executive plan for FY 1996 was placed on three major topics: the first was to evaluate the phosphating solutions and process technologies developed in the previous year, and if necessary, to reformulate their basic chemical composition

for the electrogalvanized steel (EGS) surfaces; the second focus was on developing water-based sealants for replacing a Cr acid sealant used commonly as a sealing agent of Zn×Ph coating layers; and third, to apply any new phosphating technology emerging from these two areas to mini-sized automobile door panels made from EGS in the pilot plant at Palnut Company in New Jersey. The first topic included exploring the morphological features, identifying the phases and surface chemical state of the p(AA)-modified Zn×Ph coating layers deposited onto the EGS surfaces, as well as investigating their ability to protect the zinc layers in the EGS against white rust-related corrosion. Under the second topic, our attention was paid to surveying the characteristics of water-based sealants which improve the effectiveness of Zn×Ph coatings in preventing the corrosion of EGS, and also have a great affinity for the electro-deposited polymeric primers. All the data obtained were correlated directly with the results from a full-scale feasibility test to demonstrate the reproducibility of this new coating technology.

2.0 Experimental Details

2.1 Materials

The metal substrate used was ASE 1006 cold-rolled steel coated with electroplated zinc (EGS, Ford E 60 Electrozinc 60G), supplied by Advanced Coating Technologies, Inc.. The formulation for the basic zinc-phosphate liquid was 5.0 wt% zinc orthophosphate dihydrate (Alfa Co.), 10.0 wt% H_3PO_4, 1.0 wt% $Mn(NO_3)_2 \times 6H_2O$ (Alfa Co.) and 84.0 wt% water. In modifying this standard formulation, a 25 % p(AA) colloidal solution (Rohm and Hass, Co.) added to the standard phosphating solution was 3.0 wt% of the total standard solution. The average molecular weight of the p(AA) was 60,000. As a water-based polysiloxane sealant, 3-aminopropyltrimethoxy-silane (APS) monomer, was supplied by Petrarch Systems Ltd.. The APS precursor sealant consisted of a 7 wt% APS, 3 wt% methylalcohol, 0.7 wt% hydrochloric acid and 89.3 wt% water, and had a pH of 9.96. The APS-sealed Zn×Ph coatings on the EGS test panels were prepared in according with the following sequence: As a first step to remove surface contaminants, the EGS panels were dipped for 1 min at 25°C into a pickling solution consisting of 2 wt% phosphoric acid, 1 wt% sulfonic acid, and 97 wt% water. The pickle-cleaned EGS panels were then immersed into the p(AA)-modified zinc phosphate make-up solution for » 1 min at 80°C, withdrawn slowly, followed by rinsing them with water to wash off any acid contaminants from the Zn×Ph surfaces. Next, the rinsed Zn×Ph panels were dipped for few seconds into the APS precursor sealant. Finally, the APS-wetted Zn×Ph panels were dried for 30 min in an oven at temperature of 150°C to form the polymeric APS sealant over the Zn×Ph surfaces, and to fill any voids and fissure spaces in the Zn×Ph layers.

In preparing the polymeric primer coating, all the APS-sealed Zn×Ph panels were coated with the polyurethane-modified epoxy copolymer (POWERCRON 648) by electrodeposition technology at Advanced Coating Technologies, Inc. The polymeric primer was cured in an oven at » 177°C for 30 min.

2.2 Measurements

Scanning electron microscopy (SEM) was used to investigate the degree of coverage of the EGS surfaces by p(AA)-modified Zn×Ph coatings and explore the alteration in morphological feature of crystalline Zn×Ph coatings as a function of immersion time. The surface chemical states and phase identification of the coating were carried out using x-ray photoelectron spectroscopy (XPS) and x- ray diffraction (XRD). The concentration of zinc ions dissociated from the EGS surfaces in single H_3PO_4 and $Mn(NO_3)_2 \times 6H_2O$ aqueous solutions, and in their combined medium was determined by atomic absorption spectrophotometry (AA).

DC potentiodynamic polarization measurement for data on the rate of corrosion was made with an EG&G Princeton Applied Research Model 362-1 Corrosion Measurement System. The electrolyte was a 0.5 N sodium chloride solution, made from distilled water and reagent grade salt. The test panel was mounted in a holder, and then inserted into a EG&G Model K47 electrochemical cell. The tests were conducted in an aerated 0.5 M NaCl solution at 25°C, on an exposed surface area of 1.0 cm^2. The polarization curves containing the cathodic and anodic regions were measured at a scan rate of 0.5 mv/sec in the corrosion potential range of -1.1 to -0.3 volts. AC electrochemical impedance spectroscopy (EIS) was used to evaluate the ability of coating films to protect the EGS from corrosion. The test panel was mounted in a holder, and then inserted into an electrochemical cell. Computer programs were established to calculate theoretical impedance spectra and to analyze the experimental data. Specimens with a surface area of 13 cm^2 were exposed to an aerated 0.5 N NaCl electrolyte at 25°C, and single-sine technology with an input AC voltage of 10 mV (rms) was used over a frequency range of 10 KHz to 2 mHz. The lower frequency limit was chosen because of time limitations. To estimate the protective performance of coatings, the impedance, $^3Z^3$ ohm-cm^2, was determined from the plateau in Bode-plot scans that occurred at low frequency regions. The 5% salt-spray tests at 35°C for the unprimed Zn×Ph coating panels were conducted to evaluate the degree of white rusting on unscribed panel surfaces. The salt-spray tests for the primed Zn×Ph coating panels were carried out in accordance with ASTM D 1654-79a, evaluating the blistering associated with corrosion and the loss of adhesion of the primer coating at a scribe mark, or other failure of primer film.

3.0 Results and Discussion

3.1 p(AA)-Modified Zn×Ph Coatings on EGS

Figure 1 shows SEM micrographs of crystalline Zn×Ph coatings derived from the p(AA)-modified phosphating solutions as a function of the immersion time of the EGS substrate into the phosphating bath at 80°C. As is seen, the growth of lamellar-like crystals was observed after immersion for only 2 sec (b), compared with the surface texture of the 1 sec-treated EGS (a). Immersion for 5 sec was sufficient to produce dense conversion coatings over the entire substrate surface (see Fig. 1-c). A further extension of immersing time to 10 sec (d) revealed a densely packed conformation of lamellar Zn×Ph crystals, reflecting that the EGS surface had essentially been altered and now had a rough microstructure.

Figures 2 and 3 show the high-resolution XPS spectra of P_{2p}, $Zn_{2p3/2}$, and C_{1s} core-level excitations for the Zn×Ph coatings as a function of treatment time. In the P_{2p} region (Fig. 2), no peak was found on the "as-received" EGS surfaces denoted as "OS". The coating made by 1 sec dipping (1S) exhibited two weak peaks, at 133.9 and 132.4 eV. The former peak presumably reveals the P originating from the Zn×Ph [4], and the latter may be due to the formation of zinc dihydrogen orthophosphate, $Zn(H_2PO_4)_2 \times xH_2O$ salt [5]. The intensity of peak at 133.9 eV markedly increased with an increased treatment time, while the peak at 132.4 eV vanished. The degree of coverage of Zn×Ph over EGS can be confirmed by comparing the spectral features of the $Zn_{2p3/2}$ region (Fig. 3). The single peak at the BE position of 1022.2 eV for the "as-received" EGS (OS) is due to Zn in the ZnO layers [6,7], forming on the top surface of galvanized coatings. The $Zn_{2p3/2}$ curve of the 2 sec-treated specimens (2S) is distinctive; an additional weak line at 1023.0 eV appears in the spectrum, separate from the main line. The intensity of this new line dramatically increased as the treatment time was prolonged. After 5 sec (5S), this peak eventually became the principal line, while the line at 1022.2 eV, originating from the Zn in ZnO, disappeared. Because, the peak at 1023.0 eV belongs to Zn originating from Zn×Ph [8], this result strongly supported the SEM data showing that an immersion of 5 sec is long enough to cover the whole surface of EGS with Zn×Ph. The C_{1s} region of the untreated EGS surfaces (Fig.3-OS) had a symmetrical peak at 285.0 eV, reflecting the C in the hydrocarbon, "CH_n", contaminant. When this EGS surface was treated with a phosphating solution for 2 sec, the C_{1s} spectrum (2S) revealed that the two resolvable Gaussian components at 285.0 eV as the principal component is not only attributable to hydrocarbon in the organic contaminant, but also to that in the backbone chain of p(AA). A second peak emerging at 288.7 eV corresponds to carbon originating from the carboxylic acid, COOH, in

the P(AA) [9]. Increasing the treatment time to 10 sec showed the emergence of an additional peak at 287.2 eV in the spectrum (10S). We assigned this additional peak, emerging at the BE location between a carbonyl carbon, C=O, at » 288.0 eV and a carbon-oxygen single bond at » 286.5 eV [10], to the C in the -COO^--Zn^{2+}-$^-$OOC- salt complex formation [11, 12]. Nevertheless, both the bulk and complexed p(AA) polymers appear to be present at the outermost surface site of Zn×Ph.

An important question remains to be solved: namely, why the $Mn(NO_3)_2\times6H_2O$-incorporated solution causes the rapid deposition of Zn×Ph on the EGS surfaces. To investigate the electrochemical activity of the $Mn(NO_3)_2\times6H_2O$ reagent in the increase in the conversion rate of Zn×Ph, we used three solutions without the $Zn_3(PO_4)_2\times2H_2O$ and p(AA) reagents; 1) 10.0 wt% H_3PO_4-90.0 wt% water, 2) 1.2 wt% $Mn(NO_3)_2\times6H_2O$-98.8 wt% water, and 3) 10.0 wt% H_3PO_4-1.2 wt% $Mn(NO_3)_2\times6H_2O$-88.8
wt% water. The experimental work was performed in accordance with the following sequence. First, an EGS test panel with a surface area of 100 cm^2 was immersed for 2, 5, 10, or 30 sec, into a bath containing 1L of these solutions at 80°C. After withdrawing the panel, the concentration of Zn ion in the bath was detected by A.A. to gain the information on the anodic dissolution of the Zn coating. Figure 4 shows the resulting dissolution rates, mg/ml, of Zn ion from the Zn coating, as a function of immersion times. When the EGS panels were soaked in the single $Mn(NO_3)_2\times6H_2O$ solution, » 2.7 x 10^{-4} mg/ml of Zn ions dissociate from the EGS surfaces in the first 2 sec of immersion; thereafter, the rate of Zn ion dissolution increases with increased time. The concentration of dissociated Zn ion after 30-sec immersion was » 1.8 x 10^{-3} mg/ml. Using the other single H_3PO_4 solution, the amount of Zn dissociated in 2 to 30 sec corresponded to a tenfold increase over that of the $Mn(NO_3)_2\times6H_2O$ solution. By comparison, a considerable amount of Zn ion was recorded from the combined solution of $Mn(NO_3)_2\times6H_2O$ and H_3PO_4; immersion for only 2 sec resulted in the dissociation of abundant Zn ion of near 2 x 10^{-1} mg/ml, and subsequently an increase in immersion to 30 sec referred to the dissolution of 1.1 mg/ml. In addition, the extent of hydrogen evolution which was observed by the bubbling of the phosphating solution surrounding the EGS panel was in the following order; $H_3PO_4 + Mn(NO_3)_2\times6H_2O >> H_3PO_4 > Mn(NO_3)_2\times6H_2O$ solutions. These findings verified that the addition of $Mn(NO_3)_2\times6H_2O$ to H_3PO_4 solution significantly promotes the dissolution of Zn ions from the EGS surfaces in conjunction with a more brisk evolution of hydrogen. Possible interpretation of the electrolytic corrosion of Zn layers in the H_3PO_4 electrolyte containing Mn^{2+} ions is as follows: the electrochemical reaction between Zn and H_3PO_4 leads to the anodic dissolution of Zn, Zn ® Zn^{2+} + $2e^-$, which is directly related to the corrosion of galvanized coatings. After the ejection of Zn ions, the electrons $2e^-$ generated by the

anodic reaction of Zn preferentially react with the Mn^{2+} ions dissociated from the $Mn(NO_3)_2 \times 6H_2O$ reagents. This reaction can be described as the electron-trapping reaction, $Mn^{2+} + 2e^- \rightarrow Mn^o$ [13]. The elemental Mn which is less electropositive than Zn may adhere to the Zn to create short-circuited cells with Zn acting as the anodic area and Mn as the cathode. Assuming that the creation of such a short-circuited cell is reasonable, the reaction of Zn with H_3PO_4 might be accelerated by the presence of a cathodic Mn electrode. Once the dissolution of Zn ions has occurred at anodic area, the electrons pass from Zn to Mn, and then the uptake of electrons by hydrogen ions discharged from H_3PO_4 results in a brisker evolution of hydrogen from cathodic Mn side:

$$2H_3PO_4 \rightarrow 2H^+ + 2H_2PO_4^-$$

$$2H^+ + 2e^- \rightarrow H_2.$$

From this information, we show the hypothetic conversion mechanisms of Mn-incorporated H_3PO_4 solution into zinc phosphate phase over the EGS (Fig. 5). The anodically dissolved Zn^{2+} ions react with an ionic dihydrogen phosphate, $H_2PO_4^-$, formed by the discharge of H^+ from H_3PO_4 electrolyte. This reaction leads to the formation of zinc dihydrogen orthophosphate, $Zn(H_2PO_4)_2$, and subsequently, the hydration of $Zn(H_2PO_4)_2$ aids in its conversion into $Zn_3(PO_4)_3 \times nH_2O$. A similar mechanism may occur when Mn-incorporated zinc phosphating solution was applied as a Zn×Ph-convertible solution. The only difference was that many free Zn ions, dissociated from $Zn_3(PO_4)_2 \times 2H_2O$ as the starting material, are present in the original phosphating bath before immersing the EGS plates. Thus, the anodic dissolution of Zn not only contributes to the precipitation of $Zn_3(PO_4)_2 \times nH_2O$ on the EGS, but also may have catalytical activity which increasingly promotes the rate of conversion of free Zn ions into the Zn×Ph.

Figure 6 illustrates the XRD tracing, ranging from 0.444 to 0.225 nm, of the "as-received" EGS as a control, and the p(AA)-modified Zn×Ph coatings prepared by immersing EGS panels for 1, 2, 5, and 10 sec. The XRD pattern of the control shows the presence of a single phase only corresponding to the pure Zn crystal. Although the intensity of XRD line is very weak, the Zn×Ph conversion products formed on EGS after immersing for 1 sec can be identified as the hopeite phase, $Zn_3(PO_4)_2 \times 4H_2O$. The intensity of these hopeite lines markedly increased with an increased immersion time, while the strong lines of the underlying Zn phase are still present in the pattern. The data also indicated that zinc orthophosphate dihydrate, $Zn_3(PO_4)_2 \times 2H_2O$ coexists as minor phase with the hopeite.

3.2 Water-Based APS Sealant

One drawback of the Zn×Ph coatings is the fact that some interstitial voids remain in the coating layers, so that the panels corrode in a short-term exposure to a corrosion environment. Although uniform, dense, continuous Zn×Ph coating layers were fabricated on the panels, there is a need to fill their void spaces with sealers. The goal of this part of the research was to gain technical information on the non-toxic, water-based APS sealant used to replace the conventional toxic hexavalent chromic acid as corrosion-inhibiting sealant. This involved investigating the effectiveness of APS sealer on improving the ability of Zn×Ph coating layers to prevent the corrosion of EGS panels, and also assessing the importance of the chemical affinity of APS for the electro-deposited polymeric primer in extending salt-spray resistance.

In the XPS study earlier, we found that the p(AA) polymers remain at the outermost surface sites of Zn×Ph layers. Thus, it is very important to know how the APS sealer reacts with the p(AA) polymers chemisorbed to the Zn×Ph. To obtain this information, we created a resemblant reaction model that would yield interaction products which were detectable using specular reflectance FT-IR over the frequency range 1800 to 1000 cm^{-1}. The samples were prepared by spin-casting at 4000 rpm the 7 wt% APS solution onto a 3 wt% p(AA)-coated aluminum mirror, followed by heating them in an oven at 150°C for 10 min to form the solid-transparent APS film over the p(AA) film. Also, the bulk APS and p(AA) films deposited onto the aluminum mirrors were used as the reference samples. The spectrum of polymeric APS reference film (not shown) had the absorption bands at 1650 and 1600 cm^{-1}, belonging to the CH_2 groups, at 1200 and 1140 cm^{-1}, corresponding to the Si-methoxide compounds [14], and at 1030 cm^{-1} which can be ascribed to the siloxane groups, Si-O-Si [15,16]. The formation of Si-O-Si linkage strongly verified that the transformation of monomeric APS into the polymeric APS occurred during the thermal treatment of films at 150°C. The spectrum of bulk p(AA) indicates the presence of a strong band near 1710 cm^{-1} which can be assigned to the C=O in the pendent carboxyl and the main chain CH_2 of saturated methylene at 1440 cm^{-1}. By comparison with these reference samples, the differences in spectral feature of the p(AA) film coated with the APS were as follows: (1) the disappearance of the peak at 1710 cm^{-1}, (2) the emergence of a new band at 1550 cm^{-1}, and (3) the decrease in peak intensity of the NH_2 band at 1600 cm^{-1}. Regarding the aspect (2), a possible assignment of new band is likely associated with the formation of amide groups, -CONH-, [17,18]. If this assignment is correct, the results strongly demonstrated that when the APS was attached to the p(AA), the NH_2 groups in APS

favorably reacted with the carboxyl in p(AA) to form the amide bonds. Thus, it is conceivable that the formation of interfacial amide bonds acts to link strongly p(AA) to the APS films. The hypothetical interaction mechanisms at interfaces between the p(AA)-modified Zn×Ph layer and the polymeric APS sealer are illustrated below in Figure A:

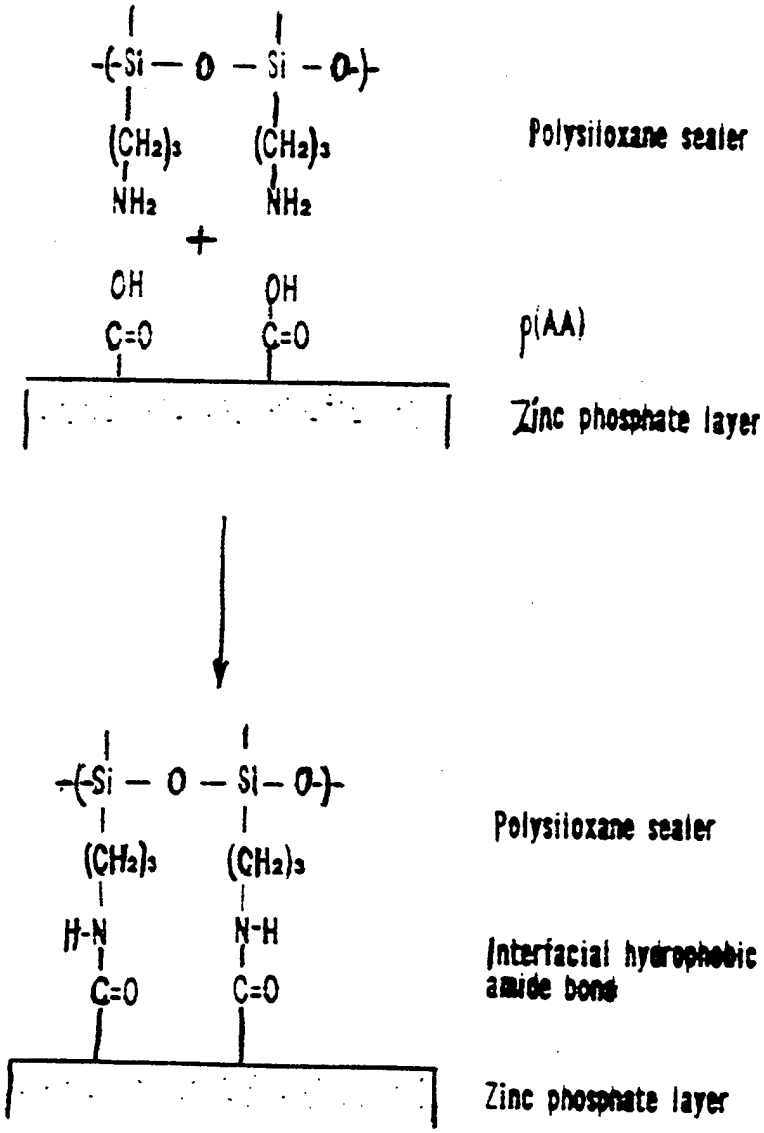

Figure A

Figure 7 depicts typical polarization curves log current versus potential for the uncoated EGS, and Zn×Ph-and p(AA)-Zn×Ph-coated EGS panels. The shape of the curves presents the transition from cathodic polarization at the onset of the

most negative potential to the anodic polarization curves at the end of lower negative potential. The potential axis at the transition point from cathodic to anodic curves is normalized as the corrosion potential, E_{corr}. When compared with those for the uncoated EGS, the striking characteristics of the cathodic curves for the coated EGS specimens are as follows: (1) a decreased current in the vicinity of E_{corr}, and (2) a lower short-term steady-state current value in the potential region between -1.2 and -1.0 V. As a result, it appears that the ability of zinc layers in the EGS to inhibit the cathodic reaction in terms of the oxygen reduction reaction, $H_2O + 1/2O_2 + 2e^- \rightarrow 2OH^-$, of the underlying steel was further enhanced by the p(AA)-modified and unmodified Zn×Ph coatings. Further inhibition of the cathodic reaction by the Zn×Ph coatings not only contributed significantly to reducing the rate of corrosion of the steel, but also extended lifetime of the zinc layers acting as the corrosion barrier. The polarization curves for the APS-sealed EGS, Zn×Ph/EGS, and p(AA)-Zn×Ph/EGS panels are shown in Figure 8. The thickness of the polymeric APS films deposited to the Zn×Ph-coated and uncoated EGS surfaces was determined using a surface profile measuring system. Their thicknesses ranged from 0.2 to 0.7 mm. A comparison of the cathodic polarization areas from the APS-sealed EGS and unsealed EGS (Fig.7) indicates two noteworthy features: (1) the short-term steady-state current value for the sealed EGS panels is a order of magnitude lower than that of the unsealed one at the potential near -1.0 V, and (2) the APS sealer leads to a shift in corrosion potential to a more positive site and a considerably decreased current in the vicinity of E_{corr}. Regarding the result (1), the lower current for the sealed EGS compared with that of the unsealed one is attributed to a low hydrogen evolution as well as a less active surface of the underlying steel, suggesting that the oxygen reduction reaction is suppressed by the APS sealer. For the second observation, applying the APS sealer to the EGS conspicuously enhanced its resistance to corrosion. When this sealer was applied to the Zn×Ph-coated EGS panels, the curve showed a better corrosion protection than that of the panels in which the APS was directly applied to the EGS; namely, the current in the potential region between -0.9 to -1.0 V became somewhat lower. In contrast, a dramatic improvement in protection by the sealer can be seen from the curve of

APS/p(AA)-Zn×Ph/EGS systems, indicating a considerable shift in current to a lower value in the potential range -0.75 to -0.85 V, as well as a large reduction in E_{corr} to a less negative potential. Thus, we believe that the formation of interfacial amide bonds by the interaction between APS and p(AA) significantly contributes to protecting steel from the corrosion, suggesting that the APS has a high potential for use as sealer of the p(AA)-modified Zn×Ph coatings.

Based upon these polarization curves, we attempted to determine the absolute corrosion rates of steel, expressed in the conventional engineering units of milli-inches per year (mpy). The equation (1) proposed by Sterm and Gery [19], was used in the first step:

$$I_{corr} = \beta_a \times \beta_c / 2.303 (\beta_a + \beta_c) R_p \text{ ---------- (1)}$$

where I_{corr} is the corrosion current density in A, β_a and β_c having the units of volts/decade of current refer to the anodic and cathodic Tafel slopes, respectively, which were obtained from the log I vs E plots encompassing both anodic and cathodic regions, and R_p is the polarization resistance which was determined from the corrosion potential, E_{corr}. When I_{corr} was computed through the equation (1), the corrosion rate (mpy) can be obtained from the following expression:

$$\text{Corrosion rate} = 0.13\, I_{corr} (EW) / d \text{ ----------(2)}$$

where EW is the equivalent weight of the corroding species in g, and d is the density of the corroding species in g/cm^3.

Table 1 gives the I_{corr} and corrosion rate obtained from this Tafel calculation for various coating panels. The corrosion rate of underlying steel for the uncoated EGS was 1.449 mpy, corresponding to I_{corr} of 3.17×10^{-6} A. This rate was reduced to 0.505 mpy by depositing Zn×Ph onto the EGS surfaces. Incorporating the p(AA) into the Zn×Ph layers has allowed a further reduction to 0.467 mpy. A significant decrease in corrosion rate can be seen from the APS-sealed panels, especially in the APS/p(AA)-Zn×Ph coating system. The rate of 0.022 mpy for this coating system was approximately two orders of magnitude less than that of the uncoated EGS.

In support, all the test panels were exposed in a 5 % salt fog chamber at 35°C to determine the extension of useful lifetime of the coatings that protect the zinc layer in EGS against white rusting. The results from these test panels are shown in Table 2. The consequent data strongly supported the information obtained from the electrochemical polarization experiment; the most promising coating system for mitigating white rust of the zinc layers was the APS-sealed p(AA)-Zn×Ph, conferring a salt-spray resistance for 750 hrs.

3.3 Electrically Deposited Primer Coatings

One important consideration for the sealed Zn×Ph coating systems is to investigate whether the sealer's layers existing at the outermost surface sites of Zn×Ph layers have a proper affinity for the polyurethane-modified epoxy primer coatings (POWERCRON 648). To gain this information, we electrically deposited the primer coatings onto the APS-sealed and unsealed Zn×Ph layers, and then examined the ability of primer coatings to further improve the protection of EGS against corrosion by AC electrochemical impedance spectroscopy (EIS) and the 5 % salt-spray tests according to ASTM D 1654-79a. The thickness of primer coatings ranged from 1 to 2 mil. A schematic representation of the entire coating system developed in this program is illustrated below in Figure B.

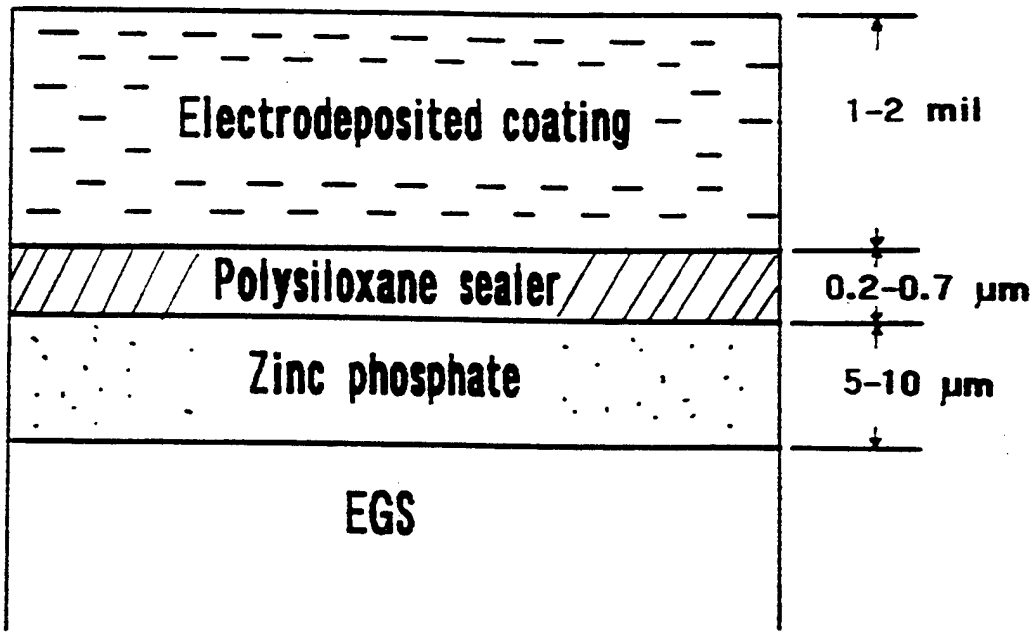

Figure B

Six different coating systems, electrically deposited primer (EDP), EDP/Zn×Ph, EDP/p(AA)-Zn×Ph, EDP/APS, EDP/APS/Zn×Ph, and EDP/APS/p(AA)-Zn×Ph, were prepared for this examination.

In the EIS tests, the curves (not shown) for all the coated EGS panels depicted the Bode-plot features [the absolute value of impedance $^3Z^3$ (ohm-cm^2) vs. frequency (Hz)]. Our particular attention in the overall impedance curves was given to the impedance value of the element $^3Z^3$, which can be determined from the plateau in the Bode plot occurring at sufficiently low frequencies. We adapted the $^3Z^3$ value at a frequency at 1.5 Hz to compare the magnitudes of ionic conductivity generated by the 0.5 N NaCl electrolyte passing through the coating layers; namely, a high value of $^3Z^3$ reflects a low degree of penetration of electrolyte into the coating films. Figure 9 gives the changes in $^3Z^3$ value for these coating panels after for up to 7 days to 0.5 N NaCl solution at 25°C. The value of $^3Z^3$ for all coatings tends to decrease slowly with an elapsed exposure time. Thus, the ability of the coatings to reduce the ionic conductivity gradually weakens during exposure, suggesting that a long-term exposure leads to the uptake of more electrolyte by the coatings. The lowest value of $^3Z^3$ for the EDP-coated EGS panels may be associated with a poor adherence of EDP to the EGS surfaces, thereby resulting in a deficient protective performance. By comparison, the EDP/APS/p(AA)-Zn×Ph and EDP/APS/Zn×Ph coating systems showed an ionically inert behavior, corresponding to $^3Z^3 > 10^7$ ohm-cm^2. Nevertheless, the effectiveness of these coatings in ensuring a low degree of penetration of electrolyte was in the following order; EDP/APS/p(AA)-Zn×Ph > EDP/APS/Zn×Ph > EDP/APS > EDP/p(AA)-Zn×Ph > EDP/Zn×Ph > EDP. Assuming that the factor contributing to the enhancement of protection is due to the chemical attraction of EDP to the substrates, the chemical reaction between the EDP and APS may yield the bond structure which links EDP to APS layers. Although there is no evidence for the chemical reaction mechanisms, we believe that such interfacial interactions play an important role in protecting EGS panels from the corrosion.

This information was correlated directly with the states of primer-coated panels after salt-spray tests for 1080 hours. A scribe of the panels down to bare metal was meant to simulate mechanical damage of the primer coating, where failure can begin easily. The delamination of coating film from the substrate corresponds to the loss of adhesion of the film at the defect, and is the major reason for the scribe. Two major failures were generally looked for in evaluating the

are shown in Table 3. The EDP-coated EGS panels without the APS sealer and Zn×Ph coating showed the failures of the protective coatings after exposure to the salt fog for only 360 hours. The two features considered as failures were 1) the average loss of 10 mm coating films from a scribe mark, and 2) the occupation of » 80 % of the inscribed areas by blisters. By comparison, the deposition of p(AA)-modified Zn×Ph and unmodified Zn×Ph coatings onto the EGS contributed remarkably to protecting EGS from salt-induced corrosion during an exposure of 1080 hours. A further improvement in protection was observed when both the EGS substrate and Zn×Ph coating were treated with the APS. Although some peeling and blistering were observed surrounding the blemished film and in the unblemished areas, the EDP coating overlaid on the APS/p(AA)-Zn×Ph layers displayed the best protective performance, compared with any other coating systems. The EDP/APS/Zn×Ph coating system gave the second best protective performance. This finding was similar to the data on the EIS: the most effective coating system for protecting EGS against corrosion was identified to be the EDP/APS/p(AA)-Zn×Ph.

3.4 Industrial-Scale Demonstration Tests

To demonstrate the reproducibility of this coating technology on mini-sized automobile door panels (25 cm x 25 cm x 5 cm in size) made from EGS, a full-scale feasibility test was carried out in collaboration with the Palnut Company, New Jersey, on December 3, 1996 (Fig. 10).

As described in the Experimental section, the optimized Zn×Ph coating process technology, except for the EDP coating, involved the cleaning, coating, rinsing, sealing, and drying (Fig. 11). The four separate solution tanks with a 1514 L (400 Gal.) were used in a whole process, excepting for the drying. First, the fifteen mini-sized EGS door panels on hangers were immersed in a pickling solution for 1 min at 25°C to remove any surface contaminants (Fig. 12). Second, the cleaned panels were soaked into the p(AA)-modified zinc phosphate make-up solution for 1 min at 80°C (Fig. 13), withdrawn slowly (Fig. 14), and rinsed with water. Third, the water-rinsed panels were dipped for few seconds into the APS sealant (Fig. 15), and finally, the APS-wetted Zn×Ph panels were dried in an oven for 30 min at 150°C to convert the precursor solution into the polymeric APS sealer (Fig. 16). Then, a visual observation was made to ensure that uniform, dense, continuous Zn×Ph layers completely were covered over the EGS surfaces (Fig. 17). The total preparation time of coatings was » 35 min. To ensure that this coating process was reproducible, the procedure was repeated ten times; all 150 mini-sized door panels were successfully coated with Zn×Ph. Half of them was sent to ACT Laboratories, INC. to make electrodeposited primer coatings. After all the primed panels are returned to us, environmental testing of these panels will

commence at Tacom, BNL, and other Army engineering laboratories.

4.0 Conclusions

We modified the surface of electrogalvanized steels (EGS) to inhibit corrosion of Zn layers and to improve their sealer-adhesion properties by immersing EGS panels into environmentally acceptable zinc phosphating solutions consisting of $Zn_3(PO_4)_2 \times 2H_2O$, H_3PO_4, poly(acrylic acid)[p(AA)], $Mn(NO_3)_2 \times 6H_2O$ and water at 80°C. The electrochemical reaction between Mn dissociated from $Mn(NO_3)_2 \times 6H_2O$ and Zn in the acid media created short-circuited cells by the flow of electrons from Zn acting as the anode to Mn as the cathode. Such a cathodic activity increasingly promotes the anodic dissolution of Zn, $Zn \rightarrow Zn^{2+} + 2e^-$, and is reflected by a brisker evolution of hydrogen from the Mn. Considering the precipitation of crystalline zinc phosphate tetrahydrate (hopeite) on the EGS surface, a high degree of ejection of Zn ions contributed significantly to the rapid growth of hopeite crystals deposited on EGS. Uniform hopeite layers completely converting over the EGS surfaces were observed on the specimens prepared by immersion for only 5 sec, thereby conferring good protection layers against corrosion. Thus, it is apparent that the service life of Zn layers as protective barriers for underlying steels could be extended. Hexavalent Cr acids known to be environmental hazards are commonly used as a sealant for the Zn×Ph layers because they improve the ability of Zn×Ph to protect the metal from corrosion. Hence, our attention was paid to find the replacing materials for the Cr acids. We succeeded in developing an environmentally acceptable water-based 3-aminopropyltrimethoxysilane (APS) sealant, which is converted into a polymeric APS sealer at 150°C. When the APS was applied to the surfaces of p(AA)-modified Zn×Ph layers, the carboxyl groups in the p(AA) existing at the outermost surface sites of Zn×Ph layers chemically reacted with the amino groups in the APS sealer to form amide bonds at interfaces between Zn×Ph and APS layers. This interfacial amid bond which linked the Zn×Ph to APS significantly contributed to protecting EGS from the white rust corrosion, which represents deterioration of the zinc layer in EGS, suggesting that the APS has a high potential as a replacing sealant. In addition, the APS sealer had a strong chemical affinity for the polyurethane-modified epoxy primer coating induced by the electrodeposition technology. Such affinity at the critical boundary zones not only led to the coverage of a smooth, continuous primer film over the Zn×Ph layers, but also acted to confer a great protection of EGS against corrosion.

We conducted a scale-up test to demonstrate the reproducibility of this coating technology on mini-sized automobile door panels made from EGS in collaboration with the Palnut Company in

New Jersey. Fifteen mini door panels were successively emersed in four separate solution tanks (holding 400 gal.), involving a cleaning, coating, rinsing, and sealing; the total preparation time was » 35 min. This process was repeated ten times and all 150 panels were successfully coated with APS-sealed Zn×Ph, thereby establishing the potential for industrial-scale feasibility of this coating technology.

5.0 Recommendations

The following five recommendations from the integration of our work performed in FY 96 as Phase II research, are described below:

1. The optimum formulation for an environmentally benign zinc phosphating solution suitable for electogalvanized steels (EGS) was 5 wt% $Zn_3(PO_4)_2 \times 2H_2O$ powder, 10 wt% (85 % H_3PO_4), 1.0 wt% $Mn(NO_3)_2 \times 6H_2O$, and 84 wt% water, in conjunction with poly(acrylic acid) [p(AA), M.W. 60,000] additive of 3.0 wt% by total weight of basic Zn Phos solution.

2. The water-based 3-aminopropyltrimethoxysilane (APS) sealant consisting of a 7 wt% APS, 3 wt% methylalcohol, 0.7 wt% hydrochloric acid, and 89.3 wt% water, can be used to replace the conventional hexavalent Cr acid sealant. The conversion of APS precursor solution into the polymeric APS sealer was carried out by heating it for 30 min at 150°C.

3. Using the process technology developed in this work, the p(AA)-modified zinc phosphate (Zn×Ph) conversion coatings with a APS sealer were prepared in according with the following sequence: 1) pickling the EGS panels in a 2 wt% H_3PO_4-1 wt% H_2SO_4-97 wt% water solution for 1 min at 25°C, 2) immersing the surfaces-cleaned EGS panels for 1 min into the p(AA)-dissolved zinc phosphate solution at 80°C, 3) rinsing the Zn×Ph-coated EGS surfaces with water, 4) dipping the water-rinsed Zn×Ph coating panels for few seconds into a 7 wt% APS sealing agent at 25°C, and 5) drying the APS-wetted Zn×Ph coating panels for 30 min in an oven at 150°C.

4. Although this coating technology is feasible for depositing corrosion-protective Zn×Ph coatings to the EGS on the industrial scale, we will need a long-term exposure in a corrosive environment to ensure that they afford an adequate protection of EGS against corrosion.

5. This coating system was responsible for improving the corrosion resistance of auto-motive body panels made of EGS by delaying the onset of "white rust", which represents deterioration of the zinc layer in EGS. However, the assessment of the potential application of this coating system to the bare steel vehicles was unfinished. Thus, again, a full-scale demonstration test will be required for verifying the industrial feasibility of the coating technology that inhibits the onset of "red rust" of various discrete parts, such as fasteners and brackets.

6.0 Acknowledgments

The authors are grateful to Dr. Robert R. Reeber, U.S. Army Research Office (ARO), for his invaluable suggestions; and to Dr. Joseph Lucas, PPG Industries, Inc., for his assistance to prepare electrodeposited topcoatings on the Zn×Ph surfaces. Discussions with Mr. Philip H. Austin, the Palnut Company, is also appreciated.

References

1. I.C. Handsy, T. Sugama, and N. Carciello, Advanced Polyelectrolyte-Modified Zinc Phosphate Coatings, Phase I, SERDP Final Report, 1995.
2. R. Sard, Plat. and Surf. Fin. 74 (1987) 30.
3. E. Breval, and M. Rachlity, J. Mater. Sci. 28 (1988) 1835.
4. T. Sugama, and R. Broyer, Surf. Coatings Tech. 50 (1992) 89.
5. M. Pelavin, D.N. Hendrickson, J.M. Hollander, and W.L. Jolly, J. Phys. Chem. 74 (1970) 1116.
6. G. Schoen, J. Electron Spectrosc. Relat. Phenom. 2 (1973) 75.
7. J.E. DeVries, J.W. Holubka, and R.A. Dickie, J. Adhesion Sci. Tech, 3 8. T. Sugama, L.E. Kukacka, N. Carciello, and J.B. Warren, J. Coatings Tech. 61 (1989) 43.
9. T. Sugama, L.E. Kukacka, C.R. Clayton, and H.C. Hua, J. Adhesion Sci. Tech. 1 (1987) 265.
10. D. Briggs, and M.P. Seach. "Practical Surface Analysis by Auger and X-Ray Photoelectron Spectroscopy", John Wiley, New York, (1985) p 385.
11. P.S. Ho, P.O. Hahn, J.W. Bartha, G.W. Rubloff, F.K. LeGoues, and B.D. Silverman, J. Vac. Sci. Tech. 3 (1985) 739.
12. F.S. Ohuchi, and S.C. Freilich, J. Vac. Sci. Tech. 4 (1986) 1039.
13. H. Leidheiser, Jr., and I. Suzuki, J. Electrochem. Soc. 128 (1981) 241.
14. A.L. Smith, Spectrochim. Acta, 16 (1960) 87.
15. G.J. Su, N.F. Borelli, and A.R. Miller, Phys. Chem. Glasses, 3 (1962) 167.
16. R. Hama, J. Am. Ceram. Soc., 48 (1965) 595.
17. I. Mizushima, T. Shimanouchi, I. Ichishima, T. Miyazawa, I. Nakagawa, and T. Araki, J. Amer. Chem. Soc., 78 (1957) 2038.
18. M.St.C. Flett, Spectrochim Acta, 18 (1962) 1537.
19. M. Sterm, and A.L. Geary, J. Electrochem. Soc., 104 (1957) 56.

Table 1.0 Tafel Analyses for Polarization Curves of Coated EGS Panels

Coating	E_{corr}(I=0) V	$ß_a$ V/decade	$ß_c$ V/decade	I_{corr} A	Corrosion rate mpy
Uncoated	-0.8711	0.0669	0.1513	3.17×10^{-6}	1.449
Zn×Ph	-0.9692	0.0472	0.1660	1.11×10^{-6}	0.505
p(AA)-Zn×Ph	-0.9609	0.0668	0.1547	1.03×10^{-6}	0.467
APS	-0.8293	0.0458	0.1312	3.10×10^{-7}	0.142
APS/Zn×Ph	-0.8453	0.0532	0.1227	2.12×10^{-7}	0.097
APS/p(AA)-Zn×Ph	-0.6421	0.1257	0.1634	4.78×10^{-8}	0.022

Table 2. Salt-Spray Resistance of Coated EGS Panels

Coating	Salt-spray resistance Hr
Uncoated	15
Zn×Ph	190
p(AA)-Zn×Ph	264
APS	340
APS/Zn×Ph	612
APS/p(AA)-Zn×Ph	750

Table 3. Evaluation of EDP-Coated EGS Panels Subjected to 5 % Salt Spray Testing

Coating	Exposure hr	Representative mean creepage from scribe mm	Area of blister formed in inscribed areas %
EDP	360	10.0	» 80
EDP/Zn×Ph	1080	8.5	» 32
EDP/p(AA)-Zn×Ph	1080	6.5	» 28
EDP/APS	1080	3.0	» 20
EDP/APS/Zn×Ph	1080	1.8	» 13
EDP/APS/p(AA)-Zn×Ph	1080	1.2	» 5

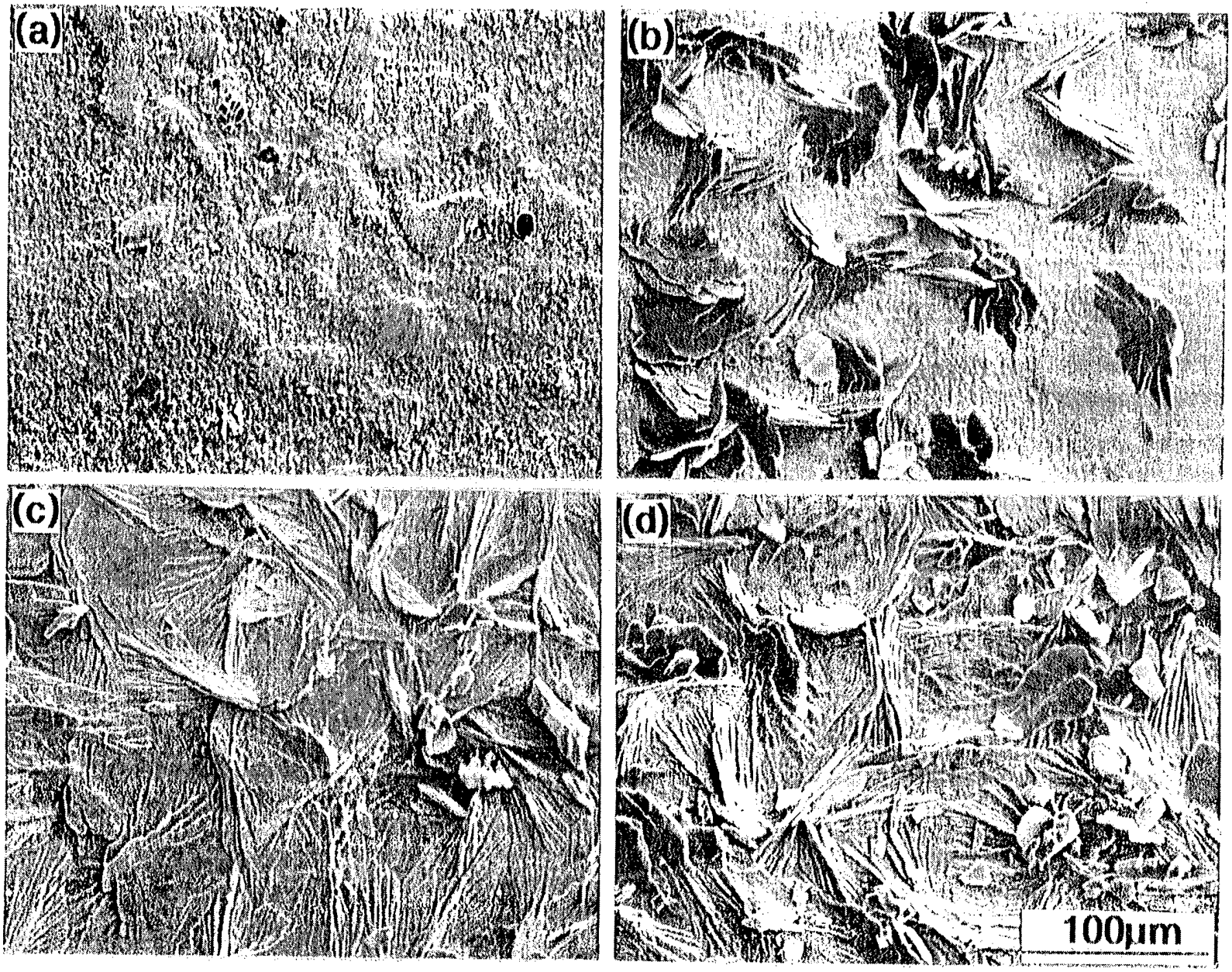

Figure 1. SEM image of p(AA)-modified zinc phosphate deposited rapidly on EGS surfaces after immersion for 1 sec (a), 2 sec (b), 5 sec (c), and 10 sec (d).

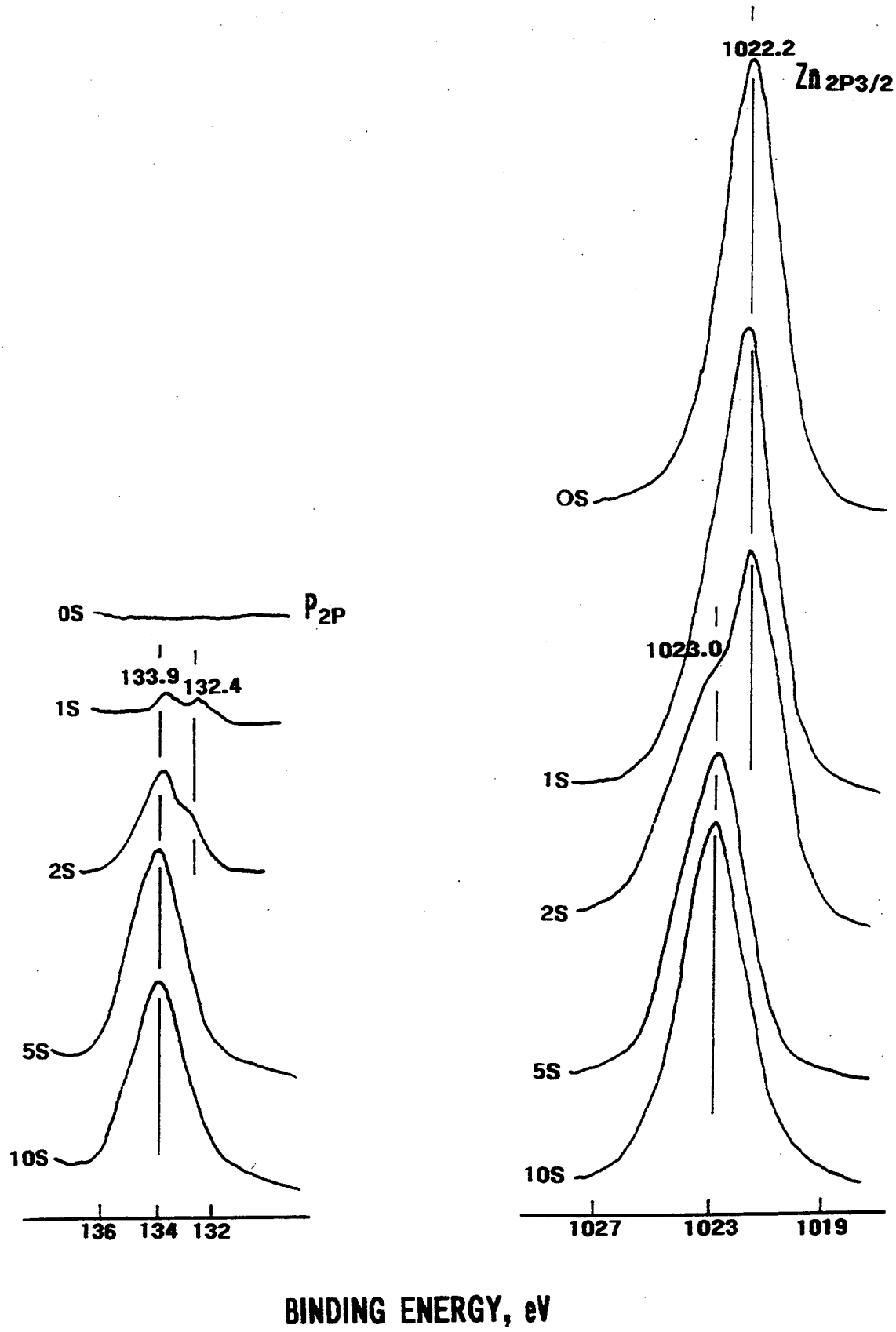

Figure 2. XPS P_{2p} and $Zn_{2p3/2}$ regions of Zn·Ph deposited on EGS as a function of immersion time.

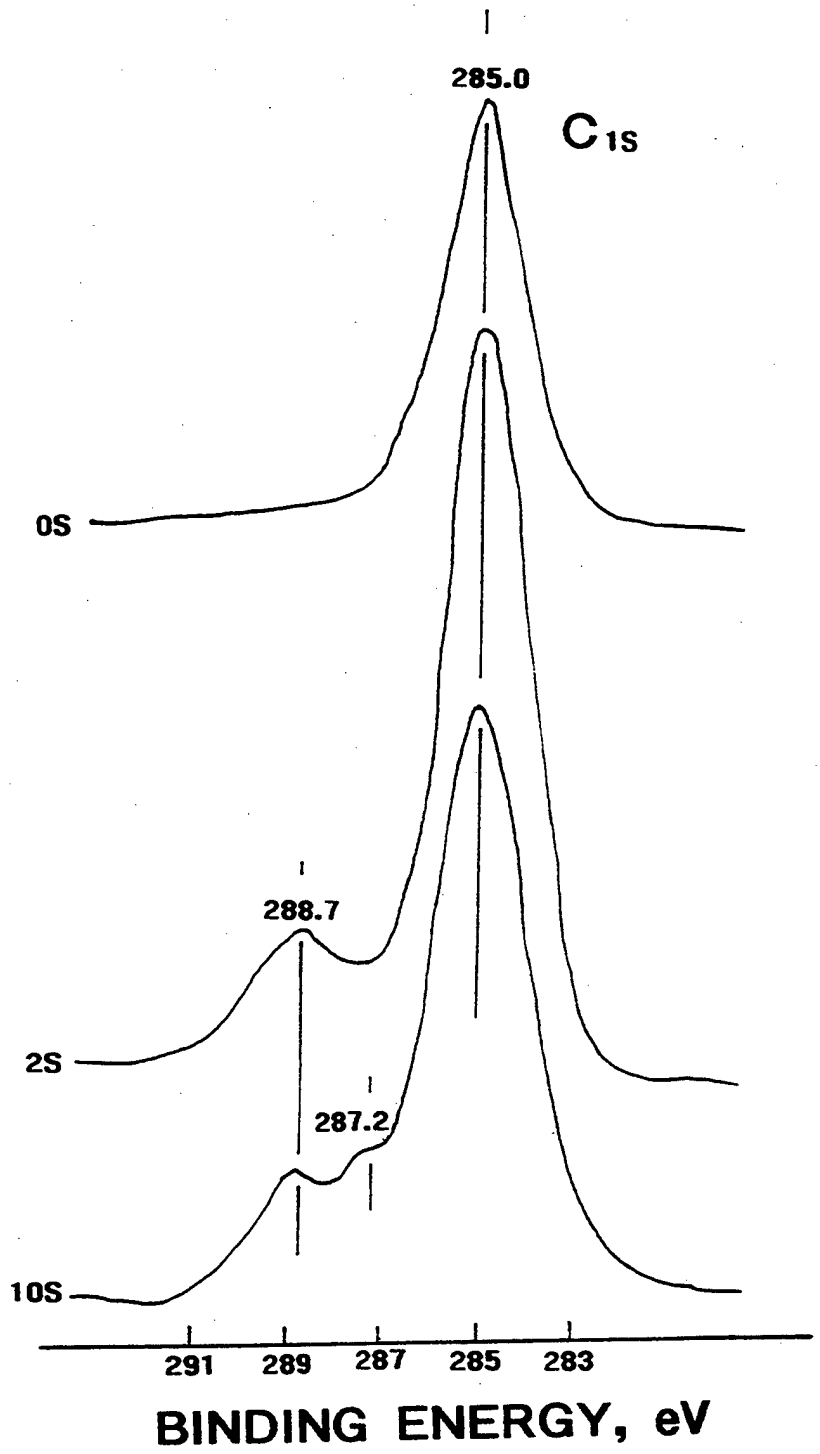

Figure 3. C_{1s} region of "as-received" EGS (0S), and 2s and 10s-treated Zn·Ph surfaces.

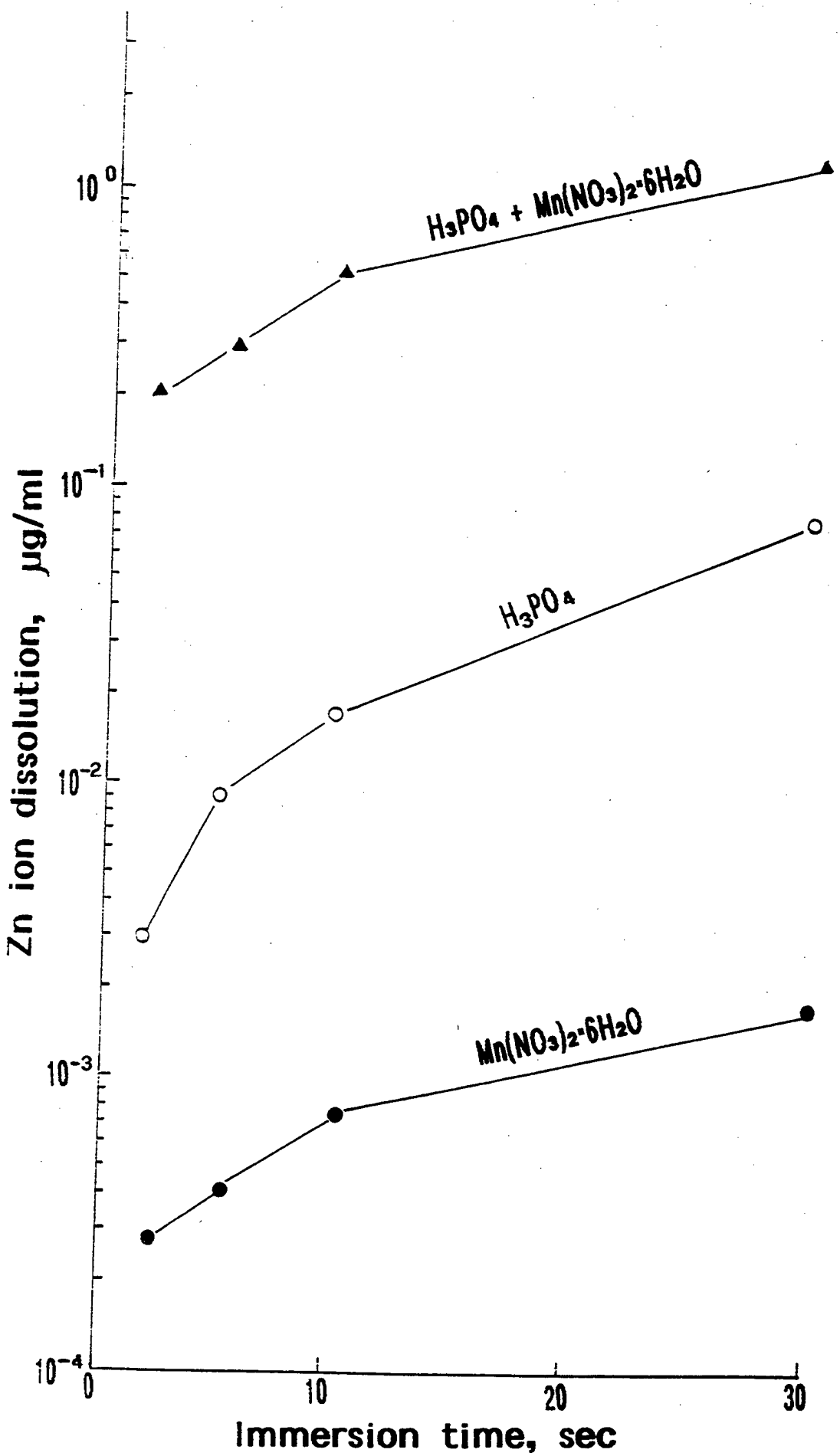

Figure 4. Changes in the concentration of zinc ions dissolved anodically from galvanized coating after immersion of EGS into H_3PO_4, $Mn(NO_3)_2 \cdot 6H_2O$, and H_3PO_4 + $Mn(NO_3)_2 \cdot 6H_2O$ solution, respectively, at 80°C.

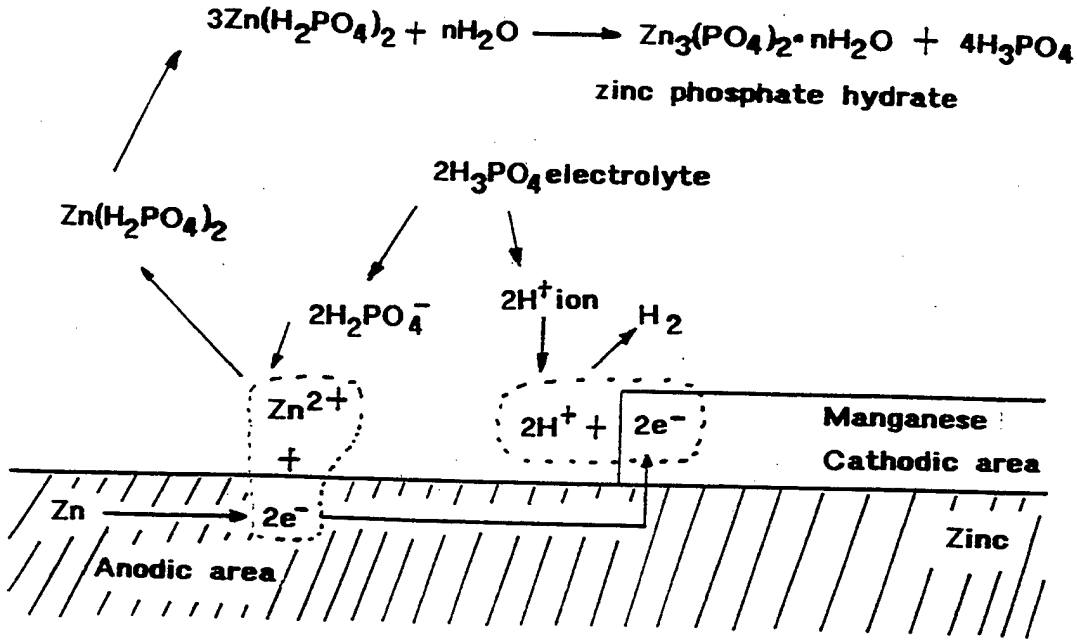

Figure 5. Hypothetical multiple reactions occurring at interfaces between EGS and Mn-incorporated H_3PO_4 electrolyte.

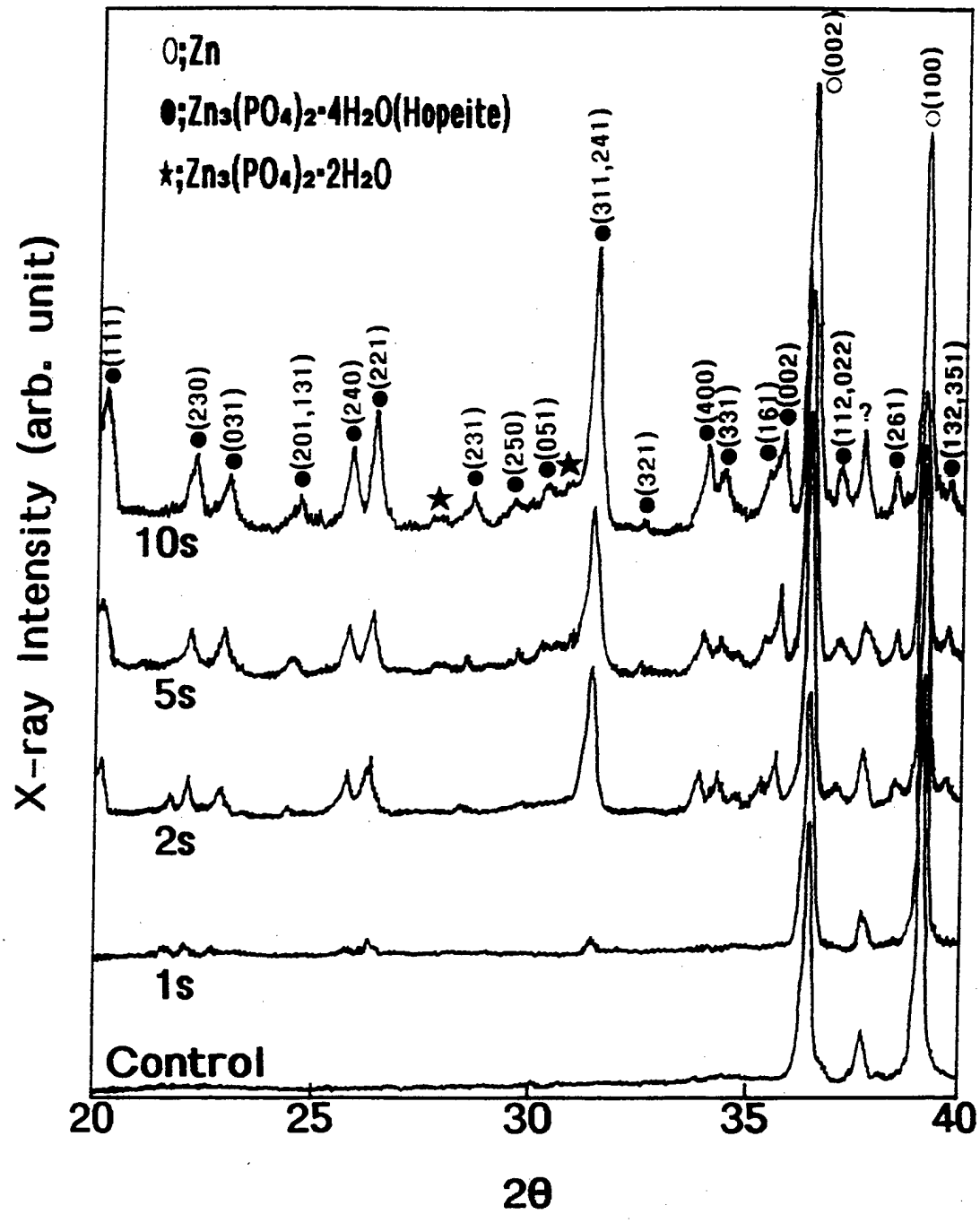

Figure 6. XRD patterns of "as-received" EGS surfaces as control, and Zn·Ph made after immersion for 1, 2, 5, and 10s.

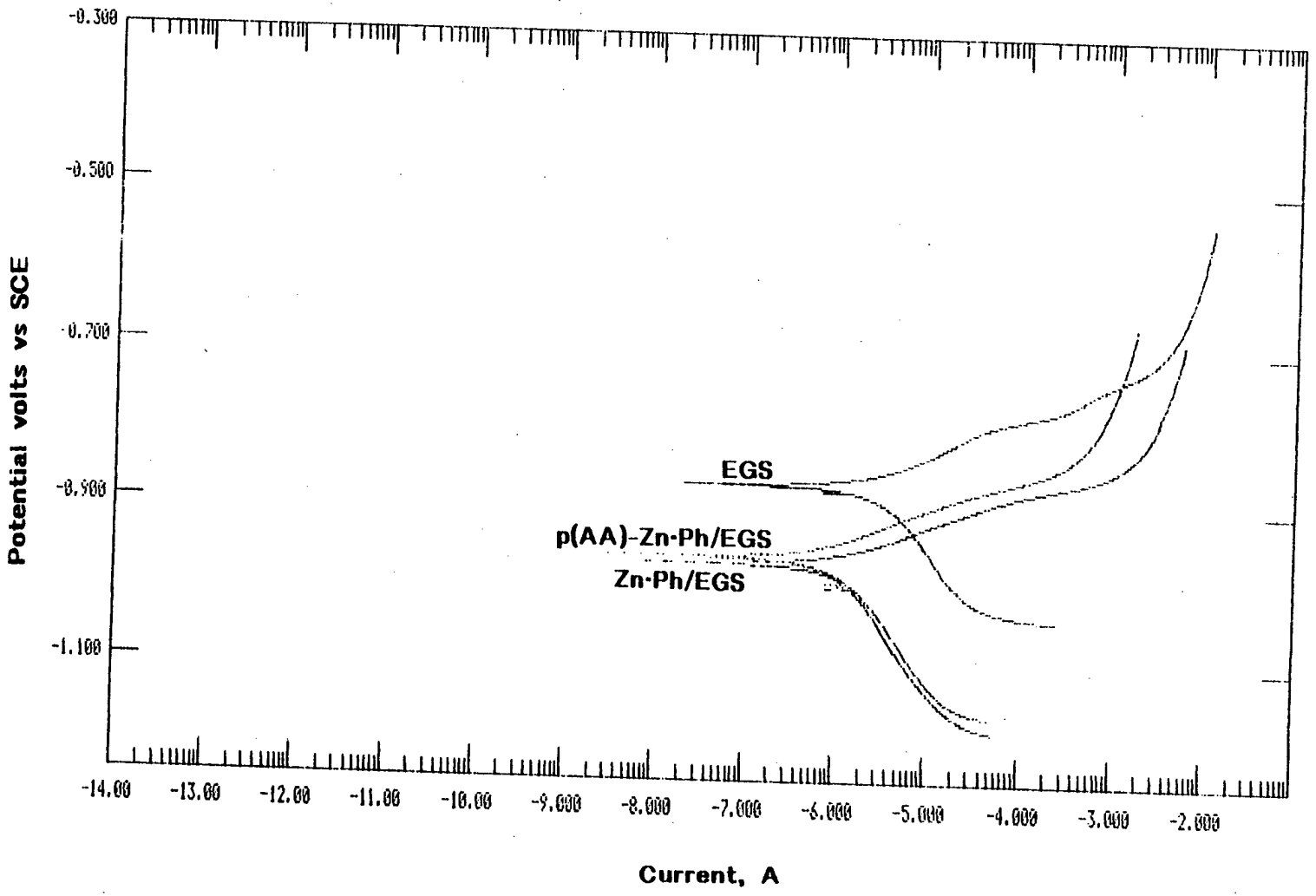

Figure 7. Polarization curves for "as-received" EGS, and p(AA)-modified and unmodified Zn·Ph coating panels.

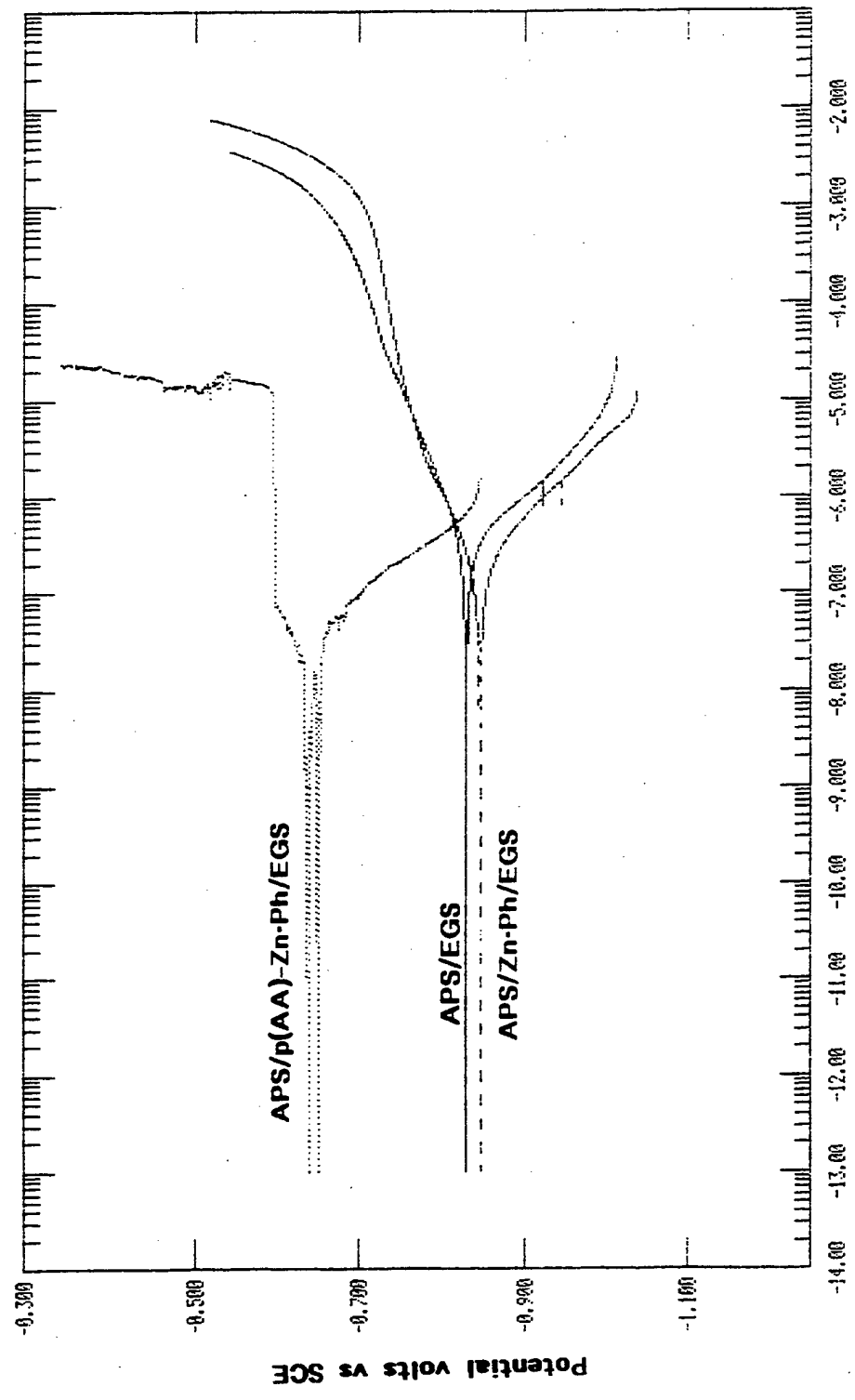

Figure 8. Polarization curves for the APS-sealed EGS, Zn·Ph, and p(AA)-Zn·Ph panels.

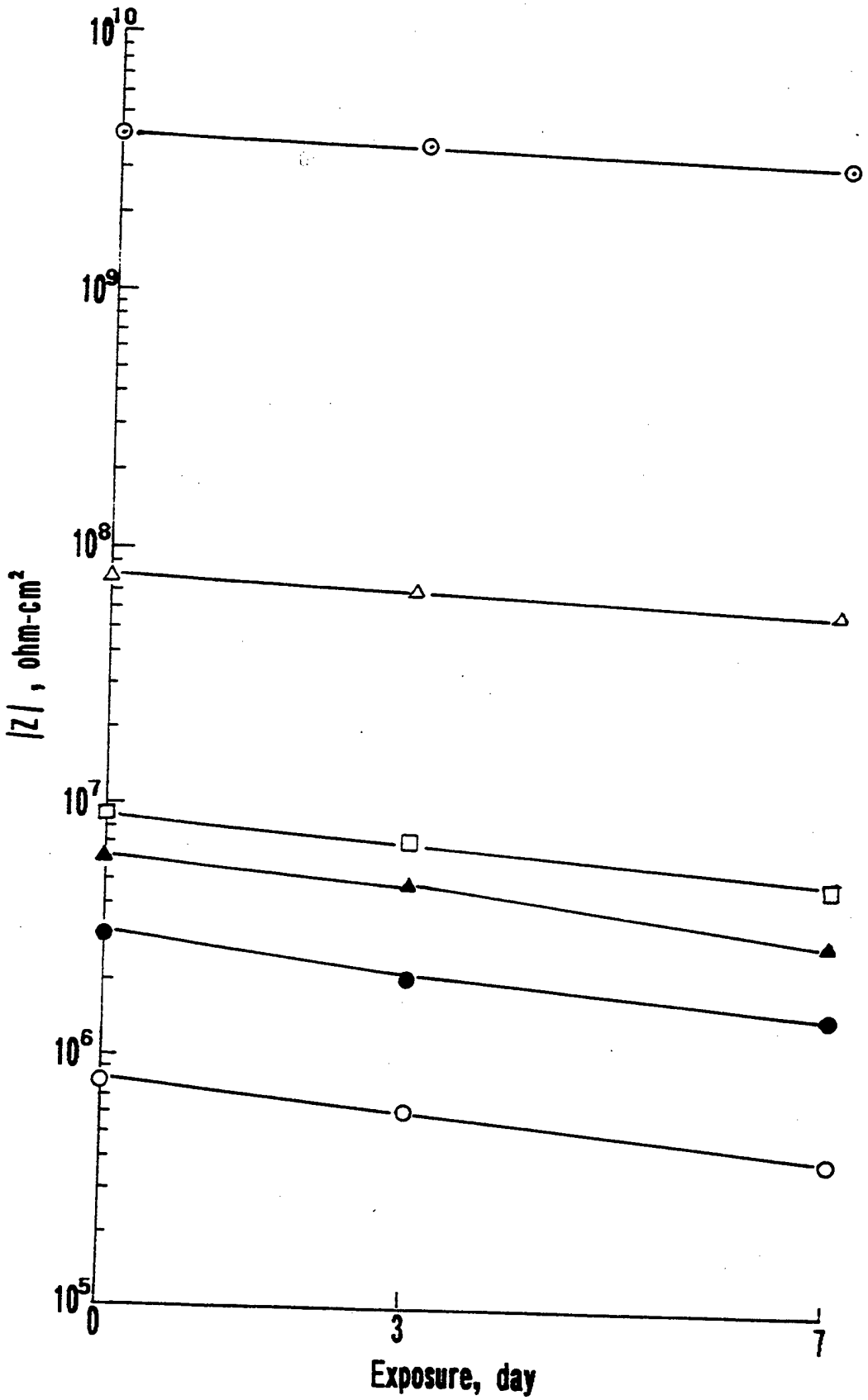

Figure 9. Changes in impedance value for (0) EDP-, (●) EDP/Zn·Ph-, (▲) EDP/p(AA)-Zn·Ph-, (□) EDP/APS-, (△) EDP/APS/Zn·Ph-, and (θ) EDP/APS/p(AA)-Zn·Ph-coated EGS panels as a function of exposure time.

Process Technology for Zn-Ph Coatings on EGS

1. Pickled (2 wt% H_3PO_4-1 wt% H_2SO_4-97 wt% water) for 1 min at 25°C

2. Immersed in zinc phosphate solution for 1 min at 80°C

3. Rinsed with water

4. Dipped in water-based polysiloxane sealant

5. Oven-dried for 30 min at 150°C

6. Electrodeposited primer coatings

Figure 10

A Chromate-Free Chemical Conversion Coating for Aluminum and Steel Alloys

J.F. McIntyre, W.J. Claffey and R.J. Brent
Man-Gill Chemical Company
23000 St. Clair Avenue
Cleveland, OH 44117

R. Conrad
Naval Surface Warfare Center
Code 683
West Bethesda, MD 20817

ABSTRACT

A novel surface pretreatment for aluminum and steel that eliminates the need for chromates is described herein. The new approach is to prepare aluminum and steel prior to the application of a polymer topcoat by bonding a reactive organic conversion coating (ROCC) to the substrate surface. ROCC films are about 20-30 nm in thickness and composed of an inorganic inner layer and an outer organic layer. The organic portion of ROCC is highly functionalized which aids in improving adhesion of organic topcoats. ROCC is equivalent to a commercial chromate conversion coating in extended salt-spray exposure. In addition, the performance of ROCC treated steel topcoated with various systems is comparable to iron phosphate pretreated substrates with chromate seals. The environmentally friendly ROCC system contains no toxic metals and the organic portion of the film is biodegradable. Processing of ROCC uses equipment and conditions that are similar to those used in phosphating operations.

BACKGROUND

Aluminum and steel alloys are used in military applications because of their ease of fabrication, varied use and their typically low cost. Aluminum alloys, for example, are used extensively in military and civilian aircraft because of their high strength-to-weight ratios. Unfortunately, these alloys are susceptible to several insidious forms of corrosion -- hence, requiring these alloys to be protected from the deleterious effects of aggressive service environments. Historically, conversion coatings and sealers containing hexavalent chromium have shown great utility as pretreatments for aluminum prior to topcoating with various polymers or, in some situations, as stand alone protection systems. An article by J. Bibber[1] describes the different types of conversion coatings available for pretreating aluminum. Bibber[1] reviews both chrome and chrome-free systems for use on aluminum. A blind study organized and monitored by the National Center for Manufacturing Sciences involved performance testing of hexavalent chromium-free conversion coatings on aluminum alloys[2]. A project committee

consisted of nine industrial, government and academic organizations, each of which participated in some portion of the testing. Twenty-nine chrome-free systems were obtained from twelve commercial, government and academic sources. The various systems were applied to one or all of the following aluminum alloys: 3003, 2024-T3, 6061-T6, 7075-T6 and 356. This report also features a section on the environmental assessment of several of the submitted chemistries. In summary, the NCMS report identified several candidate chromium-free systems for further investigation; however, pretreating AA 2024 and AA 7075 alloys remains problematic for the chromium-free alternatives.

Steel alloys are frequently pretreated with phosphate conversion coatings and subsequently rinsed with a chromium containing sealer. Recent efforts have focused on replacing chromate rinses (sealers) with non-chrome versions, including those based on titanium and zirconium chemistries, organic film forming sealers, acidic molybdates and fluoride complexes[3].

Conversion coatings and sealers that contain hexavalent chromium are carcinogens and hazardous air pollutants as defined by the Federal Clean Air and Clean Water Acts. Hence, there is a strong interest by university, industry and government research establishments to find replacements for hexavalent chromium containing films.

The following criteria are important for the development of a commercially viable chromate-free pretreatment: 1) corrosion resistance equivalent to chromate films; 2) easy to use; 3) low cost; 4) environmentally compliant; and 5) effective on multi-metals. By following these guidelines, an alternative pretreatment for preparing aluminum, steel and galvanized steel substrates prior to the application of a polymer topcoat was developed. This new technology replaces conventional chromate systems by bonding a *reactive organic conversion coating* (ROCC) to the substrate surface. The ROCC system contains no toxic metals and the organic portion of the film is biodegradable. Processing of ROCC uses equipment and conditions that are similar to those used in phosphating operations. ROCC is equivalent to iron phosphate and chromate conversion in cost. ROCC chemistry has the following attributes: 1) easy to maintain and monitor; 2) low sludging; and 3) long bath life.

ROCC CHARACTERIZATION

The ROCC system is composed of an inorganic inner layer and an organic outer layer. A schematic of the ROCC film is provided in Figure 1. The outer portion of the film is a highly functionalized, naturally-occurring organic entity. The high functionality of the organic backbone aids in promoting adhesion to organic topcoats. The ROCC film is amorphous, similar to an iron phosphate film, with a coating weight of about 30-50 mg/ft^2 (0.032 mg/cm^2).

Characterization of ROCC by scanning electron microscopy is difficult because of the film's essentially featureless, amorphous nature. Hence, the film's topography was characterized using atomic force microscopy (AFM). Photographs representative of the ROCC film on aluminum (AA 5052) and galvanized steel are shown in Figures 2-3. The top photograph in Figure 2 is

bare aluminum after alkaline cleaning; the bottom photograph is representative of the film after the application of ROCC. The AFM clearly shows the presence of a film as indicated by the surface roughness. In comparison, the ROCC film on galvanized steel (Figure 3) is thicker and rougher than observed on aluminum.

Analysis of ROCC using X-ray photoelectron spectroscopy (XPS) reveals the presence of carbon and phosphorus in the film (see Figure 4). The strong C-1s signal provides indirect evidence that ROCC has an organic component. (Direct evidence is obtained from FTIR analysis - not reported herein.) Phosphorus in the XPS spectrum is due to the inner phosphate layer of the film. A depth profile plot (see Figure 5) shows the carbon film concentration decreases steadily from the surface. Conversely, the concentration of phosphorus increases with sputtering, reaching its maximum level at about 28 nm before beginning a gradual decrease in concentration. The iron content follows a profile similar to phosphorus except its concentration continues to increase beyond 28 nm.

EXPERIMENTAL

Specimen Preparation

Test specimens pretreated with ROCC were prepared by the following process: 1) cleaning with an alkaline cleaner (3 vol %) at 57°C (135°F) for 60 seconds; 2) rinsing with overflowing tapwater at ambient temperature for 30 seconds; 3) ROCC pretreatment at a pH of 4.1-4.3 and 49°C (120°F) for 60 seconds; 4) rinsing with overflowing tapwater at ambient temperature for 30 seconds; and 5) rinsing with deionized water at ambient temperature for 30 seconds. All panels were dried prior to further processing using infrared heaters.

Aluminum Substrates

AA 3003 specimens were obtained from a national supplier of metal samples. Topcoats used in this investigation were obtained from several vendors and are listed in Table 1. The aluminum test panels pretreated with a commercial chromate conversion film were also obtained from the same supplier of metal samples. Salt-spray testing for aluminum specimens lasted 3,000 hours.

Steel Substrates

Study No. 1. Cold rolled steel (CRS) panels were obtained from a national supplier of metal test samples; they were pretreated with ROCC or iron phosphate and subsequently painted with either a commercial powder coating or E-coat.

Study No. 2. Additional tests were conducted in order to compare the properties of ROCC to a commercial iron phosphate with a chromate seal. Pretreated panels were topcoated with five (5) powder coatings from three suppliers. These included two polyesters, two hybrid

epoxy-polyesters and one epoxy. The conditions for preparing CRS panels with ROCC were similar to that described above.

Environmental and Physical Testing

Salt-spray exposure testing followed ASTM B 117 specifications. Panels were periodically removed from the test chamber and topcoat adhesion was checked using a tape pull method. The reported values reflect paint adhesion loss as a function of distance away from the scribe line as measured in millimeter (1/32 inch) increments.

The following physical properties were measured for pretreated and topcoated specimens: 1) direct impact (ASTM G14, mod.); 2) conical mandrel bend (ASTM D 522); and 3) cross-hatch adhesion (ASTM D 3354).

Marine Exposure Testing

Hot rolled steel (HRS) and AA 5086 panels were abrasively blasted with aluminum oxide to give a profile of about 50 microns (2 mils). Aluminum panels received the following surface pretreatments: chromate conversion, ROCC or as blasted. HRS panels received the following surface pretreatments: iron phosphate with a non-chrome seal, ROCC or as blasted. All panels were protected with a single coat of epoxy primer, MIL-P-24441B, type IV, formula 150 and two coats of MIL-P-24441B, type IV, formula 151. The complete system was cured at room temperature for seven days prior to testing. The total film thickness of the paint system was about 225 microns (9 mils). One set of panels is currently exposed to a marine coastal environment in Florida. A second set of panels is being exposed to a ASTM B 117 salt-spray environment. A single vertical scribe defect was introduced into several panels from each group, while one panel from each group received no intentional defect.

RESULTS AND DISCUSSION

Laboratory Testing

Aluminum. A summary of physical property values obtained for painted aluminum panels is provided in Table 2. The behavior of ROCC and the chromate treated panels were similar. Powder coatings B and F exhibited poor flexibility on both pretreatments as revealed by adhesion loss and cracking in the conical mandrel test. In addition, minor adhesion loss occurred for coating B on both pretreatments as determined by the cross-hatch adhesion test.

ASTM B 117 salt-spray testing results are summarized in Table 3. The best performance was exhibited by ROCC pretreated panels with powder coats D, E and F. All three systems survived 3,000 hours of salt-spray exposure without evidence of adhesion loss, blistering or undercutting of the topcoat. Conversely, a localized loss of adhesion occurred at the intersection of the two scribe lines for coating B. In addition, coating C exhibited localized adhesion loss along the

length of the scribes at 1,500 hours. However, additional adhesion loss did not occur between 1,500 and 3,000 hours of exposure. In comparison, all chromate conversion pretreated and painted panels survived 3,000 hours of salt-spray exposure without evidence of adhesion loss, blistering or undercutting of the topcoat.

Cold Rolled Steel (Study No.1). A summary of results for physical tests performed on painted panels is provide in Table 4. ROCC pretreated and painted CRS panels exhibited identical behavior in comparison to the iron phosphate pretreated panels.

Salt-spray performance of ROCC treated panels was equal to that of the iron phosphated panels. The adhesion loss along the scribe length was identical for powder coated panels at 250 hours of exposure and nearly the same at 500 hours for E-coated panels (see Table 5).

Cold Rolled Steel (Study No.2). Direct and reverse impact test results for the five pretreatment, topcoat systems varied. For example, ROCC pretreated and painted panels gave better impact results in comparison to iron phosphate (chromate seal) panels for systems B, C and E; however, impact values were lower for ROCC systems A and D in comparison to the iron phosphate controls.

ROCC treated panels painted with systems C, D and E exhibited no adhesion loss, blistering or undercutting along the scribe after 500 hours of salt-spray exposure. Conversely, systems A and B gave topcoat adhesion loss along the scribes of 2.4 mm at 500 hours. In comparison, no adhesion loss, blistering or undercutting was obtained for the iron phosphate (chromate seal) controls with all paint systems.

Marine Exposure Testing

After ten weeks of exposure, no changes in the appearance of aluminum pretreated and coated panels are evident. Conversely, several steel panels without surface pretreatment are exhibiting blistering of the paint system along the scribe; blisters are characterized as #8, medium density according to ASTM D 714. The paint system is also blistering along the scribe for one phosphated HRS panel; blisters are characterized as #8, few in density according to ASTM D 714. ROCC pretreated panels exhibit no adhesion loss or blistering along the scribe for HRS panels. General rusting within the scribe is occurring on all HRS specimens with intentional defects.

SUMMARY

ROCC is equivalent to a commercial chromate conversion coating on AA 3003 in 3,000 hours of ASTM B117 salt-spray exposure -- exhibiting zero adhesion loss along intentionally placed scribes. For example, ROCC pretreated AA 3003 panels with powder coats E and F passed the 3,000 hour salt-spray test with no adhesion loss, blistering or undercutting along the scribes. Powder D also exhibited no adhesion loss except for minor undercutting along one

scribe. Two other powder coatings had localized adhesion losses of 2.4 mm. These results compare favorably with those obtained for the chromate conversion coated panels. In addition, physical property data obtained for ROCC pretreated AA 3003 was essentially identical to that of chromate conversion coated AA 3003. Performance of ROCC compared well with iron phosphate on topcoated CRS in salt-spray exposure testing. As was observed for aluminum, the physical property data were similar to the control (i.e., iron phosphate). ROCC is performing better than phosphated and non-phosphated HRS panels in marine exposure testing after ten weeks. ROCC is performing equivalently to chromate conversion aluminum coated panels after ten weeks of marine coastal exposure.

A *reactive organic conversion coating* offers a number of distinct advantages over chromate conversion and chromate sealed phosphate films. ROCC is environmentally compliant, it is easier to use and offers lower life-cycle costs compared to conventional pretreatment systems. The performance of ROCC compares favorably to chromate conversion coatings and chromate sealers in salt-spray testing and is an equivalent or better promoter of topcoat adhesion. This investigation demonstrates that the ROCC pretreatment is a viable chromate-free technology for the replacement of hexavalent chromium containing films.

REFERENCES

(1) J. Bibber, "The Importance of Chrome-Free Conversion Coatings in the Pretreatment of Aluminum," Powder Coating, April, 1997: pp. 29-43.

(2) National Center for Manufacturing Sciences, "Alternatives to Chromium for Metal Finishing," NCMS Report 0273RE95, Ann Arbor, MI, 1995.

(3) G. Gorecki, "Function of Final (Seal) Rinses in a Phosphate Operation," 1997 Organic Finishing Guidebook and Directory, Publ. by Elsevier Sciences for Metal Finishing , New York, New York, Vol. 95, No. 5A, 1997: p. 123.

Table 1. Coating systems used on ROCC pretreated AA 3003.

Panel Code	Coating Type	Generic Coating Type	Cure Temperature, °C (°F)	Cure Time (minutes)
B	powder	white acrylic	190 (375)	20
C	powder	white polyester	190 (375)	20
D	powder	gray polyester	190 (375)	15
E	powder	gray polyester TGIC[(1)]	193 (380)	15
F	powder	white polyester	204 (400)	17
[(1)] Triglycidylisocyanurate				

Table 2. Summary of physical property values for ROCC pretreated AA 3003.

Coating System	Cross-Hatch Adhesion		Direct Impact, kgf.m (in.lbf)		Conical Mandrel Bend Test	
	ROCC	Chromate Film	ROCC	Chromate Film	ROCC	Chromate Film
B	6% adhesion loss	3% adhesion loss	0.07 (6)	0.06 (5)	100% adhesion loss	95% adhesion loss
C	no adhesion loss	no adhesion loss	0.05 (4)	0.15 (13)	no adhesion loss	no adhesion loss
D	no adhesion loss	no adhesion loss	0.14 (12)	0.11 (10)	no adhesion loss	no adhesion loss
E	no adhesion loss	no adhesion loss	0.23 (20)	0.21 (18)	no adhesion loss	no adhesion loss
F	no adhesion loss	no adhesion loss	0.06 (5)	0.07 (6)	5.1 cm 100% adhesion loss 10.2 cm microcracking [1]	microcracking along entire length of mandrel
				[1] 100% adhesion loss starting at small diameter end of the mandrel .		

Table 3. Summary of salt-spray exposure for AA 3003 pretreated substrates at 3000 hours.

Coating System	Topcoat Adhesion Loss along Scribe (mm)	
	ROCC	Chromate Conversion
B	0	0
C	2.4	0
D	2 small spots	0
E	0	0
F	0	0

Table 4. Summary of physical property values for ROCC pretreated cold rolled steel.

Polyester Powder	Conical Mandrel	Reverse Impact, kgf.m (in. lbf)	Direct Impact kgf.m (in.lbf)	Cross-Hatch Adhesion
A-ROCC/CRS	No Adhesion Loss	0.69 (60)	0.92 (80)	No Adhesion Loss
A1- Fe Phos/CRS	No Adhesion Loss	0.74 (64)	0.92 (80)	No Adhesion Loss
E-Coat	**Conical Mandrel**	**Reverse Impact**	**Direct Impact**	**Cross-Hatch Adhesion**
B-ROCC/CRS	No Adhesion Loss	0.92 (80)	0.92 (80)	No Adhesion Loss
B1- Fe Phos/CRS	No Adhesion Loss	0.92 (80)	0.92 (80)	No Adhesion Loss

Table 5. Summary of salt-spray exposure results on cold rolled steel pretreated substrates for study no. 1.

Polyester Powder	Paint Adhesion Loss along Scribe		
	120 hours	250 hours	500 hours
A- ROCC/CRS	0	0	NA
A1 - Fe Phos/CRS	0	0	NA
E-Coat	**Paint Adhesion Loss along Scribe**		
	120 hours	**250 hours**	**500 hours**
B- ROCC/CRS	0	0	1.6, localized
B1 - Fe Phos/CRS	0	0	0.79

Table 6. Summary of direct and reverse impact testing on cold rolled steel pretreated substrates for study no. 2

Coating System	Direct Impact kgf.m (in. lbf)		Reverse Impact kgf.m (in. lbf)	
	ROCC	Fe Phosphate	ROCC	Fe Phosphate
A	0.7 (60)	0.9 (80)	0.3 (30)	0. 5 (40)
B	1.8 (160)	1.8 (160)	1.8 (160)	1.6 (140)
C	1.6 (140)	0.9 (80)	0.9 (80)	0.5 (40)
D	0.9 (80)	1.1 (100)	0.3 (30)	0.6 (50)
E	1.8 (160)	1.8 (160)	1.4 (120)	1.6 (140)

Table 7. Summary of salt-spray exposure results on cold rolled steel pretreated substrates for study no. 2.

Supplier	Coating System	Topcoat Adhesion Loss along Scribe (mm)
		500 hours
A	polyester	2.4
B	epoxy	2.4
C	hybrid	0
D	polyester	0
E	hybrid	0
F[1]	---	0
[1] iron phosphate control with chromate seal, all coatings.		

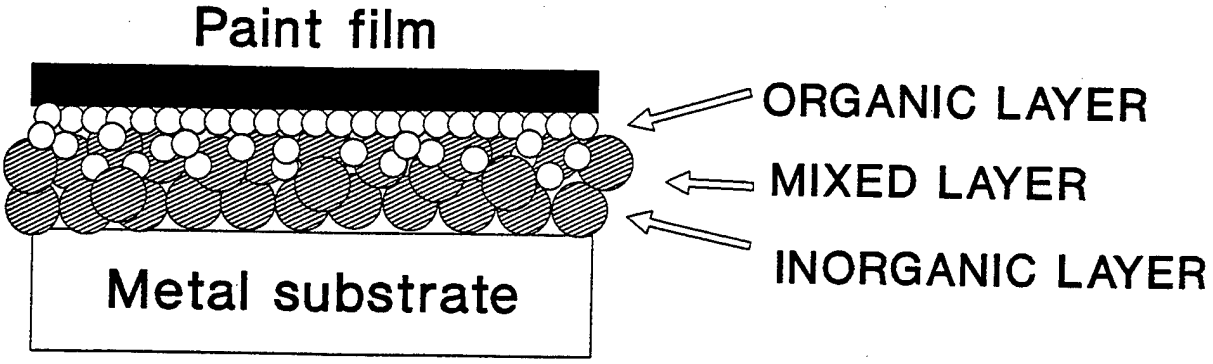

Figure 1. Schematic of Reactive Organic Conversion Coating.

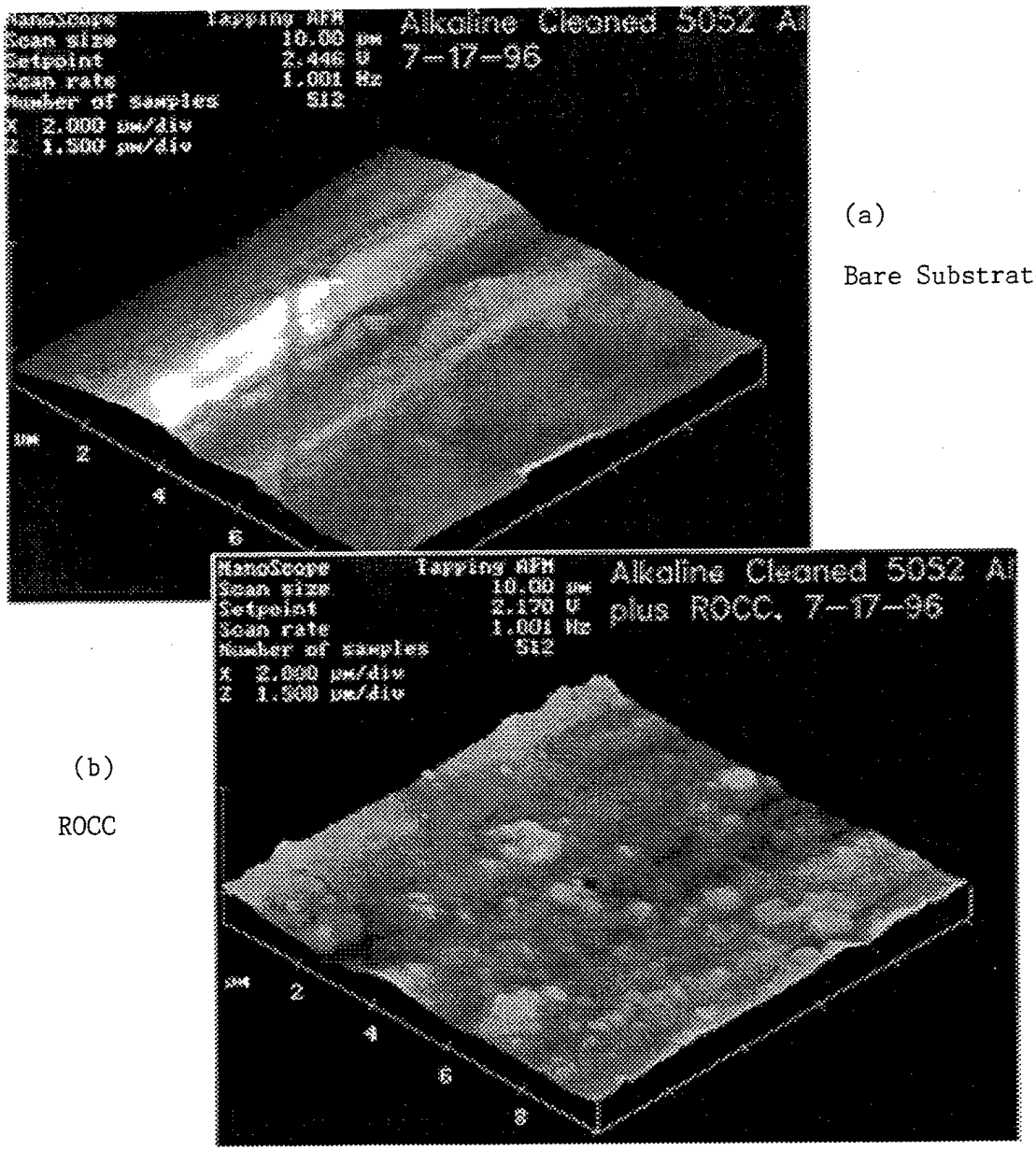

(a)

Bare Substrate

(b)

ROCC

Figure 2. Atomic Force Micrographs of AA 5052.

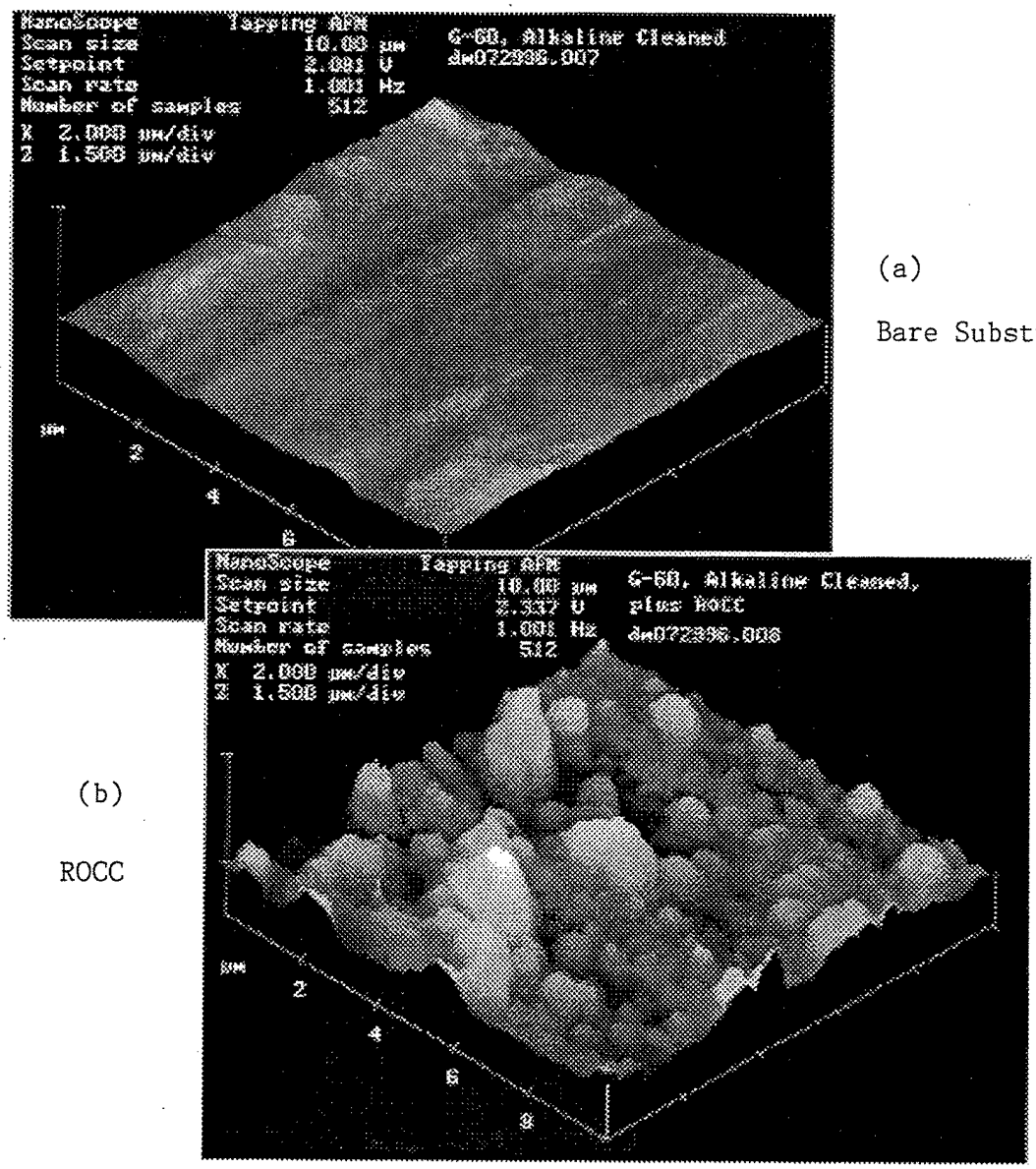

Figure 3. Atomic Force Micrographs of Galvanized Steel.

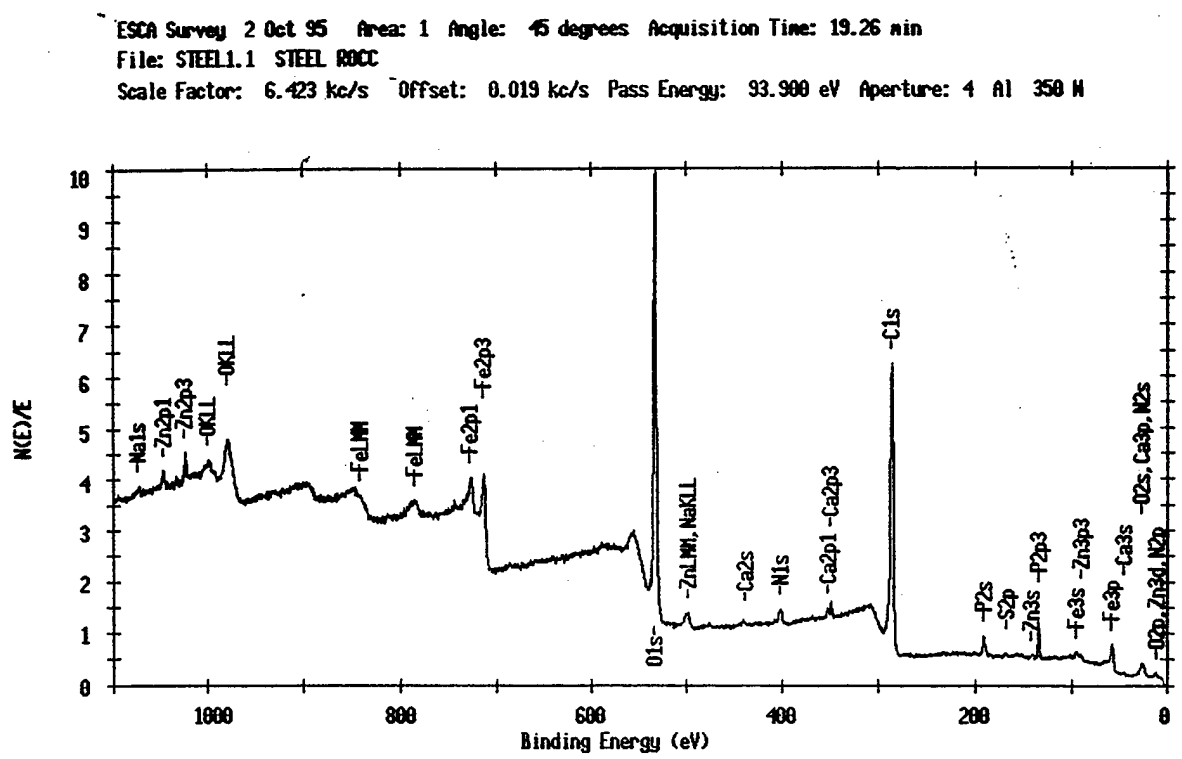

Figure 4. X-Ray Photoelectron Spectroscopy of ROCC film.

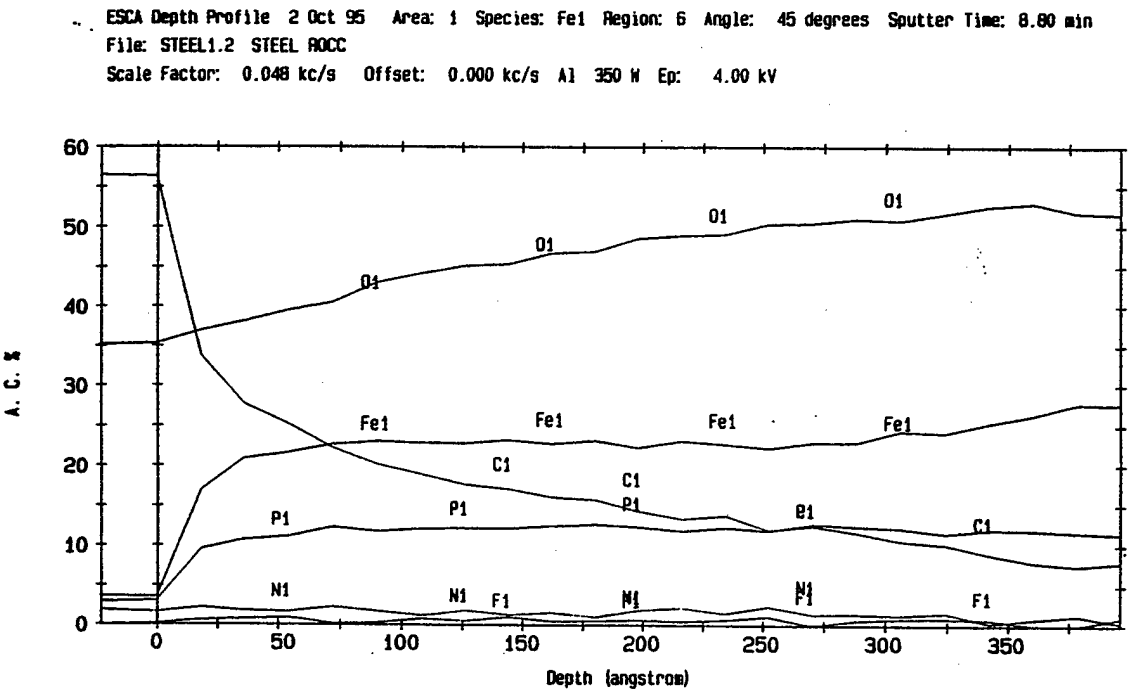

Figure 5. XPS Depth profile of ROCC Film on Steel.

NOVEL CHROMIUM-FREE SURFACE PRETREATMENT PROCESS FOR CORROSION INHIBITION

by

Francis L. Keohan, Hege J. Lizarralde, Peter Phillips and Anthony Arvanites
CAPE COD RESEARCH, INC.
East Falmouth, Massachusetts

Thomas M. Landy
U.S. Army Tank-automotive and Armaments Command
Tank-Automotive Research, Development and Engineering Center
ATTN: AMSTA-TR-E/MATL/267
Warren, MI 48397-5000

ABSTRACT

The need to eliminate hazardous materials and processes from pre-bond surface treatments has increased industrial interest in mechanical abrasion for cleaning, deoxidizing and roughening metallic adherends. The surface treatments described in this study use simpler and less hazardous means than traditional chemical etching to prepare metals for structural bonding and coating. The overall approach involved surface abrasion with both medium pressure water and abrasives and abrasive-free ultra high pressure water followed by treatment with aqueous organosilane solutions and chromium-free, waterborne primers. Both abrasive and non-abrasive pretreatments yielded excellent maintenance of paint adhesion and corrosion resistance under salt spray and GM Spec 9540P cyclic corrosion test conditions. Control adhesive pretreatments included the the P2 etch and phosphoric acid anodizing. The initial strength and durability of bonds prepared by standard and experimental pretreatment methods using bare and clad aluminum alloys of the 2XXX, 5XXX and 7XXX series and several commercial epoxy-based adhesives were measured by the tensile lap shear, floating roller peel, and wedge opening tests. The approach yielded adhesive bonds whose initial strength and durability in hostile environments met or exceeded those attained for adherends prepared by the control pre-bond surface treatments.

KEYWORDS: pretreatment, water jetting, adhesives, paint, abrasion, organosilanes, corrosion

1.0 INTRODUCTION

Abrasive blasting with high pressure water or hydrosanding is frequently used to remove paint, corrosion products and other contaminants from metallic surfaces when preparing articles for repainting. In the case of aluminum alloys, the next step in stabilizing the cleaned surface usually involves acid etching, chromate conversion coating or electrochemical anodization and the application of chromate-pigmented primers. Over the past two decades, environmental concerns have arisen regarding almost every aspect of cleaning, priming and painting metal surfaces. Present and anticipated environmental restrictions on the use of high volatile organic compound (VOC) primers and chromium compounds will have a great impact on manufacturing and repair operations. The costs of maintaining present metal finishing technologies in terms of waste stream treatment and disposal are expected to rise dramatically (1).

The combination of mechanical abrasion and organosilane coatings has been used as an alternative to traditional prebond surface treatments such the sulfo-chrome etch and chromic acid anodization (2-7). The techniques reported to date generally involve dry abrasive blasting followed by silane deposition or manual sanding in the presence of hydrolyzed organosilanes. An extension of this approach that provides simpler waste management and potentially more effective adhesion promotion is high-pressure blasting with partially hydrolyzed silane coupling agent solution and abrasive. (8) The method has been found to be effective for rapidly removing surface contaminants and metal oxides and replacing them with a primed layer containing silicate boundary layers. The PAST process incorporates the passivation of metal surfaces by the combination of mechanical abrasion from hydrosanding and interaction with hydrolyzed organosilane priming agents. The freshly exposed metal can be considered an activator for organosilane deposition and condensation. It has been demonstrated that organosilane films over ferrous and non-ferrous metals can inhibit corrosion and promote strong adhesion of paint and commercial adhesives (9).

Additional waste minimization was realized by increasing the water blasting pressure and removing solid abrasives such as aluminum oxide from the blast stream. The non-abrasive PAST (NA-PAST) process passivates metal surfaces by combining abrasive-free, mechanical abrasion from ultra high pressure water jetting and interaction with hydrolyzed organosilane priming agents. This report describes the paint removal, corrosion test results and adhesion performance of non-ferrous alloys prepared by the PAST and NA-PAST processes.

The objective was to develop an effective, easily applicable surface treatment for aluminum and titanium alloys to replace currently used prepaint methods that rely on toxic and corrosive chemicals such as chromate conversion coatings. The approach was to explore alternative methods of metal deoxidation and stabilization through hydrosanding and abrasive-free waterjet abrasion and application of an organosilane primer.

2.0 EXPERIMENTAL

2.1 PAST Pretreatment Process

The PAST process can consist of three or four steps:

1) The degreased metal substrates are first mechanically deoxidized by high pressure water/media blasting.
2) The deoxidized surfaces are treated with proprietary blends of hydrolyzed organosilanes in aqueous solution (note: the organosilane can be applied simultaneously during the hydrosanding by injecting concentrated solutions in the blast stream or it can be applied in diluted form after hydrosanding).
3) The organosilane passivation coating is dried at 93°C (200°F) for one hour.
4) A chromate-free, waterborne corrosion inhibiting adhesive primer is applied.

Four different types of abrasive media were evaluated in the PAST process: quartz sand or silica, aluminum oxide or alumina, magnetite, and sodium bicarbonate. The duration of the blasting was measured as an average of 15 seconds per 36 in^2 panel or 0.06 sec per cm^2 area. Variations of the process included different delay, or out times, between deoxidization and silane application, between silane application and priming, and between primer application and adhesive bonding. The PAST process was used to prepare adhesive bonded specimens for wedge, tensile lap shear and peel testing. In addition, PAST was used as a corrosion inhibiting pretreatment with experimental waterborne and commercial solvent-based primers on a variety of non-ferrous metals.

2.1.1 Abrasive PAST Application Equipment

The organosilanes were partially hydrolyzed by stirring in deionized water maintained at room temperature for a minimum of 45 minutes before using. Adherends were deoxidized by high pressure water/grit blasting using a Sprak Model EL-3000 hydrosander. Pressures between 1500-2500 psi at a stand-off distance of approximately 1 ft (0.3 m) were maintained during hydrosanding. In some cases, hydrolyzed organosilane was injected directly into the blast stream but generally it was applied by brush to surfaces that had been abraded with only water and media. The cleaned but still wet samples were typically dried in an air circulating oven maintained at 93°C (200°F) for one hour. These drying conditions have been found to be effective in curing organosilane coatings for adhesive bonding pretreatments (3,5).

2.2 Abrasive-Free NA-PAST Process

The NA-PAST process consists of similar steps as the PAST process, with the exception that the degreased metal substrates are first mechanically deoxidized by ultra-high pressure (30-50 ksi) water blasting.

2.2.1 NA-PAST Application Equipment

Pressures between 35-40 ksi and a stand off distance of approximately 1 ft (0.3 m) were maintained during hydrosanding. In some cases, hydrolyzed organosilane was injected directly into the blast stream but generally it was applied by brush to surfaces that had been water blasted. Blast-deoxidized surfaces would be kept wet with deionized water before silane solution application. The cleaned but still wet samples were typically dried in an air circulating oven maintained at 93°C (200°F) for one hour. These drying conditions have been found to be effective in curing organosilane coatings for adhesive bonding pretreatments (3,5).

The effects of blasting pressure, blast duration, and stand-off were studied. Blasting pressure could be controlled at the intensifier pump stage within approximately 2 ksi. Blast duration was controlled by varying the horizontal travel rate of the specimen.

2.3 Organosilane Solution Formulation and Coating Cure Study

2.3.1 Formulation of Organosilane-Based Aqueous Solutions

Preliminary surface passivating agent formulations were prepared by dissolving commercially available organosilanes such as 3-glycidoxypropyltrimethoxysilane (GLYMO) and 3-mercaptopropyltrimethoxysilane (MPTMOS) in deionized water at a concentration of 1 percent on a weight basis. The solutions were stirred at ambient temperature for a period of 45 minutes to one hour before applying to deoxidized metal substrates. Various additives including organic dyes, surfactants, acids, and other organosilanes were used in these formulations to alter such properties as hydrolysis rate, surface wetting, surface film coloration for visual quality determination, and solution stability.

Formulation Properties

Preliminary organosilane formulations were prepared by dispersing mixtures of commercially available organosilanes in deionized water. The organosilanes were chosen for their chemical compatibility with aluminum, titanium alloys and the components of typical corrosion-inhibiting primers. The degree of organosilane hydrolysis and aqueous solubility was controlled by formulation pH and by blending various organosilanes. The addition of organosilanes to water does not significantly change the viscosity but can have a dramatic effect on the surface wetting characteristics of the resulting solutions.

2.3.2 Surface Chemistry Analysis of NA-PAST-Treated Metals by FTIR

Fourier Transform Infrared (FTIR) Analysis was used to the analyze the nature of chemical bonding at the oxide surfaces prepared by PAST and NA-PAST. Thin gauge aluminum specimens were deoxidized by the NA-PAST method, treated with organosilane solution and their surface chemistry studied by FTIR. In some cases, neat samples of the organosilanes were analyzed in transmission mode between potassium bromide plates. Commercial grade aluminum

foil was also used as a substrate for depositing hydrolyzed organosilane films for surface IR analysis. A multiple internal reflectance (MIR) accessory was used to obtain the infrared spectra in most cases. The effects organosilane concentration, cure time and cure temperature on the condensation chemistry of deposited organosilane films were studied.

2.3.3 Surface Analysis by SEM-EDS, SAM and ESCA

Scanning electron microscopy (SEM) with energy dispersive X-Ray spectroscopy (EDS) is an analytical technique that qualitatively and quantitatively identifies the elemental composition of materials analyzed in an SEM. Beryllium windowed EDS detects all elements with atomic numbers greater than oxygen at concentrations greater than 0.1% and analyzes the top two microns of the sample.

Scanning Auger Microanalysis (SAM) is a surface analysis technique that determines elemental composition and some chemistry of surfaces and interfaces. SAM has a sampling depth of 2-3 nm providing analysis of films as thin as a few monolayers with a lateral resolution of 50 nm. Coating film depth determinations can be conducted by performing intermittent SAM with ion milling.

Electron Spectroscopy for Chemical Analysis (ESCA), also called X-ray Photoelectron Spectroscopy (XPS), is a surface analysis technique that provides composition and chemical bonding information about the top few atomic layers (2 nm) of the sample. ESCA can detect all elements heavier than helium. The elemental detection limit for ESCA id around 0.5 atomic percent. Like SAM, ESCA can also be combined with argon ion milling to perform depth profiling of surface layers.

2.4 DC Polarization Spectroscopy

The durability and performance of adhesive bonds and protective coatings in typical service environments depends to a large degree on the prevention of substrate corrosion. A dc polarization method was used to measure the corrosion inhibitor efficiency of the experimental and control surface treatments. Comparison of corrosion currents and corrosion voltages for treated and untreated metals allow the calculation of a corrosion rate which can be used to rank different precoating surface treatments. The analyses are performed in 5% aqueous sodium chloride solution maintained at 25°C and pH 7 using a Model 6310 electrochemical impedance analyzer equipped with a flat cell. Dc polarization plots are prepared from the electrochemical corrosion data and the corrosion rate in mils per year is then calculated.

2.5 Preparation of Aluminum Panels for Laboratory Cyclic Corrosion Testing

Corrosion test panels were prepared by the NA-PAST process for cyclic corrosion analysis. Water pressures of 40,000-45,000 psi was used to prepare Al 2024-T3, 6061-T6, and 5086-H321 panels. The experimental corrosion-inhibiting primer for this evaluation was ACP-6, which was found to yield the best and most consistent results in continuous salt spray testing (ASTM B117)

for samples prepared by the abrasive PAST process. Some of the NA-PAST-treated panels were primed with a commercial corrosion-inhibiting primer conforming to MIL-P-53022. Some of the primed panels were coated with a chemical agent resistant coating (CARC) topcoat conforming to MIL-C-46168 and some were not topcoated. These specimens and suitable controls (solvent degrease, alkaline clean, acid etch, desmut, Alodine®, MIL-P-53022) were tested in accordance with GM Spec 9540P, Method B and evaluated to ASTM D-1654, Procedure A. The test matrix is provided in Table 1.

2.6 Preparation of Test Panels for Outdoor Exposure

The PAST method (alumina media/MPD silane agent) and the optimized NA-PAST method were used to prepare coated test panels for outdoor exposure testing in Florida. Ten specimens per set were prepared for each condition. The test sample matrix is provided in Table 2.

2.7 Preparation and Testing of Aluminum Panels for Coating Abrasion and Chipping Resistance

The NA-PAST method was used to prepare sets of coated specimens for Taber abrasion testing and chip resistance testing. The test matrix is provided in Table 3.

The treated and primed panels were tested for abrasion resistance by the Taber Abraser method according to ASTM D4060-90 and for chipping resistance according to ASTM D3170-87.

2.8 Preparation of Aluminum Panels for Electrocoat Primer Application and Corrosion Testing

The set of blasting conditions (40,000 psi at a stand off distance of 0.5 in with a blasting rate of 1.25 in/s.) found most effective in promoting durable adhesive bonding was used to prepare a set of ten bare aluminum 2024-T3 panels for electrocoat primer application. The NA-PAST-deoxidized panels were exposed to a mist of hydrolyzed organosilane solution generated by an ultrasonic spray head inside a closed polyethylene chamber. The organosilane agent was specially formulated to yield a surface coating having high polarity to assist in the electrodeposition of primer. After approximately 5 minutes of exposure, the panels were cured in an air-circulating oven maintained at 93°C (200°F) for one hour.

3.0 RESULTS AND DISCUSSION

3.1 Organosilane Passivating Coating Cure Study and Surface Analysis

The hydrolysis and curing chemistry of simple organosilane films on glass and metallic surfaces have been studied at Cape Cod Research (5) and others in recent years. (10, 11) The application of aqueous organosilanes is, in essence, a form of sol-gel coating deposition. It has been demonstrated that controlling the silane film curing conditions is critical for achieving durable adhesive bonds. (3)

3.1.1 FTIR Analysis of Organosilane Passivating Films

Organosilane-treated aluminum surface characterization has revealed that MPTMOS-based wet sanding agents produce more hydrophobic surfaces than GLYMO-based agents.(6) Curing residual films of GLYMO hydrolysates at elevated temperature was generally found to produce rapid condensation of silanols. For residual films derived from 1% GLYMO solution, the extent of siloxane or silicate formation after one hour of curing at 93°C appeared roughly equivalent to that measured for room temperature curing for 24 hours. Room temperature curing of residual MPTMOS films appears to yield low and relatively stable levels of silanol functionality. The lower initial levels of silanol observed at room temperature may indicate that elevated temperature curing accelerates the hydrolysis of residual MPTMOS.

Films of the of the most effective organosilane blends used in the PAST and NA-PAST processes were applied from aqueous solution onto aluminum foil and cured under different conditions. The films were analyzed by FTIR Spectroscopy using a multiple internal reflectance technique. In this study, the TES-PDHI concentration in water was varied from 0.5% to 3% on a weight basis. Films were deposited onto clean aluminum foil from solutions that were pre-hydrolyzed in water for one hour and dried under different conditions.

For films derived from hydrolyzed TES-PDHI, the strong absorbance band at 2840 cm^{-1} corresponding to Si-OR diminished upon hydrolysis. The spectral region between 1100 and 1000 cm^{-1} corresponding to Si-O-Si bond formation and that between 3300-3100 cm^{-1} corresponding to the disappearance of Si-OH bonds were monitored to follow the silane polymerization on aluminum surfaces. In some cases, FTIR spectra of adequate signal to noise ratio could not be obtained by this technique, particularly for the films derived from 0.5% solution and those cured at elevated temperature for extended periods. Absorbance bands between 2800 and 2950 cm^{-1} corresponding to Si-OR functionality appear to be weaker for freshly deposited films (those dried at ambient temperature for under one hour) derived from the lower concentration solutions. All of these uncured films also show strong infrared absorbance in the 3500-3100 cm^{-1} region corresponding to silanol and absorbed water. Note the low level of absorbance in this region for the spectrum derived from neat TES-PDHI.

Curing or drying the film deposits at ambient temperature was not found to produce large changes in the absorbance bands. Room temperature curing appears to yield moderate and relatively stable levels of silanol functionality. Films derived from all three TES-PDHI concentrations yielded spectra having strong absorbance in the 3500-3100 cm^{-1} region due to unreacted silanol groups. Drying for over 24 hours at room temperature did not appear to significantly alter their chemistry.

Elevated temperature curing residual films of TES-PDHI hydrosylates, like those derived form GLYMO and MPTMOS was generally found to produce rapid condensation of silanols. The lower initial levels of silanol at room temperature may indicate that elevated temperature accelerates the hydrolysis of residual organosilane. For the 1% TES-PDHI solution case, curing

for one hour at 93°C produced a significant degree of silanol condensation while overnight cure at this temperature appeared to completely consume the silanol groups and dehydrate the film.

Monitoring the extent of siloxane or silicate formation over time for TES-PDHI residues on aluminum yielded somewhat less distinct curing trends. The expected behavior would be an increasing level of siloxane content with increasing time and temperature. Films derived from 0.5% and 1% TES-PDHI solutions basically showed this behavior. Absorbance bands in the region between 1100 and 1000 cm^{-1} corresponding to Si-O-Si bond formation tend to broaden, shift to lower frequency and become more intense as the films are cured at both 60°C and 93°C.

3.1.2 SEM-EDS Analysis of Metal Surfaces Treated by NA-PAST

The surfaces of aluminum panels treated by NA-PAST and control pretreatments were examined by scanning electron microscopy (SEM). Selected specimens were also analyzed for surface elemental content by energy dispersive X-ray spectroscopy (EDS). The SEM images of bare 2024-T3 panels treated with a commercial chromate conversion coating are shown in Figure 1.

The features of the chromate conversion coated panel before cyclic corrosion chamber exposure indicate that a smooth and relatively uniform surface was obtained. After corrosion testing, however, even the control treatment shows signs of pitting and corrosion. Figure 2 shows the surface of a bare 2024-T3 panel after NA-PAST treatment and silane passivation.

3.1.3 SAM and ESCA Analyses of Metal Surfaces Treated by PAST Silane Sealing Processes

The surfaces of aluminum panels treated by PAST silane sealing pretreatments after solvent degreasing were examined by scanning Auger microanalysis (SAM) for surface elemental content. The treated specimens were also subjected to argon ion milling to produce a depth profile showing changes in elemental concentration with depth. The method was used to measure the effects of the various organosilane agents and solution deposition processes on the thickness and chemical content of surface oxide layer and silane sealing layers.

The outermost surface of the untreated (degreased only) bare 2024-T3 specimen was primarily aluminum oxides 150-200 Angstroms thick. The SAM analysis uncovered the presence of sulfur and other trace elements found on the sample's surface – these presumably were contaminants that could not be removed by simple degreasing with acetone. The type of organosilane stabilizing agent and method of deposition was found to have an effect on the thickness of residual films left on the treated metal surfaces. Immersion deposition processes (20 minutes immersion followed by thorough rinsing with deionized water) appeared to yield thicker silane-rich layers for the MPD and MGAMo silanes than simple brush application with no rinsing. The method of deposition did not appear to affect the thickness of the layers of the MATG silane agent. The presence of significant quantities of elements such as sulfur, carbon, nitrogen, and phosphorus can be traced to the chemistry of the organosilane formulations. The detection of significant quantities of copper and fluorine on the treated

surfaces was somewhat puzzling. While copper is the primary alloying element in 2XXX series aluminum, these panels were clad with commercially pure aluminum. Perhaps the appearance of copper may be due to dissolution of copper ions form the unprotected sides of the specimens and deposition onto the surface. The overall thickness of the oxide was not significantly higher than before etching, however. Fluoride was not used during the processing of these panels and its source remains unresolved. Selected silane-treated aluminum and titanium 6/4 specimens were analyzed by ESCA for surface chemistry.

The NA-PAST-deoxidized and MPTMOS-sealed 2024-T3 bare aluminum surfaces were scanned to identify the presence of different elements and their chemical states. The results show the chemical states of silicon in the top few molecular layers of the treated aluminum surface. Evidence of organosilane, siloxane and silicate bonding was detected. This result is important in that it shows that the deposition and cure conditions used in the PAST process yield some degree of inorganic silicate formation which is believed essential in promoting adhesion and corrosion inhibition. When focused on the organic region, ESCA shows the presence of organosulfur groups as well as bonding states for carbon (C-O- and carbonyl) that suggest some oxidation of the organic portion of the organosilanes occurred. ESCA analysis of NA-PAST-treated titanium 6Al-4V alloy show the same organosilane, siloxane and silicate bonding observed in the aluminum sample in addition to titanium oxides.

3.2 DC Polarization Results for Aluminum Alloys Prepared by PAST, NA-PAST and Control Pretreatments

The properties of aluminum alloys treated by the PAST process and control processes were studied by dc polarization analysis. The corrosion rate in mils/year is calculated from dc polarization data taken in aqueous NaCl solution at room temperature. Aluminum specimens were treated by different deoxidation and stabilization methods including organosilane coating for polarization analysis. The different pretreatments used to prepare standard G-2 pellets fabricated from bare Al 2024-T3 alloy for dc polarization studies are described in Table 4 and the dc polarization test results are presented in Table 5.

The dc polarization corrosion test results show the expected trend of lower corrosion rates for the 2024-T3 aluminum alloy samples that had been deoxidized via the P2 etch or by hand abrading with a red Scotch-Brite pad, sealed with either hydrolyzed GLYMO or MPD organosilanes and primed with the experimental ACP-III primer as compared to that which had been simply degreased. Additional panels were prepared from bare aluminum 2024-T3 alloy panels that were water blasted by the NA-PAST method for testing in the flat cell setup.

The application and cure of two organosilane blends (MPD and MGAMo) over a ultra high pressure waterjet abraded surface were tested for corrosion inhibition. The methods used to prepare bare Al 2024-T3 alloy panels for dc polarization studies are described in Table 6 and the dc polarization test results are provided in Table 7.

Water blast abrasion followed by stabilization with the organosilane blend MPD was found to yield improved corrosion resistance over Al 2024-T3 having a native oxide coating. The higher corrosion rate observed for the water blasted aluminum alloy sealed with the polarity-modified silane blend MGAMo may have to do with the high surface area and porosity and higher ionic conductivity produced by the abrasion/silane sealing process. It should be noted that the corrosion rates measured for these samples are for unprimed metal and cannot be directly compared to the results in Table 5.

3.3 Corrosion Test Results for Specimens Treated by PAST Method

Test panels prepared by the PAST method from Al 5083-T3, Al 2024-T3, and Ti 6Al-4V adherends in conjunction with an experimental, waterborne, chromate-free corrosion inhibiting primer and a control primer formulation were tested per ASTM B117 continuously for 1,000 hours and 2,000 hours respectively. The exposed scribed specimens were rated for coating durability according to ASTM D1654. The process conditions and experimental sample matrix are described in Tables 8 and 9. The results of the corrosion testing are provided in Table 10.

The corrosion and paint durability results for titanium alloy specimens treated by the PAST-1 process was excellent. No corrosion, paint blistering of adhesion loss was observed after 1000 hours of salt spray (ASTM B117). Specimens prepared from aluminum 2024-T3 (WAB:MP/DP/N-1:24:III) showed the greatest amounts of corrosion and topcoat blistering. When blistering occurred, it tended to be between the primer and topcoat. The performance of samples primed with a solvent-based commercial primer conforming to MIL-P-53022 and the experimental waterborne primer ACP-3 was equivalent for this exposure time. The sample prepared without a topcoat had no blistering and excellent primer coat adhesion.

Samples prepared from Al 5083-H321 panels (WAB:MP/DP/N-1:50:III) generally showed less corrosion than the 2024-T3 sets. The performance of samples primed with MIL-P-53022 and the experimental waterborne primer ACP-3 was equivalent for this exposure time. The sample prepared without a topcoat had no blistering and only a slight amount of corrosion around the scribe line. The alumina abrasive PAST process was used to prepare sets of corrosion test panels to examine the effects of using a different organosilane blend after hydrosanding and omitting the organosilane passivation step completely. The process conditions and experimental sample matrix are described in Tables 11 and 12. The results of the corrosion testing are provided in Table 13. The corrosion test results for PAST-I-treated titanium specimens after 2,000 hours of salt spray testing are also included.

The corrosion and paint durability results for titanium alloy specimens treated by the PAST-1 process was excellent. No corrosion, paint blistering of adhesion loss was observed after 2,000 hours of salt spray exposure.

Specimens prepared from bare aluminum 2024-T3 showed the greatest amounts of corrosion and topcoat blistering. When blistering occurred, it tended to be between the primer and topcoat. The performance of samples primed with the experimental waterborne primer ACP-3 and MIL-

P-53022 was equivalent for this exposure time. The samples prepared without a post abrasion silane treatment had significantly more blistering and corrosion outside of the scribe lines.

Samples prepared from Al 5083-H321 panels generally showed less corrosion than the 2024-T3 sets. The performance of samples primed with ACP-3 and MIL-P-53022 was equivalent for this exposure time. The samples prepared without a post abrasion silane treatment had more blistering and corrosion outside of the scribe lines. The results of these corrosion tests also showed that the MPTMOS/DNP (9:1) silane gave superior results in the PAST process than the MPTMOS/DPE/DNP (8:1:1) silane agent when used with the ACP-3 anticorrosive primer.

Two sets of corrosion test samples were prepared from aluminum alloys 2024-T3 and 5083-H321 using the alumina abrasive/MPD silane PAST process and a new experimental anticorrosive primer, ACP-4. This waterborne formulation was formulated with different anticorrosive pigments than previously tested primers. Panels were also prepared by the same process and primer formulation ACP-3 for comparison. All primed panels were coated with a topcoat conforming to MIL-C-46168. The corrosion test results after 1,000 hours of salt spray exposure are provided in Table 14.

The paint adhesion and corrosion test results after 4 week of continuous salt spray exposure indicate that this primer may be superior in corrosion inhibiting capacity than ACP-3 or MIL-P-53022, particularly for corrosion-prone alloys of the 2XXX series. The degree of blister formation was significantly lower for PAST/ACP-4 treated 2024-T3 substrates, even at the edges of the coated panels.

Effect of Titanate Salt-Modified Silane Passivation Agents on Corrosion Inhibition

The use of acidic titanium salt solutions as co-stabilizing agents with the organosilanes was evaluated as a means of depositing titanium complexes on the surface to catalyze surface organosilane polymerization during the sealing step. Titanates are well known catalysts for promoting siloxane condensation and are frequently used themselves as coupling agents for coatings and adhesives. The titanate-modified pretreatment process PAST-II was conducted as follows: After water/alumina blasting treatment, the samples were removed, immersed in the 1 % aqueous titanate solutions for a period of 10 minutes at room temperature. After immersion, the adherends were thoroughly rinsed in tap and deionized water and dried in an air circulating oven maintained at 100 °C for 15 min. They were then treated by the usual organosilane deposition treatment and priming procedure. Corrosion test specimens prepared from PAST-treated Al 2024-T3 primed with waterborne primer formulations ACP-5 and ACP-6 were also tested by 1,000 hours of salt spray exposure. The sample preparation methods for these experiments are described in Table 15 , the sample test matrix in Table 16 and the corrosion test results in Table 17.

The effect of pretreating freshly hydroblasted aluminum with aqueous solutions of titanium salts was generally found to be positive in terms of corrosion prevention and coating adhesion. The titanium oxalate treatment, in particular, appeared to prevent the formation of blisters, even from

the sides of the coated panel. Primer formulation ACP-5, which contained a different anticorrosive agent package than previous waterborne formulations was not found to be effective in preventing blister formation. The anticorrosive agent combination used in primer formulation ACP-6, however, yielded excellent coating adhesion results with no visible blister formation.

The control pretreatment for these three alloys consisted of degreasing with acetone, cleaning with Duraprep-120 alkaline solution, deoxidizing with acidic Alumiprep 33, desmutting with Duraprep-420, rinsing with deionized water, drying under ambient conditions and priming with MIL-P-53022. The conditions used to prepare the PAST-I treated corrosion test specimens can be found in Tables 15 and 16. The Al 2024-T3, Al 6061-T6 and Al 5083-H321 alloy panels were tested for corrosion resistance under cyclic exposure (per GM Spec 9540P, Method B) and rated according to ASTM D1654. The corrosion test results after 1,000 hours of cyclic exposure are provided in Table 18.

The paint adhesion and corrosion test results after 1000 h of concurrent corrosion cycles indicate that this pretreatment and waterborne primer may be equivalent or even superior in corrosion inhibiting capacity to MIL-P-53022, particularly for corrosion-prone alloys of the 2XXX series. The degree of blister formation on the 2024-T3 alloy treated by the control method (CCC:MP:TC:24) was surprisingly high and may be a function of the pre-conversion coat cleaning and deoxidation methods used.

3.4 Corrosion Testing of Specimens Treated by Hydrogen Peroxide Etch and Anticorrosive Primer ACP-6

Two prebond surface treatments that had been used successfully used to treat aluminum alloys for bonding were also tested as corrosion inhibiting treatments for painted metals. Two sets of bare Al 2024-T3 and bare 6061-T6 were treated by : acetone degreasing, acid deoxidization with Alumiprep 33, etching with transition metal complex-promoted aqueous hydrogen peroxide, sealing with MPTMOS solution, and priming with a waterborne chromate-free experimental primer. The latter primer formulation (ACP-6) was developed and successfully tested over PAST-treated surfaces for corrosion resistance in this program. The specimens were sent to the Army Research Laboratory (ARL), Ft. Belvoir, VA for coating adhesion and corrosion testing.

The wet adhesion test was performed as an initial screen. The coated panels were immersed in room temperature water for 24 hours, scribed in a cross hatched pattern according to FED-STD-141, method 6301.2 and tested for tape adhesion. The remaining specimens were scribed to the bare metal on the lower half of the panel and aged in a salt spray cabinet for 336 hours according to ASTM B117. The condition of the scribe lines was noted after salt spray exposure and the upper half of the panels were tested for chipping resistance according to ASTM D3170-7. The results of this testing are provided in Table 19.

The results indicate that the chromium-free CM-50 etch/MPTMOS seal/ACP-6 primer performs as well as Alodine 1200 and a primer conforming to MIL-P-53030 on aluminum in terms of wet adhesion and salt spray resistance.

We also prepared panels from 2024 and 6061 alloys with each of the experimental pretreatments (without any additional primers or topcoats), scribed the panels to the bare metal and aged them in a salt spray cabinet for 1,000 hours. The ACP-6 primed panels were then evaluated for corrosion resistance according to ASTM D1654. The results are provided in Table 20.

The results obtained for both systems were comparable to the best results observed for PAST-treated Al 2024-T3 substrates. Taken with the coating adhesion results obtained at Ft. Belvoir, the CM-50 etch treatment in combination with the ACP-6 anticorrosive primer provides an effective chromium-free surface treatment for aluminum alloys. Such a process would be applicable in a manufacturing environment where treating complex shaped parts might be difficult with abrasion deoxidation methods.

3.5 Corrosion Testing of Specimens Treated by NA-PAST Method

Coated corrosion test specimens (ten specimens per condition) prepared from Al 2024-T3, 5086-H32, and Al 6061-T6 alloys by the optimized NA-PAST/MPD/ACP-6 process and control pretreatments were tested for corrosion resistance under cyclic exposure (per GM Spec 9540P, Method B) and found to exhibit excellent corrosion resistance as rated according to ASTM D1654. The corrosion test results after 2,000 hours of cyclic exposure are provided in Table 21. The NA-PAST pretreatment yielded excellent corrosion resistance for all of the aluminum alloys tested and was found to be most effective on the 5XXX series aluminum substrate. In general, the ACP-6 waterborne primer was more effective over NA-PAST-treated substrates than the control (MIL-P-53022).

Coated corrosion test specimens (ten specimens per condition) were prepared from cold rolled steel Q-Panels by the optimized NA-PAST/MPD/ACP-6 process and control pretreatments and tested for corrosion resistance under cyclic exposure (per GM Spec 9540P, Method B). The control pretreatment was a Q-panel-supplied zinc phosphate coating (ZPC). The corrosion test results, as rated according to ASTM D1654 after 200 hours of cyclic exposure are provided in Table 22. In addition, three corrosion-resistant metal alloys (titanium 6/4, 301 stainless steel, and cartridge brass) were prepared from by the optimized NA-PAST/MPD/ACP-6 process and tested for corrosion resistance under cyclic exposure. Those corrosion test results are provided in Table 23.

The corrosion resistance measured for the bare CRS substrates prepared by the optimized NA-PAST/MPD/ACP-6 process compared quite favorably with the zinc phosphate control. The most sensitivity was found for panels primed with MIL-P-53022. Zinc phosphate-coated CRS panels primed with the control primer exhibited the highest degree of blistering around the scribed areas.

Excellent corrosion prevention and primer coating adhesion maintenance was observed for the three corrosion-resistant alloys prepared by NA-PAST with both waterborne ACP-6 primer and MIL-P-53022.

3.6 Corrosion Test Results for Aluminum Prepared by NA-PAST with Electrocoat and Powder Coat Primers

The effect of modifying the silane sealing agent for better compatibility with E-coat primers produced mixed results in wedge adhesion durability tests. Silane treatment MATG appeared to yield the best results in terms of crack growth and failure mode. This treatment was used to prepare a set of 10, 3 x 5 inch bare 2024-T3 aluminum panels for E-coat primer application at the National Defense Center for Environmental Excellence (NDCEE). 2 sets of bare Al 5083-H321 aluminum panels were pretreated by NA-PAST with MGAMo silane sealer and primed by both by both E-coat and powder coat and primer application processes at NDCEE. The NA-PAST-treated panels were all successfully primed by these methods and tested for initial adhesion, primer coat hardness, impact resistance, flexibility, solvent resistance and salt spray resistance. The pretreatment performance test results are summarized in Tables 24 through 29.

The mechanical properties listed in Table 24 show that the NA-PAST pretreatment yields a substrate surface that promotes strong bonding with a commercial electrocoat primer. The corrosion inhibiting qualities of the surface were also found to be acceptable. Table 25 shows that bare Al 2024-T3 panels prepared by the NA-PAST/e-coat primer combination showed coating adhesion maintenance in excess of 400 hours in salt spray. This corrosion test rating exceeds the requirement for the U.S. Army's CARC system (MIL-C-53072B).

The mechanical and corrosion test results for panels prepared from bare aluminum armor alloy 5083-H321 by the NA-PAST/MGAMo seal process with both e-coat and powder coat primers are summarized in Tables 26-29.

The NA-PAST/MGAMo pretreatment combination appears to greatly exceed the corrosion resistance requirements of MIL-C-53072B when used with either e-coat or powder coat primers on bare Al 5083-H321 alloy. It would be recommended that this pretreatment be evaluated with other aluminum alloys and with non-abrasion deoxidation processes.

3.8 Coating Abrasion and Chip Resistance Testing of Specimens Treated by NA-PAST Method

Coated test specimens prepared from Al 2024-T3, 5086-H32, and Al 6061-T6 alloys by the optimized NA-PAST/MPD/ACP-6 process and control pretreatments were tested for Taber abrasion resistance according to ASTM D 4060-84 and for chip resistance according to ASTM D3170-87. The results are summarized in Tables 30 and 31, respectively.

It would appear that the control primer (MIL-P-53022) is somewhat more abrasion resistant than the experimental ACP-6 waterborne primer. However, the Taber abrasion test data contains too much scatter to definitively compare the primers and surface treatments. The experimental PAST and NA-PAST processes in conjunction with the ACP-6 primer produced good chip resistance on the three alloys tested.

4.0 CONCLUSIONS

The PAST process has been shown to be an effective prebond and prepaint surface treatment for aluminum and titanium structure. The method consists of hydrosanding either in the presence of aqueous organosilane solution or with water and abrasive followed shortly by organosilane deposition and by priming with a waterborne corrosion inhibiting adhesive primer (WB-CIAP). The most effective abrasive was found to be finely divided alumina. This media yielded the most uniformly abraded surfaces without severe structural deformation. The effect of delay or out time between process steps was found to be critical for optimum adhesive bond durability. The time between silane application and priming was found to be most important and should be kept below 24 hours at room temperature. The delay time between primer application and bonding was not found to be as critical. The degree of bond durability was found to be best for low copper aluminum alloys such as 5083, chromium-aluminum alloys such as 7075 and clad alloys. Tensile lap shear and roller peel test results demonstrated that the PAST abrasion/WB-CIAP primer combination yields high-strength adhesive bonds with excellent resistance to elevated temperature and humidity. Excellent retention of paint adhesion and corrosion resistance was demonstrated for non-ferrous metals pretreated by the optimized PAST process. The abrasive/water PAST method has yielded excellent bond durability and corrosion inhibition under hot/wet, continuous salt spray and cyclic corrosion conditions with a number of different aluminum alloys including bare and clad 2024-T3, 6061-T6, 7075-T6, and 5083-H321.

Specifically, the Phase II research program for development of the abrasive PAST process resulted in the following observations and accomplishments:

- Silica, magnetite, alumina and sodium bicarbonate particles were evaluated in PAST process

- PAST using 150 grit alumina found to yield the best adhesive bond durability and surface abrasion uniformity

- Organosilane solutions injected with blast media and applied after blasting
  Both methods tested and found effective in adhesive bonding applications

- Effective chromate and lead-free, epoxy-siloxane-based primers developed
  RT-curing waterborne primers prepared and tested
  Theoretical VOC content below 100 g/l

- Mechanical adhesive properties found to be equal to or better than those measured with samples prepared with control pretreatments and solvent-based primers

- Adhesion durability (as measured by wedge test) equivalent to that obtained with solvent-based and control primer and surface preparation methods

- Excellent bond durability in hot/wet exposure for alloys bare 2024-T3,

clad 2024-T3, bare 7075-T6, and bare 5083-H321

- Excellent bond and coating durability in salt spray exposure for bare alloys 2024-T3, 6061-T6 and 5083-H321

- Pretreating aluminum alloys for adhesive bonding by deoxidizing with the chromate-free P2 etch followed by MPD-1 silane agent and waterborne CIAP was also found to yield good bond durability under prolonged hot/wet exposure

- Excellent coating durability and corrosion resistance to salt spray exposure for titanium alloy Ti 6Al-4V

This research program has also demonstrated that ultra high pressure water abrasion coupled with organosilane deposition is an effective process for deoxidizing non-ferrous metals and preparing them for painting and adhesive bonding. The method consists of high pressure blasting adherend surfaces either in the presence of aqueous organosilane solution or with water followed shortly by organosilane deposition and by priming with a WB-CIAP. The non-abrasive primer activated surface treatment (NA-PAST) has been shown to be a viable alternative to corrosive chemical deoxidizing and chromate conversion coating in pre-paint treatments for metals and as an alternative to chromate etching and anodizing in prebond surface treatments.

Specifically, the NA-PAST research program resulted in the following observations and accomplishments:

- Prototype NA-PAST apparatus built and successfully tested

- Rapid paint removal and metal surface abrasion demonstrated by NA-PAST

- NA-PAST-treated aluminum specimens exhibited comparable corrosion resistance and paint adhesion to specimens treated by control methods including chromate conversion coatings after 2,000 h of cyclic corrosion test exposure (GM Spec 9540P)

- NA-PAST-treated 2024-T3 aluminum specimens readily accepted a commercial electrocoat primer and the resulting panels exhibited excellent corrosion resistance and primer adhesion durability after 2,000 h of salt spray test exposure (ASTM B117).

- NA-PAST-treated 5083-H321 aluminum specimens readily accepted both powder and electrocoat primers and the resulting panels exhibited excellent corrosion resistance and primer adhesion durability after 3,500 h of salt spray test exposure (ASTM B117).

- NA-PAST-treated aluminum specimens have exhibited comparable adhesive bond mechanical properties and bond durability under hot/wet conditions to specimens treated by control processes including phosphoric acid anodizing and chromated primers with a number of different aluminum alloys.

The most effective set of blasting conditions for adhesive bonding with aluminum alloys was found to be: 40,000 psi at a stand off distance of 0.5 in with a blasting rate of 1.25 in/s. These parameters yielded the most uniformly abraded surfaces without severe structural deformation. The effect of delay or out time between process steps was found to be critical for optimum adhesive bond durability. The time between waterjet abrasion and silane application was found to be the most important and should be kept as short as possible not exceeding one hour. The time between silane application and priming was found to be most important and should be kept below 24 hours at room temperature. The out time between silane cure and e-coat primer application for paint primers does not appear to be as critical. The degree of bond durability was found to be best for low copper aluminum alloys such as 5083.

Acknowledgments:

The authors are grateful to Mr. I. Carl Handsy and Mr. Donald T. Ostberg from the U.S. Army Tank-Automotive Research, Development and Engineering Center (Warren, MI) for their invaluable technical inputs and suggestions during the investigation and preparation of this work and final report.

5.0 REFERENCES

1. B.R.W. Hinton, Metal Finishing, 55, September, (1991).

2. U.S. Pat. 5,015,506, (May 14, 1991) W. M. Purcell, (to the U.S. Air Force).

3. R. J. Kuhbander and J. J. Mazza, SAMPE International Symposium, 38, 1225, (1993).

4. F. L. Keohan, A. J. Mitchell, C. C. Ragan, and L. J. Bialic, SAMPE International Symposium, 38, 1181, May, 1993.

5. F. L. Keohan, A. J. Mitchell, J. A. Adelstein, and A. C. Arvanites, SAMPE International Symposium, 39, 1116, (1994).

6. F. L. Keohan, A., J. A. Adelstein, and A. C. Arvanites, SAMPE International Symposium, 39, 1130, (1994).

7. S. H. McKnight and J. W. Gillespie, Jr., SAMPE International Symposium, 39, 2760, (1994).

8. F. L. Keohan, H. J. Lizarralde, A. C. Arvanites and I. C. Handsy, SAMPE International Symposium, 40, 1170, (1995).

9. L. J. Matienzo, D. K. Shaffer, W. C. Moshier, and G. D. Davis in R. A. Dickie and F. L. Floyd, eds., Polymeric Materials for Corrosion Control, ACS Symposium Series, Washington, D. C., 1986, pp. 234-249.

10. Allen, K. W. and Stevens, M. G., *J. Adhesion*, **14**, 137, 1982.

11. Shachat, N. and Li, Y.-Z., Proceedings of the 20th Water-Borne, Higher-Solids, & Powder Coatings Symposium, p 383, 1993.

Figure 1 SEM Photomicrographs of Chromate Conversion Coated Bare Al 2024-T3 Panel Before and After 20 Corrosion Test Cycles (1000X)

Figure 2 SEM Photomicrographs of NA-PAST-Treated Bare Al 2024-T3 Panel Before Corrosion Testing (500X)

Table 1
Corrosion Test Sample Matrix

Sample	Alloy	Pretreatment*	Primer	Topcoat
NAP:P-6:TC:24	2024-T3	NA-PAST	ACP-6	MIL-C-46168
NAP:P-6:24	2024-T3	NA-PAST	ACP-6	none
NAP:MP:24	2024-T3	NA-PAST	MIL-P-53022	none
CCC:MP:TC:24	2024-T3	AlC/AcD/Alodine	MIL-P-53022	MIL-C-46168
NAP:P-6:TC:60	6161-T6	NA-PAST	ACP-6	MIL-C-46168
NAP:P-6:60	6161-T6	NA-PAST	ACP-6	none
NAP:MP:60	6161-T6	NA-PAST	MIL-P-53022	none
CCC:MP:TC:60	6161-T6	AlC/AcD/Alodine	MIL-P-53022	MIL-C-46168
NAP:P-6:TC:50	5083-H32	NA-PAST	ACP-6	MIL-C-46168
NAP:P-6:50	5083-H32	NA-PAST	ACP-6	none
NAP:MP:50	5083-H32	NA-PAST	MIL-P-53022	none
CCC:MP:TC:50	5083-H32	AlC/AcD/Alodine	MIL-P-53022	MIL-C-46168

Table 2
Outdoor Exposure Test Sample Matrix

Sample	Alloy	Pretreatment*	Primer	Topcoat
NAP:P-6:TC:24	2024-T3	NA-PAST	ACP-6	MIL-C-46168
NAP:P-6:24	2024-T3	NA-PAST	ACP-6	none
NAP:MP:24	2024-T3	NA-PAST	MIL-P-53022	none
WAB:MPD-1:24B:I	2024-T3	PAST-1	ACP-6	MIL-C-46168
CCC:MP:TC:24	2024-T3	AlC/AcD/Alodine	MIL-P-53022	MIL-C-46168
NAP:P-6:TC:60	6161-T6	NA-PAST	ACP-6	MIL-C-46168
NAP:P-6:60	6161-T6	NA-PAST	ACP-6	none
NAP:MP:60	6161-T6	NA-PAST	MIL-P-53022	none
WAB:MPD-1:61B:I	6161-T6	PAST-1	ACP-6	MIL-C-46168
CCC:MP:TC:60	6161-T6	AlC/AcD/Alodine	MIL-P-53022	MIL-C-46168
NAP:P-6:TC:50	5083-H32	NA-PAST	ACP-6	MIL-C-46168
NAP:P-6:50	5083-H32	NA-PAST	ACP-6	none
NAP:MP:50	5083-H32	NA-PAST	MIL-P-53022	none
WAB:MPD-1:50B:I	5083-H32	PAST-1	ACP-6	MIL-C-46168
CCC:MP:TC:50	5083-H32	AlC/AcD/Alodine	MIL-P-53022	MIL-C-46168

* AlC = Cleaned with alkaline Duraprep™ 120 aluminum cleaner (Shipley Company, Inc.)
AcD = Deoxidized with Duraprep™ 320 acid etch (Shipley Company, Inc.)
Alodine = Alodine® 1201, chromate conversion coating (Parker+Amchem Corp.)

Table 3
Abrasion and Chipping Resistance Test Sample Matrix

Sample	Alloy	Pretreatment*	Primer
AP:P-6:24	2024-T3	PAST	ACP-6
NAP:P-6:24	2024-T3	NA-PAST	ACP-6
NAP:P-6:TC:60	6161-T6	NA-PAST	ACP-6
CCC:MP:TC:60	6161-T6	AlC/AcD/Alodine	MIL-P-53022
NAP:P-6:50	5086-H32	NA-PAST	ACP-6

* AlC = Cleaned with alkaline Duraprep™ 120 aluminum cleaner (Shipley Company, Inc.)
AcD = Deoxidized with Duraprep™ 320 acid etch (Shipley Company, Inc.)
Alodine = Alodine® 1201, chromate conversion coating (Parker+Amchem Corp.)

Table 4
Aluminum Pretreatment Conditions for Al 2024-T3
DC Polarization Test Samples

SAMPLE	SAMPLE PREPARATION CONDITIONS			
	Step 1	Step 2[a]	Step 3[b]	Step 4
2024/UC	degreased			
2024/P2/GS/ACP	degreased	P2 Etch	1% GLYMO	ACP-III prime
2024/HA/MPD/ACP	degreased	Hand abraded	1 % MPD-1	ACP-III prime
2024/P2/MPD/ACP	degreased	P2 Etch	1 % MPD-1	ACP-III prime

Table 5
Corrosion Rate Test Results for Al 2024-T3 Alloy in
3% NaCl Solution (SCE Reference)
(G-2 Pellets)

SAMPLE	I_{corr} ($\mu A/cm^2$)	E (I=0) (V)	CORROSION RATE (mils per year)
2024/UC	3.13	-0.523	1.5
2024/P2/GS/ACP	0.005	-0.650	0.002
2024/HA/MPD/ACP	0.023	-0.680	0.010
2024/P2/MPD/ACP	0.033	-0.668	0.014

Table 6
Aluminum Pretreatment Conditions for Al 2024-T3
DC Polarization Test Samples

SAMPLE	SAMPLE PREPARATION CONDITIONS		
	Step 1	**Step 3[b]**	**Step 4**
2024/UC	degreased		
2024/UHPWB/MPD	degreased	40ksi/0.5in/1.25ins^{-1}	MPD silane
2024/UHPWB/MGAMo	degreased	40ksi/0.5in/1.25ins^{-1}	MGAMo silane

a: abrasion code a/b/c: where a = water pressure, b = stand-off distance, and c = blasting rate h or rate of stepping motor moving substrate in horizontal direction

Table 7
Corrosion Rate Test Results for Al 2024-T3 Alloy in
3% NaCl Solution (SCE Reference)

SAMPLE	I_{corr} ($\mu A/cm^2$)	E (I=0) (V)	CORROSION RATE (mils per year)
2024/UC	3.13	-0.523	1.5
2024/UHPWB/MPD	1.04	-1.194	0.44
2024/UHPWB/MGAMo	8.89	-1.173	3.71

Table 8
Sample Preparation Conditions for PAST-I-Treated
Nonferrous Alloy Panels
2000 psi / 150 grit Alumina / 0.4 sec per in^2 Blast Duration
1% Aqueous Silane Applied after Grit Blasting

Sample #	Silane Solution Concentration (Wt. %)	Silane Type	Silane Dry Time Temp./Time (^oC/hr)	Primer Formulation ID #	Primer Dry Temp./Time (^oC/hr)
WAB:GLY-1:III	1	GLYMO	93/1	ACP-3	22/120
WAB:MP/DP/N-1:III	1	MPTMOS/DPE/DNP (8:1:1)	93/1	ACP-3	22/120

Table 9
Corrosion Test Sample Matrix for PAST-I-Treated Non-Ferrous Metals

Sample	Alloy	Pretreatment	Primer	Topcoat
WAB:GLY-1:Ti:III	Ti 6Al-4V	PAST-1	ACP-3	MIL-C-46168
WAB:MP/DP/N-1:Ti:III	Ti 6Al-4V	PAST-I	ACP-3	MIL-C-46168
WAB:MP/DP/N-1:24:III	Al 2024-T3	PAST-I	ACP-3	MIL-C-46168
WAB:MP/DP/N-1:24:III	Al 2024-T3	PAST-I	ACP-3	----------
WAB:MP/DP/N-1:24:III	Al 2024-T3	PAST-I	MIL-P-53022	MIL-C-46168
WAB:MP/DP/N-1:50:III	Al 5083-H321	PAST-I	ACP-3	MIL-C-46168
WAB:MP/DP/N-1:50:III	Al 5083-H321	PAST-I	ACP-3	----------
WAB:MP/DP/N-1:50:III	Al 5083-H321	PAST-I	MIL-P-53022	MIL-C-46168

Table 10
Coating Performance Ratings for PAST-I-Treated Metal Samples

Sample	Primer	Topcoat	Unscribed Area Failure (%)	Rating	Avg. Scribe Creepage (mm)	Rating
WAB:GLY-1:Ti:III	ACP-3	MIL-C-46168	0	10	0	10
WAB:MP/DP/N-1:Ti:III	ACP-3	MIL-C-46168	0	10	0	10
WAB:MP/DP/N-1:24:III	ACP-3	MIL-C-46168	4.0	7	< 0.5	9
WAB:MP/DP/N-1:24:III	ACP-3	----------	0	10	0	10
WAB:MP/DP/N-1:24:III	MIL-P-53022	MIL-C-46168	4.0	7	< 0.5	9
WAB:MP/DP/N-1:50:III	ACP-3	MIL-C-46168	0.4	9	< 0.5	9
WAB:MP/DP/N-1:50:III	ACP-3	----------	0.01	9	0	10
WAB:MP/DP/N-1:50:III	MIL-P-53022	MIL-C-46168	0.25	9	0	10

Table 11
Sample Preparation Conditions for Modified PAST-I-Treated Nonferrous Alloy Corrosion Test Panels
2000 psi / 150 grit Alumina / 0.4 sec per in^2 Blast Duration
1% Aqueous Silane Applied after Grit Blasting

Sample #	Silane Solution Concentration (Wt. %)	Silane Type	Silane Dry Time Temp./Time (°C/hr)	Primer Formulation ID #	Primer Dry Temp./Time (°C/hr)
WAB:24B:III	1	----------	93/1	ACP-3	22/120
WAB:MPD-1:24B:III	1	MPTMOS/DNP (9:1)	93/1	ACP-3	22/120

Table 12
Corrosion Test Sample Matrix for Modified PAST-I-Treated Nonferrous Alloy Panels

Sample	Alloy	Pretreatment	Primer	Topcoat
WAB:GLY-1:Ti:III	Ti 6Al-4V	PAST-1	ACP-3	MIL-C-46168
WAB:MPD-1:Ti:III	Ti 6Al-4V	PAST-I	ACP-3	MIL-C-46168
WAB:24:III	Al 2024-T3	Waterblast	ACP-3	MIL-C-46168
WAB:MPD-1:24:III	Al 2024-T3	PAST-I	ACP-3	MIL-C-46168
WAB:50:III	Al 5083-H321	Waterblast	ACP-3	MIL-C-46168
WAB:MPD-1:50:III	Al 5083-H321	PAST-I	ACP-3	MIL-C-46168

Table 13
Corrosion Test Results for Modified PAST-I-Treated Aluminum and Titanium Samples After Exposure to Neutral Salt Spray According to ASTM B117

Sample*	Primer	Alloy	Exposure Time (h)	Unscribed Area Failure (%)	Rating	Avg. Scribe Creepage (mm)	Rating
WAB:GLY-1:Ti:III	ACP-3	Ti 6Al-4V	2,000	0	10	0	10
WAB:MPD-1:Ti:III	ACP-3	Ti 6Al-4V	2,000	0	10	0	10
WAB:MPD-1:24:III	ACP-3	Al 2024-T3	1,000	0.06	9	0.02	9
WAB:24:III	ACP-3	Al 2024-T3	1,000	0.56	9	0.5	4
WAB:MPD-1:50:III	ACP-3	Al 5083-H321	1,000	0	10	0	10
WAB:50:III	ACP-3	Al 5083-H321	1,000	0	10	0.11	6

* All panels painted with CARC topcoat conforming to MIL-C-46168

Table 14
Effect of Primer on Coating Performance for PAST-1-Treated Aluminum Samples After 1,000 Hours of Neutral Salt Spray Exposure According to ASTM B117

Sample*	Primer	Aluminum Alloy	Unscribed Area Failure (%)	Rating	Avg. Scribe Creepage (mm)	Rating
WAB:MPD-1:24:IV	ACP-4	2024-T3	0	10	< 0.01	9
WAB:MPD-1:50:IV	ACP-4	5083-H321	0	10	< 0.001	9
WAB:MPD-1:24:III	ACP-3	2024-T3	0.06	9	0.02	9
WAB:MPD-1:50:III	ACP-3	5083-H321	0	10	0	10

Table 15
Sample Preparation Conditions for PAST-I- and PAST-II-Treated Aluminum Alloy 2024-T3 Panels
2000 psi / 150 grit Alumina / 0.4 sec per in^2 Blast Duration
1% Aqueous Silane Applied after Grit Blasting

Sample #	Silane Solution Concentration (Wt. %)	Silane Type[a]	Silane Dry Time Temp./Time (°C/hr)	Primer Formulation ID #	Primer Dry Temp./Time (°C/hr)
WAB:MPD/TiOx:24B:IV	1	MPTMOS/DNP (9:1)/TiOx	93/1	ACP-3	22/120
WAB:MPD/TiS:24B:IV	1	MPTMOS/DNP (9:1)/TiS	93/1	ACP-4	22/120
WAB:MPD-1:24B:V	1	MPTMOS/DNP (9:1)	93/1	ACP-5	22/120
WAB:MPD-1:24B:VI	1	MPTMOS/DNP (9:1)	93/1	ACP-6	22/120

a: TiOx = Titanium oxalate = $Ti_2(C_2O_4)_3 \cdot 10\ H_2O$, TiS = Titanium sulfate = $TiOSO_4 \cdot H_2SO_4 \cdot 8H_2O$

Table 16
Corrosion Test Sample Matrix for PAST-I- and PAST-II-Treated Aluminum Alloy 2024-T3 Panels

Sample	Alloy	Pretreatment	Primer	Topcoat
WAB:MPD/TiOx:24B:IV	Al 2024-T3	PAST-II	ACP-4	MIL-C-46168
WAB:MPD/TiS:24B:IV	Al 2024-T3	PAST-II	ACP-4	MIL-C-46168
WAB:MPD-1:24:V	Al 2024-T3	PAST-I	ACP-5	MIL-C-46168
WAB:MPD-1:24:VI	Al 2024-T3	PAST-I	ACP-6	MIL-C-46168

Table 17
Coating Performance Ratings for
PAST-I and PAST-II-Treated Al 2024-T3 Samples
After 1,000 Hours of Neutral Salt Spray Exposure According to ASTM B117

Sample*	Primer	Exposure Time (h)	Unscribed Area Failure (%)	Rating	Avg. Scribe Creepage (mm)	Rating
WAB:MPD/TiOx:24B:IV	ACP-4	1,000	0	10	0.002	9
WAB:MPD/TiS:24B:IV	ACP-4	1,000	0	10	0.01	9
WAB:MPD-1:24:V	ACP-5	1,000	0.2	9	1.1	7
WAB:MPD-1:24:VI	ACP-6	1,000	0	10	0	10

Table 18
Primer Coating Performance Ratings for Aluminum Panels Prepared by PAST-I/ACP-6 and Control Pretreatments
After 1,000 hr GM Spec 9540P Cyclic Corrosion Exposure

Pretreatment Code*	Alloy	Primer	Unscribed Area Failure (%)	Rating	Avg. Scribe Creepage (mm)	Rating
WAB:MPD-1:24:VI	2024-T3	ACP-6	0	10	0.013	9
CCC:MP:TC:24	2024-T3	MIL-P-53022	33	3	7.5	3
WAB:MPD-1:50:VI	5083-H321	ACP-6	0	10	0	10
CCC:MP:TC:50	5083-H321	MIL-P-53022	0	10	0	10
WAB:MPD-1:60:VI	6061-T6	ACP-6	0	10	0	10
CCC:MP:TC:60	6061-T6	MIL-P-53022	0	10	0	10

* All primed panels coated with topcoat conforming to MIL-C-46168

Table 19
Coating Adhesion Performance Ratings for Peroxide-Etched Aluminum Samples

Alloy	Etch	Primer(s)	Wet Adhesion Rating	Corrosion Scribe Test Remarks	Post Salt Spray Chip Resistance Rating
Bare Al 2024-T3	CM-50	ACP-6/MIL-P-53030	Pass	Some Corrosion	9B, 6A; 6A, 6A
Bare Al 2024-T3	NM-22	ACP-6/MIL-P-53030	Fail	Some Corrosion	5C, 7B; 4C, 7B
Bare Al 6061-T6	CM-50	ACP-6/MIL-P-53030	Pass	Some Corrosion	7A, 8A; 7A, 8A
Bare Al 6061-T6	NM-22	ACP-6/MIL-P-53030	Fail	Some Corrosion	9B, 4A; 5A, 4A
Alodined Al 1100	------	MIL-P-53030	Pass	Some Corrosion	7A, 6A, 7A

Table 20
Primer Coating Performance Ratings for Etched Aluminum Panels After 1,000 Hours Salt Spray Exposure Per ASTM B117

Pretreatment Code*	Alloy	Unscribed Area Failure (%)	Rating	Avg. Scribe Creepage (mm)	Rating
CM-50/MPTMOS	2024-T3	0	10	0.003	9
NM-22/MPTMOS	2024-T3	0	10	0.003	9
CM-50/MPTMOS	6061-T6	0	10	0.017	9
NM-22/MPTMOS	6061-T6	0	10	0.002	9

All panels primed with experimental waterborne formulation ACP-6

Table 21
Coating Performance Ratings for NA-PAST Treated Aluminum Samples After 2,000 hr GM Spec 9540P Cyclic Corrosion Exposure

Sample	Primer	Topcoat	Unscribed Area Failure (%)	Rating at Unscribed Area (0-10)	Average Scribe Creepage (mm)	Rating at Unscribed Area (0-10)
NAP:P-6:TC:24	ACP-6	MIL-C-46168	0	10	0	10
NAP:P-6:24	ACP-6		0	10	0	10
NAP:MP:24	MIL-P-53022		0.401	9	0.021	9
CCC:MP:TC:24	MIL-P-53022	MIL-C-46168	0.049	9	0.015	9
NAP:P-6:TC:60	ACP-6	MIL-C-46168	0.15	9	0	10
NAP:P-6:60	ACP-6		0	10	0	10
NAP:MP:60	MIL-P-53022		0.26	9	0	10
CCC:MP:TC:60	MIL-P-53022	MIL-C-46168	0	10	0	10
NAP:P-6:TC:50	ACP-6	MIL-C-46168	0	10	0	10
NAP:P-6:50	ACP-6		0	10	0	10
NAP:MP:50	MIL-P-53022		0	10	0	10
CCC:MP:TC:50	MIL-P-53022	MIL-C-46168	0	10	0	10

Table 22
Corrosion Performance Ratings for Low Carbon Steel 1010 Alloy
Pretreated by NA-PAST and Control Methods
200 hr GM Spec 9540P Cyclic Corrosion Exposure

Sample*	Primer	Unscribed Area Failure (%)	Unscribed Area Rating	Avg. Scribe Creepage (mm)	Scribed Area Rating
NAP:P-6:LCS	ACP-6	0	10	0.012 ± 0.007	9
ZPC:P-6:LCS	ACP-6	0	10	0.11 ± 0.02	9
NAP:MP:LCS	MIL-P-53022	0.05 ± 0.09	9	0.06 ± 0.02	9
ZPC:MP:LCS	MIL-P-53022	0	10	0.4 ± 0.0	9

Table 23
Corrosion Performance Ratings for Assorted Alloys
Pretreated by NA-PAST Method
500 hr GM Spec 9540P Cyclic Corrosion Exposure

Sample*	Alloy	Primer	Unscribed Area Failure (%)	Unscribed Area Rating	Avg. Scribe Creepage (mm)	Scribed Area Rating
NAP:P-6:SS	Stainless steel	ACP-6	0	10	0	10
NAP:MP:Ti	Ti 6Al-4V	MIL-P-53022	0	10	0	10
NAP:P-6:Ti	Ti 6Al-4V	ACP-6	0	10	0	10
NAP:P-6:CB	Cartridge Brass	ACP-6	0	10	0	10

Table 24
Primer Coating Mechanical Properties for Bare Al 2024-T3 Prepared by NA-PAST/MATG Silane and E-Coat Priming

CDC Sample ID Number	Test Parameter	Test Method	Test Result
95-3573-P	E-Coat Primer Thickness	ASTM B244	0.8 mils
	Reverse Impact Adhesion	ASTM D2794	>100 inch-lbs.
95-3574-P	Tape Adhesion: X-Cut (A) Cross-Cut (B)	ASTM D3359	5 No Failure 5 No Failure
	Pencil Hardness: Gouge Scratch	ASTM D3363	4H 2H
95-3575-P	MIBK Solvent Rub	PPG Cure Test	Satisfactory Rating
	Mandrel Bend	ASTM D522	Pass
95-3577-P	E-Coat Primer Thickness	ASTM B244	0.8 mils
	Reverse Impact Adhesion	ASTM D2794	>100 inch-lbs.
95-3578-P	MIBK Solvent Rub	PPG Cure Test	Satisfactory Rating
	Mandrel Bend	ASTM D522	Pass
95-3579-P	Tape Adhesion: X-Cut (A) Cross-Cut (B)	ASTM D3359	5 No Failure 5 No Failure
	Pencil Hardness: Gouge Scratch	ASTM D3363	4H 2H

Table 25
E-Coat Primer Corrosion Performance Ratings for Bare 2024-T3 Aluminum Panels Treated by NA-PAST/MATG Silane After 2,000 Hours Salt Spray Exposure Per ASTM B 117

CDC Sample ID Number	Description of Corrosion	Average Scribe Creepage Rating (0-10)	Maximum Scribe Creepage Rating (0-10)	Interval of Noticeable Adhesion Loss (hrs)	Rating at Unscribed Area (0-10)	Interval of Noticeable Adhesion Loss (hrs)
95-3595-P	C, F	9	10	NN	5	403-504
95-3596-P	C, F	8	10	NN	2	403-504
95-3597-P	C, F	9	10	NN	5	403-504
95-3598-P	C, F	9	10	NN	2	403-504

Table 26
Primer Coating Mechanical Properties for Bare Al 5083-H321 Prepared by NA-PAST/MGAMo Silane and E-Coat Priming

CDC Sample ID Number	Test Parameter	Test Method	Test Result
96-0879-P	E-Coat[a] Primer Thickness	ASTM D1400	0.85 mils
96-0879-P	Gloss at 60 Angle	ASTM D523	5.4
96-0879-P	Wet Tape Adhesion	Fed. Std. 141 Method 6301	No Failure

a: BASF Gray Cathoguard 300 electrocoat primer

Table 27
E-Coat Primer Corrosion Performance Ratings for Al 5083-H321 Aluminum Panels Treated by NA-PAST/MGAMo Silane After 3,500 Hours Salt Spray Exposure Per ASTM B117

CDC Sample ID Number	Description of Corrosion	Average Scribe Creepage Rating (0-10)	Maximum Scribe Creepage Rating (0-10)	Interval of Noticeable Adhesion Loss (hrs)	Rating at Unscribed Area (0-10)	Interval of Noticeable Adhesion Loss (hrs)
96-0875-P	A, B	10	10	NL	10	NL
96-0876-P	A, B	10	10	NL	10	NL
96-0877-P	A, B	10	10	NL	10	NL
96-0878-P	A, D	10	10	NL	9	3264-3360

Table 28
Primer Coating Mechanical Properties for Bare 5083-H321 Aluminum Panels Prepared by NA-PAST/MGAMo Silane and Powder Coat Priming

CDC Sample ID Number	Test Parameter	Test Method	Test Result
96-0884-P	Powder[a] Primer Thickness	ASTM D1400	3.32 mils
96-0884-P	Gloss at 60 Angle	ASTM D523	84.3
96-0884-P	Wet Tape Adhesion	Fed. Std. 141 Method 6301	No Failure

a: Morton Emglo Blue Epoxy powder coating

Table 29
Powder Coat Primer Corrosion Performance Ratings for Bare 5083-H321 Aluminum Panels Treated by NA-PAST/MGAMo Silane After 3,500 Hours Salt Spray Exposure Per ASTM B117

CDC Sample ID Number	Description of Corrosion	Average Scribe Creepage Rating (0-10)	Maximum Scribe Creepage Rating (0-10)	Interval of Noticeable Adhesion Loss (hrs)	Rating at Unscribed Area (0-10)	Interval of Noticeable Adhesion Loss (hrs)
96-0880-P	A, B	10	10	NL	10	NL
96-0881-P	A, B	10	10	NL	10	NL
96-0882-P	A, B	10	10	NL	10	NL
96-0883-P	A, D	10	10	NL	10	NL

Table 30
Primer Coating Abrasion Resistance Test Results for Aluminum Panels Prepared by PAST, NA-PAST and Control Pretreatments

Pretreatment	Primer	Alloy	Weight Loss[a] @ 500 cycles (mg)
PAST/MPD-1	ACP-6	bare 2024-T3	40 ± 5
NA-PAST/MPD-1	ACP-6	bare 2024-T3	37 ± 4
NA-PAST/MPD-1	ACP-6	bare 6061-T6	40 ± 20
AlC/AcD/Alodine[b]	MIL-P-53022	bare 6061-T6	30 ± 20
NA-PAST/MPD-1	ACP-6	bare 5086-H321	35 ± 3

a: CS-10 calibrase wheel with 500g weight

b: AlC = Cleaned with alkaliné Duraprep™ 120 aluminum cleaner (Shipley Company, Inc.)
AcD = Deoxidized with Duraprep™ 320 acid etch (Shipley Company, Inc.)
Alodine = Alodine® 1201, chromate conversion coating (Parker+Amchem Corp.)

Table 31
Primer Coating Chipping Resistance Test Results for Aluminum Panels Prepared by PAST, NA-PAST and Control Pretreatments

Pretreatment	Primer	Alloy	Chipping Rating[b]
PAST/MPD-1	ACP-6	bare 2024-T3	5B-7A (P)
NA-PAST/MPD-1	ACP-6	bare 2024-T3	4B-6A (P)
NA-PAST/MPD-1	ACP-6	bare 6061-T6	4B-6A (P)
AlC/AcD/Alodine[a]	MIL-P-53022	bare 6061-T6	5B-7A (P)
NA-PAST/MPD-1	ACP-6	bare 5086-H321	4B-7A (P)

a AlC = Cleaned with alkaline Duraprep™ 120 aluminum cleaner (Shipley Company, Inc.)
AcD = Deoxidized with Duraprep™ 320 acid etch (Shipley Company, Inc.)
Alodine = Alodine® 1201, chromate conversion coating (Parker+Amchem Corp.)

b For chipping resistance rating explanation, see Appendix

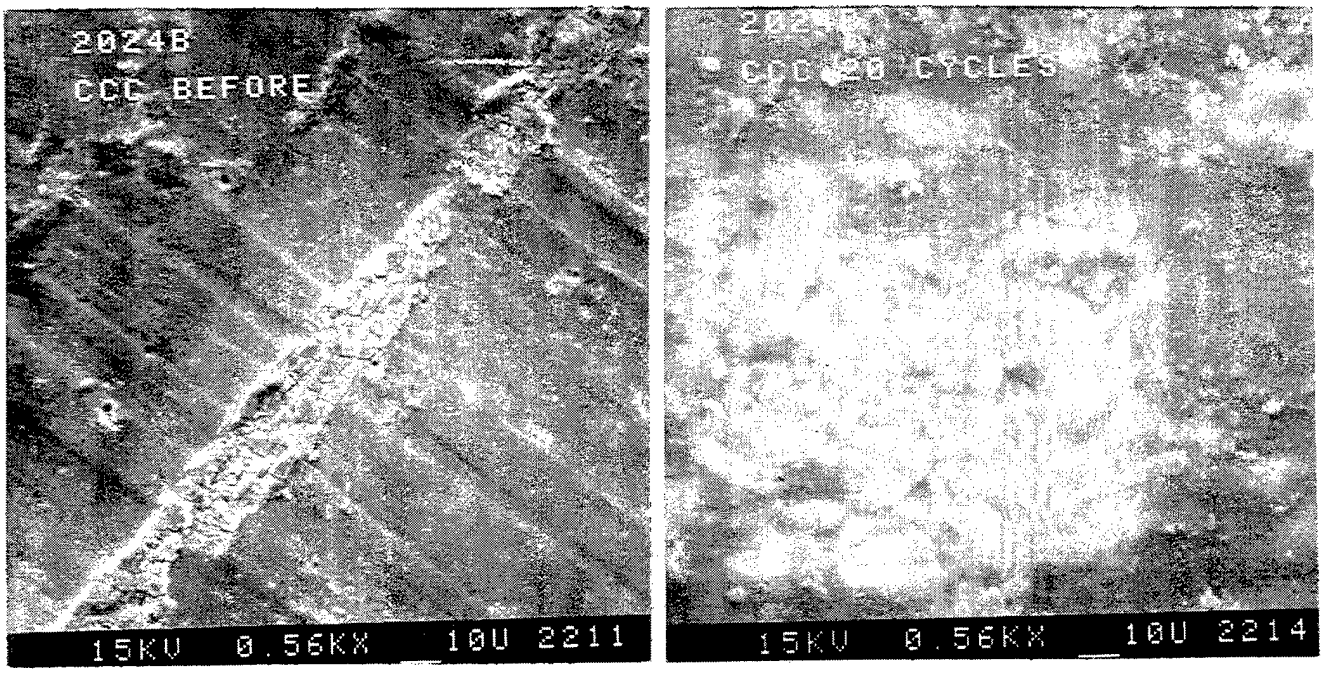

FIGURE 1. SEM photomicrographs of chromate conversion coated bare Al 2024-T3 panel before and after 20 corrosion test cycles. (1000X)

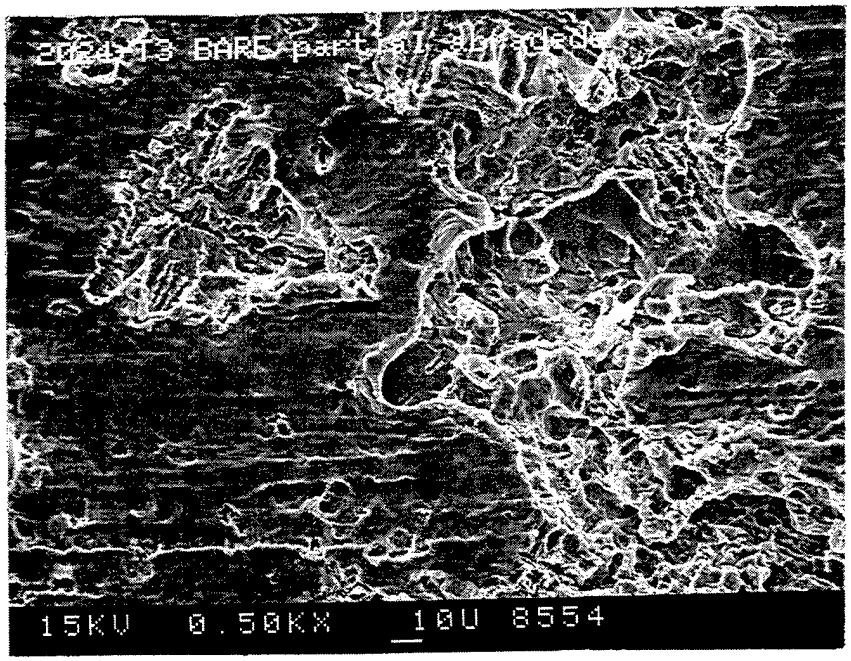

FIGURE 2. SEM photomicrographs of NA-PAST-treated bare Al 2024-T3 panel before corrosion testing. (500X)

TRIVALENT CHROMIUM CONVERSION COATING FOR ALUMINUM - A REPLACEMENT FOR HEXAVALENT CHROMIUM PRETREATMENT

Fred Pearlstein and Vinod S. Agarwala
Naval Air Warfare Center Aircraft Division
48110 Shaw Road
Patuxent River, MD 20650

ABSTRACT

A relatively non-toxic dilute trivalent chromium bath has achieved salt spray corrosion resistance and paint adhesion better or equivalent to that of hexavalent chromium (Alodine) conversion coatings for 7075-T6 and 2024-T3 aluminum. It was also demonstrated that trivalent chromium bath has less tendency for inducing hydrogen embrittlement to high strength steels than a chromating (Cr^{+6}) bath. Color coatings were successfully produced by addition of dyes to the trivalent chromium solution.

Keywords: conversion coating, trivalent chromium, low or non-toxic (environmentally friendly), aluminum alloys, corrosion resistance, paint adhesion, salt spray testing, Alodine 1200 (Cr^{+6}), chromate conversion coating alternative.

INTRODUCTION

It was reported earlier[1] that chemical conversion coatings can be applied to aluminum using trivalent chromium solution which imparts significant corrosion resistance. It is a viable alternative to use of highly toxic chromate (hexavalent chromium) baths. A typical trivalent chromium immersion treatment for aluminum after cleaning and deoxidizing was: 10 minutes at 23 ± 2 ^{0}C in 4 g/l basic chromic sulfate, $[Cr_4(SO_4)_5(OH)_2]$* bath containing 0.4 g/l Na_2SiF6 and 16 to 20 ml/l of 0.5 N NaOH. After rinsing, a post-treatment by spray or immersion in 0.3% H_2O_2 was applied (no rinse); up to 336 hours salt spray corrosion resistance was obtained on 7075-T6 and up to 168 hours on 2024-T3 aluminum alloys. The present paper reports additional studies to further improve the trivalent chromium process particularly investigation of more dilute trivalent chromium solutions and fluoride-containing compounds other than fluorosilicate.

EXPERIMENTAL PROCEDURE

Aluminum alloys 7075-T6 and 2024-T3 were prepared by soaking 10 minutes at 75^0 C in a silicated non-etch alkaline cleaner, rinsing, deoxidizing 10 minutes at room temperature in a

* 17.8% Cr^{+3} + 23 to 24% Na_2SO_4; Fluka Chemical Corp, Ronkonoma, NY

proprietary non-chromate formulation (a solution containing ferric sulfate, nitric acid and potassium bifluoride) and rinsing, prior to treatment.

It was found that addition of Na_2TiF_6 to the original bath described in Introduction [1] provided good corrosion resistance to aluminum at shorter immersion times, e.g., 3 minutes vs. 10 minutes. Therefore, 0.4 g/l Na_2TiF_6 was added to a considerably used 12 liter bath of composition shown in Introduction. Panels of 7075-T6 and 2024-T3, held on titanium rack, were treated by 3 minutes immersion at room temperature; after rinsing, panels were immersed 20 seconds in 0.3% H_2O_2 (10 ml/l 30% H_2O_2) and, without rinsing, were permitted to dry naturally. The panels, in quadruplicate, were exposed to 5% neutral salt spray (ASTM B117) and at Naval Surface Warfare Center's marine site at Dania, Florida along with bare and Alodine 1200 ** chromate conversion coated aluminum.

Baths were prepared with 4 g/l basic chromic sulfate to which was added NaF, Na_2SiF_6, K_2TiF_6 or K_2ZrF_6 singly at 0.8 g/l or in binary combinations of 0.4 g/l each. The baths were permitted to age one week before use which is necessary to develop proper bath characteristics. Panels, after rinsing from deoxidizing, were immersed into the baths for three minutes at 23 ± 2 °C with agitation for 15 seconds at start and half-way through the process. Panels were rinsed, immersed 20 seconds in 0.3% H_2O_2 solution and allowed to dry naturally. Freshly treated panels were exposed to 5% neutral salt spray (ASTM B117) for 336 hours and evaluated for corrosion resistance.

Baths were prepared with various concentrations of basic chromic sulfate and 0.4 or 0.8 g/l K_2ZrF_6 and allowed to age one week before conducting immersion tests as described above. After the baths had aged a total of three weeks from make-up, the solutions were applied by spraying, using a propellant gas, with direct impingement on panels held at a 60° angle. Panels were actively sprayed 20 seconds each minute for a total of three minutes. Solution was applied by wiping with Polybrush*** on aluminum panels in horizontal position 20 seconds each minute, periodically adding fresh solution, for a total of three minutes. Panels treated by spraying or brushing were post-treated after rinsing by spraying with 0.3% H_2O_2 (1: 9 dilution of common household peroxide with deionized water) using a common hand-trigger operated plastic bottle, and allowed to dry naturally. Panels were exposed to salt spray.

Aluminum panels (7075-T6 and 2024-T3) were trivalent chromium treated using:

0.6 g/l basic chromic sulfate
0.8 g/l K_2ZrF_6

This solution will hereinafter be referred to as "0.6Cr - 0.8Zr". Panels were immersed one or three minutes; brushing or spraying was applied three minutes. Panels were also immersed 2 or 6 minutes in 0.8 g/l K_2ZrF_6 alone. Panels solely cleaned and deoxidized were used as controls. All panels were painted with 1.0 to 1.2 mil water-borne MIL-P-95582, Type I, Class N. The painted panels were allowed to age 14 days, then submerged in distilled water at 23± 2° C for 24 hours.

** Parker Amchem, Henkel Corp, Madison Heights, MI

*** Open-Cell Polyurethane Foam on Wood Handle; Gardco Corp, Pompano Beach, Fl

Panels were dried, scribed, tape firmly applied and rapidly removed to observe any lack of paint adhesion adjacent to scribes. Panels that passed this test were immersed in distilled water 7 days at 65° C, scribed anew at another area and the procedure repeated.

The deposit weight (mass) was determined as a function of immersion time by immersing panels in the "0.6 Cr - 0.8 Zr" bath for 1, 3, 9 or 27 minutes (panels agitated in bath 15 seconds at beginning and midway through process), rinsed, dried and weighed. The panels were stripped by immersion for one minute at room temperature in 50% (vol) HNO_3 and then rinsed, dried and reweighed.

Notched 4340 steel C-rings (2" OD, 1-1/4" wide, 3/32" thick) heat treated to 280,000 PSI were stressed with a bolt to 65% of notch tensile strength. Drops of distilled water or "0.6 Cr - 0.8 Zr" solution or Alodine 1200 chromate solution were applied at the notch area and time-to-failure (indicated by spontaneous audible cracking) was noted. The time to failure is indicative of the relative tendency for the liquids to produce hydrogen embrittlement.

Aluminum panels were prepared by immersing in a "0.6 Cr - 0.8 Zr" bath that had been aged approximately 4 months and been considerably used. Spraying or brushing was accomplished with solution aged for about 4 months but unused. Panels were tested for salt spray corrosion resistance with or without application of the spray 0.3% H_2O_2 post-treatment.

RESULTS AND DISCUSSION

Fluorosilicate Plus Fluorotitanate

Panels treated in the $Cr^{+3} + Na_2SiF_6 + NaOH + Na_2TiF_6$ bath were exposed 336 hours to salt spray or one year at a marine site; corrosion resistance evaluation is shown in Table 1. Trivalent chromium coated (TCC) and chromate conversion coated (CCC) 7075-T6 exposed to salt spray were virtually identical in appearance with few traces of white salts barely visible. TCC and CCC 2024-T3 aluminum were also virtually identical with definite traces of white salts sufficient to indicate corrosion failure. The TCC and CCC 7075-T6 panels exposed one year to a Marine exposure environment at Dania, Florida, again were similar in appearance with a moderate amount of pitting and white salts; some what greater corrosion was observed on 2024-T3. Bare panels were extensively corroded in salt spray and, in marine atmospheric exposure, most of the area was pitted with considerable white salts. Exfoliation corrosion was visible at edges of bare 7075-T6 exposed at the marine site; examination under 10X magnification of pitting corrosion on bare 7075-T6 and 2024-T3 showed evidence of exfoliation corrosion initiation.

Fluoride-Containing Compounds

Solutions of 4 g/l basic chromic sulfate (17.8% Cr^{+3} + 23 to 24% Na_2SO_4) plus fluoride-containing compounds were prepared as shown in Table 2 and aged 7 days. It had been found that solutions must be aged approximately one week to develop desired properties. Aluminum was immersed three minutes, with agitation for 15 seconds at start and midway through process.

The deposit appearance varied from pale tan to pale blue/violet similarly on 7075-T6 and 2024-T3. Three of the four baths containing K_2TiF_6 had slight sediment formed; the only other bath with sediment was at the highest pH and contained 0.8 g/l NaF. With continued bath aging, the amount of sediment increased markedly in those baths and some sediment also formed in most of the other baths.

The corrosion resistance of treated panels was evaluated after 336 hours salt spray exposure. A scribe had been made on each panel to ascertain any self-healing characteristics. See Table 2. Panels treated in baths containing 0.8 g/l Na_2SiF_6 or 0.4 g/l Na_2SiF_6 + 0.4 g/l K_2TiF_6 had little or no corrosion resistance. This should not be unexpected since the pH was low (under 3.1) and previously reported work[(1)] showed that the pH of the baths containing Na_2SiF_6 must be raised to about 3.7 by addition of 16 to 20 ml/l 0.5 N NaOH. However, it is interesting to note that all baths containing K_2ZrF_6 provided good corrosion resistance and self-healing though the bath pH of one of these was 3.0 and 3 of the 4 baths were under 3.4. It was concluded that baths containing K_2ZrF_6 were less sensitive to variations in pH. It was therefore decided to conduct additional studies using this fluorocompound though some of the combinations containing K_2ZrF_6 such as NaF + K_2ZrF_6 may also be worthy of further study. Other fluoride compounds which did not appear to offer promise for trivalent chromium treatment were fluoroborate, hexafluorostannate, hexafluoroaluminate and hexafluorophosphate.

Trivalent Chromium and Fluorozirconate Concentrations

Baths were prepared as shown in Table 3 containing various concentrations of trivalent chromium salt plus 0.4 or 0.8 g/l K_2ZrF_6 . The corrosion resistance of panels immersed or sprayed as described above and post-treated by 0.3% H_2O_2 spray is shown in Table 3.

Aluminum panels immersion treated in the bath containing 4 g/l basic chromic sulfate plus 0.4 g/l K_2ZrF_6 had poor corrosion resistance; all others were intact (excluding edges) or had only traces of incipient corrosion. Also, most panels exhibited excellent or complete self-healing at scribes; all had some self-healing characteristics. Surprisingly, as little as 0.15 g/l of the chromic salt (approximately 27 ppm Cr^{+3}) provided excellent corrosion resistance.

Spray-treated aluminum had consistently lower corrosion resistance than those immersion treated. Generally, baths containing 0.8 g/l K_2ZrF_6 yielded better corrosion resistance than those containing 0.4 g/l. The effect of even higher K_2ZrF_6 concentration should be considered. Optimum corrosion resistance and superior self-healing for sprayed 7075 or 2024 Al appeared to occur with baths containing 0.6 g/l basic chromic sulfate plus 0.8 g/l K_2ZrF_6 and those containing 0.3 g/l basic chromic sulfate plus 0.4 or 0.8 g/l K_2ZrF_6 . It is possible that pH may be a factor in the results and increasing the pH of the higher chromic concentration baths may improve corrosion resistance of sprayed aluminum.

Panels were also treated by brushing with open-cell polyurethane as described above. Corrosion resistance was similar to those immersion treated and superior to those spray treated.

Based upon results of the above corrosion tests, the preferred bath of 0.6 g/l basic chromic sulfate plus 0.8 g/l K_2ZrF_6 ("0.6 Cr - 0.8 Zr") was adopted since this bath would permit significant depletion by dragout or chemical reaction without seriously decreasing corrosion resistance. This bath contains less than 110 ppm Cr^{+3} which will minimize waste treatment and may even permit direct disposal of residue rinsed from aluminum treated by immersion or brushing.

Paint Adhesion

The results of paint adhesion tests on bare and trivalent chromium coated using the preferred bath ("0.6 Cr - 0.8 Zr") are shown in Table 4. It had been found that immersion of aluminum in baths free of chromium, i.e., containing only 0.3 to 2.0 g/l K_2ZrF_6 provided some measure of corrosion resistance; up to 72 hours salt spray corrosion resistance was obtained on 7075-T6 and considerably less corrosion resistance on 2024-T3. A paint pre-treatment using 0.8 g/l K_2ZrF_6 was included in these tests. It may be possible to add other agents even more innocuous than trivalent chromium to produce an effective chemical conversion coating although initial attempts in this direction have failed to improve performance sufficiently to warrant continuing these studies at this time.

The painted panels which had simply been cleaned and deoxidized and subjected to the one day water soak test had very poor paint adhesion; the paint spontaneously curled and lifted from the entire 7075 panel and substantial paint was lifted by tape from the scribed area of 2024. All other panels passed the tape test without paint lifting or any paint blistering.

All painted panels subjected to the 7 day test had blistered paint which was generally limited to areas near edges. There was much more extensive blistering on panels treated in the 0.8 g/l K_2ZrF_6 solution (chromium-free) and tape tests at scribes caused substantial lifting of paint. All other treatments passed the tape tests. The trivalent chromium treatment provided excellent paint adhesion based upon the one day immersion test. The 7 day test is quite severe and yet good adhesion was obtained except for blistering near edges. Fluorozirconate solution (chromium-free) treatment was effective for providing paint adhesion based on the one day soak test but failed the 7 day soak test. Unfortunately, Alodine 1200 (chromate conversion coating) was not applied for comparison so it is not known whether results would be superior to the trivalent chromium treatments.

The "0.6 Cr - 0.8 Zr" bath was submitted to Naval Air Station Oceana for evaluation. Tests were conducted on actual aircraft aluminum parts by brushing on the solution using synthetic "cotton". Their tests[(2)] indicated that the process provided good corrosion resistance and excellent paint adhesion.

Deposit Weight vs. Immersion Time

Deposit weights obtained by the preferred trivalent chromium bath ("0.6 Cr - 0.8 Zr") was much lower than 40 mg/ft^2, a minimum deposit weight required for Alodine in accordance with MIL-C-81706. The rate of film formation was greater at lower immersion times indicating that initial films tend to retard continued surface chemical reactions. Even after 27 minutes immersion

coating weight did not increase further than 20 mg/ft^2. This data may be useful in developing a specification to cover the trivalent chromium process.

The effect of immersion time on corrosion resistance has not been extensively determined but there is evidence that 1 to 6 minutes is advisable. For unpainted surfaces, 3 to 6 minutes are more than adequate or preferred; for painted surfaces, 1 to 3 minutes.

Hydrogen Embrittlement

In order to get an indication as to whether the trivalent chromium bath has a tendency to produce hydrogen embrittlement of high strength steels, drops of solution were applied at the notch area of stressed steel C-rings. The time for audible spontaneous cracking is shown in Table 5. The trivalent chromium solution appeared to have a lesser tendency for hydrogen embrittlement than Alodine 1200 chromate conversion coating solution. The notched C-rings are known to be highly susceptible to embrittlement. However, it was not expected that distilled water would cause cracking since corrosion with distilled water is not expected to liberate any significant hydrogen. However, until additional tests are performed to support that the trivalent chromium bath is not seriously embrittling, steps should be taken to ensure that the solution does not inadvertently come in contact with high strength steels.

Peroxide Post-Treatment

The effect of peroxide spray post-treatment on corrosion resistance of trivalent chromium coated (TCC) aluminum with the preferred "0.6 Cr - 0.8 Zr" bath by immersion, brush or spray was determined. The results are shown in Table 6. Peroxide post-treatment applied by spray is preferred because peroxide baths will eventually decompose from presence of metal ions introduced by immersion.

The peroxide post-treatment only marginally improved the corrosion resistance and degree of self-healing on 7075-T6; marked improvement was noted for 2024-T3. All panels peroxide post-treated were able to pass the 336 hour salt spray test except for sprayed 2024-T3. 7075-T6 panels passed the 336 hour salt spray test even without the post-treatment. Aluminum alloy 6061-T6 had excellent corrosion resistance and self-healing at scribe with or without post-treatment but a powdery deposit was produced. Occasionally, powdery deposits had been observed on 7075 and 2024 which were attributable to loss of effectiveness of the deoxidizer.

The fact that significant and sometimes, excellent or complete self-healing was produced even without the peroxide post-treatment is not yet understood. In a previous study[1], self-healing of deposits post-treated with peroxide was attributed to the presence of a modicum of inhibitive hexavalent chromium (<1ppm) produced. Recent XPS analysis of TCC sample with/without peroxide post-treatment showed that a large component of surface film contained Cr_2O_3 (Cr^{+3}) with some mixture of CrO_2 (Cr^{+4}) but no evidence of CrO_3 (Cr^{+6}). Further studies may be warranted to elucidate the mechanism of healing and the inhibitive action of the process.

Preliminary tests indicated that trivalent chromium applied to electrodeposited cadmium or zinc-nickel on steel provided significant salt spray corrosion resistance retarding formation of both white salts and substrate rusting.

Dyed Trivalent Chromium Coatings

The trivalent chromium treatment imparts a pale tan to pale blue tint which is usually not readily visible. To overcome this difficulty, a number of dyes were added to the used aged "0.6 Cr - 0.8 Zr" bath. It was found that addition of 0.5 g/l Aurintricarboxylic acid[****] or Evans Blue[*****] upon three minutes immersion produced a definite attractive pink or blue coating respectively which did not adversely affect corrosion resistance. Coloring of aluminum was not as effective when applied by spray or brush. It has not been determined whether dyed coatings will provide effective paint base properties and whether the ability to provide color coatings will be degraded with long-term aging.

Future Studies

The following factors that would further improve and/or extend the trivalent chromium process will be considered in future studies: (i) effect of bath aging on effectiveness, (ii) use of surfactants to help overcome presence of any trace soils that may be present on parts during actual production use, (iii) optimization of process for production use and to improve performance on 2024-T3, (iv) applicability to other metals, alloys or deposits, (v) bath replenishment and (vi) methods to increase trivalent chromium deposit weight.

CONCLUSIONS

Trivalent chromium baths applied by immersion, spray or brush to 7075-T6 aluminum alloy, along with a dilute peroxide post-treatment, provides corrosion resistance of over 336 hours salt spray exposure. The peroxide post-treatment significantly improves corrosion resistance and is particularly important for 2024-T3. Aluminum alloy 2024-T3 also passes the 336 hour corrosion test when applied by immersion or brush; however, slight corrosion is produced when applied by spray. The preferred solution arrived at as a result of these studies is:

0.6 g/l basic chromic sulfate
0.8 g/l K_2ZrF_6

Trivalent chromium treated aluminum provides effective paint adhesion. Deposit weight of about 15 to 20 mg/ft^2 is produced by immersion in the preferred bath for 3 to 6 minutes at 22° C. The preferred bath produces hydrogen embrittlement of notched high strength steel C-rings but has less tendency than chromate conversion coating bath Alodine 1200. Color coatings can be produced during immersion trivalent chromium application by incorporating certain dyes into the preferred bath. Trivalent chromium conversion coating is a potentially viable alternative to chromate conversion coating based upon the results of this study.

[****] Eastman-Kodak Practical, Rochester, NY
[*****] Sigma Chemicals Co., St Louis, MO

REFERENCES

1. F. Pearlstein and V.S. Agarwala, Plating and Surface Finishing, 81, (1994), p.50.
2. Private communication between Mr. John E. Hagensieker, NAS Oceana, Virginia Beach, VA and Fred Pearlstein, Naval Air Warfare Center, Warminster, PA, of 6 March 1996.

Table 1

Corrosion of Bare, Trivalent Chromium Coated (TCC) or Chromate Conversion Coated (CCC) Aluminum Alloys in Salt Spray or Marine Exposure Environment

Alloy	Corrosion Rating*, Average		
	Treatment	336 Hours Salt Spray	One Year Marine
7075-T6	None (bare)	0	1
2024-T3	None (bare)	0	1
7075-T6	TCC	9	5
2024-T3	TCC	8	4
7075-T6	CCC	9	5
2024-T3	CCC	8	4

*Corrosion Rating Key:

10	No Corrosion
9 - 8	Traces
7 - 6	Slight
5 - 4	Moderate
3 - 2	Considerable
1 - 0	Extensive

Note: Rating of 8 or lower is considered to indicate corrosion failure.

Table 2

Effect of Various Fluoride-Containing Compounds Added to 4 G/L Basic Chromic Sulfate on Corrosion Resistance of Immersion Treated Aluminum alloys

Fluoride-Containing Compound, g/l				Bath Aged 7 Days		Corrosion Rating * 336 Hours Salt Spray	
NaF	Na_2SiF_6	K_2TiF_6	K_2ZrF_6	PH	Sediment	7075-T6	2024-T3
0.8	—	—	—	4.1	slight	10(SH)	8
—	0.8	—	—	3.0	none	0	0
—	—	0.8	—	3.3	slight	7	7
—	—	—	0.8	3.4	none	10(SH)	9(SH)
0.4	0.4	—	—	3.4	none	5	8
0.4	—	0.4	—	3.7	slight	9(SH)	9(SH)
0.4	—	—	0.4	3.7	none	10(SH)	10(SH)
—	0.4	0.4		3.1	none	0	0
—	0.4		0.4	3.0	none	9(SH)	8(SH)
—	—	0.4	0.4	3.3	slight	9(SH)	9(SH)

*Corrosion Rating Key - See Table I

(SH) = Considerable to complete self-healing at scribe

Table 3

Effect of Bath Composition on Corrosion Resistance of Aluminum alloys Trivalent Chromium Coated by Immersion or Spray.

Bath Composition g/l		Aged 1 Week	Corrosion Rating* - 336 Hours Salt Spray			
			Immersion		Spray	
Cr^{+3} salt*	K_2ZrF_6	pH	7075	2024	7075	2024
4	0.4	3.2	2	1	2	1
4	0.8	3.3	10	10(SH)	5	5
1.2	0.4	3.5	10(SH)	10(SH)	6	3
1.2	0.8	3.6	10(SH)	10(SH)	8(SH)	5
0.6	0.4	3.6	10(SH)	10(SH)	8	6
0.6	0.8	3.7	10(SH)	10(SH)	9(SH)	8(SH)
0.3	0.4	3.8	10(SH)	9(SH)	9(SH)	8(SH)
0.3	0.8	3.9	10(SH)	9(SH)	9(SH)	8(SH)
0.15	0.4	4.0	10(SH)	9	8	5
0.15	0.8	4.0	10(SH)	9	9	5

*Corrosion Rating Key - See Table 1

(SH) = Considerable to complete self-healing at scribe.

Table 4
Paint Adhesion on Aluminum alloys, Bare or Trivalent Chromium Treated by Immersion, Spray or Brush.

Bath	Treatment		Tape Test on Scribed Painted Panels			
	Method	Time, Min.	One Day Submersion		7- Day Submersion	
			7075-T6	2024-T3	7075-T6	2024-T3
None	None	—	Fail	Fail	—	—
"0.6 Cr - 0.8 Zr"	Immer.	1	Pass	Pass	Pass*	Pass*
"0.6 Cr - 0.8 Zr"	Immer.	3	Pass	Pass	Pass*	Pass*
"0.6 Cr - 0.8 Zr"	Spray	3	Pass	Pass	Pass*	Pass*
"0.6 Cr - 0.8 Zr"	Brush	3	Pass	Pass	Pass*	Pass*
"0.8 g/l K_2 Zr F_6"	Immer.	2	Pass	Pass	Fail	Fail
"0.8 g/l K_2 ZrF_6"	Immer.	6	Pass	Pass	Fail	Fail

*Paint blistered at areas near edges.

Table 5
Time to Cracking of Stressed Notched 4340 Steel C-Rings.

Solution Applied	Time to Cracking, Min.
Distilled Water	48
"0.6 Cr - 0.8 Zr"	18
Alodine 1200	13

Table 6
Effect of Peroxide Post-Treatment (P.T.) on Corrosion Resistance of Trivalent Chromium coated Aluminum alloys.

Alloy	Corrosion Rating* After Hours Salt Spray Exposure						
	96 Hours	336 Hours					
	Bare All	Immersion		Brush		Spray	
	No P.T.	No P.T.	Peroxide	No P.T.	Peroxide	No P.T.	Peroxide
7075-T6	0	10	10(SH)	10 (SH)	10	9	10(SH)
2024-T3	0	8	9(SH)	7 (SH)	9(SH)	5	7(SH)
6061-T6	3	10(SH)	10(SH)	—	—	—	—

*Corrosion Rating Key - See Table I
(SH) = Considerable to complete self-healing at scribe

Joseph T. Menke
U.S. Army ARDEC, AMSTA-AR-ESM-H
Rock Island, IL 61299-7300

FAILURE ANALYSIS OF ASTM F519 SPECIMENS

Introduction:

Aircraft maintenance chemicals require testing per ASTM F519 to determine the potential for hydrogen embrittlement that may arise when the solution comes in contact with steel. Since there are few, if any, bare steel surfaces on an aircraft, the test method requires the chemicals to be evaluated in contact with cadmium plated 4340 steel in the 51-54 hardness Rockwell C (HRC) condition. This apparently simulates a worse case condition and is specifically directed to fasteners, landing gear, and other highly loaded/stressed components. The cadmium plating specified is referred to as "low-embrittling cadmium." Other names that may describe this are dull cadmium, nodular cadmium, or columnar cadmium. The plating is applied without brightener and at high current densities to produce a porous cadmium that is perpendicular to the steel surface and allows hydrogen to escape during baking. This is different than cadmium plating that is applied with brightener at lower current densities. Cadmium plated under these conditions is bright/shiny and laminar (parallel to the steel surface) in structure. This cadmium structure supposedly is much more difficult to bake properly for adequate hydrogen embrittlement relief.

In a previous report[1], ASTM F519 type 1d (notched C-ring) specimens showed significant lab-to-lab variation in results. The labs in the study included commercial and government facilities. After numerous passes/failures, examination of stressed specimens revealed a crack in the cadmium plating at 42 percent of the ultimate notched tensile strength (UNTS). It was not determined if the cracks extended to the steel surface.

In this study, a maintenance chemical was evaluated by various "U.S. Air Force approved" labs using ASTM F519 type 1a (notched tensile specimens). The first test resulted in a failure and the subsequent test passed. A rewriting of the specification required another qualification test with a different lab. Again, the first test failed. When the lab was requested to provide the failed specimens for failure analysis, the response was "we don't have to provide them, all we have to do is provide the results . . . Pass or Fail." A second test was then run by a commercial lab with the understanding that the specimens would be available for failure analysis.

Approach:

Type 1a specimens (4340 at 51-54 HRC) were cadmium plated per Treatment B of ASTM F519. The specimens were loaded to 45 percent UNTS and exposed to the maintenance chemical. A second set of specimens were loaded to 75 percent UNTS for 200 hours in air. A third set of specimens were loaded to 45 percent UNTS and exposed to distilled water. Various specimens from each set which passed or failed were examined with the scanning electron microscope (SEM) to determine the surface condition and/or the failure mode. Where necessary, X-ray analyses were performed to document specific observations.

Results:

Specimens 0592, 0593, and 0594 were loaded to 45 percent of UNTS and exposed to the concentrated maintenance chemical solution. Times to failure ranged from 29.2 to 31.6 hours. Specimens 0595, 0596, and 0597 were loaded to 45 percent UNTS and exposed to a 6 percent dilution of the maintenance chemical. Times to failure ranged from 38.2 to 53.8 hours. Specimens 0589, 0590, and 0591 were loaded to 75 percent UNTS in air for 200 hours. All three specimens passed the test as required for cadmium plated and baked specimens. See Tables 1 and 2. Finally, specimens 14, 15, and 16 were loaded to 45 percent UNTS and exposed to ASTM D1193, type II water. Specimen 15 failed after 14 hours while specimens 14 and 16 passed the 150 hour exposure requirement. See Table 3.

Specimen 0592 was examined using the SEM. The fracture surface is shown in Figure 1. Intergranular attack indicative of hydrogen embrittlement is evident on the fracture surface. Figure 2 shows the condition of the cadmium plating adjacent to the fracture. Elongated voids and holes are evident in the cadmium plating. The X-ray analysis of the surface shows a significant amount of iron to be present. Thus, potential defects in the cadmium plating exposed the steel substrate to the maintenance chemical during testing.

Specimen 0590 was photographed using the SEM and the surface is shown in Figure 3. Short, medium, and long cracks can be seen on the surface. X-ray analysis shows the surface to be essentially pure cadmium. These cracks correlate with the defects noted on the surface of specimen 0592. The presence of cracks agree with the observations noted in the reference report and confirms the fact that preloading to 75 percent of UNTS results in permanent deformation (cracking) of the cadmium plating. Figure 4 shows one of the cracks and an X-ray analysis using the "spot" indicator in the center of the crack. The presence of significant amounts of iron indicates that the crack extends through the plating to the basis metal. Permanent deformation of the cadmium plating and crack extension to the basis metal were not determined in the reference report.

Specimen 15 failed the test after 14 hours exposure to distilled water at 45 percent UNTS loading. The fracture surface is shown in Figure 5 and is a typical hydrogen embrittlement failure. The condition of the cadmium plating adjacent to the fracture is shown in Figure 6. Voids/defects in the cadmium plating of 10 to 20 microns are evident and porosity greater than 0.1 micron in the coating, as deposited, is considered excessive. X-ray analysis shows that the voids penetrate to the basis metal as iron is evident. With these defects in the plating, distilled water was shown to cause hydrogen embrittlement failure. Specimen 16 passed the 150 hour test at 45 percent UNTS loading with distilled water. Figure 7 shows the condition of the cadmium plating in the notched area of specimen 16. There are no voids, cracks, or other defects in the cadmium exposing the basis metal. Examination of the cadmium surface up to 3000X did not reveal any additional defects. Examination of the cadmium plating on the shank of specimen 16 revealed a larger sized nodule deposit. See Figure 8. This indicates a current density difference or some type of

shielding in the notched area resulting in two different plating deposits/crystal structures on the same specimen. All these cadmium coatings were applied by the same plating contractor.

A photograph of cadmium plating per Treatment B of ASTM F519 on a steel "Hull Cell" specimen is shown in Figure 9. This reveals a different structure again. Crystal structures on the Hull Cell specimen varied significantly with current density. These variations may be due to the smooth/polished nature of the specimen versus the blasted surface required for the notched tensile specimens. The Hull Cell specimen was coated with cadmium by a different plating vendor.

Discussion:

Paragraph 11.1 of ASTM F519-93 states that "the accept/reject criteria are the judgments for precision and may vary depending on the applied stress and notch geometry." Based on the results of this study, it is proposed that the nature of the cadmium deposit is a significant variable affecting the precision of the test. It is also interesting to note that paragraph 11.2 states that no interlaboratory study has been made to verify bias in the test. The reference report evaluated the same maintenance chemical, same applied load, and same specimen geometry at three different labs and essentially ended up with three different sets of data. A reproduction of the data is shown in Table 4.

The interpretation of the failure analysis suggests that two different situations can exist during the test. These two situations are a direct result of potential variations in the cadmium plating. Condition I assumes a continuous cadmium plating with no porosity or other defects such as cracks that form on loading. A continuous cadmium coating would slowly dissolve in the maintenance chemical putting cadmium ions in solution with the potential formation of cadmium corrosion product. As long as the cadmium layer is continuous, only general corrosion of the cadmium would occur with no embrittlement of the steel. See Figure 10. This continuous layer was noted with specimen 16 which survived the 150 hour contact with distilled water.

Condition II assumes a cadmium plating that has pores, cracks, or other defects that expose the basis metal. A cadmium coating with defects exposing the basis metal would result in galvanic corrosion where the cadmium is an anode and steel is the cathode. Since hydrogen is generated at the cathode, hydrogen embrittlement of the steel can occur under the test condition. The maintenance chemical or distilled water simply becomes the electrolyte in a galvanic corrosion cell. This condition is summarized in Figure 11. Thus, under current conditions, the test evaluates the cadmium plating and not the maintenance chemical. If water cannot be used for aircraft maintenance, the entire concept of washing aircraft needs to be reviewed. Exposing aircraft to rain, sleet, and snow would also have to be curtailed if this is a valid test. Since aircraft have survived in these environments for years, it is obvious that this is not the problem.

The question also arises why concentrated alkaline cleaners have consistently passed this test. Above pH 10, alkaline electrolytes would passivate the steel in the defects and no hydrogen would be generated. Alkaline cleaners that have failed were probably diluted to less than pH 10 and simply became electrolyte in the galvanic reaction. Other materials, such as phosphoric acid cleaners and alodine solutions, have failed the test in two and eight seconds, respectively[2]. They obviously represent even better electrolytes for galvanic corrosion.

This paper brings into question the reproducibility/probability of testing per ASTM F519. It identifies a number of variables that need to be addressed before a valid test can be performed. The integrity/consistency of the cadmium plating with respect to specimen geometry and loading is critical to performing a valid test.

Recommendations:

It is recommended that:

(1) Some method of quality control be applied to the cadmium plating deposited on ASTM F519 specimens. The "cookbook recipe" approach currently used does not ensure reproducible deposits.

(2) A test should be conducted to determine the ability of columnar/nodular cadmium plating to be loaded beyond 40 percent UNTS without cracking on a consistent basis.

(3) Labs that are "government approved" be required to furnish failed specimens upon request. The contractor paying for the test should have the option of performing a failure analysis when the tests fail. In fact, ASTM F519 requires a failure analysis prior to retesting.

(4) A test method must be developed that ensures the integrity of the cadmium plating after loading to 45 percent UNTS and prior to exposure to the maintenance chemical.

References:

[1] Grainger, J., DeGuzman, E., and Distaso, J., Reproducibility of Hydrogen Embrittlement Testing for Aerospace Maintenance Chemicals. Presented at the First International Technology Transfer Conference on Hydrogen Embrittlement of Fasteners: Problems and Solutions, Denver, CO, 17-19 May 1995.

[2] Communication with Mr. Gene Stevens at Kelly Air Force Base, TX.

TEST REPORT

Report Number	210598
Report Date	21-NOV-94
Page	1 of 2
Client Number	**265600
Client Order	4298

RECEIVED	Approx. 80 Ounces of Test Solution (3 Containers)
IDENT AS	Batch 4279 Lot 1
MATERIAL	UBIX No. 0092
CONDITION	*
TEST TO	ASTM F519-77
TEST PER	ASTM F519-77
PURPOSE	*
PHONE	713-242-7741

PROPERTIES AS SUPPLIED

9 ASTM F519-77 Type 1a V-Notch Sustained Load Specimens (Lot A Batch A Serial Nos 0589 thru 0597) were plated per ASTM F519-77 Annex A1 Treatment B, except a 100 hour bake was used in lieu of 23 hours.

150 HR. SUSTAINED LOAD TEST: IMMERSED IN: CONCENTRATED UBIX #0092
PROCEDURE: 45% OF NOTCHED UTS PER ASTM F519-77

S/N	Notch Dia	Load KSI	Date/Time Start	Time Hrs	Visual Inspection @ 10X	Results	Disp
0592	0.175"	174.3	11/11/94 1330	29.2	-	Rupture	Off Spec
0593	0.175"	174.3	11/11/94 1330	31.0	-	Rupture	Off Spec
0594	0.175"	174.3	11/11/94 1330	31.8	-	Rupture	Off Spec

TABLE 1. TEST REPORT

TEST REPORT

Report Number	210598
Report Date	21-NOV-94
Page	2 of 2

150 HR. SUSTAINED LOAD TEST: IMMERSED IN: 6% DILUTED UBIX #0092
PROCEDURE: 45% OF NOTCHED UTS PER ASTM F519-77

S/N	Notch Dia	Load KSI	Date/Time Start	Time Hrs	Visual Inspection @ 10X	Results	Disp
0595	0.175"	174.3	11/11/94 1330	38.2	-	Rupture	Off Spec
0596	0.175"	174.3	11/11/94 1330	53.8	-	Rupture	Off Spec
0597	0.175"	174.3	11/11/94 1330	50.9	-	Rupture	Off Spec

200 HR. SUSTAINED LOAD TEST
PROCEDURE: 75% OF NOTCHED UTS PER ASTM F519-77

S/N	Notch Dia	Load KSI	Date/Time Start	Time Hrs	Visual Inspection @ 10X	Results	Disp
0589	0.175"	290.6	11/11/94 1330	200.0	No cracks	No rupture	In Spec
0590	0.175"	290.6	11/11/94 1330	200.0	No cracks	No rupture	In Spec
0591	0.175"	290.6	11/11/94 1330	200.0	No cracks	No rupture	In Spec

TABLE 2. TEST REPORT

TEST REPORT

Report Number 213453
Report Date 5-JAN-95

3 ASTM F519-77 TYPE 1A NOTCHED ROUND BARS (LOT 191532 SERIAL NOS. 14 THRU 16) WERE MANUFACTURED PER ASTM F519-77 PAR. 7.2.4 AND 7.2.5 FOR THE FOLLOWING TESTS:

SUSTAINED LOAD TEST V NOTCH SPECIMEN
IMMERSED IN ASTM D1193 TYPE II WATER

S/N	Notch Dia	Load KSI	Date/Time Start	Time Hrs	Visual Inspection @ 10X	Results	Disp
14	0.175"	174.3	12/29/94 1200	150.0	No cracks	No rupture	For Info
15	0.175"	174.3	12/29/94 1200	14.0	-	Rupture	For Info
16	0.175"	174.3	12/29/94 1200	150.0	No cracks	No rupture	For Info

TABLE 3. TEST REPORT

Initial Test Results

Type 1D Tests on Compound A
Hours to Failure
(>100hrs=DNF)

SAMPLE	LAB A	LAB B	LAB C
1	<2, <2, <2, <2	----	>100, >100, >100
2	>100, >100, >100	<1	<1, <1, <1
2a	<2, <2, <2	<1	<1, <1, <1
3	>100, >100, >100	<1, <1	<48, <48, <48
3a	30, 31	<1	<16, <16, <16
3b	>100, >100	<10	<16, <16, <16
3c	>100, >100	----	<16, <16, <16
3d	>100, >100, >100, >100	----	<16, <16, <16

TABLE 4. TEST DATA

FIGURE 1. SPECIMEN #0592 SHOWING FRACTURE SURFACE.

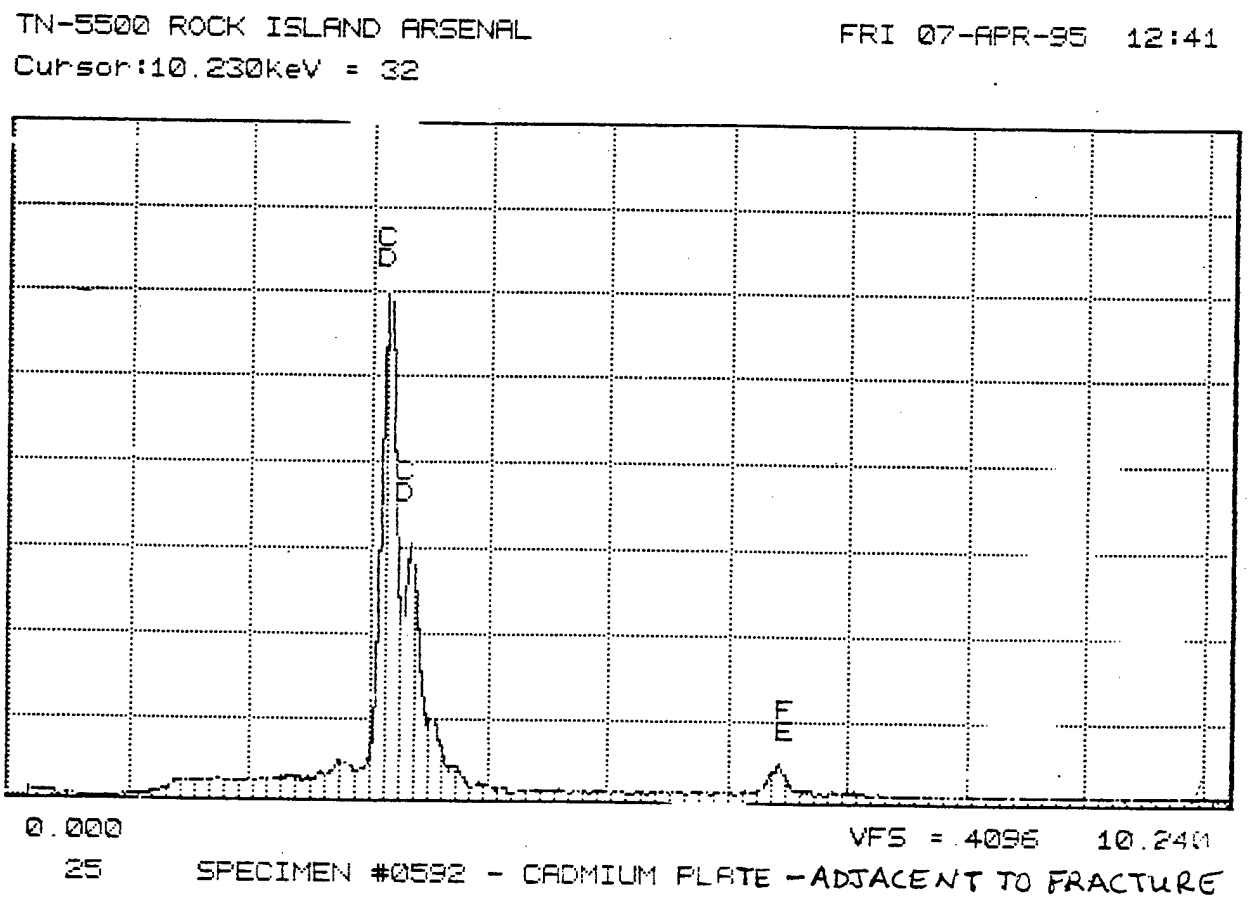

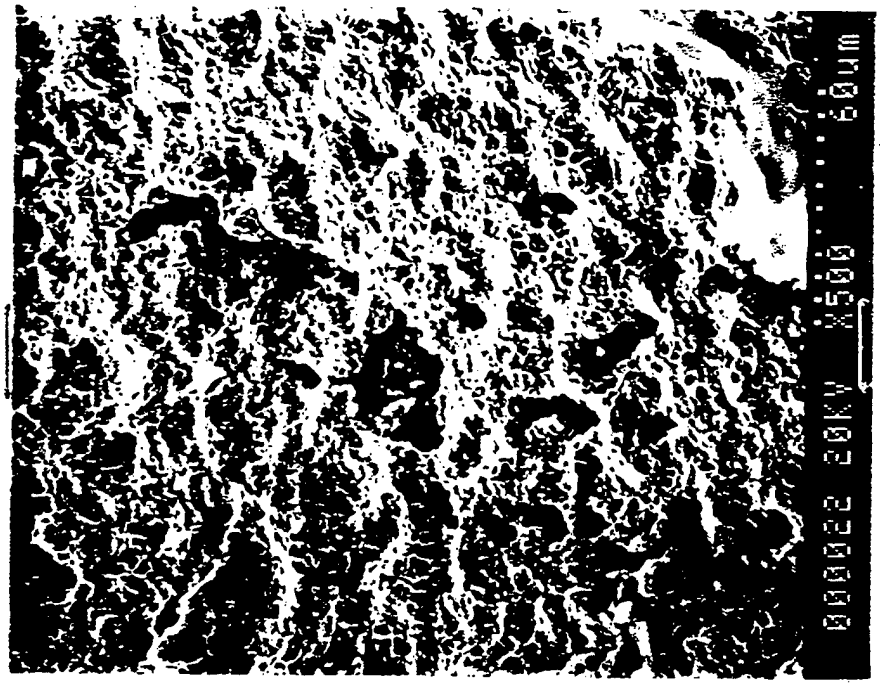

FIGURE 2. CONDITION OF CADMIUM SURFACE.

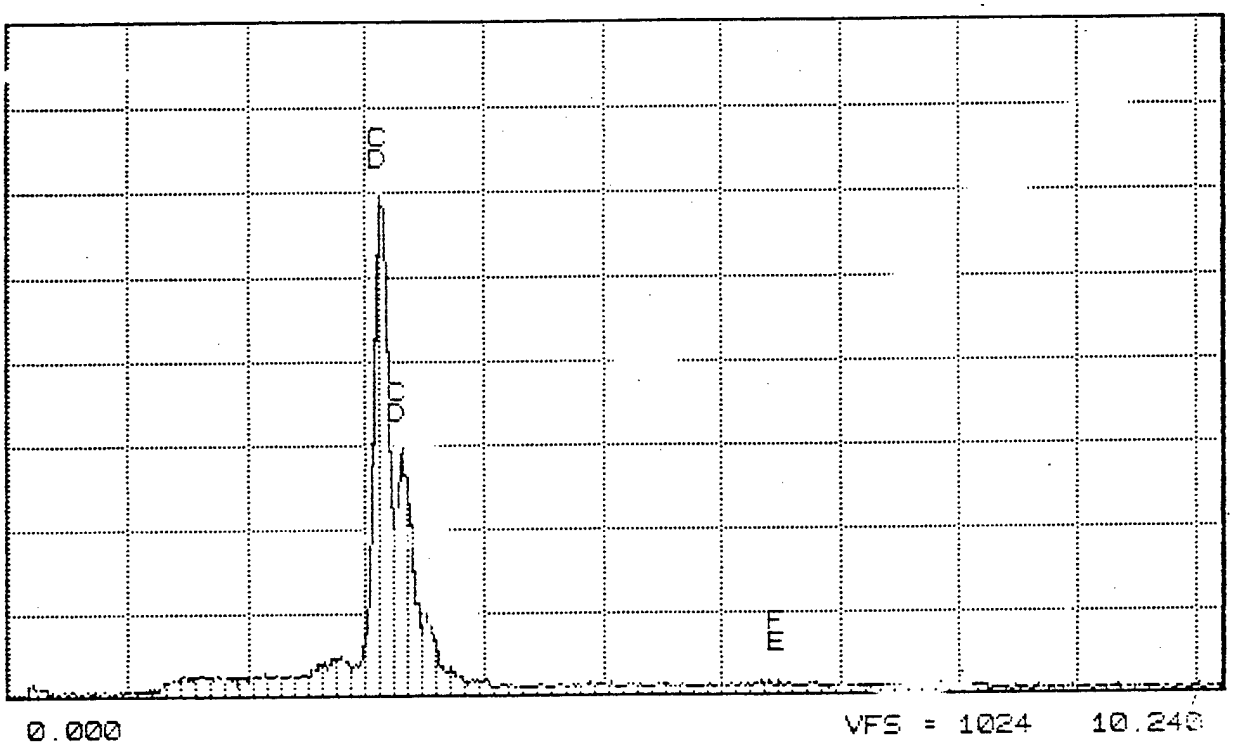

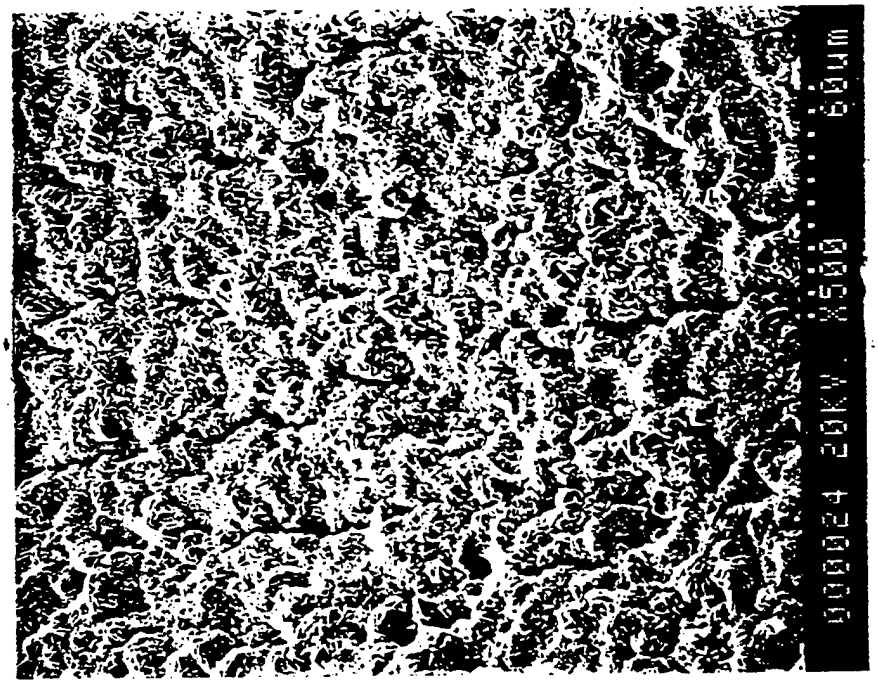

FIGURE 3. CONDITION OF CADMIUM AFTER 75% UNTS LOADING.

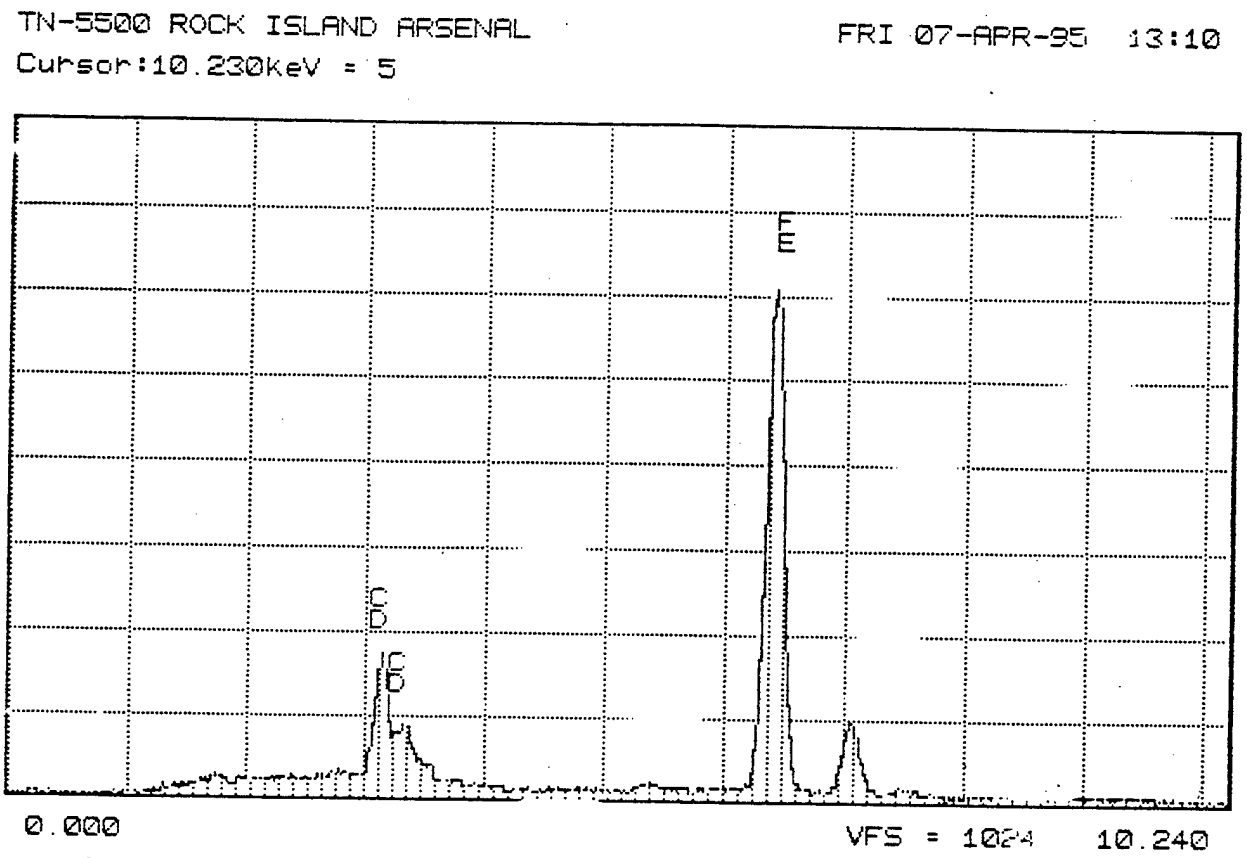

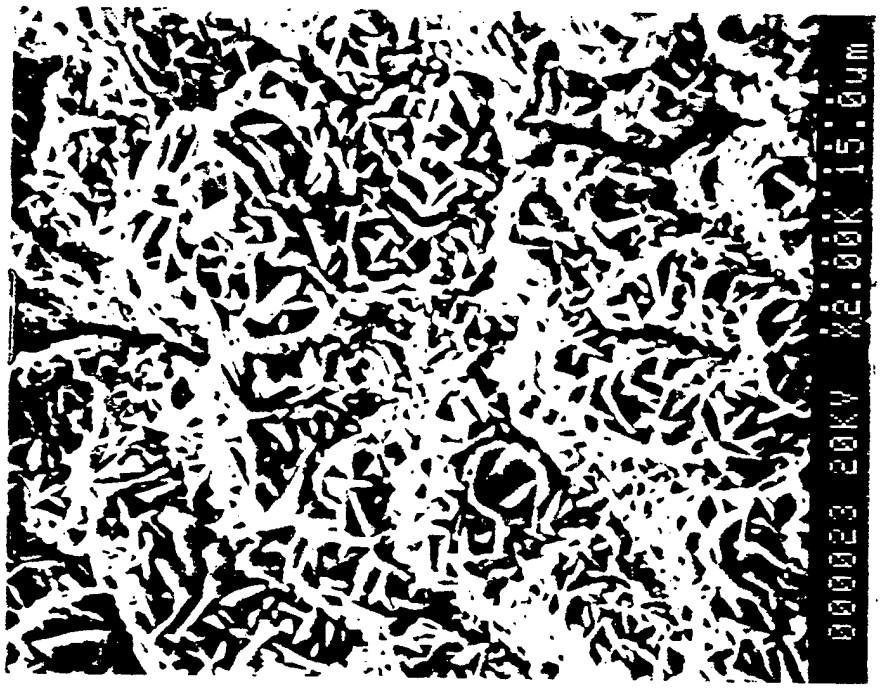

FIGURE 4. ANALYSIS OF CRACK

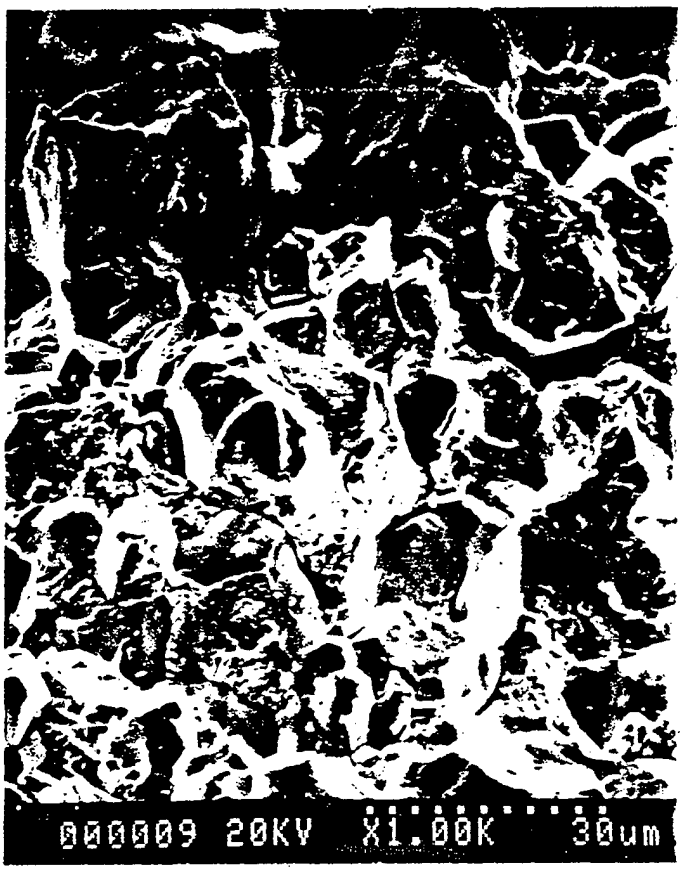

FRACTURE SURFACE SHOWING INTERGRANULAR ATTACK TYPICAL OF HYDROGEN EMBRITTLEMENT. TEST DURATION - 14 HOURS.

FIGURE 5. SPECIMEN 15 EXPOSED TO DI WATER.

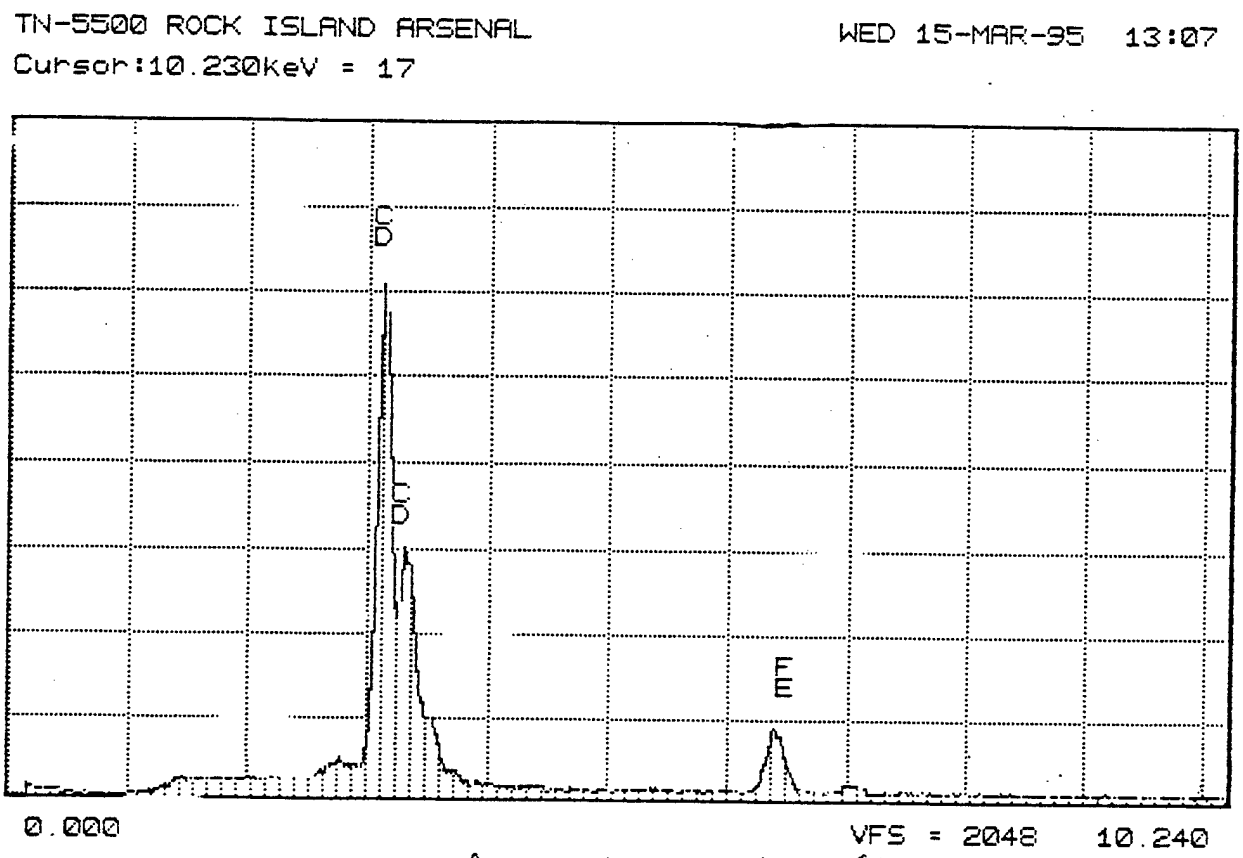

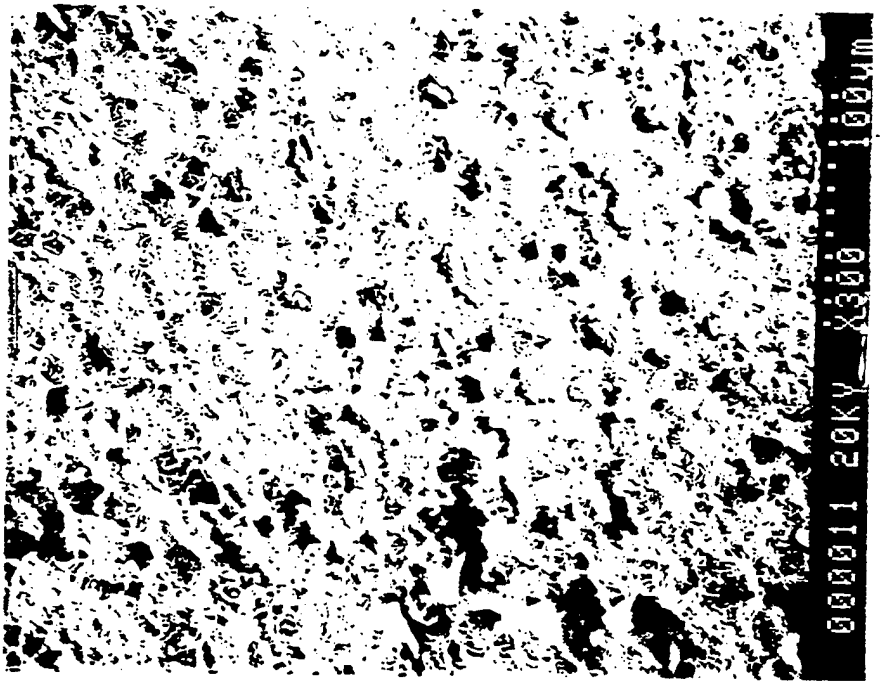

FIGURE 6. CADMIUM SURFACE ON SPECIMEN 15.

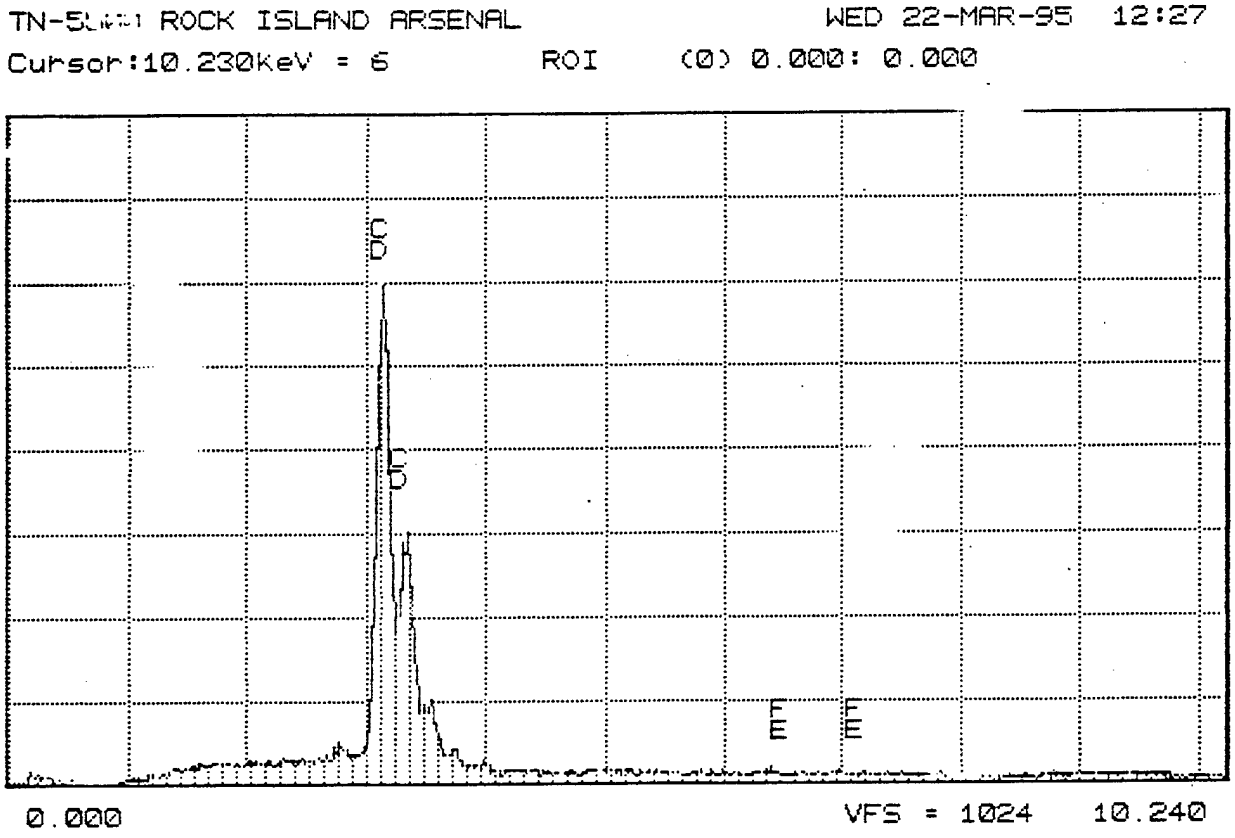

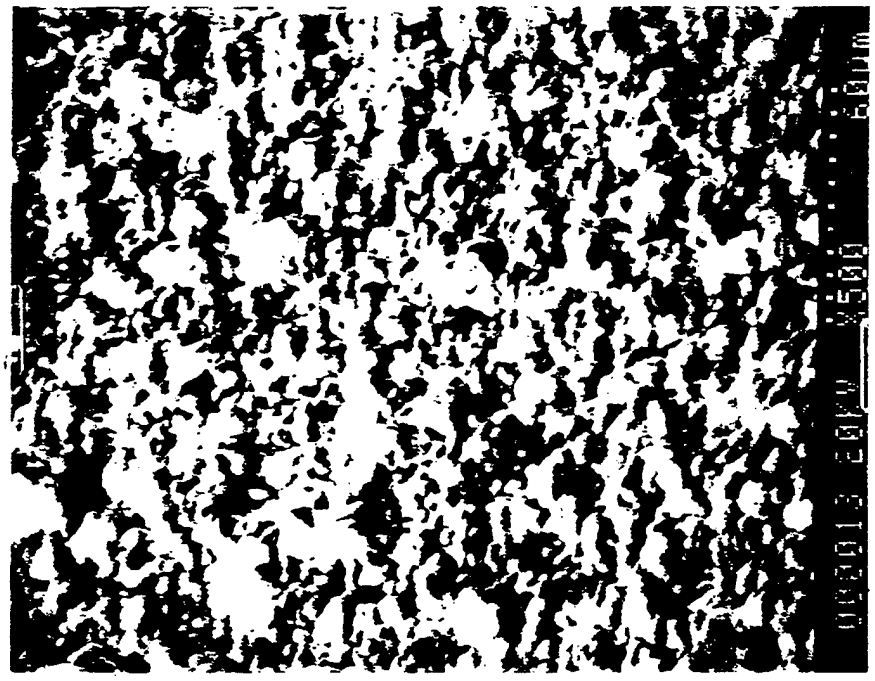

FIGURE 7. CADMIUM SURFACE IN RADIUS ON SPECIMEN 16.

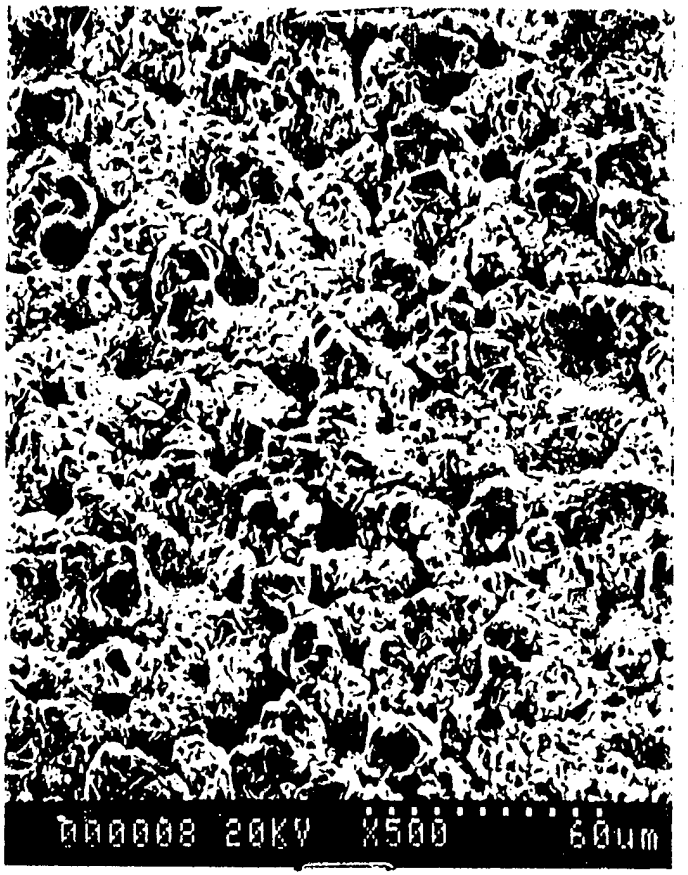

CADMIUM ON SHANK OF SAMPLE #16.
NODULES ~ 15 μm. COATING IS CONTINUOUS.

CADMIUM IN RADIUS ON SAMPLE #16.
NODULES ~ 6 μm. COATING IS CONTINUOUS, I.E., NO PORES.

FIGURE 8. SPECIMEN 16. SHANK VS. RADIUS.

FIGURE 9. PHOTO OF NODULAR (DULL) CADMIUM ON HULL CELL PLATE.

CONDITION I - Cd PLATE (NON-POROUS)

SCHEMATIC

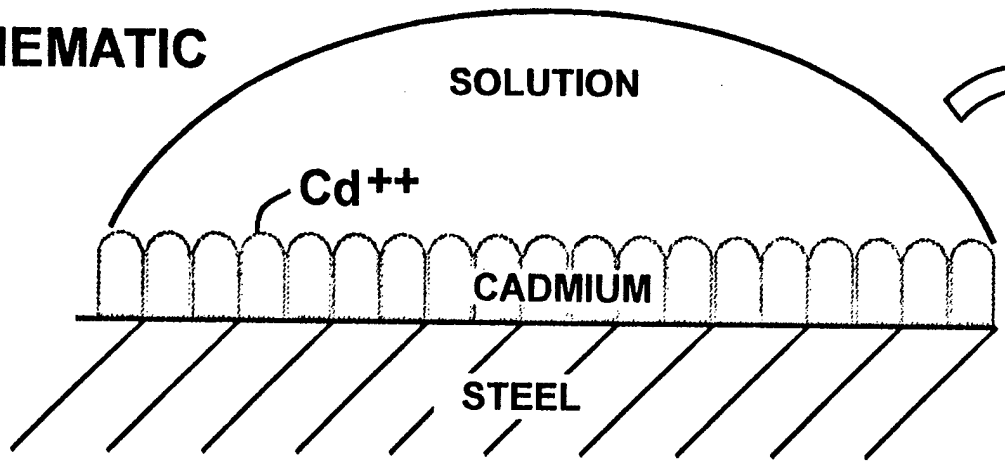

GENERAL CORROSION OF Cd IN CONTACT WITH ELECTROLYTE. NO H_2 INVOLVED

CHEMICAL REACTION: $2\,Cd + 2H_2O + O_2 \longrightarrow 2\,Cd(OH)_2$

ASTM - F519 CADMIUM PLATED SPECIMEN

FIGURE 10

CONDITION II - Cd PLATE (POROUS)

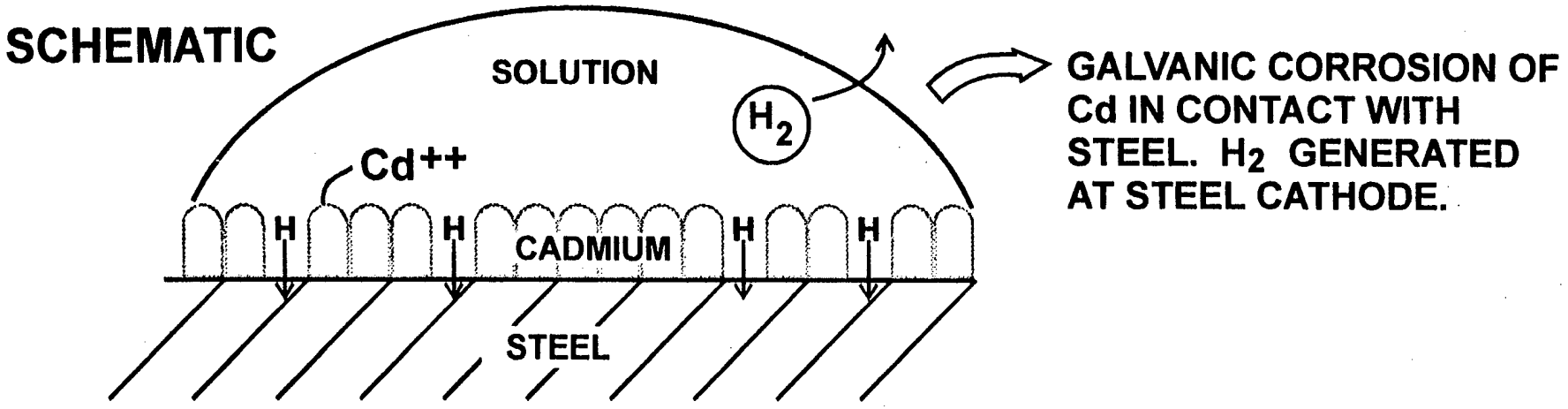

CHEMICAL REACTION: $Cd + 2H_2O \longrightarrow Cd(OH)_2 + H_2$

ASTM - F519 CADMIUM PLATED SPECIMEN

FIGURE 11

Development of an Alternate Material Selection System for Cadmium Electroplating

Paul Decker
U.S. Army Tank-Automotive & Armaments Command
Warren, MI

Keith Cramer
Ocean City Research Corporation
Ocean City, NJ

Abstract

Cadmium plating is used in many applications to protect substrates from corrosion and provide other beneficial properties such as lubricity and galvanic compatibility. There is no single alternate coating or material available that can match or exceed the performance of cadmium electroplating in all of its applications. Alternate materials are available that may perform adequately in specific applications to replace cadmium. The U.S. Army Tank-Automotive & Armaments Command, Tank-Automotive Research and Development Engineering Center (TACOM-TARDEC) tasked Ocean City Research Corporation (OCRC) to develop the first version of an Alternate Material Selection System for Cadmium (AMSS-Cd)[1] and a detailed explanation report[2] explaining the system. This work was completed through the support of the Army Acquisition Pollution Prevention Support Office (AAPPSO) of the Army Material Command (AMC). This effort was teamed with efforts from industry participants to develop an affective tool for a materials or design engineer to select an alternative material to cadmium

Introduction

Executive Order 12856 mandates that the Department of Defense (DoD) reduce their hazardous waste generation 50% by 1999. Cadmium is used on Army weapon systems as a corrosion control coating for steel and aluminum. Cadmium is a carcinogenic material and has low worker exposure and environmental discharge limits due to its high toxicity. Cadmium contributes to hazardous waste generation for Army depot facilities and contractors during both plating operations, and repair/overhaul procedures.

In "Guidance for Eliminating Cadmium from U.S. Army Weapon Systems[3]" AAPPSO estimated cadmium hazardous waste handling and disposal costs for the U.S. Army. There are some very significant costs and risks associated with the continued use of cadmium in U.S. Army weapon systems that will not only affect the life cycle cost of the systems, but may also affect readiness and fielding capabilities in some extreme circumstances.

- Hazardous waste disposal costs for cadmium at one Army depot were estimated to be $60,000 per year for treatment and disposal. This does not include administrative costs associated with compliance with RCRA, or any possible additional ordinances imposed by the state or local government.

- OSHA has set a 5 ppm 8-hour time weighted permissible exposure limit (PEL) for cadmium. Depots are required to upgrade their facilities to comply with the new regulations. One depot has committed $22M for an entirely new, OSHA-complying metal finishing facility. A second will reportedly spend $275K to upgrade an existing facility to provide shower and clean-up areas required for employees exposed to cadmium.

- The Army is also at risk from possible legal costs from worker compensation claims, class action lawsuits, and fines for compliance violations associated with the past and continued use of cadmium in weapon systems.

- International trends to minimize or eliminate cadmium have become more severe. The amount of cadmium allowed in weapon systems fielded in some foreign countries is severely limited and may be banned in the future. This will affect the Army's ability to supply, support, and operate military operations in foreign countries and could reduce some foreign military sales activities.

This Alternate Material Selection System for Cadmium (AMSS-Cd) has been developed as a tool to help guide design and material engineers along the process of identifying an appropriate non-cadmium material for U.S. Army weapon systems. Version 1 of this system focuses on the use of cadmium in plating applications. The primary types of materials discussed in this system will provide sacrificial and barrier corrosion protection to steel and aluminum substrates in typical Army weapon system environments, just as cadmium provided. Additional coatings that provide only a barrier to keep corrosive environments from substrate materials and alternate base materials are also briefly mentioned in the system because they will be appropriate alternatives for some applications.

The system requires the user to understand the requirements of the application they are examining. It then gives some suggested alternate materials and possible specifications. Industry standards or commercial specifications have been identified when possible to assist the DoD's efforts to move away from the use of military specifications and standards. The system is a guide to help the user select an alternate material. ***The responsibility for ensuring that the appropriate coating is selected ultimately falls upon the user of the AMSS-Cd.***

Alternate Material Selection System Concept

The Alternate Material Selection System is intended to help select appropriate materials to replace hazardous materials used in military systems. It is not intended to be Army policy, but rather it is intended to provide guidance to the decision-maker. The system tries to generalize the requirements for all of the different applications of a material into a few categories. The system

then gathers all possible data from many varied test programs and tries to consolidate these results into general statements on the possible performance of the materials in these categories. The performance of the materials will be dictated by both its own properties, but also its ability to be properly applied on the specific part (coating in blind holes, etc.).

The AMSS uses these generalized application requirements and the material properties to point out the alternative with the highest expected probability of success for a given application. To be a successful substitute the material must be able to perform acceptably, have minimal impact on system performance, be readily available, and have a cost that is appropriate for the application. It is up to the user of the AMSS to decide if these generalizations are not appropriate for their particular application. If the system's assumptions are not correct, the more detailed information available in the supporting reports should be consulted to make appropriate material decisions. The AMSS custodians may also be contacted to aid in difficult material selection decisions.

The AMSS is meant to be a living document, undergoing constant revision. New materials are constantly being developed and their properties are being evaluated. Periodically, the AMSS document is meant to be revised to include all additional information. All constructive criticism or sharing of additional test data associated with the AMSS will be appreciated.

Alternate Material System for Cadmium (AMSS-Cd)

The AMSS-Cd has been developed through a review of available technical information on cadmium alternatives, as well as discussions with several commercial industry representatives involved with cadmium use and substitution. The system is broken down into a series of tables to help the user identify materials which may be appropriate for their application. The tables include:

Table 1: Suitable Materials for Army Applications
Table 2: Material Properties Required for Army Applications
Table 3: Material Performance in Material Property Categories

Suitable Materials for Army Applications

Table 1 of the AMSS-Cd is titled Suitable Materials for Army Applications. This table lists the various material families listed as cadmium alternatives. It indicates if they are appropriate for use in different major application areas where the U.S. Army still uses cadmium plating. The major alternate material systems are identified along with the major applications identified for the Army's uses of cadmium platings. Table 1 has been included in the AMSS-Cd to help the user narrow down the list of all potential alternate material systems to just the material families that apply for the specific application of interest. Table 1 of the AMSS-Cd is included as Table 1 of this document.

Alternative Materials for Cadmium. Many different types and classes of materials are proposed as cadmium alternatives. The types of alternatives that may be appropriate for different applications depend on the component property requirements, dimensional limitations, environmental exposure, process restrictions, etc. Some materials which are possible alternatives to cadmium coated substrates are given below.

Material Family	Sub-Category Descriptions
Zinc Coatings	Electroplated Zinc, Hot-Dip Galvanized Zinc, and Inorganic Zinc
Zinc Alloy Platings	Tin/Zinc, Zinc/Nickel, Zinc/Cobalt, and Zinc/Iron
Aluminum Based Coatings	Ion Vapor Deposited Aluminum (IVD Al) and IVD Al alloys, Electroplated Aluminum, and Aluminum/Ceramic
Organic (Paint) Coatings	Paints, Metal-Filled Paints, and Duplex Metal Coating/Organic Coating Systems
Barrier-Only Metal Platings	Nickel, Tin, Gold, and Silver
Alternative Base Materials	Stainless Steel and Composites

All possible alternative materials have not been included in the overall summary charts. The materials excluded primarily include those which are not commercially available, or are not portrayed as large scale production coatings. They may be applicable for special parts, or may develop into large-scale production coating processes in the future.

Major Application Categories of Cadmium Plating. There are many uses of cadmium coatings on various substrate materials. These primarily include areas where cadmium protects a substrate from environmental corrosion. Cadmium also has the benefits of reducing or eliminating bi-metallic corrosion (galvanic couples), providing a lubricous surface, and providing a pore-free coating at very low thicknesses. Cadmium is used in many different applications. Three of the major TACOM application categories are discussed in this report:

Major TACOM Application Category
Fasteners
Small steel components
Electrical connectors

Material Properties Required for Army Applications

Table 2 of the AMSS-Cd is titled Material Properties Required for Army Applications. It lists the major Army applications of cadmium plating along with the key material properties that have been identified for the different types of cadmium applications. The list is meant to address performance requirements by most, but not all individual applications of cadmium within the category. Table 2 has been included in the AMSS-Cd to help the user narrow down the list of all potential material properties to just those that generally apply for the specific application of interest. If specific details are available for the application requirements, the information should be used to expand or further narrow the list of important properties for consideration when selecting an alternate material system. AMSS-Cd Table 2 is included as Table 2 of this document.

Description of Key Properties. The material properties discussed in this material selection system and explanation report do not include many specific test results. All results for the categories listed below were generalized to represent the overall performance of the materials in most situations discussed in the literature.

Alternative Material Key Properties for Major TACOM Applications

Substrates Used On
Corrosion Resistance
Material Compatibility to Aluminum
Lubricity
Hydrogen Embrittlement
Environmentally Assisted Cracking
Fatigue Properties
Wear
Adhesion
Low Contact Resistance
Maximum Temperature Limitations
Cost
Availability
Solderability
Environmental Friendliness

Material Performance in Material Property Categories

Table 3 of the AMSS-Cd is titled Material Performance in Material Property Categories. It lists 1-10 ratings (10 being good, 1 being bad) for the alternate material systems in the key material properties that have been identified for different cadmium applications. The 1-10 ratings are described in the AMSS-Cd explanation report attached to the system. ***This table is the heart of the AMSS-Cd.*** The information summarized in this table is used to select an alternative material system. Tables 1 and 2 are supplemental information that can be used to narrow down the fields of materials and properties prior to examining the performance ratings in Table 3. Sample material and property ratings from Table 3 of the AMSS-Cd are included as Table 3 of this document.

The ratings given in Table 3 are based on test data or application experience from several difference reference articles and many different types of test procedures. Whenever possible, information was used from the same test procedures to develop ratings for the same property category. This was not always possible. As an example, corrosion resistance combines data from

different natural exposures, ASTM B117 salt fog testing, and other accelerated corrosion tests to allow for comparisons between some of the alternatives.

If specific data was not available for different material system thickness and surface finish combinations, it was inferred from data available for other combinations from the same material type. In some cases data was not readily available for an entire material family for a specific material property. In this situation the rating was inferred from information available from similar types of material families for the property of interest. These ratings are underlined in the AMSS-Cd and the sample of Table 3 given in this report.

Table 3 provides ratings for all of the different thicknesses and surfaces finishes described in the referenced specification. When possible ASTM standards are referenced. ***Other commercial and industry specifications can be used for these material systems.*** Different thickness and surface finish requirements can also be specified when appropriate. ***The thickness and surface finishes listed correspond only to those listed in the referenced standards and are not meant to restrict the AMSS-Cd user to these requirements.*** Additional information on other specifications is given in the explanation report for the AMSS-Cd.

Qualitative Rating System. A number ranking system was developed to give a relative performance for comparison of the performance of the different materials in each of the categories. 1-10 numerical rankings (1 being worst, 10 being best) were developed from a review of available references on the performance of materials. An emphasis was placed on identifying references which compared several different materials. When possible, tests conducted in-service were examined and this data was referenced rather than accelerated laboratory test results.

The 1-10 ratings are listed in Table 3 for the alternate material systems for each material property. Qualitative 1-10 ratings are listed rather than actual test data. Differences in test procedures and test coating systems make it difficult to list actual test data for all of the different alternate material systems in all of the different property categories. Several different types of information are included in the AMSS-Cd explanation report to help users identify the actual expected performance of a particular material in a property category.

- When possible, the 1-10 rating descriptions refer to ranges of test performance values.
- Key reference documents are listed that discuss the performance of several alterative materials for the property category.
- Select technical papers are attached to the AMSS-Cd explanation report detailing some of the test data used to develop the 1-10 ratings for the different material systems.

The descriptions and rankings used for "good" to "bad" material systems are based on the context of performance in expected cadmium service environments and applications. For example, cadmium plating is used to effectively protect steel substrates for extended atmospheric exposure, but not seawater immersion. A material system rated as a good performer for corrosion resistance will not necessarily be a high performing system in seawater immersion.

The numerical performance ranking listed will differ from the performance measured in some test programs. If the AMSS user identifies a reliable reference that tested a wide variety of materials for their specific application, these individual test results can be substituted when alternatives are evaluated. In most situations the generalized rankings should give a realistic indication of the best types of alternate materials for an application.

Selection of an Alternate Material with the AMSS-Cd

Listed below are two examples of methods for using the ratings contained in Table 3 to help select an appropriate alternative material. Both are only suggested methods and have their own strengths and weaknesses. The AMSS-Cd user could use either method, both in combination, or develop a customized analysis system to identify appropriate alternatives.

Method 1 - Weight Multiplication Factors

In the weight multiplication factor (WMF) example, the user creates a customized table of materials and performance ratings for their own application. Each performance property rating is then given its own weight factor, as determined by the importance of the properties for the function of the application. The sum of the products of the performance ratings and their WMFs for each possible material are then compared for each material. Material systems with the highest totals are then examined according to specific details for each performance or other key property category to determine the most appropriate substitute. This technique has the advantage of being quicker, and easier to customize for the relative importance of performance differences of different key property categories. The disadvantage of this method is that it treats a unit difference in rated performance as an equivalent difference within each property. For example, the difference in lubricity between ratings of 9 and 10 is 0.10, but the difference in lubricity for ratings of 5 and 6 is 0.20. The steps of the WMF method are listed below.

1. Determine the application.

2. Note any specific requirements for your application (maximum thickness, mating materials, etc.)

3. Develop a table listing possible materials and important properties for the application. Fill in the appropriate row and column headings using Tables 1 and 2. Make sure to only focus on Properties which are important for the application.

   For many applications, non-performance issues such as cost, availability, etc. are important, but only after an alternative has been identified based purely on performance. In other cases, the non-performance issues may play a role on whether material systems that offer border line performance would be preferred. Depending on specific application requirements, one may assign weight factors to only a list of performance factors, and based on those results further down-size the list based on other non-performance requirements. If this approach is taken, one will do the analysis twice. The first analysis

would be with just key performance related properties. The second analysis would be with important non-performance related priorities and would be based on only the top ranking materials from the first analysis. Splitting the analysis will allow the user to separate out performance and non-performance related issues.

4. Examine Table 3. Fill in the performance rating for each type of coating material according to the 1-10 rating given in Table 3.

   *** The general numerical ranking can be adjusted in some circumstances. For example, if specific test data is available that directly correlates to your application, this test data can be used to make minor modifications to the given ratings for the individual application.

5. If certain properties are determined to be significantly more important that others, then that property can be "weighted" so that it more heavily influences the final material decision. An arbitrary multiplication factor can be given for the more important properties. The value of the weighting factor should reflect the relative importance of that property to the other key properties.

6. Use the sum of the weighted properties for each coating to indicate the top performers.

7. Compare the top rated materials, giving more weight to top priority properties.

8. Select the best alternate material based on weighted rank as well as personal knowledge of application and customer requirements.

Method 2 - Minimum Rating Requirements

The Minimum Rating Requirement (MRR) technique requires the user to give attention to each material rating value for each key property of their application. The process will be time consuming but does allow the user to develop an understanding of the general strengths and/or weaknesses for the different alternatives for each key property they evaluate. The process includes narrowing of the total list of alternates through the following steps.

1. Determine the appropriate major application category.

2. Identify any specific requirements for the application (maximum thicknesses, high service temperature requirements, etc.).

3. Use Table 1 to identify the appropriate material families for that application.

4. Use Table 2 to identify the appropriate key properties related to the application. (This analysis can also be done in an order to first only consider performance properties, and then non-performance issues.)

5. Prioritize the key properties according to the application requirements.

6. For every key property determine the minimum rating level you will accept for the application. Refer to the AMSS-Cd Explanation Report for a detailed explanation behind the expected performance for each rating level.

7. Start with the highest priority property and eliminate all material systems that do not meet the minimum rating needed for the application.

8. Move to the second, then third, etc. priority properties and eliminate all materials that do not meet the minimum requirements.

9. Continue until the key property categories have all been examined.

10. If needed, continue to narrow the list by assigning minimum performance rating requirements for other related factors, or increase the requirements for some properties. (Be careful to watch cost when specifying a material that will perform above the application performance requirements.)

11. If the initial list is too narrow, go back and determine if any of the minimum requirement ratings can be lowered to include more alternatives.

(Each user of the AMSS should develop their own system to identify an appropriate alternative.)

Example Problem

Problem: A Grade 5, 1/4"-13, 3" long steel bolt is used to hold together a lap joint for two steel plates on the exterior of a large structure in a marine environment, and has a specification for a QQ-P-416, class 2, type II cadmium coating. What should this specification be changed to?

Resolution:

Basics for low strength fasteners:

Table 1: Appropriate Materials

Zinc electroplating
Tin/zinc
Zinc/nickel
Zinc/cobalt
Aluminum Ceramic
Nickel
Stainless Steel

Table 2: Key Properties

Corrosion Resistance
Aluminum Compatibility (possible)
Lubricity
Fatigue Resistance (possibly)
Wear (possibly)
Adhesion (possibly)
Low Cost
Availability
Environmental Friendliness

The description of the application indicates that this will be a corrosive application. There is no indication given that this is a safety critical joint. Based on the application description, it can be concluded that there will not be contact with aluminum. Grade 5 fasteners have ultimate tensile strengths less than 150 ksi. For threaded fasteners, coatings specified at 0.5 mils or less should be used unless another thickness tolerance is specified. The performance of different alternate materials will first be analyzed.

Property:	Corrosion	Lubricity	Wear	Adhesion
Weight Factor:	5	4	1	1

From the weighted totals, the following materials performed well:

Material	Total
Cadmium, 0.3 mils, chromate	90
Zinc, 0.5 mils, zinc phosphate	77
Zinc, 0.5 mils, colored chromate	82
Zinc, 0.3 mils, zinc phosphate	72
Zinc, 0.3 mils, colored chromate	77
Tin/Zinc, 0.5 mils, chromate	82
Zinc/Nickel, 0.4 mils, bronze chromate	87
Zinc/Cobalt, 0.47 mils, bronze chromate	82
Aluminum-Ceramic	99
Nickel	47
Stainless Steel	93

The top three performing non-cadmium materials are zinc/nickel alloy plating, aluminum ceramic coating, and stainless steel. Zinc, at 0.5 mils with a colored chromate coating, and tin/zinc platings also offer fairly good performance ratings, although they are rated well below the cadmium coating currently specified. Weight factors for non-performance based properties, and the corresponding rating sums are given below for the top rated materials.

Property:	Cost	Availability	Environmental Friendliness
Weight Factor:	3	1	3

Material	Total
Cadmium, 0.3 mils, chromate	30
Zinc/Nickel, 0.4 mils, bronze chromate	46
Aluminum-Ceramic	30
Stainless Steel	31

The zinc/nickel plating has the best non-performance based rating of all three materials. An appropriate way of specifying a 0.4 mil zinc/nickel plating with a bronze chromate conversion coating (to replace a QQ-P-416, class 2, type II cadmium plating) is ASTM B841, Grade 3, Type C. Because the lubricity of zinc/nickel is lower than cadmium, the torque requirements for the fastener should be increased to achieve the same clamping load.

TACOM Implementation of the AMSS-Cd to Identify Alternatives to Cadmium

TACOM has already begun to use the AMSS-Cd to identify appropriate alternatives to cadmium platings. These efforts have been focussed on internal use and contractor distribution of the system.

The AMSS-Cd will be of use to the Army and DoD in future vehicle and weapon system design, and for any individual components requiring redesign to eliminate use of cadmium plating. It will serve as a vehicle for bringing the Army's suppliers up to speed on commercially available cadmium replacements and inform them of the work that has already been done in this area.

To aid in their replacement of cadmium in the identified major applications categories, TACOM has developed an in-house priority ranking for the different alternate materials. This listing gives the TACOM AMSS-Cd a list of alternatives that will likely be acceptable for general applications. The user is still responsible for examining the details of their application to make the final decision on the applicability of the alternate material system. Also, this list should not be used for mission-critical components. Each of these applications should receive its own detailed analysis based on the specific requirements for that application.

Future Efforts

The task of identifying alternate materials for all cadmium applications is not yet complete. Several tasks are underway to help further eliminate cadmium. Some of the specific tasks that TACOM is involved with are listed below:

- Identification of an alternative material system for use on electrical connectors.
- Identification of an appropriate lubricant for IVD aluminum on high strength fasteners.
- Identification of non-chrome conversion coatings for zinc and zinc alloy platings.
- Development of a lessons-learned database through evaluation of the performance of cadmium plating alternatives already used in military service environments.
- Development of an Internet web site to increase accessability of the AMSS-Cd, simplify the use of the AMSS-Cd analysis techniques. This will enable the military and technical community to be continually updated on new developments in cadmium alternatives.
- Continue to participate in the National Center for Manufacturing Sciences (NCMS) working group to develop a larger-scale matrix focussing on across the board industrial applications of cadmium.

Acknowledgments

The authors would like to thank the Army Materiel Command's Army Acquisition Pollution Prevention Support Office (AMC-AAPPSO) for support in the development of the AMSS-Cd and its explanation report. The authors would also like to thank the many industrial and DoD representatives who were kind enough to review the draft version of the AMSS-Cd.

References

1. Ocean City Research Corporation Final Report, "Alternate Material Selection System for Cadmium (AMSS-Cd) Version 1", prepared for U.S. Army Tank-Automotive and Armaments Command, April 1997.

2. Ocean City Research Corporation Final Report, "Details of the Alternate Material Selection System for Cadmium", prepared for U.S. Army Tank-Automotive and Armaments Command, April 1997.

3. Ocean City Research Corporation Final Report, "Guidance for Eliminating Cadmium From U.S. Army Weapon Systems", prepared for Army Material Command, Army Acquisition Pollution Prevention Support Office (AMC-AAPPSO), April 1996.

Table 1: Suitable Materials for Army Applications

Alternative Category	Sub-Category Description	Major Category	Fasteners	Fasteners	Small Steel Hardware	Small Steel Hardware	Electrical Connectors	Electrical Connectors
		Description	less than 150 ksi ultimate tensile strength	greater than 150 ksi ultimate tensile strength	Simple	Complex		
		Substrate	steel	steel	steel	steel	steel	aluminum
ALTERNATE COATINGS								
Zinc	Plating		Yes	Possibly, but Hydrogen Embrittlement and/or Environmentally Assisted Cracking (HE/EAC) possible	Yes	Yes	No	No
	Hot-Dip		Check Tolerances	Possibly, Check tolerances, EAC possible	Possibly	Possibly	No	No
	Inorganic		No	No	Possibly	No	No	No
Zinc Alloy	Sn/Zn		Yes	Yes	Yes	Yes	Possibly	Possibly
	Zn/Ni		Yes	Possibly, HE/EAC possible	Yes	Yes	Possibly	Possibly
	Zn/Co		Yes	Possibly, HE/EAC possible	Yes	Yes	No	No
	Zn/Fe		Yes	Possibly, HE/EAC possible	Yes	Yes	No	No
Aluminum	IVD		Possibly, galling possible at high stress	Possibly, galling possible at high stress	Yes	No	Possibly	Possibly
	Electroplate		Possibly, galling possible at high stress	Possibly, galling possible at high stress	Yes	Yes	Possibly	Possibly
	Al-ceramic		Possibly, Check tolerances, use lubricant	Possibly, Check tolerances, use lubricant	Yes	No	Possibly	Possibly
Paints	organic		No	No	Possibly	Possibly	No	No
	metal-filled		No	No	Possibly	Possibly	No	No
	Duplex		Possibly	Possibly	Possibly	Possibly	No	No
Barrier-Only Metal Plating	Tin		No	No	No	No	No	Possibly
	Nickel		Possibly	Possibly	Possibly	Possibly	Possibly	Possibly
	Gold, Silver, and alloys		No	No	No	No	No	Possibly
ALTERNATE BASE MATERIALS								
Stainless Steels			Yes	No	Yes	Yes	Yes	Yes
Composite with electroless nickel			No	No	No	No	Possibly	Possibly

Table 2: Material Properties Required for Army Applications

Major Application Category	Sub-Category	Substrates Material	Corrosion Resistance (1)	Material Compatibility with Aluminum	Lubricity	Hydrogen Embrittlement (HE)	Environ-mentally Assisted Cracking (EAC)	Fatigue Resistance	Wear (2)	Adhesion (2)	Low Contact Resistance	Solderability	Low Cost	Availability	Environmental Friendliness
Fasteners	Less than 150 ksi	steel	Yes	Possibly	Yes	No	No	Possibly	Possibly	Yes	No	No	Yes	Yes	Yes
	Greater than 150 ksi - Grade 8 min.	Steel	Yes	Possibly	Yes	Yes	Yes	Yes	Possibly	Yes	No	No	Yes	Yes	Yes
Small steel hardware		steel	Yes	Possibly	No	Possibly	Possibly	Possibly	Possibly	Yes	No	No	Yes	Yes	Yes
Electrical Connectors		steel	Yes	Possibly	Possibly	No	No	No	Possibly	Yes	No	Possibly	Possibly	Yes	Yes
		aluminum	Yes	Possibly	Possibly	No	No	No	Possibly	Yes	Yes	Possibly	Possibly	Yes	Yes

(1) Cadmium is used as a corrosion resistant coating. The amount of corrosion resistance required will depend on the environment the material will be exposed.

(2) This property is not typically a primary concern for cadmium applications, but it may become an issue when significantly different types of materials are substituted for cadmium (i.e. organics).

Table 3: (Sample) Material Performance in Material Property Categories

ID #	Alternative Category	Sub-Category Description	Specification	Class or Grade	Type	Min. Thick. (mils)	Finish	Corrosion Resistance (1)	Material Compatibility to Al	Lubricity (dry)	HE	EAC	Low Contact Resistance	Cost
1	Cadmium	Electroplating	QQ-P-416	2	II	0.3	chromated	8	8	9	8	9	8	7
2	Zinc	Electroplating	ASTM B633	Fe/Zn 25	II	1	colored chromate	8	6	2	8	3	8	9
3				Fe/Zn 12	II	0.5	colored chromate	7	6	8	8	3	8	9
4					IV	0.5	phosphate	6	6	8	8	3	8	9
5				Fe/Zn 8	II	0.3	colored chromate	6	6	8	8	3	8	9
6					IV	0.3	phosphate	5	6	8	8	3	8	9
7		Hot-Dip	ASTM A153			1.7		9	6	2	9	3	8	9
8		Inorganic				2		9	6	2	9	3	8	7
9	Zinc Alloy	Sn/Zn	BAC 5899	1	II	0.5	chromate treated	8	8	7	8	5	7	7
10				2	II	0.3	chromate treated	7	8	7	8	5	7	7
11		Zn/Ni	ASTM B841	1	C	0.2	bronze chromate	6	7	8	8	4	7	7
12				2	B	0.3	yellow chromate	7	7	8	8	4	7	7
13					C	0.3	bronze chromate	7	7	8	8	4	7	7
14				3	B	0.4	yellow chromate	8	7	8	8	4	7	7
15					C	0.4	bronze chromate	8	7	8	8	4	7	7
16		Zn/Co	ASTM B840	2	C	0.47	bronze chromate	7	6	8	8	3	2	8
17				3	C	0.71	bronze chromate	8	6	2	8	3	7	8
18		Zn/Fe	ASTM B842	2	A	0.47	black chromate	6	6	8	8	3	2	8
19				3	A	0.71	black chromate	7	6	2	8	3	7	8
20	Aluminum	IVD	MIL-C-83488	1	I	1	as coated	8	10	2	9	7	9	1
21					II	1	chromate	9	10	2	9	7	9	4
22				2	II	0.5	chromate	7	10	4	9	7	9	4
23				3	II	0.3	chromate	4	10	4	9	7	9	4
24		Electroplate	(none)			>0.5		9	10	4	9	7	9	3
25		Al-ceramic				>0.8		9	9	10	9	7	1	3
26	Paints	Organic				>2		3	10	2	9	10	1	10
27		Inorganic				>2		4	9	2	9	9	1	9
28		Duplex				>2.2		8	8	2	8	3	1	6
29	Barrier Only Metal Plating	Tin	ASTM B545					3	4	1	1	1	7	8
30		Nickel (electroless and electrolytic)	ASTM B656, ASTM B689					3	3	4	7	9	7	8
31		Gold, Silver, and alloys	ASTM B488, ASTM B700					2	2	1	1	1	10	1
32	ALTERNATE BASE MATERIALS													
33	Stainless Steels	Types 304, 316, or A286				---		9	6	7	10	10	7	3
34	Composite w/electroless Nickel					---		10	2	1	10	10	7	2

(1) Ratings developed from corrosion resistance reported in literature for several natural environments, salt fog testing, and other accelerated tests.

(2) Underline numbers refer to ratings developed based on performance of similar material systems rather than data for the specific material family.

Demonstration of Ozone Treatment for Cooling Towers at Thayer Hall, U. S. Military Academy at West Point, NY

Vincent F. Hock and Robert Hess
U.S. Army Corps of Engineers
Champaign, IL 61826, USA
217-373-6753

D. Piskin and N. Labbe
Puckorius and Associates
Evergreen, CO

ABSTRACT

This report covers the evaluation of ozone as a stand-alone treatment in a new cooling tower system that has been in operation for two cooling seasons (summer only) at the U. S. Military Academy, West Point, New York. The results showed that ozone appeared to have protected the water contacted equipment from mineral scale and excessive micro-biological deposits but showed increased, excessive corrosion of both copper and mild steel. The use of ozone treatment for cooling towers appears to be somewhat effective as a biocide. However, the ozone residuals were too low and too great a fluctuation at Thayer Hall for optimum effectiveness. The life cycle cost analyses compared ozone treatment to conventional chemical treatment.

INTRODUCTION

The U.S. Army operates numerous cooling towers associated with chillers and other industrial processing systems. The water circulating through cooling towers can be the source of several costly operations and maintenance (O&M) problems such as biological fouling, scaling and corrosion.

These problems can waste energy by reducing the efficiency of heat transfer, and they can wear down or damage system components. Such problems are typically mitigated through the application of chemical treatments (i.e., biocides, antiscale compounds, and corrosion inhibitors), but the use of these chemicals poses its own set of problems.

Environmental compliance issues- some of the most effective compounds, such as chromates used for antiscale treatment, are considered hazardous and are banned or tightly restricted by the U.S. Environmental Protection Agency (EPA). Chemical costs arise from the fact that different chemicals are needed for each problem, and in the case of biocides, several chemicals are often required to destroy resistant microorganisms. Monitoring and maintenance have procedures which can be very labor-intensive to conduct, but failure to conduct them will shorten cooling system life cycle. Taken together, these problems make it highly desirable for the Army to find effective, cost-efficient alternative treatment methods for cooling tower water.

For almost 100 years ozone (O_3) has been recognized for its ability to disinfect water, but ozone has been used to treat cooling tower water only since the 1970s (U.S. Department of Energy 1995). Ozone treatment system manufacturers claim that ozone is more effective than chorine in destroying disease-causing bacteria such as strains linked to Legionnaires' disease. Ozone also is attractive from an environmental standpoint because it is a short-lived form that rapidly reverts to diatomic oxygen (O_2), as opposed to chemical biocides, which concentrate in cooling systems over time and may contaminate public water treatment systems when purged via blowdown. Furthermore, anecdotal reports from ozone users and vendors suggest that ozone can control certain kinds of scale and corrosion. Consequently, interest in ozone as a stand-alone alternative to conventional chemical treatments has been growing. However, independent data are not available to substantiate the wide-ranging claims of ozone proponents.

To investigate ozone's effectiveness as a biocide in cooling towers as well as anecdotal claims about additional ozone benefits, the U.S. Army Construction Engineering Research Laboratories (USACERL) demonstrated and evaluated ozone water treatment technology on a new cooling tower installed at the U.S. Military Academy, West Point, NY. The research was conducted under the Army's Facilities Engineering Applications Program (FEAP). The objective of this project was to investigate the use of ozone as a stand-alone cooling water treatment at Thayer Hall (Building 601), U.S. Military Academy (USMA) at West Point, NY, and determine its effectiveness and cost-efficiency versus conventional chemical treatments.

EXPERIMENTAL PROCEDURES

To evaluate ozone as a stand-alone treatment, the technology's performance was monitored relative to industry standards for good protection of cooling tower system equipment. Good protection requires the prevention of scale due to water-soluble minerals, corrosion control of all system metals, micro-biological organism control and control of deposits from materials suspended in the system water. This investigation included all of the following evaluation techniques: system water analysis, corrosion rate determinations, micro-biological analysis, deposit accumulation rates and equipment inspections.

A bypass test loop shown in Figure 1, was installed around the two pumps in the circulating water system. The loop contained insertion points for two linear polarization corrosion monitor probes and eight metal specimens for corrosion monitoring, plus one BI°GEORGE™ electrode for micro-biological monitoring.

Figure 1. Schematic of test loop.

To collect baseline data, one site visit was made before ozone was fed into the system for the 1993 air conditioning season. Three site visits were made during the 1993 air conditioning season to collect data, remove and replace the steel corrosion-test coupons, remove and replace chart paper, and collect water and deposit samples for laboratory analysis. Any cooling system equipment that was accessible during the site visits was inspected-primarily the cooling tower and basin. The condenser portion of the chiller and circulating water line interiors were not available for inspection either before, during, or after the cooling season.

Site inspections were performed by Puckorius & Associates, Inc., Evergreen, CO. Water analyses and corrosion rate determinations were performed in the Puckorius laboratory. Deposit analyses were performed by a subcontractor laboratory, Structural Integrity Associates, Inc., of San Jose, CA. Ozone analyses of cooling water were performed on-site using the indigo-trisulfonate calorimetric method (Method #8311, Hach Co., Loveland CO 80539).

Physical Plant and Ozone Generator Data

Cooling System- The cooling tower system provides cooling water for the heating, ventilating, and air conditioning (HVAC) system at Thayer Hall. It consists of two York 900 ton absorption refrigeration machines, which are used one at a time. The condenser tube material is 95-5 copper-nickel. Condenser tube sheets are mild steel, as are the water boxes and all circulating piping. Valves are mild steel, and circulating pump housings are cast iron with bronze impellers.

This cooling system utilizes three 300 ton Marley cross-flow galvanized-steel towers with stainless steel basins. The three basins are connected to a common suction (supply) header. Fill is honeycombed film-fill polyvinyl chloride (PVC); fan blades are aluminum. Design temperature drop of hot to cold water through the cooling towers is 16 EF, but can range from 14 EF to 23 EF. The return water is proportioned to both ends of the three towers. See Figure 2. Each tower has a circulating water capacity of 870 gallons per minute (gpm). Thus, 2610 8pm of water is recirculated when the system is operating.

Figure 2. Schematic of cooling system.

Ozone Generator-The ozone generator was supplied by Advanced Oxidation Systems, Inc. of Wayne, NJ. The generator has a capacity of 6 lb of ozone per day. At a nominal circulation rate of 2700 8pm, the maximum theoretical concentration of ozone would be 0.185 ppm. However, the power on the generator was set below design, generally at about 50 percent of capacity. Consequently, a maximum of 0.09 to 0.10 ppm of ozone fed into the cooling water. Ozone analyses on tower sump water ranged from 0.02 to 0.05 ppm.

Ozone Feed System-The feed system utilizes a unique ozone-lift mixing system as seen in Figure 3. The ozone-air mixture from the generator is fed into a venturi that draws water from the tower sump and lifts it into a mixing chamber. The mixture of air and water has a slightly higher pressure (head) than the tower basin and therefore the water flows back into the tower basin. A vent from the mixing chamber to the top of the tower gets rid of the off-gas (nitrogen, air, and some ozone) to the atmosphere.

Two cooling towers are fed by this system. The third tower had been fed by means of an inline static mixer shown in Figure 4. However, this arrangement allowed water to flow back into the generator when the system was down, in spite of a backflow prevention loop, causing generator damage.

Figure 3. Schematic of "ozone-lift" mixing system.

Figure 4. Schematic of inline static mixer.

RESULTS

Data Collected

Water Analyses-Makeup water samples were taken at the same time as the tower water samples in order to calculate the mineral relationships The makeup water is a corrosive water with low hardness and low alkalinity, typical of Catskill-area surface water. The May 11th cooling tower water sample, taken before the ozone feed was started, had only been concentrated about two times, but the calcium and magnesium values were higher than can be accounted for by two cycles of concentration (COC). This indicates that scale deposited in the previous year, during no-treatment conditions, was being dissolved by the water. The Langelier Saturation Index (LSI), the Ryznar Stability Index (RSI), and the Puckorius Scaling Index (PSI) can indicate whether tower water is corrosive, i.e., non-scale-forming (Puckorius, September 1983). All three indices showed the water to be non-scale-forming.

The June 22nd cooling tower water sample which was taken 2 weeks after ozone feed was begun, showed about 7 COC. Calcium, alkalinity, and silica were precipitating and causing deposits. The more soluble magnesium, chloride, and sulfate ions were concentrating somewhat linearly. The LSI indicates that the circulating water was only slightly scale-forming at +1.12, assuming that an LSI of 0.00 is theoretically neither scale-forming nor scale-dissolving. However, experience has shown that a stable water may have an LSI between +1.0 and +2.0 without forming scale. Therefore, according to the LSI, the water sampled on 22 June is very nearly stable-neither scale-forming nor scale-dissolving. The RSI also indicates that the water is very nearly stable (approximately 6.0). The PSI, also approximately 6.0, shows it to be slightly scale-dissolving (slightly corrosive). The reason that the analysis of this concentrated water calculates as non-scale-forming is that some calcium and alkalinity ions have come out of solution as calcium carbonate and caused deposits, and the calculations for the indices reflect this. The water had become supersaturated with calcium and alkalinity upon concentrating, but as the calcium carbonate came out of solution, the water remained saturated with these ions (but seemingly stable).

The July 20th and August 5th cooling tower water samples, taken during routine ozone treatment, show high concentrations of magnesium, chloride, and sulfate, but lower concentrations of calcium, alkalinity, and silica. The various calcium carbonate scaling indices indicate a near-stable water, but at 15 and 19 COC this indication is not likely to be accurate. Calcium and alkalinity had precipitated out, forming deposits, and this is typical of ozone-treated tower waters. White particles are generally found in the basins of the towers, and may result in some scale on the heat exchange surfaces of the condenser, and often on the cooling tower fill. Examination was limited with the condenser not being inspected, and the cooling tower did not show appreciable deposits.

If one was to calculate a theoretical scaling index using the same number of concentrations of calcium and alkalinity as there are COCs of chlorides, the PSI for the 20 July sample would be 3.38. This is an extremely scale-forming value-one that would require an extremely high application of anti-sealant in a chemical treatment program. Even then, an anti-sealant might not work. Therefore it can be concluded that scale was being deposited within the cooling tower system.

The theoretical PSI for the 5 August sample calculates as 4.66-again a severe scale-forming condition, while the actual PSI (6.43) was non-scaling. A simple deposit analysis showed some effervescence from calcium carbonate on the mild steel test coupons when they were cleaned, but there was no reported loss of efficiency due to scaling in the operation of the chiller. Because there are two chillers operating alternately, not together, it is not known if there have been deposits within either of the condensers, or to what degree. The condensers were to be examined for scale when they are opened during the winter of 1993-1994. No data have been obtained.

Corrosion Study-Corrosion monitoring methods used in this study were indirect, and utilized both corrosion coupons of mild steel (representing the water lines and condenser tube sheet and water box); copper (typical of condenser tubing but not found at USMA); galvanized mild steel (cooling tower components); Admiralty brass (70% copper and 30% zinc-also typical of condenser and other heat exchanger tubing, but not found at USMA); copper (95%) nickel (5%), which is not typical for condenser tubes but found in the condensers at USMA; copper (90%) nickel (10%), also not normal for condenser tubes and not used at USMA; and aluminum grade AL 1100 (not common in cooling water systems and not used at West Point). The metals not used at USMA were included in the study for possible reference to metals used at other Army installations.

Another indirect corrosion monitoring technique used a linear polarization monitor that provides instantaneous corrosion rate testing. A mild steel probe was utilized on this device. A third monitoring method was used to detect specific micro-biological-caused corrosion. This method employed a specialized linear polarization monitor system called the BI°GEORGE™ biofilm monitor. Table 1 summarizes the results.

Results for Mild Steel- The test coupons were all heavily encrusted with small carbuncles of iron oxide when removed, and even had copper plated on the metal surfaces. When cleaned, all coupons showed active corrosion, including pitting. For mild steel, general corrosion rates of 5 to 7 mils per year (mpy) may be acceptable in some cooling tower systems. However, pitting corrosion in excess of these rates is unacceptable. Therefore, the results were clearly unacceptable for mild steel.

The corrosion monitor for mild steel read about halfway between the zero and 10 mpy (4-6 mpy) on the chart, which is about the same rate calculated for the test coupons. However, the monitor results did not track the actual metal loss apparent on the test coupons, possibly as the result of iron oxide accumulation on the monitor electrodes. Nevertheless, results were unacceptable because general corrosion rates were high and pitting corrosion was evident.

Results for Copper Alloy- All of the copper, Admiralty brass, and copper-nickel coupons were covered with a dark brown loosely adherent coating Except for the copper-nickel samples, all ozone-exposed samples were darker than the same metal coupons exposed to standard cooling water treatments. This dark color indicates excessive corrosion. Copper alloys that are adequately protected will be clean and close to original color and appearance. Corrosion rates of greater than 0.1 mpy for copper, Admiralty brass, and copper-nickel are unacceptable.

The results of corrosion coupons (Table 1) show copper to be high (0.18-0.34 mpy); and not acceptable. Admiralty brass corrosion was excessive (0.34-0.51 mpy); and thus not acceptable. Copper/nickel was only slightly high at 0.13 mpy, which is acceptable. Galvanized steel and aluminum coupons looked even worse than their measured corrosion rates of 5 and 7 mpy, respectively. Attack was so that neither metal should be considered for use with ozone. Only the two stainless steel coupons had corrosion rates that would be considered acceptable, at 0.080 mpy for 304 stainless and 0.103 for 316 stainless. A large amount of red iron oxide was found in the stainless pans of the towers, about 0.125 in. deep. Some white particles were separated from a deposit sample and analyzed by energy dispersive x-ray. The white particles were composed of zinc (probably as zinc carbonate), calcium (probably as calcium carbonate and calcium silicate), silica, and iron and copper corrosion products. The deposit, as found, analyzed as iron, copper, and zinc corrosion products, plus calcium as the carbonate, as indicated by effervescence in acid.

Table 1. Summary of corrosion coupon results.

Micro-biological Study-The micro-biological monitoring was performed by Structural Integrity Associates (SIA), Inc., of San Jose, CA under subcontract to Puckorius & Associates, Inc A portion of the testing was conducted using a device called the BI°GEORGE™ micro-biological corrosion monitor; the results were tracked for experimental purposes to compare with the conventional test methods employed.

The BI°GEORGE™ corrosion monitor, which uses a mild steel probe, showed that little or no biofilm had grown during the exposure period, but some big-corrosion was detected. Active corrosion-causing microbes were found on the probe, which showed considerable corrosion fluctuation and some pitting. This suggests that (1) big-corrosion had occurred during the exposure period and (2) ozone residuals had probably varied considerably from high levels to none. While the BI°GEORGE™ probe indicated relatively high counts of bacteria present in the cooling water, conventional testing of wetted tower surfaces revealed no biofilm growth.

COST ANALYSIS AND OBSERVATIONS

Life-Cycle Cost Analysis

Based on the field investigations made at Thayer Hall, reduced scaling will allow tower pumps to run more efficiently and with less maintenance. Increased efficiency of equipment will reduce energy requirements and electrical use. With less scale buildup in the lines, heat transfer also will improve. In addition to better heat transfer and reduced energy needs, the use of

chemicals is eliminated and the required amount of makeup water is reduced. The annual estimated savings for Army-wide application is approximately $2.25 million. Table 2 summarizes the potential savings reported in Appendix C.

Table 2. Estimated life-cycle cost savings for ozone treatment (versus conventional methods).

Observations

Scale and Deposits-There has been no indication of scale on heat exchange surfaces (condenser) due to loss of efficiency, but there has been no inspection of the condenser for verification. Deposits were found in the cooling tower and basin. These were analyzed and showed both scale deposits (calcium and silica) as well as corrosion products (iron oxide); copper (from condenser tubes); and zinc (from galvanized steel cooling tower).

Micro-biological Growth-No apparent biological deposits were found in the towers at Thayer Hall during the site visits. However, two other methods for monitoring micro-biological organisms and deposits were utilized. One method was the incubation of cooling water samples to determine the levels of microbes present. The use of MIC kits (Big-industrial Technologies) revealed the presence of slime-forming (deposit-producing) bacteria and corrosive bacteria (anaerobic and acid-producing). The second method was to culture deposits found on the BI°GEORGE™ biofilm probe. This method detected the same micro-organisms found in the water samples. The analysis showed levels of 105 and 106 CFU (colony-forming units) per milliliter of sample. Good levels of microbiological control range from 103 to 104 CFU/ml, so the levels detected in the water samples and on the biofilm probe in this demonstration were too high to be considered good.

CONCLUSIONS AND RECOMMENDATIONS

The conclusions for the USMA ozone technology demonstration are as follows:

- Ozone performed satisfactorily at Thayer Hall as a stand-alone biocide, but two separate testing modes detected micro-biological deposits in excess of levels normally considered desirable, and some test coupons exhibited microbe-induced corrosion.
- Scale deposits occurred during the demonstration, but no loss in system efficiency was detected. Cooling tower deposits may require frequent cleaning, however.
- Corrosion-especially pitting-was excessive and unacceptable for mild steel, galvanized steel, copper, Admiralty brass (90% copper, 10% zinc), and aluminum.
- Corrosion of copper/nickel alloy was low and acceptable.
- Corrosion of stainless steel was negligible.
- Ozone residuals generally were too low during the demonstration period, and fluctuated too much for optimum water treatment effectiveness.

The Thayer Hall cooling system contains mild steel (lines), galvanized steel (cooling tower), and copper/nickel (condenser tubing). Based on the final condition of test coupons made of mild steel and galvanized steel, it can be concluded that the lines and cooling tower experienced unacceptable corrosion rates during the demonstration treatment. This conclusion implies that continuous ozone treatment of the cooling water in the Thayer Hall system would cause premature leaks, requiring early repair or possible replacement. Based on the test findings for the copper/nickel test coupons, it may be concluded that condenser tubing stayed within acceptable corrosion rates.

It is concluded that ozone cannot serve as a stand-alone cooling water treatment for the USMA Thayer Hall cooling system, or for other systems elsewhere that are similar in terms of material composition and makeup water. USMA's dual-chiller design could provide uninterrupted cooling service to Thayer Hall using ozone treatment, but only if USMA were to make a larger investment in labor and materials for cleaning. Furthermore, because the Thayer Hall system principally comprises metals that performed poorly in ozone exposure, stand-alone ozone treatment of the cooling water would create a higher risk of equipment damage or premature failure due to corrosion.

In summary, it is concluded that ozone technology as a stand-alone water treatment technology cannot o flier the required corrosion protection provided by standard multiple chemical treatments. It is further concluded that site-specific conditions must be considered to correctly determine whether ozone treatment can either partially or entirely replace standard chemical treatments for cooling tower water. Guidelines are available in the literature (e.g., Puckorius, September 199 l) that could help other Army installations determine whether ozone treatment is a useful, cost-effective alternative to standard methods.

Recommendations

It is recommended that the ozone feed system at Thayer Hall be improved to provide better, more reliable feed and delivery. It is further recommended that the system be monitored frequently enough by operations personnel to detect and correct wide fluctuations in ozone residual levels. Also, it is recommended that a longer mixing chamber, such as on the tower at the Officers's Club, be installed on the Thayer Hall system.

REFERENCES

1. Puckorius, P.R, "Get a Better Reading on Scaling Tendency of Cooling Water," *POWER*, September 1983, pp 79-81.
2. Puckorius, P.R, "Ozone for Cooling Towers: Is it a Panacea?" Paper #212, National Association of Corrosion Engineers Annual Conference and Corrosion Show, Cincinnati OH, 11-15 March 1991.
3. Puckorius, P.R, "Ozone Use in Cooling Tower Systems: Current Guidelines-Where it Works," International Ozone Association, Pan American Committee, Toronto, Ontario, 16-18 September 1991.

Table 1. Summary of corrosion coupon results.

Coupon #	Exposure Dates	# Of Days	Weight Loss	MPY
T7921	06/23/93-07/20/93	27	0.2058 gram	6.35
T7922	06/23/93-08/05/93	45	0.3023	5.86
T2926	07/20/93-08/05/93	16	0.4638	24.15
T2923	06/23/93-10/25/93	124	0.6523	4.38
T2928	08/05/93-10/25/93	81	0.6971	7.07
T2929	08/05/93-10/25/93	81	0.7017	7.22

Copper - Grade CDA 110 (f = .737)

Coupon #	Exposure Dates	# of Days	Weight Loss	MPY
1811	06/23/93-07/20/93	27	0.0099 gram	0.270
1812	06/23/93-08/05/93	43	0.0103	0.187
D2108	07/20/93-08/05/93	16	0.0074	0.341
D2109	08/05/93-10/25/93	81	0.0211	0.192
D2110	08/05/93-10/25/93	81	0.0233	0.212

Admiralty-Grade CDA443 (f = .769)

Coupon #	Exposure Dates	# of Days	Weight Loss	MPY
A632	06/23/93-07/20/93	27	0.0122 gram	0.347
A939	07/20/93-08/05/93	16	0.0105	0.515

95:5 Cu:Ni Grade 704 (f = .733)

Coupon #	Exposure Dates	# of Days	Weight Loss	MPY
01	08/05/93-10/25/93	81	0.0144 gram	0.130

304 Stainless (f = .826)

Coupon #	Exposure Dates	# of Days	Weight Loss	MPY
04	06/23/93-07/20/93	27	0.0026	0.080

316 Stainless (f = .826)

Coupon #	Exposure Dates	# of Days	Weight Loss	MPY
A1246	07/20/93-08/05/93	16	0.0021	0.103

Galvanized Steel (f = .833)

Coupon #	Exposure Dates	# of Days	Weight Loss	MPY
52	06/23/93-07/20/93	27	0.1614	4.98

Aluminum Grade AL1100 (f = 2.419)

Coupon #	Exposure Dates	# of Days	Weight Loss	MPY
A0503	08/05/93-10/25/93	81	0.2368	7.07

90:10 Cu:Ni Grade 706 (f = .733)

Coupon #	Exposure Dates	# of Days	Weight Loss	MPY
01	08/05/93-10/25/93	81	0.147	0.133

Table 2. Estimated life-cycle cost savings for ozone treatment (versus conventional methods).

Cost Category	Savings
MAINTENANCE SAVINGS	$34K
ENERGY REDUCTION SAVINGS	$1660K
ELIMINATION OF CHEMICALS	$360K
REDUCTION OF MAKEUP WATER	$200K
TOTAL ANNUAL SAVINGS ARMY WIDE	**$2250K**

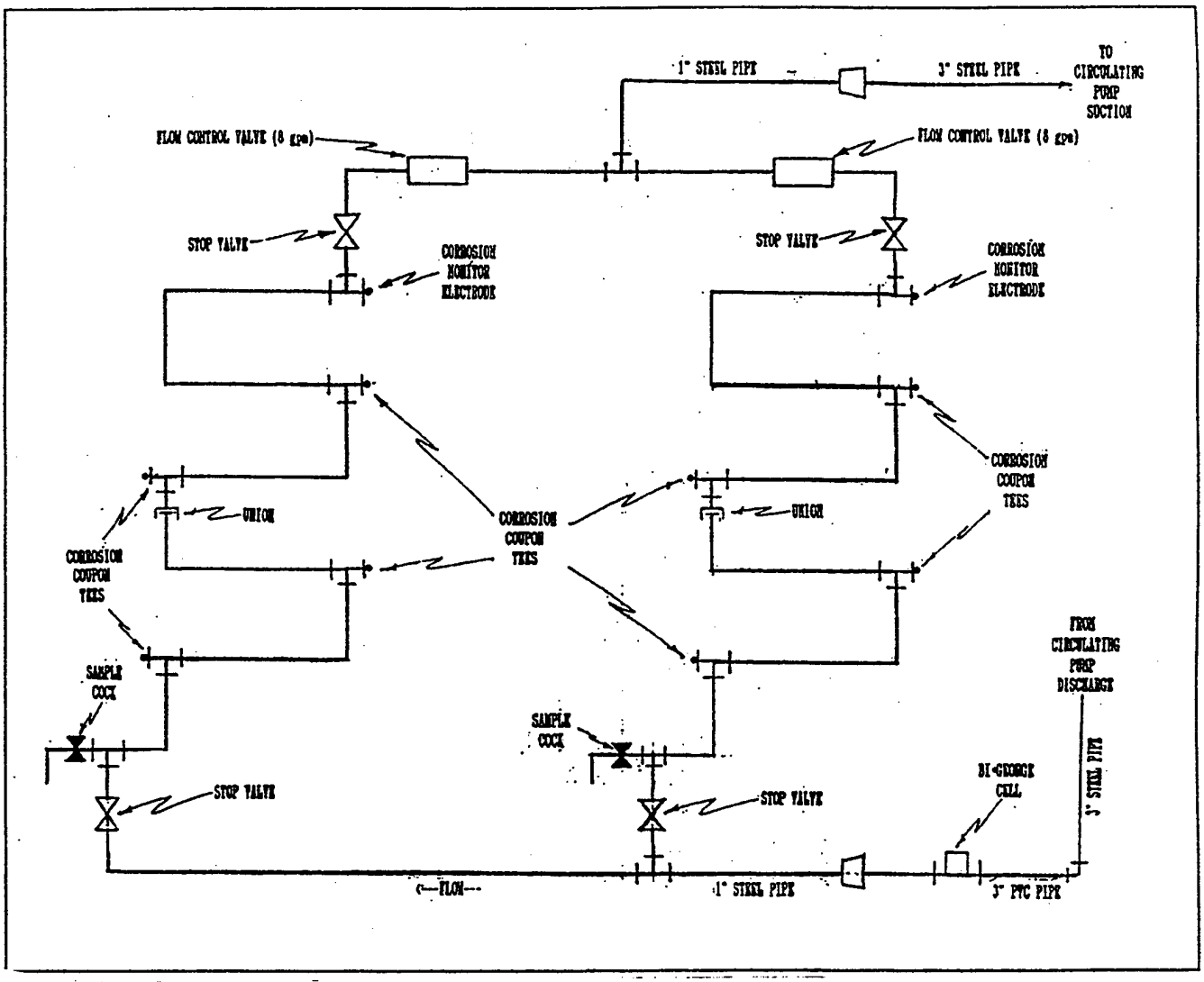

Figure 1. Schematic of inline static mixer

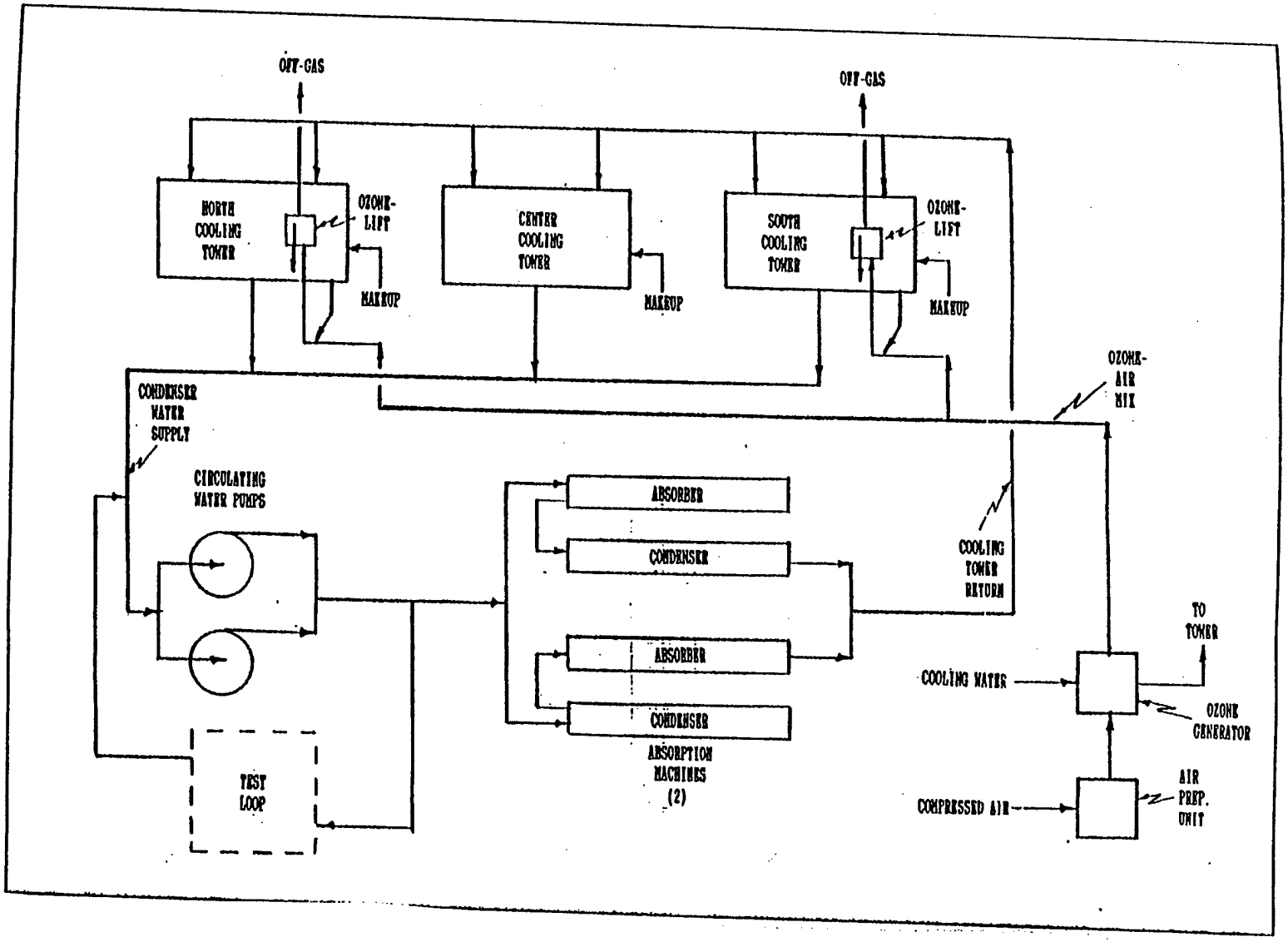

Figure 2. Schematic of cooling system

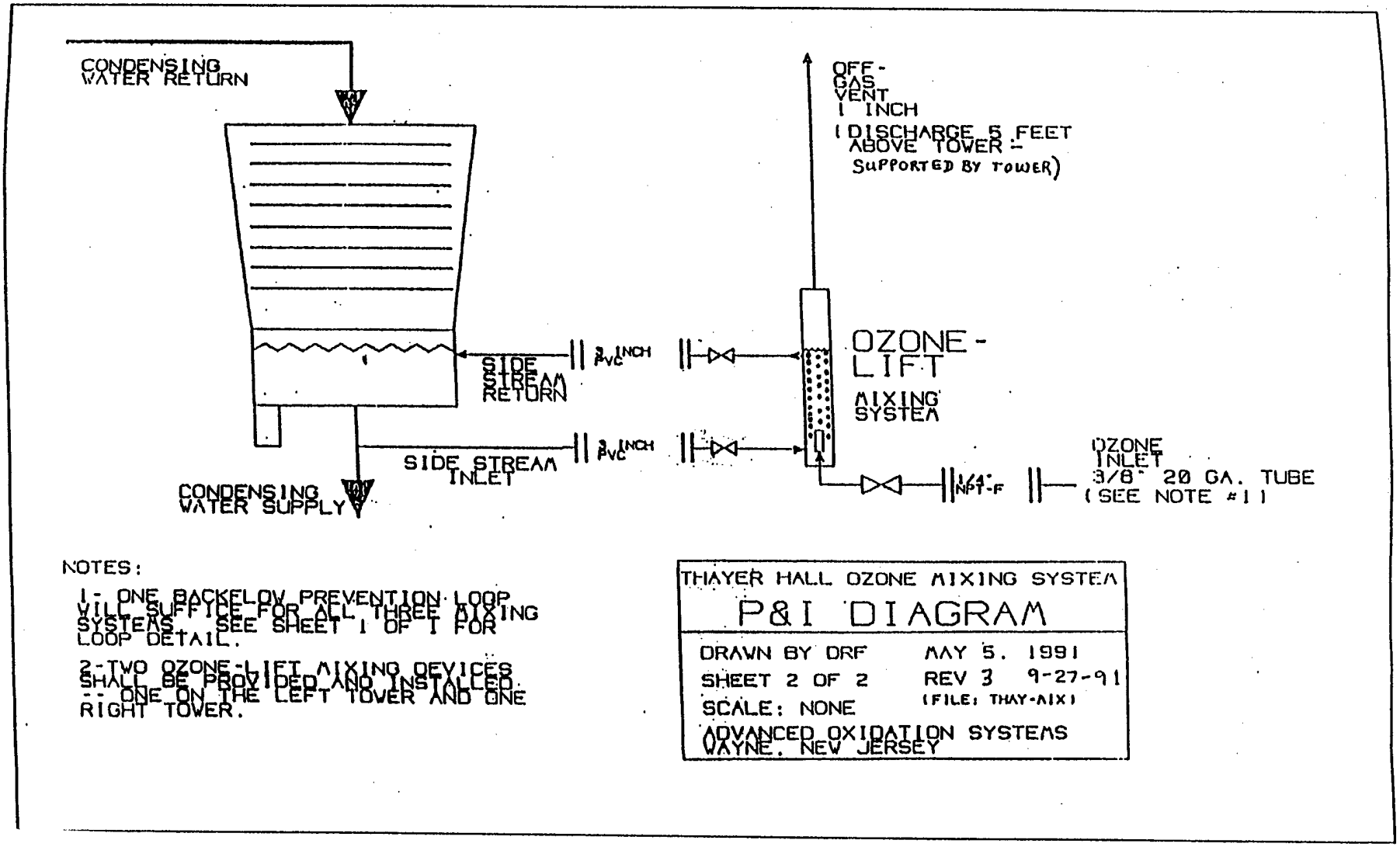

Figure 3. Schematic of "ozone-lift" mixing system.

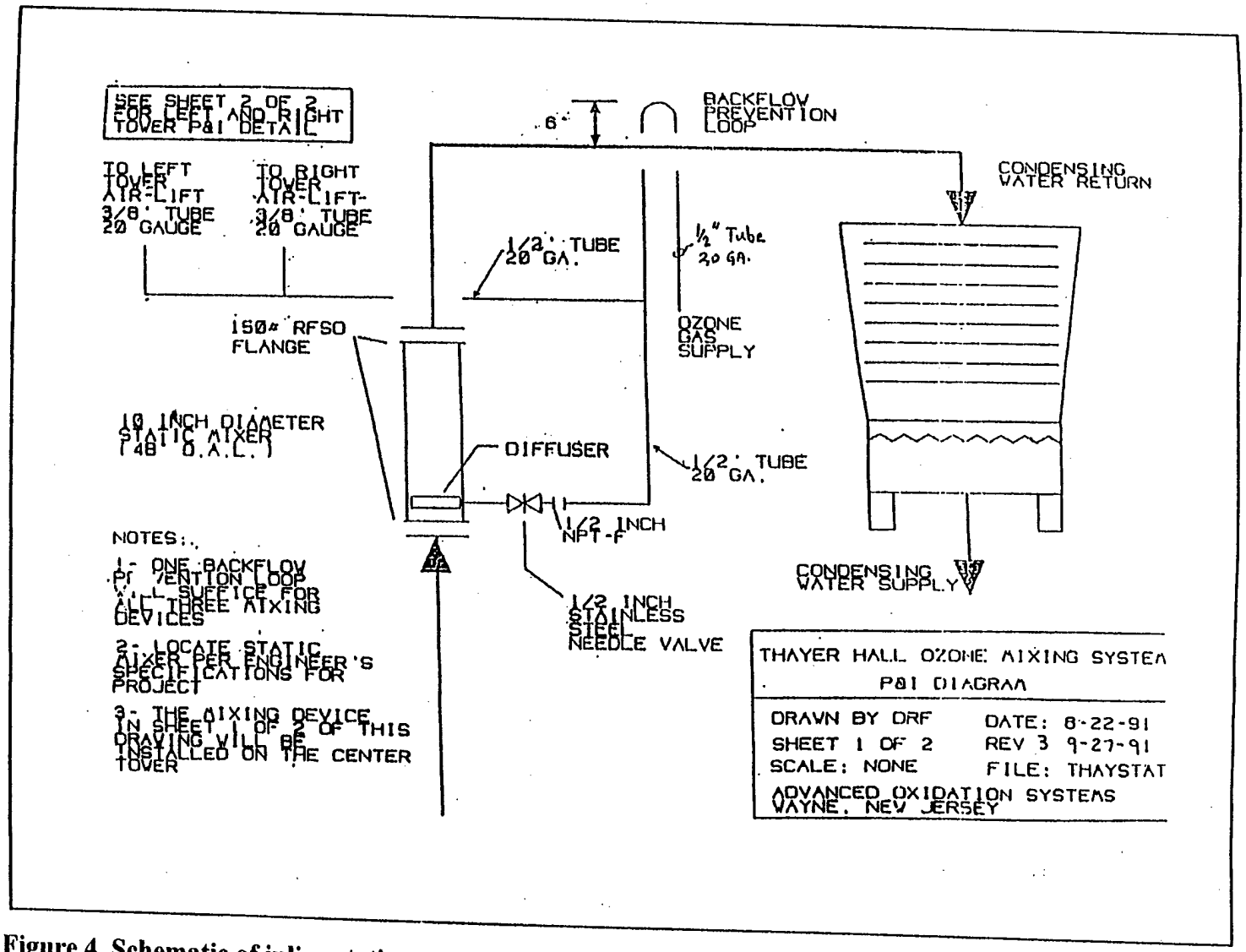

Figure 4. Schematic of inline static.

POST-PROCESSING OF THERMAL SPRAYED COATINGS USING HOT ISOSTATIC PRESSING

D.A. Davis, R.L. McCaw, and D.M. Aylor
Carderock Division, Naval Surface Warfare Center, Bethesda, MD
R.A. Hays
Proteus Engineering, Division of Analysis and technology, Inc., Stevensville, MD

ABSTRACT

Thermal sprayed coatings are currently being used in the Navy and in private industry to improve corrosion and wear resistance. While these coatings have several attractive features, there are also limitations. Two characteristics of thermal sprayed coatings which limit applications include porosity in the coating and the lack of metallurgical bonding between the coating and the substrate. In general, it has been shown that porosity is detrimental to corrosion performance. The lack of metallurgical bonding has precluded the use of thermal sprayed coatings in critical applications due to concern over debonding. The intent of the work described herein was to establish the feasibility of post-processing thermal sprayed coatings to decrease porosity levels and to establish metallurgical bonding between the coating and the substrate material.

After reviewing several potential techniques for post-processing the coatings, hot isostatic pressing (HIP) was selected due to its potential to reduce porosity and produce metallurgical bonding in a single step. Coatings applied using conventional flame spray and high velocity oxy-fuel (HVOF) techniques were post-processed using two sets of HIP parameters. As-sprayed and post-processed coatings were then comparatively evaluated metallographically, in bond strength tests, and in laboratory corrosion tests.

INTRODUCTION

Thermal sprayed coatings are currently being used in a variety of applications by the Navy and private industry to improve corrosion and wear resistance. In particular, thermal sprayed coatings for machinery element restoration and repair (MERR) have been used quite successfully in the Navy for over 15 years[1]. While the applications performed under the MERR process have generally been limited to pump shafts and shaft sleeves, strainer plugs, and valve stems, significant cost savings have been realized. Puget Sound Naval Shipyard alone estimated cost savings to the Navy of $2.3M through 1993[2]. Expansion of the number and type of applications has the potential to provide even greater cost savings to the Navy, especially in the area of high integrity repairs of costly components. Another important aspect of thermal spray repair is the ability to shorten repair times, thus mitigating mission impacts resulting from other time consuming repair techniques or long lead procurements. For example, the use of thermal spray to repair the rudder rams on USS SAIPAN (LHA 2) during December, 1994 had a direct impact on meeting the scheduled undocking date[3].

Past work has shown that bond strength and porosity level are the two primary limitations to performance of thermal sprayed coatings in corrosion prevention applications[4, 5]. As-deposited thermal sprayed coatings are mechanically bonded to the substrate and some level of porosity is inherent. The ability to develop some level of metallurgical bonding and reduce porosity

levels should substantially improve coating performance and expand applications of the coatings, especially to more critical components. The presence of metal oxides in the coatings are generally not critical to the performance of a thermal sprayed coating in a corrosion prevention application. However, high levels of oxides can make the coatings more susceptible to chipping and make machining difficult. Therefore, reducing oxide content is also generally desirable.

Several techniques for improving thermal spray coating quality by post-processing to reduce porosity and achieve metallurgical bonding have been attempted by other investigators. These include post-coating heat treatment[6] laser treatments, shot peening[7], and polymer impregnation[6]. The work described herein evaluated the feasibility of using hot isostatic pressing (HIP) as a post-processing technique. HIP was selected for evaluation due to its potential to impact both coating porosity and metallurgical bonding, its relative simplicity, and its availability.

HOT ISOSTATIC PRESSING

Hot isostatic pressing is a technique in which high isostatic pressure is applied to a powder part or compact at elevated temperatures[8]. Typical temperature ranges for powder metallurgy processing or casting densification are 60% to 70% of the melting point of the material of interest. The medium by which the isostatic pressure is usually applied is high density argon gas and typical pressures range from 3 ksi to 45 ksi. The process was initially developed at Battelle Memorial Institute for diffusion bonding of clad nuclear fuel elements. The process is now widely used in industrial production of powder metallurgy components such as nickel-based superalloy jet engine turbine disks and shafts, titanium alloy billets, and various tool steel shapes.

MATERIALS

Table (1) provides the matrix of base and coating materials used in this initial feasibility study. Nominal compositions of the substrate and coating materials are provided in Table (2). The monel (alloy 400) coatings on monel and steel substrates were applied using the plasma spray technique and were selected to represent current Navy applications in terms of materials and spray processes. The alloy 625 coating on HY-80 steel and commercially pure titanium (CP Ti) coating on alloy 625 were applied using the high velocity oxy-fuel (HVOF) technique and selected to represent advanced materials and spray processes.

EXPERIMENTAL PROCEDURE

The generalized approach to this effort was to apply the thermal sprayed coatings to coupons of the various substrates, HIP a portion of each coupon, and comparatively evaluate the HIPed and un-HIPed materials. Evaluations included quantitative metallography, bond strength tests, and polarization curve measurements.

Thermal Spray Application

All thermal sprayed coatings were applied by Norfolk Naval Shipyard (NNSY) under conditions representative of industrial production. The monel coatings on both the monel and

HY-80 steel substrates were applied by a plasma spray process using a METCO 9MB system using parameters contained in Puget Sound Naval Shipyard's Uniform Industrial Process Instruction (UIPI) for thermal spray. Coating thickness was specified as 20 ± 2 mils.

The HVOF coatings were applied using a METCO Diamond Jet system. Shorter dwell times of the feed powder in the flame and higher flame velocities of the HVOF process as compared to the plasma spray process can result in coatings with lower porosity and higher bond strengths. Since only semi-molten particles are transferred to the substrate in the HVOF process, oxide formation is also reduced compared to the plasma spray process. HVOF parameters used to apply the alloy 625 coatings were developed by METCO. The parameters used to apply the CP Ti coatings were developed by the Carderock Division, Naval Surface Warfare Center (CDNSWC). HVOF coating thickness was also specified to be 20 ± 2 mils.

Hot Isostatic Pressing

Hot isostatic pressing was performed by Pressure Technologies, Inc. (PTI). Initial parameters were selected by PTI to be typical of those used to process powder metallurgy parts similar in composition to the thermal sprayed materials. All specimens were HIPed in the as-sprayed condition and none of the specimens was encapsulated prior to HIP processing. HIP parameters are provided in Table (1).

Quantitative Metallography

Metallographic specimens of each of the coating/substrate combinations in both the HIPed and as-sprayed conditions were prepared simultaneously to minimize variability due to specimen preparation. After careful sectioning with an abrasive wheel, the specimens were hot compression mounted and automatically ground and polished. Each of the specimens was then viewed and photographed in a light microscope at 100X, 250X, and 500X magnification. After the initial viewing, the specimens were etched and photographed again in preparation for quantitative image analysis.

Porosity and oxide content were measured using a LECO 2001 Image Analyzer and Version 2.02 software. Images magnified to 200X were broken into 25 fields each for the measurements. Reported values are averages over the 25 fields.

Bond Strength Testing

One specimen of each coating/substrate combination in the as-sprayed condition and two specimens of each coating/substrate combination in the HIPed condition were tested in accordance with ASTM C633. The test consists of coating one face of a substrate fixture, bonding this coating to the face of a loading fixture, and subjecting this assembly to a tensile load normal to the plane of the coating.

The fixtures used in these tests were 1-inch diameter "buttons." Coating thickness used for the evaluation was 0.015 inch and the bonding agent was Master Bond® EP-15. Load was applied in an MTS servo-hydraulic testing machine at a cross-head displacement rate of 0.04 inch/min. Maximum load was recorded for each test.

After each test, the appearance of the failure is documented. Potential failure locations include:

- Adhesive - failure at the interface between the coating and the substrate
- Cohesive - failure within the coating
- Bonding Agent - failure of the epoxy

A true measurement of the bond strength of the thermal sprayed coating is only achieved if the failure occurs solely in the adhesive fashion.

Polarization Curve Measurement

Open circuit corrosion potentials (E_{corr}) and anodic polarization curves for each coating/substrate combination in both the HIPed and as-sprayed conditions were measured in accordance with ASTM G-5. Similar measurements were made on the uncoated substrate materials for comparison.

Approximately 3 to 4 cm^2 of each material condition was exposed in deaerated, substitute ocean water (ASTM D1141) for a period of 15-30 minutes to allow the specimen to stabilize prior to polarization. Deaeration was accomplished by bubbling nitrogen through the test solution for a period of 12-24 hours before inserting the specimen. E_{corr} measurements were made during the 15-30 minute stabilization period. Following these measurements, the specimens were immediately polarized in the anodic (electropositive) direction using a Princeton Applied Research Model 352 potentiostat. The polarization began at approximately 10 mV cathodic to E_{corr} and proceeded in the electropositive direction at a scan rate of 0.1 mV/sec to develop the anodic polarization curves. Potential and current measurements were made using a saturated calomel reference electrode (SCE) and two graphite counter electrodes.

RESULTS AND DISCUSSION

The results of this investigation are summarized in Table (3). Porosity, oxide, and tensile bond strength results are presented graphically in Figures (1) through (3) respectively. Details of the metallographic, tensile bond strength, and polarization curve evaluations are discussed in the following sections.

Quantitative Metallography

Plasma Sprayed Coatings - Examination of the plasma sprayed monel coating on the monel substrate show it to be characterized by elongated "splats" with relatively fine oxide layers in between. Remnants of the splats and associated oxides are still apparent in the coating HIPed at 1050 °C. However, the oxides are no longer continuous. In the coating HIPed at 1150 °C, the splats are no longer visible and the oxides are nearly randomly dispersed throughout the coating. Figure (4a) shows the coating/substrate interface for the as-sprayed and HIPed conditions for the plasma sprayed monel coating on the monel substrate. The mechanical nature of the bonding between the coating and substrate is apparent in the as-sprayed condition. Some level of metallurgical bonding is apparent in both HIPed

conditions. While the coating HIPed at 1150 °C appears to have recrystallized, no significant difference in the level of metallurgical bonding between the two HIP conditions is apparent.

Quantitative image analysis shows little effect of the HIP treatments on the porosity in the coating, Figures (4b and 4c). While the as-sprayed coating and the coating HIPed at 1050 °C have nominally equivalent porosity levels, an increase in the porosity level was observed for the coating HIPed at 1150 °C. Since there is no apparent reason for porosity levels to increase during the HIP process, it is possible that this result is simply reflective of variable porosity levels in the coating as it is deposited. The oxide content was reduced in both HIP conditions as compared to the as-sprayed coating.

The morphology of the plasma sprayed monel coating applied to the HY-80 steel substrate is essentially equivalent to that applied to the monel substrate as anticipated. The mechanical bond between the monel coating and HY-80 steel substrate as well as the martensitic microstructure of the substrate for the as-sprayed condition is shown in Figure (5a). The large amount of separation between the substrate and coating may be an artifact of the specimen preparation and not entirely typical of this substrate/coating combination. The metallurgical bond developed during both the 1050 °C and 1150 °C HIP cycles is readily apparent in Figures (5b and 5c). In both cases, the bond is uniform in appearance and depth. No significant increase in depth of the bond is apparent at the higher HIP temperature. While the appearance of a metallurgical bond is encouraging, it is also apparent that the microstructure of the substrate has been effected. At the 1050 °C HIP temperature, the base metal has re-austenitized and formed a microstructure of equiaxed bainite and ferrite. At the 1150 °C HIP temperature, the base metal has re-austenitized and formed a coarsened bainitic and ferritic microstructure.

Image analysis revealed little to no change in porosity levels between the as-sprayed coating monel coating applied to the HY-80 steel substrate and the HIPed coatings. As with the monel coating on the monel substrate, a slight decrease in oxide content was measured between the as-sprayed and the HIPed coatings. Very little difference in oxide content was observed between the two HIP conditions.

HVOF Coatings - The morphology of the as-sprayed HVOF alloy 625 coating applied to the HY-80 steel substrate is typical of most HVOF coatings which are characterized by more spherical shaped particles than the elongated splats found in plasma sprayed coatings. The coating also contains inter-particle oxide layers. These oxide layers tended to be broken up on HIPing at 1050 °C and even further upon HIPing at 1150 °C. No change in particle shape was apparent. The mechanical bond at the interface between the alloy 625 coating and the HY-80 steel substrate in the as-sprayed condition is shown in Figure (6a). HIPing at both 1050 °C and 1150 °C produced metallurgical bonding with the higher temperature producing a slightly broader zone of bonding, Figures (6b and 6c). As with the monel coating on the HY-80 steel, the HIP process produced undesirable changes in the HY-80 steel, changing the microstructure from martensitic to ferritic and bainitic.

Image analysis showed similar porosity levels between the as-sprayed and 1050 °C HIP coatings. A slight increase in porosity level was measured for the 1150 °C HIP coating. Oxide contents for the as-sprayed and HIPed coatings were similar with the 1050 °C HIP coating having the lowest measured oxide content.

The metallic coating particles of the CP Ti coatings applied to the alloy 625 substrate have more irregular shapes than those seen in the alloy 625 HVOF coating, but are typical of those seen in other investigations[4]. The inter-particle oxides surrounding these particles are very apparent. HIPing at 925 °C/15 ksi/2 hours appears to have broken up the bands of oxides without changing the shape of the metallic particles significantly. Increasing the HIP pressure to 25 ksi did not change the microstructure further in terms of oxide morphology or metallic particle shape. Cross-sections revealing the CP Ti coating/alloy 625 substrate interface show the mechanical bonding achieved in the as-sprayed condition and the bonding that occurred on HIPing at both the 15 ksi and 25 ksi pressures. It is probable that this bonding has occurred through the formation of Ni-Ti intermetallic compounds. Microprobe analysis to confirm this result was not performed.

Image analysis results show that the porosity content of the HIPed coatings increased dramatically as compared to the as-sprayed coating, Figure (7a). This result was unexpected and may reflect variation in as-sprayed coating porosity levels at different locations as opposed to an effect of the HIP processing. Oxide content was decreased in the HIPed coatings as compared to the as-sprayed coating, Figure (7b and 7c).

Bond Strength Testing

Results of the tensile bond strength testing are summarized in Table (3) and Figure (3). Since there were so few tensile tests conducted, interpretation of the results is somewhat difficult. However, there are some clear trends in the data. First, in the as-sprayed condition, failure occurred cohesively within the coating for each of the substrate and thermal spray coating combinations. After HIPing, the failures were a combination of bonding agent and adhesive failures. The second observation is that an increase in the stress at failure occurred for the monel substrate/monel coating, HY-80 steel substrate/monel coating, and the HY-80 steel substrate/alloy 625 coating material combinations with the 1050 °C /15 ksi HIP cycle as compared to the as-sprayed condition. In each of these cases, a slight decrease in the stress at failure occurred with the 1150 °C /15 ksi HIP cycle as compared to the 1050 °C /15 ksi HIP cycle. The largest increase in stress at failure occurred for the HY-80 steel substrate/alloy 625 coating combination. These results suggest that the metallurgical bonding and changes in coating morphology achieved at the lower HIP temperature are sufficient to produce desirable changes in properties for these coatings and substrate combinations.

HIP post-processing of the CP Ti coating on the alloy 625 substrate did not produce an increase in the tensile stress at failure. In fact, the 925 °C/25 ksi HIP cycle resulted in a significantly lower stress at failure than the as-sprayed condition or the 925 °C/15 ksi HIP cycle. This result could be due to the formation of relatively brittle Ni-Ti intermetallics at the coating/substrate interfaces.

Polarization Curve Measurement

The paragraphs below summarize the polarization curve results for each of the substrate/coating combinations. Coated specimens that had been HIPed are compared to coated specimens without HIPing and to uncoated metal substrate controls in order to assess the effectiveness of the HIPing operation in improving the corrosion resistance of the coating. The coatings evaluated in this research are all passive-film forming alloys, and an improvement

in the corrosion resistance of the coating is shown in the anodic polarization curves as a reduction in the corrosion current density at a given potential. Typical anodic polarization curves for the substrate/coating specimens are found in Figure (8). The curve on the left represents a coated specimen displaying passivity, while the curve on the right is indicative of a specimen with no passivity.

Plasma Sprayed Coatings - The uncoated monel substrate polarization curve exhibited a passive range from E_{corr} to approximately 0 mV_{SCE}. The monel substrate/monel coating baseline specimen did not display any evidence of passivity in the potential range evaluated. The E_{corr} measurement for this specimen at the onset of the anodic polarization was -24 mV_{SCE}, significantly more electropositive than the E_{corr} measured for the uncoated monel substrate (-533 mV_{SCE}). This was presumably due to a lack of deaeration in the test solution, which shifted the E_{corr} to a more electropositive potential and masked the passive range for this specimen. The monel substrate/monel coating specimen that was HIPed at 1150 °C showed a range of passivity that was increased by approximately 80 mV as compared to uncoated monel. This result shows a slight improvement in the coating's corrosion resistance.

The uncoated steel substrate polarization curve was typical for steel in aqueous chloride solutions, that of an increasing corrosion current as the potential is scanned in the electropositive direction. No passivity was evident in this polarization curve. The as-sprayed steel substrate/monel coating specimen demonstrated passivity over an approximate 345 mV range. The steel substrate/monel coating specimen that was HIPed at 1050 °C showed no improvement in the coating's corrosion resistance as compared to the as-sprayed specimen. For the 1150 °C HIP condition, the polarization curve results showed a very slight increase in corrosion resistance for the HIPed condition as compared to the as-sprayed specimen.

The marginal improvements in corrosion resistance appear to confirm the metallographic results which indicated little porosity consolidation for this coating/substrate combination. As a result, additional as-sprayed and HIPed specimens were tested after polishing the exposed surfaces with 60 grit sandpaper in an attempt to close the surface porosity. The as-sprayed steel substrate/monel coating specimen after polishing showed a passive range of approximately 850 mV. Similar improvements were found for the HIPed specimens which had been polished. These results suggest that improvements in the corrosion resistance of the coating were influenced more by polishing (closing surface porosity) than by HIPing and therefore reinforce the premise that porosity plays a large role in the corrosion performance of thermal sprayed coatings.

HVOF Coatings - Like the uncoated steel substrate specimen in the section above, the steel exhibited no passivity in the anodic polarization curve. In contrast, the HY-80 steel substrate/alloy 625 coating specimen showed a very large passive range of more than 900 mV. This demonstrates the significant increase in corrosion resistance gained by coating a steel substrate with a passive film forming alloy such as Alloy 625. The steel substrate/alloy 625 coating specimen that was HIPed at 1150 °C showed a large degree of scatter in the anodic polarization data, suggesting that the alloy 625 passive film was very unstable. No additional improvement in corrosion resistance was noted after HIP processing. These results indicate that use of coating techniques which result in low porosity (such as HVOF) have the potential to produce significant improvements in corrosion resistance in the as-sprayed condition.

The uncoated alloy 625 substrate specimen displayed a passive range in the anodic polarization curve measured. The as-sprayed alloy 625 substrate/titanium coating specimen with no HIPing exhibited minimal passivity as compared to the uncoated alloy 625 substrate specimen. These results are not typical for commercially pure titanium, which is known to have excellent corrosion resistance in room temperature aqueous chloride solutions due to its tenacious passive film that is readily formed in air[9]. The alloy 625 substrate/titanium coating specimen that was HIPed at 1050 °C demonstrated passivity that was similar to the uncoated alloy 625 substrate specimen and increased passivity as compared to the as-sprayed alloy 625 substrate/titanium coating. The alloy 625 substrate/titanium coating HIPed at 1150 °C also showed an increased passivity as compared to the as-sprayed coating, but slightly less than for the coating HIPed at 1050 °C.

SUMMARY AND CONCLUSIONS

Four thermal sprayed coating/substrate combinations were subjected to metallographic, tensile bond strength, and polarization curve characterization in the as-sprayed condition as well as after post-processing with hot isostatic pressing (HIP). The Monel 400 coating on Monel 400 substrate and monel coating on HY-80 steel substrate specimens were produced using the plasma spray process while the alloy 625 coating on HY-80 steel substrate and commercially pure titanium coating on alloy 625 substrate were produced using the high velocity oxy-fuel (HVOF) process. Based on the work described above, the following conclusions are made:

- Metallographic examination showed that some level of metallurgical bonding was achieved for all coating/substrate combinations as a result of the HIP post-processing;
- The porosity results had a large amount of scatter and were therefore difficult to interpret. However, no significant decreases in porosity were observed for any of the coating/substrate combinations as a result of the HIP post-processing. Modifications of HIP parameters may result in porosity reductions;
- The metallurgical bonding produced by the HIP post-processing generally resulted in increased coating tensile bond strength. The largest increases were seen for the alloy 625 coatings on steel substrates;
- The HIPing operation did not result in substantial improvements to the corrosion resistance of the coatings applied on the monel, HY-80 steel or alloy 625 substrates. Slight improvements were noted for some of the coated specimens, but a significant reduction in corrosion current density was not present on any of the HIPed specimens;
- Based on results for a very limited number of specimens, polishing the specimens after coating did result in a substantial increase in coating corrosion resistance. The polishing process evidently closes surface porosity present in the coating, thereby improving the overall corrosion resistance.

ACKNOWLEDGEMENTS

The authors would like to thank Mr. Arthur Dwyer of Norfolk Naval Shipyard for assisting in the preparation of the thermal spray specimens. The technical assistance provided by Mr. Al Brandemarte, NSWCCD Code 612 was critical to this effort. Mr. James Pugh provided significant logistical support to the program. Finally, the support of Dr. John Sedriks of ONR and Mr. Ivan Caplan of NSWCCD Code 0115 is gratefully appreciated.

REFERENCES

1. Brenna, R., R.A. Hays, and R. Masson, "Thermal Spray Coatings for Marine Corrosion Control," SSPC '95 Protective Coatings, Steel Structures Painting Council Conference 1995 (Nov 1995).
2. Travis, R., M. Herbstritt and J. Herbstritt, "Thermal Spraying for Shipboard Machinery Component Repair," American Welding Society Thermal Spray Symposium (Apr 1993).
3. Scandell, K.C. and R.L. McCaw, "High Velocity Oxy-Fuel (HVOF) Thermal Spray: An Alternative for Machinery Repair, Restoration, and Surface Conditioning," American Society of Naval Engineers Fleet Maintenance Symposium '95, Norfolk, VA (Oct 1995).
4. Hays, R.A. and R.L. McCaw, "Application of Commercially Pure Titanium Coatings Using the High Velocity Oxy-Fuel Thermal Spray Process Under Atmospheric Conditions," 1992 Tri-Service Conference on Corrosion, Plymouth, MA (May 1992).
5. Siitonen, P., P. Sorsa, S.L. Chen, K. Niemi, P. Vuoristo, Proceedings of the 12th Scandinavian Corrosion Congress & Eurocorr '92, pp. 363-372, Espoo, Finland (June 1992).
6. Kinos, T., P. Siitonen, P. Kettunen, and V.-J. Laurila, "Effect of Post Treatments on the Corrosion Resistance of Plasma Sprayed Duplex Stainless Steel Coating in Saltwater," Proceedings of the 7th National Thermal Spray Conference, American Society for Materials (Jun 1994).
7. Steffens, H.-D, M. Nolde, D. Dvorak, M. Dvorak, Proceedings of the International DVS-Conference, pp 156-159, Aachen Germany (Mar 1993).
8. Metals Handbook, Ninth Edition, Volume 7 - Powder Metallurgy, American Society for Metals, Metals Park, OH (1984).
9. Schutz, R.W. and D.E. Thomas, "Corrosion of Titanium and Titanium Alloys," in Metals Handbook, 9th Edition, Vol. 13, Corrosion, J.R. Davis, Editor, ASM International, Metals Park, Ohio, 1987, pp. 669-706.

Table 1. Experimental Matrix

BASE MATERIAL	COATING MATERIAL	THERMAL SPRAY PROCESS	HIP PARAMETERS		
			TEMP. (C)	PRESSURE (psi)	TIME (hr)
Monel	Monel	Plasma	--- 1050 1150	As-Sprayed 15000 15000	--- 4 4
HY-80	Monel	Plasma	--- 1050 1150	As-Sprayed 15000 15000	--- 4 4
HY-80	Alloy 625	HVOF	--- 1050 1150	As-Sprayed 15000 15000	--- 4 4
Alloy 625	CP Titanium	HVOF	--- 925 925	As-Sprayed 15000 25000	--- 2 2

Table 2. Nominal Compositions (weight %) of Coating and Substrate Materials

MATERIAL	MONEL POWDER	ALLOY 625 POWDER	CP TITANIUM POWDER	MONEL SUBSTRATE	HY-80 STEEL SUBSTRATE	ALLOY 625 SUBSTRATE
Spec.	MIL-STD-1687A	Dimalloy 1005	Manuf. Cert.	ASTM B127	MIL-S-16216K	ASTM B443
Ni	70	58.0 min	0.06	63.0 min	2.50 to 3.50	58.0 min
Cu	30			28.0 to 34.0	0.25	
Fe		5.0	0.1	2.5	Bal.	5.0
Mn		0.50		2.0	0.10 to 0.40	0.50
C		0.10	0.03	0.3	0.13 to 0.18	0.10
Si		0.50	0.04	0.5	0.15 to 0.38	0.50
S		0.015		0.024	0.008	0.015
P		0.015	0.20		0.015	0.015
Cr		20.0 to 23.0			1.40 to 1.80	20.0 to 23.0
Nb+Ta		3.15 to 4.15				3.15 to 4.15
Co		1.0				1.0
Mo		8.0 to 10.0			0.35 to 0.60	8.0 to 10.0
Al		0.40				0.40
N			0.07			
O			0.18			
H			0.35			
Ti		0.40	Bal.			0.40

Table 3. Summary of Results

SUBSTRATE	COATING MATERIAL	HIP PARAMETERS			% POROSITY	% OXIDE	BOND STRENGTH (psi)
		TEMP. (°C)	PRESSURE (psi)	TIME (hr)			
Monel	Monel		As-Sprayed		3.6	9.6	6410
Monel	Monel	1050	15000	4	2.8	3.9	7385
Monel	Monel	1150	15000	4	5.2	5.5	6560
HY-80	Monel		As-Sprayed		3	5.5	7274
HY-80	Monel	1050	15000	4	3.2	3.1	7908
HY-80	Monel	1150	15000	4	3.6	3.3	7087
HY-80	Alloy 625		As-Sprayed		1.5	6.9	7763
HY-80	Alloy 625	1050	15000	4	1.9	5.1	10501
HY-80	Alloy 625	1150	15000	4	4.2	6.6	9741
Alloy 625	CP Tit		As-Sprayed		5.4	12.6	5327
Alloy 625	CP Tit	925	15000	2	12.2	9.6	5425
Alloy 625	CP Tit	925	25000	2	9.7	8.8	4148

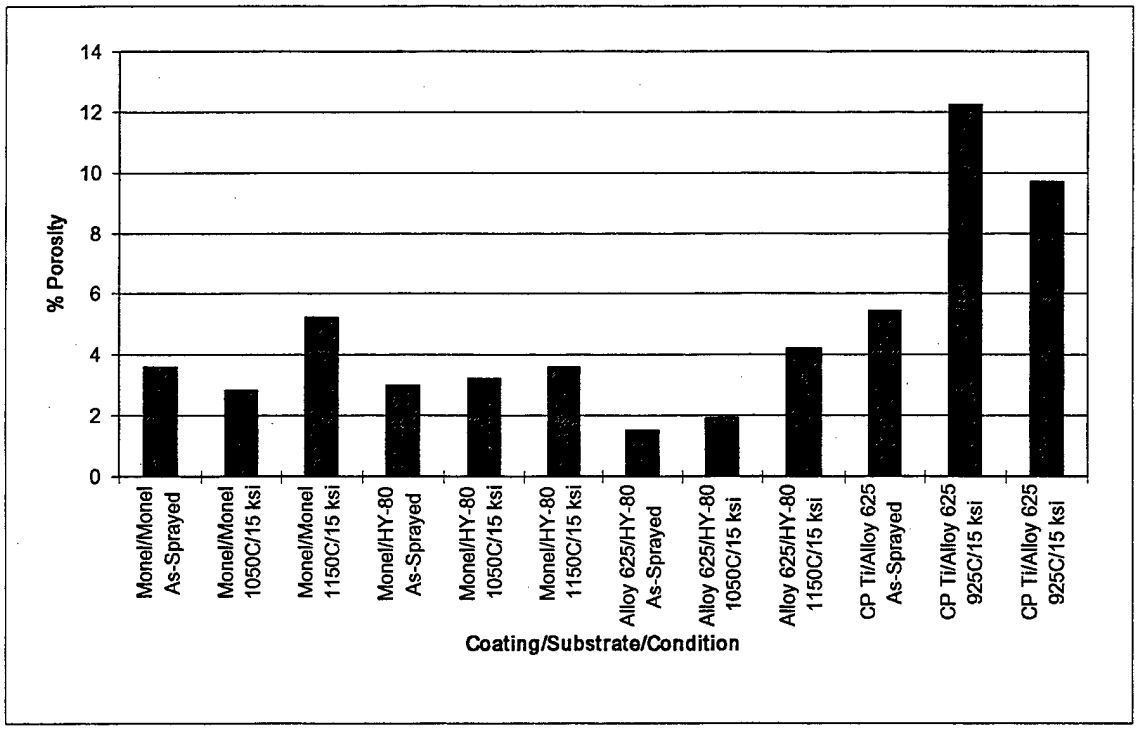

Figure 1. Porosity Content of As-Sprayed and Post-Processed Thermal Sprayed Coatings

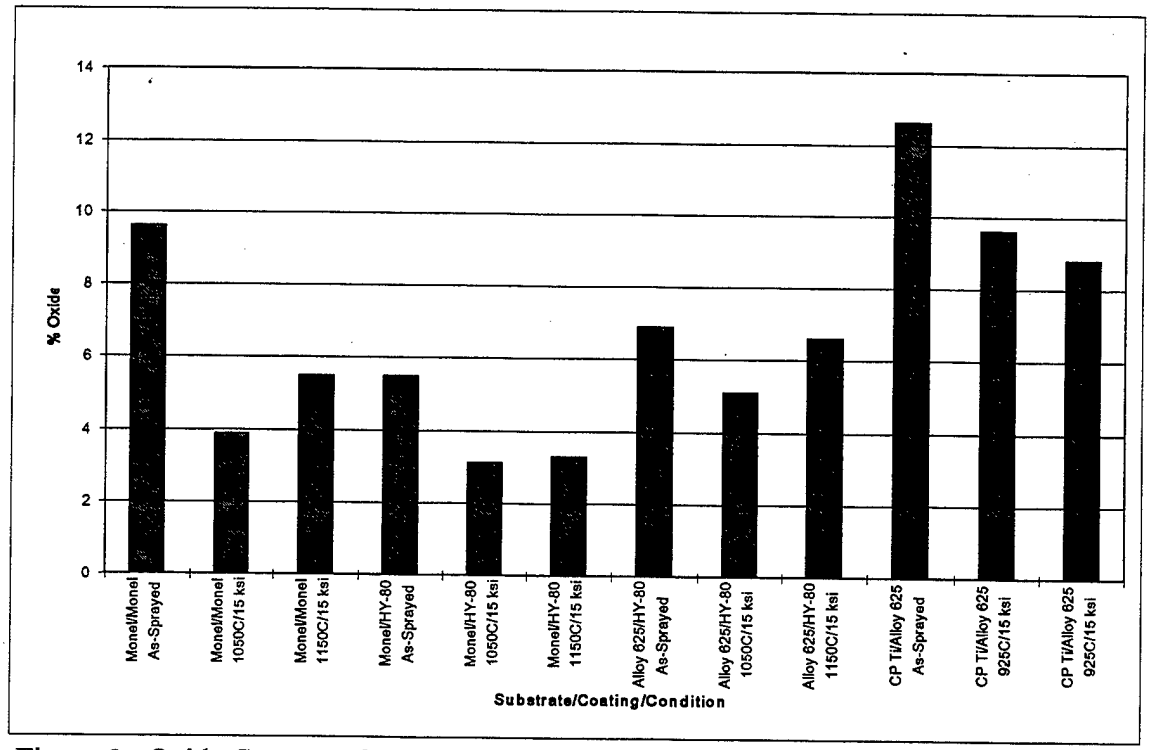

Figure 2. Oxide Content of As-Sprayed and Post-Processed Thermal Sprayed Coatings

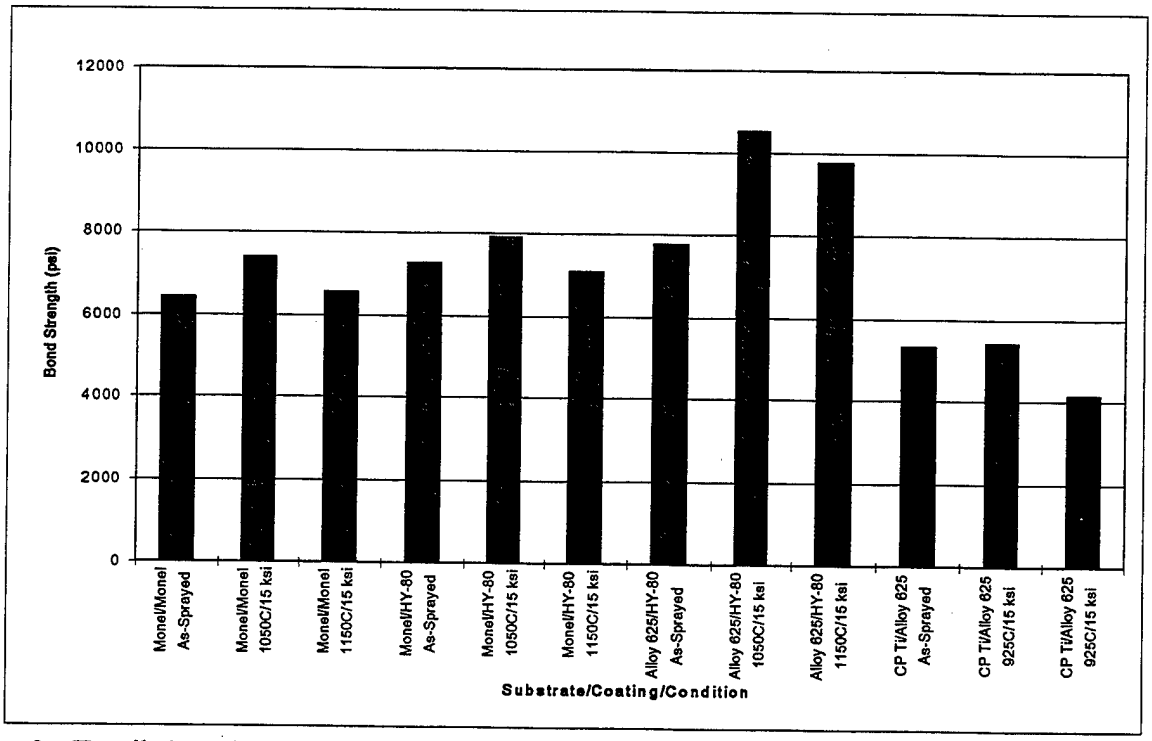

Figure 3. Tensile Bond Strength of As-Sprayed and Post-Processed Thermal Sprayed Coatings

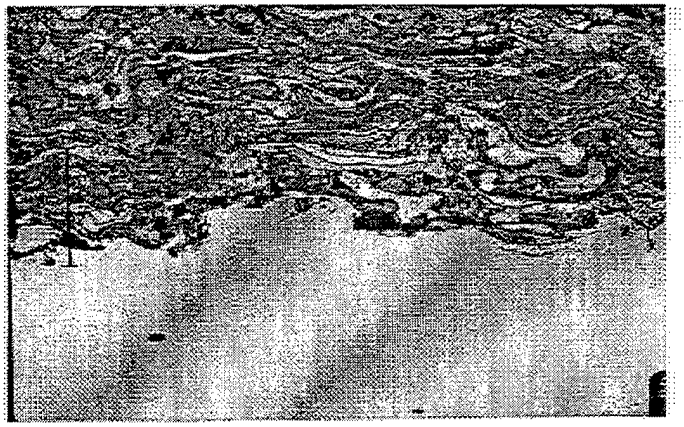

(a) As-Sprayed

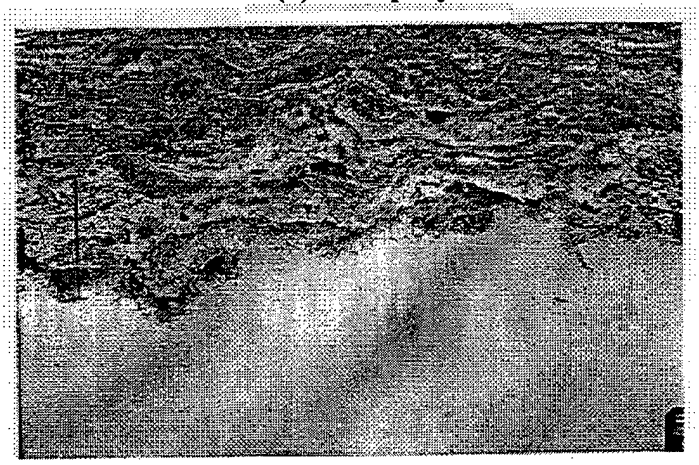

(b) HIPed @ 1050 °C/15 ksi/4 hours

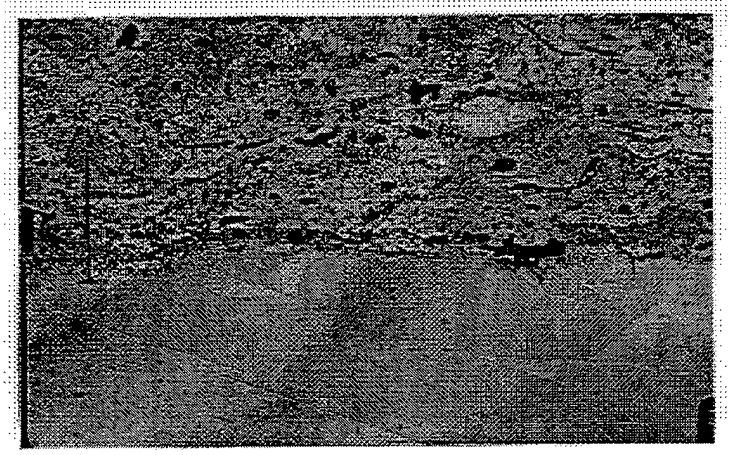

(c) HIPed@1150 °C/15 ksi/4 hours

Figure 4. Plasma Sprayed Monel 400 on Monel 400 Substrate

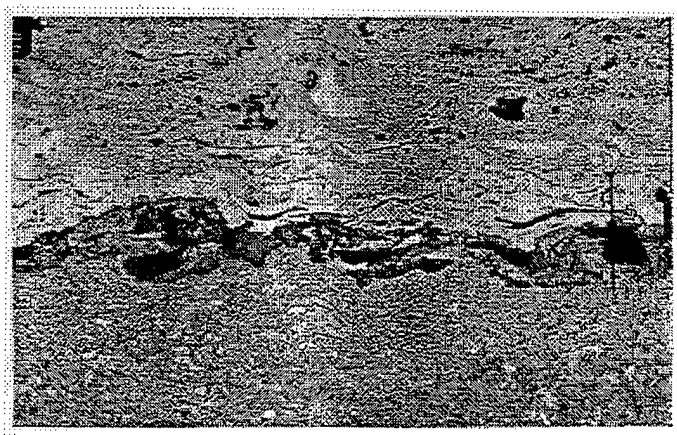

(a) As-Sprayed

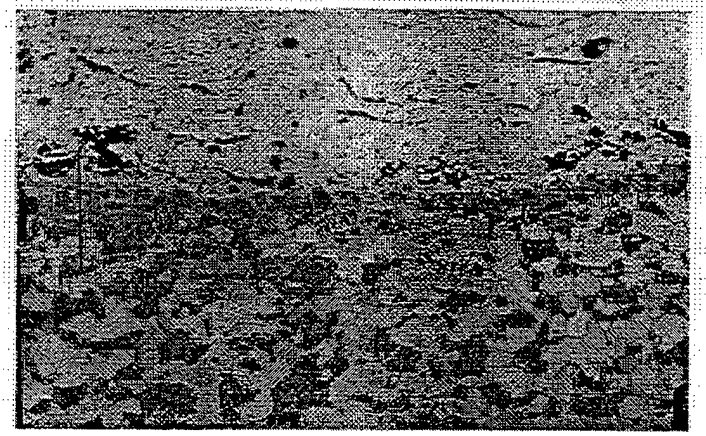

(b) HIPed@1050 °C/15 ksi/4 hours

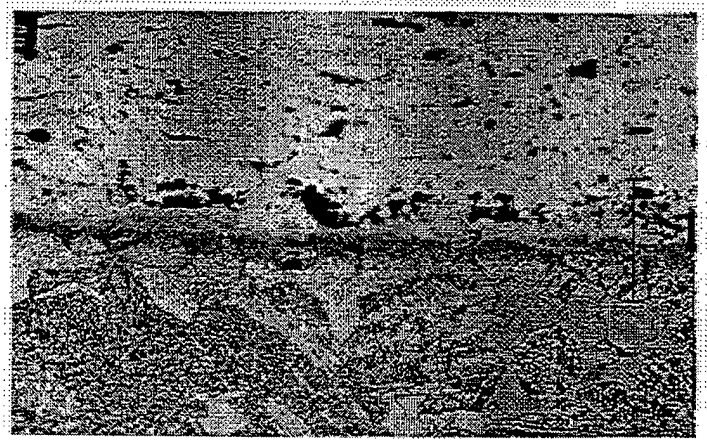

(c) HIPed@1150 °C/15 ksi/4 hours

Figure 5. Plasma Sprayed Monel 400 on HY-80 Steel Substrate

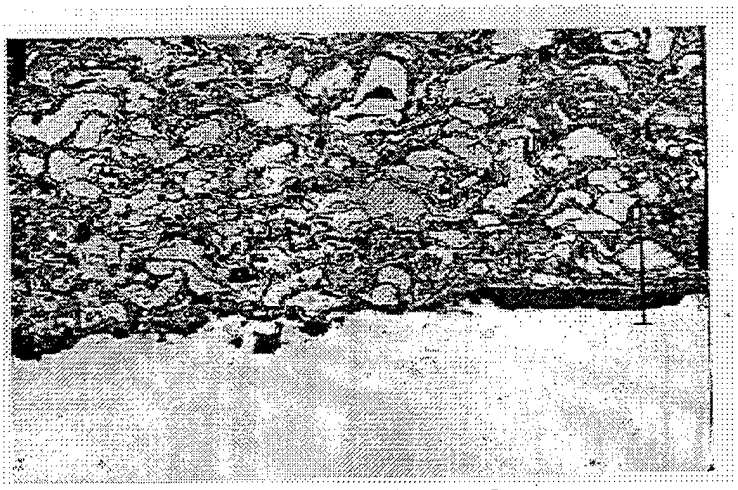

(a) As-Sprayed

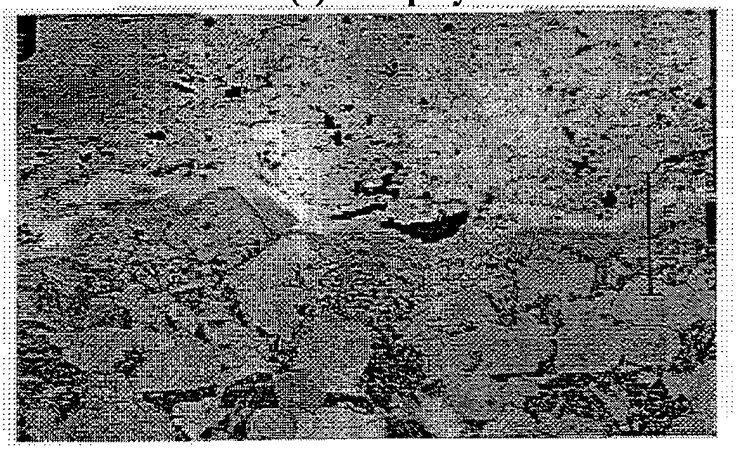

(b) HIPed@1050 °C/15 ksi/4 hours

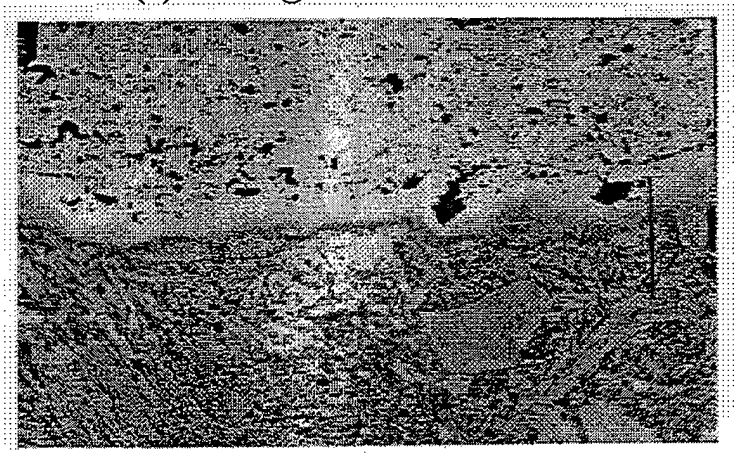

(c) HIPed@1150 °C/15 ksi/4 hours

Figure 6 HVOF Sprayed Alloy 625 on HY-80 Steel Substrate

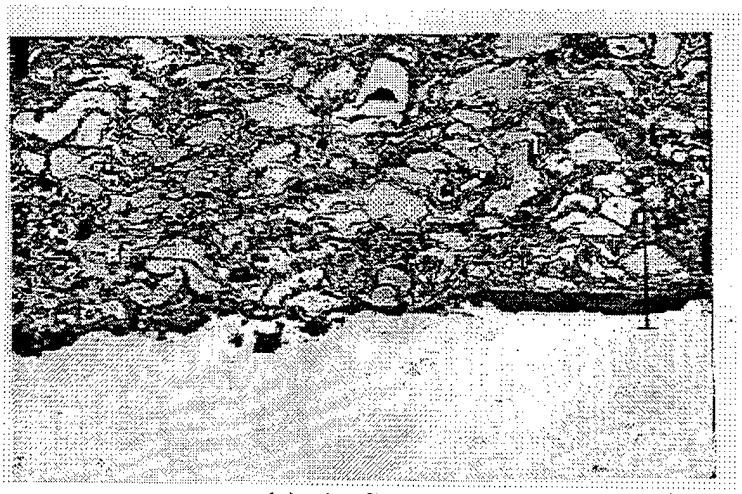

(a) As-Sprayed

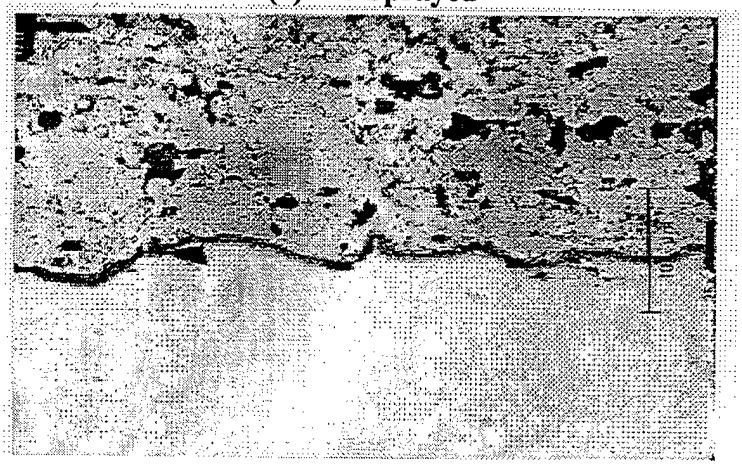

(b) HIPed@925 °C/15 ksi/2 hours

(c) HIPed@925 °C/25 ksi/2 hours

Figure 7. HVOF Sprayed Commercially Pure Titanium on Alloy 625 Substrate

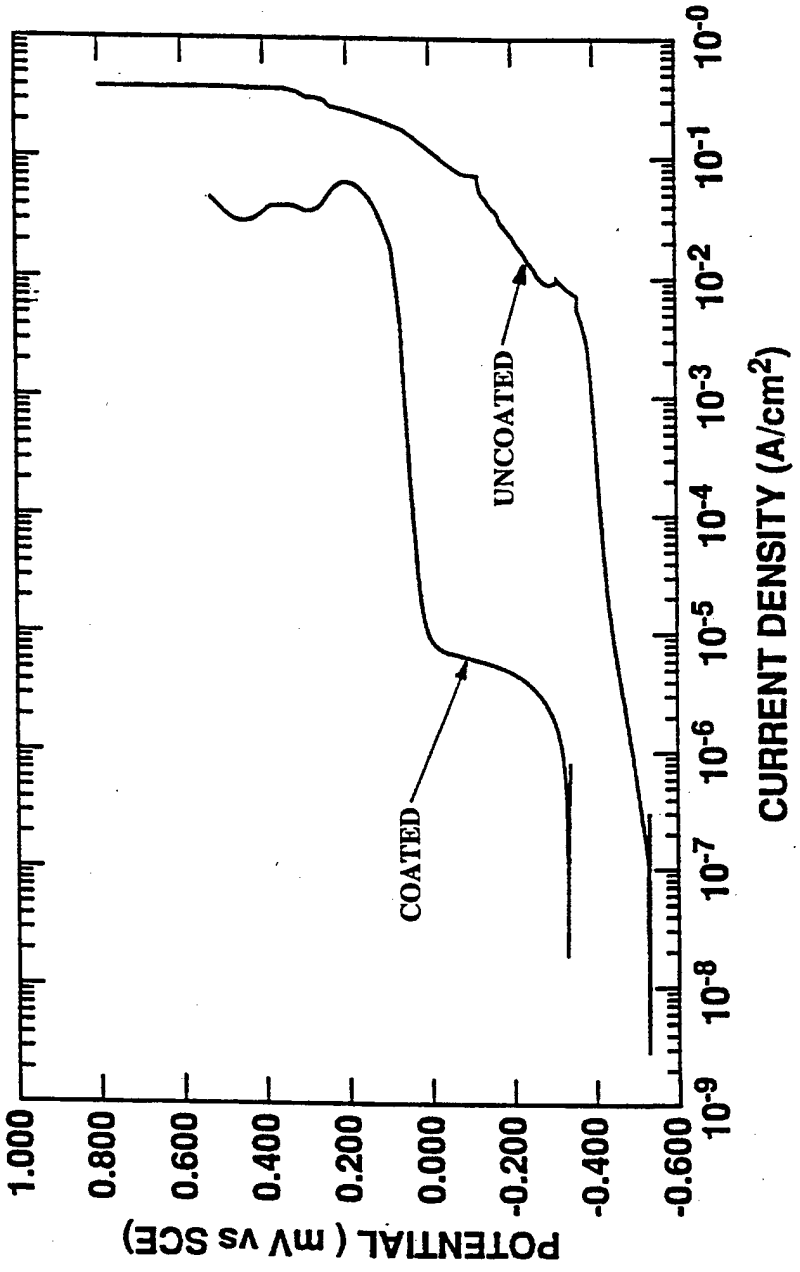

Figure 8 - Typical Anodic Polarization Curves for Substrate/Coating Specimens

Demonstration of Electro-Osmotic Pulse Technology for Groundwater Intrusion Control in Concrete Structures

Vincent F. Hock, Michael K. McInerney, and Erik Kirstein
U.S. Army Construction Engineering Research Laboratories
P.O. Box 9005, Champaign IL 61826-9005

ABSTRACT

Groundwater intrusion through a building's foundation can cause serious damage. Basement dampness can ruin expensive mechanical equipment which is often located in basement space, can increase maintenance requirements, and can make affected areas uninhabitable or even unusable. A system has been developed to apply electro-osmotic pulse (EOP) technology commercially to concrete structures by applying a pulsating electric field between the structure and the surrounding soil. EOP technology can mitigate some water-related problems from the interior of affected areas without the cost of excavation. The EOP alternative can further mitigate corrosion damage to mechanical equipment along with humidity and mold problems.

INTRODUCTION

Groundwater intrusion through a building's foundation can cause serious damage. Basement dampness can ruin expensive equipment, e.g., Heating Ventilation, and Air-Conditioning (HVAC) equipment, which is often located in basement space; can increase maintenance requirements (frequent repainting or cleaning to combat mold growth); and can make affected areas uninhabitable or even unusable (e.g., poor air quality).

A properly designed original foundation with appropriate dampproofing will avoid most water problems. However, in older buildings, such as those common on U.S. Army installations, severe damp-basement problems call for immediate action to mitigate water damage. In selective problem areas, the usual approach is to "trench and drain," in other words, to excavate in order to expose the wall area and the base of the foundation, and then to replace dampproofing on the wall surface and install a drain tile system around the building or affected area. This expensive process is further complicated by the fact that most contractors limit their warrantees against future seepage in areas with high water tables.

Electro-osmotic pulse (EOP) technology offers an alternative that can mitigate some water-related problems from the interior of affected areas without the cost of excavation. The EOP alternative can further mitigate corrosion damage to mechanical equipment along with humidity and mold problems.

Electro-osmosis is not a new technology although new applications are still being developed. In 1809, F.F. Reuss originally described electro-osmosis in an experiment that showed that water could be forced to flow through a clay-water system when an external electric field was applied to the soil. Research since then has shown that flow is initiated by the movement of cations (positively charged ions) present in the pore fluid of clay or similar porous medium such as concrete; and the water surrounding the cations moves with them. Electro-osmosis can be used to arrest or cause flow of water as well as the ions in it. Electro-osmosis has been used in civil engineering to dewater dredgings and other high-water content waste solids, consolidate clays, strengthen soft sensitive clays, and increase the capacity of pile foundations. It has also received significant attention in the last five years as a method to remove hazardous contaminants from groundwater or to arrest water flow.

A system has been developed to apply electro-osmosis commercially within concrete structures by applying a pulsating direct electric field combined with an off-period. It is called electro-osmotic pulse (EOP). The pulsating electro-osmotic sequence consists of a pulse of positive voltage (as seen from the dry side of the concrete wall), a pulse of negative voltage, and a period of rest when no voltage is applied. The pulse of positive voltage has the greater time duration. The amplitude of the signal is typically on the order of 20 to 40 Volts DC (VDC). The electrical pulse causes cations (e.g., Cl^-) and associated water molecules to move from the dry side (anode) towards the wet side (cathode) against the direction of flow induced by the hydraulic gradient, thus preventing water penetration through buried concrete structures. One of the most critical aspects of this technology is the negative voltage pulse. This allows control of the amount of moisture within the concrete which prevents overdrying of the concrete matrix and subsequent degradation. Field tests were conducted to assess the feasibility and cost effectiveness of EOP technology, in comparison with conventional dampness mitigation techniques, at selected Army installations.

BACKGROUND

If ions of one sign are preferentially adsorbed at a solid solution interface, a net charge or electric potential difference develops across the interface. This phenomenon is referred to as *electro-osmosis*. (The basic physics and chemistry of electro-osmosis can be found in several textbooks and treatises. [1, 2, 3]) It was found that when a potential difference is applied to electrodes immersed into an electrolyte solution on opposite sides of a porous plug or fine capillary tube, a flow of the solution results. Similarly, when a solution is forced through such a barrier by hydrostatic pressure, a potential difference develops between the solution on one side of the barrier and that on the other. This is called the *streaming potential*.

Descriptions of these phenomena are based on the concept of electric double layer. A layer of ions, which is approximately a single ion in thickness, of one sign is firmly adsorbed on the solid surface or particle, the sign of the charge depending on the nature of the surface and other conditions. The region as a whole is electrically neutral, and an equal number of opposite electric charges are present in an adjacent ionic atmosphere which, as the term implies, becomes more attenuated as distance from the surface increases. This is called the diffuse layer. When the solid

surface and fluid are in relative motion, there exists a velocity gradient, and a thin film of solution, together with the ions it contains, is immobilized near the wall. Part of the ion atmosphere moves with the solution, and part (together with adsorbed ions) effectively belongs to the surface. As a result, the liquid phase and the wall have different net electric charge, and the application of an external electric field produces relative motion.

For example, electro-osmosis occurs in clay soils when cations in the diffuse layer are driven by the application of an external electric field. As a result, a velocity field in the pore fluid develops (Figure 1). The velocity distribution changes rapidly near the particle's surface, but then becomes flat at the edge of the diffuse layer. Hence, electro-osmotic flow appears as plug flow through the pores of soil.

The velocity profile reaches a constant value (V_o) a short distance from the particle's surface. To determine V_o, a steady-state equation of motion is:

$$\mu \frac{\partial^2 V_x}{\partial y^2} + E_x \varepsilon \frac{d^2 \phi}{dy^2} = 0 \qquad (1)$$

where:

μ	is	the viscosity of the solution;
V_x	is	the velocity of the solution parallel to the particle surface;
y	is	the distance orthogonal to the particle surface;
E_x	is	the externally applied electric field gradient;
ε	is	the permitivity of the solution; and,
ϕ	is	the electrical potential gradient.

By the Debye-Hückel approximation, ϕ is written as

$$\phi = \xi \exp\left(-y \sqrt{\frac{2 n_i^{\infty} Z_i^2 F^2}{\varepsilon RT}} \right) \qquad (2)$$

where:

ξ	is	the zeta potential[1];
n_i^{∞}	is	the concentration of constituent i in free solution;
Z_i	is	the equivalents/mole of constituent i;
F	is	Faraday's constant;
R	is	the universal gas constant; and,
T	is	the absolute temperature.

[1] The difference of potential between the plates of a hypothetical capacitor used to model the diffuse layer.

When (1) is solved using the boundary conditions,

$$\begin{aligned} V_x &= 0 \qquad at\ y = 0 \\ V_x &= V_0 \qquad at\ y >> 0 \end{aligned} \tag{3}$$

The velocity V_o is then obtained:

$$V_o = \frac{\varepsilon \xi}{\mu} E_x \tag{4}$$

Of the four independent variables in (4), E_x can be controlled to redirect the movement of the solution.

The pulsating electro-osmotic technique consists of a positive voltage pulse, a negative voltage pulse, and a period when no voltage is applied. Figure 2 shows an example waveform for the pulsating electro-osmotic pulse or EOP system. This waveform was sampled at one of the demonstration sites. (The vertical scale in Figure 2 is 10 volts/division and the horizontal scale is 1 second/division.) The positive voltage pulse has the longest interval and the negative voltage pulse has the shortest interval. As a result of this, the pore fluid moves (on the average) in one direction.

Currently, the reasons for the increased performance of the EOP system over standard dc electro-osmosis for drying concrete are not well understood. However, it is speculated that the change in polarity results in the reversal of some of the chemical reactions occurring during electrolysis. It is also believed that the rest phase (no applied voltage) allows the system to equilibrate. As a result of these effects, undesirable side effects such as acid production and increased corrosion are avoided. Also, use of a pulse sequence might prevent the concrete from becoming too dry.

An EOP system is realized by inserting anodes (positive electrodes) into the concrete wall or floor on the inside of the structure and by placing cathodes (negative electrodes) in the soil directly outside the structure. The density of the anode and cathode placement is determined from an initial resistivity test of the concrete and soil. The objective is to achieve a certain current density in the concrete.

TECHNOLOGY DEMONSTRATIONS

Two sites were selected for the EOP technology demonstration, Building 3265 at Fort Jackson, SC and Building 5 at McAlester AAP, OK. In both cases, the location of the groundwater intrusion was through the floor and walls of poured concrete basements.

FT Jackson

Building 3265 had a history of water seepage into the concrete basement mechanical room. The mechanical room had experienced water levels within the structure as high as 36 cm. On the average, there existed about 5 cm of standing water. In addition, there was seepage from cracking in the wall, efflorescence, and poor air quality as a result of the high indoor humidity. This seepage initiated corrosion of the mechanical equipment located in the basement.

For the EOP system, eighty-three (83) rubber-graphite anodes were coated with a graphite-mortar mixture and inserted into holes drilled into all four walls, approximately 13 cm from the floor and 46 cm apart. Twenty-four feet of rubber-graphite conductive cable was installed around the base of a concrete pad that supported steel water tanks in the room. Three copper-clad steel ground rods (cathodes) were driven into the soil adjacent to the exterior side of the concrete wall. The EOP Control Unit was mounted on one wall and all wiring from the anodes and cathodes was enclosed and wired into the unit.

McAlester AAP

The basement of Building 5 had standing water in several areas. Problems similar to the basement at Fort Jackson were prevalent: water seepage from cracking in the wall, efflorescence and high indoor relative humidity (70 percent). The reduction of the indoor air humidity through the EOP system is very important, as one of the rooms is the Industrial Hygiene Office, occupied by an individual 40 hours a week.

Rubber-graphite anodes were placed 13 cm above the floor and 28 cm on center. The total number of anodes used was 95. Analysis of the water infiltration revealed that only about the half the basement was leaking, therefore not all of the basement was protected. Five copper-clad steel ground rods (cathodes), 2.44 m long, were driven into the soil adjacent to the exterior concrete wall in selected areas.

EOP OPERATIONAL DATA

FT Jackson

The EOP dc output current was within acceptable limits, varying from 0.75 amps for a high humidity environment to less than 0.2 amps for a low humidity environment. This is a result of the characteristics of the EOP system. The EOP power supply produces a voltage pulse of constant amplitude (i.e., a constant voltage power supply). The resistivity of the concrete is inversely proportional to the amount of water present in the concrete. As the water is slowly driven out, the resistivity of the concrete increases, decreasing the current load of the power supply, since current is inversely proportional to resistance (Ohm's Law). Table 1 shows measured current and voltage outputs of the EOP power supply. The slight increase in output current is due to the higher water table during July and August 1996.

Concrete moisture readings were taken at different locations on the walls. Table 2 lists the moisture measurements that were taken at three different times: at the time of installation, at the 5-month performance check, and 2 years after installation. The data are presented as the percent relative humidity of the concrete. All measurements were made at the concrete surface, not internally. The most suitable humidity for concrete structures is ≈70 percent. Note the direct correspondence between the power supply current (Table 1) and the concrete humidity (Table 2).

The corrosion potential of rebar specimens was investigated. Several small (~5-cm long) sections of 1.27-cm steel rebar were embedded in various locations in the basement walls. The purpose of these specimens was to document whether any change occurred in the native corrosion potential of rebar that might be embedded in a concrete structure when the EOP system is operating. The corrosion potential of the specimens was tracked and compared to the average corrosion potential for reinforcing steel in concrete, which is approximately -0.2 VDC. Table 3 lists the corrosion potentials for some of the specimens. These potentials were taken at the 5-month performance check on 10 January 1995. This data shows no significant difference in the corrosion potential from the native potential for the rebar specimens, however, this is just one time sample of a dynamic system. A larger record will be needed to fully document the EOP system effect on rebar corrosion potential.

The level of the water table relative to the basement floor was tracked. A monitoring well was installed just outside the basement wall for this purpose. The water table level is a good indication of EOP system performance: if the water table is above the floor of the basement and the basement remains dry, then the EOP system is fulfilling its purpose. Figure 3 shows the hydrograph for the monitoring well from September 1995 until September 1996. (Groundwater temperature just happened to be included in the standard monitoring well "package", it was not used in this study.) Note there are several times during the recording period when the water table exceeded the basement floor level, yet because of the EOP system the basement remained dry.

Rainfall data were recorded to track the months when there would be a greater potential for a higher water table. These data can be correlated to the monitoring well data points, specifically, note the correlation between the high rainfall during March 1996 and the rise in the water table during that month. Table 4 shows the rainfall data at Fort Jackson up to May 1996.

McAlester AAP

Many of the same parameters that were recorded at Fort Jackson are being recorded at McAlester AAP. The corrosion potential of rebar is sampled using a 33-cm long piece of 1.27-cm steel rebar which was grouted into the wall along with a Ag/AgCl reference half cell. The half cell was installed so as to be behind the rebar, and separated from it by about 5 cm of concrete. The humidity of the concrete is sampled using a dual humidity/temperature probe which was sealed in a small cavity in the concrete wall. Since the cavity is sealed, this probe monitors the temperature and humidity of the cavity. The humidity of the cavity should be proportional to the moisture content of the concrete, giving an indication of the effectiveness of the EOP system as it operates. Ambient room humidity and temperature sensors are monitoring the Industrial Hygiene Office.

The level of the water table outside the basement is also being monitored. In addition to these sensors and probes, the electrical power consumption of the EOP system is tracked to determine the power output of the power supply. All these monitoring devices except the rebar corrosion potential are fed into a datalogger that is installed on site and is remotely accessible via modem. The data is collected and stored in the datalogger until downloaded to a computer.

The daily rainfall, average outdoor temperature, and average outdoor relative humidity at McAlester AAP are obtained from the Oklahoma Climatological Survey. Data is downloaded monthly from their INTERNET site.

Figure 4 shows some of the recorded data, and highlights the power consumption of the EOP system in relation to the relative humidity of the wall cavity, as measured by the wall probe. Figure 4 shows that, as the power consumption drops (as a result of the decrease in current as the water is driven out), the concrete humidity drops as well. This shows that the EOP system is decreasing the moisture content in the concrete with a corresponding decrease in power requirements, both excellent indicators that the system is working properly.

Figure 5 shows the water table with respect to the basement floor. (Figure 5 gives the same information for McAlester AAP that Figure 3 gives for Fort Jackson.) Unlike FT Jackson the water table never rises above the basement floor.. Therefore the water intrusion problem at McAlester was mainly associated with the floor to wall cold joints which was associated with periodic saturation of the nearby soil.

COST/BENEFIT ANALYSIS

How to best estimate the initial cost savings of EOP over standard dampproofing methods for purposes of decision making must be based on experience and standard construction industry cost-estimating reference guides. [4, 5, 6] The comparison of the standard waterproofing technology to EOP technology is based on field experience at Fort Jackson and at McAlester AAP.

The focus of this estimate is a basement about 2.44-m deep with a concrete exterior. The standard estimate is drawn from construction cost guides, which is then compared to the results of the Army test sites.

Table 5 gives the breakdown of the costs for each facet of the standard dampproofing method, including the approximation of the cost per linear meter (lm) of the exterior foundation wall. This assumes a contract for the whole building and a standard depth of 2.44 m with average, but wet soil conditions.

The original contracts to the EOP manufacturer were analyzed and adjustments were made to the contract prices to reflect generic installations (i.e., travel, monitoring wells, report requirements, and certain extra experimental requirements have been eliminated from the base costs). The price of the EOP system based on installed costs and linear foot of wall was calculated. As for installation, both sites required some degree of interior access to the basement

level, but neither excavation nor dampproofing were required. Installation of the probes is generally based on a 30.5-cm. spacing and about 20 to 30 cm from the floor level. The price includes the EOP Control Unit, the anodes, ground rods, and all the wiring and labor for installation (Table 6).

The manufacturer of the EOP system estimates the life cycle of the system be 10 years. Therefore, one could assume a normal cycle with almost zero maintenance for that period of time. However, the system does consume energy roughly equivalent to that of a 60W light bulb left on all the time. This cost is minimal and is neglected in these calculations.

The percent savings based on capital costs is basically a comparison between the cost of trenching, dampproofing, backfilling, and installed EOP technology. The comparison is:

$$\%\ \text{first cost saved} = 100 \times \left(1 - \frac{\text{EOP per lm}}{\text{Trench \& Drain per lm}}\right) = 100 \times \left(1 - \frac{\$618.38}{\$1{,}034.41}\right) = 40\% \qquad (5)$$

Payback is based on a calculation of time taken to recoup the original investment. This is usually based on the overall reduction in maintenance and repair costs over time. The two possible approaches are *Payback Upon Price Comparison* and *Payback Over Time*. With payback upon price comparison (P_{PC}) one determines how long it would take to save investment moneys for EOP over a comparable expenditure for a trench and drain system.

$$P_{PC} = \frac{1}{\dfrac{\text{Trench \& Drain per lm - EOP per lm}}{\text{EOP per lm}}} = \frac{1}{\dfrac{\$416.03}{\$618.38}} = \frac{1}{0.67} = 1.49 \text{ years} \qquad (6)$$

Note that this is an internal return on investment, but does not represent the savings over time.

The payback over time (P_{OT}) calculation very much depends on individual circumstances. Questions regarding these circumstances are: whether the treated area can be used in the future for habitable area; whether corrosion degradation of valuable mechanical equipment will be stopped; and whether elimination of painting mold will reduce the number of cycles of painting in the future. Table 7 summarizes the savings over ten years at FT Jackson and McAlester AAP for the most important circumstances.

$$P_{OT} = \frac{\text{Total Installation Cost}}{\text{Sum of Annual Cost Avoidances}} = \frac{\$38{,}800.00}{\$41{,}973.80/10 \text{ years}} = 9.24 \text{ years} \qquad (7)$$

This value for P_{OT} should be used only as a guideline because two different sites were combined to determine this estimate.

CONCLUSIONS

In buildings with daily occupancies and mature landscaping, retrofitting a foundation wall by "trenching and draining" is not easy. The common approach to prevent water intrusion is to excavate to expose the wall area and the base of the foundation, and then to replace the dampproofing on the wall surface and install a drain tile system around the building or affected area. This is a costly endeavor. Any interior application that can mitigate some of the water-related problems will save the cost of excavation. If the alternative can also mitigate corrosion damage to mechanical equipment and humidity and mold problems it should be highly rated.

Based on the results of the demonstration and validation, this study concludes that the application of EOP technology for control of moisture in concrete basement structures is an acceptable alternative to conventional trenching and drain.

The EOP technology installed in a facility at Fort Jackson, SC successfully prevented water seepage and reduced the relative humidity of the concrete to 70 percent. The cost of installation has been determined to be 40 percent lower than the cost of the conventional trench and drain approach. The operating or energy cost of the EOP system is negligible—equivalent to the expenditure of burning a 60W light bulb.

It is recommended that the EOP technology be transferred for Department of Defense implementation as a cost effective alternative to the "trench and drain" approach for control of moisture in concrete basement structures.

ACKNOWLEDGMENTS

This study was conducted for U.S. Army Center for Public Works (USACPW) under the Facilities Engineering Application Program (FEAP); Project Title "A Demonstration of Electro-Osmotic Pulse (EOP) Technology for Control of Seepage in Concrete Structures". The assistance provided by Frank Cooper, Fort Jackson, SC; Gary Reasoner, McAlester Army Ammunition Plant; Fidel Rodriguez and Malcolm McLeod, Center for Public Works, Ft. Bevoir, VA; Dr. Charles Lozar of Architects Equities Research Group; and Roger Hayes, Arild Ottersen, Egil Bjerke, and Michael Connor, Drytronic (formerly known as Dry-Tec of North America), was essential to the completion of this work.

REFERENCES

1. Hamill, W.H., Williams, R.R. and MacKay, C., *Principles of Physical Chemistry, 2nd edition*, 1966, Prentice-Hall, Inc., Englewood Cliffs, N.J.

2. Glasstone, S., *Textbook of Physical Chemistry, 2nd edition*, 1946, D. Van Nostrand Company, Inc., Princeton, N.J.

3. Tikhomolova, K.P., *Electro-Osmosis*, 1993, Ellis Horwood Limited, Chichester, West Sussex, England.

4. *Means Cost Estimating Guides*

5. *Walker Estimating Guide*

6. *National Construction Estimator Handbook*

Table 1. Power supply dc output.

Date of Reading	DC Volts	DC Amps
1995/01/10	+37	0.20
1996/08/15	+30	0.75

Table 2. Concrete moisture readings in Building 3265.

	% Relative Humidity at Surface			
Date of Reading	A	B	C	D
1994/08/23	94	92	98.3	97.6
1995/01/10	44	43	68.3	64.3
1996/08/15	72.5	72.1	76.3	76.8

Table 3. Rebar specimen corrosion potentials.

	Potential (Volts DC)		
Specimen	Minimum	Maximum	Average
3	-0.190	-0.200	-0.195
5	-0.204	-0.224	-0.214
9	-0.145	-0.154	-0.150

Table 4. Monthly precipitation data for Columbia, SC.

Date	Total Precipitation (cm)	Date	Total Precipitation (cm)
August 1994	13.49	July 1995	19.96
September 1994	8.31	August 1995	16.99
October 1994	12.04	September 1995	14.00
November 1994	7.82	October 1995	9.17
December 1994	14.81	November 1995	7.34
January 1995	11.40	December 1995	5.56
February 1995	17.02	January 1996	7.37
March 1995	4.32	February 1996	2.95
April 1995	2.49	March 1996	16.56
May 1995	4.29	April 1996	6.04
June 1995	27.28	May 1996	6.81

Table 5. Standard approach cost estimate.

Action	Cost per lm
Site dewatering	$221.55
Wood shoring	$34.78
Excavation and backfill	$728.34
Drain tile installation	$13.78
Dampproofing	$26.25
Backfilling	$3.61
Landscaping restoration	$6.10
Total	$1,034.41

Table 6. Calculation of EOP System Based on Installed Costs and lm of Wall.

Location	Lineal Meters Installed	Cost per Linear Meter
McAlester AAP	29.0	$624.07
Fort Jackson	34.5	$612.69
Average Cost of EOP Installation for Both Sites		$618.38

Table 7. Payback over time savings estimates.

Situation	Savings
Usable space return (at McAlester)	$21,225.00
Painting avoidance (at McAlester)	$748.80
Reduced mechanical maintenance (at Jackson)	$20,000.00
Total	$41,3973.80

FIGURES

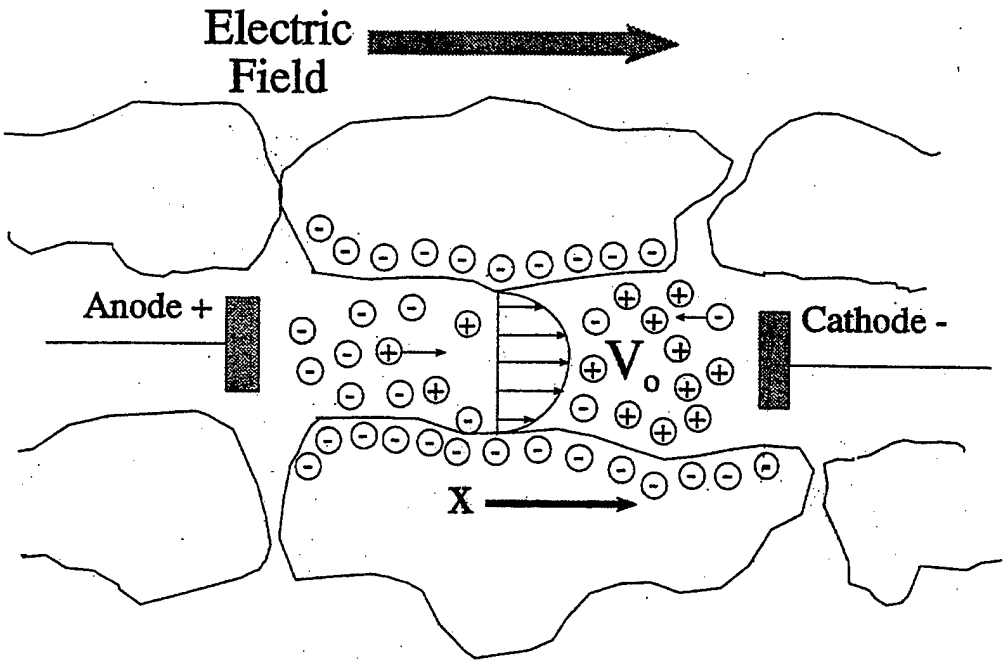

Figure 1. Movement of cations in a soil pore by electro-osmosis.

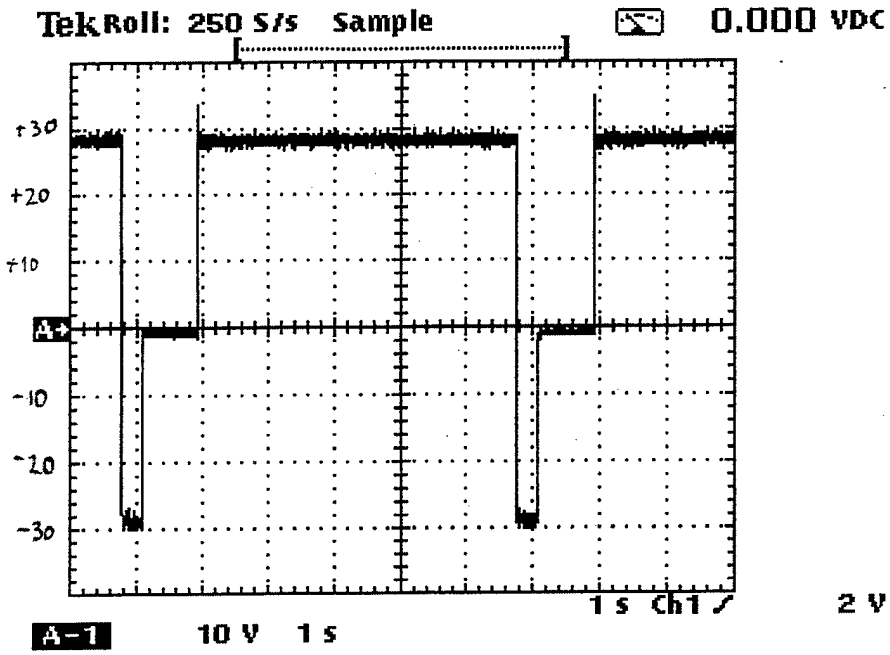

Figure 2. Example EOP voltage waveform.

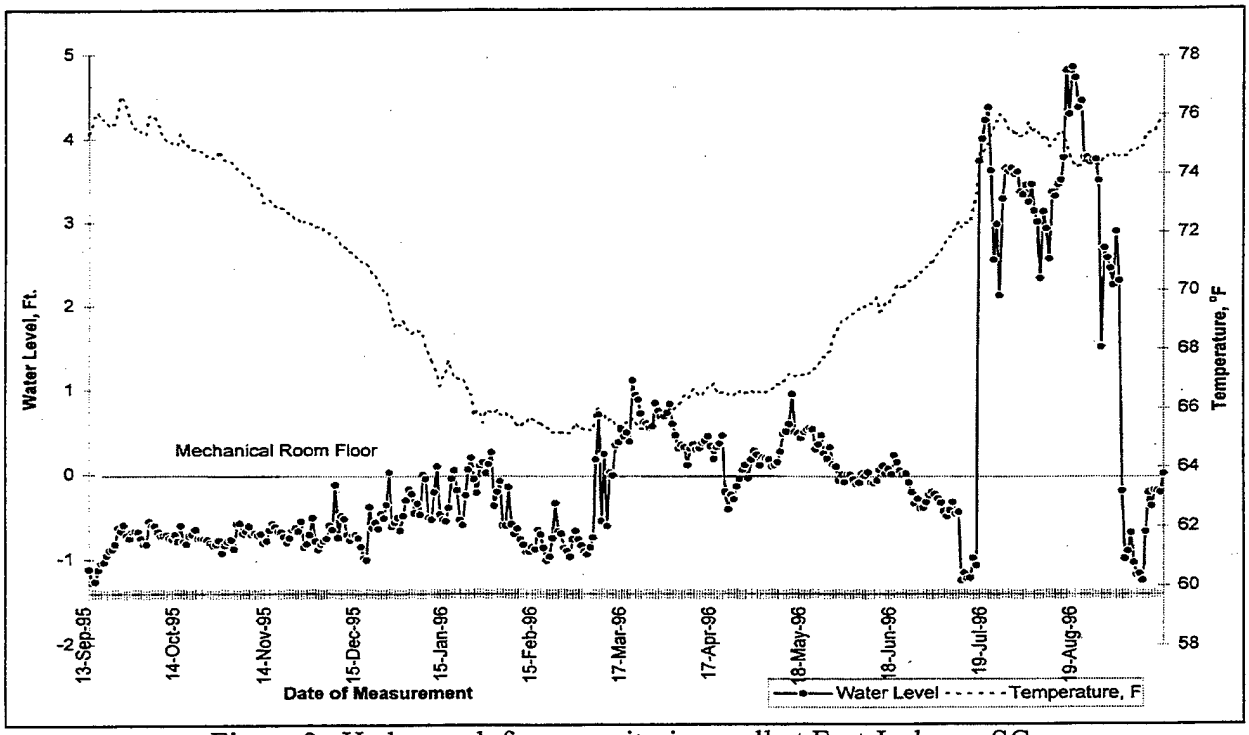

Figure 3. Hydrograph from monitoring well at Fort Jackson, SC.

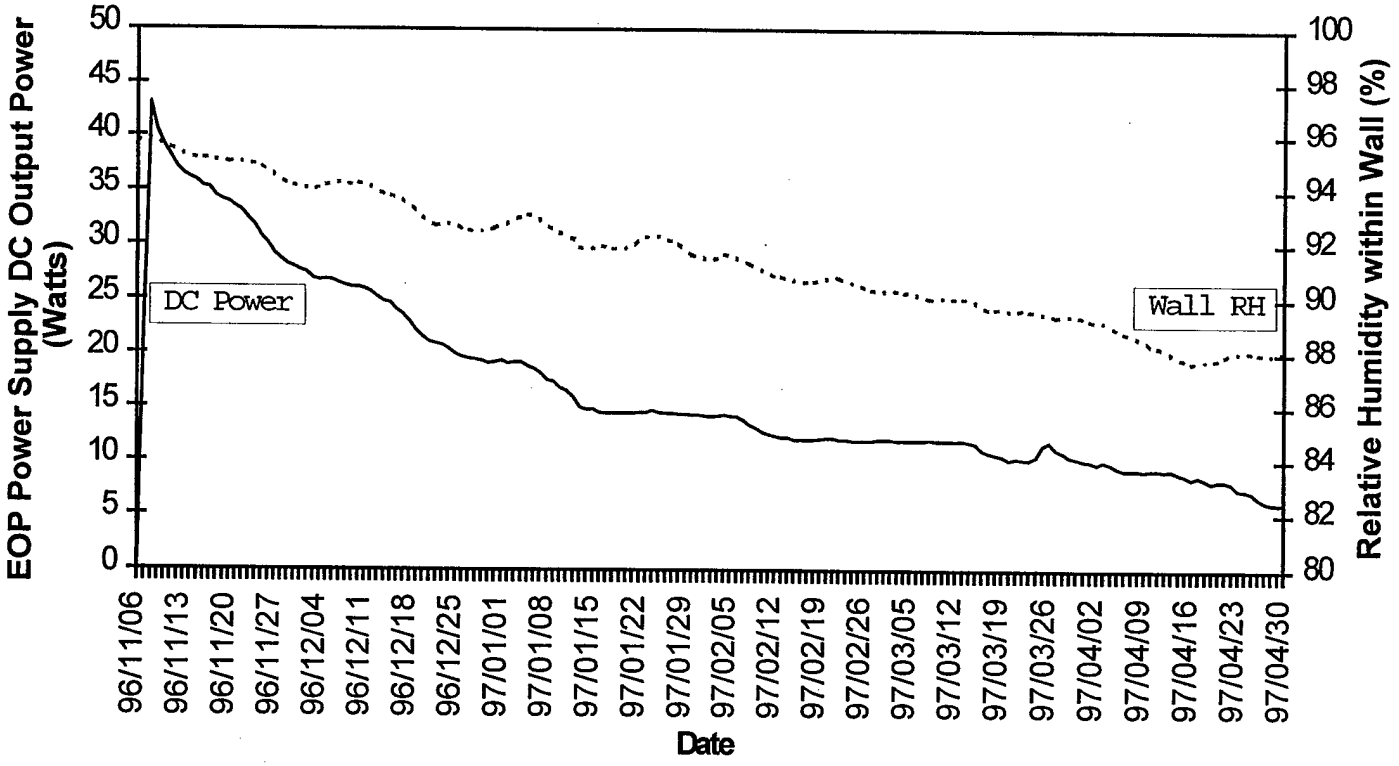

Figure 4. Power consumption of EOP system in relation to relative humidity of the wall.

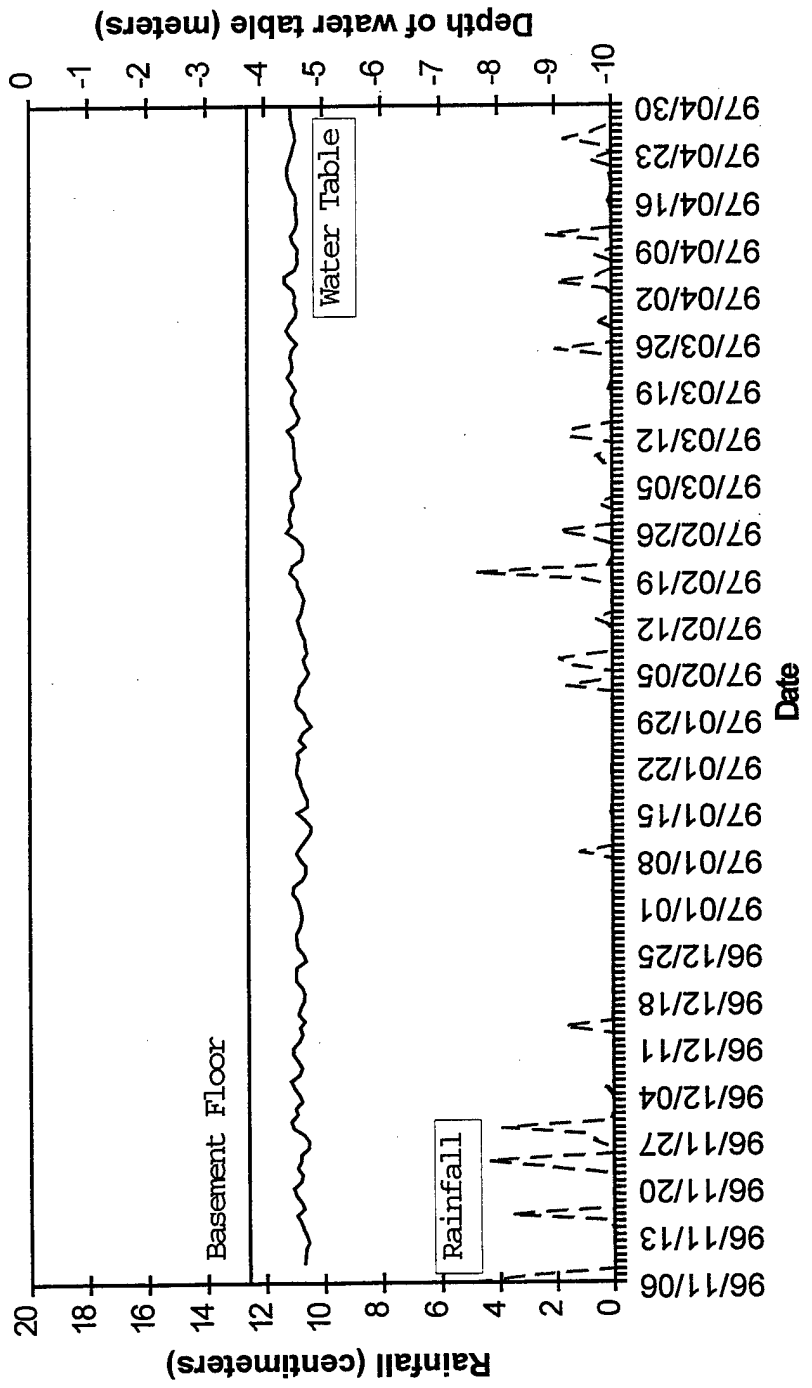

Figure 5. Water table with respect to basement floor, Bldg. 5, McAlester AAP.

Integration of Wire Arc Spray Technology for Corrosion Protection of General Purpose Bombs at the Kadena AB Bomb Renovation

Dr. Douglas H. Neale
Science Applications International Corp.
2220 Northwest Parkway, Suite 200
Marietta, Georgia 30067

ABSTRACT

The design, development, installation and operation of an automated wire arc spray system for corrosion protection of general-purpose bombs at the U.S. Air Force Kadena Bomb Renovation Plant, Okinawa, Japan is described. The zinc/aluminum metallized coating sealed with industrial water-borne direct-to-metal (DTM) acrylic latex paint replaces the previous solvent-borne primer/topcoat combination to yield an environmentally compliant lifetime corrosion protection coating system that eliminates the requirement for stripping and re-coating bombs every five years. A conservative 20-year life cycle cost analysis verifies substantial cost savings for the Air Force using metallized coatings for this application.

INTRODUCTION

The U.S. Air Force currently spends in excess of $7 million worldwide each year for corrosion protection of cast iron general-purpose (GP) bombs. Many of these bombs are stored in highly corrosive, tropical environments and require repeated renovation to maintain bomb serviceability. Currently, the bombs are returned from the field to a fixed, automated renovation facility at which the existing solvent-borne paint system and corrosion products are removed with an abrasive blast machine. The bomb casings and fuze wells are then re-coated with environmentally non-compliant solvent-borne primers and topcoats and returned to storage. The process is expensive, ineffective from a corrosion protection perspective and is responsible for generating significant volumes of hazardous air pollutants (HAPs), volatile organic compounds (VOCs), and toxic material waste streams.

The Air Force Corrosion Program Office (AFCPO) at the Warner Robins ALC (Robins AFB, Georgia), in conjunction with Science Applications International Corp. (SAIC), has conducted a review of state-of-the-art, commercially available, environmentally compliant coating technologies for corrosion prevention/protection of existing general purpose bombs. Specifically, the AFCPO has targeted corrosion problems encountered at the automated Kadena AB Bomb Renovation Plant (Okinawa, Japan) and has instituted a test evaluation program at that facility to document the performance of alternative environmentally compliant coating technologies for corrosion protection. Currently, deteriorating bombs are brought to the Renovation Plant, stripped of existing coatings and corrosion products, coated with solvent-borne chromate primers and lead-containing topcoats, stenciled, re-palletized and returned to storage either outdoors or in designated igloos. This facility is currently responsible for supporting tens of thousands of

MK-82 (500 lb.) and MK-84 (2000 lb.) general purpose bombs as well as BLU-109 penetrators. The munitions served by this plant are experiencing severe corrosion degradation with a requirement imposed by Kadena for complete coating refurbishment every 5 years. The conventional solvent-borne paints now used by the Air Force at the renovation plant are neither environmentally compliant nor effective for corrosion protection over the five-year recycle maintenance period. In the course of the investigation, SAIC and the AFCPO have identified and instituted a coating material system and process that mitigates both the environmental and corrosion problems experienced at the Kadena Bomb Renovation Plant. The technologies applied at Kadena will accrue significant cost savings for the Air Force by extending coating life, reducing facility maintenance/support requirements and substantially reducing the costs of managing hazardous/toxic waste streams.

PROJECT SUMMARY

SAIC and the AFCPO have jointly developed and executed a comprehensive plan to address the environmental and corrosion problems experienced at the Kadena Bomb Renovation Plant. The solution includes identification and implementation of effective, compatible, environmentally compliant coating processes to protect GP cast iron bomb casings as well as the formed steel sheet metal fuze well cavities located at the nose and tail of the bombs.

SAIC was initially directed by the AFCPO to evaluate the use of environmentally compliant thermoplastic powder coatings for corrosion/abrasion protection of GP bombs. SAIC conducted an extensive test program to develop the techniques required for application of these coatings on bomb casings. Powders were applied with flame spray, fluid bed and electrostatic spray systems. The electrostatically applied powders were melted and cured using convection, infrared and electromagnetic induction heating. All processes produced the desired protective coatings; however, the heat required to melt, flow and cure the powders into protective films resulted in substrate temperatures significantly higher than the bomb service temperature (165°F). SAIC concluded that powder-coating technology was not suitable for this Air Force application and reported these findings to the AFCPO. Concurrently, SAIC surveyed the industrial coatings market to evaluate alternate solutions for this application. As a result of these parallel investigations, SAIC identified metallizing technology as an excellent candidate for protection of GP bomb casings and proposed to develop this technology for use at the Kadena Bomb Renovation Plant. The use of thermally sprayed sacrificial metallized coatings for effective protection of structural iron and steel in corrosive environments is well-documented in the literature and in the field with over 50 years of proven performance. This technology's compatibility with the GP bomb renovation process has been further enhanced by the recent commercial development of portable wire-arc spray units designed and built specifically for high-production field application of metallized coatings.

After AFCPO approval, SAIC conducted a test program to evaluate and customize the metallizing process for cathodic protection of cast iron bomb casings. Extensive testing on instrumented bomb casings using portable wire arc spray equipment proved that superior coatings could safely be applied to the casings without exceeding the bomb service temperature. These

tests were reported[1] to the AFCPO and to the Air Force Weapons Safety group (WR-ALC/SEW) for review. Based on these tests, the WSC approved development of a prototype automated wire arc spray system designed specifically for the Kadena Renovation Plant. Installation of the system at Kadena was contingent on successful demonstration of the equipment and process on live bombs at the Eglin AFB test range. SAIC designed, built and successfully demonstrated the prototype automated system and process on live bombs in December 1995. After review of the Eglin range test results, the Hazard Analysis[2], and Implementation Plan[3] for the Kadena Bomb Renovation Plant, SEW approved installation and test for that site. Installation was completed in April 1996 and process/production evaluation tests have continued to the present. Program progress is documented in this report and in the Monthly Status Reports[4] for Air Force Contract No. F09603-90-D-2215, Delivery Order 0011.

Casing Protection

Primer - In the original renovation process at Kadena, bomb casings (ductile cast iron) were stripped with steel shot and primed with a solvent-borne red-oxide alkyd primer (MIL-P-11414D). A "dry" arc-sprayed zinc/aluminum alloy has now replaced the liquid primer. In the arc spray process, two electrically isolated wires of the selected coating material are given opposite DC polarity using an arc-welder power supply. The wires are simultaneously fed to an application gun where they are brought into close proximity to initiate an electric arc. The arc between the two impinging wires results in a local region of high temperature plasma and molten metal. A jet of compressed air, directed through the arc region from behind, disperses and projects the molten metal to the surface being coated. The metal droplets impinge on the substrate, solidify and bond to form a continuous barrier/sacrificial coating for cathodic protection of the munitions casing. The application gun remains 8 - 12 inches from the bomb surface and negligible heat is imparted to the casing even during extended coating activities. Bomb temperatures do not exceed ambient by more than 20°F during the process and do not approach the 165°F bomb service temperature specified in the item Technical Order.

Corrosion protection of ferrous metals with metallizing technology has been extensively documented in both Government and industrial field applications. Coating life exceeding 50 years in highly corrosive marine environments using unsealed zinc and aluminum metallized coatings on steel structures has been demonstrated. SAIC has conducted supplemental comparative corrosion resistance tests[5] at an independent certified laboratory for the AFCPO and has verified the superior performance of a variety of zinc and aluminum arc-sprayed coatings for protection of carbon steel (> 5000 hours salt fog per ASTM B117 procedure). Based on its survey of published literature, recommendations from commercial industrial sources, independent test results[6,7,8,9] and specific requirements of this application, the AFCPO and SAIC selected an 85/15 zinc/aluminum alloy (by weight) for use in the Kadena GPB application.

Proper application of these metallized coatings requires that the substrate be prepared with a near-white metal media blast (SSPC-SP10), 2 mil anchor profile (minimum). Industry specifications for zinc metallized coatings typically call for a 4-6 mil thick coating. For aluminum,

a 10-mil coating is required because of the differing protection mechanisms provided by the two metal coatings. This process produces high local noise levels and ultraviolet radiation emissions from the arc region requiring the use of earplugs and No. 6 or higher welding goggles for personnel protection in the vicinity of the application gun. In addition, smoke, metal dust and metal oxide fumes are generated requiring that operation be conducted in a well-ventilated area. The American Welding Society and ANSI[10,11] have published specifications for the process detailing the parameters for safe and effective application of metallized coatings. Also, the U.S. Navy has developed a Military Standard[12] for the use of metal sprays on shipboard. SAIC has conducted surveys of pertinent Federal, State and Local health and safety regulations and has found no cited permanent personnel health hazards related to the use of zinc, aluminum or zinc/aluminum alloys with the metallizing process. For health and safety purposes, the industry recommends that wire arc metallizing should be treated as a common arc welding process.

SAIC developed a customized automated wire arc spray system (AWASS) for application of the metallized coatings on GP bombs at Kadena. The system includes a Thermion SprayMaster wire arc spray system, a PowCon welding power supply unit and Mavrix automated electromechanical transport to apply coatings to stationary bombs suspended vertically from the nose and rotated by means of an overhead conveyor system. The AWASS is configured with a vertical mast and a horizontal telescoping arm with a pivoted arc spray gun mounted at the end. The arc spray head, offset from the bomb surface, traverses vertically at fixed speed (adjustable) between the nose and base of the bomb while coating the sides. After the spray head drops below the base of the bomb, it is indexed toward the bomb with the translating horizontal arm and is tilted upward to spray the base and provide a continuous cathodic protective coating. The coating wire is dispensed from two remote, independent drums. Wire is drawn from each drum with separate gear drives in the Thermion cabinet mounted on the vertical transport carriage. The wires receive opposite DC voltages from the PowCon powder supply and are fed continuously through separate insulated flexible conduits to the spray head. At the spray head, the wires are brought together to generate a controlled electric arc in which the metal alloy is melted. A separate compressed air stream is directed at the arc region from behind to atomize, disperse and propel the molten metal droplets onto the bomb surface. The molten metal condenses onto the "cold" bomb to form a sacrificial corrosion protection coating. Since the coating is relatively thin compared with the cast iron casing, temperature rise of the bomb wall is less than 10°F under normal operation.

The process may be conducted in either a top-to-bottom or bottom-to-top cycle to optimize production. Normal operation is in the "automatic" mode with the AWASS control logic communicating with the Bomb Renovation Plant Alan-Bradley control system; however, "manual" operation is also an option for set-up and for unique applications. The AWASS accommodates automated coating of munitions ranging in size up to MK-84 bombs by adjusting travel limits on the vertical mast and the translating horizontal arm, adjusting the vertical spray head travel speed, setting tilt angle and base coating time, and adjusting arc spray voltage/current parameters. Once the system is set up for a particular munition, no adjustments are required and coating becomes fully automatic. Changeover can be completed in less than 15 minutes. All system controls and displays are included in the local AWASS integrated Mavrix/Thermion

control center. Safety interlocks and fault reports are incorporated to terminate arc spraying if bomb rotation, vertical travel or air pressure is lost. Maximum cycle time can be set to terminate arc in the event the process does not properly shut down at the end limit positions. Loss of arc is also sensed by the system resulting in termination of travel and a fault report to the Plant Control Operating System. Spraying can be resumed after correction of a reported fault by operating a manual reset button located on the AWASS control box. A non-conducting phenolic deflector is installed at the spray head to prevent inadvertent physical contact of the wire arc tips with the bomb casing.

The AWASS was installed at Station 1 in the Renovation Plant primer booth after removal of the original automated Binks paint spray system. The entire system including assembly, operation, maintenance, safety and associated technical data is documented in the AWASS User's Manual[13].

Sealer - Although not essential for corrosion protection, application of a conventional liquid sealer over a metallized base-coat can provide somewhat enhanced coating life and can satisfy application-specific color requirements. Since there is currently a color requirement for GP bombs, SAIC selected an industrial direct to metal (DTM) waterborne acrylic latex sealant to provide olive drab color and to extend the coating system life expectancy for munitions at Kadena. Waterborne coating technology has rapidly advanced in recent years and performance now rivals that of the best conventional plural-component corrosion protection coating systems available. These low VOC (< 200 g/l) systems are environmentally compliant and are significantly easier to manage than the alkyd enamel solvent-borne paints (TT-E-516A) currently used for top-coating general purpose bombs at Kadena. Tap water may be used to thin the DTM acrylic latex when necessary and may be used for all spray system cleanup and flushing procedures. Wastewater generated in cleanup and in the waterfall paint booth used for application may be sent to the local sanitary sewer and all solid wastes (sludge, rags, etc.) may be sent to municipal landfill for disposal. SAIC evaluated five candidate DTM coatings for performance and compatibility in lab and field tests[14,15,16,17]. All of the products tested performed well and two were selected to represent the technology. These products and all acrylic DTM latex primers and finish coats are controlled by Steel Structures Painting Council Paint Specification (SSPC) Numbers 23 and 24[18].

Fuze Well Protection

The nose and tail fuze well assemblies are the most corrosion-sensitive components on general-purpose bombs. The fuze wells are formed, alloy steel, sheet metal domed cylindrical receptacles supplied with an OEM cadmium corrosion resistant coating that deteriorates during field exposure. At scheduled renovation, fuze wells are uncapped and inspected for corrosion. If no corrosion is found, no action is taken and the fuze well is capped and sealed. If corrosion is detected, the fuze well is stripped to bare metal with a portable vacuum blast machine to recover the abrasive media (typically, sand), coating and corrosion products. Currently, an environmentally non-compliant, two component epoxy primer (MIL-P-23377) is brush-applied to the fuze well to restore corrosion protection. As part of this project, SAIC conducted a comparative laboratory evaluation[19,20] of environmentally compliant alternative

coatings/treatments for the fuze wells. In addition to the current epoxy primer, alternatives tested included: including vapor corrosion inhibitor (VCI) emitters and coatings; zinc ring inserts; and a low VOC (2.1 lbs/gal, 250 g/l), organic zinc-rich cold-galvanizing compound. To simulate field conditions, the fuze wells were capped and subjected to cyclical temperature variations at high humidity in a laboratory environmental chamber. A small, calibrated weep hole in each cap allowed moisture migration to and from the fuze well cavity. Tests were sustained until the onset of epoxy primer failure was detected. It was determined that the organic zinc cold-galvanizing compound exhibited superior corrosion protection to all other systems tested. This environmentally compliant compound is 90% elemental zinc by weight with an organic solvent vehicle. While use of the galvanizing compound does not entirely eliminate solvents from this particular operation, the volume usage relative to the casing coatings is very low (<1%) and the resulting waste stream is negligible. Unlike the epoxy primer, the cold galvanizing compound does not have a limited pot life, which allows virtually total usage of the product once the container has been opened. As a result of these lab tests, ZRC cold-galvanizing compound was selected for further field evaluation at Kadena.

Life Cycle Cost Analysis

SAIC has conducted a series of comparative life cycle cost (LCC) analyses to predict the benefits of converting the Kadena bomb renovation facility to the new coating technologies. The analysis uses published and documented test technical/cost data as well as data specific to the renovation plant. A conservative twenty-year coating life expectancy for the metallized system (vs. 5 years for the existing solvent-borne system) was used. Field data[21.22.23] strongly support metallized coating life expectancy in excess of 30 years for this application.

The cases studied predict costs for renovating the entire Kadena inventory of MK-82 and MK-84 general-purpose bombs with both the current solvent-borne and metal arc-spray systems. Cost data is taken from published industry estimates[24], from information supplied by Kadena Bomb Renovation Plant employees, and from observations of plant operation by SAIC personnel. Estimated costs for solid/hazardous waste disposal from the previous solvent-borne system were understated in this analysis. Kadena personnel estimate that approximately $35,000 a year is spent on waste removal. The analysis includes amortization of the new arc-spray equipment and installation over 20 years. Maintenance of the arc-spray and solvent spray delivery systems was assumed to be the same. Labor costs (12 full time employees) are incurred only during actual plant operations and not in the period between renovation cycles (assumes plant is closed after bomb inventory is processed each cycle). Personnel safety and medical expenses are assumed to be identical for the two processes and surface preparation costs are the same regardless of the coating system applied. Analysis results are tabulated in Table 1.

In summary, the studies show that, even though the arc spray/DTM system is more expensive than the current non-compliant system to apply, the extended life and reduced waste disposal costs of the alternative system result in over $3 million in savings. The substantial life cycle cost advantage predicted by these analyses does not include the additional savings of more than fifteen years of plant operation/maintenance costs after the original bomb inventory is

metallized. If the plant were closed after completion of the current bomb inventory, it is estimated that an additional $10 - $15 million would be saved at Kadena. In another scenario, the facility can be used to continue processing munitions delivered to Kadena from other Air Force storage sites worldwide after the original Kadena bomb inventory has been renovated. The ongoing utilization of the renovation plant would continue accrual of life cycle cost savings and would further reduce Air Force waste stream volumes. Perhaps the best alternative, however, would be to mobilize the process and deliver the system to remote munitions storage locations for on-site renovation, thereby eliminating the cost of transporting bombs to the fixed Kadena renovation plant. A proposed design for mobile capability has been submitted to the Air Force.

A material cost analysis was also conducted and is presented in Table 2. The table shows that the metallized coating system in-place material cost can range from approximately two to four times the cost of common solvent-borne systems. The higher initial material cost, however, is erased in the life cycle because of the repeated applications required with the solvent-borne coatings. Significant LCC savings are realized with metallized coatings by eliminating the labor, operations, maintenance and hazardous waste management costs related to multiple applications of the solvent-borne systems.

Bomb Renovation Plant Retrofit Conversion

Installation of an Automated Wire Arc Spray System (AWASS) and associated environmentally compliant coating technologies at the Kadena AB Bomb Renovation Plant was completed by SAIC in March - April, 1996. The major elements of the conversion to the new technologies were:

1. Development of an automated wire arc spray system for the Kadena Bomb Renovation Plant
2. Obtaining process installation approval from the Air Force Weapons Safety Office
3. Integration of the AWASS with the Renovation Plant automated operating system and replacement of the existing solvent-borne primer paint/application system with arc-sprayed 85/15, zinc/aluminum alloy
4. Familiarization of Air Force personnel with operation/maintenance/repair of new equipment
5. Replacement of the solvent-borne topcoat and stencil paint systems with environmentally compliant industrial waterborne direct to metal (DTM) acrylic latex paint
6. Repair/refurbishment of the facility abrasive blast machine, replace current steel shot abrasive with angular steel grit (MHG-25, GL)
7. Replacement of two-part epoxy primer with zinc-rich cold-galvanizing compound for corrosion protection of bomb fuze wells.
8. Minor repair/refurbishment of Renovation Plant hardware to restore operation
9. Identification, documentation and recommendation of further plant/system repairs required in order to restore plant to full operation per original design specifications.

All installation requirements were completed and the plant was brought to full bomb renovation capability.

At the conclusion of installation, a two-week system checkout was conducted to verify system integration, validate operational status of the plant and establish/verify coating parameters and techniques. It was determined that the abrasive blast machine produced clean (original coating and corrosion products removed, no residual dust film) bombs with a minimum 2 mil profile as required. The AWASS operated as designed and a deposited a 4-6 mil metallized coating of 85/15 zinc/aluminum alloy over the entire bomb surface, including the base. MK-82 and MK-84 bombs require 3.5 and 10 minutes to metallize, respectively. The blast machine is capable of stripping one bomb (MK-82 or MK-84) every four minutes (approximately). Accordingly, the blast machine is the pacing item for MK-82 production while the metallizing process determines maximum production rates for the MK-84 bombs. If MK-84 production were to become critical, a duplicate AWASS system for simultaneous operation could be installed at the currently unused No. 2 station in the primer booth. In reality, however, the manual re-stencil and fuze well coating operations tend to be slower than any of the automated renovation processes at this facility and ultimately limit production with the current staffing.

No significant odor or smoke attributable to the arc spray process was detected in either the spray booth or outside the plant. The existing waterfall system in the primer booth effectively trapped the metal dust generated by the process and deposited it in the sump for recovery as scrap metal. The infrared oven formerly used to bake the solvent-borne primer was allowed to operate at reduced power to preheat the bombs before application of the topcoat. As they traverse the oven (four minute dwell, approximately) the bombs are preheated to 100°F - 110°F to accelerate curing of the waterborne acrylic latex sealer. The original Binks automated reciprocating spray system in the topcoat booth was refurbished and the gun was outfitted with a suitable spray orifice to optimize delivery of the waterborne sealer. After application of the sealer, the bombs pass through the topcoat infrared bake oven (ten-minute residence time, approximately) to complete the cure. Coatings were successfully cured by the system at 75°F, 90% relative humidity (approximate ambient conditions). The porous nature of the metallized coating allows deep penetration of the sealer and results in "dry to the touch" condition in less than 20 minutes under high humidity ambient conditions even without the benefit of baking.

After the casings are coated, the bombs are removed from the overhead conveyor and re-stenciled for identification. The original lead-containing solvent-borne stencil paint (A-A-208) dispensed in aerosol spray cans was replaced with waterborne acrylic DTM applied with a high volume, low pressure pneumatic touch-up spray gun provided by SAIC. Zinc-rich cold galvanizing compound was then brush-applied to the nose and tail fuze wells. Both coatings dried to the touch in less than 30 minutes under high humidity conditions (no heating or forced air) allowing the fuze well caps to be installed and the bombs to be re-palletized for storage. During the two-week shakedown tests, over 200 live MK-82 and MK-84 general-purpose bombs (total) were renovated with a one-day MK-82 peak production of 106 demonstrated.

After one year of operation over 1500 general purpose bombs had been completed, despite extensive down-time for facility repair and maintenance,. Less than two hours of down-time was attributed to wire arc spray system problems during the first year. The system demonstrated a coating efficiency (wire consumed to wire deposited) of 77% (70% predicted). A comprehensive arc spray system evaluation after one year's operation revealed that the unit was in excellent operating condition and that all functions were performing as designed.

CONCLUSIONS

The wire arc spray process for corrosion protection of general-purpose bombs has been successfully integrated into the Bomb Renovation Plant at Kadena AB, Okinawa. Arc spray hardware safety, reliability and effectiveness have been demonstrated under production conditions. The sacrificial metallized zinc/aluminum "primer" sealed with industrial DTM waterborne latex has virtually eliminated the hazardous and toxic waste streams associated with the original solvent-borne coatings used at this facility for corrosion protection. The use of an environmentally compliant zinc-rich cold galvanizing compound for coating the fuze wells provides a total corrosion protection package for the munitions at Kadena. The effectiveness of these coatings has been demonstrated extensively in field and laboratory tests and it is expected that the life of this coating system will easily exceed 20 years. It is probable that the munitions processed at the Kadena plant have effectively been given a permanent corrosion protection coating from which the Air Force will realize over $10 million in life cycle cost savings at this location alone. It is recommended that the Air Force initiate plans to install this technology at other existing fixed bomb renovation facilities or to develop a mobile capability for providing environmentally compliant, lifetime on-site corrosion protection for munitions deployed worldwide.

ACKNOWLEDGEMENT

The author would like to thank Mr. David Ellicks at the U.S. Air Force Corrosion Program Office (WL/MLS-OL), Robins Air Force Base, Warner Robins Air Logistics Center for his support of this project under Contract No. F09603-90-D-2215, Delivery Order 0011.

REFERENCES

1. "Test Demonstration: Metal Arc Spray Coating For Corrosion Protection of General Purpose Bombs", U.S. Air Force Contract F09603-90-D-2215, Delivery Order 0011, February 17, 1995

2. "Phase II Safety Hazard Report/Approval", U.S. Air Force Contract F09603-90-D-2215, Delivery Order 0011, August 18, 1995

3. "Conversion of Kadena Bomb Renovation Plant to Metal Arc Spray Coating Process for Corrosion Protection of General Purpose Bombs: Preliminary Design, Phase II Implementation Plan and Operational Test Plan", U.S. Air Force Contract F09603-90-D-2215, Delivery Order 0011, March 31, 1995

4. "Monthly Status Reports", U.S. Air Force Contract F09604-90-D-2215, Delivery Order 0011

5. "Certified Test Report, Salt Spray Resistance Test – 2000, 3000, 5000 Hours", Applied Technical Services, Marietta, Georgia, Ref. I06933, May 16, 1996

6. "Certified Test Report, Abrasion Resistance", Applied Technical Services, Marietta, Georgia, Ref. I53504, August 10, 1995

7. "Certified Test Report, Abrasion Resistance", Applied Technical Services, Marietta, Georgia, Ref. I53504, August 29, 1995

8. "Certified Test Report, Coating Adhesion", Applied Technical Services, Marietta, Georgia, Ref. I06823, February 13, 1995

9. "Certified Test Report, Coating Thickness", Applied Technical Services, Marietta, Georgia, Ref. I06823, February 13, 1995

10. "Thermal Spraying: Practice, Theory, and Application", American Welding Society (AWS), Miami, FL

11. "Guide for the Protection of Steel with Thermal Sprayed Coating on Aluminum and Zinc and Their Alloys & Composites", ANSI/AWS C2.18-93, American Welding Society, Miami, Florida

12. MIL-STD-21388A (SH), "Metal Sprayed Coatings for Corrosion Protection Aboard Naval Ships", 13 May 1992

13. "Automated Wire Arc Spray System – Users Manual", U.S. Air Force Contract F09603-90-D-2215, Delivery Order 0011, May 1, 1996

14. "Certified Test Report, Accelerated Weathering/Coating Adhesion – 500 Hours", Applied Technical Services, Marietta, Georgia, Ref. I53504, July 31, 1995

15. "Certified Test Report, Accelerated Weathering/Coating Adhesion – 1000 Hours", Applied Technical Services, Marietta, Georgia, Ref. I53504-1, ", August 15, 1995

16. "Certified Test Report, Accelerated Weathering – 500 Hours", Applied Technical Services, Marietta, Georgia, Ref. I55123, October 25, 1995

17. "Certified Test Report, Salt Spray Resistance Test – 500, 1000 Hours", Applied Technical Services, Marietta, Georgia, Ref. I06823, March 22, 1995

18. "Steel Structures Painting Manual, Volumes I and II", Steel Structures Painting Council, Pittsburgh, PA

19. "Certified Test Report, Fuze Well Coating Tests", Applied Technical Services, Marietta, Georgia, Ref. I00082, October 21, 1994

20. "Certified Test Report, Fuze Well Coating Tests", Applied Technical Services, Marietta, Georgia, Ref. I00082, March 16,1995

21. "Corrosion Tests of Flame-Sprayed Coated Steel, 19-Year Report", American Welding Society, Miami, Florida, 1974

22. "Thirty-Year Atmospheric Corrosion Performance of 55% Aluminum-Zinc Alloy-Coated Sheet Steel", Materials Performance Magazine, National Association of Corrosion Engineers (NACE), Houston, TX , April, 1996

23. "Performance History of Thermal-Sprayed Aluminum Coatings in Offshore Service", Materials Performance Magazine, National Association of Corrosion Engineers (NACE), Houston, TX, April, 1995

24. "Updated Protective Coating Costs, Products, and Service Life", Materials Performance Magazine, National Association of Corrosion Engineers (NACE), Houston, TX, February, 1997

		LCC PER UNIT ($)		TOTAL LCC ($)	
ITEM	NUMBER	SOLVENT	ARC SPRAY	SOLVENT	ARC SPRAY
MK-82	50,000	86.48	28.95	4,324,190	1,447,335
MK-84	10,000	102.95	77.83	1,029,524	778,321
			TOTAL	$5,353,714	$2,225,656

Table 1. Kadena Twenty Year Life Cycle Cost Summary

PARAMETER	SOLVENT-BORNE COATING SYSTEMS		
	Epoxy/Poly (Solvent)	Acrylic/Acrylic (Water)	Alkyd/Alkyd (Solvent)
Coating Weight- lb/sq.ft. (100% Deposit @ 5 mils) *	N/A	N/A	N/A
Consumption - lb/sq.ft. (70% deposit) *	N/A	N/A	N/A
Cost - $/lb **	N/A	N/A	N/A
Cost - $/sq.ft. (100% Deposit) ***	.05 + .15 = $.20	.11 + .12 = $.23	.042 + .054 = $.096
Cost - $/sq.ft. (70% Deposit)	$0.29	$0.33	$0.14
MK-82 Parameters (500 LB.)			
Area - sq.ft. (Approx.)	13	13	13
Coating weight per unit - lb/bomb	N/A	N/A	N/A
Coating Cost Per Unit - $/bomb (One Time)	$3.77	$4.29	$1.82
MK-84 Parameters (2000 LB.)			
Area - sq.ft. (Approx.)	35	35	35
Coating weight per unit - lb/bomb	N/A	N/A	N/A
Coating Cost Per Unit - $/bomb (One Time)	$10.15	$11.55	$4.90

PARAMETER	METALLIZED ALKYD /SEALER SYSTEM		
	Zinc/Aluminum (Basecoat)	Acrylic Sealer (Topcoat)	Zn/Al Topcoat with Sealer
Coating Weight- lb/sq.ft. (100% Deposit @ 5 mils) *	0.17	N/A	0.17
Consumption - lb/sq.ft. (70% deposit) *	0.24	N/A	N/A
Cost - $/lb ** (85/15 zinc/aluminum)	$1.80	N/A	N/A
Cost - $/sq.ft. (100% Deposit) ***	$0.31	$0.12	$0.43
Cost - $/sq.ft. (70% Deposit)	$0.43	$0.17	$0.60
MK-82 Parameters (500 LB.)			
Area - sq.ft. (Approx.)	13	13	13
Coating weight per unit - lb/bomb	2.2	N/A	2.2
Coating Cost Per Unit - $/bomb (One Time)	$5.59	$2.21	$7.80
MK-84 Parameters (2000 LB.)			
Area - sq.ft. (Approx.)	35	35	35
Coating weight per unit - lb/bomb	6	N/A	6
Coating Cost Per Unit - $/bomb (One Time)	$15.05	$5.95	$21.00

NOTES:
* ~ Physical Data
** ~ Vendor Quotation
*** ~ "Materials Performance" Magazine; February, 1997 (NACE)

Table 2. Material Cost Analysis

Design of Seawater Ballast Tank Impressed Current Cathodic Protection (ICCP) Systems

K. E. Lucas, M. F. Evans
Naval Research Laboratory, Key West, FL

E.D. Thomas, P.F. Slebodnick
Naval Research Laboratory, Washington, DC

E. A. Hogan
Geo-Centers Inc. Key West, FL

ABSTRACT

Impressed Current Cathodic Protection (ICCP) systems are currently employed on many of the U.S. Navy's ship hulls as a means of corrosion control. These systems are now being considered for internal areas of the ship including seawater ballast tanks. ICCP systems have been tested for use in these internal areas using the physical scale modelling (PSM) technique and prove to be a successful alternative for galvanic zinc systems. Preliminary ICCP results and comparison to galvanic systems are presented.

Keywords: impressed current, ballast tanks, physical scale modelling.

INTRODUCTION

Impressed Current Cathodic Protection (ICCP) is the standard method utilized by the Navy for the corrosion protection of hulls in seawater. These systems in conjunction with good hull coatings, provide for complete life-cycle protection and typically require little maintenance during the life of the ship. The self-regulating control feature of ICCP is achieved using a feed-back Ag/AgCl reference cell, which provides continual monitoring of hull potential and enables the establishment of target control levels for operation, typically at -800mV or -850 verses the Ag/AgCl reference cell.

The design capacity of the power supplies required for an ICCP system is determined by the amount of wetted metallic surface that will require protection, incorporating both bare and coated metallic areas into the initial assessment. Additionally, an allowance for coatings deterioration over the life-cycle is included. The design of an ICCP system requires knowledge of the geometry involved and insight into the protection current requirements. The placement of ICCP components is a critical component for balanced operation and should be such to provide all areas of the hull with uniform current distribution and current density throughout the life-cycle.

On large hulls, it has become common practice to divide the ICCP system into areas having independent control and potential monitoring capability, defined as multiple-zone systems. These systems operate more effectively, whereby the potential is sensed from a number of control points with corresponding anode current more locally placed to areas adjacent to the reference point. A good zone design typically provides much more uniform polarization over the hull and enables protection current to be supplied to specific geometric areas much more effectively without overpolarizing the remainder of the hull. The number of zones chosen is typically a function of hull geometry, wetted surface area, design criteria and economics.

In advanced applications, only a very small percentage of the hull requires significant levels of cathodic protection, due to the presence of special hull treatment over most of the wetted hull surface. The performance criteria for the sophisticated ICCP system require very precise regulation of both current output and potential control. With these new operational requirements and such minimal bare hull area, other internal spaces which have typically used galvanic zinc anodes, begin to have an effect on the ICCP operation and current distribution. The most prominent of these areas are the seawater ballast tanks, which have considerable internal surface area requiring protection and a large number of galvanic anodes internal to the outer hull, but usually open to the ICCP system through gratings.

Because of the possibility of operational interaction between the two systems (-1.04 V for the galvanic anodes verses -0.8V for the ICCP), it was necessary to change the ballast tank cathodic protection design from a galvanic anode system to an ICCP system which was compatible and integrated with the operation of the hull system. The tank ICCP design methodology utilized the following guidelines defined by NAVSEA protocol and various engineering parameters:

1. Operational Criteria:
    a) ICCP system should have two control states, i.e. a full tank condition and a residual water condition
    b) Typical driving voltages should be as small as possible to minimize gas production
    c) System required to function in conjunction with Hull ICCP control computer
    d) All tanks are considered to be coated

2. ICCP Design Protocol:
    a) Maximum power supply output is 20 A per tank
    b) Cathodic protection goal of –0.8V (0.05V for all tank areas
    c) Design for protection current density of 10-15 ma/ft2 (110 – 160 ma/m2) of bare metal and paint loss area

3. Maintenance Criteria:
    a) System performance and capacity should provide for all bare components, 12% coatings deterioration on steel and non-ferrous materials

b) Anode Components should be shipyard installed and field serviceable

c) Reference Cell Components should be shipyard installed and field serviceable

The Naval Research Laboratory, Key West, FL (NRLKW) was tasked by NAVSEA to model and design an ICCP system for ballast tanks which would perform as effectively as a galvanic anode system, but would operate in a manner equivalent to the hull ICCP system. The design for the ICCP system included: 1) design concept, 2) component engineering, 3) ICCP design configuration and 4) Ballast Tank Design Criteria. This paper reports the basic engineering design and methodology utilized for seawater ballast tank ICCP systems.

EXPERIMENTAL

The Ballast Tank program at NRL was established with the objective of designing an impressed current cathodic protection (ICCP) system for seawater ballast tanks using the physical scale modeling (PSM) design techniques. The basic technique1 of PSM utilizes exact scale models to provide the experimental platform and the use of reduced conductivity electrolyte to provide the necessary equivalent ohmic paths.

PSM has proven to be an effective tool2,3 for designing ICCP systems because of the accuracy and versatility of the technique. In designing the hull ICCP systems, it has been possible to consider problems relating to both the optimal design and geometric placement of components, as well as, the physical response of the ICCP system to life cycle changes, velocity conditions and inter-zone relationships. Special consideration can likewise be given to: 1) difficult geometries, 2) restricted areas, 3) coatings degradation and 4) sophisticated new ICCP design technology.

The input pertaining to the ballast tank design requirements such as structural configuration, ICCP system capacity availability and special component features requiring protection were supplied by NAVSEA for this research effort. Basic parameters of the ICCP system and modeling were established at the onset of the program, and included: a) the scale of the model (1/2), b) use of a two-zone design per tank and c) the maximum tank power supply size of 20A.

Two 1/2 scale steel models, illustrated schematically in Figures 1 and 2, were fabricated to represent several typical seawater ballast tank configurations and included all necessary internal structural members, component geometries and three-coat polyamide epoxy coatings system. Additionally, to facilitate the modeling aspect of the effort, bare metallic plates were installed throughout the models' hull and components to enable simulation of coatings damage and variable damage scenario percentages. Each steel section was electrically isolated from the hull and could be independently switched electrically to add or subtract it from the total steel area which required protection from the ICCP. In this manner, tank damage percentages, identified in Table 1, ranging from minimal coatings damage to a maximum of 12% coatings deterioration, could be considered without the constant necessity of recoating the tank walls for each run. Electrically,

each steel section could then be isolated from others at the remote shunt box and individual cathodic current demand monitored through a 0.1 ohm shunt resistor, as shown in Figure 3.

An array of Ag/AgCl reference cells were attached to the hull to facilitate potential measurement throughout the tank and in areas of difficult geometries. Electrically, the reference cells were set up so that any reference location could be used as the controlling reference electrode.

The water used in the modeling was from the seawater system at the Naval Research Laboratory, Marine Corrosion Facility in Key West, FL. The seawater had a pH of 8.1- 8.3 and had an initial resistivity of 18 ohm-cm. The modeling electrolyte was diluted to 36 ohm-cm at 25 (C (1/2 scale). This is done to maintain an equivalent ohmic path for current to travel as compared to a full scale scenerio. Dissolved oxygen concentration was maintained near saturation in the tank by air injection and mixing.

Models were prepared for each run by first cleaning the metallic surfaces to remove corrosion product and any previous carbonate deposition. Only the isolated metallic surfaces required preparation each time, since the actual ballast tank walls remained coated throughout the test, both internally and externally.

ICCP design was based on baseline performance of a zinc galvanic system and was instrumented to provide optimal cathodic protection under the guidelines discussed previously. Before the ICCP system was installed, a galvanic zinc system was evaluated to determine the baseline cathodic protection properties of the tank. Tank A was instrumented with 87 anodes (scaled proportionately) with 13 placed below residual waterline, while tank B had 54 anodes, with 9 placed below residual waterline. The galvanic anodes were installed so that individual anode output or groups of anodes could be monitored.

The ICCP system required both the design of the equipment as well as the corresponding component placement in the tank. Figure 4 shows a schematic representation of the ICCP system for one tank. Included in this figure are the power supply, controller, upper/lower reference cells, upper/lower anode assemblies and associated components. The relative separation between the upper and lower systems occurs at the residual water line.

RESULTS AND DISCUSSION

Evaluation of the optimal anode configuration for the tanks required the testing of multiple anode types and configurations. It was determined for this work that long wire anodes produced the best current distribution and uniform potential throughout the tanks. For durability and performance, a 3/16" (4.8mm) diameter extruded platinized-niobium wire with a copper core (3/8" full scale, (9.5mm)) was selected for use and installed in the tanks. For optimal current distribution, multiple anode segments were chosen and laid out in the tanks in a manner seen in Figure 4. Modeling design provided the optimal positioning and determination of anode surface area requirements.

Using the PSM technique, the recommended ICCP layout for ballast tanks was determined. The mounting of components relied strongly on the internal structural configuration of the tank while the protection capability relied on the relative location and size of the components. Examples of representative component placements in both radial and longitudinal structural design variations are illustrated in Figures 5 and 6.

The anode size was selected to provide a minimal drive voltage and low anode current density. Typically system drive voltages were less than 3 volts which translated into anode surface voltages of 2 volts or less during normal operation. With these low anode voltages the production of chlorine and hydrogen could be kept at production rates less than a zinc galvanic anode systems. A comparison of the operational conditions for the two tanks are given in Table 2. Included in this table are the general tank potential ranges and system current outputs for the zinc and ICCP systems measured after 20-22 hrs of protection. The current values shown in brackets indicate the maximum system output following initial immersion. Note that the operational potential of the zinc system was approximately -1.0 volt, while the set potential of the tank ICCP was -0.8 volts.

Comparable performance was noted for the ICCP system. Overall, the tank could be polarized in a similar manner to the zinc system and was not under-protected at any of the multiple reference cell array measurement points. Reference cells nearer the anodes reported values generally no more negative than -950 mV in the ICCP system. With increasing polarization time the potential distribution became more uniform, as would be anticipated with the growth of calcareous deposits and reduced cathode demand.

Current outputs between the two systems were best compared at equivalent current density, because the ICCP system easily had the capacity to polarize the system more readily. A comparison of the two systems at a current density of approximately 15 mA/ft2 (160 ma/m2) under several different damage scenarios is given in Table 3. These values illustrate the relative similarity in system outputs and general performance behavior. Additionally, at longer time periods the system the current outputs remained very similar and showed no major performance differences other than improved control capability for ICCP and lower overall set potential.

CONCLUSIONS

Results from the ICCP design modeling effort provided the following basic conclusions for ballast tanks ICCP design capability and anticipated performance:

For the ICCP System:

a) Acceptable ballast tank ICCP design @ -800 mV +/- 50 mV is possible
b) Maximum system output is within design requirements of 20 A/tank
c) Zone control was necessary for surfaced and submerged states
d) Switched lower (surfaced) and upper (submerged) reference cells are optimal
e) Gas production was minimized by increasing anode surface area so that the voltage

measured at the anode surface did not exceed 2 V

f) Increased anode surface area improved current and potential distribution

For the ICCP Components:

a) A 3/8" (9.5mm) full scale extruded platinized-niobium wire anode w/ Cu core was recommended
b) Straight or curved anodes may be installed
c) Segmented anodes should have common junction point (i.e., parallel operation)
d) Each segmented anode assembly should have same length anodes to minimize IR differences in cabling
e) Anode non-metallic mounts should be resistant to chlorine and pH <4.

ACKNOWLEDGMENTS

This research was funded by Naval Sea Systems Command, Codes PMO 450 and SEA 03M.

REFERENCES

1. K. E. Lucas, E. D. Thomas and E. A. Hogan, "Theory and Application of Physical Scale Modeling for the Design of Impressed Current Cathodic Protection (ICCP) Systems", Inter-Navel Corrosion Conference (INCC), Monterey, CA. 1992.

2. E. D. Thomas, K. E. Lucas and R. L. Foster, "Physical Scale Modeling of Impressed Current Cathodic Protection Systems" NACE Corrosion 89, New Orleans, LA.

3. K. E. Lucas, E. D. Thomas and E. A. Hogan, "Physical Scale Modeling for the Design of Impressed Current Cathodic Protection (ICCP) Systems", UMIST Advances in Corrosion and Protection Conference, Paper # 199, Manchester, England, July 1992.

TABLE 1
Metal Damage Percentages

% Damage on Model	Tank A ft^2 (m^2)	Tank B ft^2 (m^2)
3	31.6 (2.9)	20.9 (1.9)
6	61.0 (5.7)	38.2 (3.6)
12	122.8 (11.4)	86.7 (8.0)

TABLE 2
Comparison of Zinc verses ICCP Cathodic Protection

CP System	Residual Seawater		Full SW Tank	
	Potential (mV)	Current (A) [max output]	Potential (mV)	Current (A) [max output]
Zinc Anodes				
Tank A/ 20 hrs	-848 to -996	2.13 [6.19]	-928 to -1017	3.35 [12.11]
Tank B/ 20 hrs	-958 to -1029	1.40 [4.45]	-819 to -1023	1.91 [7.57]
ICCP System				
Tank A/ 22 hrs	-790 to -926	2.30 [2.85]	-788 to -966	5.58 [9.59]
Tank B/ 22 hrs	-801 to -903	0.56 [2.85]	-767 to -936	4.52 [8.51]

TABLE 3
Comparison of CP System verses Coatings Damage Scenario
(Current Density @ Approx 15 mA/Ft^2 (160 m^2))

% Coatings Damage	Tank A (Amps)		Tank B (Amps)	
	Zinc Anodes	ICCP System	Zinc Anodes	ICCP System
3	3.95	4.09	1.77	3.19
6	5.67	4.57	2.81	4.07
12	7.76	5.14	4.05	4.46

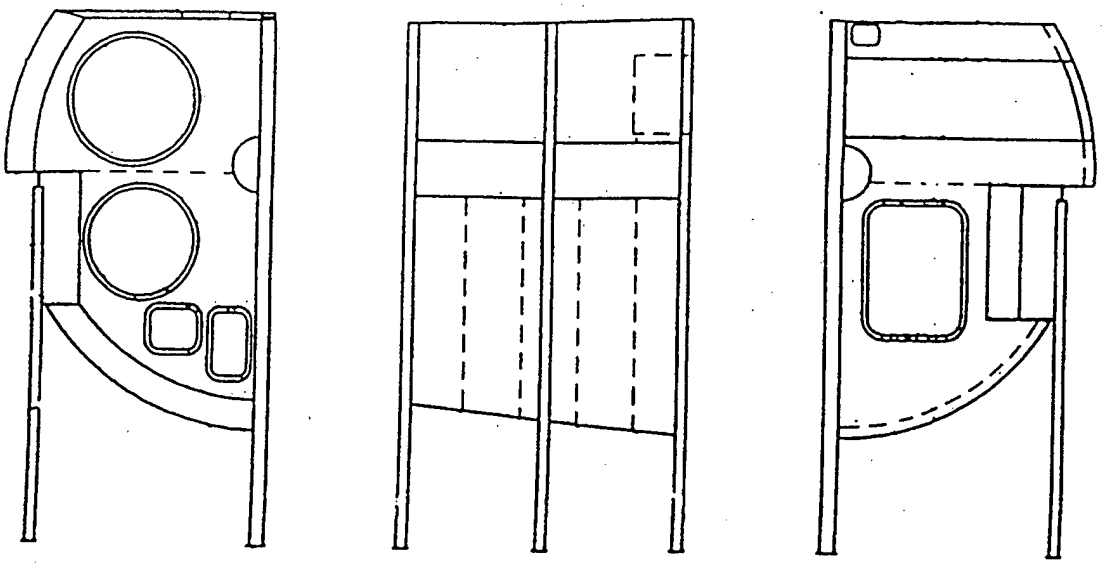

Figure 1. Graphic representation of Tank A model. Model has predominately radial structural construction.

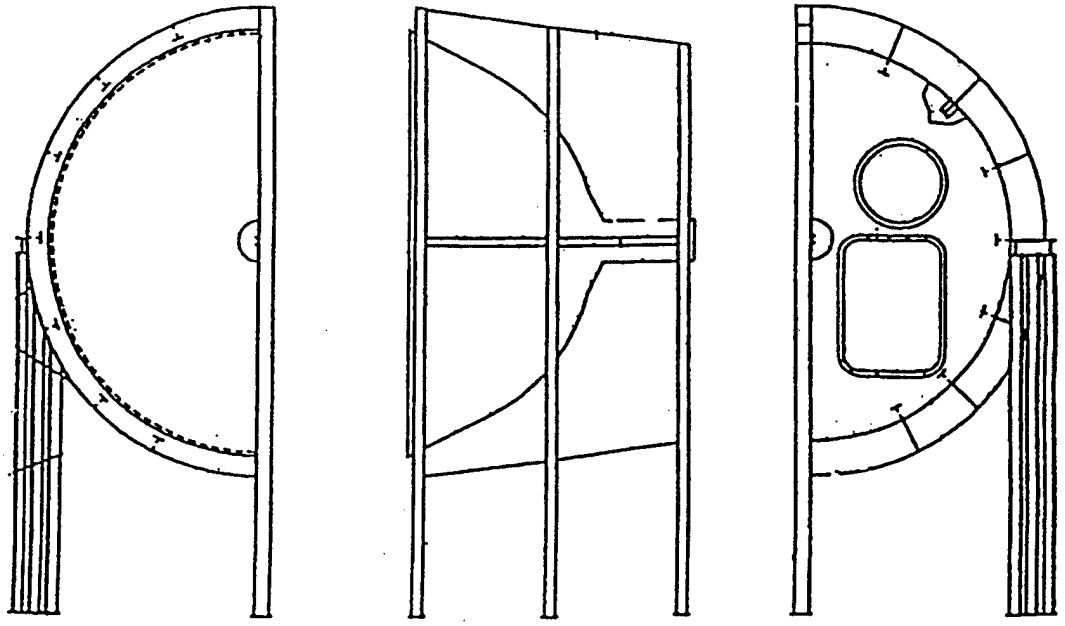

Figure 2. Graphic representation of Tank B model having predominately longitudinal structural construction, except in lower spaces.

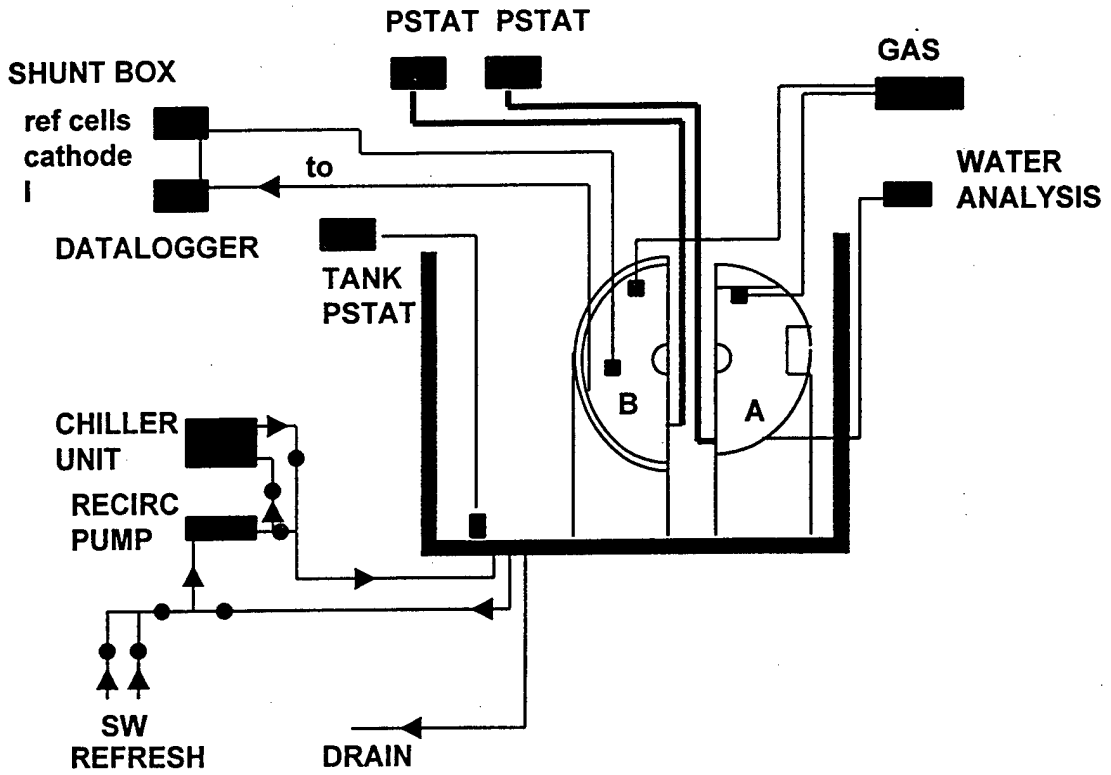

Figure 3. Basic configuration and wiring schematic for ballast tank models

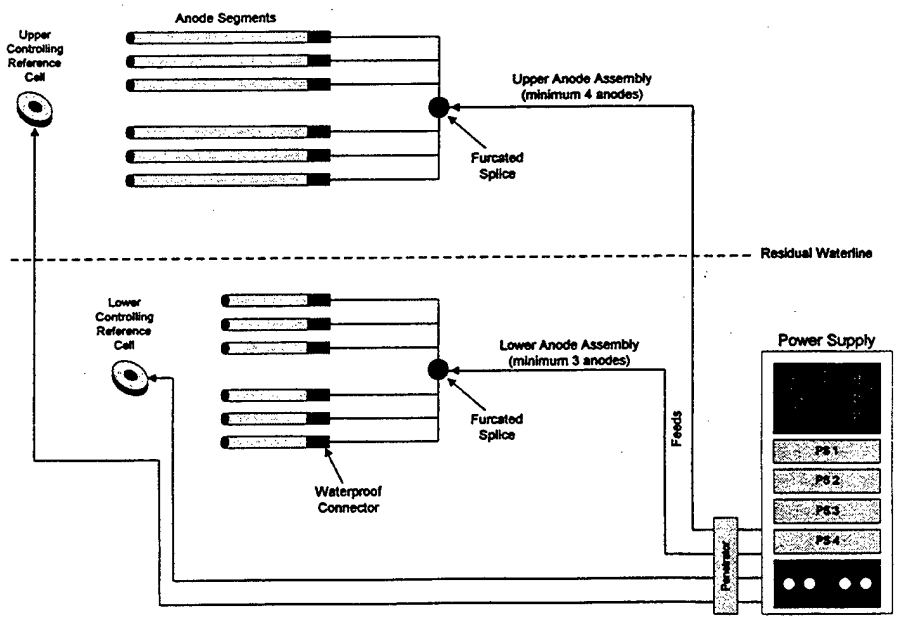

Figure 4. Schematic Layout of Ballast Tank Anode Assemblies and Components.

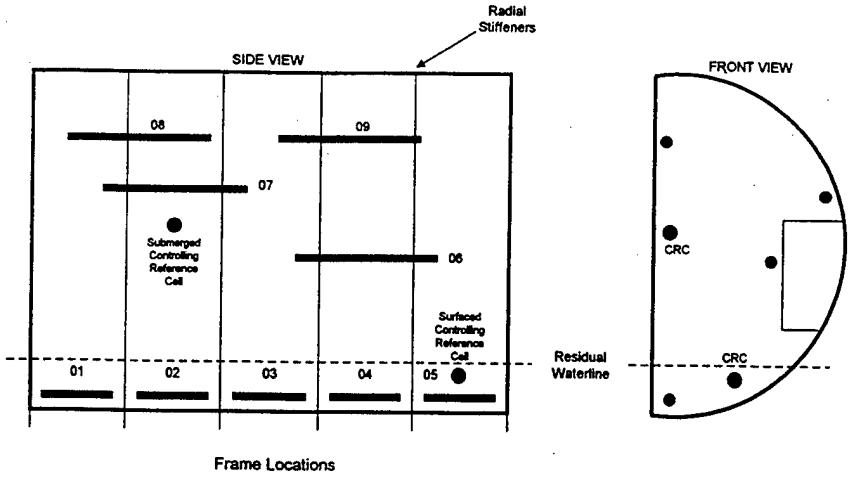

Figure 5. Schematic of Tank A ICCP system anodes and reference cells mounted on radial stiffener configuration.

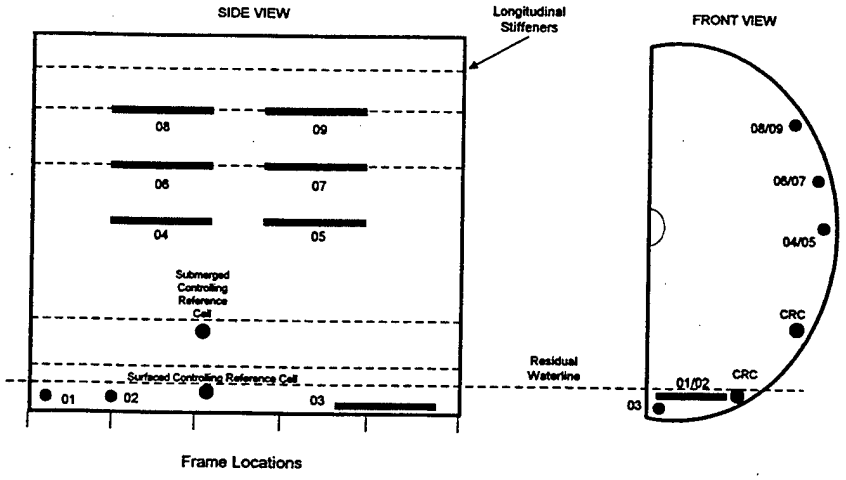

Figure 6. Schematic of Tank B ICCP system anodes and reference cells mounted on both longitudinal and radial stiffeners.

The Effect of Water Vapor on the Oxidation of Alloys that Develop Alumina Scales for Protection

Ramkumar Janakiraman, G.H. Meier and F.S. Pettit
Department of Materials Science and Engineering
University of Pittsburgh
Pittsburgh, PA 15261

ABSTRACT

Cyclic oxidation tests have been performed at 1100°C in wet and dry air on a number of alloys and coatings that form α-Al_2O_3 scales upon exposure to oxidizing conditions. The alloys that were investigated included PWA 1480, PWA 1484, CMSX 4, diffusion aluminide coatings on PWA 1480 and PWA 1484, and Co-24Cr-10.5Al-0.3Y. In cases where some cracking and spalling of the alumina scales occurred in dry air, the presence of water vapor caused the degradation rate to be increased by a factor of two. When no cracking or spalling of the alumina occurred in dry air, as was the case for low sulfur alloys, water vapor had no affect on the oxidation behavior. It is proposed that water vapor causes stress corrosion cracking at the Al_2O_3-alloy interface during cyclic oxidation.

INTRODUCTION

Water vapor is present in virtually every atmosphere to which high temperature materials are exposed. There are numerous examples that show water vapor affects the high temperature corrosion of metallic alloys and ceramics. Some effects that water vapor has been reported to cause during the oxidation of alloys are as follows:

- The presence of water vapor permits a H_2-H_2O mixture to be formed in voids which facilitates a rapid inward transport of oxygen across the pores via dissociative gas transport (oxidation-reduction process)[1,2].

- Water vapor can affect the plasticity of oxide scales. Some investigators propose that the plasticity of oxide scales is decreased and, consequently, the spalling of scales is increased[3]. Other investigators have proposed that plasticity of oxide scales is increased [2,4] with increased oxidation rates[2] or improved adherence[4].

- The presence of water vapor adversely affects the selective oxidation of aluminum and chromium in iron base alloys[5]. It has also been found that water vapor affects the selective oxidation of aluminum in TiAl[6].

- Water vapor can affect transport through oxides such as SiO_2 by causing the network structure to be changed[7].

- Water vapor can cause the vaporization of some oxides to be increased because of the formation of hydrated species with high vapor pressures[8].

- Water vapor causes the concentration of proton defects to be increased which can influence defect-dependent properties such as high temperature creep and diffusion[9,10].

Based upon the data in the literature it is evident that, depending upon the alloy and the oxidizing conditions, water vapor can affect oxidation in a number of different ways.

Most alloys and coatings that are developed for use above 1000°C rely upon the formation of an α-Al_2O_3 scale for oxidation protection. The influence of water vapor on the oxidation of alumina-forming alloys has been studied[5,11]. Kvernes et al[5] did not observe any effect of water vapor on the isothermal oxidation of an Fe-13Cr-4Al* alloy at temperatures of 680, 820 and 980°C. At 980°C these authors showed that a continuous layer of α-Al_2O_3 was formed on this alloy. Buscail et al[11] have found that water vapor decreases the isothermal oxidation rate of an Fe-21.5 Cr-5.6 Al alloy at 1000°C. The effect was not large, for example, k_p values of 2.4×10^{-13} and 2.7×10^{-13} g^2/cm^4s were obtained for water vapor pressures of 0.15 and 0.32 atm, respectively, versus 2.9×10^{-13} g^2/cm^4s for dry oxygen. These investigators proposed that the initial transient oxidation processes are affected by water vapor. Smialek[12] has shown that the scale adhesion of alumina is sensitive to water vapor and Sigler[13] has reported humidity induced spalling of alumina. Smith et al[14] have also observed that humidity may play a role in the spalling of alumina from nickel base superalloys. The results that are available indicate that water vapor does not have a substantial effect on the isothermal oxidation of alumina-forming alloys and coatings, however, water vapor may have significant adverse effects on the cyclic oxidation of such alloys. This paper is concerned with the effect of water vapor on the cyclic oxidation resistance of alloys and coatings upon which alumina scales are formed during oxidation.

EXPERIMENTAL

The cyclic oxidation experiments were performed on state-of-the-art superalloys, namely, PWA 1480, PWA 1484 and CMSX 4. The compositions of these superalloys are presented in Table I. All of these alloys have compositions such that α-Al_2O_3 scales are formed during oxidation at 1100°C after periods of some transient oxidation[15]. Aluminide coatings were also studied on the PWA 1480 and PWA 1484 alloys. One coating was formed using chemical vapor deposition techniques to establish aluminizing conditions. The other involved a pack aluminizing procedure. Scanning micrographs of these two coatings on PWA 1480 are presented in Figure 1. The pack aluminide coating was thicker than that formed by the CVD technique if the alloy interdiffusion zones were neglected. The aluminum concentration at the surface of the coatings was 61.8 at% and 42.8 at% for the pack coating and CVD coating, respectively.

In cyclic oxidation tests the adherence of the alumina scales to the substrates is an important factor. The adherence of alumina scales on alloys is affected by the sulfur concentration in alloys as well as the concentrations of reactive elements such as yttrium[16-18]. The PWA 1480 and PWA 1484 alloys contained 5-8 ppm sulfur. The CMSX 4 alloy contained 3 ppm sulfur. In order to have alloys with very good alumina adherence a casting

*All compositions are presented in weight percent unless noted otherwise.

with essentially the same composition as PWA 1484 was prepared by Howmet using special techniques to control the sulfur concentration. This casting was not a single crystal, as PWA 1484 is usually fabricated, and the sulfur concentration was 1 ppm. In order to reduce the sulfur concentration in the PWA 1484 with 5-8 PPM sulfur, thin coupons of this alloy (~0.3mm thick) were desulfurized by annealing in hydrogen for 100 hrs at 1200°C[19]. This treatment reduced the sulfur concentration to less than 1 ppm. Finally, a CoCrAlY alloy with a nominal composition as indicated in Table I was prepared to investigate an alumina forming alloy that contained the reactive element yttrium.

The cyclic oxidation specimens were coupons about 1 cm^2 and 3mm thick except for the desulfurized specimens which were 1 cm^2 but 0.3mm thick. The cyclic oxidation tests were performed in the apparatus shown in Figure 2. The specimens were cycled in and out of the furnace once every hour, 45 minutes in the hot zone at 1100°C, 15 minutes in the cool zone at 100°C. The experiments were performed in dry air with a dew point of -46°C and in wet air saturated with water at 50°C ($P_{H_2O} = 0.1\ atm$). The specimens were moved from the hot zone to the cool zone, or vice versa, in 3 minutes. The specimens were removed periodically from the apparatus and weight change measurements were performed along with visual examination of the specimens. Upon conclusion of the tests the specimens were examined in detail using optical metallography, scanning electron microscopy and X-ray diffraction.

RESULTS AND DISCUSSION

In cyclic oxidation tests spalling of the oxide scales occurs due to the development of growth and thermally induced stresses. As discussed by Evans[20] there are a number of factors, in addition to the environment, that can affect the oxide spalling process. The growth stresses are affected by the thicknesses of the oxide scale and by the thicknesses of the oxidation specimens as well as creep relaxation in the specimen. The thermally induced stresses are affected by the differences in the coefficients of thermal expansion of the oxide scale and the metallic substrate, the total temperature change and the rate of temperature change. In this investigation all of these factors were held constant for a given alloy system and the results were used to compare alumina spalling in dry and wet conditions as a function of oxidation time or increasing oxide scale thickness.

Uncoated Superalloys Oxidized in Wet and Dry Air

Weight Change Versus Time Data for the Cyclic Oxidation of PWA 1480 and PWA 1484 in wet and dry air are presented in Figure 3. The weight losses are caused by the spalling of oxide and this spalling is more severe for both alloys in water vapor compared to dry air. To compare the effects of water vapor the times of cyclic oxidation to produce the same amount of weight loss were compared. It was not possible to use the same amount of weight loss for all of the alloys tested because the rates of weight loss varied substantially. A parameter $\phi_{\Delta m}=t_{dry}/t_{wet}$ was used to compare the effects of water vapor where Δm was used to indicate the value of the weight loss (mg/cm^2) at which the comparison was made. The results obtained for ϕ for PWA 1480 and PWA 1484 are presented in Table 2 and were 2.3 and 3.7, respectively, for $\Delta m=-10 mg/cm^2$. The time required to produce the same

weight loss was about a factor of two, namely, it required about twice the time of cyclic oxidation in dry air to produce the same weight loss as that in wet air.

The results obtained for cyclic oxidation of CMSX 4 are presented in Figure 4. The weight losses for CMSX 4 in both wet and dry air were less than those observed for PWA 1480 and PWA 1484, Figure 3. It is believed that these smaller weight losses were due to the lower sulfur concentration in CMSX 4 which resulted in a more adherent oxide scale being formed on this alloy. Nevertheless, cracking and spalling of oxide did eventually occur on CMSX 4, Figure 4, and the weight losses were greater in wet than dry air. The value for $\phi_{\Delta m}$, as defined previously, was 2.4 where the value of Δm was -0.4 mg/cm^2.

As mentioned previously, PWA 1480, PWA 1484 and CMSX 4 are alumina formers. A continuous external scale of α-Al_2O_3 develops on these alloys after a transient period of oxidation during which other oxides such as NiO and Cr_2O_3 are formed. The presence of an α-Al_2O_3 scale was confirmed on these alloys using X-ray diffraction. In cyclic oxidation the oxide scales spall and the oxide formed on subsequent cycles becomes more enriched in Cr_2O_3 and NiO as an aluminum depleted zone develops in these alloys. Scanning electron micrographs comparing the depleted zones in CMSX 4 after 350 hrs of cyclic oxidation are presented in Figure 5. The depleted zone that developed in wet air, as indicated by the absence of the γ' phase, is substantially larger than that for cyclic oxidation in dry air.

Uncoated PWA 1484 with Low Sulfur Concentrations

In the case of cyclic oxidation of the desulfurized PWA 1484 and the 1 ppm sulfur PWA 1484, no spalling of oxide occurred in either wet or dry air. The results obtained after various times of cyclic oxidation in wet and dry air are compared in Figure 6. No significant difference was evident. The cyclic oxidation tests using desulfurized PWA 1484 have been performed in wet air for over 3000 hrs and in dry air for 2000 hrs. As can be seen in Figure 7, no spalling of the oxide scale is evident and there are no significant differences between testing in wet and dry air. A scanning electron micrograph of the oxide scale that formed on PWA 1484 (1 ppm sulfur) after 3500 hrs of cyclic oxidation in wet air is presented in Figure 8. The oxide adjacent to the alloy was α-Al_2O_3. Transient oxides of NiO, Cr_2O_3 as well as some tantalum oxides were above the alumina scale. This type of scale developed upon all three superalloys studied.

No isothermal oxidation experiments have been performed to determine if water vapor affects the isothermal growth of alumina. In Figure 9 weight changes obtained for the two low sulfur alloys are plotted versus the square root of the oxidation time. Even though the test was cyclic no oxide spalling occurred. These data conform to a parabolic rate law with rate constants of 1.9 x $10^{-13}$and 3.1 x 10^{-13} g^2/cm^4-s. These rate constants have values close to that for isothermal oxidation[21], 7 x 10^{-13} gm^2/cm^{4}s. These results indicate that water vapor does not have a substantial effect on the isothermal oxidation of alumina forming alloys.

Coated Superalloys

Weight change versus time measurements for cyclic oxidation of aluminide coated PWA 1484 are presented in Figure 10. Less cracking and spalling of oxide occurred in dry air and

a ϕ value of 1.9 was obtained for Δm=-10 mg/cm^2. Results obtained in wet air for the two coating on PWA 1480 and PWA 1484 are presented in Figure 11. The weight losses in this test occurred at a smaller rate initially for the pack aluminide coatings on both PWA 1480 and PWA 1484, Figure 11. The larger thickness and the higher aluminum concentration of the aluminide coating formed via pack aluminizing compared to the CVD coating may account for the observed differences in weight loss. After the coatings have been depleted of aluminum the rates of weight loss begin to approach one another, Figure 11.

CoCrAlY Specimens

Weight change measurements for the cyclic oxidation of the CoCrAlY alloy in wet and dry air are compared in Figure 12. Cracking and spalling of the oxide scale was evident on the specimen tested in wet air after about 1000 hrs. The sample tested in dry air did not exhibit any weight loss, however, a very small amount of oxide cracking and spalling was evident upon visual examination. This spalling was predominantly at the edges of specimens. Small amounts of yttrium in CoCrAl, NiCrAl and FeCrAl alloys normally results in extremely adherent alumina scales. While the cracking and spalling observed in the CoCrAlY specimen was not large, this alloy may not be representative of the optimum results that can be produced with yttrium. The yttrium concentration was 0.3%. This is large. Better results are obtained at 0.05 to 0.10%. At the higher levels of yttrium (e.g. 0.15-0.3%) yttrides are formed which preferentially oxidize to form stringers of yttria in the alumina scale and within the alloy itself.

The Effects Produced by Water Vapor

The results clearly show that water vapor does cause the cracking and spalling of α-Al_2O_3 to be more severe than in dry air. Water vapor increases the degradation by a factor of about two. However, such a condition was not observed for extremely adherent alumina scales. It appears that when cracking and spalling occurs in dry air, then water vapor causes the cracking and spalling to be more severe. When cracking does not occur in dry air, water vapor does not appear to have any influence on cracking and spalling of the alumina scales. Since the oxidation resistance of alloys is related to the times over which α-Al_2O_3 scales are developed on their surfaces, water vapor causes the lives of such alloys and coatings to be decreased. Since no effects of water vapor have been observed as yet in the low sulfur alloys, the importance of such alloys is great. Reactive elements such as yttrium may also be capable of negating the effects of water vapor, but the reactive element will have to be at concentrations and distributions to produce adherent alumina scales with no cracking nor spalling.

In order to determine if water vapor is affecting the stresses in alumina scales, the residual stresses in α-Al_2O_3 scales formed on desulfurized PWA 1484 were determined by X-ray diffraction[22]. The stresses are presented in Table III where it can be seen that no difference in residual stresses were detected after 350 hrs of oxidation in wet and dry air at 1100°C. The residual stress level did not change significantly when the oxidation time was extended to 3000 hrs at 1100°C in wet air.

The mechanism by which water vapor causes the alumina scales to crack and spall is not clear. Ramanis et al[23] have investigated the interfacial fracture toughness of gold-alumina specimens and found a large increase in the interfacial toughness in dry nitrogen compared to moist air. These investigators have proposed that this effect is due to interfacial stress corrosion cracking induced by water vapor adsorption at the crack tip. Michalski and Freiman[24] have proposed that the loss of strength in vitreous silica is associated with slow crack growth of pre-existing surface flaws due to stress corrosion by water from the surrounding environment. Michalski[25] et al showed that single crystal sapphire (Al_2O_3) had slow fracture behavior similar to silica when exposed to nonaqueous environments.

The effects of water vapor that have been observed in the current investigation seem to be consistent with interfacial stress corrosion cracking. The oxide thicknesses and the stress levels are unaffected by the water vapor, hence the stored elastic energy in the oxide scale is the same wet or dry. The oxide scales which do not readily crack under dry conditions seem to be unaffected by water vapor, which precludes stress corrosion cracking of the alumina to produce through cracks. It is possible that water vapor affects only those alloys where cracks exist in the scales thereby providing access to the alumina-alloy interface. The results obtained with the CoCrAlY alloy support this argument.

CONCLUDING REMARKS

The effects of water vapor that have been observed in the current investigation seem to be consistent with interfacial stress corrosion cracking, however, more studies are required to identify crack initiation and the effects of water vapor on this process. There are other important questions about the water vapor effect that should be investigated. For example, what is the effect of the water vapor pressure and is there some water vapor pressure below which water vapor has no effect? How important are cooling rates and hold times at room temperature? Are there any significant effects of water vapor during isothermal oxidation?

ACKNOWLEDGEMENTS

The authors are grateful for financial support from the Office of Naval Research, (contract # NOOO14-94-1-0085, A. John Sedriks, Program Officer).

REFERENCES

1. A. Rahmel and J. Tobolski, Corros. Sci., 5, 333 (1965).
2. C.W. Tuck, M. Odgers, and K. Sachs, Corros. Sci., 9, 271 (1969).
3. R.L. McCarron and J.W. Schulz, "The Effects of Water Vapor on the Oxidation Behavior of Some Heat Resistant Alloys" Proc. of Symposium on High Temperature Gas-Metal Reactions in Mixed Environments" AIME, New York, 1973, p. 360.
4. H. Bouaouine, F. Armanet and C. Coddet, International Congress on Metallic Corrosion, Toronto, Canada, (1989).
5. I. Kvernes, M. Oliveira, and P. Kofstad, Corrs. Sci., 17, 237 (1977).
6. R. Kremer, and W. Auer, Materials and Corrosion, 48, 35 (1997).
7. E.A. Irene, J. Electrochem. Soc., 121, 1613 (1974).
8. J.F. Cullinan, "The Oxidation of Carbon-Carbon Composites between 300°C and 900°C in Oxygen and Oxygen/Water Vapor Atmospheres", M.S. Thesis, University of Pittsburgh, 1989.
9. A.J. Sedriks, "Corrosion of Stainless Steels", 2nd Edition, John Wiley and Sons, Inc., New York, (1996).
10. P. Kofstad, in Microscopy of Oxidation, M.J. Bennett and G.W. Lorimer, eds., P2, The Institute of Metals London, 1991.
11. H. Buscail, S. Heinze, Ph. Dufour and J.P. Larpin, Oxid. of Metals, 47, 445 (1997).
12. J.L. Smialek, Met. Trans., 22A, 739 (1991).
13. D.R. Sigler, Oxid. Met., 40, 555 (1993).
14. M.A. Smith, W.E. Frazier and B.A. Pregger, Mat. Sci. and Eng., A203, 388-398 (1995).
15. M. Levy, P. Farrell and F. Pettit, Corrosion, 42, 708 (1986).
16. J.G. Smeggil, A.W. Funkenbusch and N.S. Bornstein, "A Relationship between Indigeneous Impurity Elements and Protective Oxide Scale Characteristics", Met. Trans. 17A, 923-932, (1986).
17. J.L. Smialek and B.K. Tubbs, "Effect of Sulfur Removal on Scale Adhesion to PWA 1480", Mt. Trans. 26A, 427-435, (1995).
18. G.H. Meier, F.S. Pettit and J.L. Smialek, Sulfur Removal on the Adherence of Alumina to Ni-and Fe-Base Alloys", Werkstoffe und Korrosion, 46, 232-240 (1995).
19. J.L. Smialek, Met. Trans., 22A, 739-752 (1991).
20. H.E. Evans and M.P. Taylor, "Creep Relaxation and the Spallation of Oxide Layers", to be published in Proceedings of the 24th International Conference on Metallurgical Coatings, San Diego, CA., April 21-25, 1997.
21. F.S. Pettit, Trans. Met. Soc. of AIME, 239, 1296 (1967).
22. C. Sarioglu, J.R. Blacheré, F.S. Pettit and G.H. Meier, "Room Temperature and In-Situ High Temperature Strain or Stress Measurements by XRD Techniques", Microscopy of Oxidation, in press.
23. I.E. Ramanis, B.J. Dolgleish, M. Brahy, M. Rühle and A.G. Evans, Acta Metall., 38, 2645 (1990).
24. T.A. Michalski and S.W. Freiman, J. Amer. Ceramic Soc., 66, 284-288 (1983).
25. T.A. Michalski, S.W. Freiman and B. Bunker, Amer. Ceram. Soc. Bull., 61, 414 (1982).

Table I

Compositions (wt %) of the Alloys

Alloy Designation	Ni	Cr	W	Ta	Al	Co	Ti	Mo	Re	Hf	Y	Sulfur Concentration
PWA 1480	Bal	10	4	12	5	5	1.5					5-8 PPM
PWA 1484	Bal	5	6	8.7	5.6	10		2	3	0.1		5-8 PPM
PWA 1484 Desulfurized	Bal	5	6	8.7	5.6	10		2	3	0.1		< 1 PPM, sulfur removal by heating in hydrogen for 100 hrs. at 1200°C
PWA 1484 1 PPM S	Bal	5	6	8.7	5.6	10		2	3	0.1		1 PPM prepared using special techniques to control sulfur concentration
CMSX 4	Bal	6.4	6.3	6.5	5.7	9.5	1	0.6	2.9	0.1		3 PPM
CoCrAlY		24			10.5	Bal					0.3	

Table II

The Ratio of Times to Produce a Given Amount of Oxide Spalling Δm

	$\phi_{\Delta m} = \frac{t_{dry}}{t_{wet}}$
PWA 1480 Δm = -10mg/cm^2	2.3
PWA 1484 Δm = -10mg/cm^2	3.7
CMSX 4 Δm = -0.4mg/cm^2	2.4
PWA 1480/CVD Diffusion Aluminide Δm = -10mg/cm^2	1.9

Table III

Residual Stress in Desulfurized PWA 1484 after Oxidation at 1100°C

Environment	Time hrs	Residual Compressive Stresses (MPa)
Dry air	350	-3890
Wet air (P_{H_2O}=0.1atm)	350	-3760
Wet air (P_{H_2O}=0.1atm)	3000	-3710

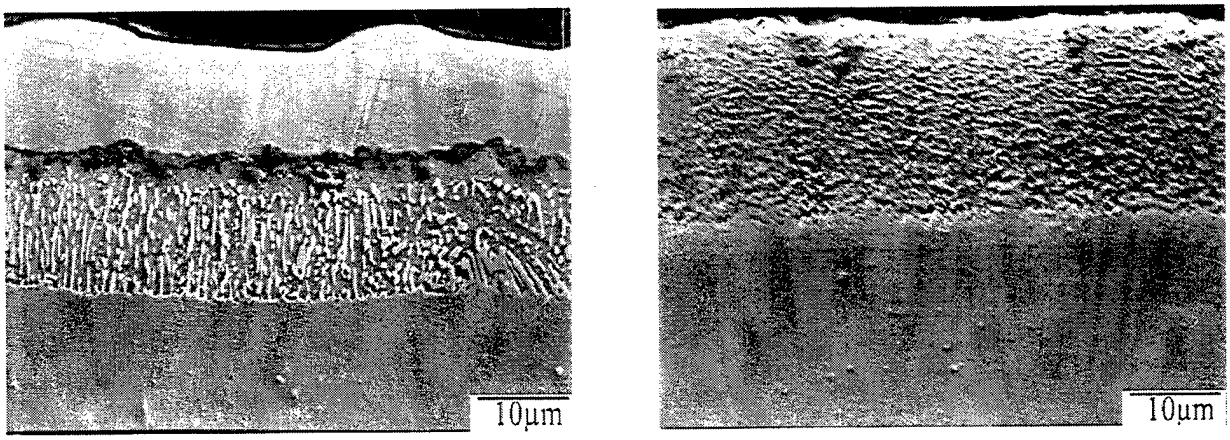

(a) (b)

Figure 1. Scanning micrographs of PWA 1480 coated with aluminide by (a) chemical vapor deposition and (b) pack alumnizing method.

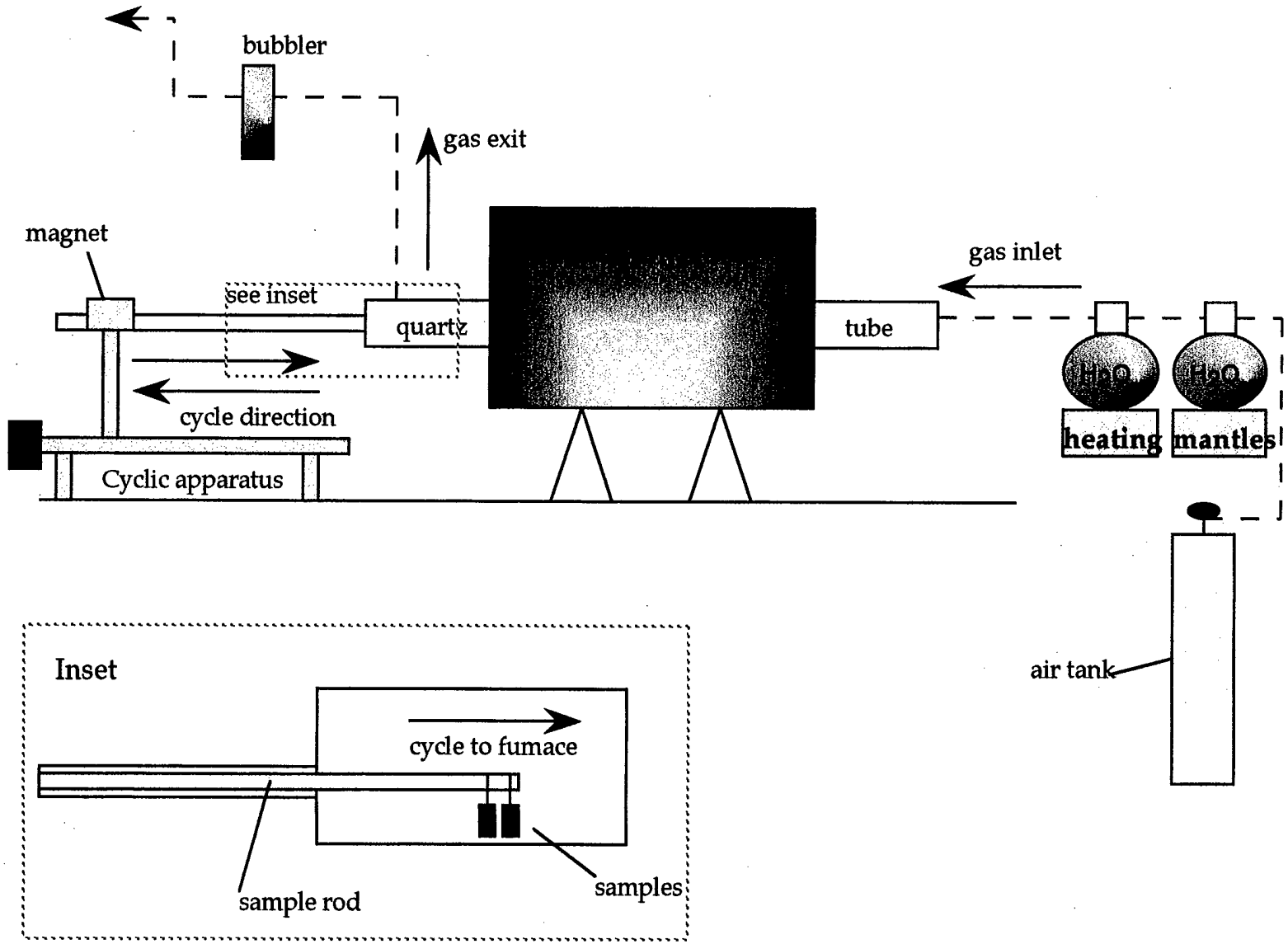

Figure 2. Schematic diagram to show the apparatus to cyclically oxidize coupon specimens in gases with defined and controlled amounts of water vapor.

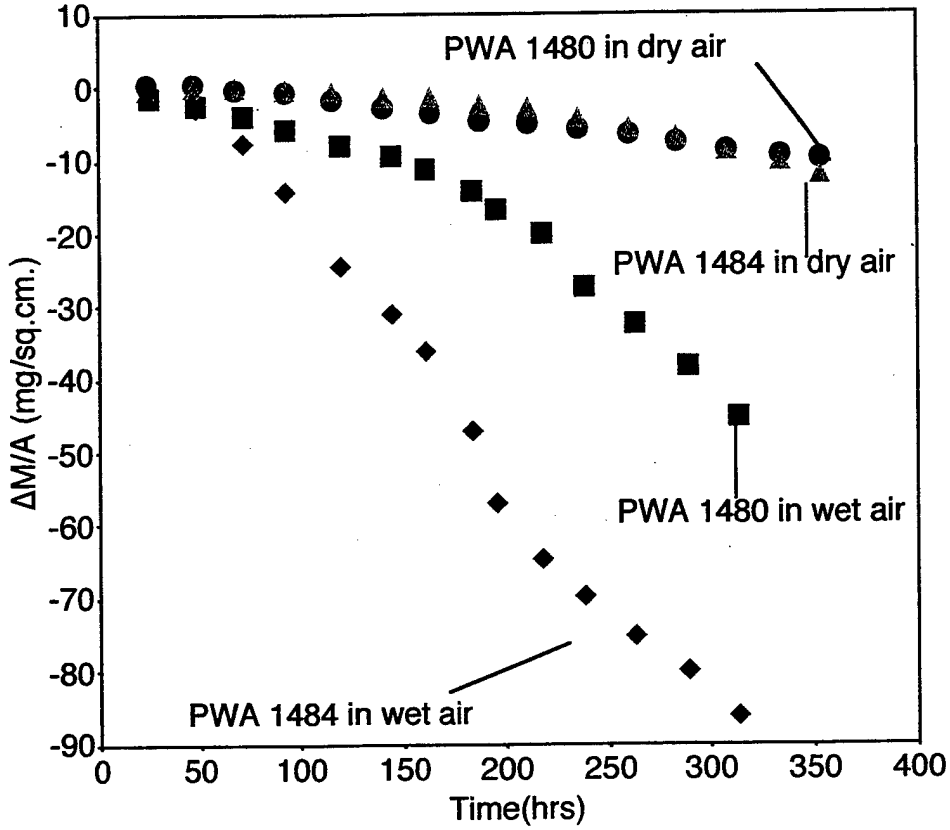

Figure 3. Weight changes versus time data for the cyclic oxidation of PWA 1480 and PWA 1484 in wet (P_{H_2O} = 0.1 atm) and dry air at 1100°C.

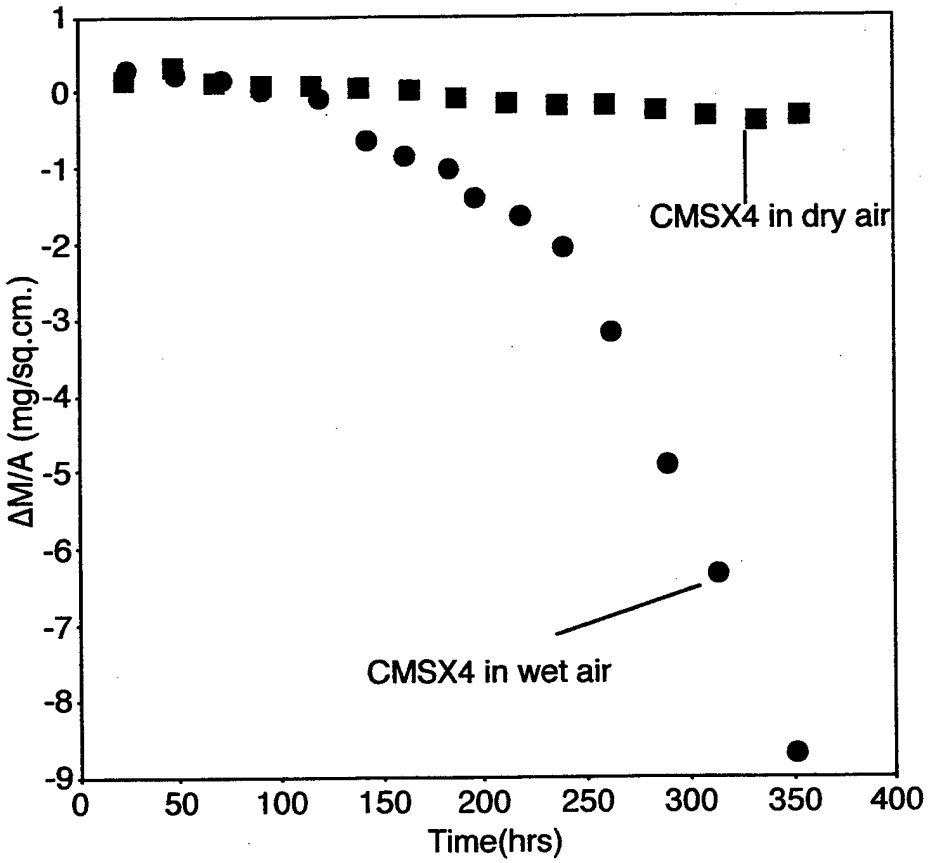

Figure 4. Weight changes versus time data for the cyclic oxidation of CMSX4 in wet (P_{H_2O} = 0.1 atm) and dry air at 1100°C.

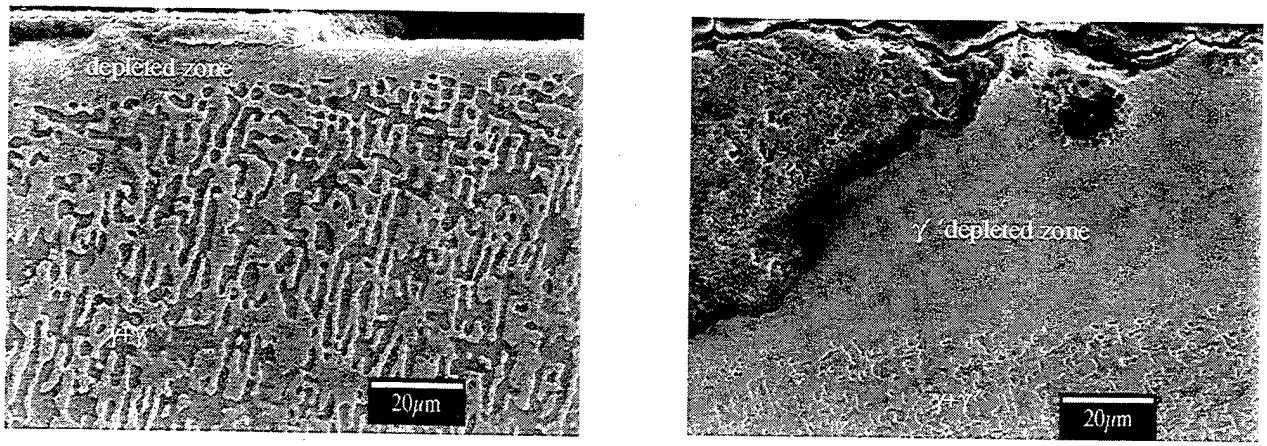

(a) (b)

Figure 5. Scanning micrographs of CMSX4 after 350 hrs of cylic oxidation at 1100°C in (a) dry air and in (b) wet (P_{H_2O} = 0.1 atm) air.

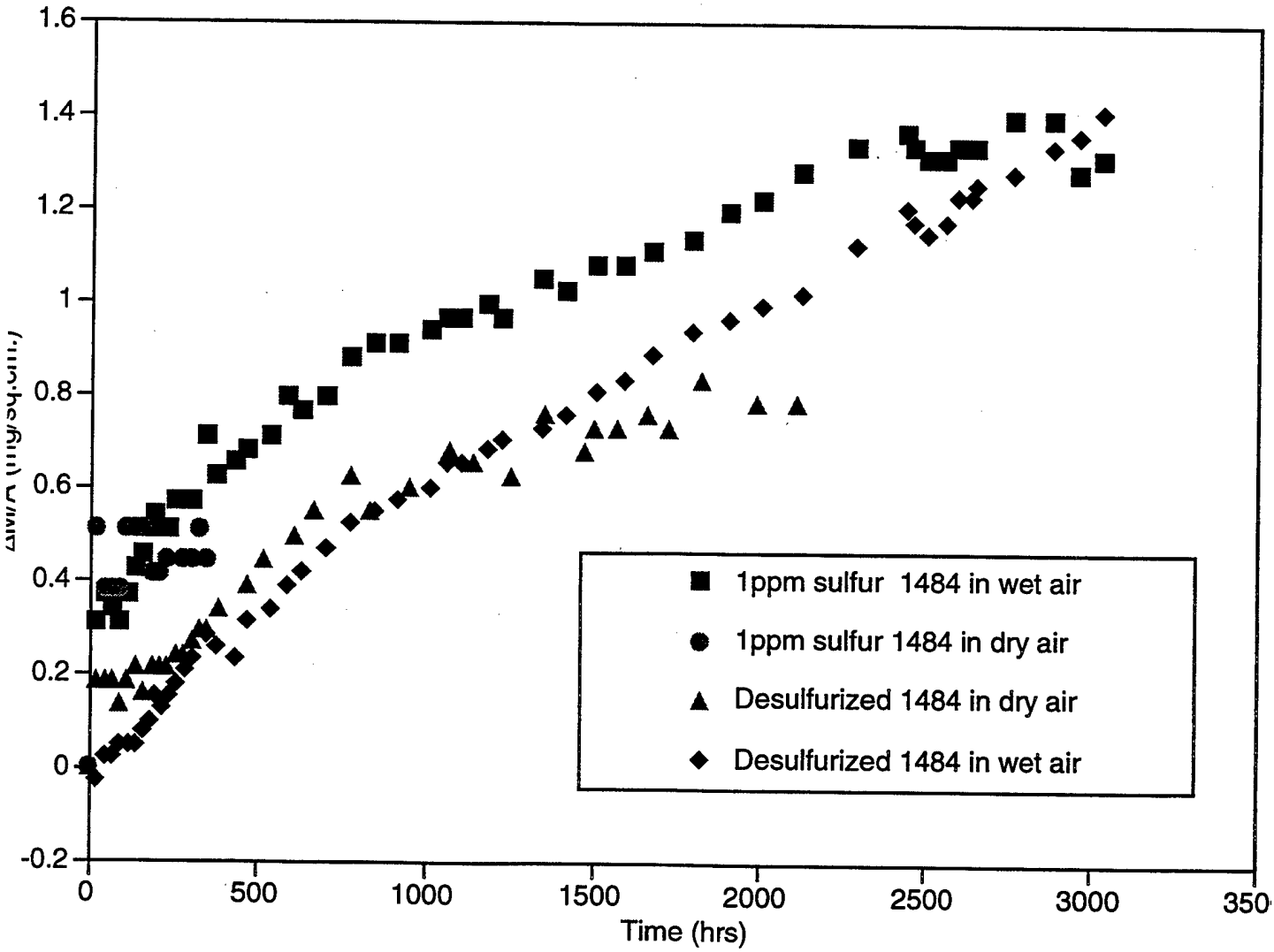

Figure 6. Weight change versus time data for the cyclic oxidation of desulfurized and low sulfur PWA 1484 in wet (P_{H_2O} = 0.1 atm) and dry air at 1100°C.

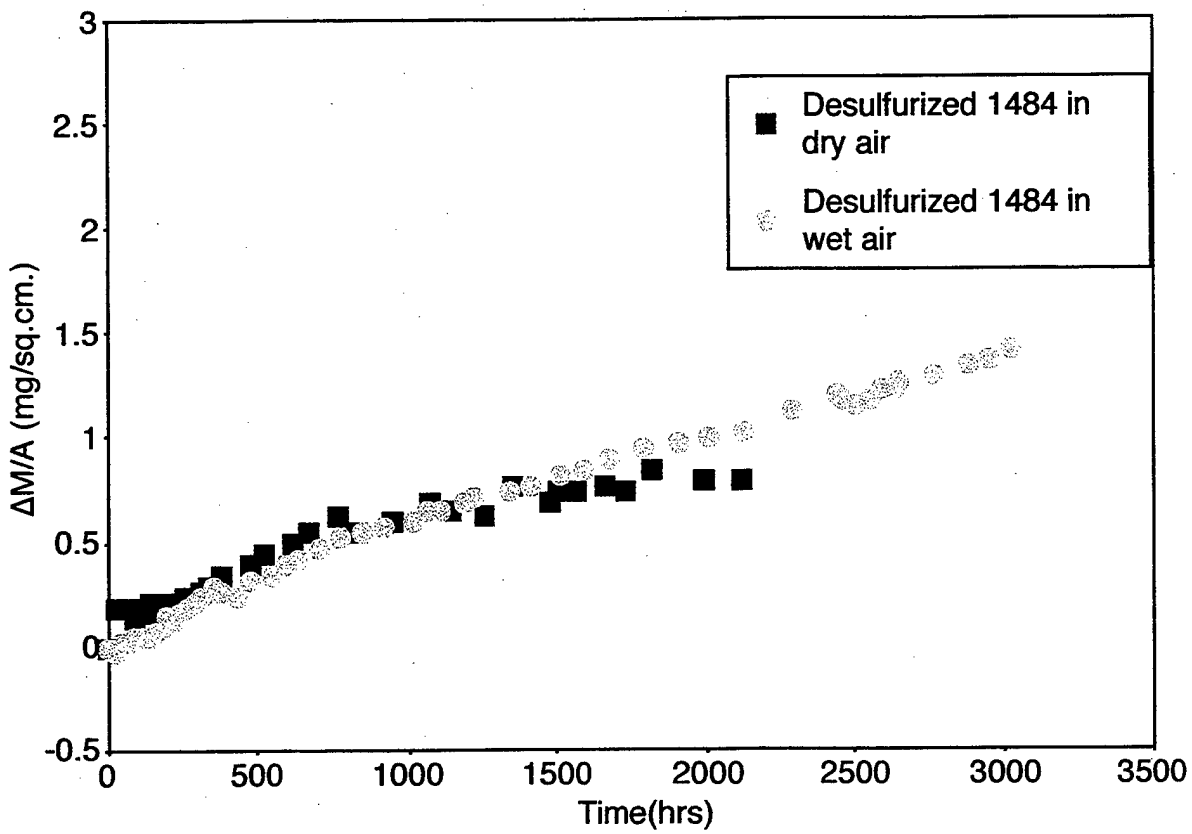

Figure 7. Weight change versus time data for the cyclic oxidation of desulfurized PWA 1484 in wet (P_{H_2O} = 0.1 atm) and dry air at 1100°C.

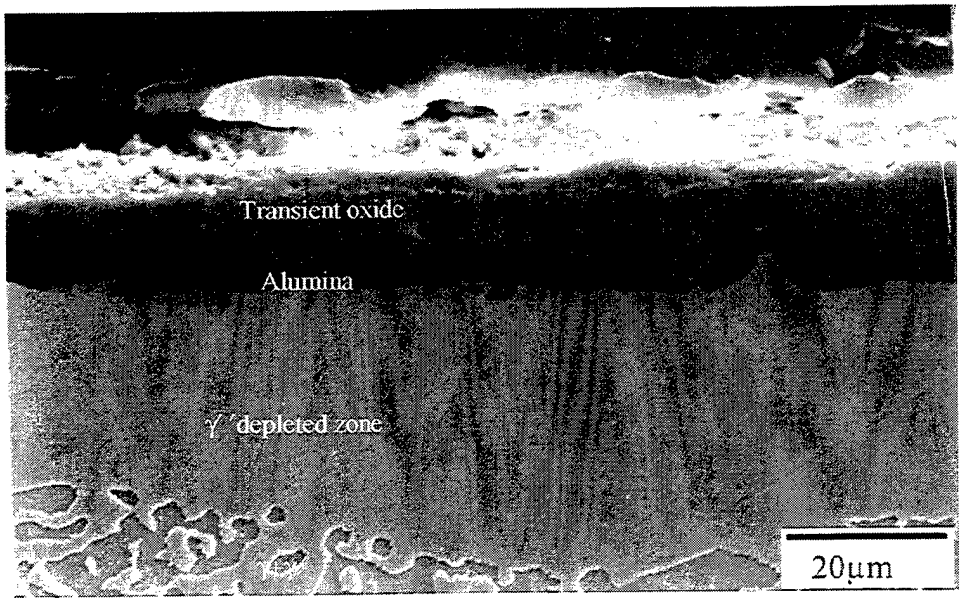

Figure 8. Scanning micrograph of PWA 1484 (1PPM, sulfur) after 3500 hrs of cylic oxidation in wet (P_{H_2O}= 0.1 atm) air at 1100°C.

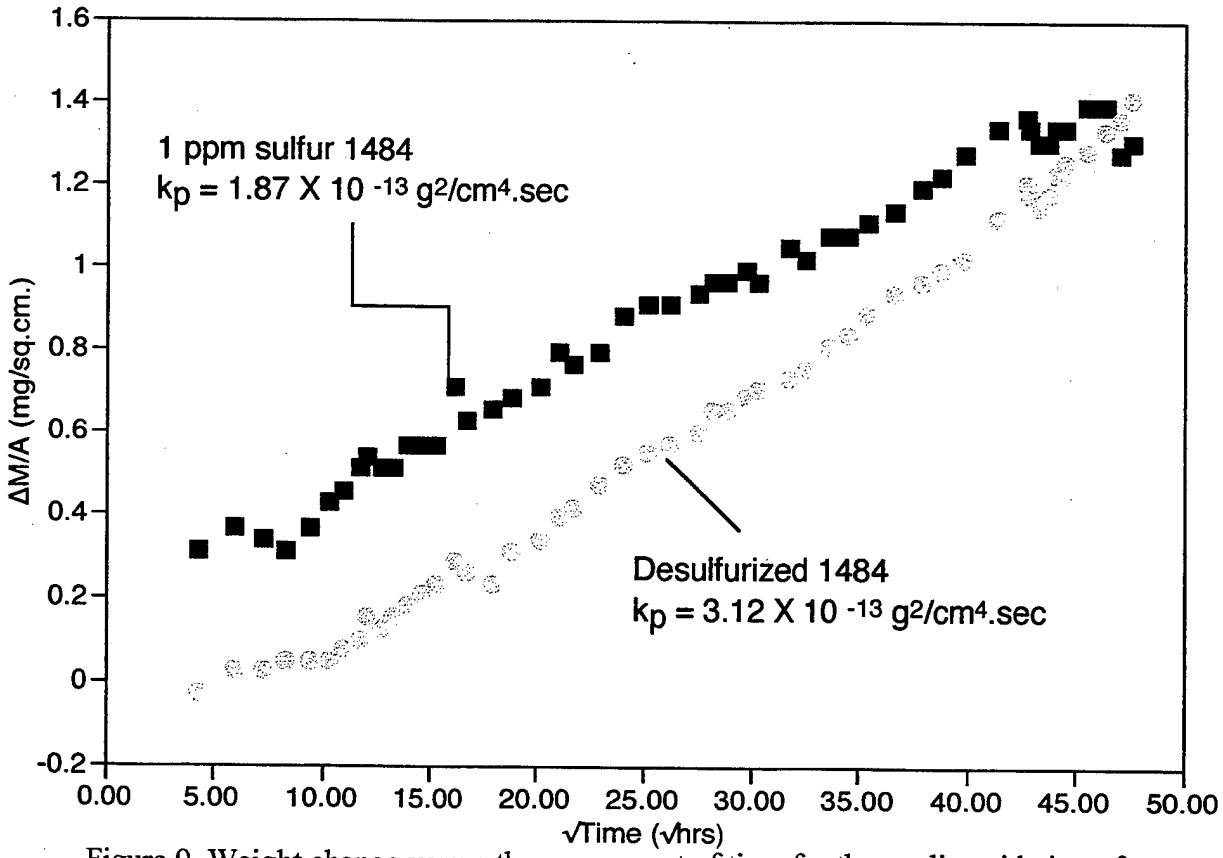

Figure 9. Weight change versus the square root of time for the cyclic oxidation of desulfurized and 1 PPM sulfur PWA 1484 in wet air (P_{H_2O} = 0.1 atm) at 1100°C. The data conform to a parabolic rate law with rate constants as shown in the figure.

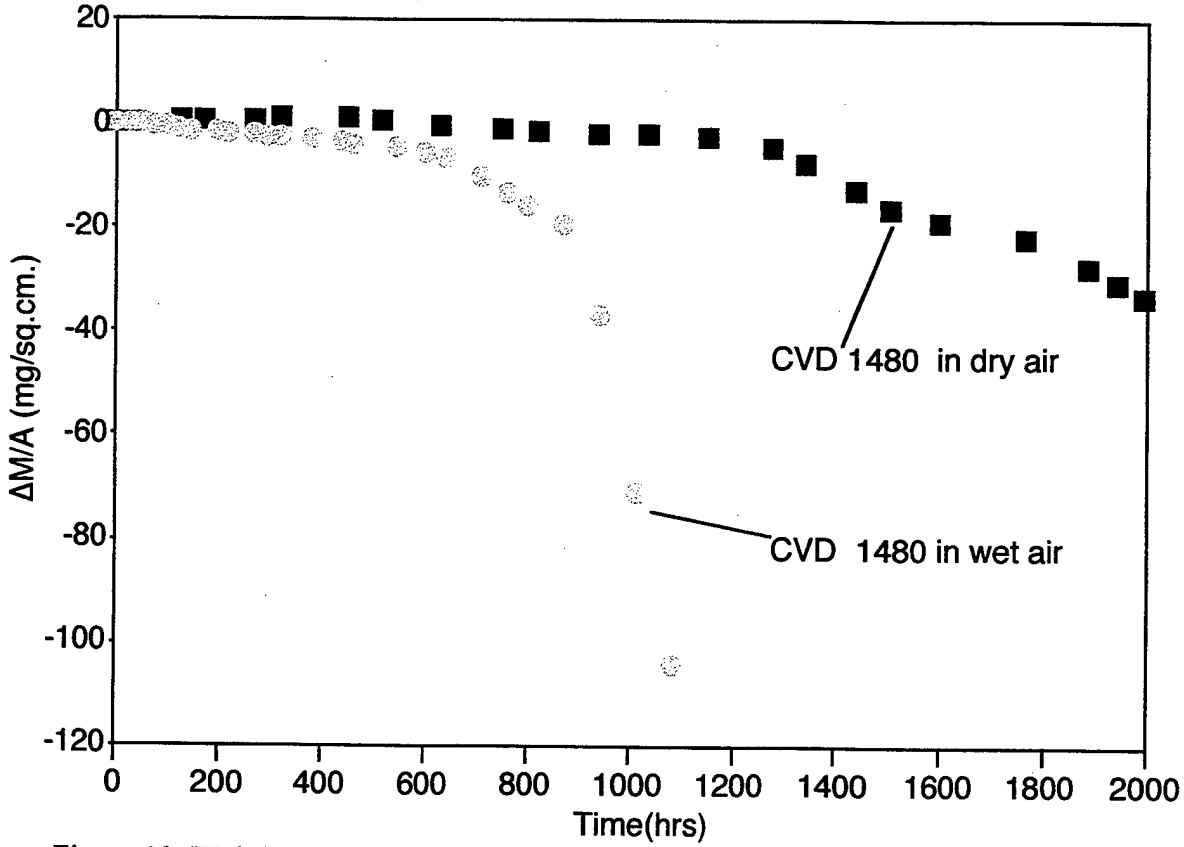

Figure 10. Weight change versus time data for the cyclic oxidation of aluminide coated PWA 1480 in wet (P_{H_2O} = 0.1 atm) and dry air at 1100°C.

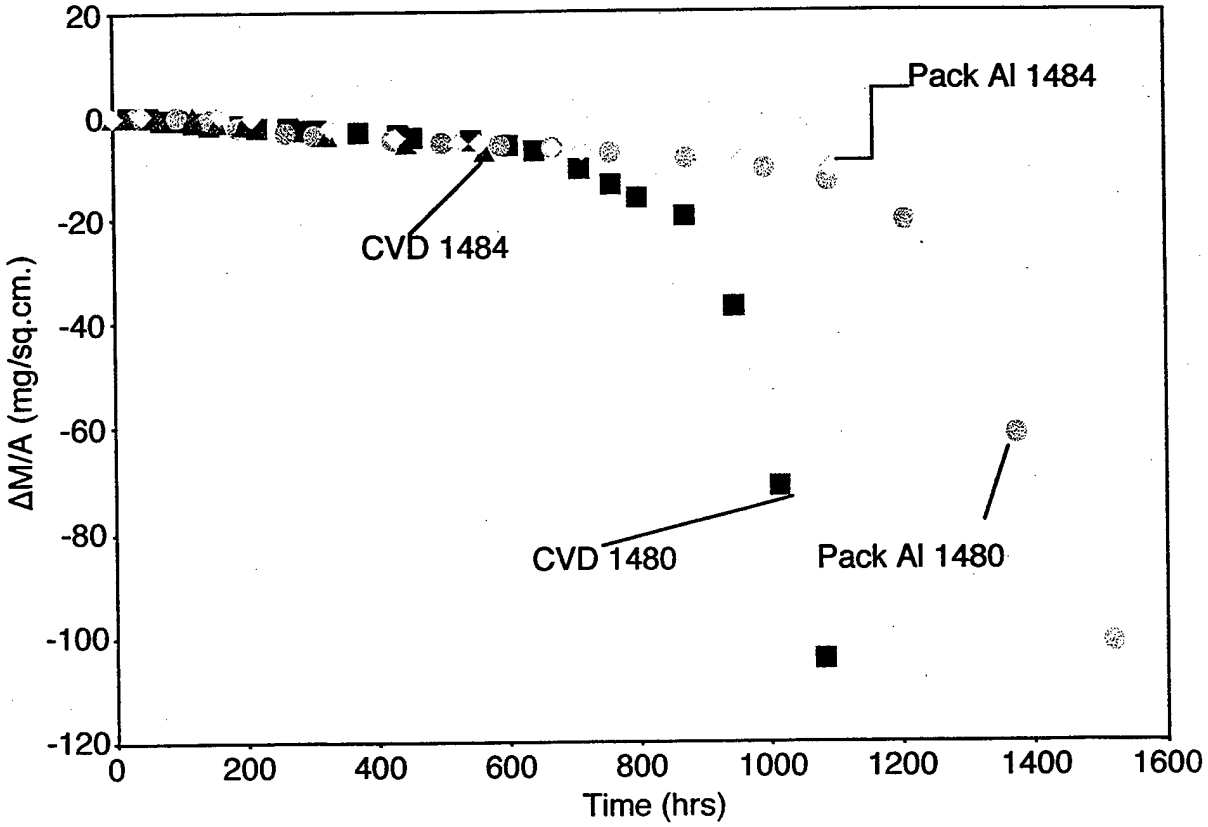

Figure 11. Weight change versus time data for the cyclic oxidation of aluminide coated PWA 1480 and PWA 1484 in wet (P_{H_2O} = 0.1 atm) air at 1100°C.

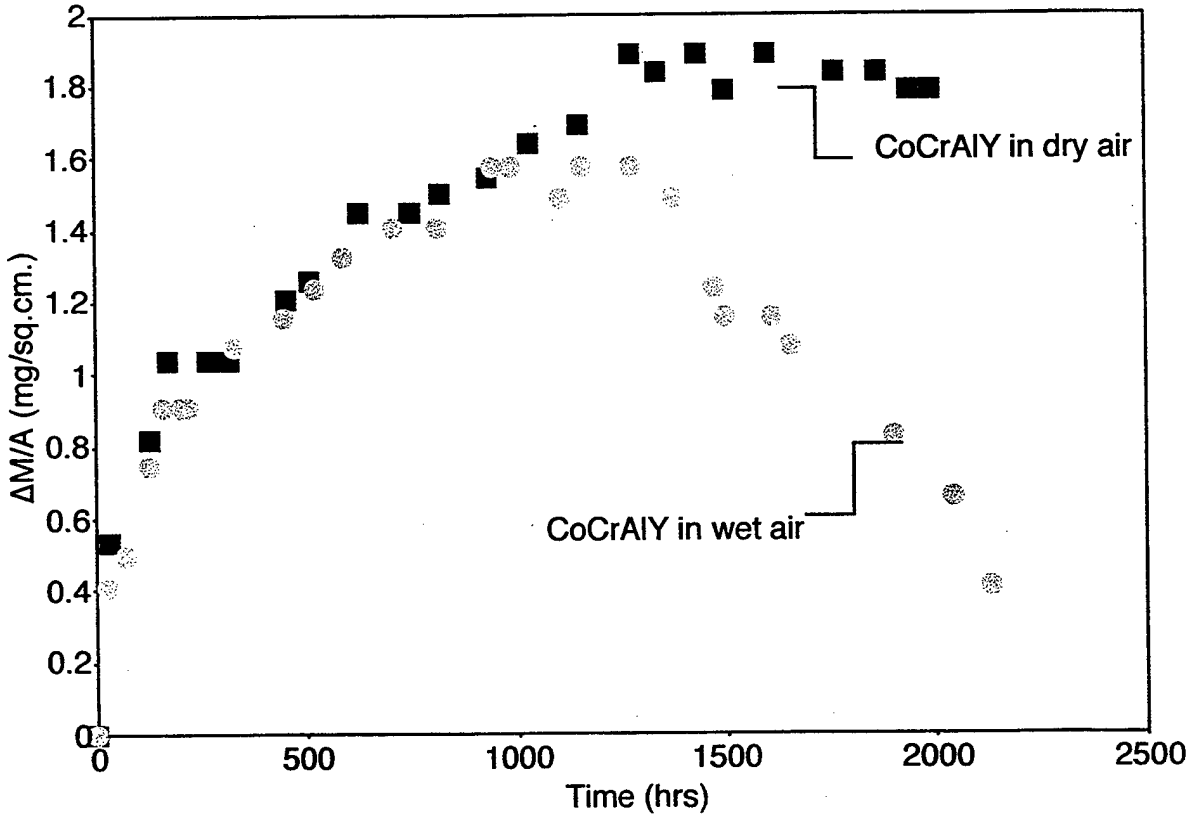

Figure 12. Weight change versus time data for the cyclic oxidation of CoCrAlY in wet (P_{H_2O}= 0.1 atm) and dry air at 1100°C.

Corrosion Control for the AN/BQG-5A(V)1 Wide Aperture Array

by
Harvey Hack, Ph.D., P.E.*
Julie Pinkham**
David G. Tipton*

The Wide Aperture Array is a passive receive submarine sonar system. The system consists of several subarrays attached to each side of the submarine pressure hull. Each subarray consists of hydrophones, outboard electronics, noise decouplers, structural and attachment members. These components are packed in layers in a large patch on the submarine pressure hull. The high density presents some unique challenges for corrosion protection, since the sea water cross section through which cathodic protection current must be distributed is small. In addition, the internal components are difficult to inspect and the hull is shielded from the submarine cathodic protection system. Early designs of this array were constructed of several types of metals and had limited cathodic protection. Limited cathodic protection caused the submarine hull to experience corrosion damage on the prototype Advanced Development Model (ADM) version of the system. Limited fastener corrosion was associated with the production Engineering Development Model (EDM), or AN/BQG-5, Wide Aperture Array. Corrosion details of both systems are described. The design of the new AN/BQG-5A(V)1 array is then described in detail. Materials used, component cross sections, cathodic protection design lifetime calculations and anode placement are presented to show how corrosion control is managed in this complex marine structure.

* Northrop Grumman Corporation
** Naval Undersea Warfare Center Newport Division

Distribution Statement A: Unlimited Distribution

Paper presented at the Tri-Service Corrosion Conference, 17-21 November, 1997, in Wrightsville Beach, NC.

INTRODUCTION

The Wide Aperture Array (WAA) is a passive receive submarine sonar system. The system consists of three subarrays attached to each side of the submarine pressure hull. Each subarray consists of hydrophones, outboard electronics, noise decouplers, structural and attachment members. These components are packed in layers in a large patch on the submarine pressure hull. The high density presents some unique challenges for corrosion protection, since the sea water cross section through which cathodic protection current must be distributed is small. In addition, the internal components are difficult to inspect and the hull is shielded from the submarine cathodic protection system.

HISTORY

ADM - The first Wide Aperture Array actually installed on a submarine supported the prototype Advanced Development Model (ADM) system. This system was installed on the SSN-710 (USS AUGUSTA) in 1986, and was removed in 1993, giving an in-service time of 7 years. This early design was constructed of several different metal alloys. The signal conditioning plate was made from HSLA steel, painted with Navy Formula 150 series epoxy, and had cathodic protection sacrificial anodes installed on its under side. This plate sustained significant material loss due to corrosion, particularly at the edges where the paint was more likely to be damaged. The subarrays were held on to the hull using bimetallic studs, with alloy 625 threads and an HY-80 steel base, with a maximum diameter of 5/8-inch. The submarine hull had limited cathodic protection, located on the hull under the forward and after fairing sections. Hull corrosion damage was revealed beneath the studs upon stud removal. This pitting damage is believed to have initiated at crevices around the base of the studs. On one port subarray, 170 of the 226 total 3/8-inch diameter stud locations exhibited hull damage, 26 areas were considered large (greater than 1.25-inches in diameter), with depths varying from slight to over ½-inch. In order to repair the damage under the studs, material had to be removed in a few cases to depths exceeding 1-inch. One starboard subarray had 67 pits, with 4 considered large. Components such as the Vibration Isolation Mounts, the support bar, and the compliant tube baffle fasteners, which were not isolated from the hull but were made of Alloy 625, showed little corrosion degradation. However, extensive crevice corrosion attack of stainless steel cable clamps and wire ties which were isolated from the hull was observed.

One of the principal contributors to the corrosion problems on the ADM was the inadequacy of cathodic protection. The original cathodic protection system for this array was designed for a three-year life, with inspections required much more frequently. However, the array was never inspected and the anodes were not replaced during the 7-year service life. Anodes were probably completely depleted during the fourth year of service. Many of the various materials used for construction were electrically connected to the hull, leading to galvanic corrosion problems as well.

EDM - The first production version of the array, called the Engineering Development Model (EDM), or AN/BQG-5, replaced the ADM on the SSN-710 (USS AUGUSTA) in

1993, and has been in service for 4 years. Details of the construction of this array are shown in Figure 1. Studs were attached to the hull to hold on the various components. Vibration Isolation Mounts (VIM's) for holding the fairings and the signal conditioning plate were also attached to the hull, and surrounded by various noise isolation components and a fairing toe piece. Mounted outboard of these components were additional noise decouplers and cables for the transducers. Next was the signal conditioning plate, to which was mounted the hydrophones and additional noise decoupler material. Surrounding the signal conditioning plate were segmented fairings attached to the hull, and transition pieces between the fairings and the signal conditioning plate. This array was fairly thick and heavy.

This design incorporated a number of improvements to enhance corrosion performance. Fewer studs were used on the hull by attaching the inner decoupler material to the underside of the signal conditioning plate instead of to the hull. Studs up to 7/8-inch diameter were used. A sealing compound was used on the fasteners to try to exclude water contact. Dissimilar metals were electrically isolated from each other by the use of plastic bushings and isolation pads. The number of sacrificial anodes used for cathodic protection was also significantly increased to provide a design lifetime of 15 years. Anodes were placed on the outer surface of the signal conditioning plate, on the hull around the perimeter of the acoustic module, and on the hull under the longitudinal and end fairings, as shown in Figure 2. A switch of hull anodes was made to MIL-A-24779 aluminum anodes from MIL-A-18001 zinc anodes to decrease weight. Efforts were also made to provide anode locations that equally distributed the protection current. As a result, this design had no corrosion problems on the hull as did the ADM array, but still experienced some corrosion damage. Crevice corrosion of 34 nickel-copper K-500 bolt heads under the coatings sometimes resulted in extensive metal removal, and was attributed to poor bonding of the sealant materials. The nickel-aluminum bronze fairing support bars had minor corrosion damage on their edges, and aluminum transition pieces showed slight damage in several localized areas, probably due to galvanic corrosion.

The second EDM was placed on the SSN-21 (USS SEAWOLF), with several major differences in construction from the first EDM, but with the same alloys. The fairing perimeter was attached, in this case, with all-alloy 625 studs, which were stick welded rather than shot onto the hull.

NEW DESIGN

Overview - The design of the new AN/BQG-5A(V)1 array, shown in Figure 3, capitalizes on the lessons learned from the previous versions. These lessons included the use of more sacrificial anodes, electrical isolation of as many metal components as possible, and special treatment of stud bases. It is constructed principally from non-metallic materials. For example, the signal conditioning plate, now renamed the array support plate, is made of glass-reinforced plastic. Much of the metallic structure has been removed completely by careful design changes. The primary purpose of this was to reduce weight in the system, but the changes also support a corrosion resistant design. When metal

components are used, they are made of either titanium-6Al-4V (ELI grade) or alloy 625, both alloys which are, by themselves, highly corrosion resistant in seawater, and galvanically compatible with each other. Great effort has been made to electrically isolate these materials from the hull to minimize the possibility of galvanic corrosion. Where isolation is impractical, for example on the outboard electronics bottles, physical separation and painting of the titanium are used to minimize the effect. The titanium is also anodized to AMS 2488 and epoxy coated with MIL-P-24441 to minimize galvanic corrosion effects. The electrical hull penetrators are made from a combination of nickel-copper alloys 400 and K-500, which have proven to be corrosion resistant and to cause no adjacent corrosion problems on the previous versions of WAA. A long life sacrificial aluminum cathodic protection system has been designed, with improved emphasis on uniform current distribution, Figure 4. Anodes had to be fit into spaces close around the active array area to provide protection to the steel hull in this area without placing them inside the area where they would act as acoustic shorts, creating some tight geometrical configurations, Figure 5.

Component Cross-Sections and Materials - Mounting details for the hydrophones, damping tiles, and noise baffles are shown in Figure 6. Notice that all materials are non-metallic except the fasteners, which are titanium-6Al-4V ELI. The noble titanium-6Al-4V ELI is not electrically coupled to any other metals. All metals in the array are coated with an epoxy anti-corrosion paint and an anti-foulant.

The VIMs that hold the array support plate are shown in Figure 7. Rubber electrically separates the titanium-6Al-4V ELI stress rings on the array support plate from the rest of the structure. The VIM and bolts are all titanium-6Al-4V ELI as is the foundation. All metals are carefully electrically isolated from the hull by the use of G-10 fiberglass spacers and washers and by heat-shrinkable tubing around the bi-metallic studs. The studs themselves are HY-80 steel bases with alloy 625 threads and titanium-6Al-4V ELI nuts and washers. Titanium is galvanically compatible with the alloy 625, and these materials are prevented from causing galvanic corrosion of the stud bases by the hull-mounted cathodic protection system and by the limited access of oxygen into the area of the stud bases. Since neither the steel nor the alloy 625 are prone to significant crevice corrosion, this is not an issue under the heat-shrinkable tubing around the studs.

The design of the snubber assemblies, shown in Figures 8 and 9, is a mixture of the above two concepts. The array support mounted portion of the snubber is all titanium-6Al-4V ELI and electrically discontinuous from any other metals, while the hull mounted portion, which is also titanium-6Al-4V ELI, is electrically isolated from the hull in the same way as the VIMs.

Figure 10 shows the complex mounting of the outboard electronics bottles. The bottles and associated fasteners are all made from titanium-6Al-4V ELI. Although some portions of the fastening system are electrically isolated, the bottles and those fasteners directly attached to them are electrically shorted to the hull through the electrical signal ground wires internal to the bottles. Galvanic corrosion of the hull from this connection

is minimized by the lack of a seawater path through the baffle plates and by the cathodic protection system anodes mounted on the hull nearby. Electrical connectors that attach to these bottles, Figure 11, are also made from the titanium-6Al-4V ELI.

Nickel-copper alloys 400 and K-500 are used for the electro-optical through-hull penetrator, shown in Figures 12 and 13. These materials, although not as corrosion resistant as titanium or alloy 625, have proven to last well in previous WAA applications because they receive cathodic protection from the hull and associated sacrificial anodes. The nickel-aluminum bronze and nickel-copper K-500 connectors that attach to this penetrator, Figure 14, are protected in the same fashion.

Cathodic Protection Design Lifetime Calculations - The assumptions used in the cathodic protection design calculations were as follows:

Life (hardware):	15 years with normal maintenance 30 years with refurbishment
Life (anodes):	2 years minimum; replacement when strap exposed (per ref. 1) (roughly 79% consumption for an AHC-10). Longer lifetimes are desired if anodes are to be placed in areas difficult to access.
Cathodic current:	2 mA/ft^2 (painted steel) (per ref. 1) 15 mA/ft^2 (uncoated metals) (per ref. 1)
Anode area ratios:	1 ft2 anode per 400 ft^2 painted steel (per ref. 1) 1 ft2 anode per 50 ft^2 uncoated metal (per ref. 1)

As a derived requirement, WAA anodes must provide cathodic protection to the portion of the ship's hull shielded by the fairing.
MIL-A-24779 aluminum anodes may replace MIL-A-18001 zinc anodes one for one per current Navy practice on surface ships.

Tables 1 and 2 list each of the metallic materials that are electrically coupled to the hull under the WAA fairings, and which will therefore receive protection current from the anodes, both for the latest design and for the design used on SSN-710. Table 1 shows the total surface area of painted metals in the latest design to be 597.4 ft^2, and the total surface area of uncoated metals to be 24.9 ft^2. Table 2 shows that the total surface area of painted metals on the SSN-710 design was 1116.9 ft^2, and the total surface area of uncoated metals was 41.1 ft^2.

Anode Areas Needed for Latest Design

	Area, ft^2	per ft^2	total anode ft^2	protection current required, mA
Painted Metal	597.4	1/400	1.5	1194.8
Uncoated Metals	24.9	1/50	0.5	373.5
Total			2.0 ft^2	1568.3 ~ 1.6A

For comparison, the current required for the SSN-710 design was significantly higher, about 10A.

A minimal design for the latest system would provide 2.0 ft^2 of anode surface area. To get this area requires 4.0 AHC-10 anodes (at 0.5 ft^2 per anode), or 6 AHC-10 anodes (at 0.3 ft^2 per anode) if they are cut down to 4-inches width, which is required for the anodes to fit into the available space.

An AHC-10 anode has a minimum weight of 8.7 lb, of which roughly .85 lb is due to the steel core. This leaves 7.85 lb of aluminum. If the anode is to be replaced when 75% of this aluminum is consumed, each anode has 5.89 pounds of usable aluminum. The reduced width anodes have roughly 2/3 this amount of aluminum, or 3.93 pounds.

The minimal design which incorporates 6 cut-down anodes therefore has 6 X 3.93 = 23.5 pounds of usable aluminum. For this amount of aluminum to supply the required 1.6A current, at an efficiency of 87% or 0.000850 lb/A-hr (7.45 lb/A-yr), Faraday's Law calculations indicate a lifetime for the minimal design of 1.98 yr.

The new WAA design actually implemented uses 18 cut-down AHC-10 anodes and 11 full-size AHC-10 anodes, for a total of 18 X 3.93 + 11 X 5.89 = 135.5 pounds usable aluminum. Faraday's Law calculations indicate a lifetime for the latest design of 11.36 yr. Given the difficulty of inspecting or replacing certain of the anodes under the fairings, and assuming a safety factor of two, this lifetime should be sufficient to last between major array support plate removals.

A two-year inspection was performed on the SSN-710 WAA installation. Theoretically, after 2 years anode depletion of 2/15=13.3% should be observed. The actual anode depletion observed was 15-28%, slightly higher than should be the case for that design at this point in time, but in good agreement given the inaccuracy in estimating anode depletion.

The minimal 6-anode configuration does not take into account the distribution of the protection current. The WAA configuration encloses a narrow channel of water which is additionally filled with components and acoustic tile to give a small effective seawater cross-section for the ionic component of the protection current to flow through. This restricted seawater path cross-section leads to a high seawater resistance to current flow, and therefore to large potential gradients. This makes it difficult to "throw" protection current very far from each anode. The ADM array used only a few anodes, and experienced corrosion problems due, in part, to inadequate current distribution. The EDM array used many more anodes than required for a minimum design to increase lifetime to 15 years, and current distribution problems were greatly reduced. The latest design incorporates fewer anodes than in the EDM design, but more than required for a minimal design, and gives an estimated lifetime of about 11 years.

Placement of anodes in the WAA is restricted, since they constitute an acoustic short if they are located under the array support plate. Anodes placed under the edges of the array support plate near the snubbers or under the transition fairings cannot be easily accessed, since the array support plate and these fairing sections are seldom removed. The best that can be done is to provide as many anodes as possible around the array support plate edges to aid in current distribution. The use of more anodes also will increase time required between anode inspections/replacements for the hard-to-access areas. Computer modeling could be used to evaluate the current distribution from the latest anode placement, and we have the in-house expertise to perform this type of analysis, but the results would likely indicate that anodes are required under the center of the array support plate, where they cannot be put for acoustic reasons. It is unlikely that any improvement in anode placement could be effected by the use of computer analysis.

One technique that could be used to improve the current distribution difficulties would reduce the current demand throughout the under-fairing area and reduce the amount of protection required at the metal remote from the anodes. This technique is the use of flame sprayed aluminum. Extensive investigations at NSWC and performance history on surface ships both show that flame sprayed aluminum is very effective, and there are no adverse affects of its use even if it were not to perform as expected. Flame sprayed aluminum has not been used on submarines before, and so there is a natural reluctance towards its use in this application.

CONCLUSIONS

The new WAA design uses significantly less metal, and most metal used is not electrically coupled to the hull. Titanium-6Al-4V ELI and alloy 625 have been used throughout the design to minimize corrosion. A long life cathodic protection system using sacrificial aluminum anodes has been designed with an emphasis on current distribution within the limited spaces inside the WAA. This new design should have improved corrosion performance over the previous two versions of the WAA.

REFERENCE

Naval Ships Technical Manual, Chapter 633, Cathodic Protection, S9086-VF-STM-010/CH-633, Sept 1993.

Table 1
AN/BQG-5A(V)1 MATERIALS COUPLED TO HULL AND SURFACE AREAS

PART DESCRIPTION	NO.	MATERIAL	ORGANIC COATING	AREA, EA, in^2	AREA, ALL, in^2	AREA, ALL, ft^2
hull	1	steel	yes	81343	81343	564.9
VIM stud base	116	steel	yes	1.47	171	1.2
snubber stud base	12	steel	yes	1.47	18	0.1
anode stud base	58	steel	yes	0.59	34	0.2
baffle stud base	128	steel	yes	0.59	76	0.5
VIM stud threads	116	alloy 625	no	10.3	1195	8.3
snubber stud threads	12	alloy 625	no	10.3	124	0.9
anode stud threads	58	alloy 625	no	3.53	205	1.4
baffle stud threads	128	alloy 625	no	3.53	452	3.1
5/8" nuts	128	titanium	no	3.93	503	3.5
3/8" nuts	186	titanium	no	2.06	383	2.7
5/8" washers	256	titanium	no	1.57	402	2.8
3/8" washers	372	titanium	no	0.88	327	2.3
OBE bottles	16	titanium	yes	212	3392	23.6
OBE connector, small	16	titanium	yes	8.25	132	0.9
OBE connector, large	16	titanium	yes	19.63	314	2.2
EOHP	1	Ni-Cu K-500	yes	134	134	0.9
coupling ring	1	Ni-Al-Bronze	yes	10.6	11	0.1
EOHP connectors	8	Ni-Cu 400 & Ni-Al-Bronze	yes	50.27	402	2.8
TOTAL COATED					86027	597.4 ft^2
TOTAL UNCOATED					3591	24.9 ft^2

Table 2

AN/BQG-5 (EDM) MATERIALS COUPLED TO HULL AND SURFACE AREAS

PART DESCRIPTION	NO.	MATERIAL	ORGANIC COATING	AREA, EA, in^2	AREA, ALL, in^2	AREA, ALL, in^2
3/8 stud cluster	3	Ni-Cu 400	yes	2.2	6	0.0
5/8 stud cluster snubber	1	Ni-Cu 400	yes	2.2	2	0.0
3/8 stud cluster	2	Ni-Cu 400	yes	8.2	16	0.1
3/8 stud cluster	5	Ni-Cu 400	yes	4.3	22	0.1
3/8 stud cluster	6	Ni-Cu 400	yes	1.2	7	0.0
3/8 stud cluster	2	titanium	yes	3.8	8	0.0
3/8 stud cluster	3	titanium	yes	1.6	5	0.0
3/8 stud cluster	10	titanium	yes	6.5	65	0.5
5/8 stud cluster snubber	1	titanium	yes	1.9	2	0.0
7/8 stud cluster	3	Ni-Al-bronze	yes	43	129	0.9
Electric Hull pen	2	Ni-Cu 400	yes	142	284	2.0
Acoustic, SCPL outer	1	alloy 625	yes	1945	1945	13.5
Acoustic, SCPL outer	1	steel	yes	19200	19200	133.3
Acoustic, SCPL outer	1	steel	yes	15800	15800	109.7
Acoustic, SCPL inner	1	steel	yes	19200	19200	133.3
Acoustic, SCPL inner	1	steel	yes	17500	17500	121.5
hull	1	steel	yes	81343	81343	564.9
EHP cable support	2	CRES	yes	72	144	1.0
OBE bottles	64	titanium	yes	80.5	5152	35.8
7/8 stud cluster	4	alloy 625	no	147.2	589	4.1
7/8 stud cluster	4	Ni-Cu 400	no	83.4	334	2.3
7/8 stud cluster	4	titanium	no	43.2	173	1.2
7/8 stud cluster	2	alloy 625	no	63.8	128	0.9
7/8 stud cluster	8	Ni-Cu 400	no	42	336	2.4
7/8 stud cluster	2	titanium	no	19.2	38	0.3
7/8 stud cluster	10	alloy 625	no	43.2	432	3.0
7/8 stud cluster	6	titanium	no	20	120	0.8
7/8 stud cluster	4	titanium	no	4.4	18	0.1
7/8 stud cluster	2	alloy 625	no	17.6	35	0.2
7/8 stud cluster	2	Ni-Cu 400	no	18.4	37	0.3
7/8 stud cluster	2	titanium	no	14.4	29	0.2
7/8 stud cluster	8	alloy 625	no	24	192	1.3
7/8 stud cluster	12	Ni-Cu 400	no	14	168	1.2
7/8 stud cluster	8	titanium	no	10	80	0.6
7/8 stud cluster	4	alloy 625	no	30	120	0.8
7/8 stud cluster	4	titanium	no	11.6	46	0.3
3/8 stud cluster	4	alloy 625	no	6	24	0.2
3/8 stud cluster	10	alloy 625	no	10.6	106	0.7
7/8 stud cluster	3	alloy 625	no	9	27	0.2
3/8 stud cluster	1	alloy 625	no	3.5	4	0.0
3/8 stud cluster	1	alloy 625	no	4.3	4	0.0
5/8 stud cluster snubber	1	alloy 625	no	5.9	6	0.0
7/8 stud cluster	3	Ni-Cu 400	no	10	30	0.2
Acoustic, SCPL inner	1	alloy 625	no	734	734	5.1
Acoustic, SCPL inner	1	Ni-Cu 400	no	1224	1224	8.5
Acoustic, SCPL outer	1	Ni-Cu 400	no	298	298	2.1
Acoustic, SCPL outer	1	titanium	no	592	592	4.1
TOTALS COATED					160830	1116.9 ft^2
TOTALS UNCOATED					5923	41.1 ft^2

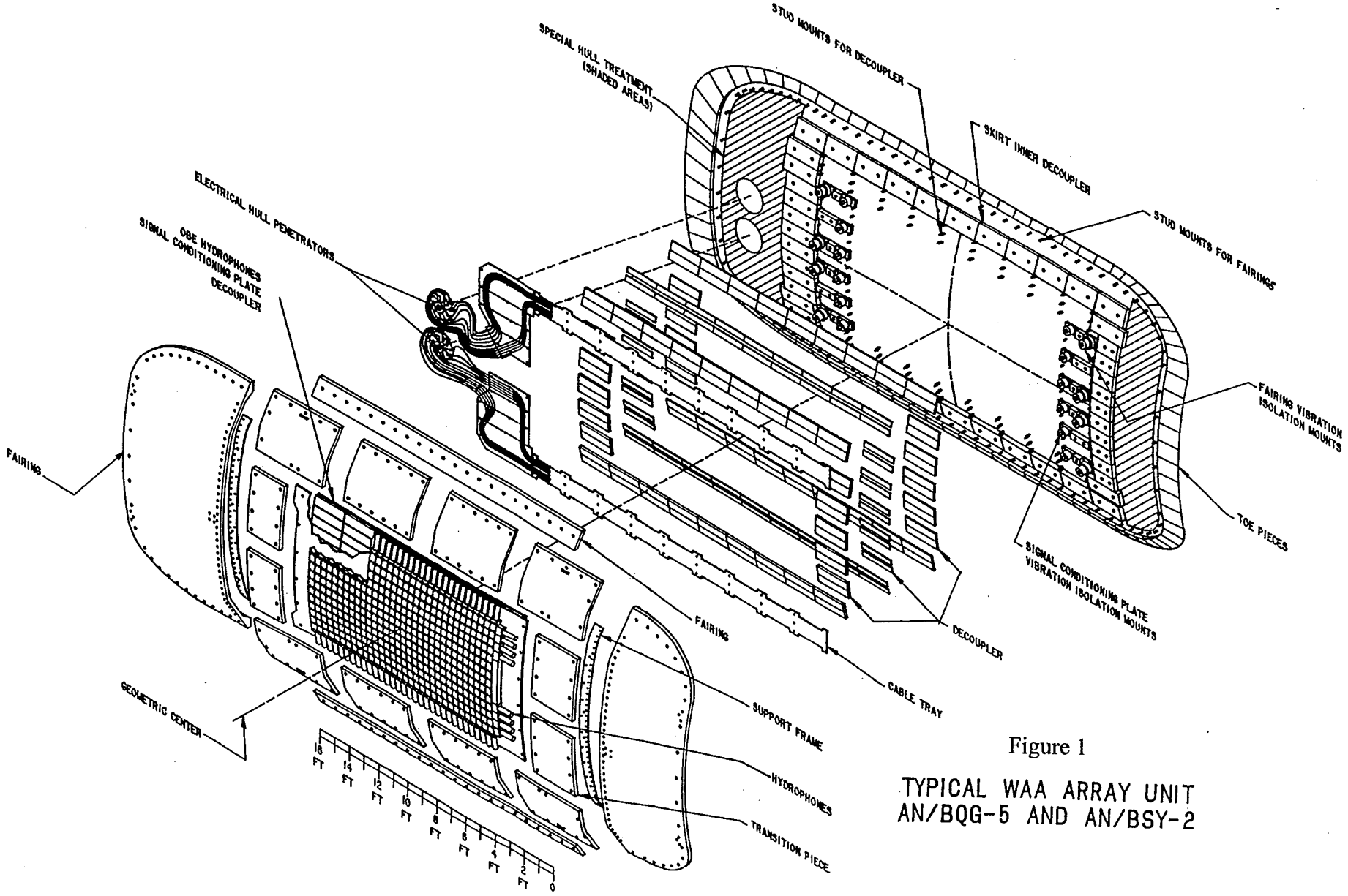

Figure 1

TYPICAL WAA ARRAY UNIT
AN/BQG-5 AND AN/BSY-2

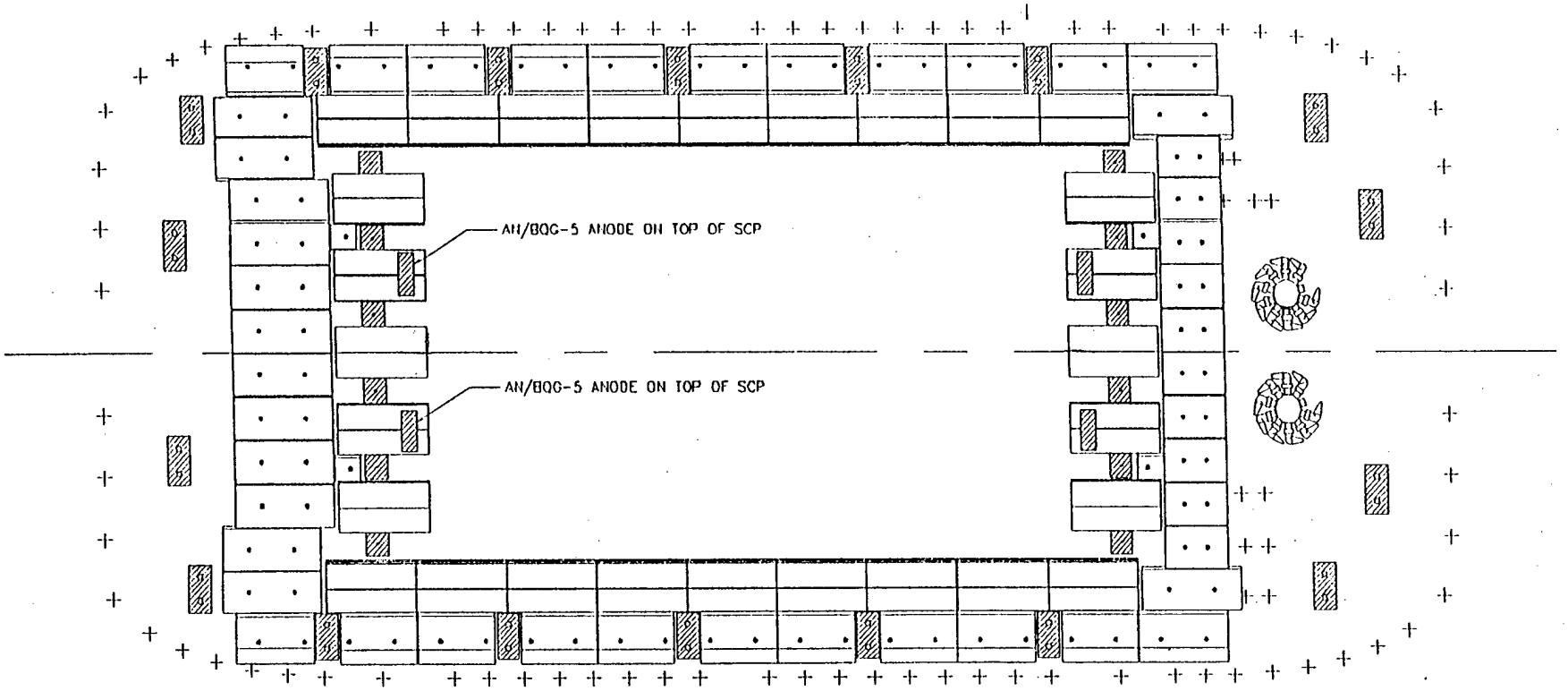

Figure 2

AN/BQG-5 WAA
SACRIFICAL ANODE LOCATIONS

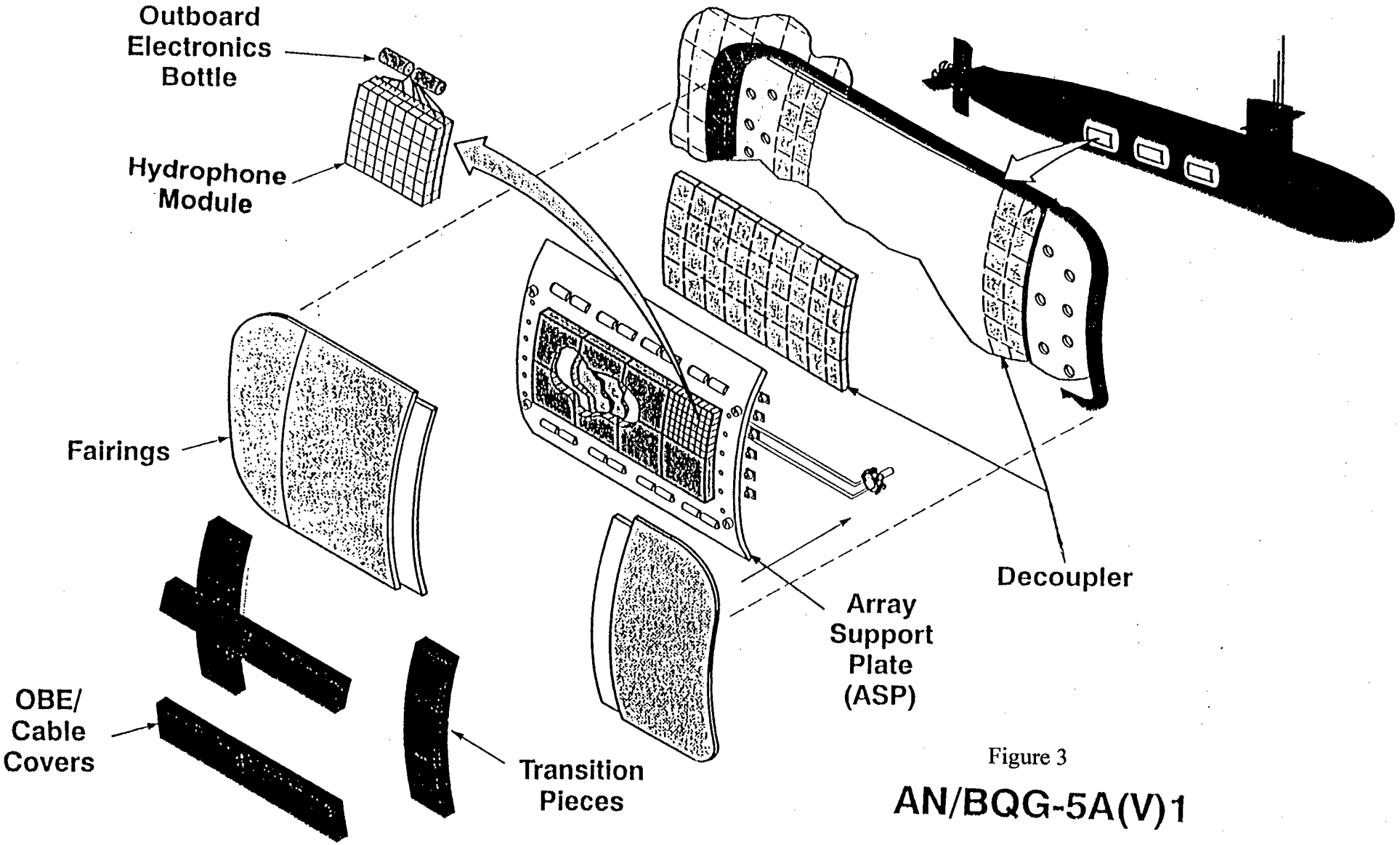

Figure 3

AN/BQG-5A(V)1

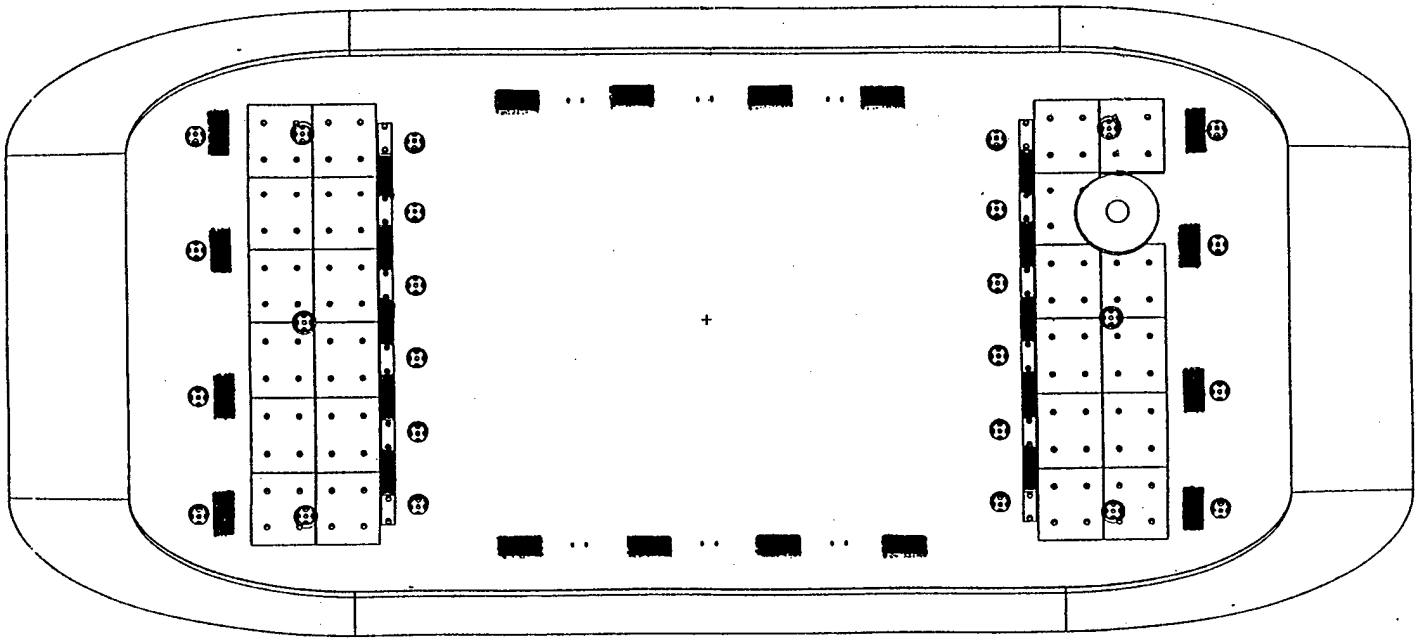

Figure 4

AN/BQG-5A(V)1 ANODE LOCATIONS

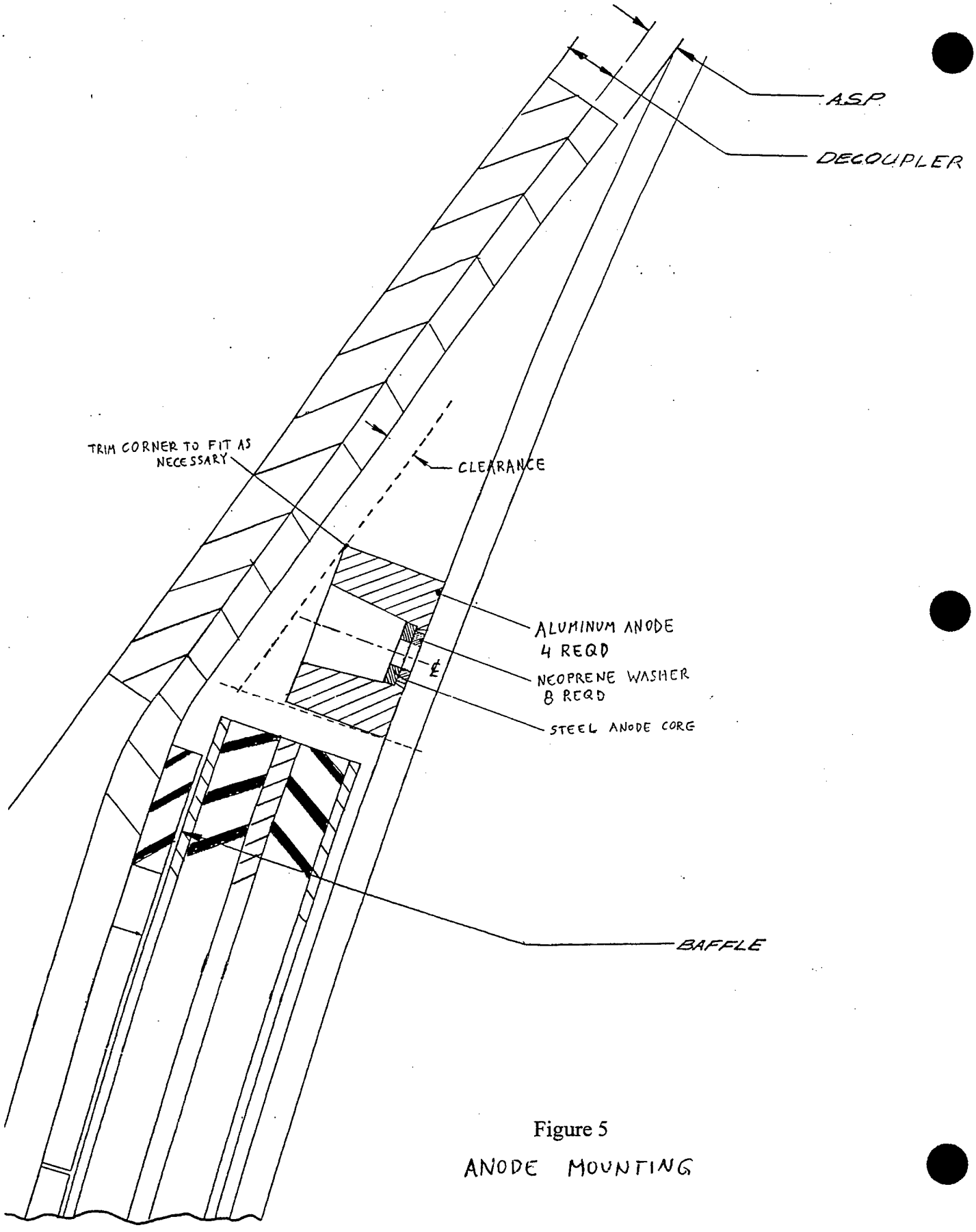

Figure 5

ANODE MOUNTING

Figure 6

HYDROPHONE MOUNTING

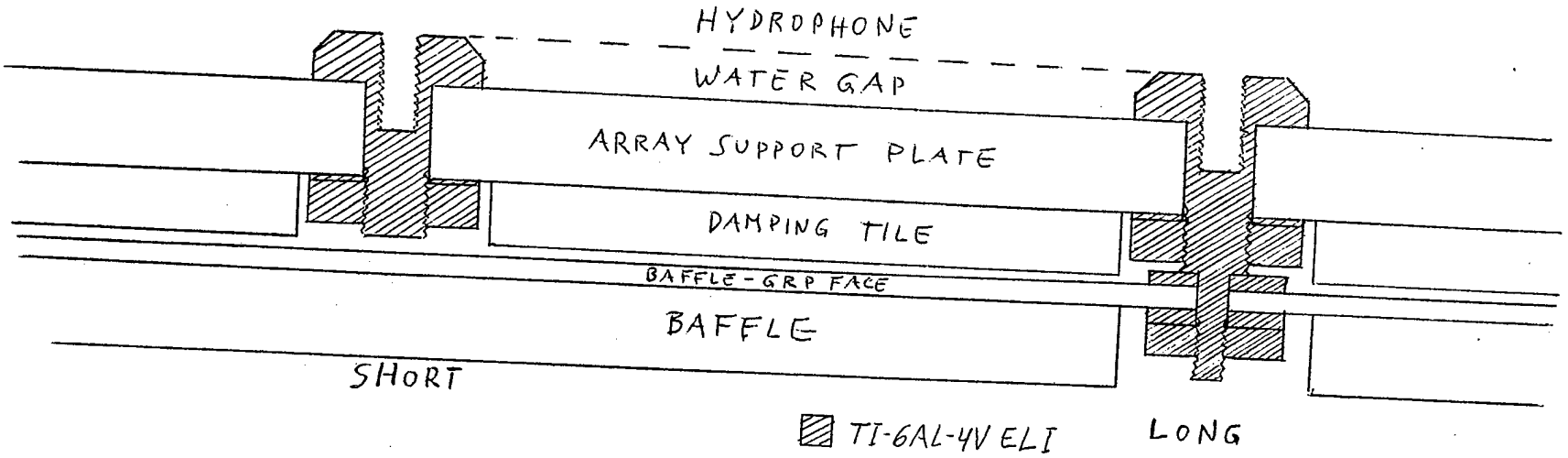

Figure 7
VIM MOUNTING

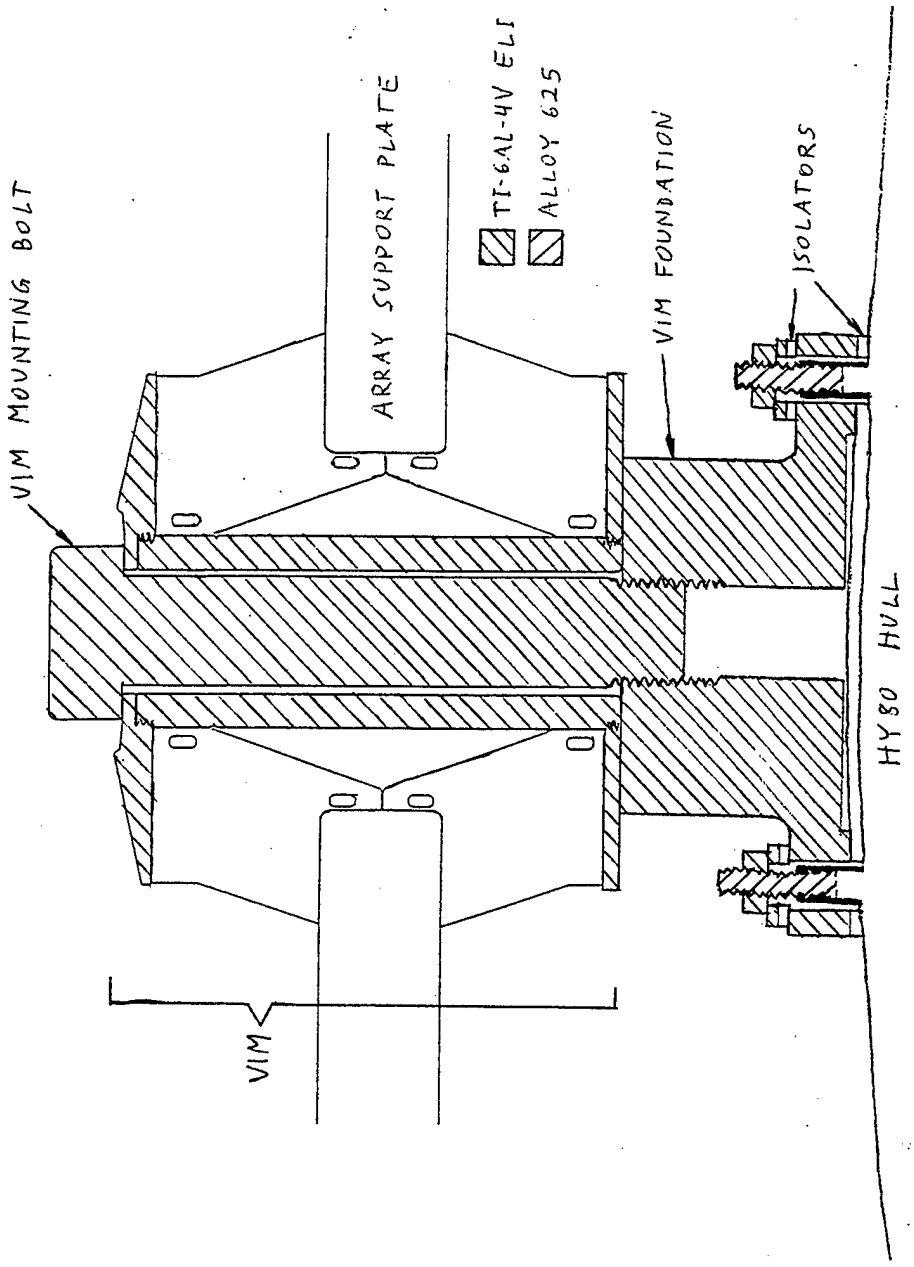

Figure 8

SNUBBER MOUNTING

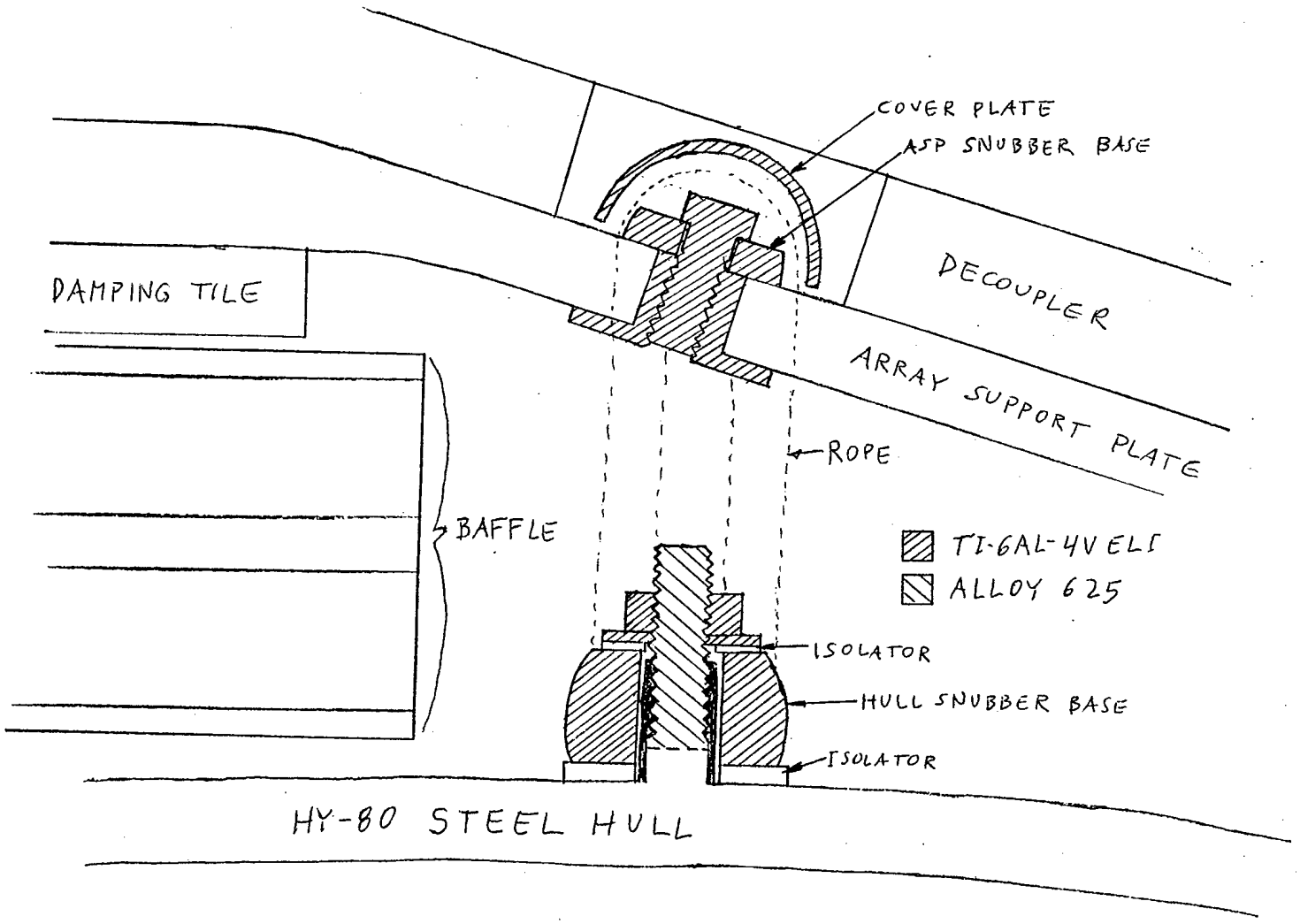

Figure 9

SNUBBER MOUNTING

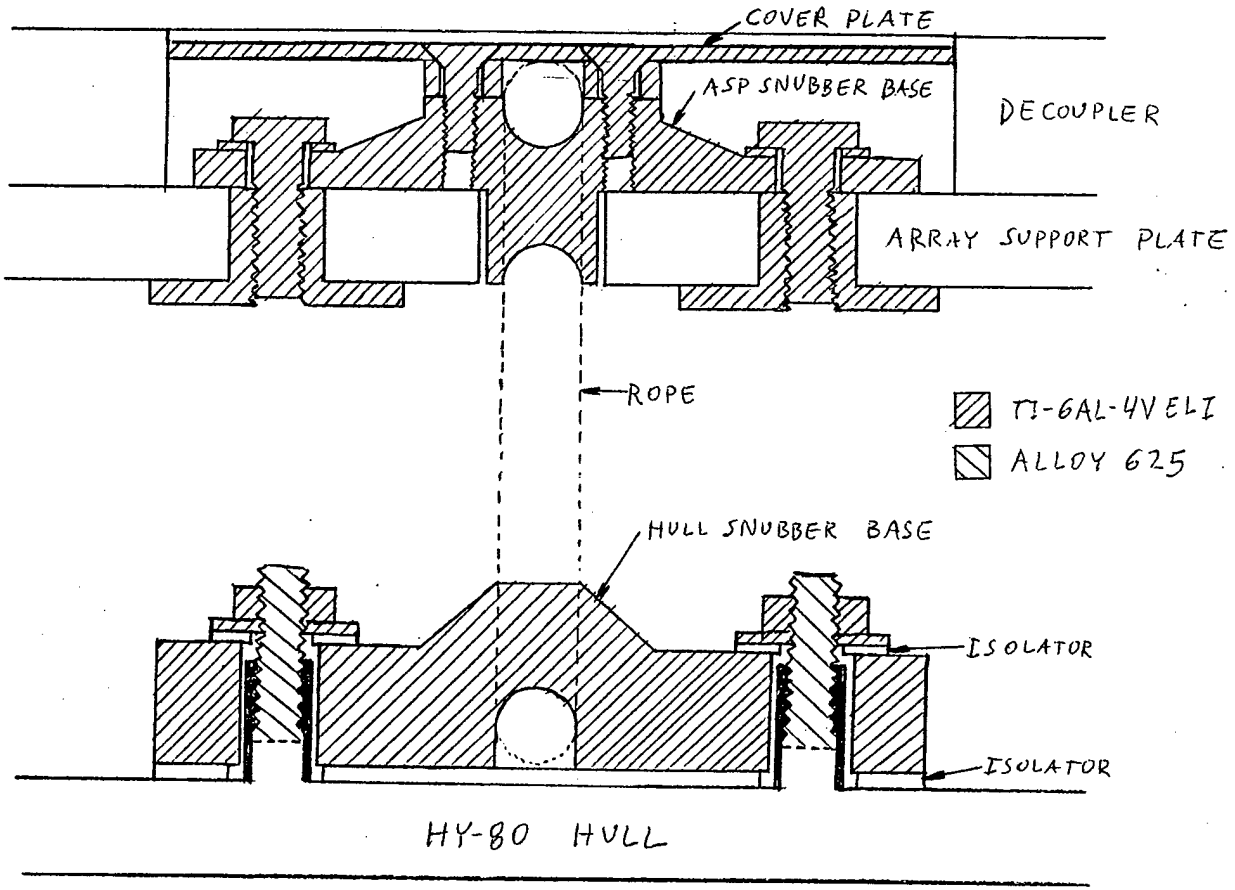

Figure 10

OBE BOTTLE MOUNTING

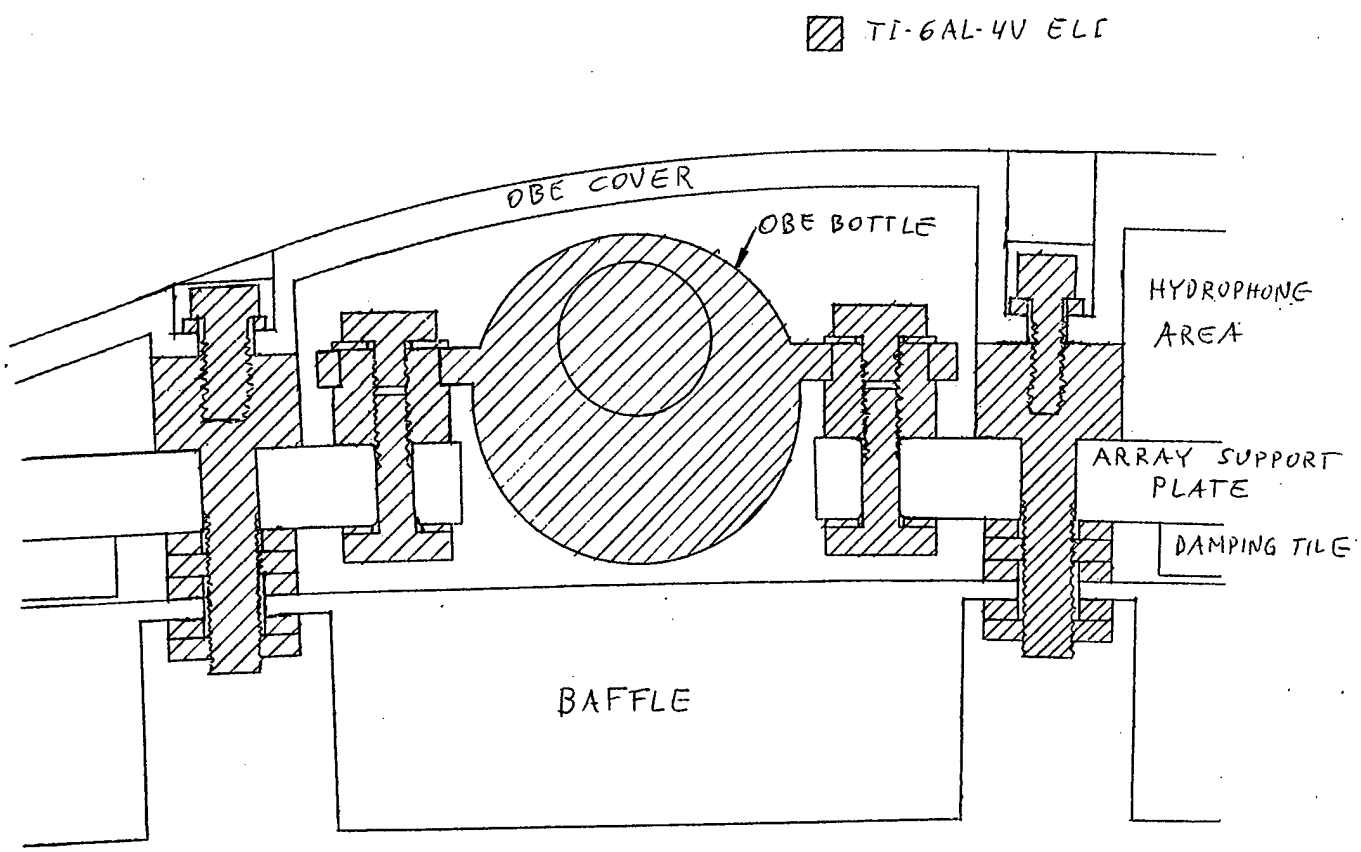

Figure 11

OBE ELECTRO-OPTICAL CONNECTOR

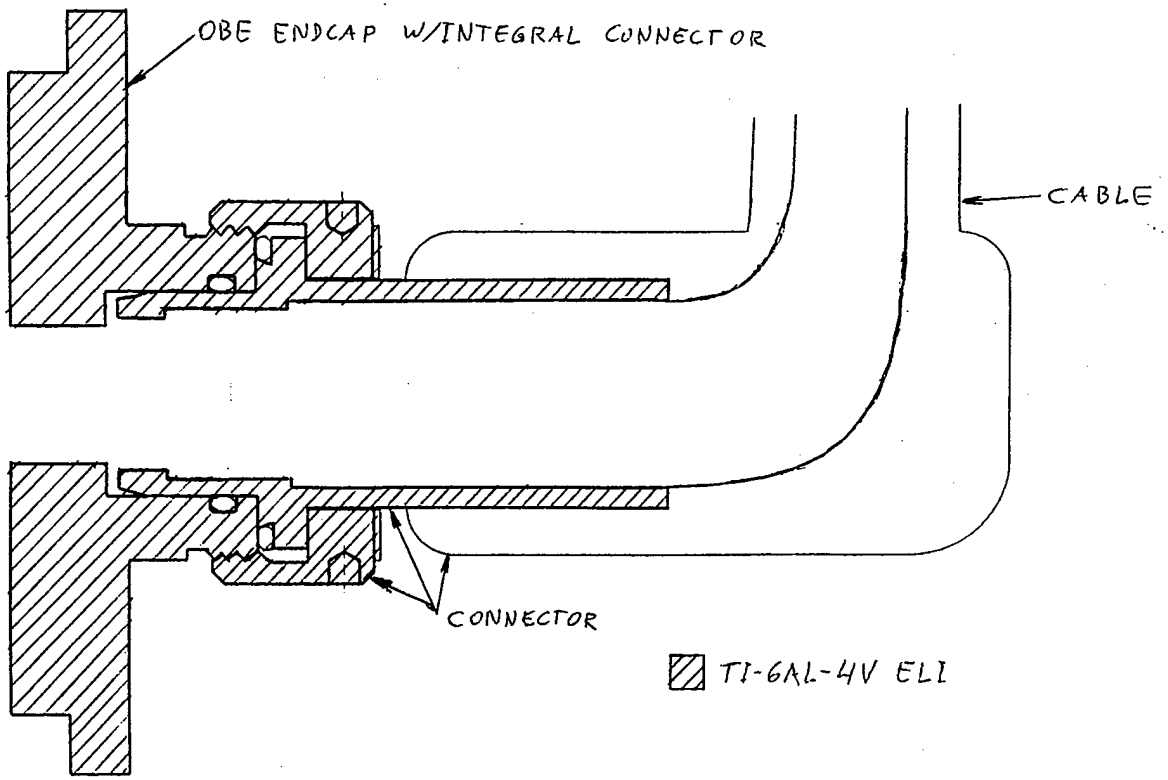

Figure 12

ELECTRO-OPTICAL HULL PENETRATOR AND CONNECTORS

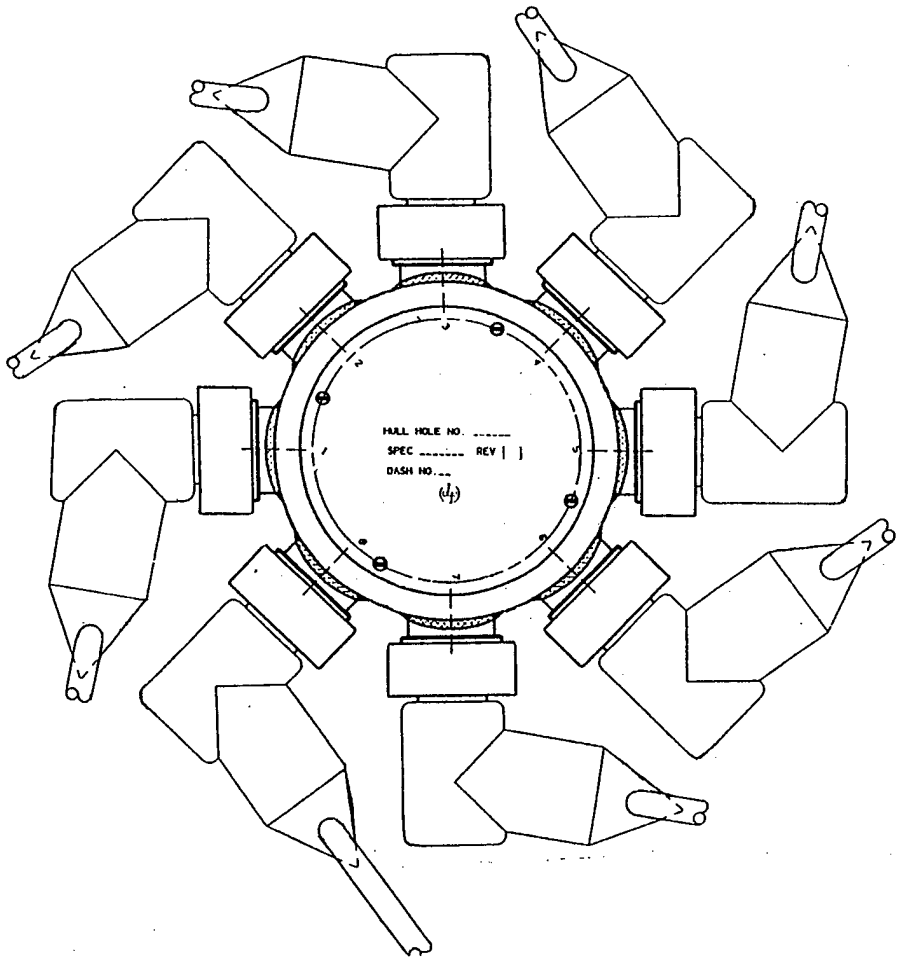

Figure 13

ELECTRO-OPTICAL HULL PENETRATOR

CROSS SECTION

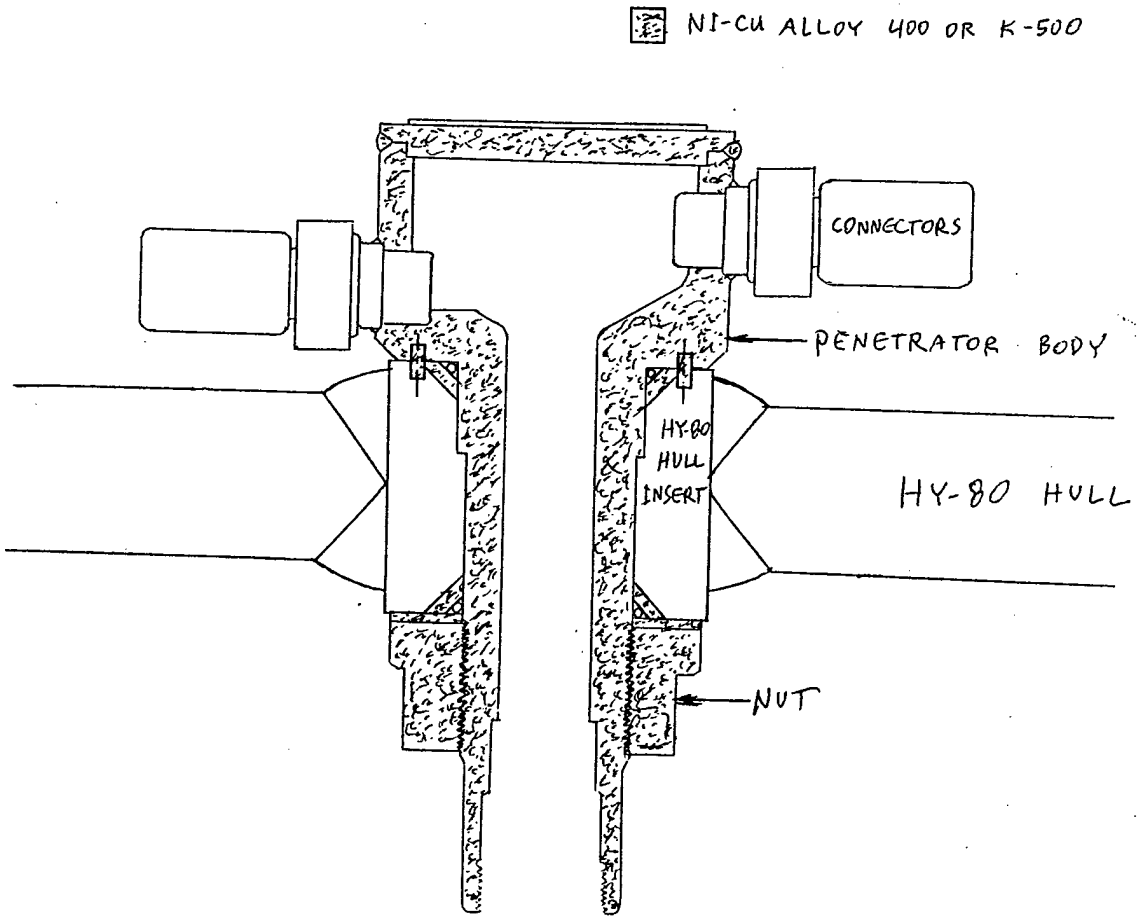

Figure 14

HULL PENETRATOR ELECTRO-OPTICAL CONNECTOR

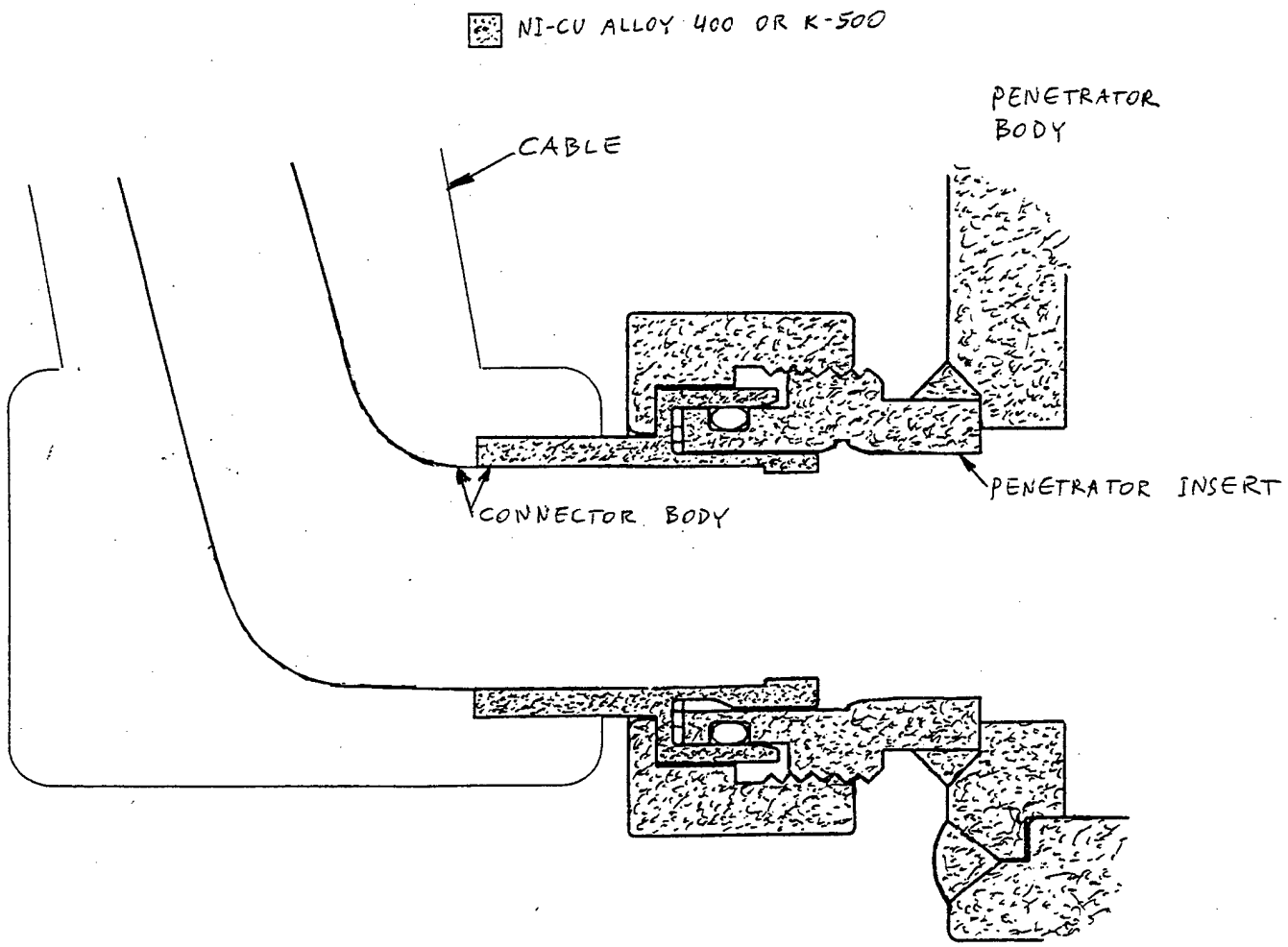

Inhibition of Microbiologically Influence Corrosion

P. M. Natishan[1], J. Jones-Meehan[1], G. I. Loeb[2], N. Gray[2],
B. J. Little[3], R. Ray[3], and M. Beard[4]

Naval Research Laboratory[1]
Washington, DC

American University [2]
Washington, DC

Naval Research Laboratory [3]
Stennis Space Center, MS

Naval Surface Warfare Center
Carderock Division[4]
West Bethesda, MD

ABSTRACT

Two areas of work designed to provide a better understanding on the nature of microbial colonization of surfaces and microbiologically influenced corrosion are discussed. The first approach examined a mechanical sensing model to describe microbial colonization. Results obtained after the exposure of a group polydimethylsiloxane polymers to an estuary environment provide support for this model. The second approach sought to determine if there is a relationship between microbial colonization of certain metallic substrates and corrosion. Exposure of zirconium, chromium, niobium, tantalum, molybdenum, tungsten and 4340 steel to Postgate medium with 2.5% NaCl and sulfate reducing bacteria (SRB) resulted in biofilms being formed on all samples. In the case of the zirconium, chromium, niobium, and tantalum samples, the weight loss after two years of exposure was negligible.

INTRODUCTION

Bacteria and other microorganisms attach and colonize the surface of metals that are exposed to aquatic environments and form biofilms [1-6]. The physical presence and metabolic processes of the microorganisms in the biofilm produce chemical changes at the biofilm/metal interface. In particular, the biofilm alters the dissolved oxygen concentration, pH, and the concentration of organic and inorganic species at the metal surface. These changes, in turn, alter the electrochemical characteristics of the metal and thereby influence its corrosion behavior. This process is referred to as microbiologically influenced corrosion (MIC). Biofilm formation resulting in MIC has been recognized by the engineering community as a significant factor in reducing the useful lifetime of equipment [2-5].

It is well known that microorganisms can change their surface characteristics in response to changes in the environment [6-9]. For example, it has been demonstrated that physiological differences exist between the sessile and planktonic cells of the same

bacterium[6-9]. The characteristic that is emphasized here is the exceptional ability of microorganisms to respond to environmental stimuli. The exact nature of the stimulus/stimuli that trigger phenotypic changes in microorganisms allowing them to become irreversibly adsorbed onto metal surfaces is not totally clear and could be chemical and/or physical in nature. This paper summarizes the research, to date, on two areas of work that were designed to provide a better understanding of colonization on surfaces and provide means to prevent the colonization which can lead to biofouling and/or MIC. The first approach discussed is based on an assumption that the major prerequisite for microbial colonization is a solid surface. The second seeks to determine if there is a relationship between microbial colonization, the type of metallic substrate, and corrosion. This paper reviews results presented elsewhere [10,11].

Dimethylsilcones and the Mechanical Sensing Model

Microbes do not colonize all surfaces equally, but exhibit preferences among immersed materials. There are two classes of materials which seem to be much more effective than others in resisting colonization: the dimethylsilicones (DMS) and the polyethylene oxide (PEO) linear polymers. The monomeric units of which these polymers are composed are quite different in their properties. DMS is a hydrophobic material with exposed methyl groups, while the PEO chain is a hydrophilic material due to the exposed ether oxygen atoms present in every monomeric unit, and which are hydrogen bonding sites available for interaction with water. The difference implies that if there is a common mode for preventing attachment by these materials, it must lie in the properties of the polymer as a whole. There is a group of properties of these polymers which is shared: it is their chain mobility and consequent high configurational entropy, and low resistance to deformation of the polymer chains at the material surface.

Belas et. al. [12] have shown that certain marine vibrio bacteria, which can be cultured in either a liquid medium or on a solid gel surface, change form depending on the situation. This change is quite dramatic with the cells from liquid medium having flagellae at one end with which they swim; while cells from a solid medium have lateral flagellae which grow out from a large number of sites along the lateral surface of the cells. The change between these forms is controlled by the activation of a particular set of genes when the organism senses that it is on or close to a surface. The only stimulus which has been found to induce this change (other than the presence of a surface) is a great increase in the viscosity of the medium in the presence of low iron concentrations[13]. Thus, it appears that a mechanical sensing mechanism is involved. There are many mechanical sensory cells known in biology and they seem to operate in the same way. That is, a deformation of the cell membrane causes a change in the ionic currents across it, which are controlled by membrane pore structures. In addition to this mechanism having been found in sensory cells whose function is to sense mechanical stimuli, recent reports indicate that this phenomenon is more general. Cells which normally function in a coherent tissue require a surface on which to grow if they are to function properly. These cells are called "anchorage dependent". Their functioning seems to depend upon their approaching a surface suitable for them (upon which they lose their rounded liquid-medium shape) and spread out to a much flatter cell with an increased number of attachment points to the immersed surface. Surfaces upon which strong attachment points do not seem to form do not lead to the change in cell shape which is correlated with their normal functioning. Leonid Margolis and co-workers [14-16] reported that attachment of animal tissue cells to such surfaces causes a change in the ratio of cellular ionic fluxes, so that the internal pH of cells changes when they accomplish proper attachment.

Thus, a signal dependent on the stressing of the cell membrane, thereby affecting membrane ion flux, appears to be required for the transformation of anchorage-dependent cells into their characteristic form for normal function on a surface or in a tissue. A surface which has very little tendency to induce such changes in cells is poly-DMS.

Metals

When a bare metal is exposed to a saltwater environment, it interacts electrochemically with the environment. The result is that metal ions can be present in the near surface region at concentrations greater than in the bulk aqueous environment. It has been observed that many microorganisms are able to sense and move toward nutrients and other attractants while moving away from harmful substances or other repellents. Movement toward chemical attractants and away from repellents is known as chemotaxis. Microorganisms can respond to very low levels of attractants on the order of 10^{-8} molar with the magnitude of the response increasing with attractant in this low concentration range[17]. Thus, it might be expected that metal ions produced by the anodic reaction and which microorganisms need as metabolites could attract microorganisms to the metal surface and/or stimulate or trigger attachment of the microorganisms leading to biofilm formation. MIC has been documented for metals exposed to sea water, fresh water, process chemicals, food stuffs, soils, aircraft fuels, human plasma, and sewage. The surface to which microbes attach plays a major role in biofilm processes during biofilm accumulation[4]. SRB may initiate anodic processes on metal surfaces by direct contact in a biofilm or by-products of bacterial metabolism (i.e. hydrogen sulfide) can contribute to corrosion processes. The purpose of this work is to compare biofilm development on pure metallic substrates using environmental scanning electron microscopy (ESEM) to characterize the topography of the wet biofilm. Weight loss measurements were done to evaluate whether metallic corrosion had occurred after a 2 year exposure to marine, SRB consortia.

EXPERIMENTAL

Dimethylsilcones

Two candidate silicone formulations (PEG-015 and PEG-060) were purchased from United Technologies. PEG-015 and PEG-060 are polydimethylsiloxane polymers with the 15 and 60 designations referring to chain length before catalytic cross-linking (polymerization). Films of varying rigidity were prepared by mixing the two liquid components, a prepolymer and a catalyst, in varying ratios (by weight). The films of varying rigidity were used to examine the significance of the mechanical sensing mechanism in regard to microbial attachment

Samples were cut from a 1 inch in diameter rod of type 4340 steel in segments that were 1/2 inch in thickness and were polished to a 600 grit finish. The samples were then coated with either the PEG-015 or PEG-060 using a mold technique. A mold was made and placed around the polished face and the PEG compounds were poured into the mold and allowed to dry. The thickness of the coatings ranged from 230 to 850 μm. Film thickness was measured by light section microscopy, making a refractive index correction by comparison with a sample of a silicone film cast on a microscope slide thick enough to be measured with a micrometer.

Silicon coated 4340 steel samples were also prepared by dip coating. Rectangular coupons (0.75" by 2") with a 600 grit surface finish were suspended in the liquid resin and withdrawn vertically using an electric motor at a rate of 1 mm per minute. Coupons were hung to cure in an air-conditioned room at 25° until the residual liquid in the mixing cup became rigid, usually 24 hours. Coating thicknesses ranged from 22 to 60 μm. In initial tests, corrosion occurred at the edges of the dipped sample due to thinning of the coatings at the sharp edges. After dipping and curing, samples were then held in contact with a small amount of additional liquid resin in a trough to cover the edges and these additional portions of polymer were allowed to cure. This process provided a very thick (1-2 mm) covering of polymer at the edges of the samples. Samples were then examined in abiotic electrochemical tests. Also, silicone samples were immersed in the estuary at the Smithsonian Laboratory in Edgewater, Maryland for six weeks.

Abiotic, electrochemical measurements were made in quiescent 0.6M NaCl solution using a three-electrode set-up in a conventional corrosion cell. Samples were immersed in the solution for 24 hours prior to polarization to establish a steady state open circuit potential. Anodic and cathodic polarization curves for treated and untreated 4340 steel samples were determined potentiostatically by stepping the potential in 25 or 50 mV increments from the open circuit potential in the anodic or cathodic direction and allowing the current to reach a steady state value. Usually 15 to 20 minutes were required at each potential. The polarization curves were used to detect defects in the coating. The *ac* impedance measurements were made during a 10 day period in quiescent 0.6M NaCl solution using a conventional corrosion cell. Potentials are reported relative to the saturated calomel electrode (sce).

Exposure of Pure Metals to Sulfate Reducing Bacteria Consortia

MIC has been documented for metals exposed to sea water, fresh water, process chemicals, food stuffs, soils, aircraft fuels, human plasma, and sewage. The surface to which microbes attach plays a major role in biofilm processes during biofilm accumulation[4]. SRB may initiate anodic processes on metal surfaces by direct contact in a biofilm or by-products of bacterial metabolism (i.e. hydrogen sulfide) can contribute to corrosion processes. Multiple samples (1/2" square) of tantalum, tungsten, chromium, niobium, molybdenum, zirconium, and 4340 steel were exposed to either a hydrogenase positive (49Z) or a hydrogenase negative (CG-59) SRB culture, as well as, Postgate medium (Control; no bacteria added). The isolation, maintenance, and characterization of sulfate reducing bacteria (SRB) communities have been described elsewhere [18-21]. The medium used was Postgate's medium with lactate as the electron donor and carbon source. The medium was supplemented with 2.5% (wt/vol) NaCl and the cultures were grown anaerobically at room temperature. Weight loss values were determined to evaluate whether corrosion had occurred after a two year exposure. Samples were also examined using ESEM after one year and after 21 months of exposure to determine the presence of microorganisms and/or the formation of a biofilm.

RESULTS AND DISCUSSION

Dimethylsilcones and the Mechanical Sensing Model

Abiotic Electrochemical Measurements - In initial tests with the dip coated samples, as discussed above, corrosion occurred at the edges of these sample due to thinning of the coatings and bare areas on sharp edges. Defects were readily detected when the samples were immersed in the chloride solution and polarized anodically (i.e. current densities increased as the potential was made more positive). See for example the curve in Figure 1 labeled "PEG Coated Steel Defect in Coating". Also, corrosion was visibly evident at the edges of the sample. These results are important in that they show that the polarization technique could be used to quickly determine the presence of pores or defects.

Figure 1 also shows anodic polarization curves for two 4340 steel samples and two PEG coated steel samples without defects. Anodic polarization curves show that the current density of untreated 4340 steel samples increased as the potential increased (made more positive) indicating general corrosion. However, current densities on 4340 samples with defect-free PEG-015 coatings (produced by dipping) remained very low (less than 0.6 nA/cm^2). Subsequent, examination of the defect free silicone coated 4340 steel surfaces using optical and scanning electron microscopy showed no sign of general or localized corrosion. In contrast, untreated 4340 steel experienced uniform corrosion with some pitting. Visible corrosion was noted on untreated 4340 samples after less than 1 hour of exposure to the chloride solution. Corrosion rates for untreated 4340 steel and nominal corrosion rates for defect-free PEG coated steels are listed in Table 1. Measured current values for PEG coated samples were at the lower detection limit of the potentiostat so that calculated current densities and corrosion rates presented in Table 1 are nominal values. The important point is that defect free PEG coatings were produced in thicknesses of engineering significance and these coatings provided an effective barrier layer that prevented the underlying metal from corroding.

Figure 2 shows polarization resistance values obtained from 4340 steel and 4340 steel coated with PEG-060 immersed in quiescent, 0.6M NaCl solutions for 10 days. These values were determined using *ac* impedance. Impedance results and visual examinations show that the 4340 steel undergoes corrosion shortly after immersion. Polarization resistance values for the silicone coated 4340 steel remain high (10^8 ohm/cm^2) for the 10 day period indicating that the PEG was a good barrier coating i.e. there were no pinholes in the coating and the protective nature of the PEG did not degrade during exposure. A decreasing value of polarization resistance would indicate that ions or water penetrated the coating or that ions were being transported through the film, and that charge transfer reactions were occurring at the coating/metal interface. In general, a polarization resistance value of 10^6 $ohm\text{-}cm^2$ or below indicates a non-protective coating.

Exposure of PEGs to an Estuary Environment - PEG-015 samples were made in four degrees of rigidity by use of different ratios of pre-polymer to cross-linking catalyst. The silicones were then immersed in the estuary at the Smithsonian Laboratory in Edgewater, Maryland for six weeks. The intent of this work was to determine if macroorganisms such as barnacles would attach to the PEG surfaces. No barnacle settlement was observed on the silicone samples but barnacles did settle on the polystyrene rack used to hold the samples during immersion. There was some algal growth starting at the edge of the samples where the silicone samples were in contact with the sample holder. This growth progressed toward the center of the silicone samples. No sample was completely overgrown and all showed a

"clear" area in the central area of the samples. Microscopic observation of the "clear" area showed a sparse population of the remnants of larval tubes of invertebrates such as amphipods, a few nematodes, swarming organisms similar to paramecia, and a few strands of algal forms traversing the surface. All could be easily dislodged from the surface with a dissecting needle, unlike the barnacles, tubeworms, or bryozoans that were firmly attached on the hard surfaces of the test rack. The most significant finding of this work was that when samples were arranged in the order of apparent overgrowth, the order was that more growth was observed on the more cross-linked samples, the least growth on the least cross-linked samples, with the exception of one highly cross-linked surface which remained relatively "clean". This ordering would be predicted by a mechanical sensing mechanism of microbial attachment.

Results of exposure to the estuary waters showed that the degree of colonization by organisms was less on the silicone surfaces than on the rigid surfaces. As mentioned above, a property of silicones which may be pertinent in preventing or inhibiting colonization by microorganisms is the high chain mobility [22-25]. If mobility is very high, there may not be perceptible stresses induced in an attaching organism so that stress-induced change in the membrane ion flux ratio does not occur. In short, the organisms do not know that they are near a solid surface and therefore do not undergo the metamorphical changes necessary for attachment. Another possibility for the resistance to colonization of these materials is that their interaction with the surface of potential colonizing organism surfaces is weak because no strong bonding can occur. This latter idea is supported by the observations in the medical community that stainless steel heart valves polished with stearic-acid resist "fouling" in the blood stream. Baier[25] observed that the polishing process coats the metal with a layer of the long-chain fatty acid, so that the surface presented to the medium is a close-packed layer of terminal methyl groups. This surface was suggested to be responsible for the non-fouling nature of the surface because the clean stainless steel became "fouled" within a short time after implantation. Dimethylsilicone chains also present a surface rich in methyl groups to the environment, so that there is an element of support for this mechanism, especially since the close-packed chains of long-chain fatty acids are not generally considered to be mobile. As other materials bearing methyl-terminated alkyl chains have not proven to be as non-fouling as DMS, it is possible that both factors are involved in the non-fouling phenomenon.

Metals

The metals that were exposed to the media with and without SRB were selected to determine if there is a relationship between microbial colonization, the type of metallic substrate, and corrosion . In general, tantalum, tungsten, chromium, niobium, and zirconium are neither a major or minor nutrient required by microorganisms; molybdenum is used as trace nutrient, and iron (from 4340 steel) is a major nutrient [26]. Results from the two year exposure show that weight loss varied as to whether the greatest weight loss was observed for the samples exposed to the SRB or the Control (no bacteria added to the Postgate's media). Table 1 lists the weight loss where each value is the average for at least two samples. A ranking as to the weight loss (from highest to lowest) for a given substrate in the various media is given below.

steel	49Z > Control > CG59
tantalum	CG59 > 49Z > Control
chromium	CG59 > 49Z > Control
tungsten	Control > 49Z > CG59
molybdenum	Control > 49Z > CG59
niobium	Control > CG59 > 49Z
zirconium	Control = CG59 = 49Z = 0

As can be seen in Table 1, the weight loss for the 4340 steel was clearly highest for samples exposed to 49Z SRB (191.6 mg), whereas, the weight loss in CG59 SRB (94.6 mg) was lower than the weight loss for the Control (136.2 mg). In prior work, dealloying of chromium was observed in 4340 steel coupons exposed to 49Z and CG59 SRB consortia after a 6 month exposure period[19]. For tantalum and chromium there was no weight loss in the Control media and a very small weight loss for the samples exposed to SRB.

Weight loss for the tungsten samples exposed to Control media alone was the next highest weight loss value observed (29.5 mg); while molybdenum samples exposed to Control media had the third highest weight loss value (15.4 mg). These weight loss values were significantly higher than the values observed for the tungsten and molybdenum exposed to the media with SRB. Weight loss for molybdenum samples exposed to the 49Z and CG59 (6.1 and 2.0 mg, respectively) was greater than the weight loss of the tungsten samples exposed to the 49Z and CG59 (2.4 and 0.7 mg, respectively). In the case of niobium, there was a small weight loss for the Control sample and essentially no weight loss for the samples exposed to SRB. Zirconium had the best results in that no weight loss was observed for samples exposed to any of the media.

ESEM was used to characterize the surfaces at one year and at twenty-one months after exposure to the CG59 and 49Z SRB. The ESEM examination showed that all metal samples were colonized to some extent and that patchy biofilms were present. These biofilms were not noticeable by visual examination of the samples.

The highest weight loss values observed occurred for the 4340 steel samples in all media. The next highest weight loss values observed were for the molybdenum. When the weight loss values for the molybdenum and tungsten samples exposed to SRB were compared to the Control samples, the weight loss for the samples exposed to the SRB were significantly less than those of the Control, i.e. there was an inhibitory effect on dissolution. This inhibitory effect was also observed for the 4340 steel exposed to CG59 consortia as compared to the Control. The observation that some SRB cultures can have an inhibitory effect on metal dissolution has been previously reported[27]. With the exception of tungsten exposed to 49Z (2.4 mg weight loss), the weight loss values for tantalum, chromium, niobium, and zirconium were negligible (below 1.0 mg).

SUMMARY

Two candidate polydimethylsiloxane polymers (PEG-015 and PEG-060) were selected to test a mechanical sensing mechanism of microbial attachment. The steel coated with these materials had essentially non-existent corrosion rates, extremely stable anodic and cathodic polarization behavior, and high polarization resistance values. These results show that the silicone compounds produce an effective barrier to abiotic corrosion in 0.6M NaCl solutions. The most significant finding of this work was that, after exposure to an estuary environment, more colonization was observed on the more cross-linked samples and the least growth was seen on the least cross-linked samples, with the exception of one highly cross-linked surface which remained relatively "clean". This ordering would be predicted by a mechanical sensing mechanism.

Environmental scanning electron microscopy (ESEM) characterization of zirconium, chromium, niobium, tantalum, molybdenum, tungsten, and 4340 steel to Postgate's media containing sulfate reducing bacteria (SRB) showed that patchy biofilms formed on all samples. The weight loss for the 4340 steel and the molybdenum were significantly higher

than weight loss for other metallic samples. In the case of the zirconium, chromium, niobium, and tantalum samples, weight loss after a two year exposure was negligible.

ACKNOWLEDGMENTS

The authors gratefully acknowledge of A. John Sedriks, Office of Naval Research, Arlington, Virginia. The authors would also like to acknowledge the contributions of Gabrielle T. Peace in sample preparation and electrochemical testing.

REFERENCES

1. W. G. Characklis, "Microbial Biofouling Control" in Biofilms, W. G. Characklis and K.C. Marshall, Eds., p. 585, John Wiley and Sons, Inc., New York, NY (1990).
2. J.F. Walko, *Chemical Engrg., 79(24)*, 129 (1972).
3. A.K. Tiller, "A Review of the European Research Effort on Microbial Corrosion between 1950 and 1984" in Biologically Induced Corrosion, p.8, National Association of Corrosion Engineers, Houston, TX (1986).
4. B. Little, P. Wagner, and F. Mansfeld, *International Materials Review, 36,* 253 (1991).
5. D.H. Pope, D. Duquette, P.C. Wayner, and A.H. Johannes, "Microbiologically Influenced Corrosion: A State of the Art Review", MTI No. 13, Materials Technology Institute of the Chemical Process Industries, Columbus, OH (1984).
6. S. C. Dexter and P. Chandrasekaran, in Critical Factors in Localized Corrosion, P. M. Natishan, R. G. Kelly, G. S. Frankel, and R. C. Newman, Eds., p. 188, The Electrochemical Society, Pennington, NJ (1996).
7. B. J. Little, P. A. Wagner, W.G. Characklis, and W. Lee, "Microbial Corrosion" in Biofilms, W. G. Characklis and K.C. Marshall, Eds., p.195, John Wiley and Sons, Inc. , New York, NY (1990).
8. W. P. Iverson, *Advances in Microbiology, 32,* 1, (1987)
9. J.W. Costerton and G.G. Geesey, "The Microbial Ecology of Surface Colonization and Consequences of Corrosion" in Biologically Induced Corrosion, p.8, National Association of Corrosion Engineers, Houston, TX (1986).
10. "Inhibition of Microbiologically Influenced Corrosion", P. M. Natishan, D. C. Hansen, and G. I. Loeb, NRL Publication NRL/PU/6310-96-302 (1996).
11. P. M. Natishan, Joanne Jones-Meehan, G. I. Loeb, N. Gray, B. Little, R. Ray, and Mary Beard, submitted to Corrosion (8/97).
12. R. Belas, M. Simon, and M. Silverman, *J. Bacteriol 167*, 210 (1986).
13. L. McCarter and M. Silverman, *Molecular Microbiology, 4,* 1057 (1990).
14. S.I. Galkina, G.F. Sud'ina, and L.B. Margolis, *Exp. Cell Res., 200,* 211 (1992).
15. L.B. Margolis and S.V. Popov, *J. Cell Sci., 98,* 369(1991)
16. Yu. Yu. Sharovskaja, L.M. Chailakhjan, and L.B. Margolis, *Exp. Cell Res.,175,* 404 (1988).
17. J. Adler, *Scientific American, 234(4),* 40 (1976).
18. J. Jones-Meehan, M. Walch, B. J. Little, R. I. Ray, and F. B. Mansfeld in 92-JPGC-NE-7, ASME, New York, NY (1992).
19. B. Little, R. Ray, P. Wagner, and J. Jones-Meehan, paper #101, Corrosion/91, NACE International, Houston, TX (1991).
20. M. B. McNeil, J. M. Jones, and B. J. Little, *Corrosion 47*, 647 (1991).
21. J. Jones-Meehan, J. W. Cofield, B. Little, R. Ray, P. Wagner, M. McNeil, and J. McCay, Paper #29, "1995 International Conference on Microbially Influenced Corrosion", New Orleans, LA (1995).
22. G.R. Llanos and M.V. Sefton, *Biomaterials, 13*, 421 (1992).

23. A.K. Harris, *J. Biomech. Engng. 106*,19 (1984).
24. Baier, R.E.; in "Adhesion in Biological Systems", R.S. Manly, p. 15, New York, Academic Press (19700.
25. R.E. Baier, in "Applied Chemistry at Protein Interfaces", Adv. in Chem series 145, R.E. Baier, ed., Am. Chem. Soc., Washington D.C. 1975 chap. 1, and private communication.
26. L. M. Prescott, J. P. Harley, and D. A. Klein, "*Microbiology*", p. 93, W. C. Brown Publishers,Dubuque, IA (1990).
27. M. Walch and J. M. Jones, paper #112, Corrosion/90, NACE International, Houston, TX (1991).

Table 1. Abiotic corrosion behavior of 4340 steel with and without silicone treatments exposed to quiescent, 0.6 M NaCl solutions.

Treatment	Exposure (Days)	Coating Thickness (μm)	Corrosion Current Density ($\mu A/cm^2$)	Corrosion Rate (mils/year)
None	1	-	9	4.8
PEG-060	1	860	1×10^{-3}*	4.6×10^{-4}
PEG-060	10	250	1×10^{-3}*	4.6×10^{-4}
PEG-015	1	230	1×10^{-3}*	4.6×10^{-4}
PEG-015	1	47	1×10^{-4}*	4.6×10^{-5}
PEG-015	1	22	1×10^{-4}*	4.6×10^{-5}

*Nominal values - the measured current values are at the lower detection limit of the potentiostat.

Table 2 . The weight loss data for 4340 steel and pure metals after a two year of exposure.

Material	Control	CG-59 (hydrogenase -)	47Z (hydrogenase +)
	grams ($x10^{-3}$)	grams ($x\ 10^{-3}$)	grams ($x10^{-3}$)
4340 steel	136.2	94.6	191.6
chromium	0	0.4	0.3
molybdenum	15.4	2.0	6.1
tungsten	29.5	0.7	2.4
zirconium	0	0	0
niobium	0.5	0.1	0
tantalum	0	0.9	0.4

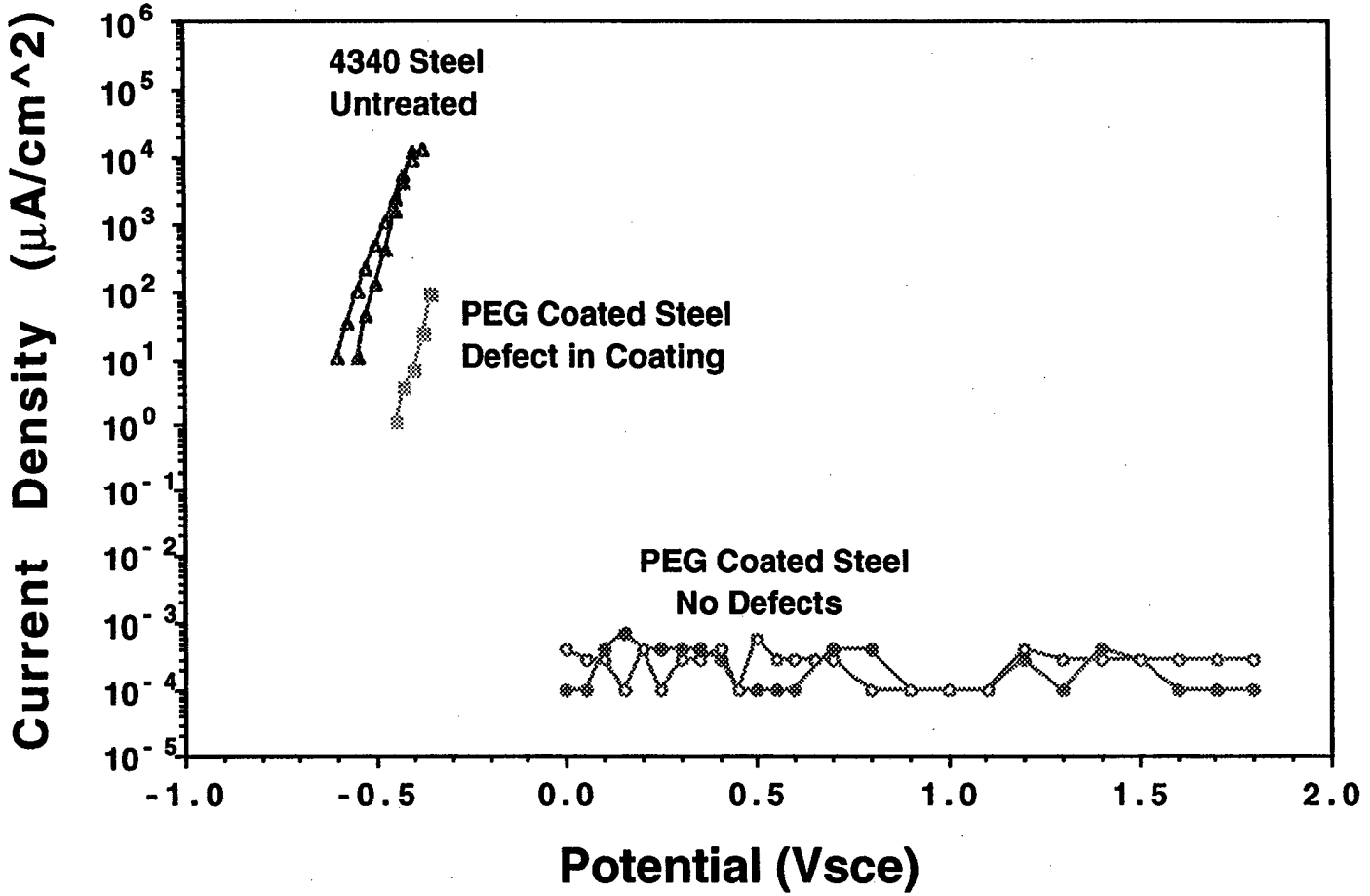

Figure 1. Anodic polarization curves for two 4340 steel samples, a PEG coated steel sample with a defect(s) in the coating, and two PEG coated steel samples without defects.

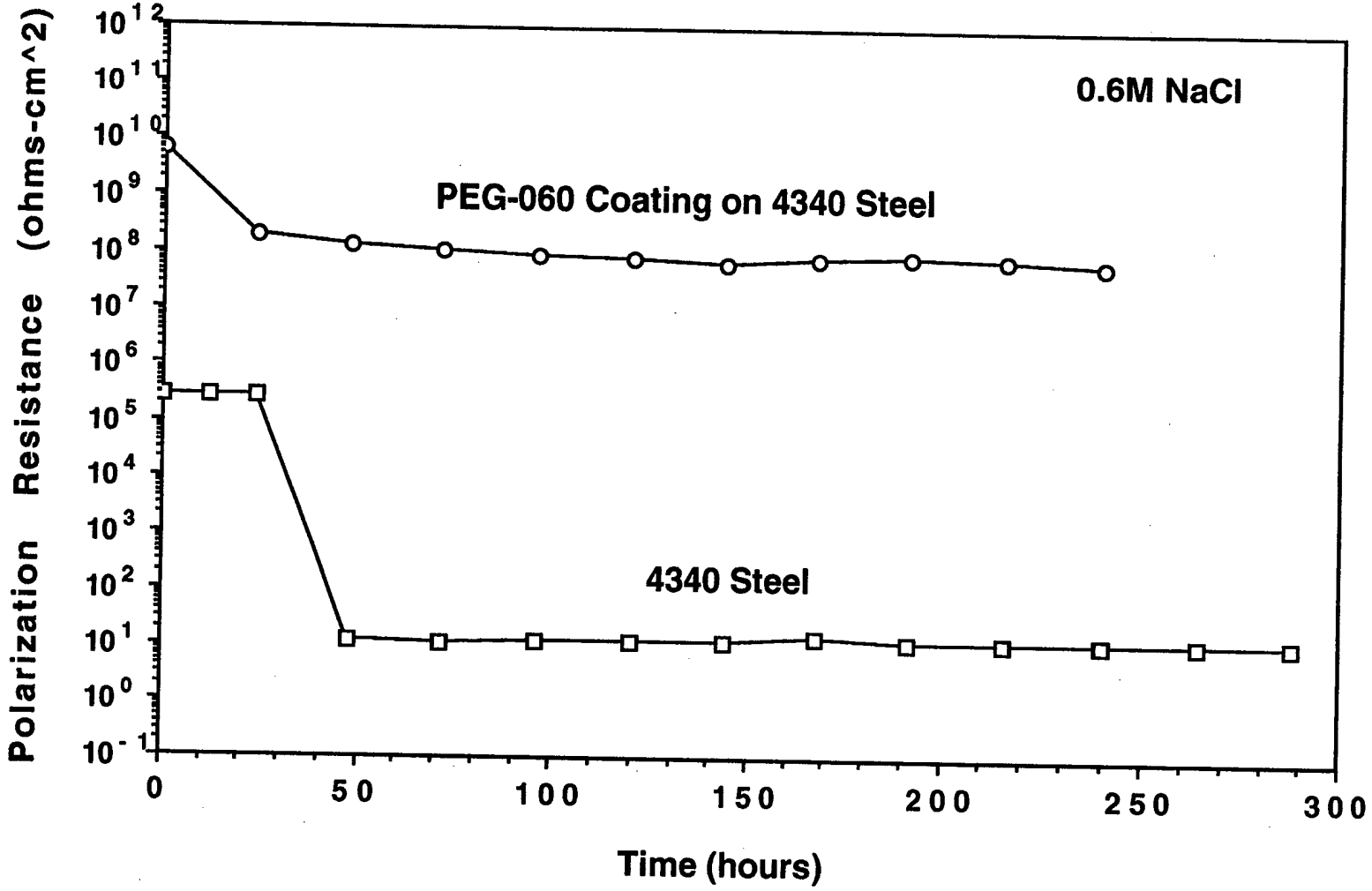

Figure 2. Polarization resistance vs. time for 4340 steel with a PEG-060 coating and untreated 4340 steel.

Fungal Degradation of Military Assets

Brenda Little, Patricia Wagner, Dennis Lavoie and Richard Ray

Naval Research Laboratory
Stennis Space Center, MS 39529

Keywords: wire rope, corrosion, fungi

ABSTRACT

Three case histories of biodeterioration due to fungi are reviewed. Fungal accelerated deterioration has recently been documented in aircraft fuel storage tanks, painted interior surfaces of helicopters, and wire highlines stored in humid environments on wooden spools. In addition to the obvious esthetic problems requiring expensive, labor intensive amelioration, growth of fungi can cause microbiologically influenced corrosion (MIC).

INTRODUCTION

Biodeterioration due to fungi has been documented for the following: cellulosic materials (paper, composition board, and wood); communication wire; cable splices; telephone cable; cable sheaths; photographic film; polyvinyl chloride films; sonar diaphragm coatings; map coatings; paints; metals; crude oil; fuel oil; jet fuel; kerosene; greases; waxes; lubricants; adhesives; asphalt; hydraulic fluids; rain repellents; textiles (cotton and wool); vinyl jackets; leather shoes; feathers and down; natural and synthetic rubber; optical instruments; mechanical, electronic, and electric equipment (radar, radio, flight instruments, wire strain gauges, helicopter rotors); hammocks; tape; thermal insulation; brick masonry; medicines; museum valuables; concrete, and processed tobacco. Fungi are nonphotosynthetic organisms having a vegetative structure known as a mycelium that is the outgrowth of a single microscopic reproductive cell or spore. Mycelia are capable of almost indefinite growth in the presence of adequate moisture and nutrients so that fungi often reach macroscopic dimensions. Yeasts are fungi that multiply by forming buds instead of mycelia. Fungi are ubiquitous in atmospheric and aquatic environments where they assimilate organic material and produce organic acids including oxalic, lactic, acetic, and citric. Fungi produce spores, non-vegetative dormant stages, that can survive long periods of unfavorable growth conditions, e.g., drought and starvation. When conditions for growth are favorable, spores germinate. Despite the extensive data base that has been developed on biodeterioration and biocides, fungi remain a modern problem for shipment, storage, and use of military assets. The following case studies document problems in wire rope storage, jet fuel storage, and helicopter operation due to the presence and activities of fungi.

Wire Rope

One-inch carbon steel wire ropes or highlines used for transporting equipment and people between U. S. Navy ships are prepared according to a federal specification with six

individual strands around an independent wire core coated with a thick maintenance grease and wrapped onto wooden spools (Fig. 1).[1] U. S. Navy standards further require that spools be wrapped in plastic prior to storage. Wire rope may be stored for weeks to months before being transported to U. S. Navy vessels. Any visible sign of corrosion disqualifies the rope for its intended purpose. Between May 1992 and February 1993, corrosion inspection statistics were compiled for 117 spools and compared with storage conditions. Five of fifty-eight highlines stored indoors showed some sign of corrosion whereas forty-two of the fifty-nine spools stored outdoors were unsuitable for use because of localized corrosion. Time in storage was not a factor. Further statistics were collected for highlines that had been removed from plastic packaging and were currently in use. Four of thirty-four highlines installed on winches were rusty when inspected. Fungal growth was observed on interiors of some wooden spools stored outdoors. Corrosion was most severe on wraps of wire in direct contact with the wooden spool flanges. There were numerous reports of a musty odor associated with spools when plastic packaging was removed.

Sections of wood from spool interiors and pieces of brown shipping paper from spool rim edges (Fig. 2) were removed. Wood and paper samples with fungal fruiting bodies, spores, or mycelia were placed in Petri dishes with potato dextrose agar (PDA) and incubated in a dark room at 37°C. After a 1-week incubation, fungal species were identified as *Aspergillus niger* and *Penicillium* sp. The pH of the condensate within Petri dishes and in areas adjacent to growing fungi were monitored using a microelectrode with a tip diameter of 2.4 mm vs. saturated calomel reference electrode. Condensate in Petri dishes where either isolate was grown dropped from a pH of 7.0 to 4.9 in three weeks. Coated wire rope was exposed to pH 5.0 citric acid solution. Localized corrosion (Fig. 3a, b) was observed in each location the acid solution touched the rope.

Wire rope received directly from the manufacturer was exposed on wooden tongue depressors in enamel trays containing PDA. Some trays were inoculated with fungi, covered with a clear plastic, and placed in a dark, 30°C environment. Other trays were inoculated but remained uncovered. Controls were uninoculated and covered. Wire rope in contact with wooden tongue depressors inoculated with either isolate developed localized corrosion in areas in direct contact with either the wood or the agar within four days (Fig. 4a, b). Fungi were attached directly to the wire and were associated with corrosion products in all inoculated trays (Fig. 5a, b, c). In the open, inoculated tray no additional corrosion was observed. No corrosion was observed in the abiotic, covered control. In the covered inoculated trays, corrosion developed in areas where condensate dripped onto the wire from the clear plastic in addition to areas in direct contact with wood and agar. Localized corrosion was observed on wire surfaces where the grease coating was thin or missing due to handling. In these cases, fungal cells were not associated with pitting and corrosion products. The maintenance coating is an amber-colored wax with organic corrosion inhibitors. The product, which has negligible solubility in water, was evaluated as a source of nutrients for the fungi by melting the grease in a Petri dish, allowing it to solidify, inoculating it directly with the isolates, and comparing to an abiotic control. Fungal isolates did not grow on the maintenance coating. Fungal growth could not be demonstrated on corroded rope sections not in direct contact with wood or agar.

Both *Aspergillus niger* and *Penicillium* sp. produce copious amounts of citric acid as a result of hydrocarbon degradation.[2] Localized corrosion of the wire rope in direct contact

with fungal-contaminated wood may be due to either organic acid production or to initiation of corrosion nucleation sites. Citric acid solution at pH 5.0 did penetrate the protective grease and cause corrosion. Wire rope in direct contact with inoculated wood and agar was colonized by fungal mycelia and fungi were associated with corrosion products. In addition to organic acid production, fungi produce copious amounts of carbon dioxide. Carbon dioxide reacts with water to form carbonic acid. In our laboratory studies, condensates in covered, inoculated trays were in the range of pH 4.0–5.0. The acidic condensate penetrated the protective maintenance coating. Areas where the maintenance coating had been mechanically removed were particularly vulnerable to attack by acidic condensates.

Laboratory data and field statistics strongly implicate the practice of storing carbon steel highlines in humid conditions wrapped in plastic with MIC. The replacement of plastic wrapping with paper packaging and redesign of wooden spool flanges to include slats one-half inch apart to promote ventilation are currently being evaluated as corrosion control measures.

Microfungal Degradation of Polyurethane Paint and Corrosion of an Aluminum Alloy in Military Helicopters

Military helicopters operating in humid environments mildew or mold on interior surfaces (Fig. 6).[3] Cleaning accounts for a significant amount of the labor expended in field maintenance activities. In extreme cases, fungal growth has been known to form thick masses, especially in areas of the craft not regularly cleaned in the field, such as the bilge, behind sound insulation blankets, within tight spaces in the overhead, and behind fixed equipment such as electronics racks. Growth in such areas may not be discovered until aircraft are sent for depot-level maintenance after 5 to 7 years. Occasionally, aircraft placed in storage for a short time are so badly contaminated with noxious growth that they are unusable and must be returned for costly, depot-level recleaning.

Five H-53 aircraft at various stages of depot-level maintenance, including salvage storage, were surveyed and whole portions of contaminated surfaces were sampled for microscopic examination in the laboratory. Fungal contamination was observed in all aircraft examined. To isolate and identify fungi, culture plates containing potato-dextrose agar (PDA) were inoculated by pressing the agar surface directly against contaminated surfaces of the aircraft. Plates were incubated in the laboratory at room temperature until colonies could be picked for isolation, identification and maintenance. The following nine genera of fungi were identified: *Pestolotia*, *Trichoderma*, *Epicoccum*, *Phoma*, *Epicoccum*, *Aureobasidium*, *Stemphylium*, *Penicillium*, and *Hormodendrum*.

Paint exposure tests were carried out using 1-inch square coupons of 2024 T-6 aluminum alloy coated with chromate primer and type 36321 polyester polyurethane paint according to Federal Specifications TT-P-2756A, MIL-P-85582 and TT-L-20A. A parallel set of coupons was prepared for comparison using lacquer coating. Coatings were scratched vertically down the center to expose bare aluminum to simulate mechanical damage that might be expected in the field. Coupon surfaces were swabbed thoroughly with 75% ethanol and dipped (with the scratch vertical) halfway into a solution of household bleach (~5.25% sodium hypochlorite). One third of the coupons was used without further treatment, while

one third of the coupons was swabbed on one side with hydraulic oil, and the remaining third was swabbed on one side with a lanolin-based preservative to simulate operating and storage conditions, respectively. Sets of three coupons (one each of alcohol, hydraulic oil, and lanolin treatments) were placed on PDA in Petri dishes with treated sides up, and agar surrounding each coupon was inoculated with fungal spores from an isolate to initiate growth of a thick fungal colony around each coupon that would either overgrow the coupon or provide a source of inoculum to the coupon surface. To further encourage growth, inocula were smeared on the center of each coupon. The following five fungal isolates were used as inocula: *Trichoderma*, *Aureobasidium*, *Stemphylium*, *Penicillium*, and *Hormodendrum*. The resulting experimental matrix was: 5 isolates × 2 bleaching treatments (bleached or not) × 3 surface treatments (alcohol only, oil, or lanolin). Incubation was carried out in the dark at 26°C.

Coupons were photographed to document the extent of growth over their surfaces at 4, 8, 23, and 32 days. At 32 days, coupons were examined visually with a binocular microscope and qualitatively scored for surface contamination. Cleaning efficacy was tested using a 75% ethanol-dipped swab to clean a spot on each coupon. Both swabbed and unswabbed areas were examined using environmental scanning electron microscopy (ESEM). ESEM micrographs of coupon surfaces before exposure to fungi demonstrate that the polyurethane coating was noticeably smoother (Fig. 7a) than the sharp, porous surface of the lacquer (Fig. 7b). After 30-day exposure to growing fungi, polyurethane-coated coupons exhibited no corrosion or blistering; however, blisters were observed close to the experimental scratch on lacquer-coated coupons.

Qualitative estimates of fungal growth on the surfaces of painted coupons after 30 days were made. Lacquer-coated coupons were more susceptible to fungal colonization than polyurethane-coated coupons. Of the 5 isolates tested, *Hormodendrum* was the most aggressive in its growth on both coatings; almost half of each coupon was covered after only 4 days exposure. Many fungi grow on solid surfaces given a modicum of organic material as a carbon source. During normal operation, interiors of military helicopters usually become coated with a thin film of hydraulic oil, and during storage, a lanolin-based coating is applied to interior surfaces as a preservative. Both materials are potential carbon sources, and, along with normal dirt accumulation, increase fungal growth, and exacerbate deleterious effects on surface coatings.

Fungi on polyurethane surfaces appeared well established, with mycelia and conidia (Fig. 8a), and germinating spores (Fig. 8b), but there was no obvious degradation at attachment points. Figure 9 illustrates incomplete removal of fungal structures by simulated field cleaning procedures. Hyphae were present in the experimental scratches on many coupons, and occurred in association with both occasional corrosion products in unbleached portions and thick corrosion products on the bleached portions.

Fungi isolated from these aircraft are ubiquitous, so contamination of the airframes could have occurred virtually anywhere during their duty cycle. At least one of the isolates, *Aureobasidium,* has been reported to cause superficial discoloration on latex paint.[4] *Hormodendrum* (reported as *Cladosporium resinae*) causes corrosion of 2024-T6 aluminum alloy in the presence of water, salts, and diesel oil,[5] a situation that might be expected in

the bilge areas of aircraft operating in a maritime environment. Aluminum alloy exposed in scratches or other mechanical damage to painted surfaces may be particularly vulnerable to corrosion exacerbated by fungal growth. In this study, although there was some spatial relationship between fungi and corrosion products in the unbleached portion of the experimental scratches, the data do not indicate a causal relationship. Corrosion in the bleached portion of the experimental scratches was due to oxidation by the bleach solution. In addition to exposing aluminum, a broken paint surface may be susceptible to additional failure at the paint-substratum interface, as illustrated by blisters observed in lacquer paint near the experimental scratch. The data cannot support a conclusion of a causal relationship between blisters and fungi, although the spatial relationship suggests an interaction.

The lower colonization rates for polyurethane compared to lacquer suggest this coating was less susceptible to initiation of fungal growth. In this short experiment, no surface degradation of polyurethane coatings was observed microscopically where fungal hyphae were attached. Simulated field cleaning/disinfectant procedures using 75% ethanol physically removed most fungal structures from paint surfaces; the viability of the few remaining fungal structures was not assessed. Operationally, short term exposure of polyurethane paints to fungi (on the order of weeks) appears to result in no physical damage to the coating surface, and alcohol cleaning appears to be effective. Prolonged or multiple exposures to fungal contamination may have a cumulative effect on coating performance. Performance also may be a function of substratum, as indicated by the observation that polyurethane paint disbonded from a glass fiber composite structure under a thick fungal colony while the surrounding surface remained intact.

Fungal influenced corrosion may occur in two ways. Fungi may directly attack unprotected aluminum alloys. At least one species of the genus *Cladosporium* in liquid culture can accelerate corrosion of unprotected 2024 T-6 alloy, the type used in military helicopters, by organic acids production during metabolic breakdown of hydrocarbons.[6] Fungi may indirectly cause corrosion when bleach (~5.25 % sodium hypochlorite) is used to remove fungal stains untouched by the authorized cleaning/disinfectant agent, 100% isopropyl alcohol. Sodium hypochlorite solution readily corrodes aluminum alloy upon contact in scratches or other holidays in the protective coating.

Jet Fuel Storage

MIC of metals is a problem in the extraction, production, distribution, and storage of hydrocarbon fuels. MIC has been identified for coated and uncoated carbon steel and aluminum. Ships with seawater displacement fuel tanks, in which seawater replaces fuel as it is consumed, are particularly susceptible. In addition, bacterial and fungal contamination in jet fuel causes fuel pump, gauge, filter, and coalescer malfunction due to clogging and blockages. Fungal contamination of fuel oils causes a deterioration in the quality of the product and, when contaminated fuel is used, can cause plugging in fuel lines and filters. Mechanisms proposed for MIC in fuel water systems are as follows: production of acids derived from the degradation of hydrocarbon chains; establishment of concentration cells; formation of tubercles by the symbiotic association with bacteria; and direct removal of metallic ions from the surface by extracellular enzymatic activity.

Extensive localized corrosion of the bottoms of carbon steel jet fuel storage tanks with subsequent leakage of fuel oil was recently investigated. *Hormoconis* (formerly *C. resinae*), *Aspergillus*, *Penicillium* and *Fusarium* were identified in the fuel/water mixtures. Corrosion attack was located near the tank bottom at the fuel/water interface where an active microbiological population was associated with free water. Fungi were observed growing over the entire surface of oil droplets and within suspended water droplets (Fig. 10). In the absence of water, no fungi were detected. Water soluble biocides are routinely added to fuel to prevent microbial growth. Problems occur when the biocides are exhausted or the amount of water has been underestimated. Attempts to form emulsions of fuel/water combinations accelerate fungal growth by increasing the surface fuel/water interfacial area and, therefore, the availability of oil, oxygen, and nutrients.

ACKNOWLEDGMENTS

This work was performed under Program Element 0601153N, NRL contribution number NRL/PP/7333--97-0024. Fungi were identified by Dr. Raymond Scheetz, University of Southern Mississippi, Hattiesburg, MS. Statistics related to wire rope storage and specimens of wire rope were provided by Mr. Chuck Boyle, Naval Surface Warfare Center, Port Hueneme, CA.

REFERENCES

1. B. Little, R. Ray, K. Hart, P. Wagner, Fungal Induced Corrosion of Wire Rope in Humid Atmospheric Conditions. CORROSION/95, paper no. 190, (Houston, TX: NACE International, 1995).

2. American Type Culture Collection Catalogue of Filamentous Fungi, (Rockville, MD: 1991) 18th Edition.

3. D. Lavoie, B. Little, Fungal Contamination of H-53 Aircraft. NRL/MR/7333--96-7725, Naval Research Laboratory, Stennis Space Center, MS, 1996.

4. C. J. K. Wang, R. A. Zabel, Identification Manual for Fungi from Utility Poles in the Eastern United States, (Rockville, MD: American Type Culture Collection (ATCC), 1990).

5. R. C. Salvarezza, H. A. Videla, Acta Cientifica Venezuelan, 35(1984): p. 244.

6. H. Videla, "The Action of *Cladosporium resinae* Growth on the Electrochemical Behavior of Aluminum," Proceedings of the International Conference on Biologically Induced Corrosion, (Houston, TX: National Association of Corrosion Engineers (NACE), 1986), p. 215.

Figure 1 – Wooden spool on which wire rope was stored; pieces of paper are attached to rim edges.

Figure 2 – Inside surface of wooden spool; white deposits are the result of fungal growth.

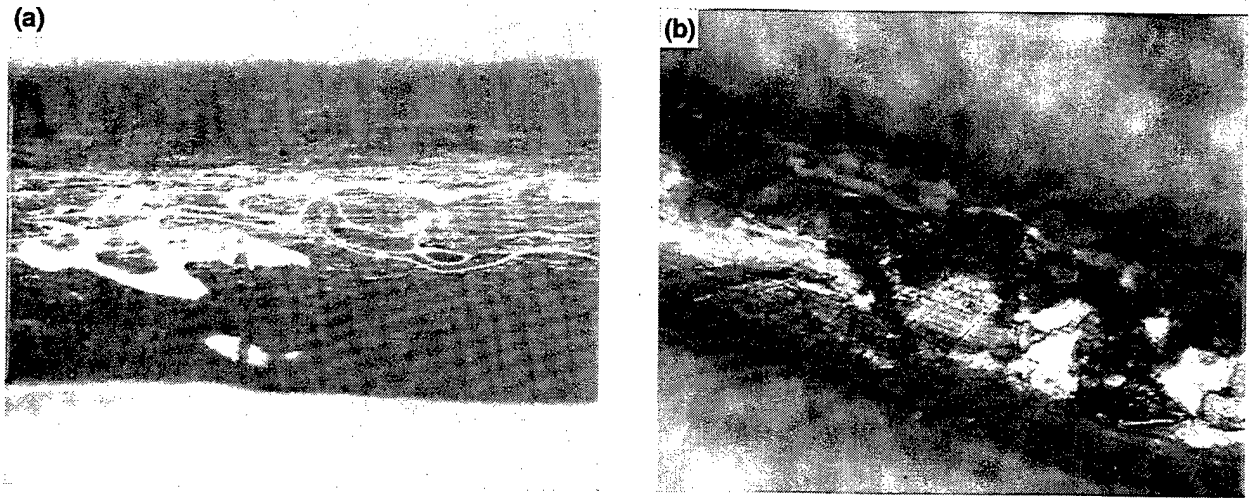

Figure 3 – (a) Strand of wire with protective grease intact before exposure to acidic solution, 30×. (b) Localized corrosion after exposure to citric acid solution at pH 5.0, 40×.

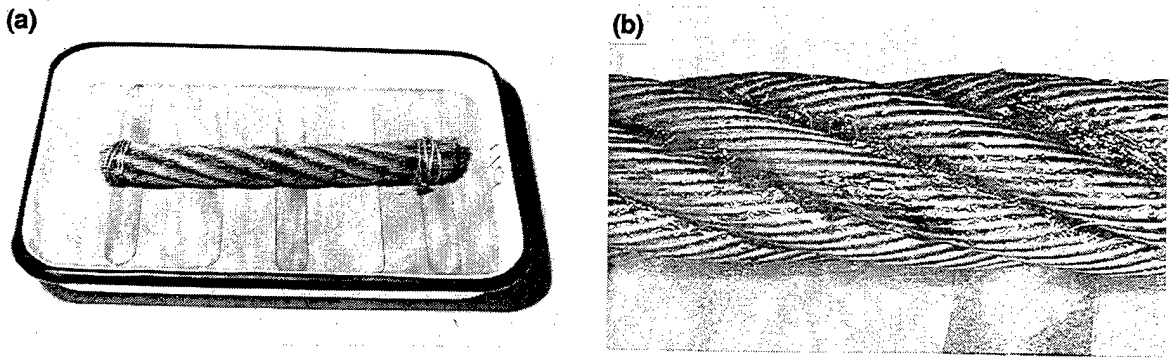

Figure 4 – (a) Wire rope placed on wooden tongue depressors in a tray containing PDA inoculated with *Aspergillus niger*. (b) Wire rope that had been in contact with wood and PDA inoculated with *Aspergillus niger*. Rope rolled aside to show localized corrosion after contact with agar or wood.

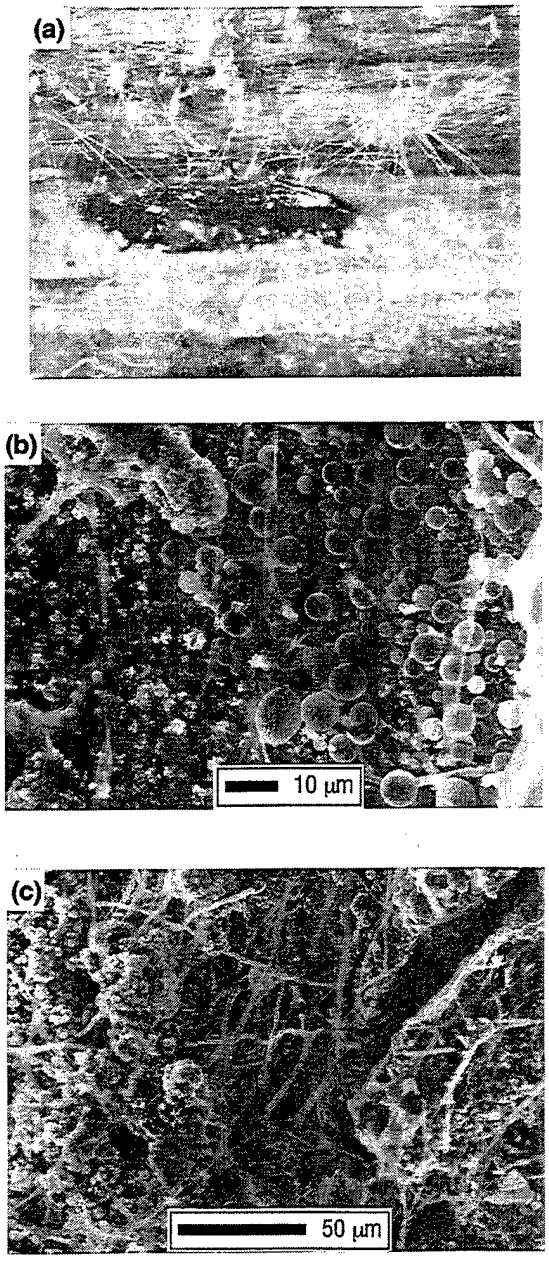

Figure 5 – (a) Light microscope photograph showing fungal mycelia attached directly to wire and associated with localized corrosion, 40×. (b) ESEM micrograph showing mycelia in association with corrosion products, 500×. (c) ESEM micrograph showing mycelia in association with corrosion products, 1000×.

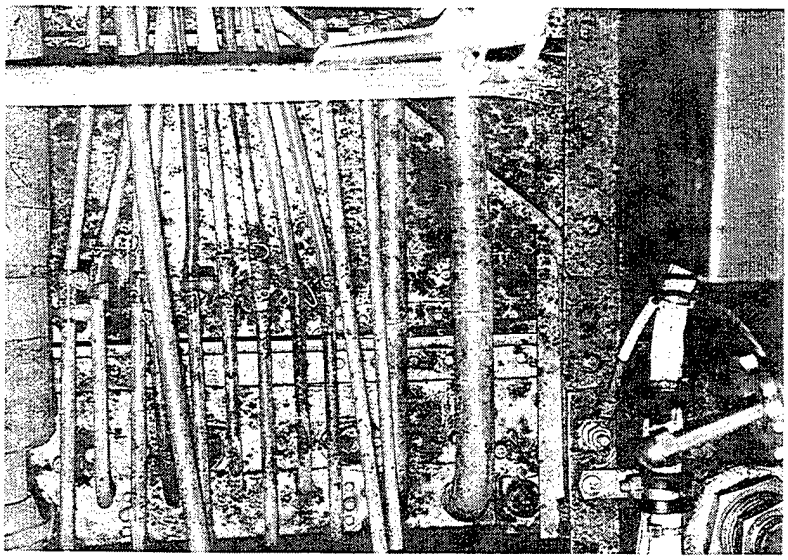

Figure 6 — Fungal growth on interior of H-53 helicopter.

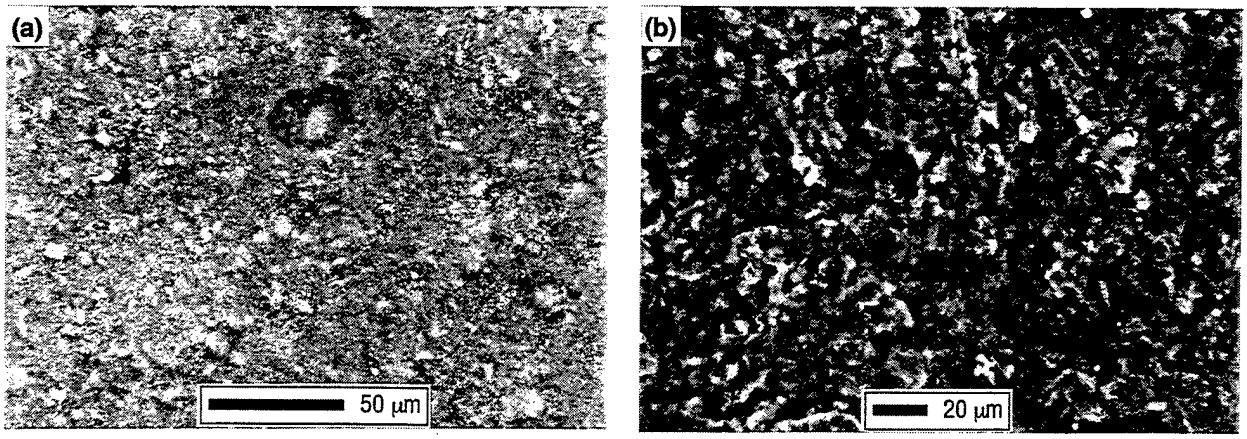

Figure 7 — (a) Polyurethane paint surface before exposure (500×) and (b) lacquer paint surface before exposure (500×).

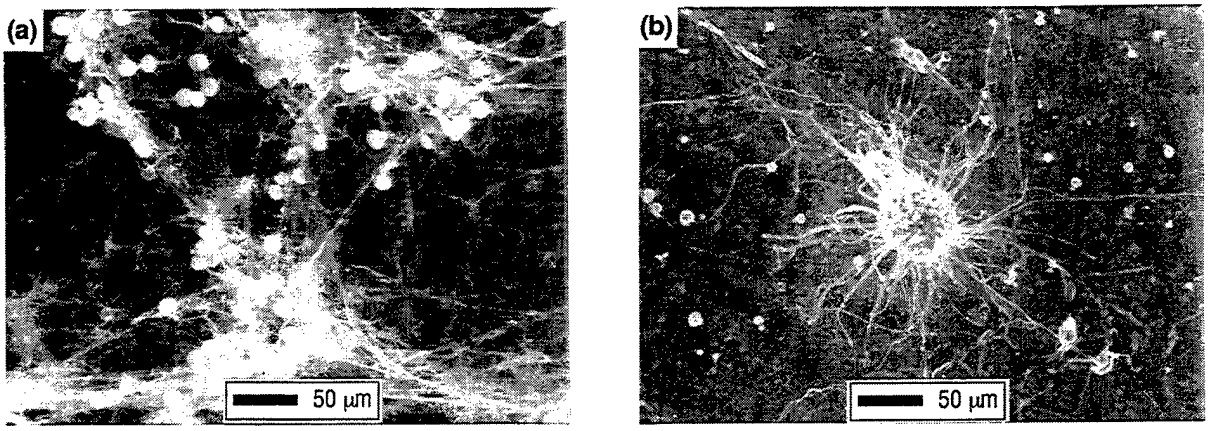

Figure 8 — (a) Mycelial mass on polyurethane coated coupon after 30 days (250×) and (b) germinating mycelia on polyurethane coated coupon after 30 days (250×).

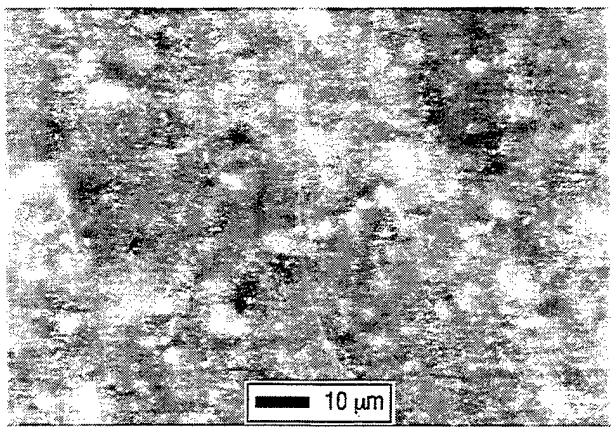

Figure 9 — Polyurethane coated coupon surface after alcohol cleaning (1000×).

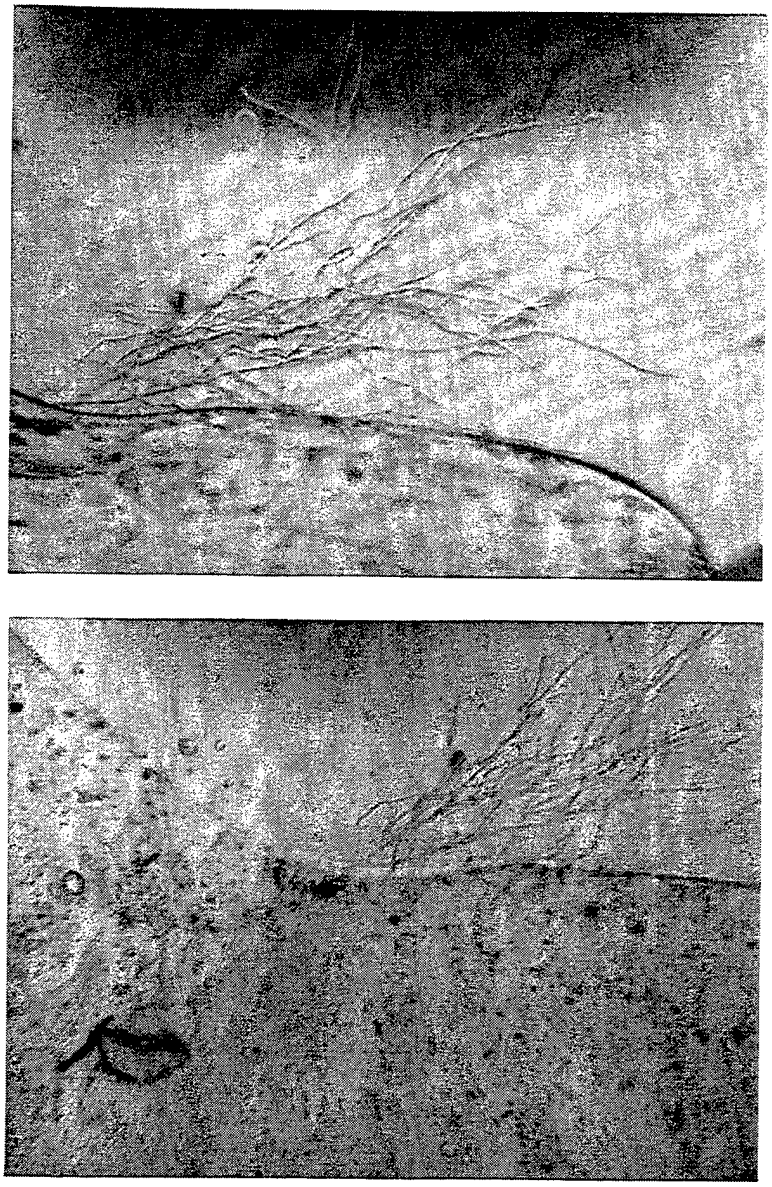

Figure 10 — Fungal mycelia in association with water droplets in jet fuel.

Material Considerations for the Navy Shipboard Waste Destruction System

David A. Shifler
Carderock Division, Code 613
Naval Surface Warfare Center
9500 MacArthur Boulevard
West Bethesda, MD 20817-5700

Catherine Wong
Carderock Division, Code 612
Naval Surface Warfare Center
9500 MacArthur Boulevard
West Bethesda, MD 20817-5700

ABSTRACT

Compliance with MARPOL environmental regulations has required the design of a waste management system to reduce the volume of solid shipboard waste and treat it so that it is safe to carry aboard ship. The U.S. Navy in cooperation with industry has developed a conceptual design of a plasma arc waste destruction system (PAWDS) capable of meeting strict shipboard weight, size and operational criteria that has precluded the use of traditional commercial systems. The innovative system design has involved a thorough examination of candidate materials that should be capable of withstanding the processing of a variable waste stream that may include highly corrosive constituents. The structural components of the PAWDS should insure safety to personnel and ship by resisting degradation through high temperature corrosion, erosion, thermal cycling, and other effects.

INTRODUCTION

U.S. Navy Operational Concept and its strategy "Forward --- From the Sea" requires the Fleet to execute its presence anywhere in the world at any time. Local, national, and international environmental regulations and statutes controlling overboard discharge of liquid and solid wastes and air emissions have become more stringent for ships deployed at sea. The Navy's ability to operate in littoral and selected areas around the world may be compromised unless alternative solid waste management processes are utilized. Existing ships do not have sewage and solid waste holding capabilities to hold wastes for more than a few days.

The International Convention for the Prevention of Pollution from Ships in 1973 and the 1978 Marine Pollution Protocol, collectively known as MARPOL 73/78[1] were early initiatives to control waste disposal in the marine environment.

[1] MARPOL refers to the International Treaty for the Prevention of Pollution for Ships. The United States is a party to this convention by S. Treaty Document No.3, 100th Congress, 1st Session

An integrated technology for Navy ships to comply with this solid waste and liquid waste discharge prohibition is not currently available commercially. The marine environment and Naval warfare requirements present significant and unique challenges for technical solutions of waste disposal problems for U.S. Navy ships deployed at sea without significant impact to operations and deployment. Unlike land-based systems, solutions aboard ships will impose considerable constraints on space and must operate reliably in a corrosive, marine environment. The Navy has significant space, weight, reliability, maintainability, and operability constraints which require that any system minimize its impact on ship operations,. ship systems, manpower requirements, maintenance, and loss of mission-oriented space.

The Naval Studies Board[2] (NSB) has recommended that the Navy continue its program of research into advanced thermal waste destruction technologies that may eventually serve as the principal shipboard waste reduction methodology. A comprehensive survey, as shown in Table 1, of thermal destruction technologies for shipboard solid waste was conducted. The survey identified electrically-heated, plasma-arc pyrolytic thermal destruction technology as the most promising because of its potential for greater reliability, compact size, higher processing temperatures, better temperature control, and greater capacity relative to standard incinerators.

Ultra-high reaction temperatures derived from plasma energy can achieve waste treatment without combustion. Plasma is produced by passing a gas through a high current electric arc; temperatures within the arc range from 18,000-36,000 °F (10,000-20,000 °C). Temperatures in the outer plume of a plasma flame can range from 5,000 to 11,000°C. This combustion-independent plasma heating process allows for extremely high heating rates which can translate into practical reactor configurations having small destruction volumes, high processing rates, short residence times and high destruction efficiencies. A PAWDS can rapidly change the physical and chemical nature of shipboard waste materials. Plasma energy can change organic wastes to their elemental constituents while inorganic solid wastes produce fly ash and a pool of liquefied inorganic-metallic material. The environment in a plasma destruction chamber may be either oxidizing or reducing; the choice of either environment can affect the material selection for the chamber.

CONCEPT DESIGN

Among the many issues involved, the reliability and design of the final PAWDS will be dependent on the materials of construction. One of the primary operational factors, the focus of this paper, is the corrosion resistance of candidate materials; the discussion of many of the other issues is beyond the scope of this paper. Complex processes occur in incineration of solid wastes which involve thermal and chemical reactions that occur at various times, temperatures, and locations. Pyrolysis via high reaction temperatures derived from plasma energy will also encompass complex reactions, dynamic gas flows, particulate and deposition effects,

[2] Shipboard Polution Control, U.S. Navy Compliance with MARPOL Annex V, Committee on Shipboard Pollution Control, Naval Studies Board, Commission on Physical Sciences, Mathematics, and Applications, National Research Council, National Academy Press, Washington DC, p.4 (1996)

mechanical and chemical mixing, and residence times of the reaction species. The operational mode, the temperatures existing within the primary combustion chamber eductor, secondary combustion, and other system components, composition of the waste stream, the chamber chemical environment, the waste stream abrasiveness, the aforementioned space constraints, safety, maintainability, and reliability will affect the choice of construction materials. The amount of Navy Solid Waste (NSW)[3] generated on average (Table 2) has been studied, but the waste stream at any given time is variable. The composition of the ship solid and liquid waste generated on warships at sea can depend in part, on ship size and class, type of mission, length of ship's mission, and location of deployment.

Several designs have been considered based on different operating scenarios and different materials. They are: (1) hot wall (refractory lined, minimal cooling), (2) air-cooled cold wall, and (3) water-cooled cold wall.

Hot Wall Design

The first design concept considered for the PAWDS was a refractory-lined, hotwall primary chamber (Figure 1) which would have an approximate service wall temperature of about 1500 °C. The use of a plasma arc would produce a plasma plume temperature of about 5300 °C near the outer plume envelope. Most alloys will degrade in environments with prolonged service temperatures above 1000 °C. Refractories can exist at higher temperatures. Refractories are mainly high-melting point metallic oxides, but also include substances such as carbides, borides, nitrides, and graphite (Table 3). Maximum service temperatures will always be less than the melting points of pure ceramics because refractories usually contain minor constituents and actual incinerator and pyrolytic environments are vastly different from simple oxygen atmospheres. Refractories are used to act as a thermal barrier between the high temperature PAWDS environment and an ambient temperature outside the chamber skin to maximize safety to ships functions and personnel[4]. Refractory suitability depends on its resistance to abrasion, maximum service temperature, corrosion resistance to liquids, gases and slag, erosion resistance, spalling resistance, resistance to thermal cycling, shock and fatigue from high thermal gradients, oxidation or reduction reactions, its mechanical strength, and its inspection and maintenance requirements. Refractories are available in either shaped (bricks) or unshaped, monolithic forms such as castable plastic refractories, ramming mixes, ceramic fiber blankets, or gunning mixes.

There are often property tradeoffs required to attain the desired optimum, serviceable refractory. Insulating refractories generally have lower density, strength, corrosion resistance,

---

[3] "U.S. Navy Shipboard Solid and Plastics Waste Management Program Plan (The Green Book)", Naval Sea Systems Command, NAVSEA 05V Enviromental Engineering Group, April 1993

[4] M. Heilberger, S. Chapelle, P. Valentine, "Development of a Thermal Destruction System for Treatment of U.S. Navy Shipboard Waste Using Plasma Arc Pyrolysis - Refractories and Slag Removal Methods Survey and Evaluation", CARDIVNSWC-TR-63-95/05, General Atomics, chaps. 3,4,6 (June 1992)

erosion resistance, and higher porosity and void fraction than stronger, less insulating refractories. Refractories are generally susceptible to thermal shock and spalling. Monolithic refractories are often more susceptible to thermal shock than shaped refractories. Dense refractories tend to have high thermal conductivities, low porosity, relatively high strength, and improved corrosion resistance, but tend to be susceptible to thermal shock. Insulating refractories have higher porosity which improves thermal shock resistance, but provides numerous pathways for molten and gaseous materials to promote corrosion and spalling.

The corrosion resistance of refractories is based on the thermodynamics of the potential corrosion reactions, the reaction rates and kinetics of these possible reactions, the composition and form of the refractory material, and the surface chemistry of the refractory with corrosive gaseous, liquid, or solid environments. The spontaneous direction of the possible corrosion chemical reactions can be calculated which can indicate which reactions are theoretically possible. The reaction kinetics will be dependent on the specific environment (gaseous, liquid, or solid), surface chemistry, the material microstructure and composition, refractory phase(s), and the temperature. All ceramics or refractories used in an oxygen-rich environment are oxides or develop a protective oxide on their surface (such as SiO_2 on SiC or Si_3N_4). Though oxide ceramics are inert, and resist oxidation and reduction, they are not chemically inert. Ceramic corrosion between ceramic oxides and molten salt deposits generally can be explained as oxide/acid-base reactions [1]. To determine if a particular slag is acidic or basic, the ratio of lime to silica in the slag is commonly used. As a general rule the slag is basic if the CaO/SiO_2 ratio (or $CaO + MgO/SiO_2 + Al_2O_3$ ratio) is greater than one, If the ratio is less than one, the slag is considered acidic [2]. Gases and liquids can penetrate deeply into highly porous refractories which can exacerbate spalling and accelerated corrosion. Oxidizing gases such as NO_x, Cl_2, O_2, CO_2, H_2O, and SO_2, reducing gases (NH_3, H_2, C_xH_y, CO, and H_2S), and vapors of volatile elements and compounds may react with different refractories. Hydrodynamic mass transport by either convection or diffusion can markedly affect the corrosion rate of a refractory in an environment. Non-wetting refractories are relatively resistant to corrosion with liquids or gases. Molten aluminum, iron, silica, and other constituents derived from the waste stream can react with the crucible refractory to form new compounds or phases which can have different melting temperatures, dimensional stabilities, and corrosion resistances. The new phases or compounds can cause dimensional changes which can cause problems in the chamber. High purity refractories are more corrosion-resistant because certain minor impurity components have microstructures, phases, and defect structures which can introduce significant corrosion. High purity refractories improve corrosion resistance by avoiding low-melting eutectics. Alkali impurities should be minimized as much as possible. Solids, either as fine particulates or dust, can cause degradation of refractories through abrasion or deposition.

Silicon carbide, high alumina, and alumina-chromia refractories were considered the best candidates for a working refractory in a hotwall PAWDS. Alumina-based refractories are usually available with silica and generally offer good corrosion resistance. However, high alumina refractories degrade rapidly in HF, chlorides, molten or strong hot aqueous alkalis, and some molten metals [3]. Alkalis flux the alumina-silica system. Chlorides cause increased porosity and removal of alumina or silica. Chromia (Cr_2O_3) improves the corrosion resistance of high alumina refractories, by reducing slag or liquid penetration [4]. Favorable performance

of alumina-chromia occurs even when the slag has a high iron content, but the use of chromia may introduce environmental questions. Silica contained in high alumina refractories reacts with iron oxide and alkalis from slag to form a glassy surface layer over the refractory which eventually exposes new surfaces to further reaction. Silicon carbide is not attacked by acids, but reacts readily with fused caustic, halogens, and certain metal oxides Silicon carbide is also abrasion resistant and less prone to thermal shock than other refractories [5]. The operating temperature of SiC should be limited to 1300 °C in reducing N_2-H_2-CO environments when no steam is present [6]. Other refractories such Si_3N_4 and ZrO_2 are considered too expensive to use in a full-size PAWDS. Some of these working refractories are listed in Table 4.

There are several limitations to the use of refractories in the PAWDS design. First, a layer of a working refractory such high purity alumina, silicon carbide, or alumina-chromia is required to be used since these refractories have the highest resistance to corrosion reactions with slag, liquids, or gases, are abrasion and spall resistant, have low porosity, and have a limited thermal shock resistance. Since these refractories also have a high thermal conductivity, an insulating refractory must be inserted between the chamber shell and the working refractory. To reduce the temperature from 1500 °C on the inner wall surface to about 100 °C on the outer shell, the combined thickness of the two refractory layers can be 12 inches (30 cm) or more. This adds an unacceptable weight for a shipboard PAWDS capable of processing the level of solid wastes generated by the fleet.

Second, refractories may crack because of thermal shock and react with the shipboard waste to corrode or wear away, thus requiring repair. Eight or more hours are required for the crucible chamber to cool before repairs can initiate. Repair would require the use of plastic refractories, mortar materials, or patching mixes for quick repairs or more a more time-consuming reinstallation of refractory brick. Refractory repair work would require specialized training of shipboard personnel and an assignment of larger number of shipboard personnel to a PAWDS operation. This is counter to the present downsizing "Smartship" philosophy of the U.S. Navy. Storage of patch materials or replacement crucible/chambers is also not feasible because of size and weight limitations.

Cold Wall Design

Driving forces for a cold wall design include the reduction of weight and size, improvement of reliability, operability and maintainability, and increased safety, while maintaining environmental compliance of the PAWDS. The gas temperature in the primary chamber is about 1200 °C with possible hot spots above 1370 °C. Thermal shock occurs during start-up, shutdown, and in the event of water leaks. The chamber environment would contain N_2, CO_2, H_2O vapor, NO_x, and small quantities of alkalis and acid gases (HCl, SO_2). Particulates in the gas stream could cause erosion and abrasion damage. A conventional refractory wall consisting of a working refractory and insulating refractory would be over 12 inches (30 cm) thick and weigh 120 lb/ft^2. A more advanced commercial refractory wall of ceramic fiber and a working refractory is about 7 inches (18 cm) and weighs 70 lb/ft^2. Both conventional and advanced refractory walls would have a limited life expectancy.

A light-weight refractory wall was proposed for a PAWDS with about a 4-inch (wall) and predicted to have a 10,000 hour life[5]. As shown in Figure 2 the light-weight wall consists of a thermal barrier coating (TBC) on a 1-1.3 cm thick superalloy shell such as UNS N07718. The TBC/superalloy wall is cooled by air. A ceramic fiber insulation layer is placed between the air-cooled channel and an outer water-cooled jacket. The TBC consists of a partially stabilized zirconia (PSZ) about 150 μm thick and an MCrAlY (M=Ni or Co) bond coating about 50-75 μm thick for corrosion protection and resistance to high temperature oxidation. This technology has been successfully employed for use in marine gas turbines to prolong the life of alloys in high temperature areas for times exceeding 10,000 to 12,000 hours[6]. The TBC serves to reduce the substrate alloy temperature by up to 300 °F (150 °C) [7]. The thermal barrier coating can be applied by either air plasma-spraying (APS) or electron beam-physical vapor deposition (EB-PVD). The bond coat reduces the stresses and the temperature gradient between the PSZ layer and the alloy substrate. APS provides slightly better heat insulation while EB-PVD coatings have superior spalling resistance. Failure of APS coatings appear to occur under oxidative thermal cycle conditions by the formation and linkage of microcracks with the zirconia layer just above the bond coat [8]. EB-PVD coatings are believed to fail primarily from cracks that develop within the thermally grown oxide that forms on the bond coat surface [9]. It is for this reason that the preferred cooling is via air and not by water since the latter causes increased thermal stresses and induces premature failures of the TBC. The PSZ usually consists of about 8% yttria stabilized zirconia, but this type of PSZ is susceptible to degradation by steam at 100-200°C [10], by molten salt deposits from sulfide, vanadium, and sodium fuel contaminants, and by P_2O_5 and various sodium phosphates at 700 and 900 °C [11,12]. Zirconia-based TBC can be stabilized with scandia (Sc_2O_3) rather than yttria to avoid many hot corrosion problems [13].

A water-cooled design for the PAWDS, shown in Figure 3, consists of an eductor with a plasma torch pyrolyzing the waste material as it is drawn through the tube, around the plasma torch, and into a secondary combustion chamber. The eductor has a coil of cooling tubes brazed to the outside of a metal tube. Inside of this tube a layer of felted insulating fiber slows the heat loss from the inner iron or nickel-based alloy liner. The inner liner is maintained between 900 and 1000 °C. The ability of the liner alloy to resist corrosion is dependent on its protective surface oxide film. Conditions which can damage the oxide and the substrate alloy in PAWDS are probably similar to that experienced in waste incinerators such as: (1) alternating oxidizing and reducing environments at high temperatures which may interfere with oxide formation and oxide maintenance resulting in porous films; (2) mechanical stresses such as residual stresses derived from fabrication and welding processes, cyclic thermal stresses that deform the alloy substrate because of rapid cooling rates, or crack or spall the oxide layer because of tensile or compressive stresses; (3) impingement/erosion which removes the oxide when fluid (gas or liquid) flow exceeds a threshold velocity; (4) reaction with corrodents, moisture condensation; (5) deposits of low-melting point mixtures; (6) flame impingement; (7)

[5] Plasma Arc Waste Destruction System (PAWDS) - Mid-Term Status Review, MSE Technology Applications, Inc., PERMA, Inc., Applied Ordnance Technology, Inc, April 18, 1996

[6] Private communication, Robert Clarke, Code 613, CDNSWC

crevices or defects encouraging galvanic attack; (8) changing metal properties with prolonged exposure at high temperatures; (9) chlorides; and (10) alkali sulfates [14]. Reaction of the slag with the chamber wall must also be considered.

A number of candidate alloys (Tables 5 and 6) have been considered for the coldwall primary reaction chamber and components of the PAWDS. Wall temperature is a major factor in determining the best material. The specific environment in the chamber (temperature, corrosive constituents in feed, air-cooled versus water-cooled, etc.) also will contribute to many possible corrosion problems. The internal surface temperature of a water-cooled primary chamber is around 330-530 °C while an air-cooled chamber will have a surface temperature of about 1000 °C. The actual chamber temperature will dictate the available materials for providing reliable, long-term service for a PAWDS.

Corrosion in High Temperature Environments

Candidate materials for high temperature waste pyrolysis need to be corrosion resistant under a number of potential degradation processes which can occur in waste incineration systems or thermal pryolysis: (1) oxidation, (2) carburization, (3) sulfidation, (4) chloridation, (5) hydrogen interactions, (6) hot corrosion, (7) dewpoint, acid corrosion, (8) galvanic corrosion, (9) crevice corrosion, (10) localized, pitting corrosion, (11) impingement, erosion-corrosion, (12) liquid metal embrittlement, (13) aging reactions, sensitization, (14) creep damage, (15) fatigue and corrosion fatigue, and (16) environmental cracking.

As mentioned previously, most metals and alloys in an oxidizing environment are protected to varying degrees by an oxide layer. Iron oxides alone are not protective above 550 °C [15]. Oxidation of carbon steels from air or steam forms an oxide scale along the metal surface which grows and thickens with time. The scales, depending on chemical composition, can be mildly insulative to very insulative. The scale growth rate increases with a rise in temperature. Chromium, aluminum, and/or silicon assist in forming scales which are more protective at higher temperatures [16]. Chromium oxide is stable up to 983 °C above which the oxide volatizes to gaseous CrO_3. Mechanical damage by spallation or cracking of the oxide film from cyclic oxidation of chromia and alumina oxides formed on nickel-based alloys is due to the mismatch of thermal expansion coefficients between the oxide and the base alloy [17]. Small additions of lanthanum, yttrium, tantalum, ceria, zirconia, and/or niobia improve the scale adhesion and scale resilience to cyclic oxidation [15]. Table 7 lists the degree of corrosion damage from commercial tests in static and dynamic, cycling environments as well as other probable corrosive scenarios which can be expected in the shipboard PAWDS.

Carburization alone usually does not result in corrosion or alloy wastage, but adsorption and diffusion of carbon into the base alloy can lead to significant changes in the alloy mechanical properties and leading to possible alloy embrittlement. Carbon dioxide produced in an oxidizing environment is less corrosive than carbon monoxide, CO, which is the prevalent carbonaceous gaseous species in a reducing environment. Stainless steels will react with hydrocarbons and/or carbonaceous gases at elevated temperatures to carburize at its surface.

Under conditions where hydrocarbons are present in the gas stream and/or with the introduction of oily components, nickel-based alloys are susceptible to severe carburization called "green rot" [18]. Green rot occurs when internal chromium carbides are formed during carburization; subsequent oxidizing of the carbides at the grain boundaries may result in embrittlement. Deterioration and material wastage by metal dusting in carburizing gases at 426-815 °C result in pitting and overall wastage of stainless steels with or without an oxidizing environment [19,20]. Corrosion products in the pits consist of metal carbides, metal oxides, and graphite. The attack is localized and carburization is confined to the pit. Metal dusting has been encountered in chromia-containing alloys such as ferritic and austenitic stainless steels, nickel-chromium alloys, and cobalt-chromiun alloys. Nickel-based alloys are more resistant to carbon diffusion than most other alloys and alloys with higher nickel content are superior to low-content nickel alloys. Carburization appears to be appreciable in nickel alloys at 650-700 °C (penetration 0.2-0.8 mm in 50-55 days). Nickel-chromium alloys containing titanium, niobium, and aluminum are better than basic nickel-chromium alloys in CO_2 atmospheres at 700-800 °C. The Al_2O_3 scale appears to be much more resistant to carburization than the Cr_2O_3 scale [21].

Sulfidation is a reaction of a metal or alloy with a sulfur-containing species to produce a sulfur compound that forms on or beneath the surface of the material. In most environments, Al_2O_3 or Cr_2O_3 form preferentially to the sulfides, but destructive sulfidation attack occurs at oxide crack sites [22]. The reduced species, H_2S, is more corrosive than the oxidized species, SO_2. Sulfates are contained in marine air used in cooling shipboard systems. Sulfidation of nickel results in the formation of eutectic Ni_3S_2 which has a melting point of 635 °C with sulfur solubility of 0.005% [23]. This eutectic formation causes the initiation and propagation of intergranular corrosion. Chromium improves resistance to sulfide attack. Increased chromium content increases the temperature limit in a sulfidizing environment. Chromium sulfide formed below the surface of the protective oxide layer may lead to depletion of chromium and breakaway corrosion. Nickel-chromium alloys have been successfully used at service temperatures of 750-1200 °C. Manganese, silicon, and aluminum additions improve the resistance of nickel alloys to sulfur attack [24].

Chlorides accumulate rapidly on metallic surfaces of a test probe. Typical deposits contained 21-27% Cl when the flue gas contained 40-140 ppm HCl [25]. Municipal wastes were characterized by Krause as having a 0.5% halide dry content of which 60% was derived from organic, polymer sources [26]. Chloride salts have melting temperatures as low as 175 °C, which can act as a fluxing agent and dissolve protective oxide films. Air in a marine environment used in cooling the hotwall surfaces of a shipboard PAWDS will be laden with chlorides. Molten $SnCl_2$ (m.p. 246 °C), $SnCl_2$ +NaCl (m.p. 199 °C), $ZnCl_2$ (m.p. 283 °C), eutectic $PbCl_2/FeCl_3$ (m.p. 175 °C), and eutectic $ZnCl_2$/ NaCl (m.p. 262 °C) [27] may cause rapid corrosion of carbon steel, if present. Attack by halogens at elevated temperatures occurs through the volatility of the reaction products. Oxides that form in combustion gases will be porous and prone to fracture. Stainless steels are generally passive, but surface pitting may occur in chloride-containing environments. Nickel-based alloys can be expected to have superior corrosion resistance as compared to stainless steel alloys [28]. Clay containing aluminum silicate may inhibit chloride-related corrosion by raising the melting points of

chloride salts through the formation of sodium aluminum silicates which expel HCl and SO_3 [29]. Problems with chlorides can be mitigated if plastic is removed from the waste stream and remaining sources of chlorides in the solid waste stream are minimized. Increasing the oxygen content and adding water vapor has also reduced the corrosion rate of various alloys by chlorides in a simulated waste incinerator environment [30].

Steam may decompose on metal surfaces at elevated temperatures to form hydrogen and oxygen. The plasma torch in the PAWDS is capable of producing atomic hydrogen and atomic oxygen. Loss in tensile ductility of steels and nickel-based alloys has been observed in gaseous environments with a total hydrogen content of 0.1 to 10 ppm at -100 to 700 °C. Hydrogen attack or hydrogen damage occurs when gaseous hydrogen diffuses into the steel and reacts with the carbides to form methane, $4\ H+Fe_3C \Rightarrow CH_4+3Fe$, and internal microcracks leading to brittle rupture. The reaction rate is dependent on hydrogen concentration, diffusion, and total gaseous pressure and occurs at 200-600 °C. Hydrogen damage has been observed in utility boilers as low as 316 °C [31]. Atomic hydrogen diffuses readily in steel which may cause cracking and decarburization of steel. Hydrogen damage can occur in other high-strength alloys resulting in loss of tensile ductility. Nickel alloys are much less susceptible to hydrogen damage than ferrous-based alloys.

Hot corrosion is the degradation of materials by the presence of a liquid deposit or ash. Type I corrosion occurs primarily at metal temperatures ranging from 850 to 950 °C. This attack involves molten ash and deposits containing sodium sulfate and/or potassium sulfate salts. Very small amounts of sulfur and sodium or potassium can produce sufficient Na_2SO_4. In gas turbine environments, a sodium threshold level below 0.008 ppm by weight precluded type I hot corrosion. Other impurities such as vanadium, phosphorus, lead, chlorides, and unburned carbon can be involved in lowering salt melting temperatures. High chromium content (>25-30% Cr) is required for good resistance to hot corrosion. Nickel alloys with chromium and aluminum show improved resistance to hot corrosion.

Type II or low temperature hot corrosion occurs in the temperature range of 650 to 750 °C. This type of hot corrosion results in pitting from the formation of low melting mixtures of Na_2SO_4 in Ni-Cr, Co-Cr, Co-Cr-Al, and Ni-Cr-Al alloys [32]. If more components are added, the melting temperature can further lowered. In the presence of molten ash products, the oxide, even in oxidizing environments, becomes unstable and dissolves. Alkali sulfates deposited on the fireside surfaces of boilers may react with SO_3 or SO_2 to form alkali pyrosulfates (m.p. 400-480 °C) or alkali-iron trisulfates [33]. A $NaCl\text{-}Na_2S_2O_7$ mixture can have a eutectic melting temperature of 622 °C. Molten pyrosulfates (such as $Na_2S_2O_7$) reacts with carbon steels at 335-410 °C by dissolving the protective oxide film and then reacting with iron to cause accelerated wastage. A few ppm of vanadium accelerates this reaction. The melting point of these deposits on waterwall tubes ranges from 335 to 410 °C. Several references have evaluated the corrosion resistance of different alloys in incinerator environments [14, 34,35].

When the PAWDS is shutdown during idle periods or while the ship is at port, temperatures can fall below the condensation temperature of flue gases containing HCl and/or

When the PAWDS is shutdown during idle periods or while the ship is at port, temperatures can fall below the condensation temperature of flue gases containing HCl and/or H_2SO_4, and may form aqueous solutions of these acids. The dewpoint temperature of sulfuric acid (SO_3+H_2O) is 120-150 °C and rises with an increase in SO_3 concentration, but above 35 ppm the dewpoint temperature is constant at 150 °C. HCl has little effect on carbon steel below 260 °C, but in an excess of air, may form $FeCl_2$ on the carbon steel surfaces. Austenitic stainless steels subjected to moist deposits high in chlorides can suffer from chloride stress corrosion cracking [36].

Galvanic corrosion can occur if two metals of different electrochemical potentials are adjacent and electrically connected. Galvanic action also can proceed for the same metal if present at significantly different temperatures. At temperatures where gases prevail (400-1700 °C), the electrical conductivity should be low enough that galvanic action would not likely be a problem. The relatively noble potential of nickel-based alloys and stainless steels will not generally cause galvanic effects.

Carbon is more cathodic than platinum in the galvanic series for seawater and may be equally cathodic to the candidate chamber alloy in the PAWDS environment. The corrosion rate due to galvanic effects will be dependent on the conductivity of the steam/gaseous environment and the temperature fluctuations along the crucible wall. Deposition of soot (carbon) on the chamber walls may lead to galvanic attack if the conductivity of condensed fluids during idle periods is sufficiently high. Large sooted areas versus bare steel areas could increase the severity of galvanic attack. Soot or deposits may be porous and can lead to concentration of deleterious constituents through the porous layer. For instance caustic levels, caused by selective deposition of NaOH at high heat flux areas, have concentrated 100 ppm NaOH in bulk boiler water to over 200,000 ppm through a process called wick boiling [31].

Compositional changes of liquids or gases in crevices may be severe. Crevices may be formed at mechanical joints or under porous, but occluding deposits. Crevices leading to severe corrosion can occur if oxidizing conditions and a soluble species are present; such conditions usually occur during idle times when moisture is present [14]. Alloys high in molybdenum typically possess higher resistances to pitting and crevice corrosion attack. Surface deposits or crevices formed by joints or connections may be subject to crevice corrosion of stainless steels. Gasket materials containing sulfur or graphite can also accentuate crevice corrosion.

Grain boundary segregation may result in localized corrosion if the grain boundaries are not as resistant as the alloy matrix or segregation causes depletion of corrosion resistant elements. Pitting is another form of localized corrosion. Both dissolved oxygen and carbon dioxide can promote pitting of carbon steels. An alkaline pH can diminish corrosion with the evolved gases likely to be neutral to acidic. Ash deposition, thermally induced stress, and particulate erosion may cause conditions that accelerate localized corrosion by cracking the protective oxide layer. Grain boundaries may be susceptible to operating conditions or room temperature corrosion when condensed water solubilizes corrodents from deposits or soot.

In the shipboard PAWDS, the components may be subjected to ash and soot deposition, thermally induced stresses, and possible particulate erosion [14]. The primary chamber wall may suffer from erosion if the flame, high-velocity gases, or particles impinge on the wall. Local reducing conditions will increase the rate of erosion over conditions existing in oxidizing environments due to the increased difficulty of the alloy to repair and reform a passive oxide film. Flame impingement can produce local overheating which can cause distortion. Erosion may also cause protective scale removal. Impingement of liquid spray droplets on hot walls could cause spalling, dissolution, or erosion of the oxide layer. Alloy modification for erosion resistance may not be compatible with corrosion resistance. Stainless steels and most nickel-based alloys generally provide good resistance to impingement or erosion.

The crucible alloy material reportedly will be protected from molten slag by a oxide/slag skull in the PAWDS. However in the event of possible contact with molten slag, it is important to know the corrosion resistance to slag of the candidate materials. Liquid metal corrosion may cause dissolution of a surface directly, by intergranular attack, or by leaching. Liquid metal attack may also initiate alloying, compound reduction, or interstitial or impurity reactions. Carbon and low alloy steels are susceptible to various molten metals or alloys such brass, aluminum, bronze, copper, zinc, lead-tin solders, indium, and lithium at temperatures from 260 to 815 °C. Plain carbon steels are not satisfactory for long-term usage with molten aluminum. Stainless steels are generally attacked by molten aluminum, zinc, antimony, bismuth, cadmium, and tin [37]. Nickel, nickel-chromium, and nickel-copper alloys generally have poor resistance to molten metals such as lead, mercury, and cadmium. In general nickel-chromium alloys also are not suitable for use in molten aluminum [38]. Liquid metal embrittlement (LME) is a special case of brittle fracture that occurs in the absence of an inert environment and at low temperatures [39]. Decreased stresses can reduce the possibility of failure in certain embrittling molten alloys. Stainless steels suffer from LME by molten zinc. Small amounts of lead will embrittle nickel alloys, but molybdenum additions appear to improve lead LME resistance. There are no known metals or alloys totally immune to attack by liquid aluminum [40]. The selection of fabricating processes must be chosen carefully for nickel-based superalloys. Liquid metal embrittlement can occur when brazing precipitation-strengthened alloys such as UNS N07041 [41]. Many nickel superalloys crack when subjected to tensile stresses in the presence of molten (B-Ag) brazing filler alloys.

Long-term aging effects can cause metallurgical changes that alter the mechanical and corrosion properties of materials. Graphitization is a microstructural change that can occur in carbon and low alloy steels. Pearlite (alternating ferrite and Fe_3C platelet structure) normally found in such steels will transform in time to graphite and ferrite at temperatures above 425 °C which causes loss of ductility and promote embrittlement. Alloying additions of at least 0.7% Cr and 0.5% Mo to steels markedly improve resistance to graphitization. Weld sites are particularly susceptible to graphitization. Heat treatments or operating conditions that heat ferritic and austenitic stainless steels to 500-900 °C cause segregation at the grain boundaries by the precipitation of complex chromium carbides, the formation of sigma phase or the precipitation of other deleterious phases. The properties of precipitation-strengthened

superalloys (processed at 535-815 °C) such as UNS N07041 may be altered by brazing [41]. Normal welding can induce susceptibility of stainless steels without postweld heat treatment. Careful control of heat treatment can avoid intergranular corrosion of unstabilized stainless steels containing more than 0.03% C. Nickel-based superalloys are also susceptible to grain boundary segregation. Nickel-based superalloys can be embrittled by less than 20 ppm sulfur segregation to alloy grain boundaries.

PAWDS candidate materials such iron, nickel and cobalt superalloys owe their unique strength up to a fairly high threshold temperature to the presence of strengthening particles such as inert oxide dispersoids, carbides, coherent ordered precipitates, and solid solution strengthening agents in a face-centered cubic (with appropriate nickel additions) structure. Introduction of precipitates into the alloy through solid solution reactions require specific alloy chemistries and heat treatments to achieve the desired mechanical properties [41,42]. However, at prolonged exposures to high temperatures (760-1000 °C), the phase rule alone suggests that a large number of new phases could nucleate within multicomponent superalloys to form a number of microstructural instabilities [43]. These instabilities can include transformation of a metastable phase to a more stable, but incoherent phase as in carbide transformation, stress induced differential diffusion of solute atoms (coarsening of $M_{23}C_6$ at grain boundaries), or dissolution of strengthening precipitates in critical areas of the microstructure. Structural instabilities of superalloys at elevated temperatures can also include the formation of new phases such as sigma, mu, and Laves phases which are brittle and possess crack-like morphologies that can adversely affect alloy tensile and stress rupture ductility and impair resistance of the alloy to crack growth [43].

Creep is a time-dependent strain of a material under stress. Rupture of a metal or alloy can occur when it is subjected to stress at elevated temperatures for a sufficiently long time. Stresses are significantly lower than that necessary to cause rupture in room temperature or during short-term tensile tests. Higher temperatures and/or higher stresses will tend to decrease the time required for creep rupture. Creep embrittlement can occur in the temperature range of 425-595 °C for alloys having a ferrite and carbide microstructure [44]. The embrittlement is most detrimental after the steel has been cooled below 260 °C. For temperatures above 760 °C, metallic liners will have a limited life because of the microstructural instabilities that develop in many of the superalloys with prolonged exposure. One possible alloy is UNS N06671 [45] which can be used to 980 °C with temperature excursions of 1100 °C [14]. This alloy, however, is not widely available and is difficult to fabricate. Other possible selections would be alloys UNS N07041 and UNS N06230, which have good high-temperature strength and resistance to long-term thermal degradation. However, their resistance to hot corrosion, sulfidation and chloride-containing salts is not known.

Frequent cycling may reduce the design life of the PAWDS walls from that predicted for operation at steady state. The hot gas environment within the PAWDS will influence the corrosion fatigue resistance of candidate alloys [46]. Cyclic temperature conditions accelerate attack mainly through the loss of the protective scale [14]. Depending on the severity of the thermal cycles in the water-cooled design, spallation of thermal barrier coatings, chromized,

and aluminized coatings is probable. Corrosion fatigue is the combined action of a repeated or fluctuating stress and a specific corrosive environment that usually lowers the minimum stress level and/or the number of cycles that will cause failure than in a inert environment. Corrosion fatigue cracking and stress corrosion cracking often initiate at stress risers such as pits. In certain instances such as in nickel-based superalloys in high-temperature oxidizing environments, the aggressive conditions can slow the fatigue fracture propagation. Stainless steels have good corrosion-fatigue limits when compared to other steels.

Stress corrosion cracking (SCC) is a brittle fracture of an otherwise ductile material which occurs under the combined action of a residual or applied tensile stress and an alloy-specific corrodent. SCC is affected by alloy composition and heat treatment, the exposure time, temperature, and solution medium. Fluctuating temperatures can accelerate stress corrosion cracking of austenitic stainless steels in the presence of chlorides, particularly at high stress points from design, operation or fabrication. Nickel alloys have improved resistance to environmental cracking over steels and stainless steels although nickel alloys are not immune to SCC. SCC of certain nickel alloys has occurred in high-temperature halogen ion environments, high-temperature waters, and high-temperature alkaline systems and environments containing acids and H_2S. SCC is dependent on the stress level, chloride concentration, alloy composition, and temperature. Susceptible temperature ranges vary from 175-330 °C. Higher temperatures will tend to lower the chloride threshold concentration and stress levels required for cracking. Ferritic stainless steels are usually not considered susceptible to SCC. Stressed martensitic stainless steel grades can crack in chloride environments.

CONCLUSIONS

Compliance with environmental regulations has required design of a waste management system to safely treat and reduce the volume of solid shipboard waste for the U.S. Navy. The U.S. Navy in cooperation with industry has developed conceptual designs for a plasma arc waste destruction system (PAWDS) capable of meeting strict shipboard weight, size and operational criteria.

A hotwall design considered a refractory lined chamber to process shipboard waste. Silicon carbide, high purity alumina, and alumina-chromia working refractories were considered the best candidates for the hotwall PAWDS design. Weight and size limitations, maintainability, and reliability of the hotwall design led to the consideration of alternative PAWDS designs.

The final candidate material in the coldwall PAWDS will not be the most corrosion-resistant alloy in all possible environments. The protective chromia, alumina, and silica oxides scales formed on the alloys have different growth kinetics, mechanical properties, and corrosion resistances to oxidizing and reducing atmospheres, sulfidation, chloridation, hot corrosion, dewpoint corrosion, galvanic attack, hydrogen interactions, and environmental assisted cracking. The alloys also have different long-term mechanical properties at high temperatures.

For the water-cooled coldwall design with temperatures below 600 °C, alloy UNS N06022 would provide optimum resistance to corrosion processes possible in the PAWDS. Similar alloys that could provide possible service are: UNS N10276, UNS N06455, and UNS N06059. These are resistant to pit initiation due to a high level of molybdenum present in the alloys. For adequate to good resistance, alloy UNS N06625 is recommended. It does not have as high a resistance to pit initiation as UNS N06022, but has better high-temperature strength which may prove acceptable in a coldwall environment. None of the alloys recommended have a long-term (creep) stress rupture strength existing over 3 ksi. The chamber wall will have to be thick enough to compensate for this lack of high-temperature strength. The alloys considered thermally degrade with time at temperatures above 600 °C.

For an air-cooled or water-cooled chamber where the temperature is around 1000 °C, alloy UNS R30556 is recommended to provide the best service for a combination of oxidation, carburization, chloridation, and hot corrosion resistance. Alloy UNS N08120 may also provide adequate service in the air-cooled environment. These alloys maintain good high-temperature strength up to 900 °C, but the long-term high-temperature stability of these alloys still needs to be established. Two other alloys, UNS N06230 and UNS N07041, have better high-temperature strength and resistance to long-term thermal degradation of the alloy microstructure, but their resistance to hot corrosion, sulfidation and chloride-containing salts is not known at this time. The selection of fabricating processes must be chosen carefully for nickel-based superalloys. Liquid metal embrittlement can occur when brazing precipitation-strengthened alloys such as UNS N07041. Many nickel superalloys crack when subjected to tensile stresses in the presence of some molten filler metals.

Testing is strongly recommended in high-temperature environments that properly simulate the conditions in the PAWDS - particularly, environments that simulate the abrasive conditions, corrodents, and the temperature fluctuations generated by the plasma arc torch on the candidate test alloys. Alloys need to be tested in a simulated PAWDS environment and under similar operating conditions envisioned for the eventual shipboard PAWDS. High temperature erosion testing of several candidate materials is presently being planned.

ACKNOWLEDGEMENTS

This work was sponsored by the Naval Sea Systems Command Research, Development, and Standards and the Office of Naval Research, Program Element 060223N, Environmental Quality and Logistics. The program manager of the PAWDS Working Group is Dr. Eugene Nolting, Code 634, of the Environmental Quality Department, Carderock Division, Naval Surface Warfare Center. The authors would like to thank Roy Richards of Geo-Centers for the eductor figure. The Corrosion Branch, Code 613, is under the direction of Mr. Robert J. Ferrara.

REFERENCES

1 - R.L. Jones, *High Temperature Technology*, v. 6 187 (1988).

2 - Handbook of Refractory Practice, 1st ed., Harbison-Walker/Indresco Inc, Pittsburgh, PA, PR-12 (1992).

3 - L.M Sheppard, "Corrosion Resistant Ceramics for Severe Environments", *Ceramic Bulletin*, v.70, 1146 (1991).

4 - H.E. Wolfe, P.A. Beaulieu, "Update on Refractories for Hazardous Waste Incineration", *Corrosion/89*, paper 551, NACE International, Houston, TX (1989).

5 - *Ceramic Industry*, v. 154, 114 (1996).

6 - D.P. Butt, R.E. Tressler, K.E. Spear, "Corrosion of Silicon Carbide Materials in Metallurgical Heat-Treatment Environments", *American Ceramic Society Bulletin*, v. 71, 1683 (1992).

7 - S. Manning-Meier, D.N. Nissley, K.D. Sheffler, "Status of Ceramic Thermal Barrier Coatings - Gas Turbine Application and Life Prediction Methods", Proceedings of the 1990 Coatings for Advanced Heat Engines Workshop, Catine, ME, U.S. Department of Energy, II-57 (1990).

8 - R.A. Miller, C.E. Lowell, "Failure Mechanisms of Thermal Barrier Coatings Exposed to Elevated Temperatures", *Thin Solid Films*, v. 95, 265 (1982).

9 - S.M. Meier, D.N. Nissley, K.D. Sheffler, "Thermal Barrier Coating Life Prediction Model Development", NASA Contractor Report 189111, NASA Lewis Research Center, Cleveland, OH (July 1991).

10 - I. Nettleship, R.Stevens, *International J. High Technology Ceramics*, v. 3, 1 (1987).

11 - S.C. Singhal, R.J. Bratton, *Trans. ASME - J. Engineering for Power*, v.102, 770 (1980).

12 - R.L. Jones, "The Development of Hot Corrosion Resistant Zirconia Thermal Barrier Coatings", Proceedings of the 1990 Coatings for Advanced Heat Engines Workshop, Catine, ME, U.S. Department of Energy, II-67 (1990).

13 - R.L. Jones, "Experiences in Seeking Stabilizers for Zirconia Having Hot Corrosion Resistance and High Temperature Tetragonal Stability", NRL/MR/617--96-7841 (April, 1996).

14 - Materials of Construction for Shipboard Waste Incinerators, National Research Council, National Academy of Sciences, Washington, DC, 91-92 (1977).

15 - P. Elliot, "Practical Guide to High-Temperature Alloys", *Materials Performance*, v. 28, 57 (1989)

16 - F.H. Stott, G.C. Wood, J. Stringer, "Influence of Alloying Elements on the Development and Maintenance of Protective Scales", *Oxidation of Metals*, v. 44, 113 (1995).

17 - M. Shütze, "Mechanical Properties of Oxide Scales", *Oxidation of Metals*, v.44, 29 (1995).

18 - Corrosion, 2nd ed, L.L. Sheir, ed., Newes-Butterworths, London, 7:101 (1976).

19 - W.B. Hoyt, R.H. Caughey, "High Temperature Metal Deterioration in Atmospheres Containing Carbon-Monoxide and Hydrogen", *Corrosion*, v.15, 627t (1959).

20 - P.A. Lefrancois, W.B. Hoyt, "Chemical Thermodynamics of High Temperature Reactions in Metal Dusting Corrosion", *Corrosion*, v.19, 360t (1963).

21 - G.Y. Lai, *Proceedings in High Temperature Corrosion of Energy Systems*, M.F. Rutman, ed., The Metallurgical Society, 45 (1980).

22 - S. Mrowec, "The Problem of Sulfur in High-Temperature Corrosion", *Oxidation of Metals*, v. 44, 177 (1995).

23 - Corrosion, 2nd ed, L.L. Sheir, ed., Newes-Butterworths, London, 7:90 (1976).

24 - ibid. 7:93.

25 - P. Ganesan, G.D. Smith, L.E. Shoemaker, "The Effects of Exclusions of Oxygen and Water Vapor Contents on Nickel-Containing Alloy Performance in a Waste Incineration Environment", *Corrosion/91*, paper 248, NACE International, Houston TX (1991).

26 - H.H. Krause, *J. Materials for Energy Systems*, v.7, 322 (1986)27 - Metals Handbook, Corrosion,, v.13, 10th ed., ASM International, Materials Park, OH, 997 (1987).

28 - G.D. Smith, P. Ganesan, L.E. Shoemaker, The Effect of Environmental Excursions within the Waste Incinerator on Nickel-Containing Alloy Performance, *Corrosion/90*, paper 280, NACE International, Houston TX (1990).

29 - C.T. Wall, J.T. Groves, E.J. Roberts, "How to Burn Salty Sludges", *Chemical Engineering*, v. ,7 (April 14, 1975).

30 - P. Ganesan, G.D. Smith, L.E. Shoemaker, "The Effects of Excursions of Oxygen and Water Vapor on Nickel Containing Alloy Performance in a Waste Incineration Environment", *Corrosion/91*, paper 248, NACE International, Houston TX (1991).

31 - J.F. Wilkes, D.A. Shifler, "Historical Perspectives of Intergranular Corrosion of Boiler Metal by Water", *Corrosion/93*, paper 44, NACE International, Houston, TX (1993).

32 - K.T. Chiang, F.S. Pettit, G.H. Meier, "Low Temperature Corrosion", in High Temperature Corrosion, NACE-6, R.A. Rapp, ed., NACE International, Houston, TX, 519 (1983).

33 - W. T. Reid, External Corrosion and Deposits - Boiler and Gas Turbines, Fuel and Energy Science Series, J.M. Beer, ed., American Elsevier, New York, 104 (1971).

34 - G. Wacker, W.L. Wheatfall, "Corrosion Problems Associated with Shipboard Waste Incineration Systems", 1976 Triservice Corrosion Conference, Philadelphia, PA, 185, October, 26-28, 1976.

35 - P. Elliott, "Materials Performance in High-Temperature Waste Combustion Systems", *Materials Performance*, v.32, 82 (1993).

36 - H.H. Krause, D.A. Vaugn, P.D. Miller, "Corrosion and Deposits from Combustion of Solid Waste", *Trans. ASME - J. Engineering Power*, v.95, 45 (1973).

37 - R.M. Davison, T. Debold, M.J. Johnson, "Corrosion of Stainless Steels", Corrosion,, v.13, 10th ed., ASM International, Materials Park, OH, 559 (1987).

38 - R.A. Smith, S.R. I. Saunders, Corrosion, 3rd ed., L.L. Sheir, R.A. Jarman, G.T. Burstein, Butterworth-Heinemann, London, 7:136 (1994).

39 - M.H. Kamdur, "Liquid Metal Embrittlement" , Corrosion,, v.13, 10th ed., ASM International, Materials Park, OH, 171 (1987).

40 - M.G. Fontana, N.D. Greene, Corrosion Engineering, 2nd ed., McGraw-Hill, New York, 294 (1978)

41 - Superalloys- A Technical Guide, E.F. Bradley, ed., ASM International, Materials Park, OH (1988).

42 - Alloy and Microstructural Design, J.K. Tien, G.S. Ansell, eds., Academic Press, New York (1976).

43 - J.K. Tien, S. Purushothaman, "The Metallurgy of High Temperature Alloys", in Proceedings: Properties of High Temperature Alloys - with Emphasis on Environmental Effects, v. 77-1, Z.A. Foroulis, F.S. Pettit, eds., The Electrochemical Society, Pennington, NJ, 3 (1976).

44 - Metals Handbook, *Properties and Selection: Irons, Steels, and High-Performance* Alloys, 10th ed. v.1 , 626-7 , ASM International, Materials Park, OH (1990).

45 - Metals Handbook, *Properties and Selection: Stainless Steels, Tool Materials, and Special-Purpose Metals,* 9th ed. v.3 , 144, ASM International, Materials Park, OH (1980).

46 - F.S. Pettit, J.K. Tien, "Hot Gas Environment - Alloy Reactions and Their Relation to Fatigue", Corrosion Fatigue: Chemistry, Mechanic, and Microstructure, NACE 2, NACE International, Houston, TX, 576 (1972).

47 - Alloy Data, Carpenter Technology Corporation, Carpenter Steel Division.

48 - High Temperature Product Literature and Hastelloy Corrosion-Resistant Alloy Product Literature, Haynes International, Kokomo, IN, 1991-1996.

49 - Product Information, The Carborundum Company, Refractories Division

Table 1 - Thermal Destruction Technologies[2]

Technology	Operational Temperature	Application/ Destruction Characteristics	Gas Products	Solid Products	Waste Reduction	Remarks
Incineration • Starved Air • Excess Air	900 °C 1650 °F	Solids & Liquids by Exothermic Combustion	CO_2, H_2O, N_2 Some: Hydrocarbons NO_x,SO_2	Particulates (Flyash) • Ash • Metal • Glass	High	Low Energy Input Available Units Generally Produce Excessive Air Emissions and Hazardous Ash
Wet Air Oxidation	316 °C 600 °F	Liquids by Low Temperature Pressurized Oxidation	CO_2, H_2O, Hydrocarbons	Particulate • Char • Inorganics	Moderate	Moderate Energy Input Incomplete Conversion of Organics. Fairly easy to design, build, and control.
Supercritical Water Oxidation	374 °C 705 °F	Liquids by Medium Temperature High Pressure Oxidation	CO_2, H_2O	Particulates Salts	Maximum	Moderate Energy Input (Depends on Waste Stream) Can Produce Complete Oxidation of Organics.
Plasma Arc • Pyrolysis • Incineration	1500-5000 °C 2700-9000 °F	Solids & Liquids by Very High Temperature/ Gasification Reactions	CO_2, H_2O, N_2	Inert Maximum Density Slag	Maximum	Very High Energy Input Air Emissions control is easier with conventional Incineration. Ash can be vitrified, making it inert.

Table 2
Green Book Navy Solid Waste (NSW) Generation Rates[3]

Average Generation Rates		
Waste Stream Constituents	lb/man/day	Weight %
Paper/Cardboard	1.11	35.35
Food	1.28	40.76
Metal	0.41	13.06
Glass	0.13	4.14
Plastic*	0.21	6.69
Total	3.14	100.00

* Note: Plastics are not planned to be processed by PAWDS

Table 3
Melting Points of Common Refractories

Nomenclature	Formula	Melting Point (°C)
Corundum, Alpha Alumina	Al_2O_3	2054
Baddeleyite, Zirconia	ZrO_2	2700
Periclase, Magnesia	MgO	2852
Chromic oxide, Chromia	Cr_2O_3	2330
Lime, calcia	CaO	2927
Cristobalite, silica	SiO_2	1723
Carborundum, Silicon Carbide	SiC	2700 (sublimes)
Silicon Nitride	Si_3N_4	1800 (dissociates)
Boron Nitride	BN	3000 (sublimes)

Table 4 - Candidate Working Refractories [2,49]

PARAMETER	CarboFrax® M SiC	Alfrax®	Refrax ®20 SiC	Tufline® 95DM	Aurex® 75 SR	Corundum® DM	Ruby® SR
Composition	89.2-SiC;0.5-CaO;1.0 Fe_2O_3 1.0-Al_2O; 6.3-SiO_2	96-Al_2O; 3.9-CaO tr-others	75-SiC 23.4-Si_3N_4 tr-others	94.2-Al_2O; 2.0 SiO_2; 3.6-other oxides, 0.1-Fe_2O_3,CaO	72.6- Cr_2O_3 20.7-Al_2O; 5.7- ZrO_2 1- other oxides	99.7 -Al_2O; 0.2-SiO_2 0.1- Fe_2O_3	83.6-Al_2O_3 10.2-Cr_2O_3 1.9-SiO_2; 3.5-other oxides
Max. Operating Temperature, °C	1480	1815	1760	1870	>1925	1870	1815-1870
Density g/cm^3/lb.ft^3	2.33/145	2.73/170	2.62/163	3.35/209	4.08/255	3.33/208	3.19/199
Apparent Porosity, %	17	--	15	12	15.8	12.9	18.1
Thermal Cond. @1477°K W/m°K	15.7	--	16.3	3.60	2.59	2.45	3.31
Permanent linear change, % 20-1727°C	-0.1 (est)	--	--	-0.1	+0.3	negligible	-0.2
Thermal shock resistance [2]	--	--	--	40+ cycles	14 cycles	3 cycles	22-25 cycles
Rupture modulus (MPa/psi)	215/3000	401/5600	445 /6300	21 6/3020	147/2060	320/4500	149/2080
Compressive Strength (MPa/psi)	1434/20,000	--	1434/20,000	993/13,860	609/8500	322/4500	910/12,700

Carbofrax, Alfrax, Refrax are registered trademarks of The Carborundum Company
Tufline, Aurex, Corundum, and Ruby are registered trademarks of Harbison-Walker, a division of INDRESCO, Inc

Table 5 - Candidate PAWDS Alloys - Chemical Compositions[46,47]

Alloy ASME or UNS Number	C	Mn	P	S	Cr	Ni	Co	Mo	Si	Cu	Fe	Al	Ti	W	Cb+Ta	Others
SA 414 Gr A	0.15	0.90	0.035	0.040							bal					
K11789	0.17	0.40-0.65	0.30	0.30	1.00-1.50	---	---	0.45-0.65	0.50-0.80	---	bal	---	---	---	---	---
S31008	0.08	2.00	0.045	0.030	24.00-26.00	19.00-22.00	---	----	---	---	---	---	---	---	---	---
S31603	0.03	2.00	0.045	0.03	16.0-18.0	10.0-14.0		2.0-3.0	1.00							
N06022	0.010	0.50		0.08	22	56	2.5	13	0.08	--	3			3		0.35
N06059					23 nom	59 nom		16 nom			1 nom					
N06600	0.10	1.00		0.015	14.00-17.00	72.00 min	---	---	0.50	0.50	6.00-10.00	---	---	----	----	----
N06601	0.10	1.0		0.015	21.0-25.0	58.0-63.0			0.50	1.0	rem	1.0-1.7				
N06625	0.10	0.50	0.015	0.015	20.0-23.0	55.0 min	1.00	8.0-10.0	0.50--	---	5.00	0.40	0.40	----	3.15-4.15	---
N06671	0.05 nom				48.0 nom	bal							0.35 nom			
N06690	0.03 nom				30 nom	60.5 nom					9.5 nom					
R30556	0.05-0.15	0.5-2.0	0.04	0.015	21-23	19-22.5	16-21	2.5-4.0	0.2-0.5	---	bal	0.10-0.50	---	2.0-3.5	0.30-1.25 Ta ;0.30 Nb	0.005- 0.10 La; 0.001-0.10 Zr; 0.10-0.30 N; 0.04
N12160	0.05	0.5			28	37	30	1	2.75	---	3.5 max	---	0.45	1	1.0 max	
N08120	0.05	0.7			25	37	3	2.5	0.6	---	33	0.1	0.1	2.5	0.7	0.004 B;0.2 N
N07214	0.5 nom	0.5			16 nom	75 nom	---	---	0.2	---	3 nom	4.5 nom	---	---	---	0.1 Zr;0.01 B; 0.01 Y nom
N06230	0.05-0.15	0.3-1.0			20.0-24.0	bal	5	1.0-3.0	0.25 0.75		3	0.20-0.50		13.0 15.0		0.005-0.50 La;0.015 B
N07041	0.05-0.12	0.10		0.015	18.0-20.0	55.0 nom	10.0-12.0	9.0-10.50	0.50		<0.3	1.40-1.60	3.0-3.30			0.0030-0.010 B
R30188	0.05-0.15	1.25			20.00-24.00	20.0-24.0	bal	---	0.20 0.50	---	3.00	----	---	13.0 16.0	---	0.03 -0.15 La

Table 6 - Candidate Alloy Physical and Mechanical Properties [46,47]

Alloy UNS Number	ASME max temp/ other max service temp °C	ASME strengt criteria	1% Creep-rupture strength 500 C/10^5h	Thermal conductivity W/m- °K 500 °C	Thermal conduct. W/m- °K 800 °C	Expan. Coeff. µm/m-°C 500 °C	MP °C	Density g/cm^3	Specific Heat kJ/kg-°K @ 871°C	UTS ksi @ 982°C	0.2% YS ksi @ 982°C	Percent elong. @ 982 °C
SA414-A	400-500	425	4.5-6 ksi	40	26	16.4						
SA213-T22	580 °C	595	6.5-7.3 ksi	37	26	15.4				2.4 max @650°		
S31008			13			17.5		8.00	0.500 @100	13	---	57
S31603	760	815	19 est.							6.1 max @650°		
N06600	982			22.5	27.6	15.1	1393	8.498	0.625	7.5	4.0	118
N06601				19.5	24.4	15.2	1301-1368	8.11				
N06625			649 -27.5 871-2.5ksi 10^5 hr	16.9	21.4	13.9	1288-1349	8.442	0.620	25.8	13.0	143
N06671						15.0	1305-1350	7.86	0.456 RT.	14	9	
N06690				22.1	26.6	16.2 @ 649 °C	1345-1375	8.08	0.6 est	15	10	
R30556	900	650		18.3	22.7	16.2		8.23	0.600	30.3	20.2	56
N12160	816		16.3 @ 593	19.8	26.1	14.9			0.562	20.4	10.8	90
N08120				18.7	24.9	16.1			0.558	27.9	19.4	81
N07214			16 @ 760	21.0	29.7	14.8	>1345	8.05	0.724	16	7	80
N06230	899	899	11.5 @ 760			14.0	1301-1371	8.97	0.605	32.5	17.3	70.5
N07041							1252-1371	8.25	0.452	90@870	50@892	19
R30188			13.5 @ 760	19.3	24.8	14.6	1302-1330	9.13	0.568	37.7	24.7	86

Table 7 - Corrosion in Various High Temperature Environments [47]

ALLOY UNS number	Static Air Oxidation Temperature[1]		Dynamic Air Oxidation Temperature[2]	Reducing Sulfidation[3,4]		Hot Corrosion[5,8]		Chloridation[6]	Carburization[7] mg/cm^2/mil depth
	980 °C	**1204 °C**	**980 °C**	**871 °C**	**593 °C**	**675 °C**	**760 °C**	**1000 °C**	**980 °C**
S31008	1.1	10.3	16.5	14		12	13.0 (35)		7.7/84.2
N06601	1.3	2.6 @1090 7.5**	20.0	perforated >21.7				9.0 @ 900	
N06625	0.7	>47.6	7.6			5		10.5 @ 900	
N06690							2.8(nil)		
N07214	0.2	0.7	1.2					6.0@900	
N08120	3.7	7.7 @1090							0/0
R30556	1.1	>150	6.2	35.6	121	2.5		6.0@ 900/11.8	1.0/18.0
N06230	0.7	7.9	3.5						0.4
R30188	0.6	>21.7	4.2	23.6	151		46.6 (9)		0.5

1) Average metal affected, results in mils (0.001" = 1 mil) Static Oxidation in Air ; lab test for 1008 hour with specimens cycled to room temperature once every 168 hours, ** large internal voids not included for N06601 reading.

2) Maximum metal affected, results in mils (0.001" = 1 mil) Dynamic Oxidation in Air ; lab test for 1000 hour with specimens cycled to room temperature once every 30 minutes

3) Ar- 5%H_2-5% CO-1% CO_2- 0.15% H_2S, PO_2 =3x10^{-19} atm, duration 500 hours except 310SS which was for 215 hours, maximum depth of attack

4) H_2-46% CO-0.8% CO_2- 1.7% H_2S at designated temperatures.

5)Recuperator of aluminum remelting furnace flue gases. Mode of corrosion combined attack by alkali sulfates, chlorides with oxidation for 1150 hours, maximum metal affected.

6) Ar+20% O_2- 0.25% Cl_2 for 400 hours at 1000 °C, average metal affected, mils.

7) packed Carburization resistance for 500 hours in packed graphite , mg/cm^2 at 982°C.

8) Burner rig test with combustion products of No. 2 fuel oil (1.0%sulfur), thermal shock frequency 11/500 hours, average corrosion rate, corrodent urine; mils/year (max penetration, mils).

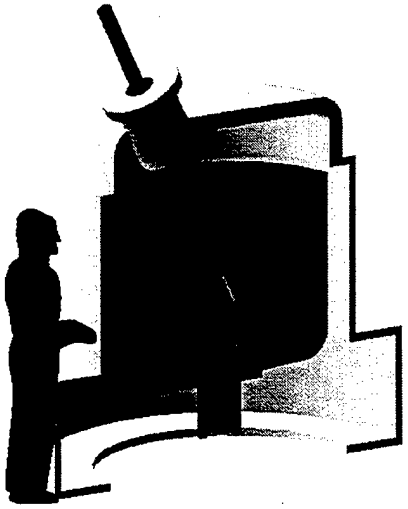

Figure 1- Cross-section of refractory-lined hotwall PAWDS.

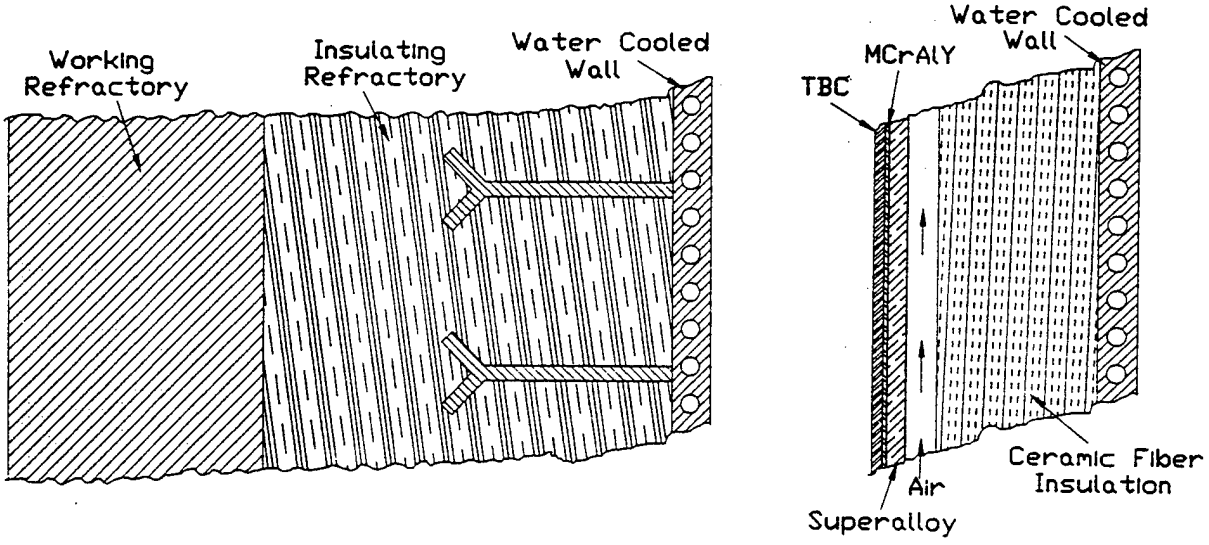

Figure 2 Comparison of thick refractory required for hotwall design (left) and air-cooled coldwall design using a TBC on a superalloy (right).

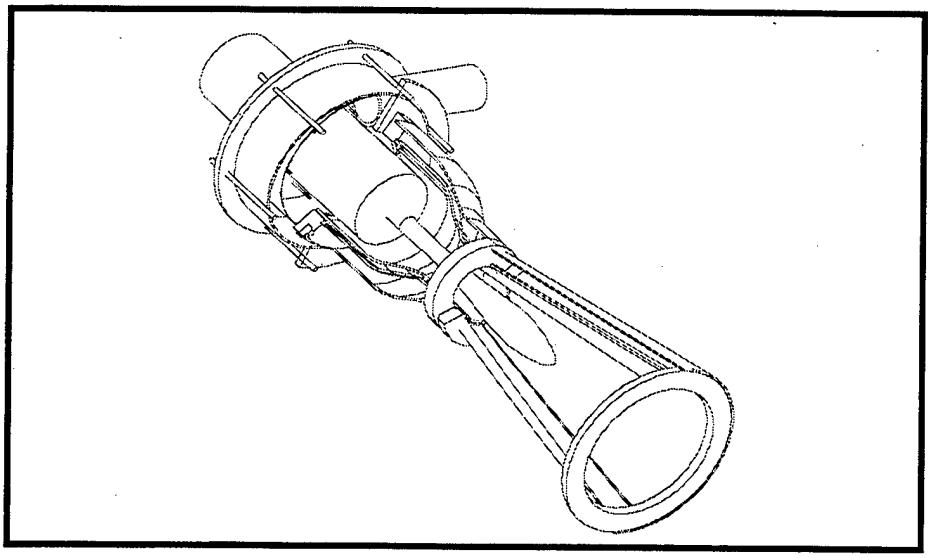

Figure 3 - Diagram of eductor consists of a central plasma torch which will process organic shipboard waste drawn through the tube and into a secondary chamber.

Localized Corrosion Behavior of Aluminum-Lithium Alloy, 2097

J. T. Hunter and J. F. Dante
University of Dayton Research Institute
300 College Park Avenue
Dayton, Ohio 45469-0137

ABSTRACT

The localized corrosion behavior of 2097-T8, an aluminum-lithium alloy, was studied in response to the replacement of 2124-T851 aluminum alloy on an F-16 bulkhead. Standard corrosion tests conducted included accelerated corrosion tests, atmospheric exposure, and electrochemical polarization. The tests revealed 2097 has a higher resistance to localized corrosion than 2124. Chromic acid anodize and chromate conversion coating pretreatments were found to limit pit growth more effectively on 2097 than on 2124.

INTRODUCTION

Significant fatigue cracking on flight and safety critical bulkheads attached to the vertical tail of F-16 fighters has resulted in a material replacement. Based on improved mechanical properties and a 5% density reduction Alcoa's recently developed 2097-T8 aluminum-lithium alloy was chosen to replace 2124- T851 (UNS A92124). Although extensive work has been performed to verify extended life of 2097 for this application, limited attention has been given to characterization of its corrosion behavior. Lockheed Martin has performed stress corrosion and exfoliation resistance testing, which indicates superior resistance of 2097 on both accounts.[1] However, the susceptibility of 2097 to localized corrosion and the effects of pretreatment have not been evaluated and are the focus of this work.

To obtain a broad characterization of the corrosion behavior of 2097, electrochemical, salt fog, cyclic, and atmospheric tests were run. Conventional surface pretreatments used for corrosion prevention on aluminum alloys in aerospace applications were examined, with and without application of a finishing system. The test matrix in Table 1 summarizes this work.

EXPERIMENTAL PROCEDURE

Materials

The aluminum and aluminum-lithium alloys were received from Lockheed Martin. The Al-Li coupons, 10 x 25 x 0.64 cm, were machined from 14 cm thick plate, and the 2124 coupons, 10 x 12.5 x 0.5 cm, were machined from 4 cm thick plate. A chemical analysis of 2097 using an inductively coupled plasma technique is shown in Table 2. Mechanical properties of 2097-T8 and 2124-T851 are shown in Table 3.

Surface Preparation at Lockheed Martin- Chromate conversion coated and chromic acid anodized coupons were first alkaline cleaned with 15-25 vol. % Turco 3878 at 52-57 °C for up to 15 minutes. They were then rinsed with ambient city water for five minutes. Acid cleaning was performed for up to 15 minutes at ambient temperature using a 10-22 total vol. % solution of nitric, hydrofluoric, and chromic acid. During the acid desmut process the coupons were immersed in a 9-11 vol. % ambient solution of nitric acid with Henkle Surface Technologies Deoxidizer 6/16 (chromated) for three minutes. This was followed by a two-stage rinse with ambient city water for two and four minutes, respectively. An Alodine 1200S chromate conversion coating per Mil-C-5541, Class 3 or a chromic anodize per Mil-A-8625, Type I, Class 1, with a sodium dichromate seal was then applied. These pretreatments were used for each test method except for the electrochemical measurements.

Surface Preparation at Wright Laboratory- Bare coupons were cleaned using an alkaline solution of 10 vol. % Brulin GD815 at 60 °C for 20 minutes, followed by a water break-free rinse with ambient distilled water. All Al-Li coupons, including those received from Lockheed Martin were then dry sheared across the width to double the number. The 2124 coupons were already cut to the desired size. Bare coupons were used for each test method. A sulfuric anodize per Mil-A-8625, Type II, Class 1 was applied to some of the bare coupons. Some of the anodized coupons were coated with Mil-P-85582 epoxy primer and Mil-C-85285 polyurethane topcoat. The coating was then scribed with an "X" exposing the bare metal to simulate service damage. The sulfuric anodized and coated materials were used only for atmospheric testing.

Preparation of Electrochemical Samples- Bare samples were polished to a 6 micron finish using a diamond paste. Prior to the application of a chromic acid anodize per Mil-A-8625, Type I, Class 1, samples were polished to a mirror finish. Bare and chromic acid anodized samples of each alloy were cut into 2 x 2 cm squares. Prior to testing, each sample was rinsed in isopropyl alcohol and deionized water to remove contaminants.

Testing Procedure

The ASTM B117 salt fog and ASTM G85 Annex 5 cyclic tests were used as accelerated techniques to gauge the susceptibility of the alloys to pitting corrosion. The cyclic test consisted of wet (1 hour at ambient temperature) and dry (1 hour at 35 °C) conditions with a 0.05 wt. % NaCl and 0.5 wt. % $(NH_4)_2SO_4$ electrolyte. Although the cyclic test was developed for coatings on steel substrates, it is of interest to investigate the correlation of this test to outdoor exposure on aluminum alloy substrates. Despite the difference in operating conditions, the rating procedure between the two tests was the same. Representative panels of each alloy and condition were removed periodically, cleaned per ASTM G1, photographed, and rated according to Table 4. As the table indicates, the severity of corrosion increases from five to zero. After a one to two day rating process the coupons were returned for further exposure.

Atmospheric exposure of bare, pretreated, and coated coupons was performed to investigate corrosion behavior in a more realistic environment. Coupons were exposed to a seacoast/UV environment at Key West, FL. Panels were positioned 8 meters from the ocean, facing south and angled at 45°. After a one year exposure a bare panel of each alloy was removed

for analysis. Pretreated and coated coupons were not removed; however, corrosion performance was documented. Subsequent analyses will be performed every other year of exposure.

In addition to the visual rating performed on coupons exposed to accelerated tests, metallographic examination was used to measure the depth of pitting under the localized corrosion product at the conclusion of salt fog and atmospheric exposure. Coupons were cross-sectioned and polished using conventional metallographic procedures. The cross-sections were examined under an optical microscope at 250X. The total area examined was consistent for each alloy and condition. All pits deeper than six microns were measured and counted. Pit depths are reported in Figures 3-6.

Consideration was given to where the cross-sections should be made. Pits were clustered on all Al-Li coupons. Because the depth of pits are significant in terms of acting as stress concentrators, 2097 panels were sectioned at the pit clusters so pit depth could be measured. In contrast, the 2124 coupons were uniformly pitted, which allowed the cut to be made anywhere along the panel surface to obtain results representative of the entire surface. Therefore, the *number* of pits reported on 2097 coupons is an exaggerated representation of the entire surface.

Electrochemical potentiodynamic polarization scans were performed on bare and chromic acid anodized samples as a method to quantitatively gauge relative corrosion behavior. A three electrode cell was used to analyze a 1 cm^2 surface area. The alloys were evaluated in two different test solutions: (1) the more conventional 0.6 M NaCl solution, and (2) an artificial rainwater (ARW) solution containing 26.0 mM ammonium sulfate, 23.7 mM sodium nitrate, and 8.6 mM sodium chloride. The pH of the rainwater solution was adjusted to 4.8 with nitric acid. The ARW solution was used to better represent an aircraft environment compared to the 0.6 M NaCl solution.

Polarization scans were initiated 40 mV below the open circuit potential (OCP) and were continued by polarizing the sample anodically at 0.2 mV/sec until the pitting potential was reached. The scans were reversed in the cathodic direction when the current density reached 1×10^{-4} A/cm^2. Scans were run in both aerated and deaerated solutions. The solutions were deaerated by bubbling argon gas into the test cell during the scan in order to stabilize the surface oxide. Prior to running the polarization scans, the samples were immersed for 2 hours deaerated when exposed to the NaCl solution. Stabilization of samples in the ARW solution required 17 hours aerated followed by 4 hours deaerated immersion. This procedure was used to obtain reproducible data. The OCP, passive current density, pitting potential, and repassivation potential were measured for each alloy in each solution.

RESULTS

Accelerated Corrosion Tests

The extent of corrosion observed on coupon surfaces exposed to salt spray and cyclic tests is shown in Figures 1 and 2, respectively. The surfaces of both bare and pretreated 2097 coupons were more corrosion resistant than either bare or pretreated 2124.

Metallographic analysis of the degree of pitting from salt fog testing of bare coupons is shown in Figure 3. Although 2097 panels were cross-sectioned at major pitted areas, pitting of 2124 was still found to be more severe. Pits on 2124 were observed to be both wider and deeper than those on 2097.

The pit depth frequency distributions for the chromic acid anodized and chromate conversion coated conditions are shown in Figures 4 and 5. Pitting performance of pretreated 2097 was improved over bare 2097. A significant reduction in pit depth was observed on the pretreated 2097 coupons. While frequency of pitting was not significantly affected, pit depth distribution for each pretreatment shifted from 100% of pits over 1.27 microns deep to 100% of pits under 1.27 microns deep. In contrast, pretreatments on 2124 reduced the frequency of pits. However, there remained pits on pretreated 2124 of significant depth.

Atmospheric Exposure

One year atmospheric exposure results on untreated alloys are shown in Figure 6. For both alloys, 2097 and 2124, the pits observed on these panels were not as deep as those resulting from salt fog testing. According to metallographic analysis both alloys contained approximately the same number of pits after atmospheric exposure, but deeper pits were observed on the 2124 material.

Less than 5 "pinhole-type" pits were found on the surface of one 2097 coupon with chromic acid anodize. Approximately 15-20 similar pits were found on the sulfuric acid anodize panel. The chemical conversion coating offered the least protection of the three pretreatments. There was no evidence of corrosion along the scribe of coated 2097 coupons.

Electrochemical Measurements

Figure 7 illustrates the polarization curves for bare 2124 and 2097 in both deaerated 0.6 M NaCl and deaerated artificial rainwater. The pertinent data is summarized in Table 4. Each entry represents the average of three tests. The open circuit potential, pitting potential, and the repassivation potential are significantly higher in the ARW solution. The passive current density is approximately an order of magnitude lower for samples in the 0.6 M NaCl solution.

Table 5 shows the OCP for bare 2124 and 2097 in NaCl and ARW under aerated conditions. The data in Table 5 represent the average of three tests. Again, the OCP was much higher in the artificial rain water solution.

No evidence of pitting was observed on either 2124 or 2097 when the surface was anodized. Very low current densities on the order of 10^{-8} A/cm^2 were measured.

DISCUSSION

Trend of Localized Corrosion

The tendency of localized corrosion observed throughout testing was that 2097 formed pits that were more shallow and narrow compared to those formed on the 2124 alloy. Shallow pitting of 2097 was even more prominent when pretreatments were applied. Referring to Figures 4 and 5, both the conversion coating and the anodize were much more effective on the 2097 alloy than on the conventional aluminum alloy. This behavior has been observed in a study by Parzuchowski et al.,[2] wherein a complete finish system offered more protection on Al-Li alloys than on conventional aluminum alloys.

Although the reason for the improved corrosion resistance of 2097 over 2124 was not part of the scope of this investigation, other authors have related the resistance of Al-Li alloys to the amount and type of coprecipitates.[2-3] The precipitation of S′ (Al_2CuMg) and T_1 (Al_2CuLi) phases has been shown by these studies to contribute more to localized corrosion than δ′ (Al_3Li) and δ (AlLi) phases. As the chemical composition in Table 2 indicates, magnesium is not used as a major alloying element in 2097. Therefore, further studies may reveal that the low Mg concentration in 2097 is a contributor to its improved localized corrosion resistance.

Comparison of Accelerated Test Methods

Historically a chromic acid anodize offers better protection against corrosion than a chemical conversion coating on aluminum materials. Visual observations of coupon surfaces exposed to the Key West environment support this claim. However, the ASTM B117 salt fog test results indicate that the conversion coating is more protective than the anodize. Referring to Figure 2, the cyclic test method showed better protection from the anodize compared to the chemical conversion coating on the 2124 alloy, and equivalent protection between the two pretreatments on the 2097 alloy. This suggests that the cyclic test may correlate better to marine environments compared to conventional salt fog testing. Other studies have shown that the combination of ammonium sulfate in the solution and wet/dry cycling is more representative of materials exposed to marine environments.[4-6]

Electrochemical Measurements

The last column of Table 6 describes where the aerated open circuit potential were located relative to the pitting potential. The aerated OCP for 2124 was in a stable pitting environment, above the pitting potential. However, the aerated OCP for 2097 was in a metastable pitting environment, below the pitting potential (and above the repassivation potential). This would suggest that deeper pits would form on 2124 than on 2097, which is in agreement with both salt spray and outdoor weathering. Pit depth was not measured on samples exposed to the cyclic test.

Less Cl^- ions in the ARW solution significantly increased the pitting potential for both alloys compared to the 0.6 M NaCl solution. However, the strong oxidizers in the ARW and a

smaller negative surface charge (due to less Cl^-) compensated somewhat for this effect, resulting in a higher OCP.

Chromic acid anodized 2124 and 2097 samples showed no signs of pitting in either test solution. This lack of pitting is in contrast to the results from salt fog, cyclic, and outdoor weathering tests. The less aggressive nature of the electrochemical immersion solutions compared to the other test environments may explain this result. In agreement with other test results, the anodized samples performed better than the bare samples.

CONCLUSIONS

The resistance to pitting of aluminum-lithium 2097 alloy measured by salt fog, cyclic, electrochemical, and outdoor exposure methods is superior to the conventional aluminum 2124 alloy. Bare 2097 had at least equivalent corrosion resistance compared to pretreated 2124 according to salt spray and cyclic testing.

The chromic acid anodize offered more protection than the chromate conversion coating in cyclic and atmospheric testing. The salt fog test failed to substantiate this trend. However, both pretreatments offered more effective protection on 2097 than on 2124 in salt fog and cyclic testing.

The tendency for 2124 to form deeper pits than 2097 can be explained by electrochemical measurements. The aerated open circuit potential for 2124 was over the pitting potential, while the aerated OCP for 2097 was between the pitting and repassivation potentials. This relationship was observed for both 0.6 M NaCl and artificial rainwater solutions.

ACKNOWLEDGMENTS

This effort was undertaken as part of an Logistical Support Materials program at Wright-Patterson Air Force Base under contract F33615-94-C-5601. The authors would like to thank Lockheed Martin for providing the 2097 and 2124 materials. A note of appreciation is also extended to Mr. Ken Chitwood of the University of Dayton Research Institute for his assistance in preparing samples and administering the accelerated and atmospheric tests.

REFERENCES

1. L.K. Austin, Lockheed Fort Worth Company, "Al-Li Alloy 2097/2197 Review," briefing, May 1995.
2. M.J. Parzuchowski, E.J. Tuegel, K.K. Sankaran, "A Study of the Corrosion Characteristics of Aluminum-Lithium Alloys for Aircraft Applications," Proceedings of the International Aluminum-Lithium Conference, 1992, pp. 777-782.
3. J.P. Moran, E.A. Starke, Jr., G.E. Stoner, G.L. Cahen, Jr., "The Influence of Composition and Microstructure on the Corrosion Behavior of Two AlLiX Alloys," Corrosion, V. 43, n. 6, June 1987, pp. 374-382.

4. N.D. Cremer, "Prohesion Compared to Salt Spray and Outdoors Cyclic Methods of Accelerated Corrosion Testing," C. & W. Specialist Equipment Ltd., Shropshire, England, Reprinted by The Q-Panel Company, Report # L-8120.
5. C.H. Simpson, C.J. Ray, B.S. Skerry, "Accelerated Corrosion Testing of Industrial Maintenance Paints Using a Cyclic Corrosion Weathering Method," Journal of Protective Coatings & Linings, V. 8, n. 5, May 1991, pp. 28-36.
6. B.S. Skerry, C.H. Simpson, "Combined Corrosion/Weathering Accelerated Testing of Coatings for Corrosion Control," Proceedings of NACE Annual Conference and Corrosion Show, March 1991.

TABLES

Table 1. Corrosion test matrix

Condition	Salt Spray ASTM B117	Cyclic ASTM G85	Atmospheric ASTM G50	E-Chem ASTM G	
				0.6 M NaCl	ARW
Bare	3	3	3	3	3
Mil-A-8625 Type I Class 1	3	3	3	3	3
Mil-C-5541 Class 3	3	3	3		
Mil-A-8625 Type II Class 1			3		
MIL-A-8625 Type I Class 1, MIL-P-85582, MIL-C-85285			3		

Table 2. Chemical composition of 2097-T8 and 2124-T851

	2097		2124
	Measured ICP wt. %	Registered Limits	AMS 4101
Copper	2.73	2.5-3.1	4.4
Lithium	1.54	1.2-1.8	-
Magnesium	0.084	0.35	1.5
Manganese	0.291	0.10-0.60	< 0.90
Zirconium	0.102	0.08-0.16	-
Zinc	0.103	0.35	< 0.20
Silicon	0.015	0.12	< 0.20
Iron	0.016	0.15	< 0.25
Titanium	0.012	0.15	< 0.15
Chromium	-	-	< 0.10
Others, Each	< 0.01	0.05	< 0.05
Others, Total	< 0.06	0.15	< 0.15
Aluminum	Remainder	Remainder	

Table 3. Mechanical property data for 2097-T8 and 2124-T851

	2097-T8 Measured; 14 cm plate	2124-T851 AMS 4101; 13-15 cm plate
Yield Strength, 0.2% offset, MPa		
L	421	372
LT	415	372
45°	410	
Tensile Strength, MPa		
L	453	434
LT	467	434
45°	462	
Elongation, %		
L	16.6	6
LT	13.0	5
45°	14.1	

Table 4: Corrosion rating scale used for visual analysis of salt spray and cyclic accelerated chamber testing.

Rating	Description
5	No visible staining or corrosion product
4	Slight staining or pit initiation
3	Minor amount of localized corrosion product build-up
2	Moderate amount of localized corrosion product build-up
1	Major amount of localized corrosion product build-up
0	Severe amount of localized corrosion product build-up

Table 5. Electrochemical parameters for 2124 and 2097 in 0.6 M NaCl and artificial rainwater under deaerated conditions.

Alloy	Solution	E_{corr} (V vs. Ag/AgCl)	I_{pass} $\mu A/cm^2$	E_{pit} (V vs. Ag/AgCl)	E_{rp} (V vs. Ag/AgCl)
2124-T851	0.6 M NaCl	-0.945	0.32	-0.734	-0.865
	ARW	-0.55	3.08	-0.362	-0.526
2097-T8	0.6 M NaCl	-0.993	0.195	-0.637	-0.947
	ARW	-0.607	6.675	-0.081	-0.566

Table 6. Open Circuit potentials for 2124 and 2097 in 0.6 M NaCl and artificial rainwater under aerated conditions.

Alloy	Solution	E_{corr}	E_{pit} - E_{corr}
		(V vs. Ag/AgCl)	(V vs. Ag/AgCl)
2124-T851	0.6 M NaCl	-0.702	-0.032
	ARW	-0.344	-0.018
2097-T8	0.6 M NaCl	-0.661	0.024
	ARW	-0.251	0.170

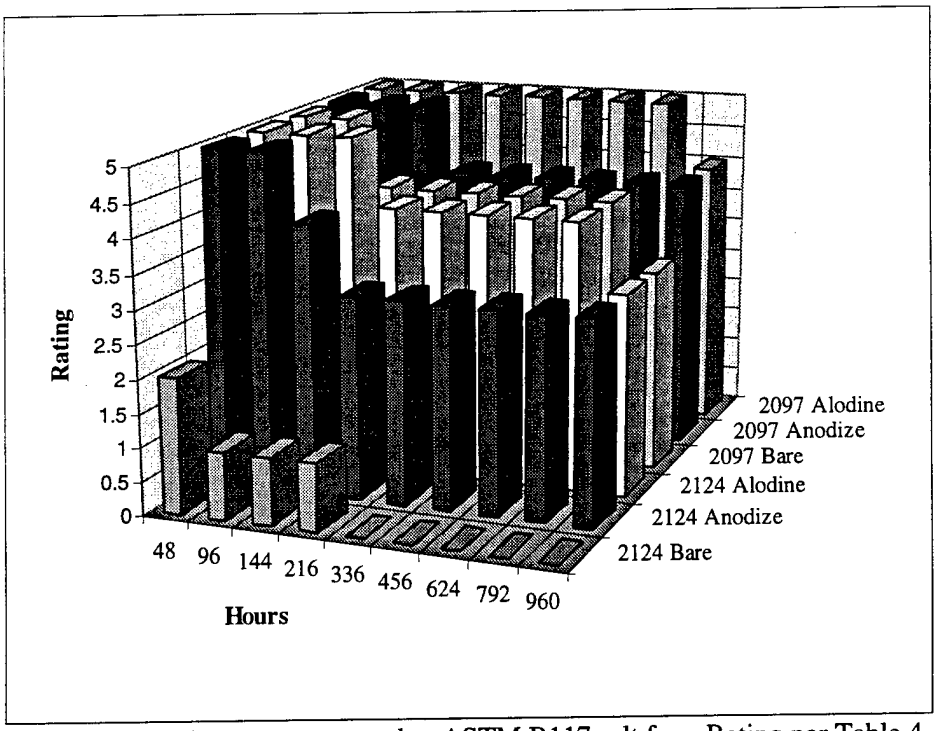

Figure 1: 2097 and 2124 coupons exposed to ASTM B117 salt fog. Rating per Table 4 represents average of three coupons. Five is no corrosion on the surface, and zero is severe corrosion. Anodize per Mil-C-8625, Type II, Class 1. Conversion coating Alodine 1200S per Mil-C-5541, Class 3.

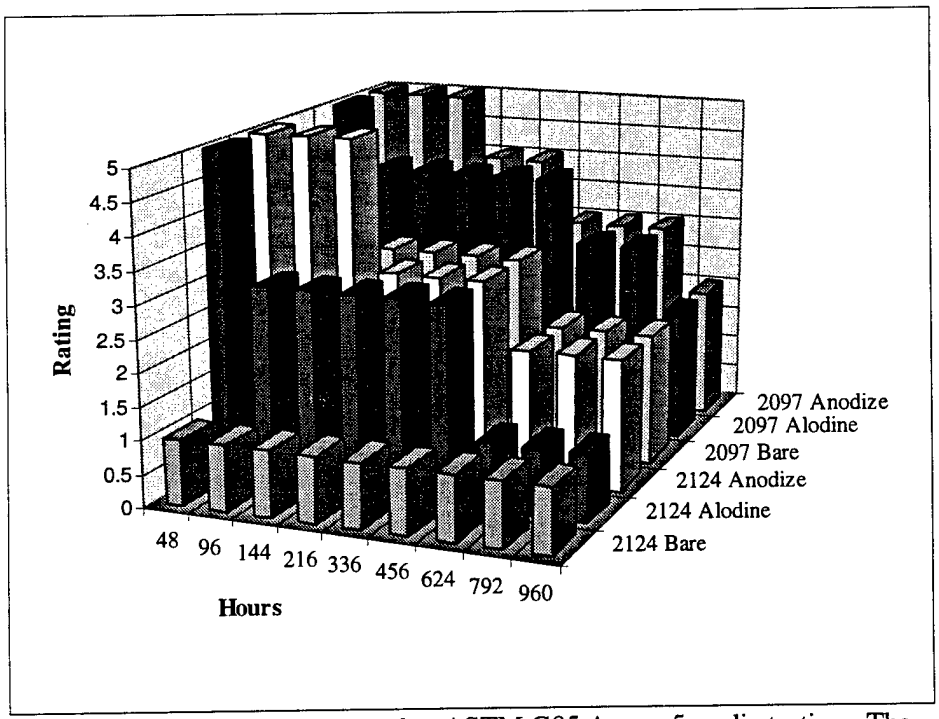

Figure 2: 2097 and 2124 coupons exposed to ASTM G85 Annex 5 cyclic testing. The anodize and Alodine pretreatments are in reverse order from Figure 1.

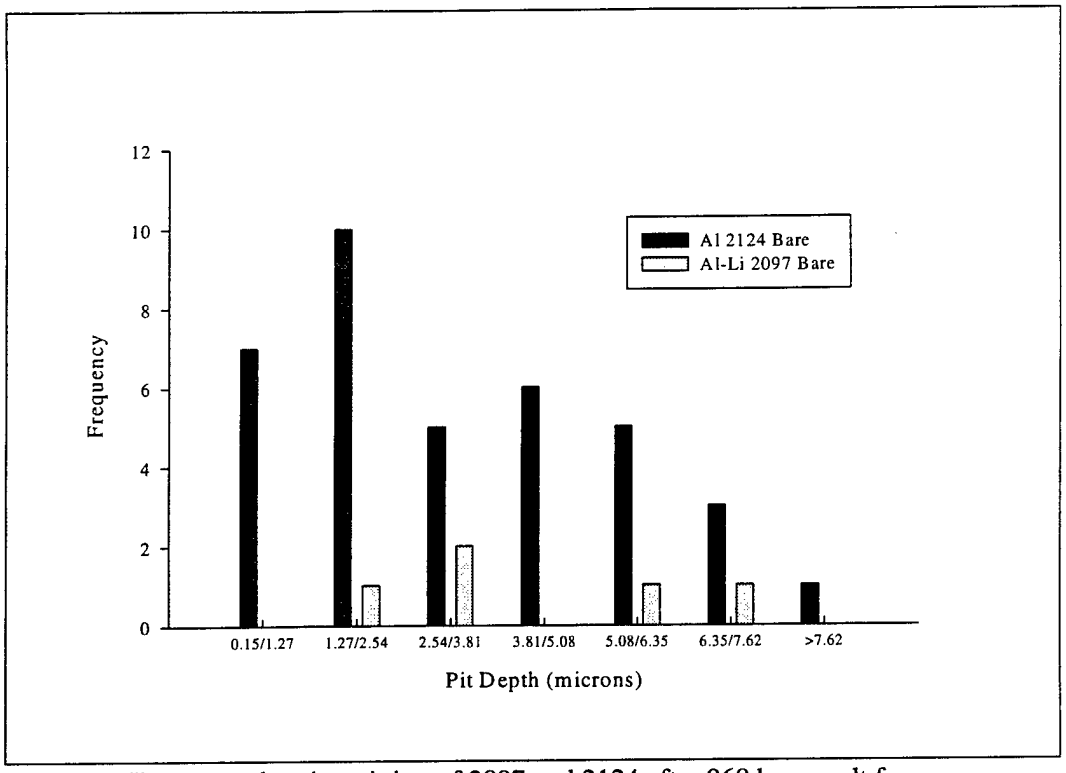

Figure 3: Histogram showing pitting of 2097 and 2124 after 960 hours salt fog.

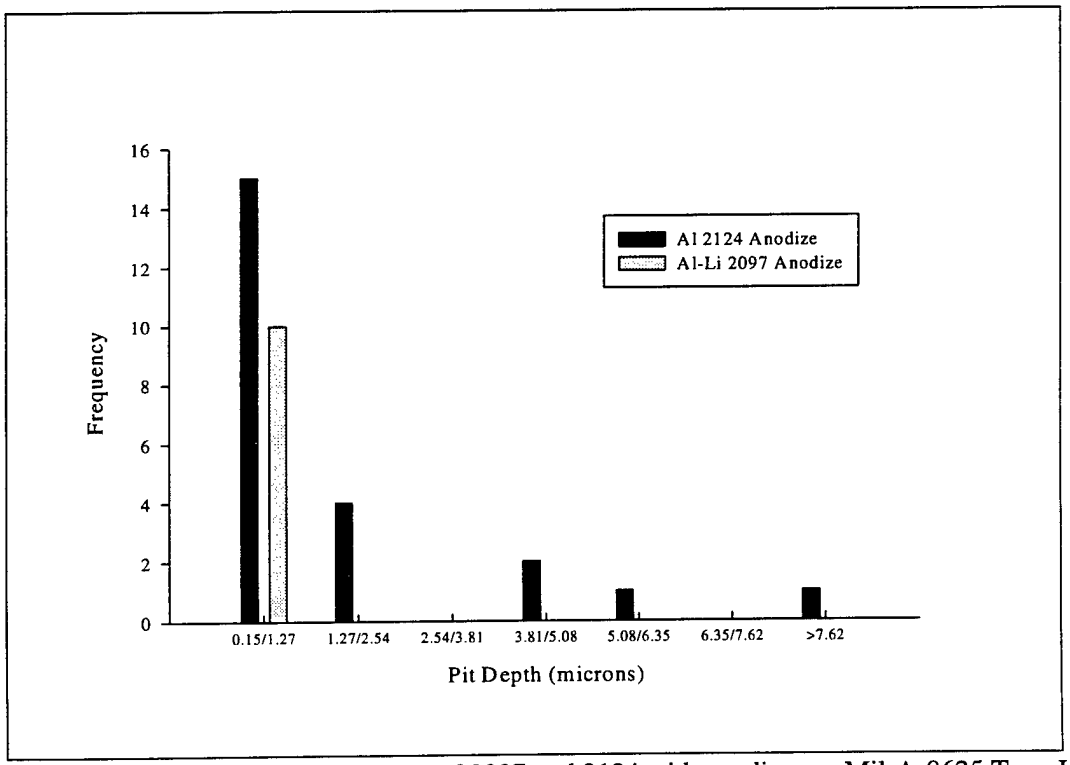

Figure 4: Histogram showing pitting of 2097 and 2124 with anodize per Mil-A-8625 Type I, Class 1 after 960 hours salt fog.

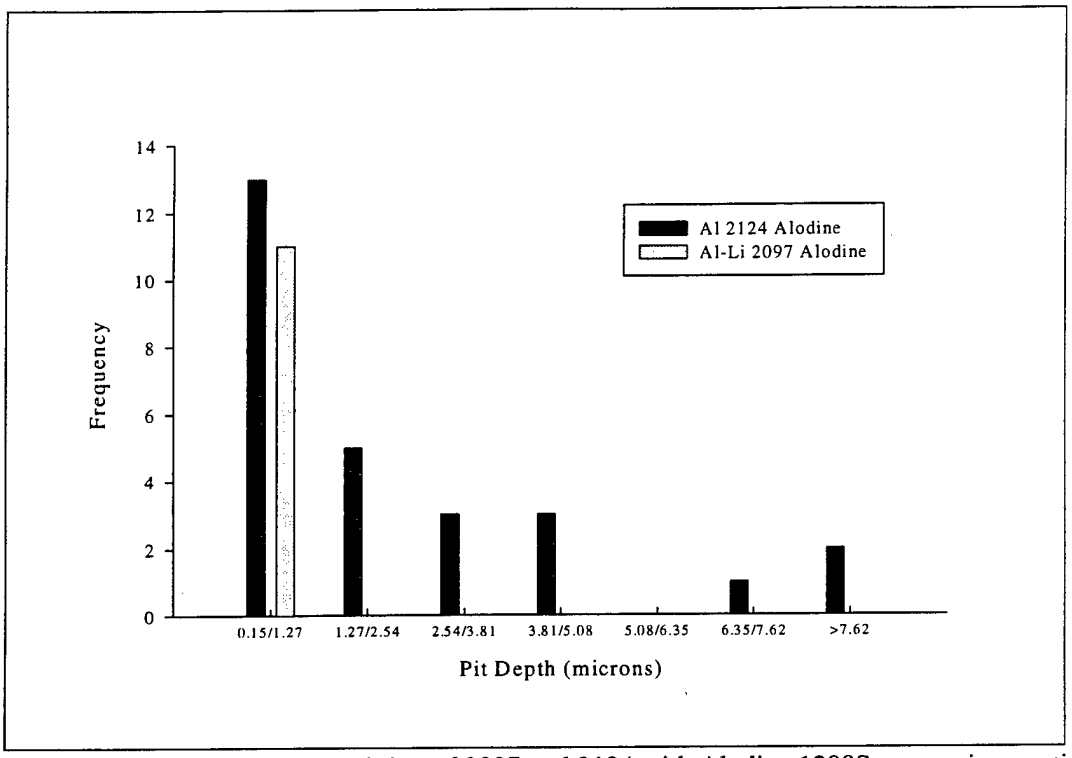

Figure 5: Histogram showing pitting of 2097 and 2124 with Alodine 1200S conversion coating per Mil-C-5541, Class 3 after 960 hours salt fog.

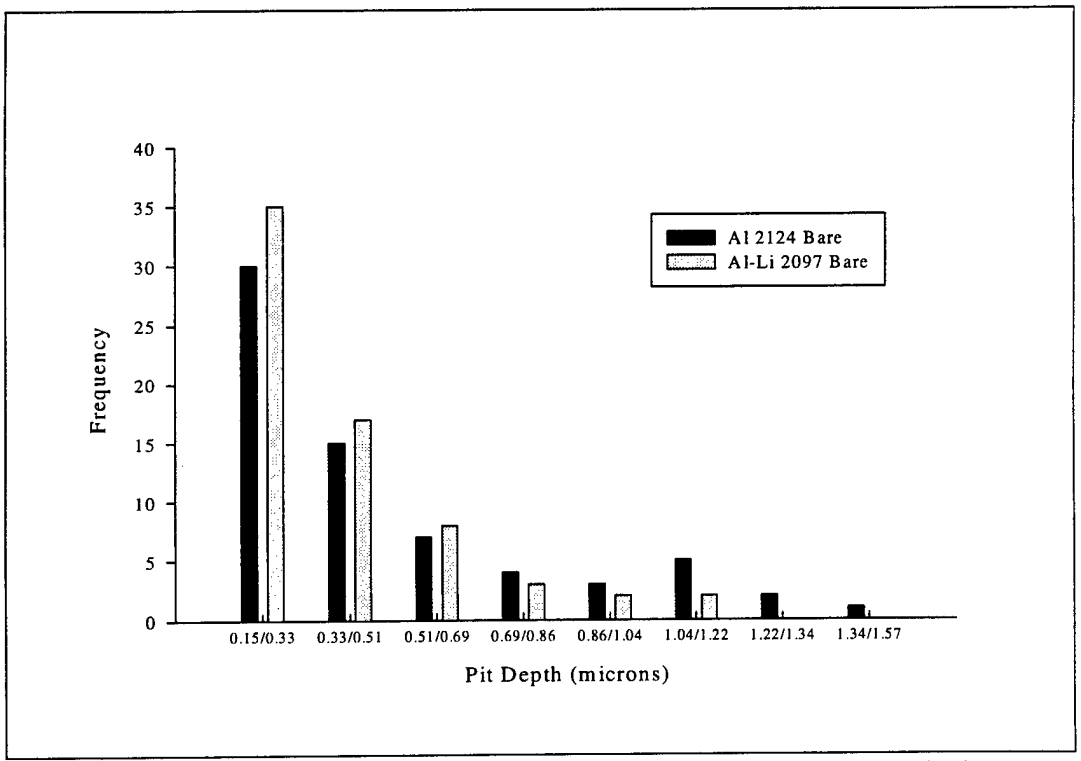

Figure 6: Histogram showing pitting of 2097 and 2124 bare after 1 year atmospheric exposure at Key West, Fl.

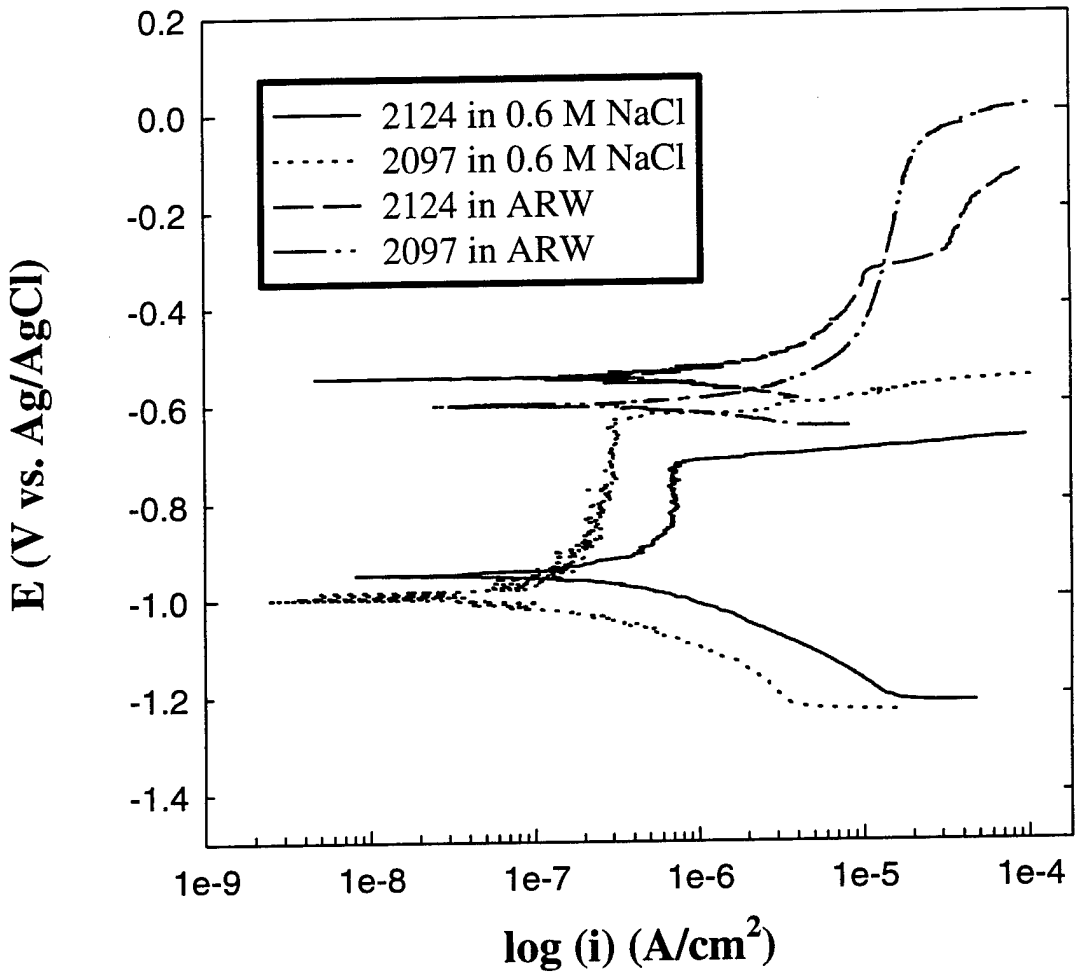

Figure 7: Polarization curves for 2124-T851 and 2097-T8 in deaerated 0.6 M NaCl and deaerated artificial rainwater.

The Determination of the Corrosion Behavior of a Developmental Al-Mg-Li-Ag Alloy

T. A. Carmody

B. A. Shaw

Penn State University

Abstract

Aluminum-Lithium alloys have attracted the attention of the aerospace industry in the last few decades. The prospects of Al-Li alloys have also spawned an interest by the marine industry. Hence, the development of corrosion resistant Al-Li alloys is currently in vogue.

The focal point of this investigation was a comparative overview of the corrosion resistance of the developmental Al-Mg-Li-Ag alloy, Weldalite 050. The Weldalite 050 and 9 other alloys were subjected to a battery of tests designed to both compare the corrosion resistance of the Weldalite 050 to that of the other alloys and to evaluate the mechanism by which Weldalite 050 was prone to attack. The other alloys selected for this comparison were: the aerospace alloys, 6013, 2090 and 8090; the common commercial alloys 1100, 5083, 6061, and the 6061-Al_2O_3 metal matrix composite; and the more elusive Soviet alloys, 1420 and 1421.

The test matrix for this investigation included both laboratory and field exposure testing and resulted in the production of an extensive database of corrosion information for all 10 of the alloys included in the study. Electrochemical polarization, laboratory immersion, filtered seawater, and atmospheric exposure testing were performed to blend an understanding of both the accelerated and in-service corrosion susceptibilities of these materials.

As a result of this study, it was shown that though Weldalite 050 is susceptible to exfoliation-type pitting, this new alloy does show improved corrosion performance over the more common, commercial Al-Li alloy compositions. Likewise, though the outcome of electrochemical testing did not prove effective in ranking the corrosion performance of this alloy, cyclic electrochemical testing results appeared to be capable of at least identifying the mechanism of corrosion, exfoliation-type pitting.

INTRODUCTION

Currently, much of the metals industries' interest is focused on achieving lower production and maintenance costs, longer service lives, and lower density materials. Light-weight, durable, and inexpensive Al alloys have been developed to address some of these issues. The inherently attractive strength of aluminum can be greatly and inexpensively enhanced by simply alloying with common elements, such as copper, zinc, and manganese. In fact, some aluminum alloys have strengths in the range of many steels. In response to the interests in strengthened materials and the high costs of redesigning processing methods, many high-strength aluminum alloys have been developed for easy substitution into existing production lines.

Though relative to other metals aluminum is considered reactive, its naturally occurring, strongly adherent oxy-hydroxide film makes it highly corrosion resistant. This film spontaneously forms on the metal's surface. As this film is tightly bonded to the metal's surface and has an inherent thickness limit of less than 100 angstroms,[1] the base metal is virtually shielded from further oxidation activity, in non-abrasive, non-aggressive environments. The protection against further oxidation which is offered by this bi-layer film is essentially protection against general corrosion. However, localized corrosion in the form of pitting, crevice corrosion, and exfoliation are common to Al alloys and are of special concern in marine environments, which are naturally aggressive because of high chloride concentrations.

As the developmental alloy in this study was formulated with specific applications in mind, it was decided to compare the corrosion performance of this alloy to that of alloys already in use in several of these proposed applications. The new alloy would then be ranked accordingly.

Subsequently, this report has two major points of focus. The primary focus is the generation of corrosion data and evaluation of these data to determine the mode of localized

corrosion of the newly developed Weldalite 050. By examination and evaluation of pit character in long term and accelerated testing, some postulates regarding the mechanism of attack were developed.

The secondary focus, the production of a comparative database for the 10 aluminum alloys included in this study, was the offspring of the first goal. By subjecting the comparison alloys to the same battery of tests performed on the Weldalite 050, generation of comparable data was achieved.

EXPERIMENTAL PROCEDURE

In efforts to produce a meaningful comparison of these materials, an exhaustive study of: the types of tests to be conducted, the rational of these testing procedures, and the applicability of the resulting data was pursued. After careful consideration a variety of tests were selected.

It must be mentioned here that though the materials were of various compositions and product forms, it was believed that the mechanisms of the degradation processes of each material would present themselves clearly enough to render a more meaningful comparison among the alloys.

To compare long term test data and accelerated test data the test matrices presneted in Tables 1.1 and 1.2 were composed. A discussion of the ASTM Standards[2], the other tests chosen to be conducted, and modifications or diversions from the test standards made during this project is provided.

MATERIALS

The history of the materials obtained for this study is as follows:

The 1100 sheet, 5083 plate and 6061 sheet alloys were purchased from commercial vendors. The tempers and thickness were 1100-H14, 0.063 inches, 5083-H116, 0.25 inches, and 6061-T6, 0.063 inches. The vendor-certified chemical compositions for the commercially provided alloys appeare in Table 2.1.

The alloys 1420, 1421, 2090, 6013, 7039, and 8090 (SPF), were donated by researchers who had done previous work with these alloys. No temper designations, heat treatment, nor further processing history was available for these materials. All chemical compositions were assumed to be nominal.

The alloy composite 6061 Al_2O_3 was provided by the manufacturer. The specimen was a 10 vol. % Al_2O_3.discontinuous particulate reinforcement in a 6061-T6 aluminum matrix. The specimen was extruded and rolled to a 0.25 thickness. Chemical composition information of the matrix is assumed to reflect nominal values.

The Weldalite 050 was provided by the developer of the alloy, Martin Marrietta. This specimen had been produced from an extruded ingot. Rolled from 10-inches to 0.5 inches at a speed of 50 surface ft/min, at temperatures between 110 to 125 °F. After quenching, the plate was stretched 4.5%. The plates were then heat treated at 875 °F and water quenched. Just prior to shipping the specimen, the plate was exposed to periods of heating at 176 °F, over a several day period, until 36 hours of heat exposure had been realized. The chemical composition of the alloy was provided by the developer and was presented in Table 2.1.

LABORATORY TESTS

Laboratory Immersion, ASTM Standard G-31: In the long term laboratory immersion test, specimens were exposed to artificial seawater (ASTM standard D-1141) while suspended from glass rods. There were three positions on the mounting apparatus, allowing exposure of specimens at levels of complete immersion, partial immersion, and fully above the solution. All

solution levels were marked at the onset of testing. Solution levels did not appear to shift throughout the duration of the tests.

The 6013 coupons were tested in the as-received surface condition. All other materials received a 600 grit polish prior to exposure. The 1-inch thick 7039 specimens were sliced to half their original thickness. The interior surfaces of these specimens were masked with a marine epoxy prior to testing.

Electrochemical Measurements: For the purpose of potentiodynamic polarization studies, the materials were secured in an electrochemical flat cell and exposed to artificial seawater (ASTM standard D-1141). All testing was performed using Gamry potentiostats and the Gamry CMS 100 software, referenced to a saturated calomel reference electrode (SCE), using a platinum counter electrode. Artificial seawater solutions were adjusted to a pH of 8.2.

Anodic Polarization: Anodic polarization was chosen as an initial test for all materials. For comparison, three sets of parameters were used for each material: quiescent conditions on specimens in the as-received-surface and polished to a 320 grit surface finish, and under deareated conditions on polished specimens. The quiescent set-up consisted of being open to the lab air environment, with no air purging or solution disturbance. It was decided that 0.05 mV/s proved the most satisfactory scan rate with respect to result replication.

Cyclic Polarization: These potentiodynamic tests were conducted under quiescent conditions in artificial seawater using the same test cell set-up as the anodic polarization testing. Within several of the individual materials' cyclic polarization test series, scan rates were adjusted and apex currents were varied. This variation in parameters allowed determination of both the affects of scan rate and pit severity, on the ability of pits to repassivate.

Corrosion Potential Tests, ASTM Standard G-69: The standard's test solution is NaCl augmented by the addition of H_2O_2. This standard suggests a test duration of one hour. The ASTM standard procedure states that reported corrosion potential is to be the average potential, calculated over the last 30 minutes of testing.

Based on the wide range of degradation seen between the materials in this study, several of the corrosion potential tests were conducted under the following different conditions: some tests were conducted for up to twelve hours, with averages over 30 minute intervals being calculated; some tests were performed in solutions which had been prepared up to 3 days in advance of testing to determine if solution age affected test results.

FIELD EXPOSURE TESTS

Alternate and Continuous Immersion, ASTM Standard G-52: Filtered seawater exposure, ASTM standard G-52, was conducted on all of the materials. In conjunction with the alternate immersion testing, continuous filtered seawater exposure was conducted. Specimens were tested at the LaQue Center for Corrosion Services' corrosion testing facility in Wrightsville Beach, North Carolina. At the LaQue Center seawater was drawn directly from the Wrightsville Beach harbor area, filtered to 5μm, and supplied to the test tanks.

Specimens for both the continuous and alternate immersion filtered seawater exposure were held in a common test tank. This tank had a continuous circulation of filtered seawater throughout testing. At the end of one week the tank was allowed to drain half way, exposing specimens mounted in the upper half of the tank. These specimens were allowed to air dry and remain exposed to air for a period of one week. At the end of the week-long air exposure period, the fluid level of the tank was raised to cover the specimens. This two week cycle was repeated throughout the duration of the test.

Atmospheric Exposure, ASTM Standard G-50: All materials undergoing long term atmospheric exposure were exposed as per ASTM Standard G-50. No coating was used to mask the edges of any of these specimens.

All atmospheric exposure specimens were cut using a band saw and the edges were de-burred. Most specimens were made into panels measuring 4-inches by 6-inches on the surface. Because of material availability, the Weldalite 050 specimens were prepared as 4-inch by 4-inch panels, and the 1420, 1421, and 8090 panels measured 4-inches by 3-inches.

In most cases, specimen surface preparation for the atmospheric exposure testing was limited to cleaning the as-received surface with Alconox, followed by a DI rinse, a methanol rinse, and a second DI rinse. The heat treated surfaces of the Weldalite 050 and 9 of the 2090 panels were treated to a 320 grit polish prior to testing and cleaned in the same manor as the other specimens.

RESULTS AND DISCUSSION

Laboratory Immersion, ASTM Standard G-31: Table 3.1 presents the average evaluation results for the fully immersed specimens. The pit number density was purely a pit count and did not take into consideration a total measured area of pitted compared to non-pitted surface. When evaluating pit size and depth, the largest and/or deepest pit was selected from each material and those measured values were reported in Table 3.1.

The bar charts shown in Figure 1 demonstrate the ranking for fully immersed specimens exposed in the Laboratory Immersion Study by: preliminary corrosion rate, pit number density, pit size, and pit depth. By comparing the rankings of each parameter-grouping, it is evident that performance ranking is entirely dependent upon which feature is chosen for comparison. A particularly vivid example of this ranking difference can be seen when looking at the ranking of the Weldalite 050, which ranked moderately for pit number density, but showed the most severe pit depths and sizes. Clearly, each of the features presented must be weighted differently when evaluating overall corrosion performance.

In general, none of the immersion specimens which were exposed only to the solution vapor showed evidence of discoloration or corrosion. The exceptions to this finding were some discoloration on the 6013, 6061, and the Weldalite 050 specimens. The 6013 and 6061 specimens showed signs of solution evaporation on the specimens, and it is assumed that these specimens were splashed during set-up. These "splashed" regions developed pits. The Weldalite 050 displayed non-uniform discoloration with no evidence of being splashed, and no evidence of pitting.

All partially submerged specimens demonstrated some signs of exposure. In many instances exposure was merely indicated by the discoloration of the submerged area. On all of the alloys, except the 1420 and Weldalite 050, this discoloration was uniform in color. On the 1100, 1420, 5083, 6061 Al_2O_3, and Weldalite 050 the solution-atmosphere interface region demonstrated a type of corrosion discoloration which did not appear the same as the submerged portion of these specimen. The severity of this "water-line" corrosion was worse on the Al-Li alloys, 1420 and Weldalite 050, which developed pits in the water-line region. On the alloy 5083, this water-line was actually the only evidence of attack on the 5083 partially submerged specimens.

The specimens exposed to full immersion were the most heavily corroded samples obtained for each material. Most of the coupons from this test position also developed uniform discoloration. Again, the exceptions to this were the 1420 and the Weldalite 050, which developed a non-uniform surface coloration. Among the fully immersed specimens, the most

severe pitting attack was seen on the two Al-Li alloys, 1420 and Weldalite 050. The worst general corrosion, as determined by calculating corrosion rates, was seen on the Weldalite 050 and alloy 7039. The 1421 showed little, if any, evidence of attack.

In SEM micrographs from immersion test specimens both before and after the destructive cleaning processes were observed. The images taken before abrasive cleaning showed evidence of the residual dehydrated barrier film. This film was clearly not present after the final cleaning process. Prior to the abrasive cleaning process, the 1100, 1420, 6013, 6061 and 6061 Al_2O_3 specimens show the presence of a "halo" around the pits. Though this halo was evident optically on all five alloys, it was barely detectable under SEM on the 1100 and 6013 specimens, appearing as nothing more than a slightly charged (SEM) artifact. The SEM charging of the halo region on these alloys suggests that the halo is composed of the dielectric oxide film.

In SEM micrographs of the 6061 and 6061 Al_2O_3 pits, the halo region had quite a different appearance. Microscopy showed that this halo region coincided with the absence of the barrier oxide. By comparing the two types of halos produced on the alloys 6061 and the 6013, it can be inferred that either the compositions, integrity, brittleness, or strength of the passive films were notably different for these two alloys, or that high OH^- of the local chemistry in and around the cathodic region at the pit opening[3] on the 6061 alloys was more hostile to the composition of the oxide film. (Note Al oxide films are unstable at extreme pH values.[4])

After immersion testing of the 6013 and 6061 alloy specimens, the abrasive cleaning process was severe enough to remove the more shallow pits entirely from the specimens' surfaces. Also, the character of the pits seen in the 6061 and 6013 alloys were more affected by the abrasive cleaning process.

Imaging of 6013, 6061, and 6061 Al_2O_3 before abrasive cleaning revealed the surfaces of grains within the pits. This SEM study showed that the surfaces of the 6013 grains had a "spongy" appearance indicative of "de-alloying" of the grain surfaces. De-alloying of the 6013 grains resulted from the alloy chemistry. Though the addition of Cu could raise the potential of the solid solution, the alloy 6013 does not contain enough Cu to provide this affect. Hence most of the Cu in this alloy would be found in the anodic $CuAl_2$ phase. The presence of the more noble $CuAl_2$ phase near the grain boundaries would have behaved as a cathode to the more reactive solid solution and Mg_2Si phases. As the grain boundaries were attacked, loosened grains fell out of the pits. The location of the cathodic reaction at the grain boundaries (within the pit itself), also explains the absence of the intense cathodic halo around the pits seen on the 6013 alloy specimens. The 6061 and 6061 Al_2O_3 alloys both showed a smoother nature on the grain surfaces suggestive of uniform dissolution of the grains. This type of attack would have been supported by the presence of the cathodic region outside the pit, imposed by pit geometry, while both the solid solution and the Mg_2Si, which have relatively close solution potentials,[2, 4] behaved as the anode. This proposed mechanism would result in the more evenly dissolved, smoother, faceted grain surfaces seen in SEM.

The Weldalite 050 specimens from every exposure position showed non-uniform discoloration on the planar surfaces and some pitting. The through-thickness surfaces of the Weldalite 050 displayed graded discoloration toward the outside edges with preferential pitting attack observed in the darker regions. A directionally-elongated nature of the pits was observed. The elongated orientation of the pits did not follow the path of gravitational forces. Examination of the planar surface and the exposed long-transverse (LT) surface showed that attack followed the layered structure of the Weldalite 050 alloy. These two views revealed layers, or leaves of

the remaining material at the interior surface of the pit. These layers indicate that corroded material may have flaked away, a process reminiscent of an exfoliation-type of attack.

Over all, the best performer in this laboratory immersion study was the 1421 alloy, followed by the 5083 and the 6061 alloys. The 6013 alloy, which was the only material subjected to this test without polishing, only developed pits along previously existing scratches. The worst performers in terms of pitting corrosion were the 1421 and Weldalite 050 alloys, and the Weldalite 050 and 7039 alloys for weight loss corrosion rates.

Electrochemical Measurements

Anodic Polarization: The plot in Figure 2 compares the anodic curves showing the best pitting potential for several of the materials tested with the polished surfaces under quiescent conditions. The alloy 1420 had the highest E_p. Another point of interest was the very low passive current density of the alloy 1420. In this plot, it can be seen that alloy 7039, though showing the lowest pitting potential, had the largest passive range.

For all of the anodic polarization tests, several regions depicted on the curves were selected as values of interest to this study. Two of the points of interest were the open circuit potential (E_{corr}), and the breakdown or pitting potential (E_p). For the purpose of standardizing our interpretation of results, an increase in potential of 0.05 mV, with a corresponding current increase of 1 μA was also used to identify the breakdown potential.

An attempt to was made to select one particular potential at which to evaluate the anodic polarization current response for all of the alloys tested. This presented a problem, as these alloys demonstrated a very wide range of both open circuit and breakdown potentials. In fact, some of the alloys tested showed open circuit potentials above the breakdown potentials of other of the alloys. (Refer back to Figure 2.) Therefore, it was decided to select the open circuit potential of each test series as the datum and to report the current response at overpotentials of 100, 150, and 200 mV with respect to that datum.

One final value of interest was the range of the passive region. This was accomplished by first determining where a series of steps in potential resulted in a relatively negligible change in current density. This negligible shift in current density was identified as an indication of passive behavior. Breakdown potentials were used to identify the end of passive behavior. This potential range between the onset of passivity and breakdown was calculated and recorded as the passive potential range.

The geometric mean of the values described above are presented in Table 3.2. The values presented are based on a minimum of 5 identical test runs. A limited number of tests were disregarded because of results which were clearly out of range, presumably as a result of experimental or equipment error.

The graphs in Figure 3 present the ranges found for the breakdown potentials for the three polarization parameters setups described previously. Here it can be seen that the range of breakdown potentials narrows considerably with surface preparation. However, the mean breakdown potentials obtained for polished-quiescent and deaerated tests results, are relatively the same. This would suggest that though surface finish has an effect on breakdown potential, deaeration does not affect effect breakdown potential results. Notice that the breakdown potentials identified were less negative for the Li-containing alloys.

When examining the character of the pits generated by anodic polarization testing the following points must be made: In SEM images of pits generated on specimens of the alloys Weldalite 050, 1420, 1421, and 1100, it was seen that the pitting attack appears as localized "clusters" of a series of small pits. This clustered morphology should not be confused with the

"lace -like" pits, which Pickering[3] attributes to the crevice nature of developing pits. The pitted regions found on the alloys listed here did not have sufficient aspect ratios to support crevice behavior. The SEM images suggested that either pitting originated through many locally weak regions in the passive film, or that once the film was breached, dissolution continued under the oxide film, undermining the film metal interface, and eventually bursting through the film from beneath. In higher magnification micrographs of these regions it was apparent that the film remaining at the edges of the pitted regions was forced upward. Comparison of these anodically induce pits with pits of immersion testing specimens, suggests that the pit sites are indicative of dissolution of thin layers of the alloy and that forces produced by the increased volume of the corrosion product ruptured the oxide films.

In SEM microscopy of anodically generated pits on a 6061 specimen, it was seen that the attack was much more localized. Though these specimens showed a hint of the halo region seen previously on immersion study specimens, the anodically induced halo-region did not present the same surface characteristics. Though the halo produced on the polarized specimen appeared as a lighter region in the micrographs, the halo was not indicative of an absence of passive film. This can be explained by two factors. In the polarization study a counter electrode acts as the cathodic site, whereas during the immersion study, it appears that the metal surface region surrounding the pit served as the cathodic site. In the case of the polarized specimen, the oxide surrounding the pit would not have encountered the extreme pH chemistries which coincide with the cathodic reaction. Therefore the oxide remaining at the pit mouth was more stable.

An additional point to be made regarding the pits concerned the nature of the surface of the remaining grains lining the pit. It was previously disclosed that the surface of grains within pits on the alloy 6061 from long term laboratory immersion studies had a smooth appearance, indicative of general uniform dissolution of the grains. Microscopy of anodically generated pits showed the surface morphology of these remaining grains were sponge-like, an indication of de-alloying. The differences displayed under these two different test conditions can also be attributed to the nature of the cathodic reaction. Under anodic polarization conditions a larger potential difference is imposed on the specimen, than that potential difference which would naturally develop in the localized pit-region on the immersion specimen. As the Mg_2Si phase found near the grain boundary is more anodic[4,5] than the solid solution, the Al matrix was leached out first under the artificially induced overpotential, weakening the grain boundary interfaces, causing grains to fall out. This scenario also accounts for the deeper more localized nature of the pits seen in the 6061 matrix and composite alloys, and in the 6013 alloy. By comparing the pits from the immersion and anodic studies, it was apparent that the mode of attack generated by the two test conditions is different. This would suggest that though accelerated testing is commonly used to compare and rank aluminum alloys, the mode of attack produced under accelerated conditions should be considered with suspicion.

Cyclic Polarization: The notable values obtained from cyclic polarization testing include the protection potential[6] (E_{pp}) and repassivation potential (E_{rp}). Many authors define E_{pp} as the point at which the forward and reverse scans cross. Others select a return to a "no net current flow" condition to define E_{pp}. For the purpose of this investigation the point of crossover was used to define the value E_{pp}.

The geometric mean values of the protection potentials, repassivation potentials, and metastable pitting range are listed in Table 3.3. It can be seen by these numbers that the metastable pitting range is very narrow for most of the Al-Li alloys. The mean values of the protection potential values generated during cyclic polarization testing are presented in Figure 4.

In the cyclic polarization studies, the E_{pp} was found to be very consistent for the alloys: Weldalite 050, 1420, 1421, 6061, 6061 Al_2O_3, and 7039.

Additionally, for the purposes of this study a metastable pitting activity range was defined as the potential range between the breakdown potential and the protection potential E_{pp}. Examples of the metastable pitting range are presented in Figure 5. When considering the plot of the 5083 cyclic data, there exists a wide range from the onset of pitting, to the point where the pits were seen to repassivate (i.e. a large metastable pitting range was evident). This would suggest that though 5083 demonstrates relatively high E_p's, once pitting has initiated, corrosion can continue over a wide range of potentials. Alternatively, the Weldalite 050 portrays a very narrow band of metastable activity. Essentially, though the Weldalite may experience pitting, a small negative shift in potential can easily terminate corrosion activity.

Looking again at the pit morphologies may provide and understanding of the magnitude of this metastable activity range. Recall that as presented in the anodic polarization section of this report anodically induced pits on the Al-Li alloys (those showing the shorter metastable range) were not as deep nor localized, as the pits generated on the alloys 5083, 6013, and the two 6061 alloys (those demonstrating a larger metastable activity range). It could be argued that the different pit geometries and the resultant localized potential gradients within the pits exhibited by these classes of pit morphologies, could serve as a controlling factors in the pit repassivation event.

As demonstrated by the data found in Table 3.3, and in a study conducted by Campbell[7] in conjunction with this work, it was seen that the protection potential values for these alloys proved to be repeatable when materials were subjected to increased apex currents and increased apex potentials. The consistency of E_{pp} values, coupled with the pit morphological studies presented, suggest that the E_{pp} is a more revealing data value when using potentiodynamic results to evaluate, rank, and investigate the mechanism of corrosion for aluminum alloys.

Corrosion Potential Tests, ASTM Standard G-69: Corrosion potential tests conducted in the 5% NaCl solution, augmented by H_2O_2, as dictated by this standard, produced consistent results within each alloy group. In these tests all alloys developed stable E_{corr} values within the first hour of testing and were able to maintain these stable values for at least the three hour duration of testing. The quickly achieved and long lived stability of the corrosion potentials can be seen in the example plot of corrosion potential data shown in Figure 6.

The E_{corr} values obtained in this corrosion potential test can be found in Table 4.5. All of the results are presented as calculated averages based on the average E_{corr} values obtained for a minimum of 5 tests for each material. The range of corrosion potential test results, and the calculated average E_{corr} values for each material are presented in the plot of Figure 7. The mean E_{corr} values obtained were within ranges reported by other researchers with the exception of the alloys 7039 and 8090. However, it must also be mentioned that the E_{corr} values presented in the published literature, do not necessarily agree from one report to another. It was therefore accepted that both the 7039 and 8090 results were within reasonable limits.

It should be noted that although corrosion potentials per the ASTM Standard G-69 are frequently published, care must be taken when assessing what these values represent. When ranking of these materials, based on the average E_{corr} values obtained in this test series, the more positive (noble) potentials are generated by the Cu-containing alloys 6013 and 2090. Higher electropotentials would be expected for Cu-containing alloys, as Cu is known to raise the potential of Al in solid solution[5]. The corrosion potential test results which are more positive do not necessarily translate to more corrosion resistant behavior. By comparing the corrosion

susceptibility rankings from the immersion studies, shown in Figure 1, to the ranking of these materials by the E_{corr} values, it is evident that less negative potentials do not correspond to lower corrosion rates.

Filtered Seawater Tests

Alternate and Continuous Immersion, ASTM Standard G-52: The specimens from the filtered seawater exposure tests at the LaQue Center for Corrosion Studies, Wrightsville Beach, NC were collected and evaluated at removal periods of 6 and 12 months. Though some specimens were subjected to continuous immersion while others underwent alternate immersion conditions, all filtered seawater specimens were exposed in a common test tank.

All of the filtered seawater specimens evaluated and ranked for the occurrence of crevice corrosion, as well as for their performance relative to preliminary corrosion rate, pit evaluation, and final corrosion rate.

Tables 3.5 and 3.6 provide the average preliminary corrosion rates, pit evaluation data, and the final corrosion rates from this series of tests. The bar charts of Figure 8 present the ranking of seawater immersion specimens based on the evaluation procedures previously described.

Upon removal of the first series of filtered seawater specimens, several trends were noticed. First, among the specimens which were subjected to alternate immersion, all panels showed non-uniform discoloration. The top of each specimen generally showed less severe corrosion, in spite of the presence of the crevice former. Likewise each specimen displayed less discoloration toward the bottom of each panel. This trend was repeated on the specimens which were removed after 12 months. This discoloration pattern was not seen on any of the continuous immersion specimens, which, with the exception of the alloy 2090, displayed a uniform discoloration of the exposed surfaces.

Among the 6-month continuous immersion panels, an adherent green algae-like substance was found on only 6013, 6061 and 6061 Al_2O_3 specimens. After removal of this algae it was found that no pits were found beneath the substance. Also, the surface which was covered by the algae did not show the uniform discoloration seen on the remainder of these panels. After 12 months of exposure this algae-like substance was, again, found only on these materials. Though these algae covered surfaces still showed no general discoloration on the surface beneath the algae, the 12-month specimens did show significant pitting attack beneath the algae.

One further anomaly seen on several of the specimens was the presence of the loosely adherent white crystalline deposit. This deposit was seen: on all of the alternate and continuous immersion specimens of the alloy 6013; on all of the alternate immersion specimens and some of the continuous immersion of the alloy 6061 Al_2O_3; and only on the alternate immersion specimens of the alloys 6061 and 8090. (Note that there were no continuous immersion specimens of the alloy 8090.) All of these white crystalline deposits were located over pits.

When examining specimens for the presence of crevice attack, it was seen that the alloys which formed the white crystalline deposit showed heavier deposits at the crevice former. These heavy deposits also coincided with the most severe attack around the crevice formers. In some instances, these heavy deposits produced excellent conditions for crevice attack, causing pits to penetrate through the thickness of the specimens.

Though other alloys showed increased biological deposits in the region of the crevice formers, these biological deposits did not coincide with increased pit activity. None of the alloys developed more severe attack under the crevice formers than on the exposed specimen surfaces.

Finally, pits located beneath the crevice formers were not seen to differ between the continuous and alternate immersion specimens.

The most heavily attacked specimens, by weight loss calculations, were the Cu-containing Al-Li 2090 specimens. This material was exposed in two conditions, as-received and with a 320 grit polish. Both conditions developed strongly adherent, rough, white deposits, on the all specimens. The alloy 2090 continuous immersion specimens also demonstrated the loosely adherent white crystalline deposits and the severe associated attack, as previously described for the 6013 and 6061 alloys. The 2090 specimens randomly displayed both the uniform and non-uniform attack distributions. This random character was likewise repeated front-to-back on some specimens. The nature of this attack, though often localized, could not be considered "pitting". Rather, it appeared as localized regions of "general" corrosion, as the regions of attack were very broad and uniformly corroded. The 2090 specimens were also the only specimens to develop a distinct continuous cathodic-type ring of deposit around the edge of the crevice former-washer. This ring of deposit was of the same character as the other strongly adherent white deposit seen on the rest of the specimen.

The alloy 6013 showed the most severe pitting attack in the continuous submersion portion of the test. This severe pitting was in all instances associated with presence of the heavy, loose, white crystalline deposits. These specimens were the first to develop pits (as early as 6-months) through the thickness of the panels. This through-thickness pitting was seen first along the edges of the 6013 panels, and later near, but not under, one of the crevice formers. The 6013 specimens exposed to alternate immersion did not develop the heavy white deposits, nor did they perform as poorly as their continuously immersed counterparts.

The 6061 specimens which were continuously immersed ranked second worst, for pitting attack. These specimens also developed pits through the thickness of the panels. However, fewer of these through-pits were developed than on the 6013 specimens.

The 6061 Al_2O_3 specimens which were not polished prior to exposure also developed severe pitting under the loose white deposits, after as little as 6 months of continuous immersion. This scenario of pit formation was also present on the 12-month alternate immersion specimen which was not polished, but was less severe than on the continuous immersion 12-month samples. It must be noted that these pits were more severe both in number and in pit depth than their 6061 matrix counterpart. The only criteria for ranking these specimens as less severe than the 6061 matrix-only specimens, was the infinite depth found on the 6061 matrix-only samples. The polished 6061 Al_2O_3 did not develop these deposits.

When comparing the attack encountered on the alloys 6013, 6061, and 6061 Al_2O_3, from these long term studies and the laboratory studies, it can be extrapolated that the presence of the white crystalline deposits produced or assisted in the development of crevice conditions which served to greatly accelerate the distruction of these alloys.

In the filtered seawater studies, the Weldalite 050 specimens performed very well when compared to the four previously described alloys. Pitting number density , depth, and overall severity were generally moderate to minimal. These specimens did show a propensity for larger pits toward the edges on the 12-month specimens. Only one specimen (a 12-month continuous immersion panel) displayed visible material loss. This attack was in the form of the exfoliated-type pitting previously described for planar surfaces on the Weldalite 050 in the laboratory immersion study. There was no incidence of obvious material loss on the LT surface of any of the Weldalite seawater immersion specimens.

Though the orientation of the elongated pits was in the direction of gravity, with respect to how the specimen was mounted, striations, indicative of rolling direction follow this same orientation. Based on this orientation observation and a similar evaluation of the laboratory immersion specimens, it was determined that the directionality of the attack was dependent upon material grain orientation and not the affects of gravity.

The remaining Al-Li alloys (1420, 1421, and 8090), displayed minimal to severe pitting attack. The order of ranking from best to worst was 1421>1420>8090. The 1420 and 8090 specimens demonstrated obvious exfoliation as the ultimate form of degradation. The alloys 5083 and 7039 were more generally affected by weight loss, than by pitting. The 7039 panels did not develop any visible pits.

Environmental Exposure Test

Atmospheric Exposure, ASTM Standard G-50: All of the specimen test panels exposed at the LaQue Center for Corrosion Services' 50 meter lot in Kure Beach, NC were subjected to the same preliminary cleaning, pit evaluation, and final cleaning steps performed for the Laboratory Immersion Study. The removal of the first series of specimens from the LaQue Center for Corrosion Services' 50 meter lot in Kure Beach, NC, occurred after 6-months of exposure.

The data in Table 3.7 provides the results of the long term environmental exposure testing. In this table are the corrosion rates determined by both the non-destructive preliminary cleaning, the pit evaluation, and the corrosion rate determined by the destructive final cleaning procedure. Rankings of these materials based on the preliminary corrosion rate, the pit evaluation, and the final corrosion rate is depicted in the bar graphs of Figure 9.

After six months, all specimens, with the exception of the Soviet 1420, demonstrated a trend based on panel orientation. All of these specimens exhibited larger pit sizes on the underside of the panels. Along with increased pit size, the number density of the pits on the underside of the panels appeared to be less then the pit number density on the sun-facing side of the panels. At the end of the 12-month removal period, the specimens continued to display the trend of increased pit size and decreased pit density on the underside of the panels.

A contrasting corrosion event was seen on the alloy 1420 at the 6-month removal time. The 1420 specimen clearly showed the presence of blister-type formations. These blisters were uniformly distributed across the surface and no noticeable difference existed between the top and under sides of the specimens. Though this specimen was not scheduled to be removed at the 6-month mark, a portion of the specimen was collected for SEM investigation. In a verbal report provided by the LaQue staff, describing this specimen after 18-months of exposure, it was stated that the 1420 specimen showed, "substantial exfoliation-type pitting attack under the surface, with approximately 35% of the surface being affected." It was also reported that the attack had parallel elongated shapes following the rolling direction of the specimen.

Microscopy showed that these blisters were elongated in the specimen rolling direction. This orientation was consistent across the panel surface. A through section of the attack site showed exfoliation of the specimens surface layers. By visual inspection, no other specimens displayed this mode of attack at the 6-month mark.

At the 6-month time interval, though no Weldalite 050 specimens were scheduled for removal, photographic evidence was obtained to record a corrosion phenomena not evident on any of the other specimens. The Weldalite 050 specimens showed signs of non-uniform pit distribution. This non-uniform attack was in the form of increased pit number density toward the

edges of the specimens, with these more numerous pits being much smaller in size than pits seen elsewhere on the surfaces. This mode of attack was much more pronounced at the corners of the specimen, and was likewise repeated on both the front and back edges of the panels. With the exception of this edge phenomena, the remainder of these specimens' exhibited the increased pit size, decreased pit number density trend which was common to the other alloys tested.

By the time of the 12-month evaluation, the Weldalite 050 specimens had also developed the blisters which were previously only apparent on the Soviet alloy 1420. However, the blisters seen on the Weldalite 050 were not seen at the edges of the specimens, where pit densities were still pronounced. As with the 1420 specimen previously discussed, the Weldalite 050 alloy appeared to be undergoing a form of exfoliation attack within the surface layers.

While comparing the exfoliated pits generated on the 1420 and Weldalite 050 alloy atmospheric specimens, with pitting attack initiated on these alloys by laboratory testing some correlation can be drawn. In the electrochemically induced attack, it appeared that corrosion product had forced it's way through the residual protective film from beneath. In the cross-section of the 1420 specimen the attacked region is clearly lifted away from the layers beneath.

One final notable observation made at the 6-month mark was the vast difference in appearance between the heat treated 2090 T-84 specimens which had been ground to a 320 grit finish prior to exposure and those which were exposed with the heat-treated surface intact. The unpolished 2090 specimens displayed the strongly adherent, rough, white-colored deposit (previously seen on the 2090 seawater immersion specimens) distributed over much of the surface. Like the 2090 seawater immersion specimens, this deposit distribution was not uniform in all instances. The 2090 specimens which had been polished prior to exposure also displayed rough areas. But, these deposits were gray in color, and were smaller in size and more evenly distributed. The edges of the polished 2090 specimens also showed a non-uniform pit density toward the edges, much like the Weldalite 050.

The 7039 materials experienced the highest corrosion rates in mpy. The mechanism of attack on this alloy was seen predominantly as only uniform discoloration of the protective bi-layer. This discolored film was easily removed by the destructive cleaning process. Though this material was in the form of a 1-inch thick plate, no differences in corrosion was apparent on the surfaces of these specimens which could be attributed to the material thickness. Attack of the through-thickness surfaces were likewise unremarkable. All pits, while insignificant relative to the general corrosion of this alloy, were uniformly distributed.

Verbal descriptions were also provided by the staff at the LaQue Center, for the atmospheric exposure panels of the alloys 1421 and 8090. These specimens were described as displaying one or two "exfoliated blister" sites, with "speckles" being evident on the surfaces. Though the 1421 specimen was reported to be more speckled than the 8090 panel, the 1421 specimen was reported to be by far the smoothest of the specimens between the 1420, 8090, and 1421. An estimated 10:1 difference was provided as a description of the magnitude of the severity of attack between the 1420 and the 1421. No specimens of these alloys (1420, 1421, and 8090) will be removed from the LaQue test site until 24 months of testing has been completed.

All of the other (1100, 5083, 6013, 6061, and 6061 Al_2O_3) specimens displayed the pitting distributions previously described in this section. The pits were surrounded by a halo region similar to those found on the laboratory immersion specimens.

CONCLUSIONS

Regarding the mechanism of corrosion for the developmental alloy, Weldalite 050:

- The elongated plates composing the layered grain structure must have higher concentrations of the anodic Al_2Li δ' phase, facilitating the dissolution of the aluminum matrix and the onset of pitting.
- The geometry of this corrosion susceptible planar grain boundary provides an ideal environment for creviceing, leading to exfoliation.
- This mode of attack is similar to that found in other non-recrystallized Al-Li alloys, 1420, 1421, 2090, and 8090, with the lesser incidences of elongated attack in the material forms with less severe grain orientation (i. e. the 2090 and 8090)
- That the heat affected zone (as that produced in the region produced by cutting the material) was harsh enough to the chemistry of the alloy, to affect the Li-constituent and alter the mode of attack in those heat affected regions.
- That electrochemical data could not be relied upon to predict the severity of in-service exfoliation of the Weldalite 050.
- That the Weldalite 050 demonstrated improved corrosion performance over several of the commercially available Al-Li alloys.

Regarding the mechanisms of corrosion demonstrated by the other alloys:

- The Al-Li alloys exhibited localized attack very similar to that encountered by the Weldalite 050 alloy.
- The alloy 2090, in the polished condition, was the only alloy, other than the Weldalite 050, to exhibit a different mode of pitting toward the cut-edges of the specimen panels.
- The severe degradation seen on the unpolished 2090-T84 alloy specimens, in both the long term and accelerated tests, reflects the detrimental corrosion resistance characteristics imparted by heat treatment of this Al-Li alloy.
- Exfoliated pitting and exfoliation have the potential for being the most detrimental in-service modes of degradation for the Al-Li alloy series.
- The Al-Mg alloys, though susceptible to grain boundary attack, did not support the geometry's necessary for exfoliation, instead supporting much deeper more localized attack in all types of testing.

Regarding the confidence in the validity of the test results and comparisons:

- Based on the range of electrochemical testing results, ranking by such parameters as E_p and E_{corr} do not necessarily suggest how well aluminum alloys might perform in long term or in-service corrosion situations, relative to each other.
- Accelerated laboratory corrosion tests were capable of generating consistent pit morphologies. Careful evaluation of the morphology of degradation, coupled with alloy phase information seems a viable predictor of mechanism of attack.
- The evaluation of cyclic polarization metastable pitting loops may be an excellent predictor of morphology of pitting attack.
- The use of corrosion rate measurements, based on weight losses, do not adequately predict the service life of aluminum alloys, which fail predominantly due to localized attack.

RECOMMENDATIONS

•SEM microscopy of the Field Exposure specimens may provide further support regarding the mechanistic predictability of laboratory studies.

•Statistical evaluation of the ranking orders obtained from the different test series might provide a weighted value to the merit of the test procedure for predicting corrosion performance.

•Continued studies of the cyclic polarization testing results in predicting pit morphologies is suggested.

•Completion of the original test matrix may provide additional weighting support, but will not likely add to the understanding of the mechanism of corrosion of the developmental

REFERENCES:

1. Van Horn, *Aluminum: Properties, Physical Metallurgy and Phase Diagrams*, 1967, American Society of Metals
2. *1994 Annual Book of ASTM Standards*, American Society for Testing and Materials, 1994
3. Ateya, B. G., Pickering, H. W., Journal of the Electrochemical Society, Vol. 122, No. 8, p. 1019, 1975
4. Pourbaix, M., *Lectures on Electrochemical Corrosion,* NACE International, Houston, TX, 1995
5. Jones, D. A., *Principles and Prevention of Corrosion*, Macmillan Publishing Co., 1992
6. Szlarska-Smialowska, Z., *Pitting Corrosion of Metals*, 1986
7. Campbell, L. G., *Corrosion Behavior of an Alumina-Reinforced AL Metal Matrix Composite*, 1996

Table 1.1: Field Exposure Test Plan

Test Standard	Filtered Seawater	Alternate Immersion	Atmospheric Exposure
Material	Perspex, G-52	G-52, G-44, G-50	G-50
1100	YES	YES	YES
1420		YES	YES
1421		YES	YES
2090	YES	YES	YES
5083	YES	YES	YES
7039	YES	YES	YES
Weldalite 050	YES	YES	YES
6061	YES	YES	YES
6061 Al2O3	YES	YES	YES
6013	YES	YES	YES
8090		YES	YES

Table 1.2: Laboratory Test Plan

	Artificial Seawater	Exfoliation	Exfoliation	Polarization	Corrosion Potential	Electrochemical Scratch
Material	G-31	G-34, G-112	G-85, Annex 2	G-5, G-59, cyclic	G-69	
1100	YES	YES	YES	YES	YES	
1420		YES		YES	YES	
1421	YES	YES	YES	YES	YES	
2090		YES		YES	YES	
5083	YES	YES	YES	YES	YES	YES
7039	YES	YES	YES	YES	YES	
6061	YES	YES	YES	YES	YES	YES
6061 Al_2O_3	YES		YES	YES	YES	YES
6013	YES			YES	YES	
8090		YES		YES	YES	
Weldalite 050	YES	YES	YES	YES	YES	YES

Table 2.1: Test Alloy Compositions (wt. %)

Al alloy ID	Fe	Si	Cu	Cr	Mg	Mn	Li	Ag	Ti	Zn	Zr
1100 [7,8]	0.32	0.33	0.20			0.05				0.10	
1420 [9]	0.06	0.06	0.07		5.09		2.05		0.011		0.075
1421 [9,10]					5.09		2.05				0.10
2090 [7,11]	0.012	0.10	2.70	0.05	0.25	0.05	2.25		0.15	0.10	0.12
Weldalite 050*	0.06	0.04	<0.02	<0.01	4.2	<0.01	2.24	0.39	0.02	0.02	0.15
5083 *	0.2	0.07	0.04	0.09	4.7	0.7			0.02	0.03	
6013 [12]	0.3	0.75	0.9	<0.1	0.95	0.35			<0.1	<0.25	
6061 *	0.45	0.63	0.25	0.18	0.94	0.09			0.02	0.04	
7039 [7]	0.22	0.1	0.05	0.18	2.89	0.24			0.02	4.15	
8090 [7,11]	0.03	0.2	1.3	0.1	0.95	0.1	2.45		0.1	0.25	0.1

Table 3.1: Laboratory Immersion Test Results for Fully Submerged Specimens

Alloy Designation	Preliminary Corrosion Rate (mpy)	Pit Density (#/cm^2)	Maximum Pit Size (cm^2)	Maximum Pit Depth (mm)	Final Corrosion Rate (mpy)	Pitting Factor
1100	0.00450	0.207	0.447	0.171	0.08555	1.999
1420	0.01449	1.434	1.038	0.114	0.10727	1.063
1421	0.01920	0.039	0.456	0.022	0.01616	1.361
5083	0.00052	0.867	0.835	0.026	0.02432	1.069
6013	0.02580	0.260	not available	not available	0.04903	
6061	0.00000	0.103	0.354	0.029	0.01794	1.617
6061 Al_2O_3	0.00000	0.075	0.584	0.263	0.00881	22.852
7039	0.17667	0.000	0.000	0.000	0.2080	0
Weldalite 050	0.19674	0.736	1.656	5.339	0.3038	17.574

The data in this table represents the average corrosion rate calculations for fully submerged aluminum alloy specimens in the Laboratory Immersion Test, ASTM Standard G-31. These results reflect the corrosion rates as determined by the two different cleaning procedures mentioned in the Experimental section. Pit size and depth evaluations reflect the most severe pit dimensions recorded for each material. Pitting Factors were calculated using the final corrosion rate reported. All tests were conducted for 90 days in an artificial seawater solution.

Table 3.3: Cyclic Polarization Results

Alloy Designation	E_{pp} (mV vs. SCE) Average	E_{rp} (mV vs. SCE) Average	Metastable Range
Weldalite 050	-725.93	-716.63	21.97
1100	-722.84	-723.58	34.32
1420	-771.9	-765.20	122.00
1421	-770.95	-758.13	46.23
2090	-672.40	-672.40	*
5083	-753.58	-753.58	59.72
6013	-718.17	-710.82	50.01
6061	-736.43	-737.95	44.88
6061 Al_2O_3	-732.60	-732.50	42.44
7039	-863.80		
8090		-660.90	

This table lists the pitting potential (Epp) and repassivation (Erp) values obtained during cyclic polarization studies. The metastable ranges are based on the mean pitting potentials minus the protection potentials. Tests were conducted in artificial seawater, under quiescent conditions.

Table 3.2: Results of Anodic Polarization Studies

Quiescent	E_{oc} (V)	i_{oc+100} (A)	i_{oc+150} (A)	i_{oc+200} (A)	E_p (V)	Range (V)	$E_{10\mu A}$ (V)
Weldalite 050	-0.7492	0.040599	0.278319	0.278	-0.70897	0.04027	-0.71703
1100	-0.8721	1.21E-06	3.83E-06	6.59E-06	-0.69987	0.15978	-0.6829
1420	-0.7496	2.45E-05	0.000149	0.002129	-0.65455	0.095	-0.64975
1421							
2090	-0.6917	0.000116	0.00152	0.0161	-0.63205	0.05962	-0.63157
5083	-0.838	2.10E-06	4.38E-06	4.72E-06	-0.6869	0.15105	-0.68181
6013	-0.8388	3.39E-06	4.80E-06	0.000112	-0.68874	0.15013	-0.68228
6061	-0.9124	9.93E-07	1.38E-06	4.68E-06	-0.70941	0.20302	-0.69867
6061 Al_2O_3	-1.0043	8.95E-07	1.13E-06	1.36E-06	-0.70875	0.29559	-0.70199
7039	-0.9256	2.87E-06	1.13E-05	0.002826	-0.7485	0.17707	-0.7455
8090	-0.706	0.000212	0.001568	0.003933	-0.64588	0.05076	-0.63659
Polished	**Eoc (V)**	**Ioc100 (A)**	**Ioc150 (A)**	**Ioc200 (A)**	**Ep (V)**	**Range (V)**	**$E_{10\mu A}$ (V)**
Weldalite 050	-0.8147	0.000235	0.016892	0.273966	-0.73386	0.08086	-0.72903
1100	-0.7492	0.000679	#NUM!	#NUM!	-0.71026	0.03891	-0.70012
1420	-0.8464	2.92E-07	3.84E-07	1.80E-07	-0.64698	0.199418	-0.6594
1421	-1.0724	4.81E-07	4.22E-06	5.99E-07	-0.73594	0.33643	-0.73051
2090	-068642	7.63E-05	0.00366		-0.576	0.1105	-0.60491
5083	-0.8894	9.54E-07	1.96E-06	1.24E-05	-0.68592	0.20346	-0.68163
6013	-0.8165	1.36E-06	4.86E-06	6.02E-06	-0.66511	0.15139	-0.64796
6061	-0.8637	1.06E-06	1.30E-06	2.41E-06	-0.68504	0.1786	-0.6716
6061 Al_2O_3	-0.9824	6.82E-07	1.06E-06	5.66E-06	-0.67342	0.30899	-0.65254
7039	-0.8984	5.13E-05	0.000576	0.002398	-0.81813	0.08027	-0.81564
8090	-0.7722	2.62E-06	4.98E-06	0.000123	-0.65649	0.11162	-0.64059
Deaerated	**Eoc (V)**	**Ioc100 (A)**	**Ioc150 (A)**	**Ioc200 (A)**	**Ep (V)**	**Range (V)**	**$E_{10\mu A}$ (V)**
Weldalite 050	-1.2353	1.03E-06	1.37E-06	1.68E-06	-0.7156	0.51969	-0.70986
1100	-1.1698	1.23E-06	1.40E-06	1.75E-06	-0.7048	0.49403	-0.69648
1420	-1.2556	1.07E-06	1.35E-06	1.34E-06	-0.74604	0.50934	-0.74081
1421							
2090	-0.9587	6.67E-07	1.14E-06	1.44E-06	-0.62177	0.33696	-0.61815
5083	-1.045	1.52E-06	3.36E-06	6.48E-06	-0.71314	0.31757	-0.70585
6013	-1.19769	6.27E-07	6.99E-07	1.20E-06	-0.65394	0.54375	-0.64494
6061	-1.1085	1.15E-06	1.16E-06	1.86E-06	-0.69099	0.41754	-0.67378
6061 Al_2O_3	-1.33216	1.10E-06	1.54E-06	1.79E-06	-0.63502	0.69715	-0.62463
7039							
8090	-1.1971	9.69E-07	1.35E-06	1.71E-06	-0.64143	0.55069	-0.62914

This table lists the geometric mean results of anodic polarization testing of aluminum alloys. The value headings are as defined in the previous paragraphs. All potentials are recorded versus SCE. All tests were conducted in artificial seawater.

Table 3.4: Corrosion Potential Test Data

Alloy Designation	Mean E_{corr} (mV vs. SCE)	Max E_{corr} (mV vs. SCE)	Min E_{corr} (mV vs. SCE)
Weldalite 050	-0.76562	-0.76013	-0.77208
Soviet 1420	-0.78702	-0.78358	-0.79038
1100	-0.74769	-0.74645	-0.74855
2090	-0.72446	-0.71727	-0.73215
5083	-0.77439	-0.76353	-0.79433
6013	-0.72087	-0.68985	-0.73168
6061	-0.7504	-0.74803	-0.75232
6061 Al_2O_3	-0.74507	-0.7398	-0.74962
7039	-0.80402	-0.75513	-0.88915
8090	-0.75447	-0.7484	-0.7580

These corrosion potentials were obtained using ASTM StandardG-69, Corrosion Potential Test

TABLE 3.5: Alternate Immersion Test Results

Alloy Designation	Preliminary Corrosion Rate (mpy)	Maximum Pit Size Ranking	Maximum Pit Depth (mm)	Final Corrosion Rate (mpy)	Pitting Factor
1100	0.031	1	0.0120	0.113	0.106
1420	0.024	3	0.0616	0.112	0.550
1421	0.025	3*	0.0725	0.096	0.755
2090 (unpolished	0.029	3*	Not available	1.776	
2090 (polished)		>5*	Not available	Not available	
5083	0.247	2	0	0.333	0
6013	0.131	4	0.1760	0.198	0.903
6061	0.076	>5	0.007	0.246	0.028
6061 Al_2O_3	0.094	>5	0.1365	0.155	0.882
7039	0.168	0	0	0.237	0
8090	-0.096	>5	0.1280	0.085	1.506
Weldalite 050	0.029	3	0.0975	0.110	0.888

This table presents the most severe corrosion values obtained in alternate immersion testing in filtered natural seawater. Preliminary corrosion rate was based on weight loss before performing an abrasive cleaning procedure commonly used in weight loss studies. The final corrosion rate was calculated after conducting the more common specimen cleaning procedure. Pit ranking is based on the ASTM standard pit ranking values and reflects the single largest pit found on each specimen evaluated. Values which are absent reflect work in progress. *These measurement were of areas displaying uniform-localized corrosion, rather than pitting.

TABLE 3.6: Continuous Immersion Test Results

Alloy Designation	Preliminary Corrosion Rate (mpy)	Maximum Pit Size (Ranking)	Maximum Pit Depth (mm)	Final Corrosion Rate (mpy)	Pitting Factor
1100	0.691	0	0	0.18379	0
2090 (unpolished	0.852	>5*	Not available	1.6887	
5083	0.088	0	0	0.3026	0
6013	1.775	>5	Through		Infinite
6061	0.255	>5	Through	0.4212	Infinite
6061 Al_2O_3	0.701	>5	2.3395	0.2288	10.216
7039	0.271	0	0	0.4988	0
Weldalite 050	0.069	>5	0.2095	0.1832	0.115

This table presents the most severe corrosion values obtained in continuous immersion testing in filtered natural seawater. Preliminary corrosion rate was based on weight loss before performing an abrasive cleaning procedure commonly used in weight loss studies. The final corrosion rate was calculated after conducting the more common specimen cleaning procedure. Pit ranking is based on the ASTM standard pit ranking values and reflects the single largest pit found on each specimen evaluated. Values which are absent represent work in progress. *These measurement were of areas displaying uniform-localized corrosion, rather than pitting.

TABLE 3.7: Environmental Exposure Test Results

Alloy Designation	Preliminary Corrosion Rate (mpy)	Pit Density (#/cm^2)	Pit Size Ranking (averaged)	Maximum Pit Depth	Final Corrosion Rate (mpy)	Pitting Factor
1100	-0.1852	45.75	2.3		0.4511	
2090 (unpolished)	-4.7410				4.0164	
2090 (polished)	-0.3698				0.1892	
5083	-0.1346	22.43	1.7		0.5771	
6013	-0.1811	34.8	2.1			
6061	0	37.82	1.8		0.3763	
6061 Al_2O_3	0.0960	20.88	1.7		0.4316	
7039	0.4323				1.7711	
Weldalite 050	-0.3719	56.99	2.2		0.4517	

This table presents the worst corrosion results encountered in environmental. Unless otherwise noted corrosion rates were worse at the time of the 6-month removal. Pit densities were calculated averages based on the data presented in the tables found in Appendix D. For the pit evaluation information the letter and number designate the side of the panel (F =front, B =back) and the removal period (6-months, 12-months), respectively. The Weldalite 050 and alloy 6013 were not scheduled for 6-month removal.

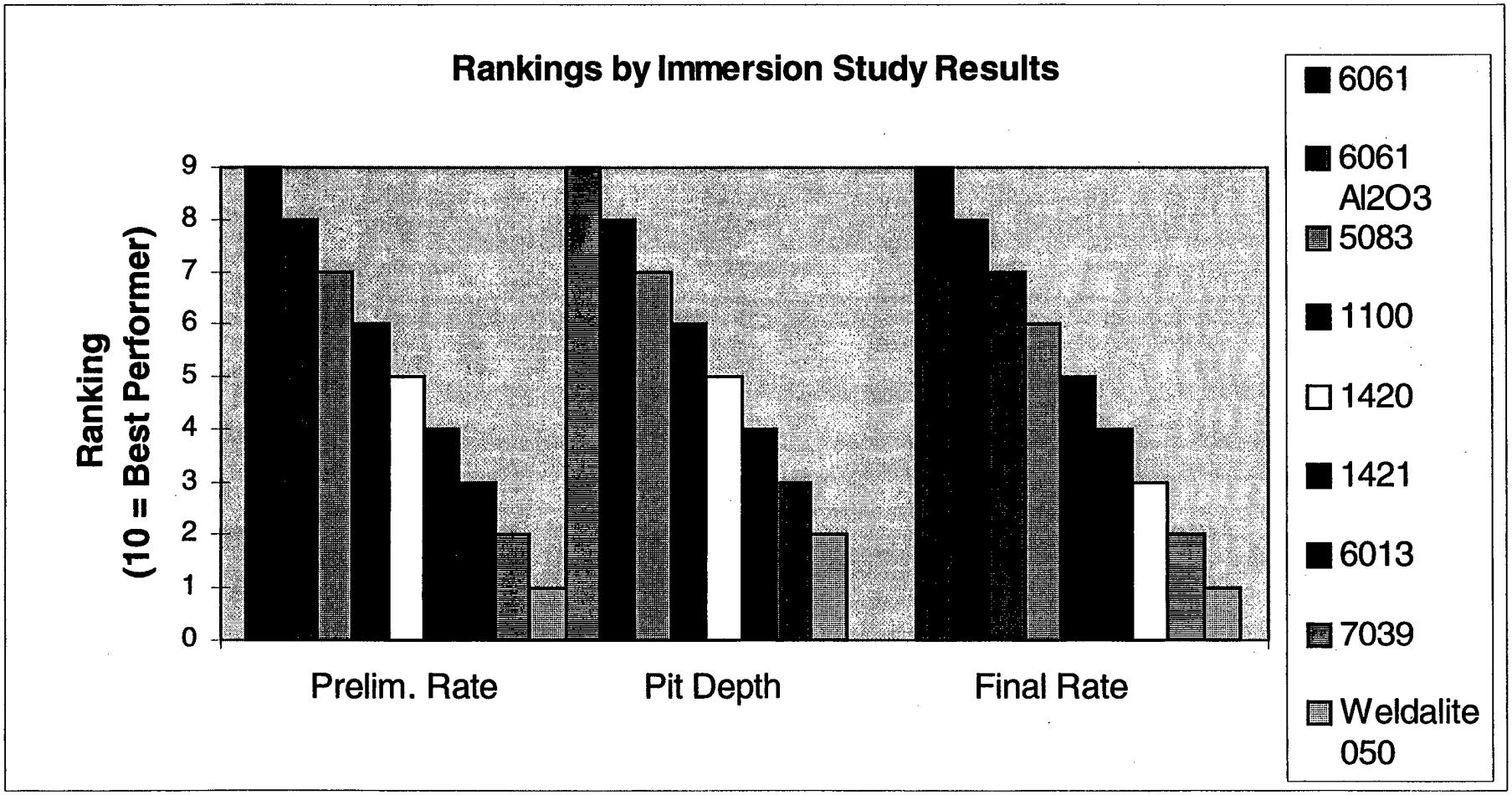

Figure 1: This figure represents the relative ranking of several aluminum alloys, based on results of laboratory immersion studies. All materials were tested in artificial seawater for a period of 90 days.

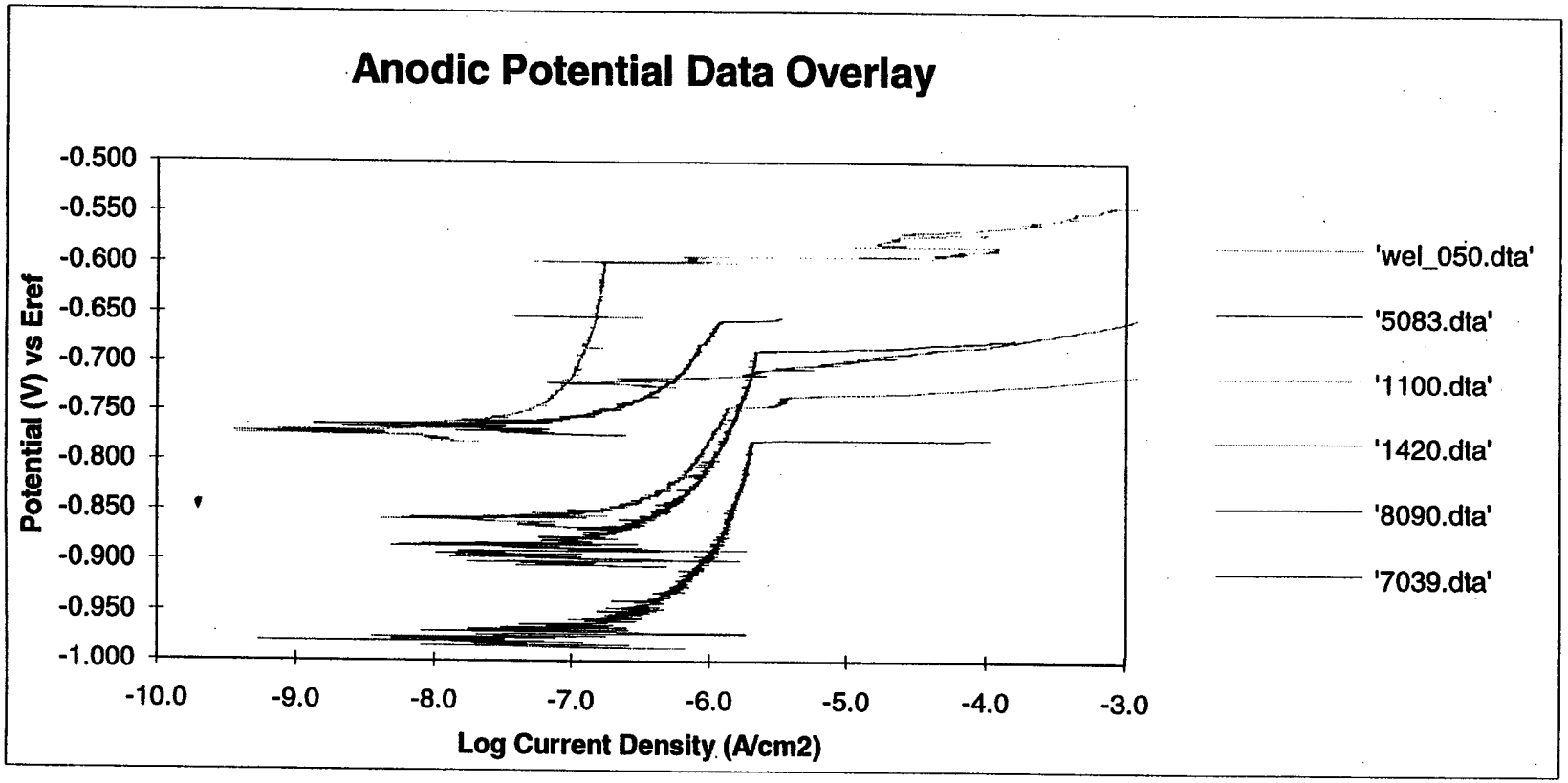

Figure 2: This figure shows the anodic polarization testing results of the aluminum alloys Weldalite 050, 1100 , 1402, 5083, 7039, and 8090. All tests were run under quiescent conditions, in artificial seawater. Potential values are reported relative to a SCE.

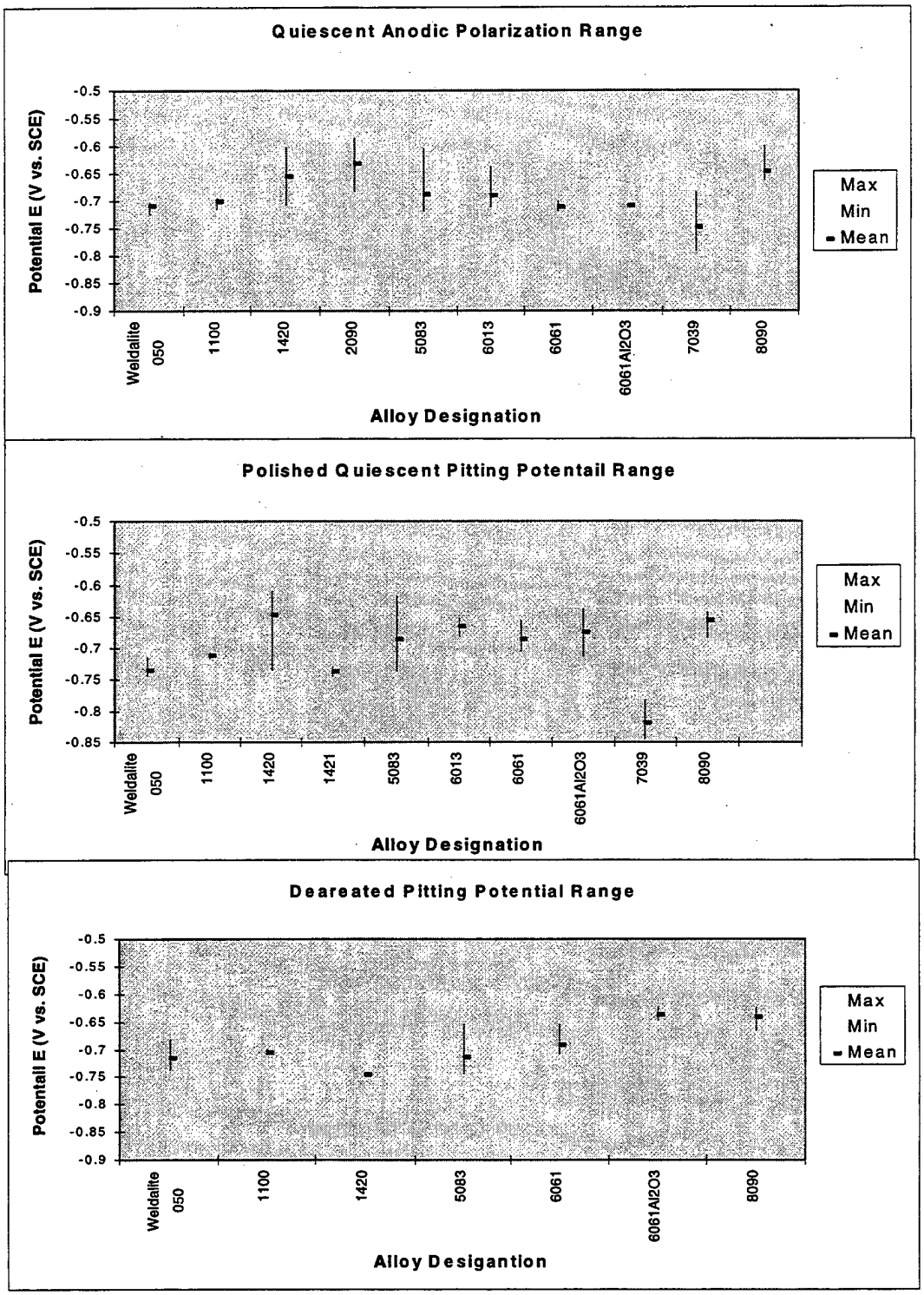

Figure 3: These figures show the ranges and mean values of the breakdown potentials E_p, as determined by anodic polarization. It can be seen that between

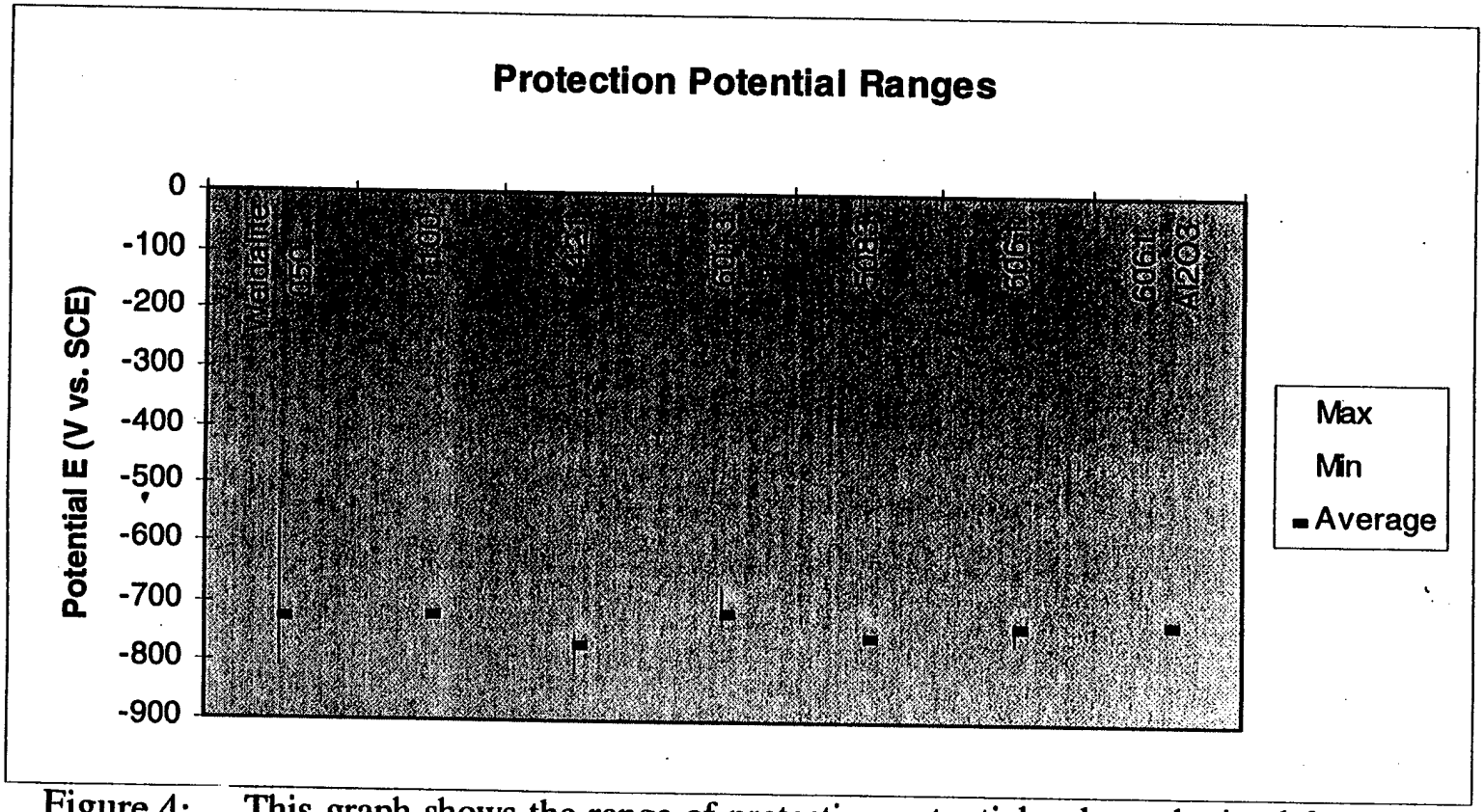

Figure 4: This graph shows the range of protection potential values obtained for materials in cyclic polarization testing. All test were conducted in artificial seawater, under quiescent conditions.

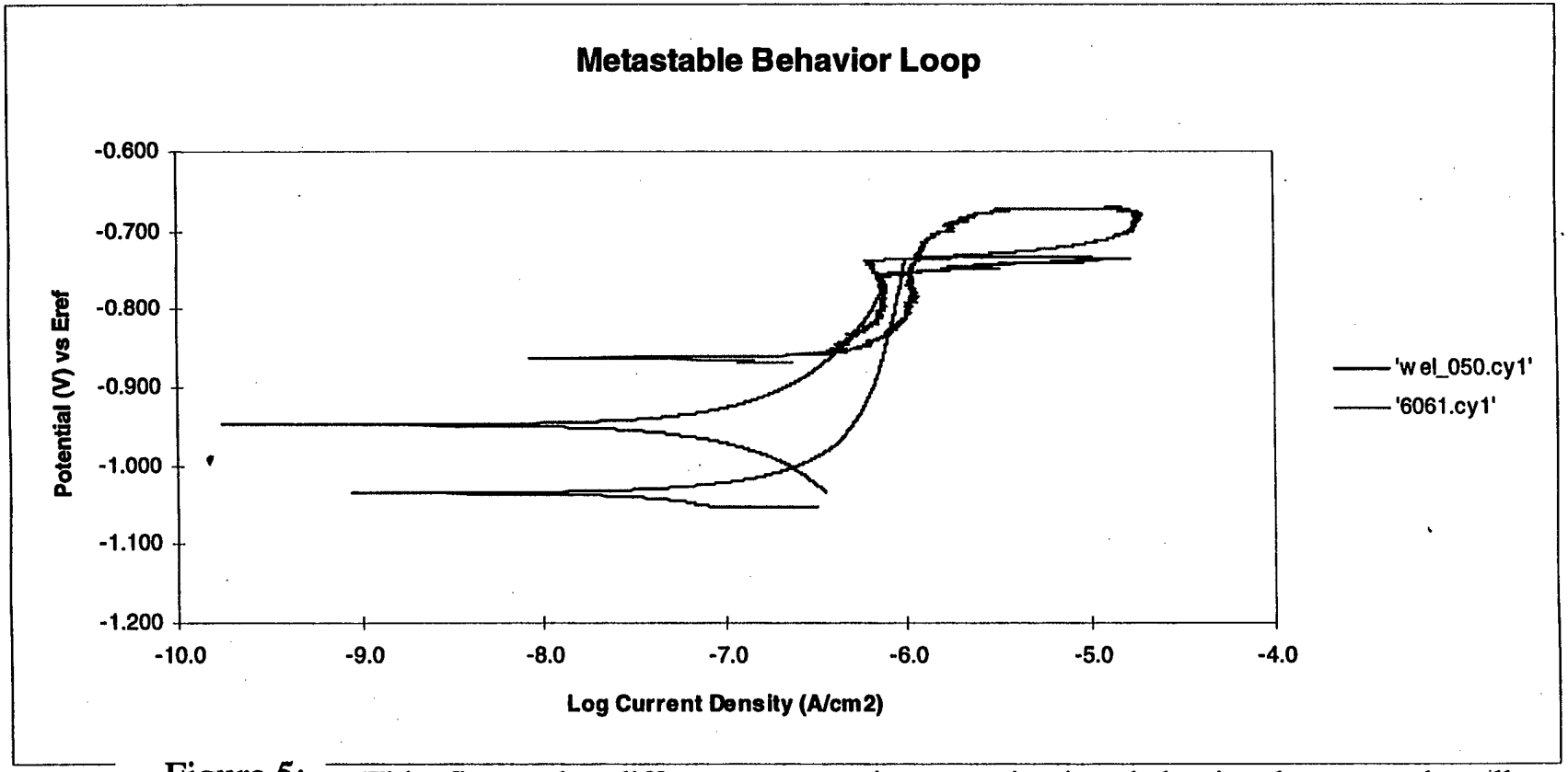

Figure 5: This figure the differences seen in repassivation behavior between the alloys Weldalite 050 and 6061. The curve Weldalite 050 curve shows a quicker return to passive behavior.

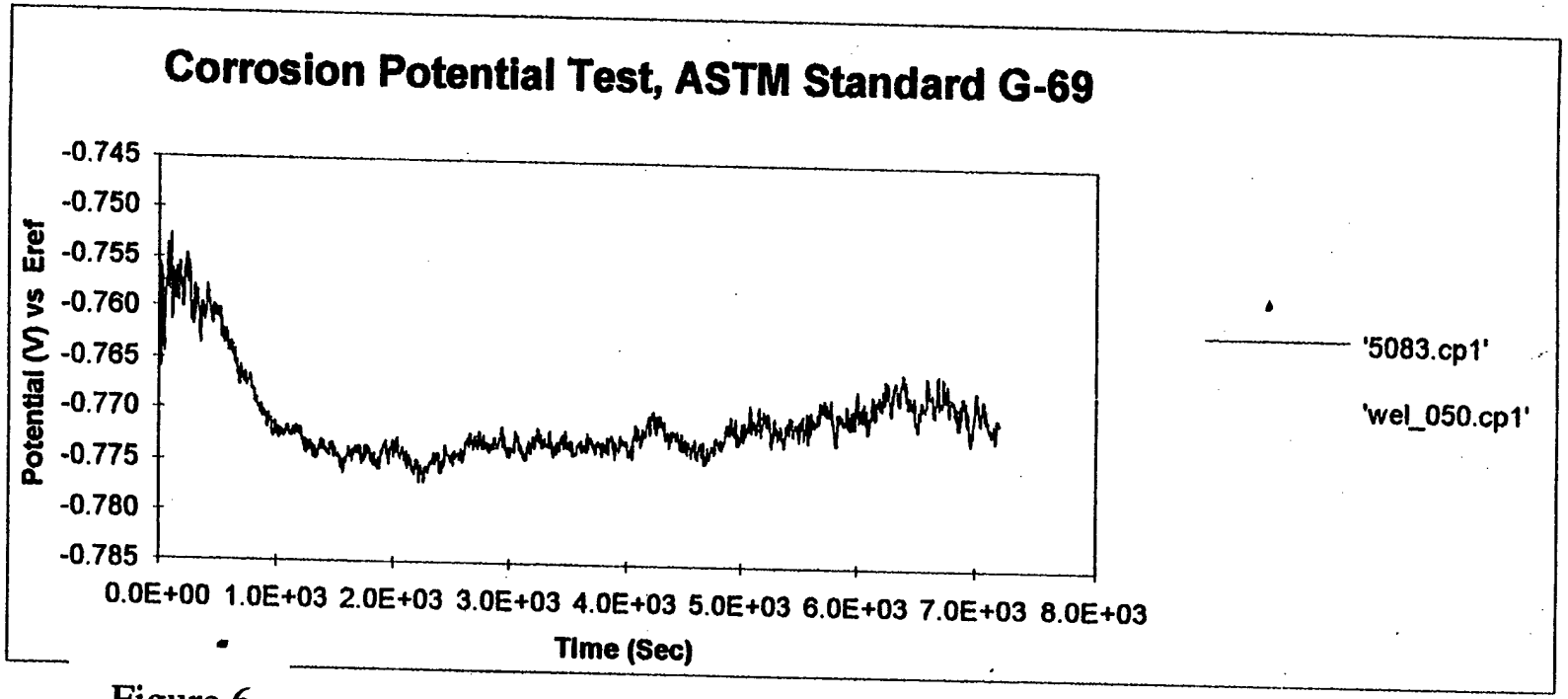

Figure 6 This plot represents the results of three hours of exposure to the ASTM Standard G-69 NaCl + H_2O_2 solution used for corrosion potential evaluation. Though some of the alloys tested displayed noticeable potential drops within the first half hour of testing , as seen for the 5083 curve, all specimens achieved stable potentials by the 30 minute mark and remained stable throughout at least three hours of exposure.

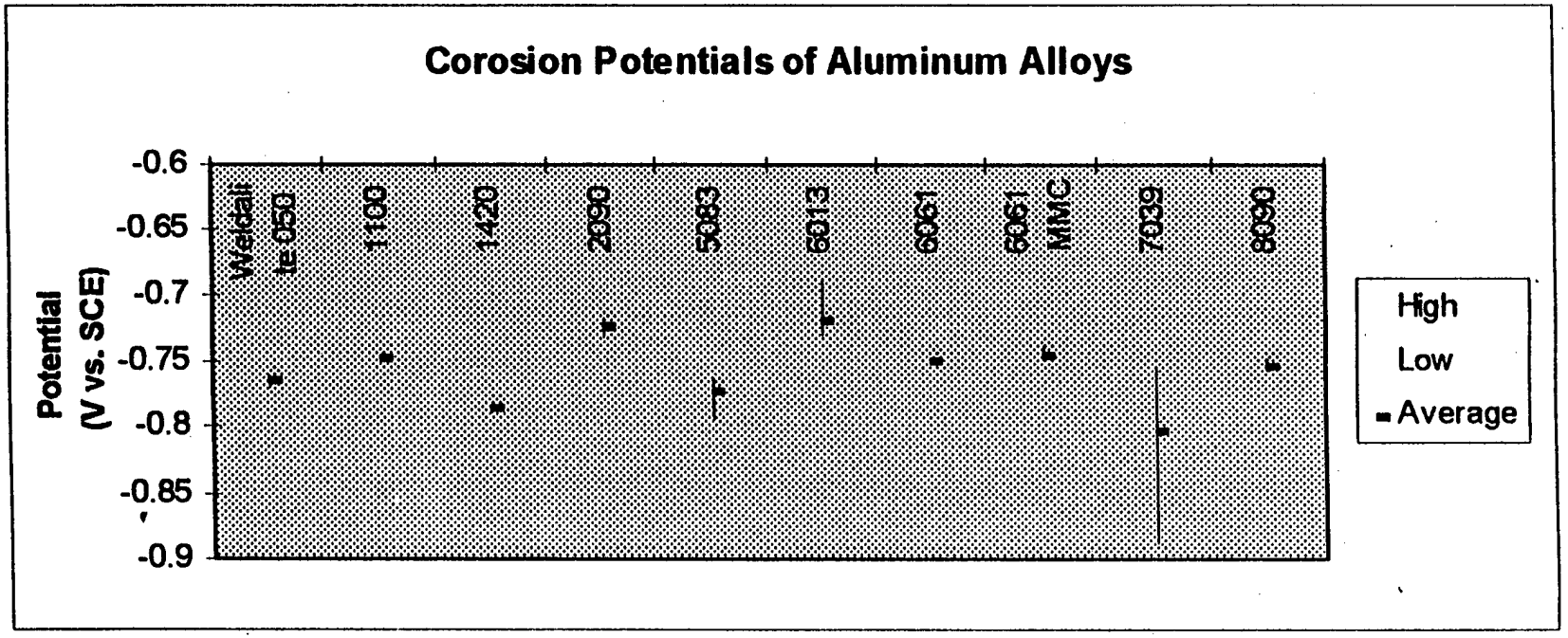

Figure 7 This plot shows the ranges and averages of E_{corr} values obtained during the ASTM G-69 testing of Al alloys. All potentials were calculated as per the ASTM standard.

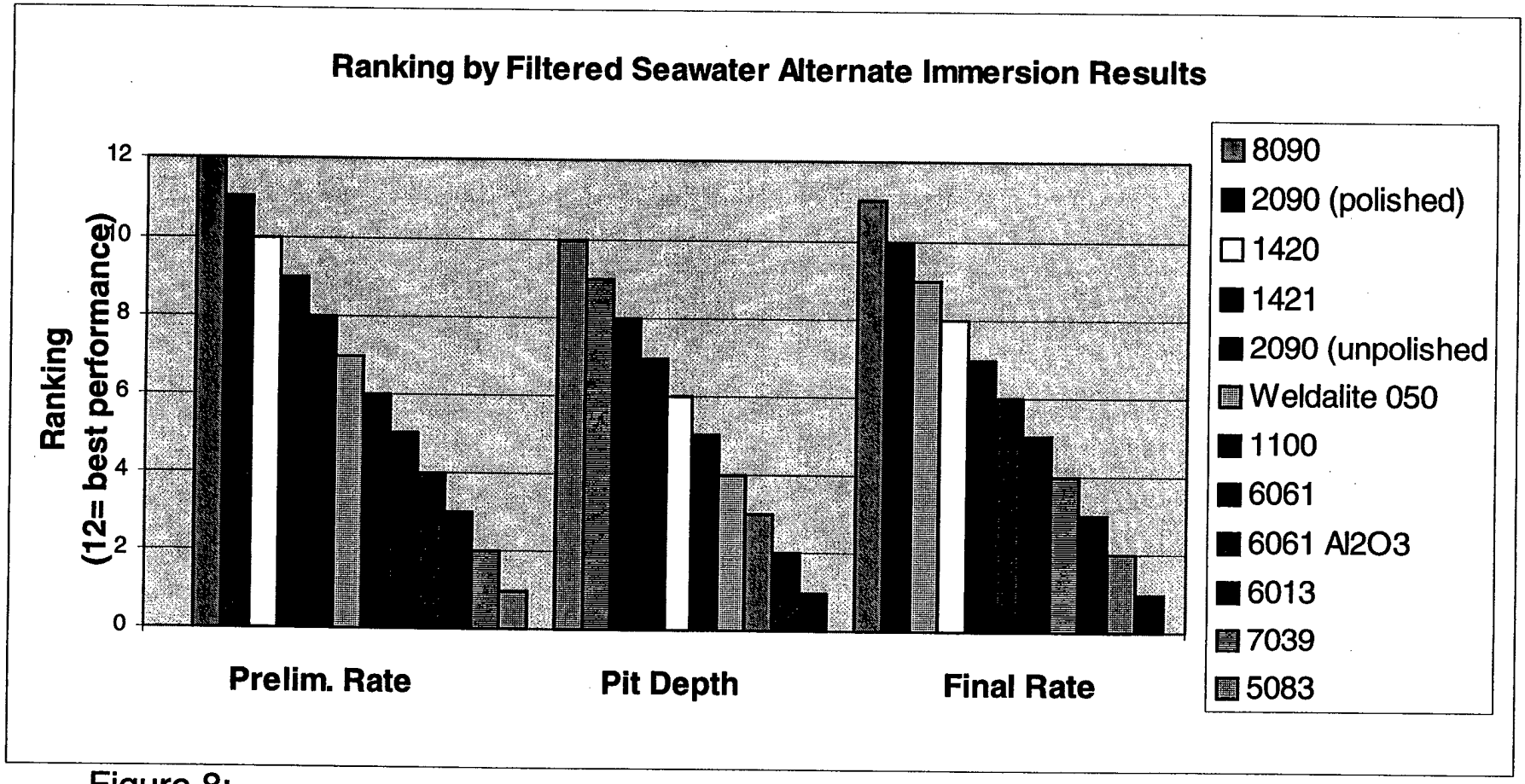
Ranking by Filtered Seawater Alternate Immersion Results
Ranking
(12= best performance)
12
10
8
6
4
2
0
Prelim. Rate
Pit Depth
Final Rate
8090
2090 (polished)
1420
1421
2090 (unpolished
Weldalite 050
1100
6061
6061 Al2O3
6013
7039
5083

Figure 8:

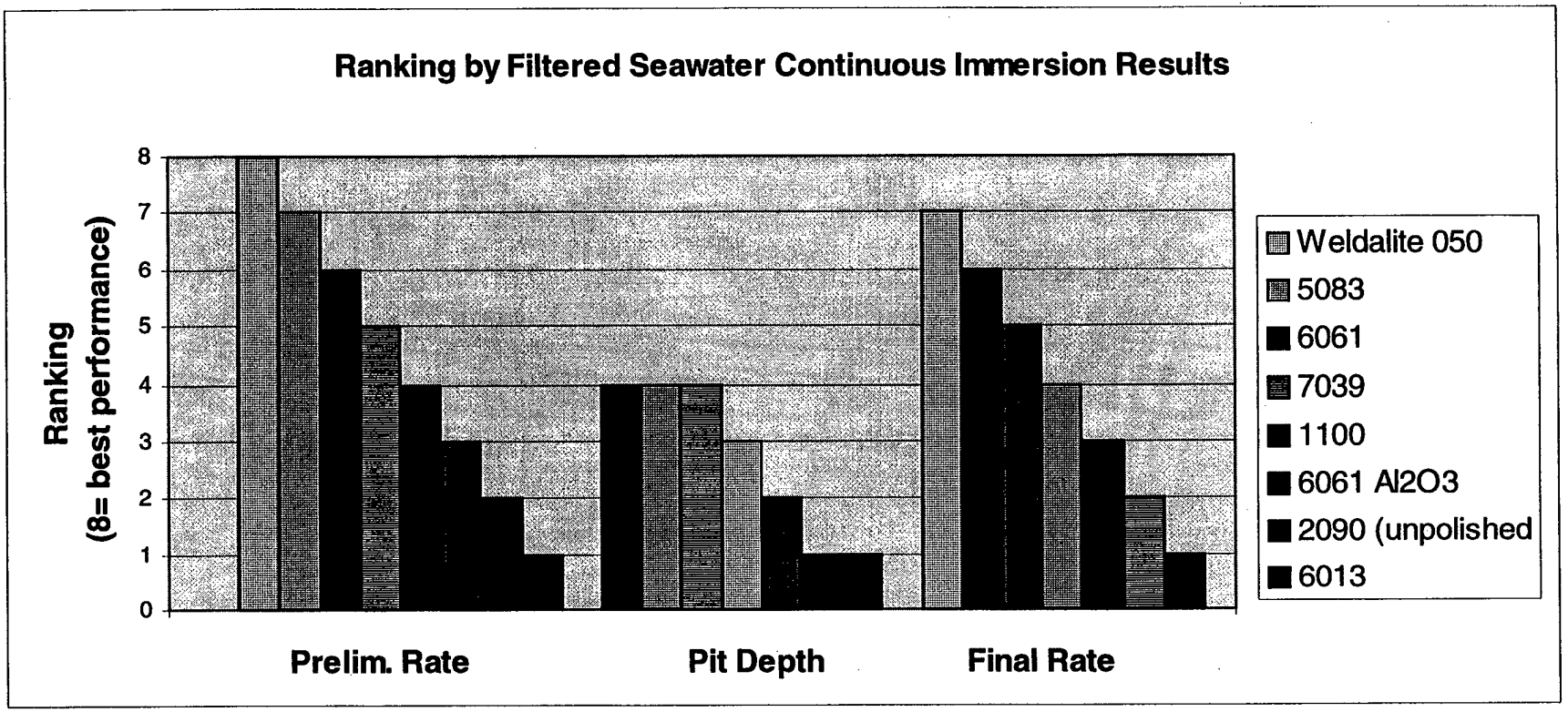

Figure 8: These bar charts demonstrate the relative rankings of Al alloys based on the specified criteria. All specimens considered in this ranking were exposed to 12-momths of filtered seawater exposure at the LaQue Center for Corrosion Testing Services.

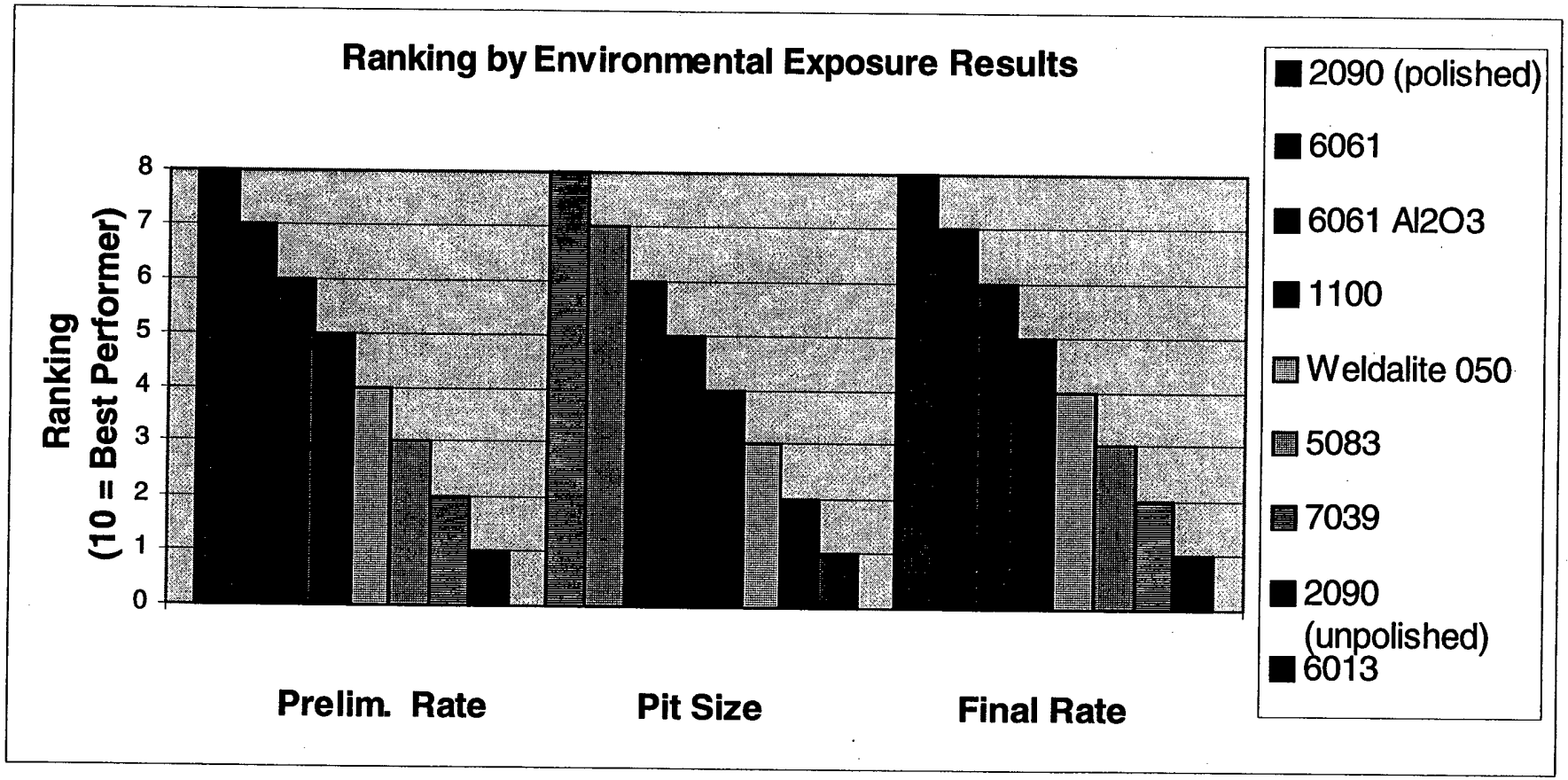

Figure 9: This bar chart shows the ranking of the Al alloys subjected to environmental exposure testing at the LaQue Center for Corrosion Services, Kure Beach, NC.

Preparation and Properties of Corrosion-Resistant Thin Ceramic Coatings on Metallic Substrates by Sol-Gel Processing

Azar Nazeri, and Paul Slebodnick
Naval Research laboratory
Environmental Effects Branch, Code 6310
Washington, D. C. 20375

ABSTRACT

Thin films of ceramic oxides were deposited on metallic substrates by dipping in liquid precursors prepared by sol-gel processing. The amorphous and porous coatings deposited on low temperature alloys such as aluminum and bronze were then treated in a room temperature process for further densification. Coatings on high temperature alloys such as stainless steel were heated to several hundred degree centigrade for consolidation and crystallization. Resultant coatings along with uncoated metallic coupons have been characterized and evaluated by electron microscopy, x-ray diffraction, salt-fog spray exposure and electrochemical measurements.

INTRODUCTION

Lack of surface stability of many metals and alloys in aggressive environments has increased the need for economical and high performance coatings which can resist such surroundings. Structures susceptible to aqueous corrosion and high temperature oxidation are currently protected by surface modifications, paints, thin and thick metal coatings or intermetallic alloys. Many metals form a protective oxide scale under high temperature conditions. However, these oxide scales are prone to spallation due to mechanical strains and temperature cycling. Ceramic coatings exhibiting high-temperature stability and resistance to hostile environments do exist; however, they are expensive, difficult to process and usually feature poor adhesion and require intermediate layers. Overall, there are serious inadequacies and inherent drawbacks associated with most coatings and the various techniques used to produce them.

Sol-Gel Processing

The sol-gel process is a cost-effective and non-hazardous method for processing ceramic coatings of pure or multi-phases with controllable composition and microstructure. This technology has been successfully used for preparation of ceramics, glasses, fibers and thin films in the past two decades and has shown considerable advantages over conventional ceramic processing especially in the area of thin films[1,2]. Multi-component oxides can be formed by formulating a solution of different precursors. Sol-gel deposition of

thin films offers a great potential for forming dense oxide thin films on complex shapes such as turbine blades through dipping or spraying of the solution which is not possible through "line-of-sight" deposition techniques. In this process, precursor chemicals are dissolved in an appropriate solvent, deposited as a thin film by dipping or spinning. Heat-treatment decomposes the organics and forms an amorphous oxide. Crystallization and densification of the oxide takes place upon further heating.

Sol-gel coatings are amorphous and porous as deposited at room temperature. In order to fully exploit the ceramic properties of these coatings, in most cases it is essential to densify and consolidate the films into their final structures by heat-treating them at elevated temperatures. This might not be a problem when high temperature alloys are coated. However, it could be detrimental to low temperature alloys by changing their microstructure or heating too close to their melting point. In this work, coatings on stainless steel were densified by treating them at high temperatures either in the air or inert atmosphere. Coatings on low temperature alloys though, were only dried or were treated at room temperatrue with a plasma treatment. This treatment is expected to densify a very thin layer at the surface and therefore make the porous coating impervious to the harsh species.

Ceria-Titania Coatings

It is well known that small additions of rare earth elements (cerium, yttrium, hafnium ...) or their oxide dispersions to high temperature alloys, containing chromium or aluminum, greatly improves their oxidation resistance [3,4]. Coatings of cerium oxide particles were reported to markedly improve the oxidation resistance [5]. Ion implantation and reactive sputtering have also been used to obtain cerium oxide coatings for high temperature protection of iron-chromium alloys [6]. Coatings from solutions however, offer the advantages of lower cost, ease of application, homogeneous coverage and concentration of the reactive element on the surface.

In the present work, thin layers of cerium oxide and titanium oxide are prepared through sol-gel processing of aqueous and organic precursors. Aqueous corrosion of 304 stainless steel with and without the sol-gel coatings is investigated. The effect of processing parameters such as the maximum temperature of heat-treatment and atmosphere on the structure and properties of the coatings is also discussed. Furthermore, the use of titania as a refractory overlayer on cerium dioxide in enhancing the aqueous corrosion resistance is investigated.

Zirconia Coatings

Zirconia is a ceramic well-known for its superior hardness, high temperature properties, mechanical, and chemical durability. Zirconium coatings are used as thermal barriers and oxidation resistant coatings. The stable form of zirconium oxide at room temperature is monoclinic. Zirconium

then undergoes two transitions: between 950°C and 1250°C it becomes tetragonal, and at 2370°C changes to a cubic fluorite structure. The volume change associated with the low-temperature to high-temperature transformation is about 4% and results in internal stresses in the ZrO_2 body large enough to cause fracture or substantial weakening. In attempts to avoid this problem, it has been discovered that appropriate additions of MgO, CaO, CeO_2 or Y_2O_3, to ZrO_2 produced a cubic form that did not undergo a transformation and was thus useful over a broad temperature range.

These oxide stabilizers form solid-solutions with zirconia. Alumina, however, is not soluble with ZrO_2 and stabilizes it through another mechanism called "Constraint" [7,8]. Essentially the critical nucleus size of zirconia particles is increased by a constraining matrix (alumina) that has a higher modulus than that of zirconia. Stabilized ZrO_2 films have long been deposited by plasma spraying, a line-of-sight process involving spraying a jet of plasma on the substrate [9,10]. Recently, films prepared by physical vapor deposition (PVD) techniques such as magnetron sputtering were found to have advantages over those prepared by plasma spraying [11,12].

The present work will investigate the possibility of forming Al_2O_3 stabilized ZrO_2 through sol-gel processing. Due to the thinness of these films (usually <1μm) these coatings are not intended as thermal barrier coatings, but rather as protective layers against corrosion and oxidation.

EXPERIMENTAL

Ceria-Titania

Ceria coatings were formed by dipping metal samples into a precursor solution formed in the following manner: cerium hydroxide was prepared by mixing ammonium cerium nitrate and ammonia. The resultant hydroxide precipitate was washed with water until a neutral pH was achieved. Dilute nitric acid was added to the precipitate at 60°C to obtain a pH of 1. A transparent yellow solution resulted which was further concentrated by heating. Titanium isopropoxide (TIP) was dissolved in isopropanol and subsequently diethanolamine (DEA). Diluted water in isopropanol (W) was added to the mixture to obtain a molar ratio of 1:1:1 of TIP:DEA:W. The concentration of this solution was 0.4 M. Substrates were coated by dipping in the appropriate solutions and withdrawn at a constant rate. They were then heated on hot plates at 150°C and 550°C for 20 minutes each. The deposition process was conducted in a glove box with a relative humidity at about 20%. Films were then treated to higher temperatures in the air or in graphite for further densification. Composite coatings of ceria/titania with an approximate thickness of 0.5μm were obtained by depositing two underlayers of ceria and firing at 550°C and then additional eight layers of titania. Samples were treated at 900°C after every two coats of titania. Aqueous corrosion resistance was

evaluated by potentiostatic polarization experiments in 0.05 N NaCl solution deaerated with argon. Details of this procedure have been described previously [13,14].

Zirconium Coatings

Zirconium-n-propoxide 70% in propanol (Johnson & Mattey) and aluminum di(isopropoxide) acetoacetic ester chelate (Alfa) were mixed in 2-propanol and acetylacetone. Four different atomic ratios of Zr : Al, 93:7, 90:10, 70:30, and 62:38 were prepared to find the minimum amount of alumina necessary to stabilize the tetragonal phase of zirconia. Solutions were prepared with no water added. Substrates were cleaned with ethanol prior to deposition. Solutions were deposited on silicon wafers, polished fused silica coupons, and unpolished stainless steel (304) coupons by dipping. Films were then dried for less than an hour on a hot-plate kept at about 160°C. After every two coats, the samples were annealed at various temperatures between 400-1000°C by inserting them into pre-heated ovens [15].

Silica Coatings

Tetraethoxyorthosilicate (TEOS) was used as the source of silica. It was mixed with ethyl alcohol and water at two ratios of 1:2:1 and 1:4:1 of TEOS: ethanol: water. Coupons measuring 2" x 3" of Navy Brass and 6061-T6 aluminum were coated. The coupons were coated after washing in soapy water and rinsing in alcohol by dipping them halfway at a constant speed in the solution. Samples were then dried at 120°C for 1 hour. Some coated samples were treated with an argon plasma at a pressure of 300 millitorr and power input of 276 W for various times. Both plasma treated and simply dried samples were then exposed in a Salt-Fog spray cabinet for 1000 hours.

RESULTS AND DISCUSSIONS

Low Temperature Coatings

Silica Coatings-There were a total of 12 brass samples and 12 aluminum samples put in the Salt-Fog (SF) cabinet with 4 of them not plasma treated. All brass samples without exception looked shinny and yellow on the side which was coated by sol-gel silica (Figure-1). This was true for both plasma treated and not plasma treated samples. The uncoated parts were extensively oxidized with black, blue and copper-color corrosion products. The samples were left in the SF upright, with the uncoated part at the top. This caused some corrosion products to run down over the coated parts. Since there were no distinguishable differences between the plasma treated samples and untreated ones, no conclusion regarding this treatment can be drawn. Figure-2 shows the X-ray diffraction patterns of the base brass metal, the uncoated and coated part

of a sample after 1000 hours in the salt fog spray cabinet. The XRD patterns of the sol-gel coated and base metal are similar while, there are few new peaks that appear in the pattern of the corroded part. The corrosion products were not identified. Scanning Electron Microscopy (SEM) was done on the coated and uncoated sections of the samples after their exposure in the salt-fog cabinet. Figure-3a shows the interface between the coated and uncoated sections of a sample. Examination of the coated area showed that the coating was still present and had kept its integrity with no sign of peeling or cracking. There was no sign of cracking. Figure-3b shows the one sample at higher magnification.

Aluminum samples behaved similar to the brass ones. The coated areas of the aluminum coupons kept their reflective appearance and very few and shallow pits were observed. However, the uncoated parts suffered general corrosion and looked dull. SEM showed that the coating was adherent to the aluminum and did not peel off. It was observed that the processing parameters such as the concentration of the solution or plasma treatment did not make any obvious difference in the performance of different samples.

High Temperature Coatings

Ceria-Titania Coatings-Ceria coatings were successfully formed on polished 304SS. Transparent, crack-free and adherent coatings up to 0.5μm were obtained. Cerium dioxide coatings obtained by multiple dipping and heat-treating at 900°C suffered much less corrosion, pitting and crevice corrosion in polarization tests than ceria coatings heated to lower temperatures. Figure-4 shows the anodic polarization curves for two ceria coated samples. Comparing the polarization behavior of the two samples heat-treated to 900°C (C900) and 750°C (C750), it can be seen that final temperature of heat-treatment has a direct effect on the performance of the coating. C900 has a higher pitting potential, Ecorr is shifted to the anodic direction and ip is also decreased by about two orders of magnitude. This is thought to be the result of higher densification attained at higher temperatures for coatings prepared by the sol-gel process. When these curves are compared to the curves of preoxidized 304SS, it is seen E_{corr} decreases significantly and the corrosion current increases. This behavior increases the anodic reaction rate in the presence of the film. Although the ceria coating provides the steel with improved resistance to pitting corrosion, the increase in i_p suggests the coating interferes with passivation and the protective properties of the normal passive film [13,14].

It was possible to obtain good quality multilayer titania films with an underlayer of ceria. The ceria undercoat seemed to greatly enhance the resistance of the substrate to oxidation. Figure-5 shows the anodic polarization curves for titania-ceria composite coatings (CTA1 and CTR with anatase and rutile structures respectively). A substantial difference in the electrochemical and corrosion behavior of these two samples is evident. Rutile sample (CTR) shows almost 5 orders of magnitude smaller ip but higher Ecorr and lower Epit

than CTA. This difference could be the result of different microstructure and surface morphology between the two sets of samples. CTA1 and CTA2 have a predominantly anatase structure and a smooth morphology, while CTR of mostly rutile structure has a rough surface. It can be concluded that rutile structure is more desirable in titania as far as the passivity is concerned. These results indicate the complex coating renders the heat-treated metal more resistant to crevice and pitting corrosion, and interferes with passivity to a lesser extent than the ceria coating. The significant decrease in the passive current observed for the ceria/titania coatings as compared to the ceria coating suggests the composite coating provides a more protective barrier for the metal substrate. This fact is substantiated by a correspondingly greater E_{pit} and the fact that no crevice corrosion was observed on the ceria/titania samples our most encouraging result. Despite the above differences in polarization behavior of CTA's and CTR, the physical appearance of the three samples after the exposure was very similar. All samples suffered no crevice corrosion and only few pits were observed on them. Tablel summarizes the polarization data (average values) for sol-gel coated and uncoated 304 stainless steel in deaerated 0.050 N NaCl.

Our most encouraging result is that the composite coating eliminates crevice corrosion of the steel as evidenced in all the polarization experiments. This could be because the coating forms a physically smoother, crevice-free surface at structural interfaces than uncoated steel. Furthermore, the composite coatings were able to keep their integrity and adherence even around the pits (Figure-6). Cracking of films at the pit sites did not propagate to other areas while undercutting of the corrosion below the films can vividly be seen. This is an unexpected performance from brittle ceramics which warrants further study of the mechanical properties of these films.

Zirconium Coatings-Thin coatings of various compositions of ZrO_2-Al_2O_3 were deposited on different substrates. Films were transparent and did not suffer any spallation and peeling after heat-treatment or upon cycling. The ZrO_2/Al_2O_3 films deposited by sol-gel processing showed an amorphous structure as deposited. The cubic phase precipitated upon heating to 600°C for one hour. The cubic phase was the only phase that crystallized in all samples prepared, regardless of the substrate and the composition. Particle sizes of the films calculated by using XRD data showed that they decreased upon higher alumina content. A significant advantage of these sol-gel films over similar PVD films are the low crystallization temperature (600°C) and low aluminum concentrations (7%.) necessary for achieving a cubic phase. Layers of Zr:Al composition of 93:7 were deposited on stainless steel coupons by dipping the coupons half way in the solution. Subsequently the coupons were fired at 900°C for various durations of time. X-ray diffraction patterns showed that cubic phase zirconia had crystallized after annealing. A significant observation was that the coated area maintained a reflective surface while the uncoated part was dulled and oxidized. This observation was also valid for samples heated for 50

hours at 800°C. These samples were taken out of the furnace and quenched in air several times. No sign of peeling or cracking was observed in the films.

CONCLUSIONS

Using sol-gel processing, thin, transparent, adherent and crack free films of ceria, titania, alumina-stabilized zirconia and silica were deposited on metallic substrates. Coatings on low temperature metals such as aluminum and brass were either dried or plasma treated for further consolidation. All coatings provided some protection against aqueous corrosion and a definite improvement of coated section over the uncoated sections was observed regardless of their plasma treatment. SEM showed that the thin ceramic coatings preserved their integrity throughout the area applied and remained adherent. Sol-gel coatings of oxides on stainless steel (ceria, titania, and zirconia) were heat treated to as high as 900°C for crystallization and consolidation. They increased high temperature oxidation resistance of the metals by reduction in scale formation and spallation and improved aqueous corrosion of stainlees steel by eliminating the crevice corrosion.

It is intended to further characterize these coatings by doing cyclic accelerated testing such as GM9540, outdoor atmosphere exposure, sea water immersion and compatibility tests with top coats and sand-blasted surfaces depending on the application intended.

REFERENCES

1.C. J. Brinker and G. W. Scherer,"Sol-Gel Science, The Physics and Chemistry of Sol-Gel Processing", Academic Press, San Diego 1990.

2.J. D. Mackenzie, J. Non-Crystalline Solids,48, 1 (1982).

3-G. M. Ecer, R. B. Singh and G. H. Meier, Oxid. Met., 18 (1982) 55.

4-S. Seal, S. K. Bose, and S. K. Roy, Oxidation of Metals, Vol. 41, Nos. 1/2, 1994

5-F. Czerwinski, and W. W. Smeltzer, J. Electrochem. Soc., Vol. 140, No. 9, 1993

6-R. J. Hussey, P. Papaiacovou, J. Shen, D. F. Mitchell and M. J. Graham, Materials Science and Engineering, A120 (1989) 147-151

7. FF.. Lange, J. Mater. Sci. 17, 225, (1992).

8. F.F. Lange, J. Mater. Sci. 17, 247, (1992).

9. E. Schwarz, A. R. Nicholl, H. Gruner and R. Prince, Proc. First INt. Conf. Surf. Engng, Brighton, UK, 25-28 June 1985, The Welding Institute (1985)

10. A. R Nocholl, H. Gruner, G. Wuest and S. Keller, Proc. Conf. Protective Systems for High Temperature Gas Turbine COmponents, Royal Society, London, 13-14 Nov. 1984, Materials Science and Technology 2 (March 1986) pp 214-218

11. T. N. Rhys-Jones and F. C. Toriz, High Temperature Technology, Vol. 7, N0. 2, May 1989 pp73-81

12. S. B. Qadri, C. M. Gilmore, C. Quinne, E. F. Skelton, and C. R. Gossett, Phys. Rev. B 39, 6234 (1989).

13.P. P. Trzaskoma-Paulette and A. Nazeri, J. Electrochem. Soc., Vol. 144, No. 4, April 1997.

14. A. Nazeri and .P. P. Trzaskoma-Paulette, To be published in the J. Sol-Gel Sci. & Technology.

15.A. Nazeri and S. B. Qadri, Surface & Coating Technology 86-87 (1996) 166-169.

Tablel polarization data (average values) for sol-gel coated and uncoated 304 stainless steel in deaerated 0.050 N NaCl.

	Ecorr (VSCE)	**ipass** (mA/cm2)	**Epit** (VSCE)
As-received steel	0.080	0.0004	0.975
Heat-treated steel	0.089	0.0008	0.450
ceria coating	-0.345	0.900	0.700
ceria/titania coating	-0.215	0.045	1.000

Figure-1 A bronze coupon coated at the bottom with silica, after exposure in salt-fog cabinet for 1000 hrs.

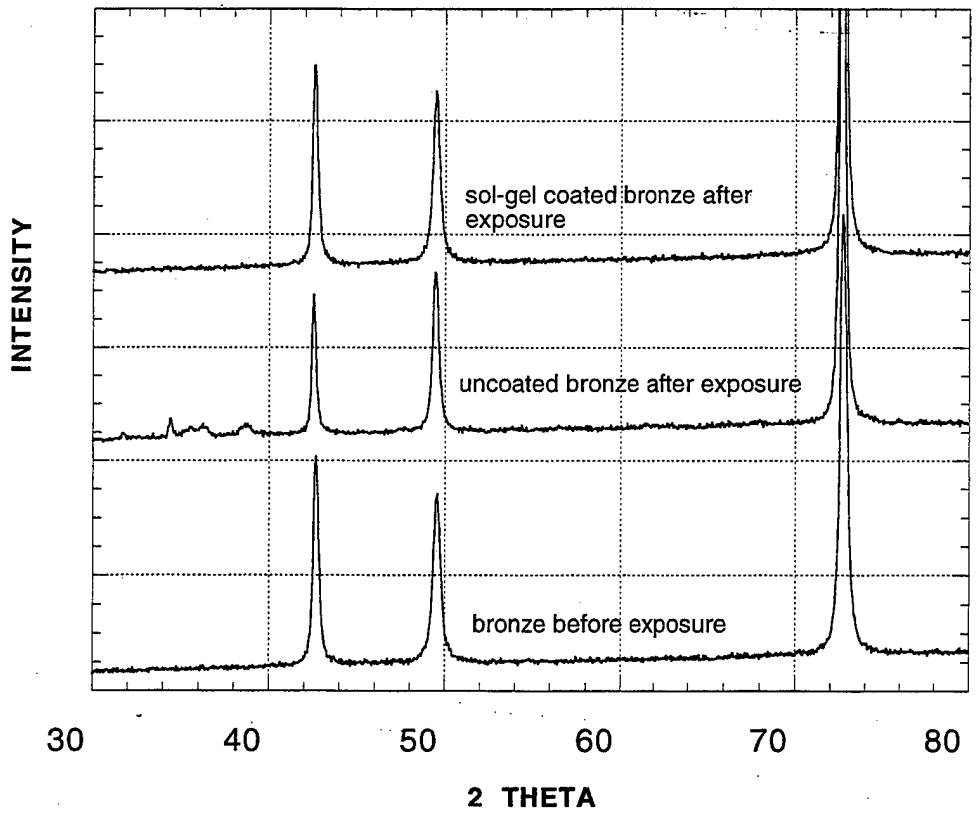

Figue-2 XRD patterns of a bronze coupon, a silica coated bronze and an uncoated bronze coupon after exposure to salt-fog cabinet for 1000 hrs.

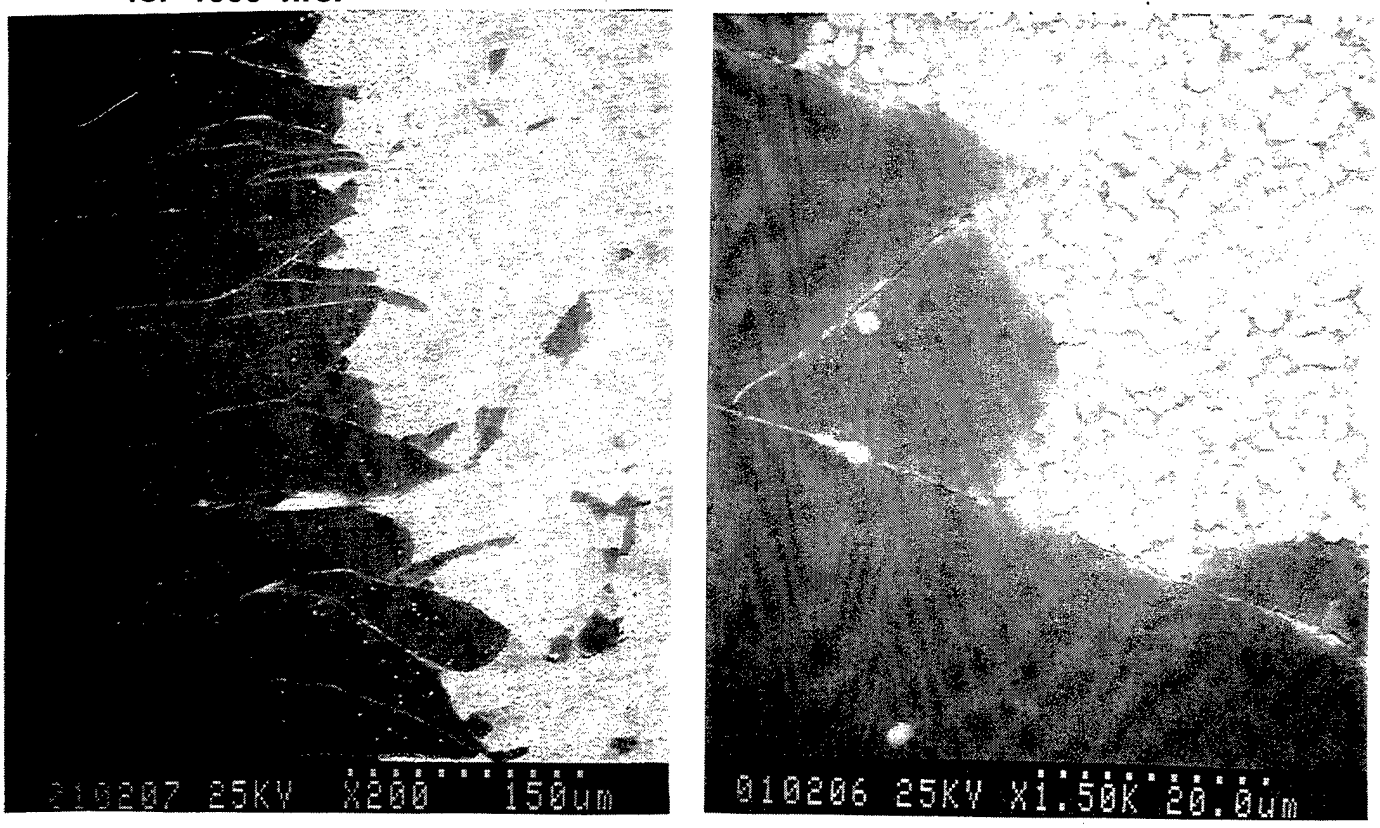

Figure-3 SEM pictures of interface between coated and uncoated parts of a bronze coupon after salt-fog exposure for 1000 hrs.

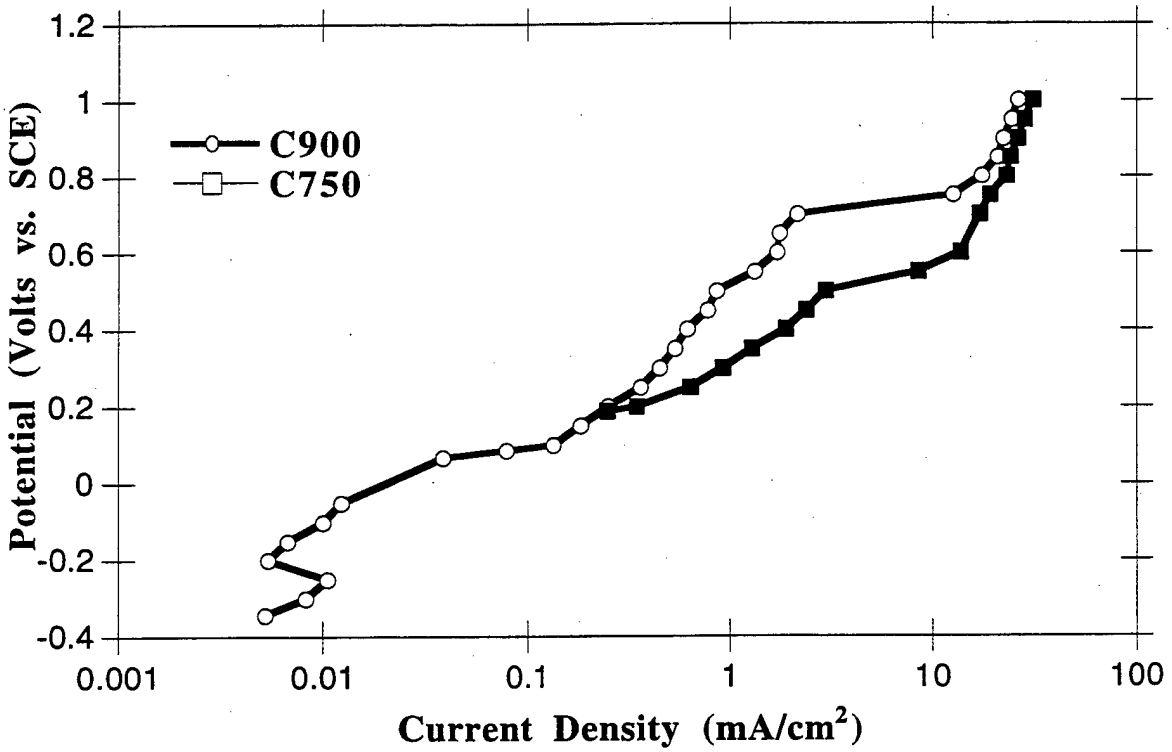

Figure-4-Polarization curves of ceria coatings on 304 stainless steel in 0.050 N NaCl solution

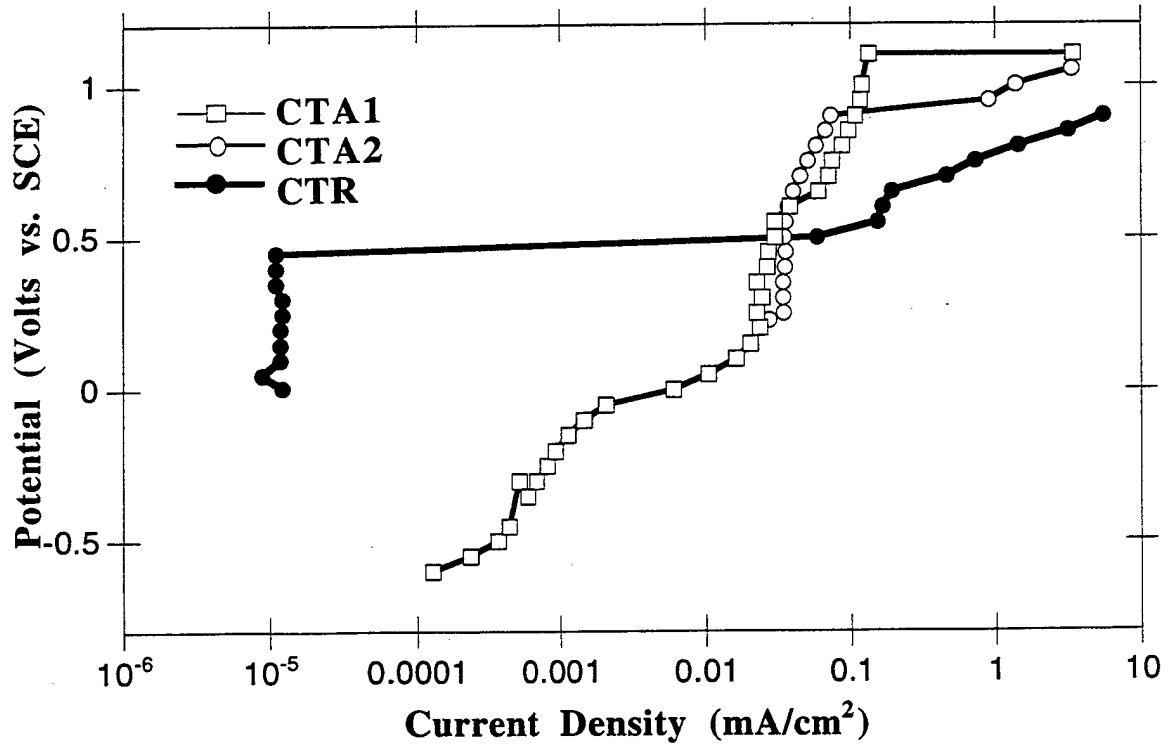

Figure-5-Polarization curves of two ceria/titania composite ccoatings with different titania crystal structure

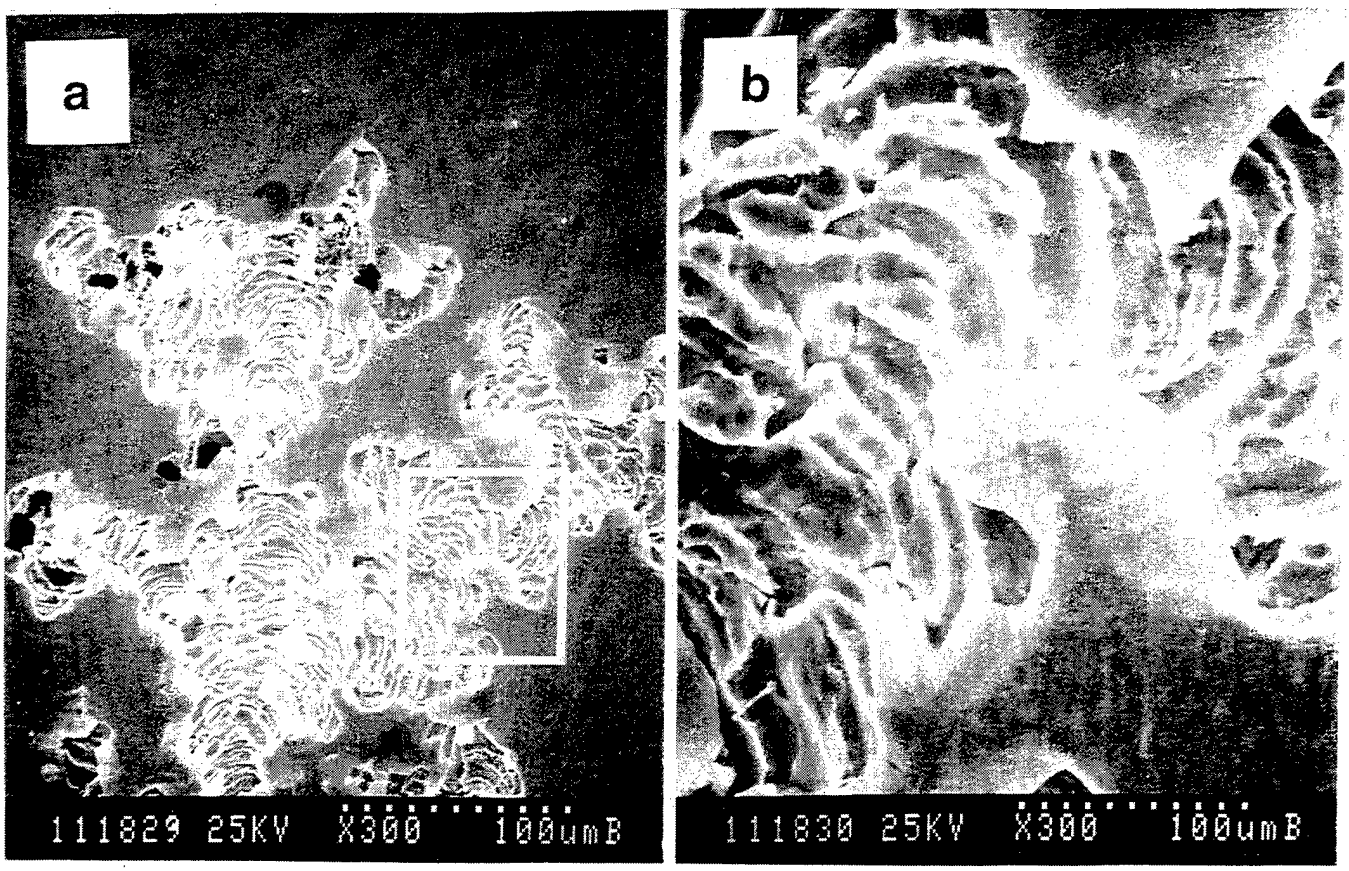

Figure-6 SEM pictures of ceria-titania coated stainlesss steel; pit formation following anodic polarization in 0.05 N deaerated NaCl.

Oxidation and Embrittlement of Titanium Aluminides

J. Rakowski, R. Cerchiara, F. S. Pettit, and G. H. Meier
Department of Materials Science & Engineering
University of Pittsburgh
Pittsburgh, PA 15261

ABSTRACT

The oxidation behavior of γ-TiAl and "orthorhombic" Ti-Al-Nb alloys in the temperature range 500-900°C is described. The effects of atmosphere composition and surface preparation on the composition of the oxide scales and the resultant oxidation kinetics are described. Particular emphasis is given to the phase transformations in the alloys immediately under the oxide layers. These layers, which are formed as the result of Al-depletion and inward diffusion of oxygen, can produce dramatic degradation of the alloys' mechanical properties, even when the layers are quite thin (<1 μm). Mechanisms for the development of the oxidation morphologies and the mechanical property degradation are presented.

INTRODUCTION

Alloys in the Ti-Al system are of interest for high temperature systems such as aircraft engines because they have low density and maintain strength at high temperature. However, their resistance to oxidation and interstitial embrittlement is a concern. Those alloys which form alumina scales have excellent resistance to surface recession while those which form titania-rich scales oxidize at much higher rates. The modification of the microstructure immediately beneath the oxide layer, resulting from interstitial dissolution and/or selective removal of one or more alloy component, is of particular concern since it can cause a substantial loss of mechanical properties.

Thermodynamics

An important aspect of the oxidation of Ti-Aluminides, compared to the aluminides of Ni and Fe, is the small difference in standard free energy of formation between alumina and the oxides of titanium, which is accentuated by a negative deviation from ideal solution behavior in the Ti-Al system. The aluminum activity is much smaller than unity in Ti_3Al and TiAl. In fact, combining the activities with standard free energy data for the oxides indicates that TiO is more stable in contact with the alloy than is Al_2O_3 for atom fractions of Al much less than about 0.5[1,2]. Thus, Al_2O_3 is unstable in contact with binary α_2 and is only marginally more stable than TiO in contact with γ-TiAl.

Oxidation of Orthorhombic Alloys

There are relatively few oxidation data available on alloys in the Ti-Al-Nb system with significant volume fractions of the orthorhombic phase. However, data are becoming available

which indicate that the amount of Nb necessary to stabilize the orthorhombic phase results in more rapid oxidation than the α_2 alloys because of the formation of discrete Nb-oxides in the reaction products[3]. The parabolic rate constant for the oxidation of Ti-25 at%Al at 800°C decreases with increasing Nb content up to the 5-10% range but increases with further additions[4,5]. Additions of Ta have been found to reduce the oxidation rate slightly at a given Nb content[3]. The rate at 700°C has been reported to decrease with Nb additions up to 10 at%[6]. Additionally, alloys with Nb contents typical of the "orthorhombic alloys" undergo breakaway oxidation following an initial parabolic period. This phenomenon which is more prominent at the higher oxidation temperatures has been shown, using acoustic emission , to result from oxide cracking as the scale is enriched in Nb-oxides[3]. During oxidation the alloy microstructure is modified beneath the oxide layer causing embrittlement.

Oxidation of γ-TiAl

Choudhury et al., in a classic paper[7], studied the oxidation of TiAl (50 at% Al) in O_2 and air over the temperature range 800 - 1200°C. In O_2, cast TiAl which was abraded through 120 grit SiC formed alumina and exhibited k_p values $\approx 10^{-9}$ $g^2cm^{-4}hr^{-1}$ at 950°C but polished specimens formed TiO_2-rich scales and exhibited k_p values of about 10^{-5} to 10^{-6} $g^2cm^{-4}hr^{-1}$. Extruded TiAl formed alumina scales regardless of surface preparation. Choudhury et al. explained the effects of extrusion in terms of the absence of macroinhomogeneities which existed in the cast structure. The "surface finish effect", observed for the cast material was presumed to result from coarse grinding homogenizing the alloy at the surface. A Ti_3Al layer was reported to form between the oxide and the alloy for all the exposures. Oxidation behavior in air at 950°C was independent of specimen preparation or fabrication method with titania-forming kinetics (k_p about 10^{-5} - 10^{-6} $g^2cm^{-4}hr^{-1}$) observed in all cases. The scales were similar to those formed on polished specimens in O_2 at 950°C. Experiments to determine the species responsible for the difference between exposures in O_2 and air indicated that CO, CO_2 and H_2O impurities were not responsible nor was the difference in p_{O2}. It was, therefore, concluded that the increased rate of oxidation in air was a "nitrogen effect" although no N_2-containing phases were identified in the scale or substrate. The oxidation of TiAl also exhibited a "temperature effect" in that kinetics for all alloys at 1100 and 1200°C, regardless of surface preparation or exposure atmosphere, indicated TiO_2 formation. Internal oxidation was also observed at the two higher temperatures.

The "surface finish effect" for oxidation temperatures below 1000°C has been shown to result from recrystallization of the ground surface[8]. The deformed layer, produced by grinding, recrystallizes during the initial oxidation exposure to produce γ grains with a grain size on the order of 1 μm from a starting γ grain size on the order of 100 μm. No recrystallized layer forms on the polished surface. It has been suggested[8] that enhanced Al diffusion in the fine-grained layer promotes the formation of continuous alumina in the same manner as that reported by Giggins and Pettit[9] for the development of chromia films on Ni-Cr alloys.

The proposal that the "nitrogen effect" involved formation of nitrides which prevented the alumina from becoming continuous has been verified by elemental spectroscopic imaging (ESI) in a transmission electron microscope[10].

Electron microscopy has also revealed an intermediate layer between the oxide and the γ phase. This zone is depleted in Al and was originally thought to be α_2[7]. However, an important observation was made by Dowling and Donlon in 1992[11] when they identified a cubic phase with a lattice parameter of 0.69 nm and a Ti/Al ratio of approximately 2/1. These observations were confirmed and the cubic phase was found to have 432 point group symmetry[12]. Extensive TEM investigation of this phase using convergent beam electron diffraction (CBED)[13] showed it to belong to one of two space groups, P432 or $P4_232$, and EDS analysis indicated an approximate composition of 57 at%Ti-33at%Al-10at%O[14]. Increased exposure times and/or higher oxidation temperatures result in the Al-depleted zone becoming two-phase as the result of nucleation of α_2 at the interface between the cubic phase and the parent γ[14]. The influence of the depleted zone on the oxidation behavior of γ alloys is not yet clear, however, it is crucial to the mechanical properties.

Embrittlement of Titanium Aluminides

The effects on mechanical properties of exposure to oxidizing atmospheres constitutes what is currently the most important area of study regarding the use of intermetallics as high temperature structural materials. The creep resistance and ductility of α_2 at high temperature are much lower in air than in vacuum[15] and room temperature fracture toughness is severely degraded by exposure to oxygen at elevated temperatures[15,16-18]. Ward et al[16] found that embrittlement of Ti-25Al-10Nb-3Mo-1V during tensile testing in air at 550 and 650°C was strain-rate sensitive and proposed a dynamic process whereby oxygen embrittled the alloy in the region of a propagating crack. Rakowski et al[4] found that room temperature ductility of Ti-21Al-11Nb was severely degraded by exposures to oxidizing atmospheres at temperatures from 600 to 900°C and that the embrittlement was sensitive to the composition of the exposure environment. Oxygen caused severe embrittlement whereas high-purity nitrogen or argon did not. However, the presence of water vapor in the nitrogen or argon caused embrittlement and analysis of the fracture behavior suggested a synergistic effect between hydrogen and oxygen. The detailed mechanisms of these phenomena have not been studied and the effect of alloying additions have not been extensively investigated.

The orthorhombic alloys have been reported to be less susceptible to environmental embrittlement than the α_2 alloys[19], however, more recent work[3,20] has indicated that this is not generally the case.

The fracture toughness[21] and ductility[11, 22-23] of γ alloys are also reduced by exposures in air at elevated temperatures as a result of the layers which form beneath the oxide, as described above. Exposures at temperatures as low as 315°C and for times as short as six minutes at 650°C were found to embrittle Ti-48Al-2Cr-2Nb[22]. An additional factor in the embrittlement is the effect of temperature and atmosphere during the mechanical test. Shrouding the test in argon or raising the test temperature to 150°C negates most of the embrittling effects of the prior exposure at elevated temperature[22]. Clearly there is a need for a detailed understanding of the mechanisms for influence of environmental exposures on the mechanical properties of the titanium aluminides.

EXPERIMENTAL

Orthorhombic alloys were provided by Wright Laboratories in the form of hot pressed foil ("neat panels") of Ti-22Al-23Nb (at%) and by G.E. Aircraft Engines in the form of cast and forged monolithic Ti-22Al-26Nb (at%). These alloys will be designated as "22-23" and "22-26", respectively, in the following. Gamma alloys were provided by G.E. Aircraft Engines in the form of cast Ti-50Al and Ti-46 or 47Al-2Nb-2Cr (at%). The latter alloy will be designated "46-2-2" and "47-2-2", respectively. Oxidation coupons were exposed with a 600 grit or 1 μm diamond surface finish to dry air at temperatures between 500 and 900°C. Oxidation kinetics were followed by continuous mass change measurements using either a Cahn 1000 or Cahn 200-D microbalance.

Mechanical test specimens (bend and tensile) were cut from the Ti-22Al-26Nb, Ti-46Al-2Nb-2Cr, and Ti-47Al-2Nb-2Cr and finished by low stress grinding. The specimen dimensions are given in the following table.

Specimen Type	Gage/Bar Length(mm)	Width (mm)	Thickness (mm)
Tensile	38	6.3	3.2
Bend	35	11.1	9.5

Mechanical test specimens were pre-exposed in dry air at various temperatures in a horizontal tube furnace with a fused silica reaction chamber. Bend and tensile testing was performed on an MTS machine linked to a PC. The tensile strain rate was 0.5 mm/min and the bend test strain rate was 10^{-3}/min.

A wide variety of analytical techniques were used for characterization of as-received and exposed specimens. X-ray diffraction (XRD), both in normal and in thin film glancing angle mode (GAXRD), was used to analyze starting material and to reveal the phase chemistry of thin thermally grown oxide films. The morphologies and compositions of the oxidation products were analyzed using both light optical microscopy (OM) and scanning electron microscopy (SEM). The SEM used was a Philips XL30 equipped with a field emission electron source and an x-ray energy dispersive spectrometer (XEDS) detector capable of detecting characteristic x-rays down to carbon. Characterization of fine structure and determination of phase chemistry on the local scale was done using transmission electron microscopy (TEM/AEM) of specimens prepared in cross-section. A JEOL 2000FX microscope equipped with a light element XEDS detector was used for the bulk of the analysis. A Zeiss Omega 910 microscope was employed to generate energy filtered compositional images.

RESULTS AND DISCUSSION

Orthorhombic Alloys

The starting microstructure of the 22-23 neat panels consisted of three phases B2(β), orthorhombic (O), and $D0_{19}$ (α_2) with thin two phase (β+O) layers at the foil/foil and external

interfaces. The 22-26 was entirely two phase, consisting of a β matrix with O distributed uniformly as submicron, acicular precipitates.

Oxidation Behavior

The oxidation kinetics of 22-23 are presented in Figure 1 and those for 22-26 are presented in Figure 2. The oxidation kinetics were observed to follow a parabolic rate law at temperatures of 700°C and below for times as long as 700 h. However, at temperatures of 800°C and above the kinetics are initially parabolic but become linear as oxidation continues. This "breakaway oxidation" occurs at shorter times as the oxidation temperature is increased.

Analysis of the oxide scale on the 22-26 alloy before breakaway reveals a scale made up exclusively of titanium oxides. Figure 3 is a cross-section TEM micrograph of the scale formed after 96 hours of oxidation at 800°C in air. The scale is approximately 1.75 μm thick. A selected area ring pattern taken across the thickness of the scale, along with convergent beam microdiffraction analysis of single grains, indicates that the oxide is rutile TiO_2. XEDS analysis reveals that the composition of the scale is nearly identical to that of the alloy. Therefore, scale growth must be predominantly inward with little diffusion in the substrate and incorporation of the Al and Nb into the rutile. Figure 4 is a cross-section of 22-26 after 180 h oxidation in air at 800°C. The external scale was shown by XRD to consist of TiO_2 and $AlNbO_4$ at this stage i.e. after breakaway. At shorter times and lower temperatures the Nb and Al were in solution in the TiO_2. Therefore, the breakaway phenomenon is associated with the formation of discrete Nb-oxides which tend to crack and lead to the linear kinetics.

Figure 4 also indicates that the alloy below the oxide is affected by the oxidation process. Zones enriched in oxygen termed "Interstitial Affected Zones" (IAZ) are clearly evident. In zone 1 the alloy microstructure is refined and contains a new phase which is dark in compositional backscattering imaging. Zone 2 is similar in microstructure but does not contain the dark phase. Zone 3 has the same microstructure as the starting material. Microhardness profiles indicated that the IAZ was hardened substantially by the changes in composition and microstructure.

Mechanical Behavior

The effects of the IAZ on mechanical properties were evaluated using both 3-point bend and uniaxial tension tests. A baseline pre-exposure for the bend tests was chosen as 8 h at 650°C. This pre-exposure resulted in a very thin scale and IAZ totalling approximately 400 nm, as observed by SEM and XTEM. Bend testing was carried out at temperatures ranging from 25 to 750°C in air. In addition, some bend tests were carried out using pre-exposed specimens with a 100 μm surface layer removed ("reground specimens"). The resulting data are plotted as percent plastic elongation versus test temperature in Figure 5. There is notable embrittlement for the specimens tested in bending at 25°C. Increasing the test temperature to 200°C results in the restoration of a large portion of ductility. In addition there was a concomitant decrease in yield strength with increasing test temperature. Increasing the test temperature resulted in incremental gains in ductility which plateaued at higher temperatures. For test temperatures of

600°C and above, the results are similar to testing of unexposed material. In addition, testing at 750°C resulted in significant creep in the β-phase. The "reground specimen" showed complete restoration of ductility when tested at room temperature.

Additional bend testing was done at room temperature using "mild" pre-exposures, Figure 6. Little change was noted for a 72 h, 300°C pre-exposure but , both 8 and 72 h pre-exposures at 400°C and 55 minutes at 650°C resulted in significant losses. Similar results were obtained in the tensile tests. In all cases for room temperature testing, the fracture features were very large and the crack path appeared to correspond to the prior β grain boundaries, Figure 7. The tensile faces of the pre-exposed bend bars and the gage faces of the tensile bars cracked in a periodic fashion upon application of a load, Figure 8. It is apparent that negligible plastic deformation occurred in the surface layer and that exposures which do not produce a significant thickness of the IAZ still embrittle orthorhombic alloys. Typically the total scale and interstitial affected zone thickness for "mild" exposures is in the range of 5 μm or less. The embrittled surface layer relieves tensile stresses by cracking in a periodic manner, rather than deforming plastically. When tested at room temperature, these cracks cannot be blunted by the matrix and produce early failure. The loss of ductility can be mitigated by increasing the test temperature. Therefore, the intrinsic toughness of the unaffected alloy plays a major role in minimizing effects of thin, brittle surface layers.

Gamma Alloys

The gamma alloys studied were Ti-50Al, which consisted of essentially 100% equiaxed $L1_0$ (γ) grains and 47-2-2 which is a duplex alloy consisting of equiaxed γ grains and lamellar $\gamma+\alpha_2$ grains.

Oxidation Behavior

The "surface finish effect" for oxidation temperatures below 1000°C is illustrated in the mass gain vs. time plot in Figure 9 for Ti-50at%Al oxidized at 900°C. The ground (600 grit) surface results in very slow kinetics in O_2 as the result of continuous alumina formation. The polished (1μm diamond) results in greatly accelerated kinetics as the result of the formation of a continuous layer of a mixed oxide. Part of the beneficial effect of grinding may be in homogenizing the surface, as proposed originally by Choudhury et al[7]. However, an additional important effect is the recrystallization of the ground surface as illustrated in the transmission electron micrographs in Figure 10. The deformed layer, produced by grinding, recrystallizes during the initial oxidation exposure to produce γ grains with a grain size on the order of 1 μm from a starting γ grain size on the order of 100 μm. No recrystallized layer forms on the polished surface.

The "nitrogen effect" is also illustrated the mass gain vs. time plot in Figure 9. The kinetics in air are essentially independent of surface preparation and are much faster than those for a ground surface exposed in pure O_2. The scales formed in air surfaces are intermixed TiO_2 + Al_2O_3. The proposal that the "nitrogen effect" involved formation of nitrides which prevented the alumina from becoming continuous has been verified by elemental spectroscopic imaging (ESI) in a transmission electron microscope [10]. An ESI map for the elements Ti, Al, O, and

N from a cross-section of the scale/alloy interface of Ti-50at%Al oxidized in air for one hour at 900°C is presented in Figure 11. These maps indicate that the alumina is broken up by islands of TiN.

The effect of nitrogen on the oxidation of 46-2-2 and 47-2-2 is similar. The effect of decreasing temperature has been documented. At 700°C the interface consists of the previously described mixed titanium nitride/ aluminum oxide layer. Decreasing the exposure temperature to 650°C results in the formation of an inhomogeneous oxidation morphology. A specimen exposed at 650°C for 168 h in air forms an oxide scale which is thin (70 nm) and uniform, consisting of a mixture of titanium and aluminum oxides. At regions corresponding to α_2 laths in the starting material the scale thickens into an oxide nodule. The nodules are between 300 and 500 nm thick and grow down the α_2 laths (Figure 12). XEDS analysis in the AEM indicates a lack of nitrogen segregation at the scale/TiAl interfaces but nitrogen is present at the scale/α_2 interfaces. A corresponding specimen oxidized at 600°C did not exhibit oxide nodules or nitrogen segregation at the scale/alloy interfaces. These results indicate that the oxidation mechanism of γ-TiAl is changing in the temperature range 600-700°C.

Mechanical Behavior

Figure 13 shows the bend ductility of 46-2-2 and 47-2-2 as a function of pre-exposure. There is some scatter in the data but the general trend is for decreased ductility as the pre-exposure temperature is increased. This loss of ductility is associated with interstitial penetration which, at high temperature, results in a well-defined transformation layer (Figure 10) but , even a low temperature exposure results in significant hardening of the alloys, Figure 14. For short times or low temperatures the hardening is primarily in the lamellar grains, indicating oxygen dissolution is primarily in the α_2. As the severity of the exposure is increased the single-phase γ grains also harden and the embrittlement becomes more severe.

CONCLUDING REMARKS

Orthorhombic Alloys

i) Oxidation is parabolic at temperatures of 700°C and lower. Oxide scale formation is almost exclusively by inward growth. The scale composition is similar to the bulk alloy composition.

ii) Oxidation is initially parabolic at 800°C but breakaway oxidation occurs after approximately 100 h. This is the result of the formation of discrete Nb-oxides which lead to scale cracking.

iii) Oxidation results in the formation of a significant IAZ. The IAZ takes the form of an extremely refined substrate microstructure containing an oxygen-rich phase.

iv) Mechanical behavior is degraded after exposure to an oxidizing environment, even for "mild" exposures.

The bend test is very sensitive to this effect.
Increasing the test temperature to 200°C or higher restores ductility.
Removal of the affected surface layer restores ductility.

Periodic cracking of tensile faces results from the embrittled layer.

These results all indicate the extreme sensitivity of orthorhombic alloys to surface condition.

Gamma Alloys

i) Thermodynamically, an alumina scale should be stable in contact with γ-TiAl. However, oxidation exposures typically result in the formation of a mixed scale, indicating kinetic factors play a major role.

> Surface Finish: Near surface deformation promotes the formation of an alumina scale in oxygen. The result of the deformation is the development of a layer of recrystallized γ-TiAl grains which are orders of magnitude smaller than the substrate grains. Increased grain boundary area may improve the ability of Al to diffuse to the alloy/oxide interface by short circuit diffusion. Also, compositional fluctuations, i.e. regions lean in Al, may be removed. The surface finish effect is not observed in air because of the nitrogen effect.
>
> The Nitrogen Effect: The reaction of Ti with N at elevated temperatures forms Ti-nitrides at the scale/alloy interface which prevents the alumina from developing continuity and leads to the formation of a mixed oxide scale. The nitrogen effect does not occur at low oxidation temperatures (600°C).

ii) Gamma TiAl alloys are embrittled by elevated temperature exposures. The effect has been documented for exposures in the range 650-800°C. Microhardness analysis indicates that, for a duplex alloy, the lamellar grains in hardness initially. More severely embrittled specimens also exhibit hardening of the gamma constituent. This indicates that oxygen is initially segregated to the α_2 laths, which have a high solubility for oxygen. At some point the α_2 becomes saturated and the oxygen content of the gamma increases. The gamma phase essentially controls the plasticity so the oxygen dissolution results in more severe embrittlement.

REFERENCES

1. *A. Rahmel, P. J. Spencer*: Oxidation of Metals, 35, (1991), 53.
2. *K. L. Luthra*: Oxidation of Metals, 36, (1991), 475.
3. *R. Cerchiara, J. Rakowski, F. S. Pettit, and G. H. Meier*: Unpublished Research, University of Pittsburgh, 1993.
4. *J. Rakowski, G. H. Meier, R. A. Perkins*: The Oxidation and Embrittlement of α_2 (Ti_3Al) Titanium Aluminides, in Microscopy of Oxidation 2, Inst. of Materials, 1993, p.476.

5. *M. Khobaib and F. W. Vahldiek*: "High Temperature Oxidation Behavior of Ti_3Al Alloys", Second International SAMPE Metals Conference, F. H. Froes and R. A. Cull eds., Covina, Ca, 1988, pp.262-270.
6. *C. H. Koo, J. W. Evans, K. Y. Song, T. H. Yu*: Oxid. Metals, 42, (1994), 529.
7. *N. S. Choudhury, H. C. Graham, J. W. Hinze*: "Oxidation Behavior of Titanium Aluminides", in Properties of High Temperature Alloys, Z. A. Foroulis and F. S. Pettit eds., The Electrochem Soc., 1976, p. 668.
8. *J. M. Rakowski, G. H. Meier, F. S. Pettit, F. Dettenwanger, E. Schumann, M. Rühle*: "The Effect of Surface Preparation on the Oxidation Behavior of Gamma TiAl Base Intermetallic Alloys", Scripta Mater., 35, (1996) 1417.
9. *C. S. Giggins, F. S. Pettit*:Trans. Met. Soc. AIME, 245, (1969), 2509.
10. *J. M. Rakowski, F. S. Pettit, G. H. Meier, F. Dettenwanger, E. Schumann, M. Rühle*: Scripta Met. et Mater., 33, (1995), 997.
11. *W. E. Dowling Jr., W. T. Donlon*: Scripta Met. et Mater., 27, (1992) 1663.
12. *R. Field, J. Schaeffer, C. Austin, T. Kelly*: unpublished, GE Aircraft Engines, 1993.
13. *Y. Cheng, F. Dettenwanger, J. Mayer, E. Schumann, M. Rühle*: Scripta Met. et Mater., 34, (1996), 707.
14. *F. Dettenwanger, E. Schumann, J. Rakowski, G. H. Meier,d M. Rühle*: 48, (1997) 23.
15. *S. J. Balsone*: "The Effect of Elevated Temperature Exposure on the Tensile and Creep Properties of Ti-24Al-11Nb" In Oxidation of High Temperature Intermetallics, T. Grobstein and J Doychak eds., TMS, 1989, p. 219.
16. *C. H. Ward, J. C. Williams, A. W. Thompson*: Scripta Met., 28, (1993), 1017.
17. *C. H. Ward*: Internat. Mater. Rev., 38, (1993), 79.
18. *Y. Saitoh and K. Mino*: Mater. Trans. JIM, 34, (1993), 393.
19. *P.R. Smith, J. A. Graves, C. G. Rhodes*: "Preliminary Mechanical Property Assessment of a SiC/Orthorhombic Titanium Aluminide Composite" in Structural Intermetallics, R. Darolia, J. J. Lewandowski, C. T. Liu, P. L. Martin, D. B. Miracle, M. V. Nathal eds., p. 765, TMS (1993).
20. *F-C Dary, T. M. Pollock*: "Effects of High-Temperature Air or Vacuum Exposures on the Room Temperature Tensile Behavior of the (O+B2) Titanium Aluminide", submitted to Mater. Sci. and Eng.
21. *L. Singheiser*: ASEA Brown-Boveri Research Laboratory, Private Communication, 1992.
22. *C. M. Austin, T. J. Kelly*: "Development and Implementation Status of Cast Gamma Titanium Aluminide" in Structural Intermetallics, R. Darolia, J. J. Lewandowski, C. T. Liu, P. L. Martin, D. B. Miracle, M. V. Nathal eds., p. 143, TMS (1993).
23. *T. Takasugi, S. Hanada, M. Yoshida*: J. Mater. Res., 7, (1992) 2739.

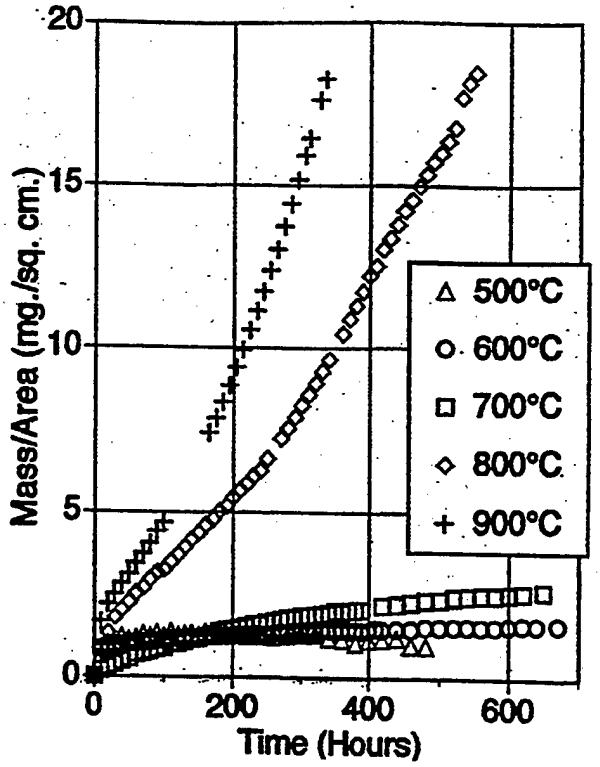

Figure 1. Weight change versus time measurements for oxidation of neat panels of Ti-22Al-23Nb at several different temperatures.

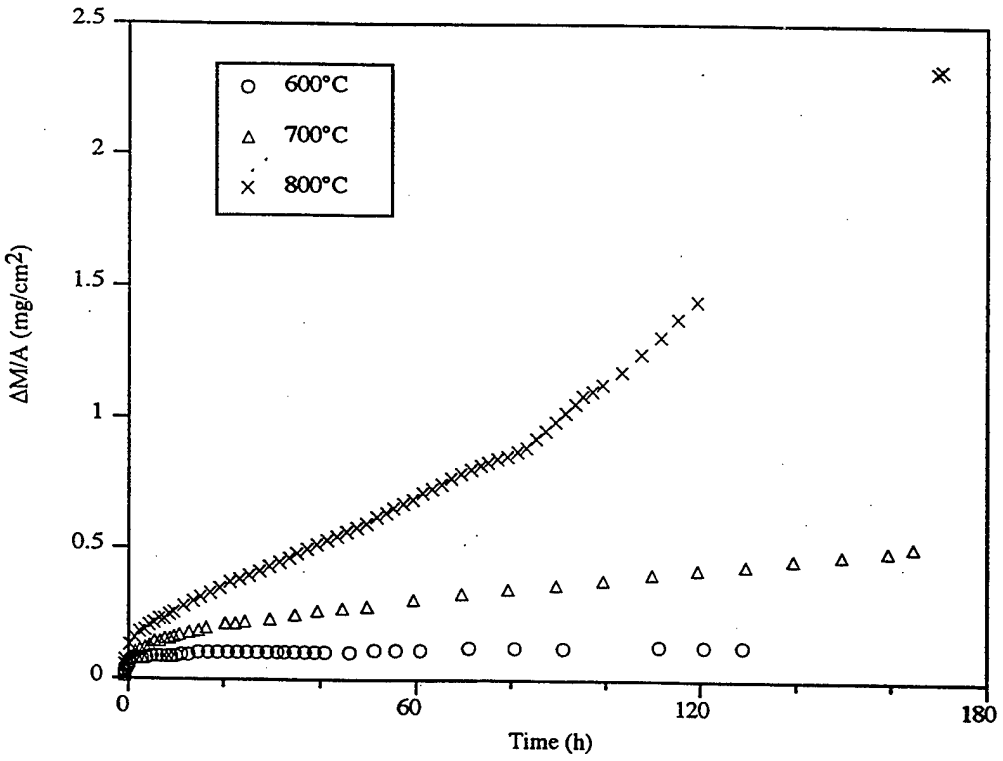

Figure 2. Weight change versus time measurements for oxidation of Ti-22Al-26Nb at several different temperatures.

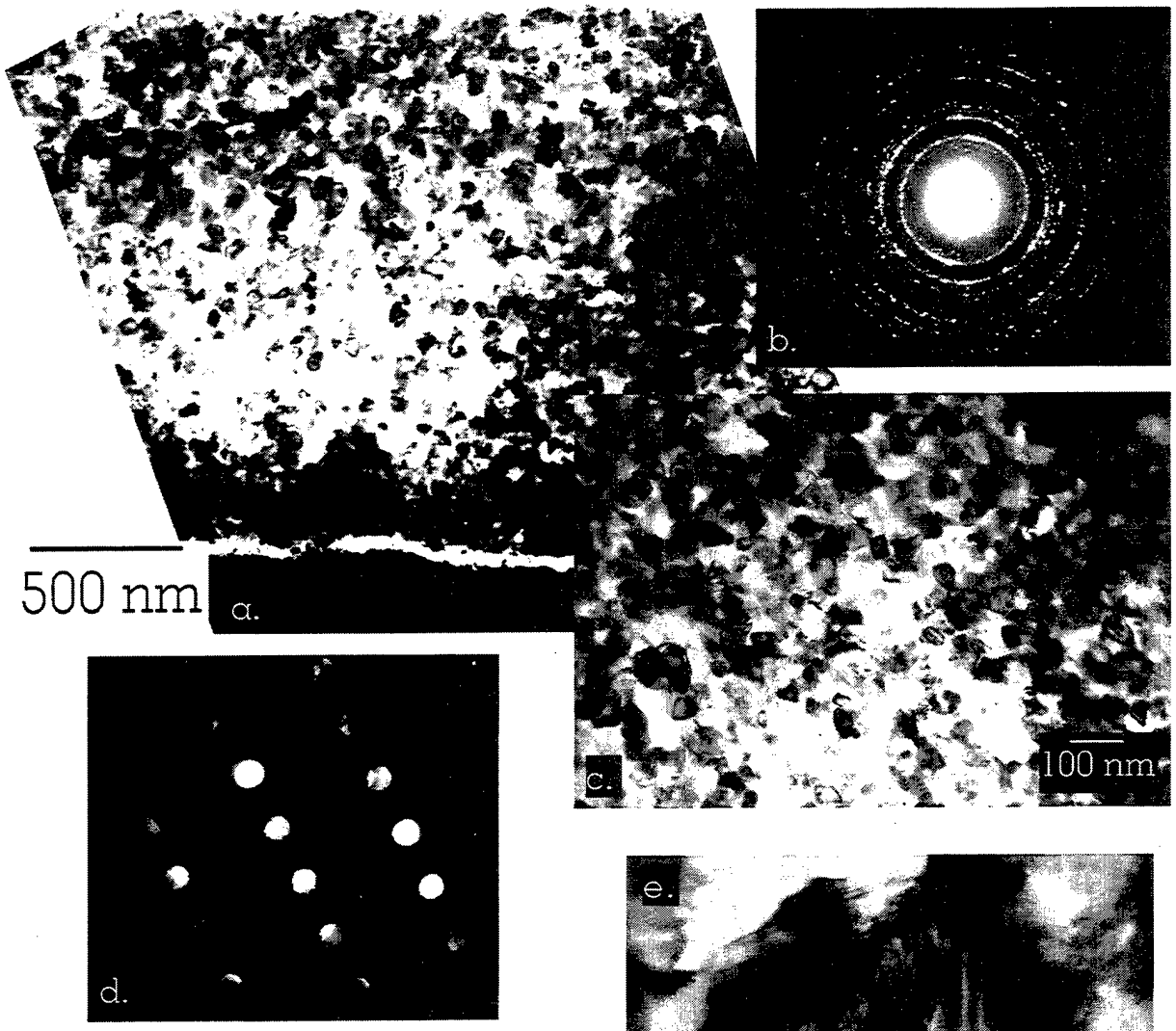

Figure 3. Cross–section TEM analysis of 22–26 exposed in air at 800°C for 96 hours.
a) Scale and alloy.
b) Rutile TiO_2 ring pattern (SAD).
c) Scale high magnification.
d) [010] ZA rutile TiO_2 spot pattern (MBDIFF).
e) Subscale interstitial penetration zone.

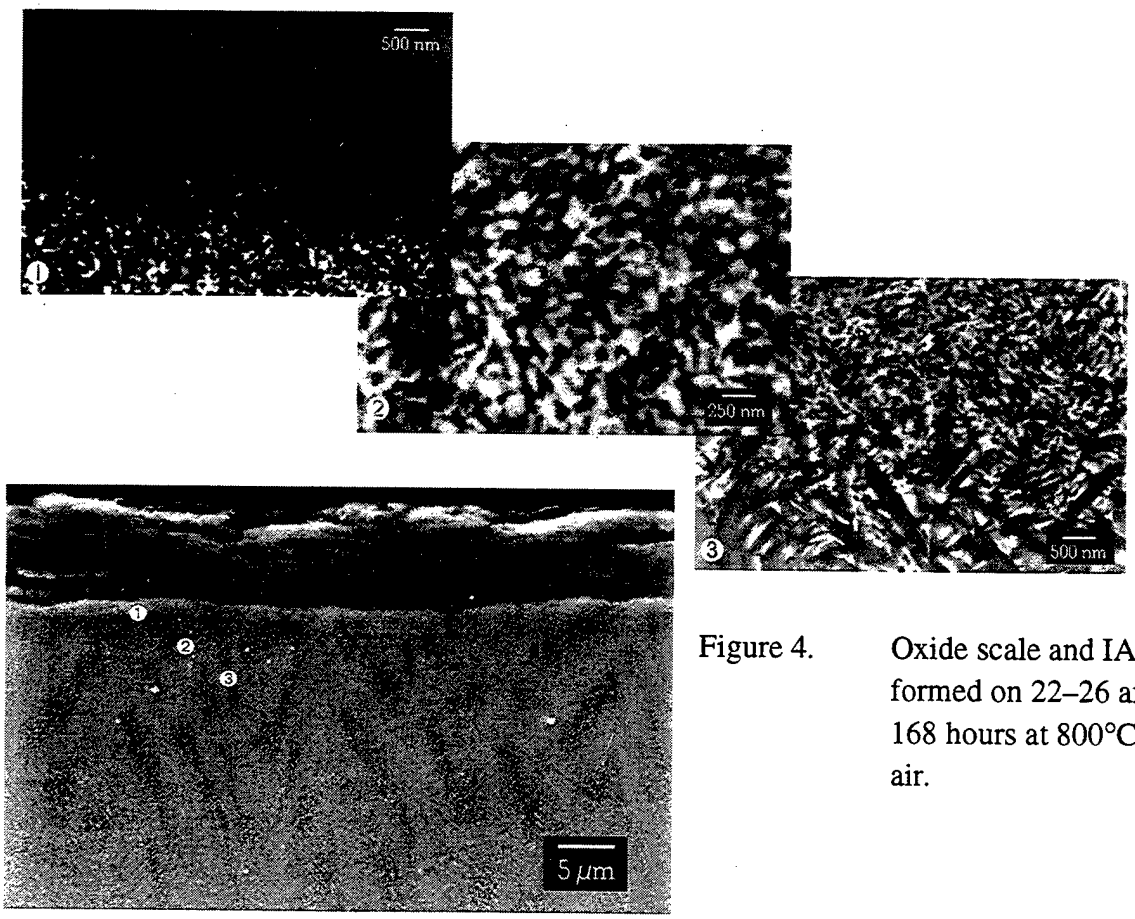

Figure 4. Oxide scale and IAZ formed on 22–26 after 168 hours at 800°C in air.

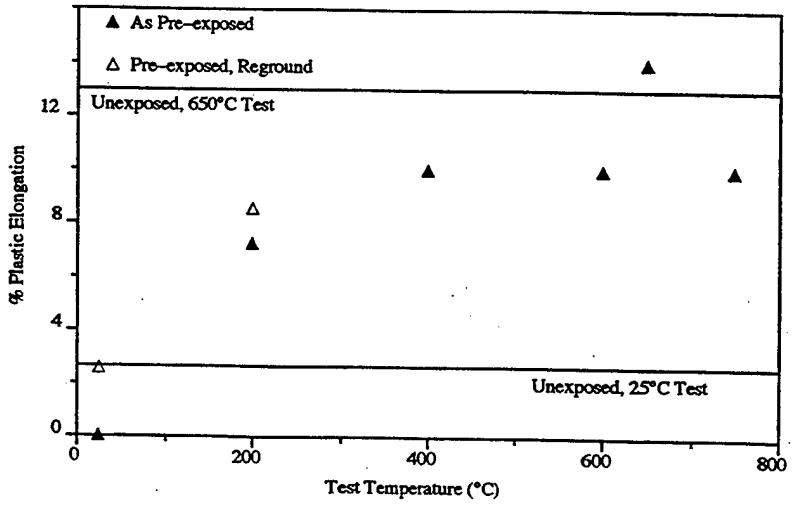

Figure 5 Ductility in bending for 22-26 specimens pre-exposed for 8 h at 650°C in air, then tested at various temperatures.

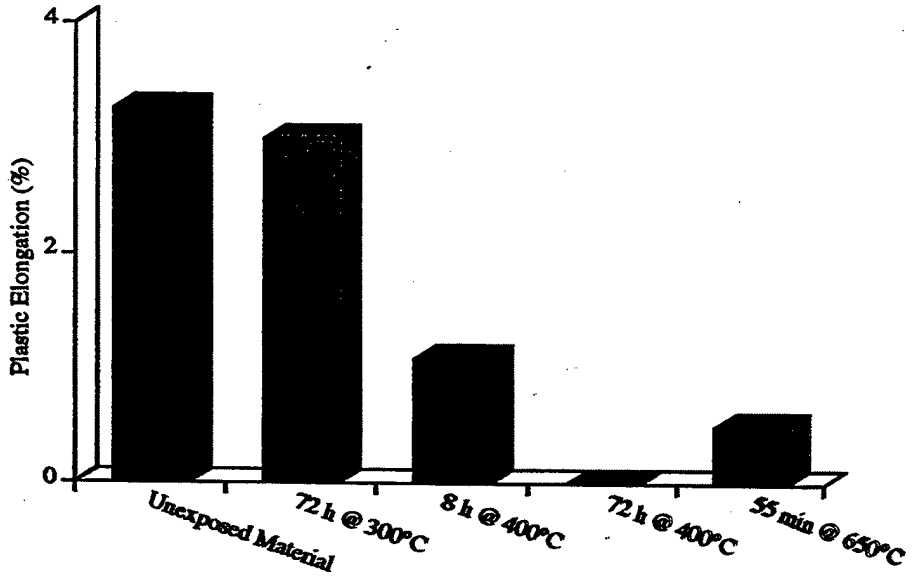

Figure 6. Ductility in bending for 22-26 specimens with "mild" pre-exposures tested at room temperature.

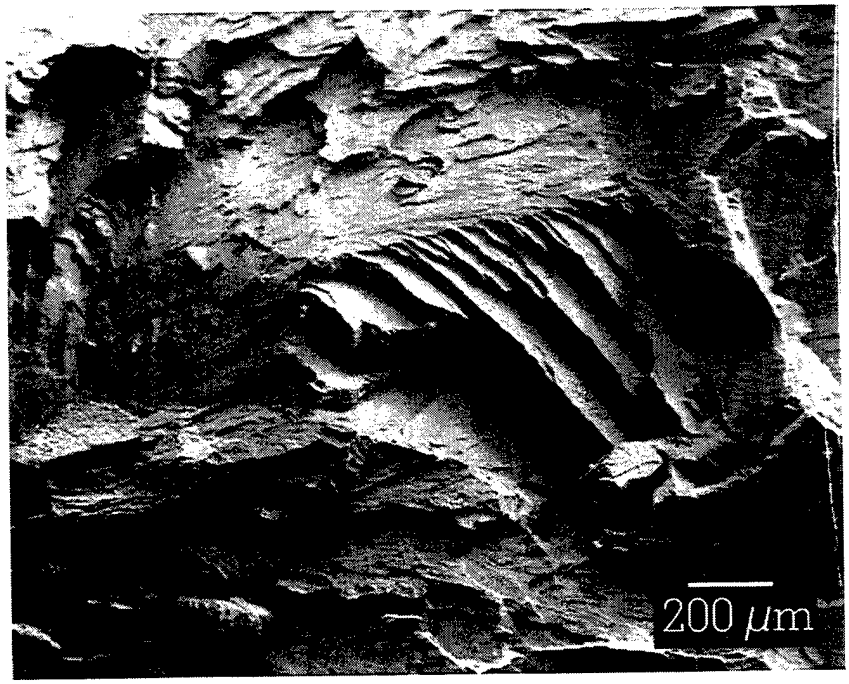

Figure 7. Fracture surface of 22–26 after pre–exposure for 8 hours at 650°C and testing at 25°C.

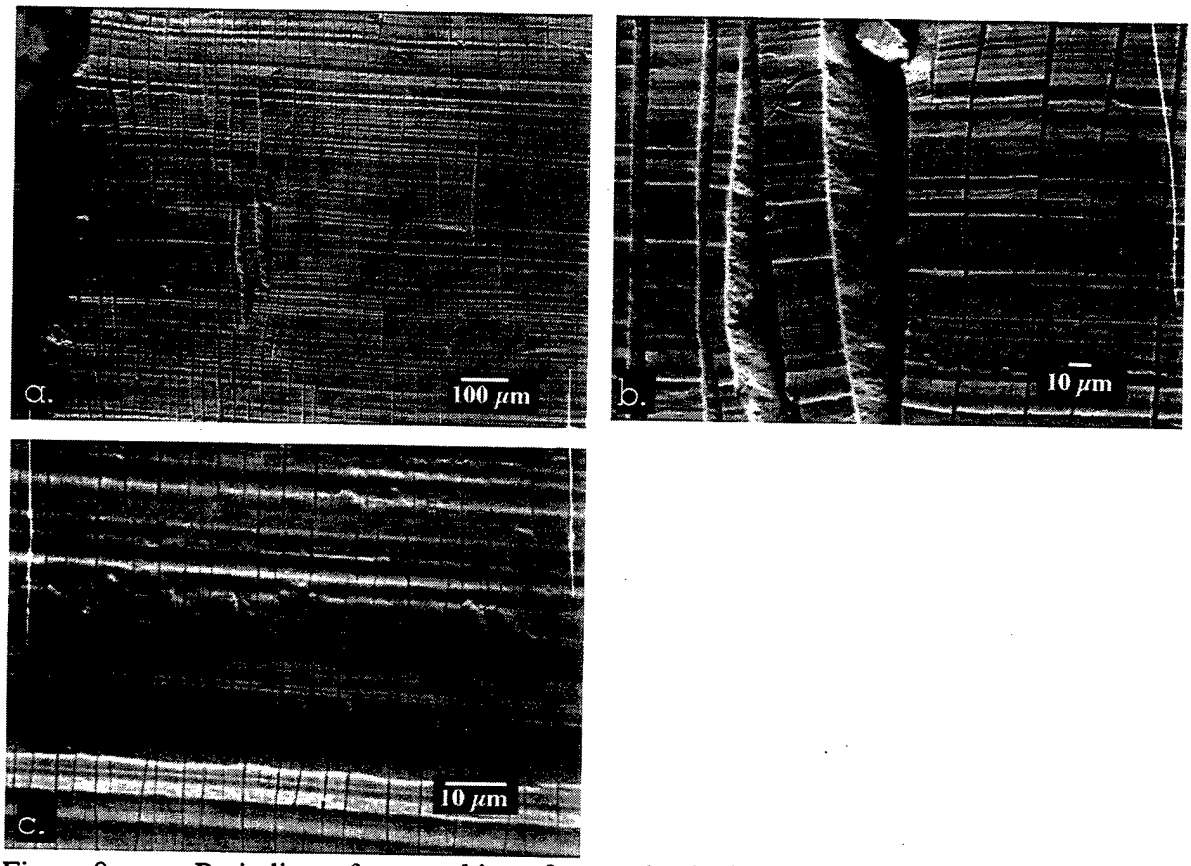

Figure 8. Periodic surface cracking after mechanical testing. a),b) Tensile specimen, 8 h, 650°C pre–exposure, 200°C test temperature. c) Bend specimen, 72h, 350°C pre–exposure, 25°C test temperature.

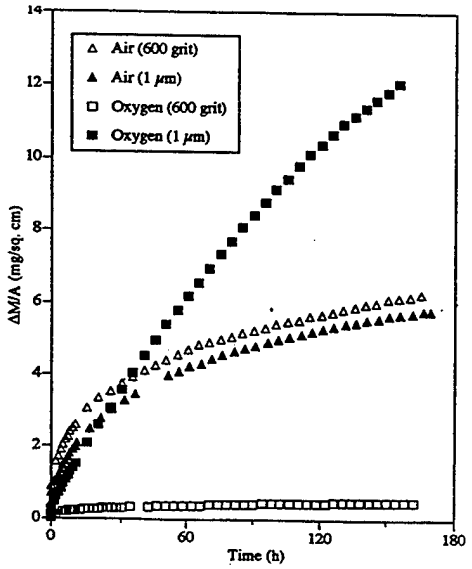

Figure 9. Effect of surface finish on the oxidation of γ-TiAl.

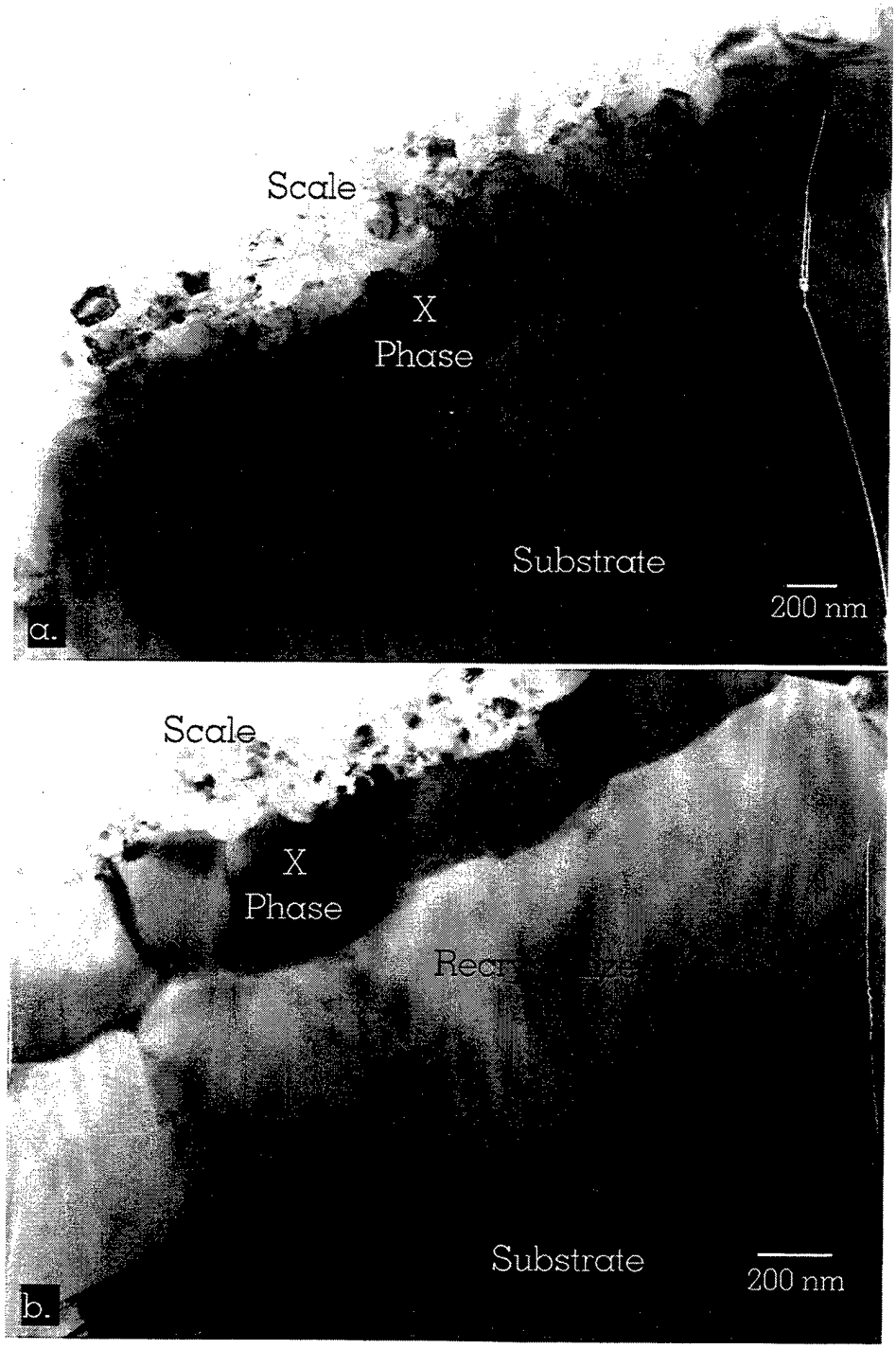

Figure 10. Cross–section TEM micrographs of Ti–50Al, exposed to oxygen for 1 hour at 900°C. a) 1 micron surface finish. b) 600 grit surface finish.

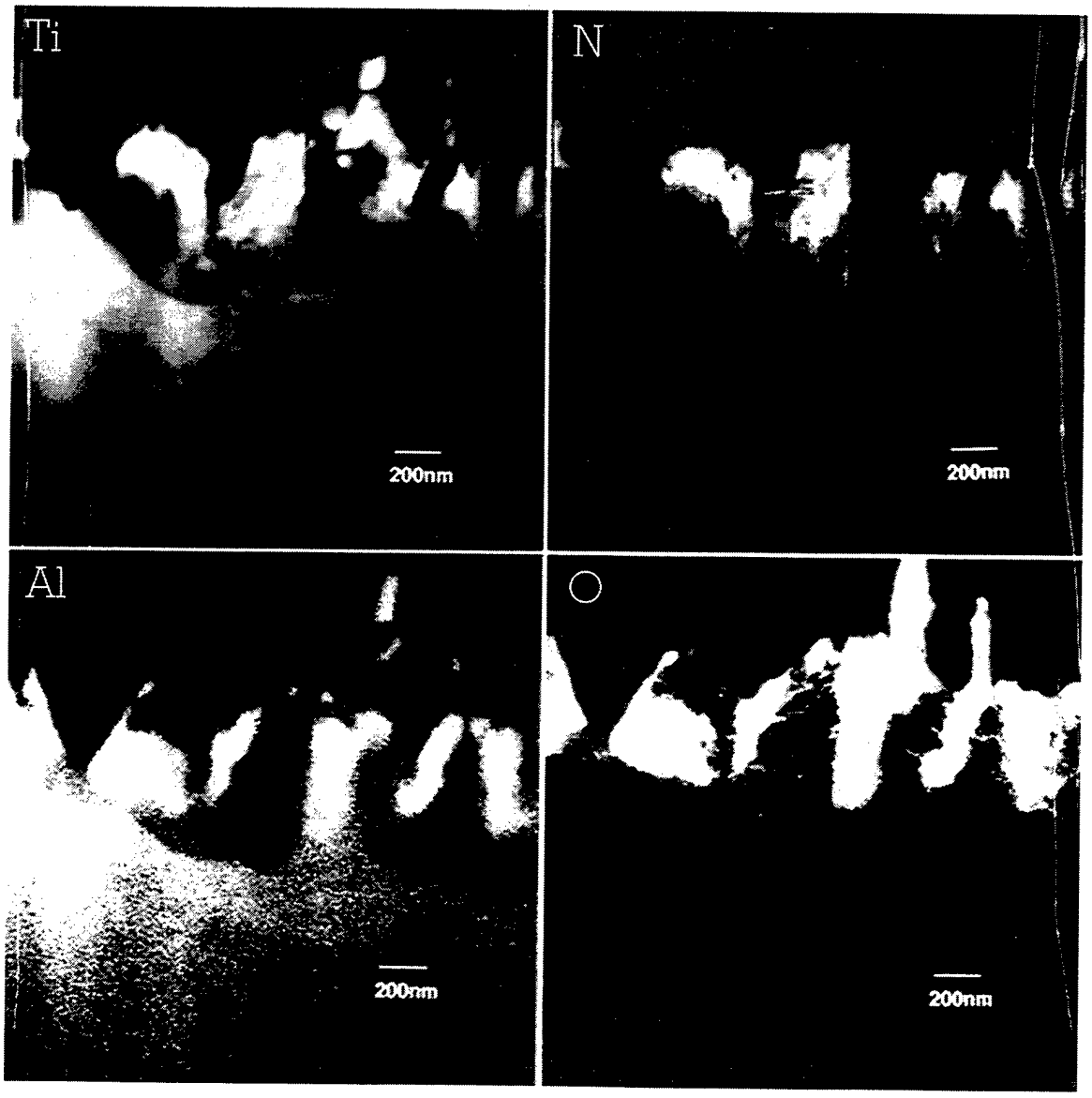

Figure 11. Cross–section TEM elemental maps, Ti–50Al, 1 hour oxidation in air at 900°C.

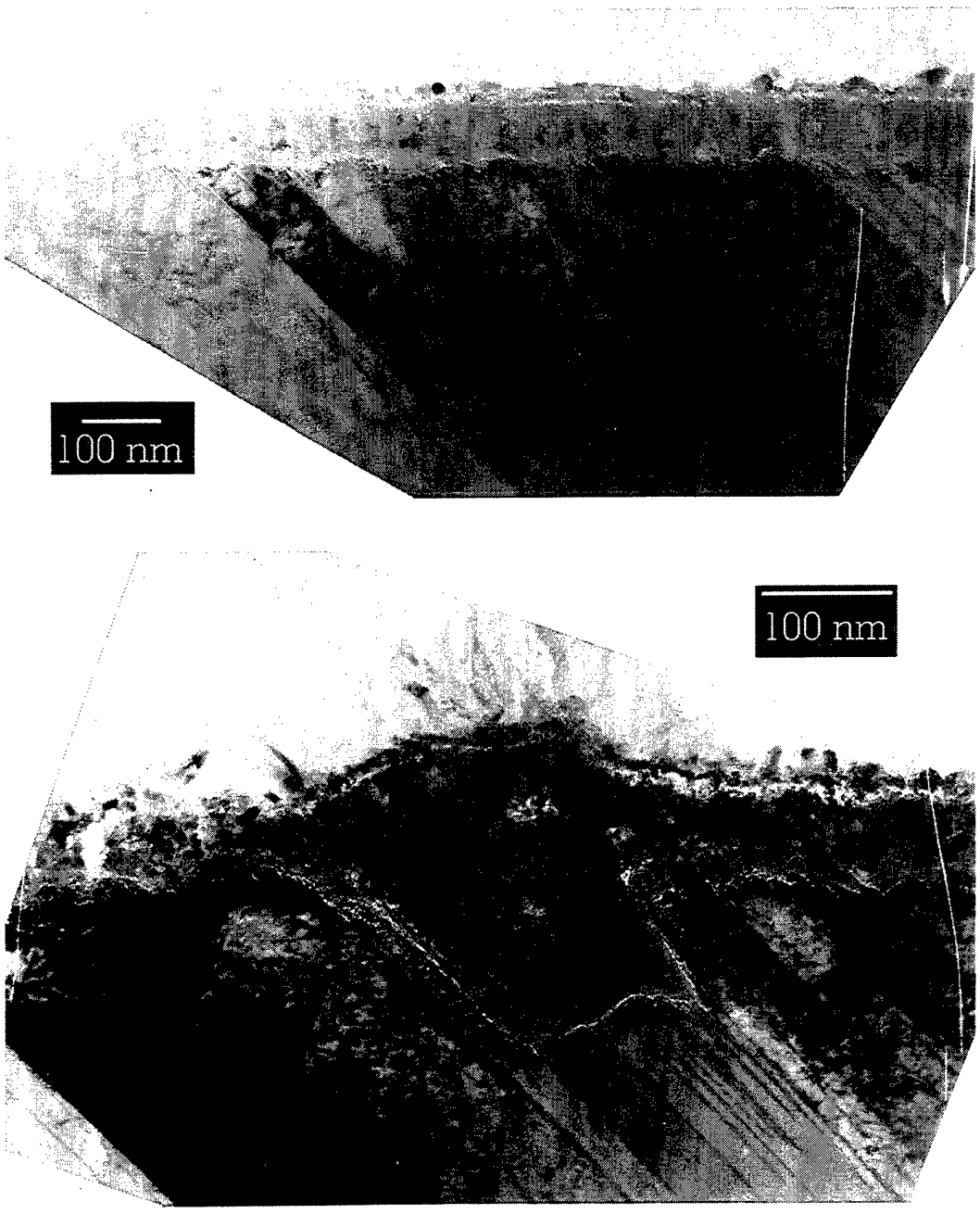

Figure 12. Cross–section TEM micrographs of the oxide scale formed on 47–2–2 exposed in air at 650°C for 168 hours.

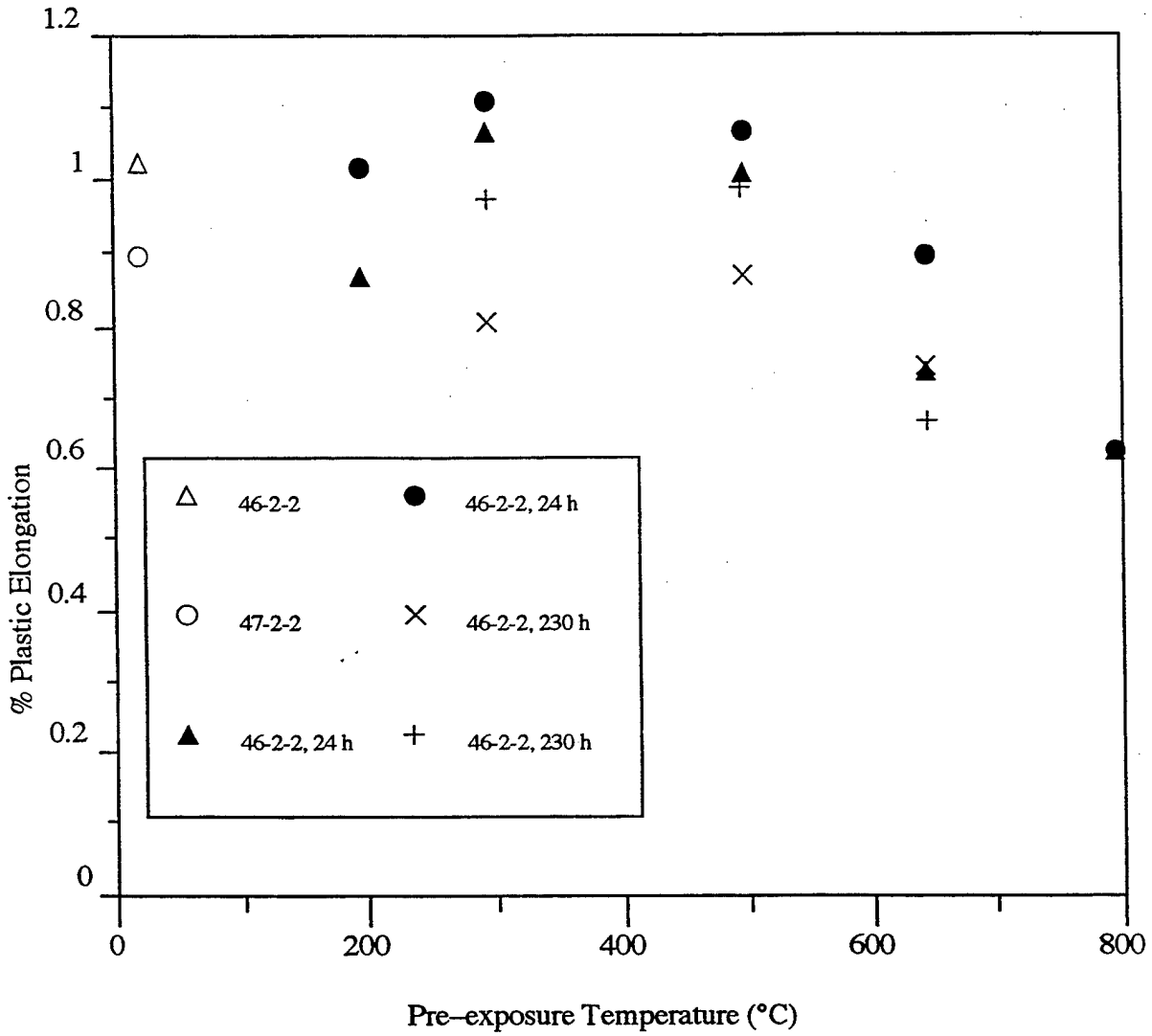

Figure 13. Plastic elongation for gamma tensile specimens as a function of pre-exposure temperature.

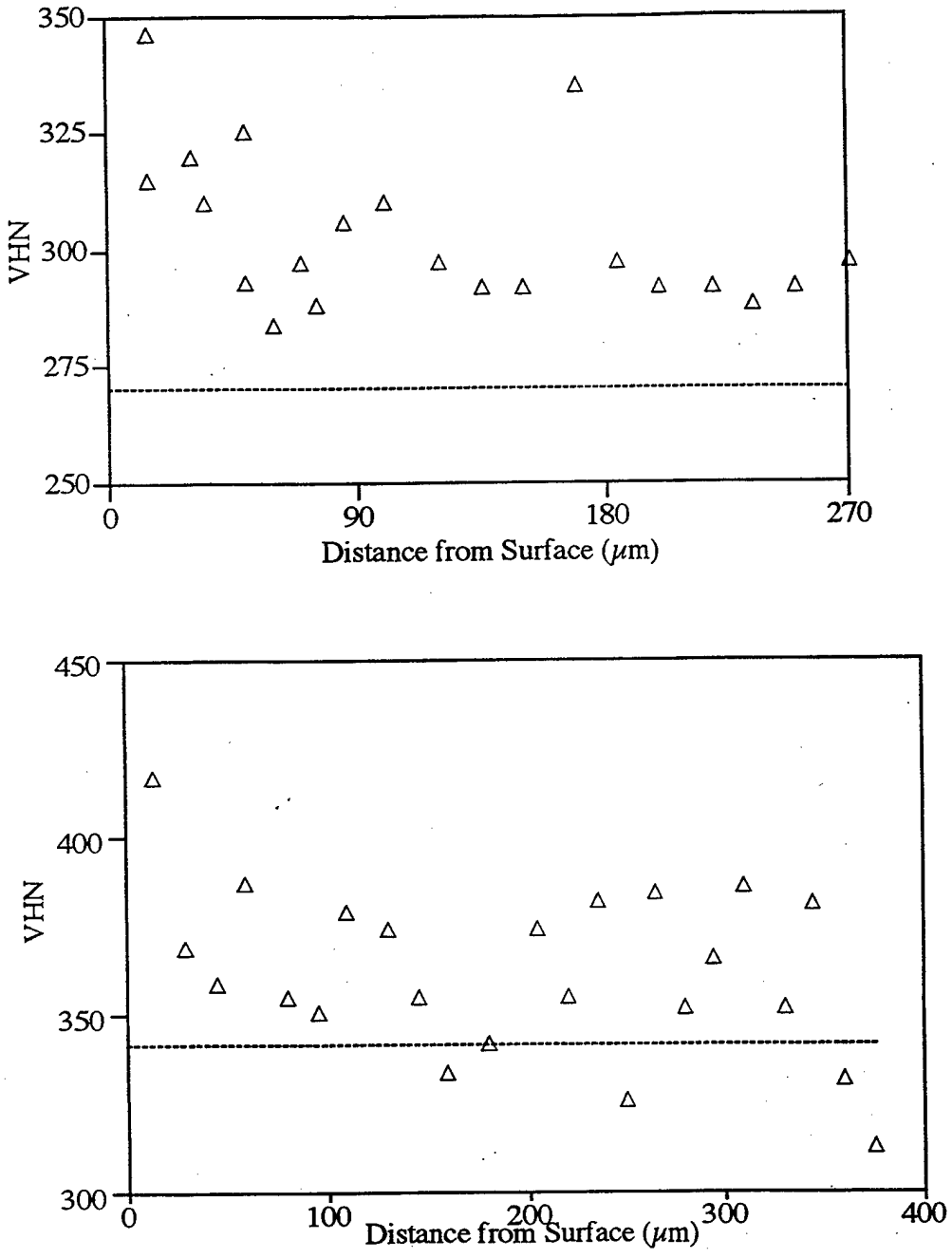

Figure 14 Microhardness analysis from transverse sections of fractured gamma TiAl tensile specimens pre-exposed for 8 h at 800°C. (a) Gamma grain. (b) Lamellar grain.

Development Of A Nano-Particle Composite Material With Corrosion Resistant EMI Shielding Properties

David S. Dixon
Naval Undersea Warfare Center
Newport, RI 02841
and
Dr. James Masi
Western New England College
Springfield, MA 01119

Abstract:. Both military and commercial organizations have concerns about obtaining electromagnetic shielding performance using materials that do not corrode in today's increasingly hostile shipboard and commercial environments. This paper discusses the evaluation of a method of achieving improved electromagnetic interference (EMI) shielding performance by impedance mismatching between various layers of materials. Three different concentrations of ferrites and layered composites were synthesized and tested In addition, several unique (Patent Pending) layers of various nano-particle materials combined in a composite matrix were also evaluated.. Theoretical and experimental values were obtained and compared. The measured values differed somewhat from the theoretical expected values. Analyses and testing results are discussed in the light of the newer materials.

INTRODUCTION

Military Environment: Over the years, electronics components and systems in Navy ships and aircraft have been required to be increasingly resistant to the electromagnetic interference (EMI) as well as the corrosive effects associated with combat and sea water environments. Stringent requirements were established for EMI resistance through the Mil Spec system, ensuring that equipment installed in ships and aircraft were sufficiently "hardened." More recently, however, acquisition reform (AR) initiatives have led to the introduction of commercial-off-the-shelf (COTS) systems and components as well as non-developmental items (NDI) into military platforms, due to their associated cost savings. Many COTS materials have difficulty meeting the military requirements, because they were not initially designed for the military environment. Similarly, many of these items were not designed to cope with the inherently corrosive operating environments encountered in Navy ships and aircraft. Therefore, to render COTS and NDI components acceptable for naval and military use, they must be adapted to meet the rigors of their intended operating environment.

CommercialEnvironment: Similarly the commercial environment has become increasingly hostile due to both the airborne environment as well as the increased usage of the electromagnetic spectrum. For example low frequency powerline fields often require attenuation due to either EMI or heath concerns. These low frequency fields have typically required the use of thick and high permeability materials in order to provide

reasonable levels of shielding performance. These new materials and fabrications may provide the same degree of shielding performance using lighter, corrosion resistant materials which will permit that performance to be maintained over long periods of time.

Today, various companies, such as Amuneal Corp. are able to provide material to shield against AC and DC magnetic interference, both at the source and the location of the sensitive component. This material however is often heavy, expensive and prone to change from heat, shock, and other environmental hazards. Magnetic shielding is bi-directional in that it can shield magnetic flux at the location of the source as effectively as it can shield fields away from a specific sensitive component. [1]

OBJECTIVES

The objective of this research was to develop, fabricate, and test shielding material created using organic (plastic) material with ferrites and also other nano-particle mixtures of conductive, non-conductive, magnetic and non-magnetic materials to operate in these hostile environments. To quickly and efficiently evaluate the performance of these materials at low frequencies, a simple test apparatus was constructed using two solenoid coils for input and output.

BACKGROUNDTHEORY

Shielding

An electromagnetic wave is rapidly attenuated in a conducting medium. In fact, in a good conductor the attenuation is so rapid that at high radio frequencies the wave penetrates the conductor only at a small depth. This depth of the penetration in both conductors or any medium, for that matter, is of considerable interest. To calculate it, let us first develop a wave equation in E_y for a plane wave in a conducting medium. From a solution of this equation, an expression of the depth of penetration is then obtained. [2] From Maxwell's equations we have for linearly polarized wave traveling in the x direction with **E** in the y direction. Assuming harmonic variation of E_y with respect to t, we may write

$$E_y=E_0e^{j\omega t}.$$

Taking the first and second derivatives with respect to t and substituting these values gives

$$\frac{\partial^2 E_y}{\partial x}-\left(j\omega\mu\sigma-\omega^2\mu\varepsilon\right)=0$$

Let $\quad \overline{\gamma}=\sqrt{j\omega\mu\left(\sigma+j\omega\varepsilon\right)}$

Then the above reduces to

$$\frac{\partial^2 E_y}{\partial x}=\gamma^2 E_y$$

This equation is a simplified form). The time t does not appear explicitly, harmonic variation with time being assumed. γ is called the complex ***propagation constant.*** [2]. A solution for a traveling wave in the positive x direction is then

$$E_y=E_0e^{-\gamma x}.$$

Thus, γ has a real and an imaginary part. Putting $\gamma=\alpha+j\beta$, we see that α, the real part, is associated with attenuation and β, the imaginary part, is associated with phase.

Continuing the discussion of the preceding section, let us now obtain a quantitative measure of the penetration of a wave in a conducting medium. Consider the wave that penetrates the conducting medium, i.e., the transmitted wave. Let $x = 0$ at the boundary of the conducting medium, so that x increases positively into the conducting medium. [2] Let the above be written in the form

$$E_y=E_oe^{-x/\delta}e^{-j(x/\delta)}$$

where $\delta = \sqrt{2/\omega\mu\sigma}$. At $x = 0$, $E_y = E_0$. This is the amplitude of the field at the surface on the conducting medium. Now δ has the dimension of distance. At a distance $x=\delta$ the amplitude of the field is

$$\left|E_y\right| = E_0 e^{-1} = E_0 \frac{1}{e}$$

Thus, E_y, decreases to $1/e$(36.8 percent) of its initial value, while the wave penetrates to a distance δ. Hence δ is called ***the 1/e depth of penetration.***

Note: depth of penetration of a plane electromagnetic wave incident normally on a good conductor like copper [2] is as follows.
The penetration decreases in inverse proportion to the square root of the frequency (resulting in fields near to the skin of the conductor [3]) or often called ***skin effect***. It also explains the shielding by conductors. Thus a high frequency field is damped out as it penetrates a conductor in a shorter distance than a low frequency field. [2]

Phase velocity is given by the ratio ω/β. In the present case of the good conductor, a=b = 1/δ so that the phase velocity in the conductor is

$$v_c = \omega\delta = \sqrt{\frac{2\omega}{\sigma\mu}}$$

Since the $1/e$ depth is small, the phase velocity in conductors is small. It is apparent that the velocity is a function of the frequency and hence of the wavelength. In this case, $dv/d\lambda$ is negative, where λ is the free space wavelength. Index of Refraction in the conductor is

$$\eta = \frac{c}{v_c} = \frac{c}{\omega\delta} = \sqrt{\frac{\sigma}{2\omega\varepsilon_0}}$$

which is dimensionless.[2]

To find wavelength λ_c, in the conductor, we have from that $\lambda_c f = \omega\delta$, or

$$\lambda_c = 2\pi\delta$$

Both λ_c and δ are in the same units (m) of length. Hence the wavelength of the conductor is 2π times $1/e$ depth. Since the $1/e$ depth is small for conductors, the wavelength in conductors is small. It is interesting to note that the electric field is damped to 1 percent of its initial amplitude in about 0.75λ in a metal. Since the penetration depth is inversely proportional to the square root of the frequency, a thin sheet of conducting material can act as a low-pass filter for electromagneticwaves.[2]

A summary of formulae for the properties of good conductors is given in Table 1. It should be noted that this tabular summary is modified somewhat for dielectrics and poor dielectrics.

Signal Amplifier

The secondary amplifier circuit schematic shown in Figure 1 was constructed. The amplifier circuit is one component of a larger system which was tested for gain vs. frequency. Even though the emphasis was on lower frequency performance the values of gain were plotted from 0-M Hz, as shown in Figure 2.

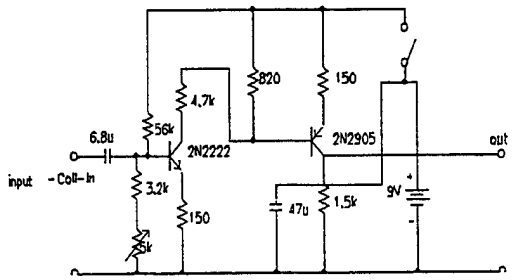

Figure 1: Amplifier Circuit

Table 1

propagation constants

propagation constant $=\overline{\gamma}=\sqrt{j\omega\mu(\sigma+j\omega\varepsilon)}$ (dimensionless)
attenuation factor = $\alpha=\exp\left(-\sqrt{\frac{\omega\mu\sigma}{2}}x\right)$ (dimensionless)
phase factor=$\beta=\exp\left(-j\sqrt{\frac{\omega\mu\sigma}{2}}x\right)$ (dimensionless)
Phase Velocity = $v_c=\omega\delta=\sqrt{\frac{2\omega}{\sigma\mu}}$ (m s^{-1})
Index of Refraction = $\eta=\frac{c}{v_c}=\frac{c}{\omega\delta}=\sqrt{\frac{\sigma}{2\omega\varepsilon_0}}$ (dimensionless)
Wavelength = $\lambda_c=2\pi\delta$ (m)
Relaxation time = $T_r=\frac{\varepsilon}{\sigma}$ (s)
Impedance = $\dot{Z}_c=\sqrt{\frac{\mu\omega}{\sigma}}\angle 45^\circ$ (Ω)
Absorption loss (of the wave(electric/magnetic)) = A = 1.314 $(f\mu_r\sigma_r)^{1/2}d$ (dB)
Reflectance Coefficient = $\Gamma=\frac{Z_1-Z_2}{Z_1+Z_2}$ (dimensionless) Note: reflection losses are effective for magnetic fields at low frequencies.

where $\omega = 2\pi f$ = radian frequency, rad s^{-1}
f = frequency, Hz
μ = permeability $\approx 1.26\mu H\ m^{-1}$ If no magnetic material is present
ε = permittivity, F m^{-1}
σ = conductivity, S m^{-1}

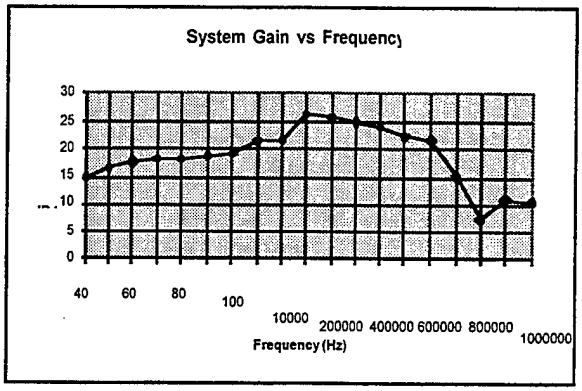

Figure 2
Amplifier Gain

Two 1 mH solenoidal coils were wound on a nylon spool using a copper wire. The number of turns required for the 1mH solenoidal coils were calculated to be 238 turns. The two coils are shown in Figure 3.

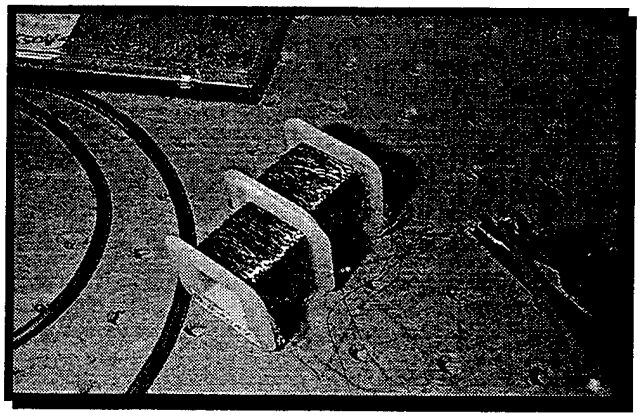

Figure 3
Two 1mH Solenoidal Coils

The primary coil has a crisp waveform going into it at 60 Hz (high output max. amplitude setting) and the secondary coil with the induced EMF caused by a changing magnetic flux (out of phase by 90°) is the noisy signal which will is cleared up by the apparatus. This waveform is shown in Figure 4. The primary coil had a 2.5V peak and the secondary coil had a 16 mV peak (noisy single).

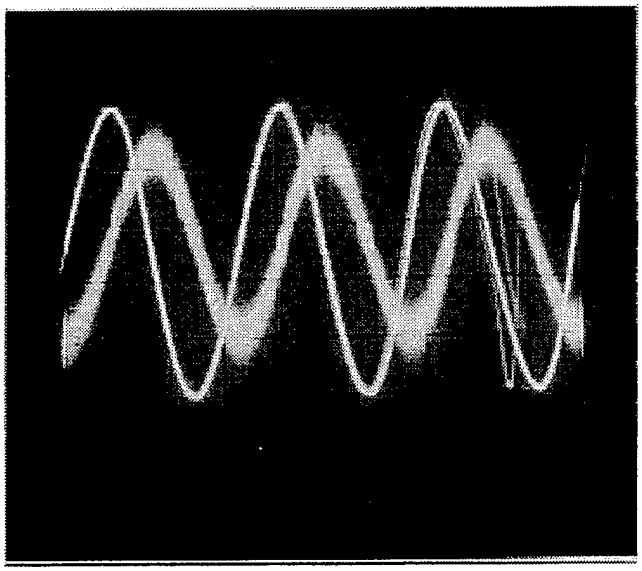

Figure 4
Wave forms: Primary (crisp) , Secondary (noisy)

The magnetic flux density was measured across both pole pieces (laminated Si/Fe) coils, in order to determine the amount of **B** field in the coil, depending where the probe was placed. The **B** field in the coil should be the greatest in the center of the air core coils (same as the **H** field). Depending on where the probe was placed the **B** field varied. (60 Hz pumping into the coil) Running the probe top to bottom, back and forth,--parallel to the coil side. **B** field ranged from ~3.3 -4.8 Gauss and were relatively uniform over a 9 square cm. area on the axis of the coil. The resonant frequency is at 10 kHz, well above the low frequency harmonics of interest, at L = 1mH. The capacitance in the system was determined to be C = 0.253μF.

The Magnetic Materials

There are few materials which capture the essence and the mystery of materials science as those which can be fabricated by gel and sol-gel methods. The unique properties and the control of the chemistry leading to these properties make these methods excellent teaching, research, and learning tools. Certain of these synthetic materials are now deemed potentially useful as magnetic materials for such applications as magnetic devices (transformers, inductors, etc.), high frequency magnetic and electromagnetic devices, shielding materials, and magneto-optic devices. The development of sol-gel methods for the production of nanoscale materials allows the scientist to tailor both properties and physical characteristics in fabrication by thick film, casting, firing or baking, dipping, or spraying. These methods produce nanoparticulate materials which have properties different from those formed by conventional chemical and calcining techniques. There are a few different forms of sol-gel. The one chosen for this work involves the use of an organic compound as the complexing agent. The organic compound is ethylene-diamine-tetra acetic acid (EDTA). One of the reasons EDTA was chosen is because it bonds well with most metallic elements and that it is comprised of an amine and an acid, fundamental for the gel.

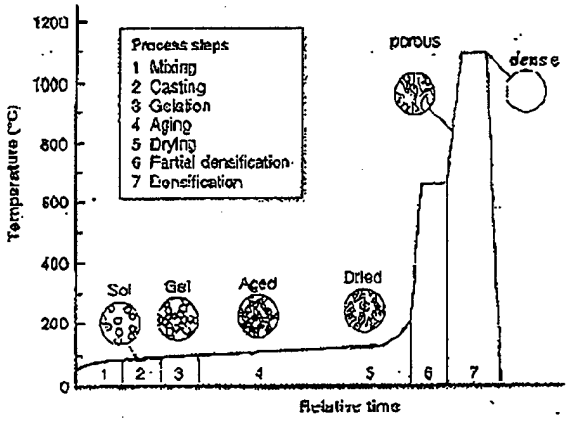

Figure 5
Stages of sol-gel

Figure 5 shows a typical depiction of the stages of the sol-gel process. Nanoparticles (particles with sizes in the range of a few nanometers) form up to and including step five. Some growth

occurs in step six, and even larger particles result from firing (sintering) in stage 7. In this study, the regions 1 through 6 are pertinent to the unique properties obtained by sol-gel processes. It is these regions which we will use for most of the materials described.

Since standard powder techniques would not allow us to reach our target, a modified sol-gel approach was studied. The change in properties at the nanocrystalline size scale for magnetic materials are the following: (a) Initially there is an increase in the magnetic coercivity down to a critical crystallite size in the nanoscale size regime; and (b) below a critical crystallite size, there is a decrease in coercivity leading to superparamagnetic behavior, high frequency response, and higher than expected permeabilities at these frequencies. [1] This approach initially involved the complexing of aqueous solutions of iron, nickel, and zinc cations in complex nitrate gels. This method consisted of complexing the solution with two mole citric acid/mole of cation and adjusting the pH of the mixture with ammonium hydroxide in the range of 7 to 11, dependent on the morphology of the powder desired. The solutions used $FeCl_3$, $NiCl_2$, $MnCl_2$ and $ZnCl_2$ in an aqueous solution. The final materials used in the complexing were Fe, Mn, and Cr chlorides, since the Ni was carcinogenic and the zinc did not behave well in the mixtures. Due to time restrictions and lack of distinct benefit over the Fe/Mn materials, the chromium oxides were abandoned. Ethylene diamine tetraacetic acid salt (EDTA) was added to obtain the sol-gel, typical of that shown in Figure 6. The pH was adjusted upward and downward using aqueous NH_4OH and HCl respectively.

The following equations (typical for iron oxides but applicable to other oxides as well) govern the gel formation in this type of formulation. The chemical reactions involve either the basic equations where nitrates are made from basic, large particle oxides or the starting point is the nitrate of the ferromagnetic metal ion itself. i.e. $Fe_2O_3 + 6HNO_3$ ------- > $2Fe(NO_3)_2 + 3H_20$, the right hand side of the equation being the starting point, as mentioned above. MnO_2 and Cr_2O_3 can be used in like manner, or, alternately, the chlorides can be used. A mixture of EDTA and ammonia are next made as a complexing agent for the gel/foam formation. i.e. $H_4EDTA + 4NH_3$ -------- > $EDTA^{4-} + NH_4$. The metal nitrate and EDTA mixtures are themselves mixed at room temperatures forming a gel. this gel is then heated on a hotplate at 220° C until gel/foam forms (approximately 15 minutes), shown in Figure 6.

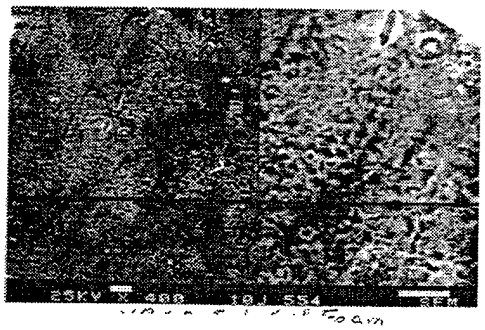

Figure 6
Sol-Gel Foam

The next step was the fabrication acrylic composite materials. Acrylic mounting liquid and acrylic mounting powder were mixed in with Ferrite . Three samples were made in three different concentrations, as shown in Table 2.

Table 2
w% Concentrations

TYP	POWD	LIQ	Ferrite	Total
I	44.4	22.2	33.3	100
II	50	25	25	100
III	57.1	28.6	14.3	100

Most Acrylic plastics are based on polymers of methyl methacrylate, which may be modified by copolymerizing or blending with other monomers. Acrylics are hard and stiff. They are also relatively strong plastic; their tensile strength ranges from 5,000 to about 11,000 lb/in^2. [1] In the vinyl synthesis we are interested in using Ferrite. Ferrites are ceramic, homogeneous materials composed of oxides containing iron oxide as the main constituent. The design advantages are: high resistivity, wide range of operating frequencies, low loss combined with high permeability, time and temperature stability, large material selection, versatility of core shapes, and low cost. [4] Since the soft ferrites have such high permeabilities, the higher the concentration of the ferrite the higher the attenuation the EM waves passing through. Combine this with the aforementioned impedance mismatch, and the attenuation becomes higher than conventional conductive shields.

The samples have to be molded into hockey puck type disks which need to be 2" diameter with a 0.25" thickness. The liquid was placed in the tray first then the powder mixed into the liquid immediately after the ferrite was mixed into the acrylic which had to stand for 2-3 hrs to harden in the container. The container was first sprayed with a silicone release agent in order to ease removal of the samples from the shells. The samples had to be sanded so they would have a flat surface.

The Test Apparatus

The cross section of the test apparatus, shown in Figure 7, was altered in dimensions to meet the requirements of the coils. The purpose of the tester is to measure shielding effectiveness (SE) at the frequency of 60 Hz. The tester was used to quickly evaluate the SE of its outer skins and the vinyl samples. Using a set of solenoidal coils as the core of each half of the tester tied in with the broad band amplifier shown in Figure 1.

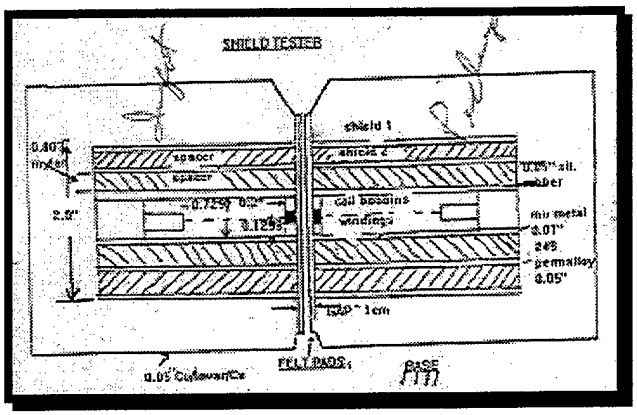

Figure 5
Test Apparatus Cross-Section

The exterior layers of the apparatus are copper/1018 steel/copper. Two BNC connectors are required to be placed on each end of the tester where the coils will be soldered to one end and coaxial cables will be connected to the other end for frequency input and measuring output. The other materials that are required for the interior of the apparatus are: felt, Silicone Rubber [5], Mylar. [1]

Once the exterior layers were made the BNC cable connectors were placed on the inside. A piece of Si/Fe ferromagnetic steel was placed inside the core of the coils to enhance the induced signal in the secondary. This would also allow for a crisper waveform and a larger waveform. The felt pads placed on the ends will allow the sample to be slid in between the two sides for testing.

The cans were placed on a piece of plexiglas which small pieces of wood would be placed on the sides for extra support (Figure 8). A sample was placed in-between to set to correct distance on the inside.

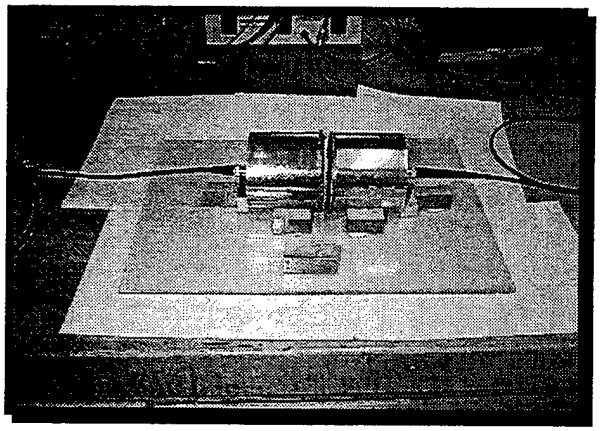

Figure 6
Expanded view of tester

TESTING SAMPLES

Sheets of copper and steel were cut into small pieces which were tested for shielding effectiveness. Relative permeabilities of 1 for copper and 1000 for steel were utilized. The resistivity in copper is $1.72 \times 10^{-8} \Omega m$ and steel is $20 \times 10^{-8} \Omega m$. Using the formulas in Table 1 values for both copper and steel can be obtained. The thickness of the sheets were Copper = 0.02" = 0.05cm and Steel = 0.028" = 0.071cm.

The theoretical results for calculations relating to both copper and steel samples are listed in Table 3. Using the test fixture assembled for these measurements provided the shielding effectiveness results listed in Table 4. The primary measurement frequency for these particular tests was 60 Hz. As shown in the Figure 2 amplifier gain curve shielding effectiveness test results can be obtained at frequencies up to 1 M Hz. As an example of one of the best performers among the standard materials the boundaries of Cu/Steel/Cu/Steel/Cu produced shielding effectiveness values of almost 23 dB at 60 Hz.

Table 3 : Values Calculated for Cu & Steel

Test Frequency 60 Hz	Copper	1018 Steel
skin depth= δ (m)	8.52×10^{-3}	9.19×10^{-4}
1 percent δ (m)	391.92×10^{-6}	42.34×10^{-6}
propagation constant	$166 \angle 45°$	$1539 \angle 45°$
phase velocity (m/s)	3.21	0.346
Index of Refraction	9.35×10^{7}	8.67×10^{8}
Wavelength(m)	0.0535	0.00577
Relaxation Time (s)	1.5×10^{-19}	1.77×10^{-18}
Impedance (Ω)	377	11913
Reflection Coefficient	for steel/copper is	0.939
Complex Impedance (Ω)	$2.85 \times 10^{-6} \angle 45°$	$3.1 \times 10^{-4} \angle 45°$
Reflection Coefficient	for steel/copper is	0.982
Absorption Loss (dB)	0.517	7.24

Table 4 : dB Attenuation Measured for different but standard materials

Material Center filling	V ratio (empty/ material)	dB attenuation
Cu	1.375/1.325	0.322
Cu,Cu	1.375/1.275	0.656
steel	1.375/0.345	12.0
steel,steel	1.375/0.2	16.8
Cu,steel	1.375/0.32	12.7
Cu,steel,steel,Cu	1.375/0.16	18.7
Cu,steel,Cu	1.375/0.34	12.1
Cu,steel,Cu,steel,Cu	1.375/0.1	22.8
Cu,5 part Ferrite,Cu	1.375/0.4	12.0
Cu,10 part ferrite,Cu	1.375/0.34	12.1
Cu,15 part ferrite,Cu	1.375/0.32	12.7

New Materials

In addition to the standard materials discussed above, nano-particle combinations were developed and evaluated in the same apparatus. As shown in Table 5, the nano-particle oxide mixture produced impressive results for very thin samples

Corrosion Characteristics

During early development efforts on composite shielding materials suitable for hostile marine environments, the ITO and the ITO/NI-flake samples were tested [6] to determine their electrochemical potential in flowing brine solutions vs 50XX aluminum. The ITO samples adjusted to less than 65 mVolts after 15 seconds , while the ITO/NI-flake samples reduced in potential from 1.89 Volts to 0.8 Volts in the same time. The ITO/Ni-flake samples eventually (after 5 minutes) reduced in potential to 0.22 Volts showing some compensatory effect.

Thus these oxide mixtures electrochemical properties, because of their high free energy of formation, are quite cathodic (resistant to corrosion). They also seem to adjust their potential [4] when in contact with more anodic materials, acting as a graded potential layer.

Additional related discussions on the electromagnetic properties of these materials are discussed in [7].

Table 5 -Measured Values for Nano-Particle Mixtures @ 60 Hz

Material & Mixture	Material Thickness	Test Results S.E. dB @ 60 Hz	Comment
Nanoparticle Oxide Mixture	100 μm film	**22**	PAINT Isoporone binder with cyclo hexane solvent
SOC/Steel Mixture	3/32 in. tile ABS/PET	**8 to 10**	TILE
SOC Mixture	3/32 in. tile Acrylic Epoxy copolymer	**6**	TILE
Oxide Mixture on glass	100 nm films 5 stacked	**9-11**	FILM
Metallic Mixture on glassien paper	100 nm films 5 stacked	**3-6**	FILM

Note: SOC = Semiconductor-Oxide-Conductor

CONCLUSIONS

The concepts of impedance reflection at the interface does indeed enhance the shielding effectiveness. Utilizing impedance mismatch and the proper scattering materials, materials with unusually high shielding properties can be developed for low frequency applications..

This leads to the conclusion that a multilayer "stack" of metals with an air interface on either side is often more effective as a shield at low frequencies than large homogeneous layers. Therefore, a three pronged approach was taken to fabricate shields, namely paint with nanoparticles of oxides, composite shields (tiles) with Dixon/Masi Patented materials in polymers, and evaporated oxides mixtures on glass, and metallic mixtures on paper (glassein).

Initial testing of NUWC Team developed materials, formulated as paints, as tiles and as films (to be applied to various materials including glass), have yielded very impressive shielding effectiveness test results against 60 Hz magnetic fields (near field). To achieve 22 dB of SE with a 100 um thickness, against this type of EMI source, is a significant accomplishment. As a comparison, many low frequency shielded rooms are constructed of two layers of steel each approximately 1/4 inch thick separated by plywood. These rooms typically have a maximum specified SE performance of 30 dB. It is obvious from this comparison that the Dixon/Masi developed materials do not electromagnetically behave like solid metals. As has been shown by Dixon/Masi in previous Patents and/or papers, non-metallic or composite materials have unique electromagnetic characteristics which allows them to significantly out perform other non metallic materials of similar thicknesses.

ACKNOWLEDGMENTS

The contribution of Mr. Adam Sedzikowski, of Western New England College, in building the test apparatus is greatly appreciated.

REFERENCES

1. " The Definitive Guide to Magnetic Shielding." Amuneal Manufacturing Corp., INFO. 1996.
2. Kraus, John D. ELECTROMAGNETICS . McGraw Hill Book Company. 1973.
3. Rao, N. N.. Elements of Engineering Electromagnetics. Prentice Hall: 1991.
4. "Soft Ferrites - A user's Guide." Magnetic Materials Producers Association: September 1991.
5. Brady, George S. Materials Handbook 14th Ed.. McGraw Hill, Inc.,: 1997.
6. Masi, J. V., Dixon, D.S.., "Development of a Composite Material with Long-Term EMI Shielding Properties", SAMPE Journal 25(6) pp.31 ff. 1994.
7. Masi, J. V. and Dixon, D.S., "The Use of Finite Element Methods and Closed Form Solutions for Electromagnetic Shielding Employing Conductive Composites." IEEE Proc., Tel Aviv, March , 1992.

Corrosion Behavior of Aluminum-Beryllium Alloys

Thomas J. Garosshen & Vincent C. Nardone

United Technologies Research Center
411 Silver Lane
East Hartford, CT 06108

ABSTRACT

Aluminum-beryllium alloys offer a unique combination of strength, high stiffness and low density. This combination of properties has resulted in their use for special applications in advanced aircraft such as the Commanche helicopter, F-22 fighter, and the V-22 VTOL. The long term corrosion behavior of this relatively new class of alloys is not well understood. In addition, little is known about the corrosion products that forms on Al-Be alloys. Beryllium oxide is a toxic substance when inhaled; special precautions must therefore be taken when using beryllium containing alloys. The corrosion product that forms on Al-Be alloys contains beryllium oxide; the corrosion process must therefore be well understood.

In this paper we present the results of: (1) Auger analysis of the native oxides that form on a cast and a PM (powder metallurgy) Al-Be alloy, (2) polarization curves for a cast and a PM alloy in 3.5% NaCl and seawater, and (3) analysis of the corrosion product and substrate after exposures in 3.5% NaCl solutions. The findings are discussed in regard to applications for this class of alloys.

INTRODUCTION

Due to the low density of the two major alloying elements, aluminum-beryllium alloys offer an attractive combination of: low density, high stiffness, and reasonable strength. An aluminum-beryllium alloy (Lockalloy) was first used for a folding ventral fin in the SR-71/YF-12a, and, for an interstage skirt in Minuteman III ICBMs[1]. The Lockalloy alloy subsequently found limited applications due to its cost and processing issues and disappeared from production. Aluminum-beryllium (Al-Be) alloys have since been rediscovered and improved upon by the Brush-Wellman Company and Nuclear Metals Inc.

Al and Be are virtually insoluble in each other in the solid state. This mutual insolubility results in an alloy that consists of an essentially pure HCP Be phase surrounded by an FCC Al matrix. The Al matrix gives Al-Be alloys significantly greater ductility than Be alloys, which lack significant ductility due to a limited number of active slip systems. Alloying elements can be added to Al-Be alloys to improve castability and to strengthen the Al matrix. Al-Be alloys exhibit excellent modulus/density ratios as shown by the comparative data in Table 1. This

makes them good candidates for stiffness-critical aerospace applications. Al-Be alloys also have good thermal conductivity and are used for applications that require good heat transfer properties such as heat sinks.

Table 1. Comparison of the Stiffness and Density of Various Materials

Material	Density (gm/cm^3)	Elastic Modulus (GPa)	Modulus/Density
Al-62%Be	2.13	190	90
Magnesium	1.85	45	24
Aluminum	2.72	69	25
Titanium	4.5	114	25
Steel	8.3	207	25

Al and Be are active metals. In seawater, they are next to each other on the very active anodic end of the galvanic series with Be being slightly more active than Al. Both metals exhibit corrosion resistance because of the formation of a thin tenacious oxide film on their respective surfaces. The oxide film that forms on Be is BeO. It is important to note that BeO particles, which are inhaled into the lungs, can cause a dangerous health condition known as chronic beryllium disease or berylliosis[1]. Soluble Be salts such as chlorides and sulfates also can be toxic[1]. In aqueous environments the presence of chloride and sulfate ions can significantly increase the corrosion rate of Be alloys and cause pitting corrosion[2].

Al is generally stable in water over a pH range from 4 to 8.5 due to the formation of the thin protective oxide. Pure Al, as well as 2000, 5000 and 6000 series wrought Al alloys, are also very stable in environments that contain chlorides and sulfates, such as seawater. However, other Al alloys, such as 2000 and 7000 series, are quite susceptible to corrosion (including localized corrosion) in solutions containing chlorides and sulfates. For both Al and Be alloys, corrosive attack is promoted by the presence of contamination and second phase particles in the alloys, which act as local anodes and cathodes.

Although it may be expected that Al-Be alloys behave similar to the base metals, the corrosion behavior of Al-Be alloys is not well understood. The development and utilization of new and improved Al-Be alloys in advanced aircraft warrants an understanding of their corrosion behavior. In addition, the potential health hazards associated with the corrosion products of Al-Be alloys demands attention.

EXPERIMENTAL PROCEDURE

Material: Preparation, Composition, Properties and Structure

The cast alloy examined in this study was purchased from Nuclear Metals Inc., and is referred to as Beralcast 363. The PM alloy examined was purchased from the Brush Wellman

Company and is known as AlBeMet 162. The PM alloy is fabricated by extruding compacted powder which is produced via inert gas atomization. Table 2 contains the nominal compositions of the two alloys studied in this investigation.

Table 2. Nominal Chemical Compositions of Al-Be Alloys (wt.%)

Alloy	Al	Be	Ag	Ge	Co
Beralcast 363	Bal.	65	3	1	1
AlBeMet 162	Bal.	62	-	-	-

For reference purposes, Table 3 contains the basic room temperature tensile properties and densities for the two alloys. Further information on the mechanical properties of the alloys can be found in references 3 and 4.

Table 3. Room Temperature Tensile Properties and Densities

Alloy	Elastic/Modulus GPa (MSI)	0.2% Y.S. MPa (ksi)	UTS MPa (ksi)	Failure Strain %	Density gm/cm^3
Beralcast 363	231 (33.5)	232 (33.7)	277 (40.1)	2.5	2.19
AlBeMet 162	202 (29.3)	262 (40.0)	345 (52)	4.0	2.10

Figure 1 contains optical micrographs of the two alloys. Coarse Be dendrites surrounded by an Al matrix are apparent in the cast Beralcast 363 structure shown in Figure 1A. The AlBeMet 162 microstructure is significantly finer and shows variations in the size of the Be particles along with a directional microstructure due to the PM fabrication process, see Figure 1B. Both alloys contain approximately 60 vol. % of the Be phase.

EXPERIMENTAL RESULTS

Analysis of Native Oxide Layer

Scanning Auger Microscopy (SAM) was utilized to determine the nature of the oxide layer that forms on Al-Be alloys. Specimens of the two alloys, Beralcast 363 and AlBeMet 162, were polished to a one micron metallographic finish and then allowed to sit in air for several weeks at room temperature prior to analysis. The specimens were then subjected to SAM (Perkin Elmer 660) analyses to determine the composition and thickness of the oxide film that forms. The sputtering rate calibration used for the depth profile analyses was based upon the sputtering rate of Al_2O_3, which is a reasonable approximation for the subject oxide films.

Figure 2 contains SEM micrographs of the areas subjected to AES (Auger Electron Spectroscopy) analysis for the Beralcast 363 and AlBeMet 162 alloys.

Representative AES spectrums of the surfaces of the Be particles and the Al matrix for the Beralcast 363 alloy after 31 days are contained in Figure 3. As shown, the oxide film over the Be phase consists of Be and O. Whereas, the oxide layer on the Al matrix contains both Al and Be along with O. The presence of Be in the oxide film over the Al matrix phase is most likely due to the high diffusion rates generally associated with Be. The oxide film was subjected to depth profile analyses to determine the thickness of the respective oxide films on the two phases. Typical depth profile analyses are found in Figure 4. As shown, the oxide layers that formed on both the Al and Be phases was 30-40 Å thick after 31 days of growth.

Figure 5 contains AES spectrums of the oxide films on the Al and Be phases for the AlBeMet 162 alloy after 36 days in air. As shown, the oxide film over the Al matrix phase consists of a mixture of Al and Be. Whereas, the oxide film over the Be phase does not contain any Al. The depth profile analyses for this alloy are found in Figure 6. The thickness of the oxide film on the AlBeMet 162 alloy was ~40 Å, similar to that on the Beralcast 363 alloy. Note that the C observed on both alloys during SAM analysis is believed to be the result of contamination and is not an integral part of the observed oxide films.

As indicated by the above analyses, Al-Be alloys form very thin protective oxide films that inhibit rapid oxidation under benign conditions. BeO is a major constituent of the oxide film that forms on this class of alloys.

Potentiodynamic Polarization Analysis

Specimens of Beralcast 363 and AlBeMet 162 were subjected to potentiodynamic polarization analyses in aerated 3.5% NaCl solutions and seawater (Westerly, RI) according to ASTM G 5 in order to determine their respective corrosion rates. The specimens' surfaces were prepared to a 600 grit SiC finish and the scan rate was 1V/hr. The Ag/AgCl reference electrode was used for the potentiodynamic polarization analysis.

The resulting polarization scans for the Beralcast 363 alloy are contained in Figure 7. As shown, the alloy exhibits relatively low corrosion current densities at E_{corr} in both 3.5% NaCl and seawater. The corresponding corrosion rates in millimeters per year are found in Table 4.

The polarization scans for the AlBeMet 162 alloy are contained in Figure 8. As shown, this alloy exhibits lower corrosion current densities at E_{corr} in both 3.5% NaCl and seawater as compared to the cast alloy. Table 4 also contains the corrosion rates for this alloy in the two solutions. Based upon the measured E_{corr} values, the Al-Be alloys will be on the active end of the galvanic series at a potential similar to Be, which is slightly more active than Al alloys[5].

Table 4. Corrosion Rates for Al-Be Alloys from Polarization Scans

Alloy/Solution	E_{corr} (V)	i_{corr} (A/cm^2)	Corrosion Rate (mm/yr.)
Beralcast 363 / 3.5% NaCl	-0.95	$1x10^{-5}$	0.14
Beralcast 363 / Seawater	-0.89	$1x10^{-6}$	0.015
AlBeMet 162 / 3.5% NaCl	-1.03	$2x10^{-6}$	0.03
AlBeMet 162 / Seawater	-1.1	$1x10^{-7}$	0.002

Cyclic polarization scans also were performed in the 3.5% NaCl solution according to ASTM G 61 to determine the susceptibility of the alloy to pitting corrosion. The larger the hysteresis loop between the forward and reverse scans, the greater the tendency for an alloy to exhibit pitting corrosion[6]. This is because the hysteresis loop represents an area where the oxide film on the metal surface is metastable; it can therefore breakdown locally and allow localized corrosion to occur.

As shown by the observed hysteresis loops between the forward and reverse scans for both Al-Be alloys, Figure 9, they have the potential to exhibit localized corrosion such as pitting. For the Bealcast 363 alloy the voltage hysteresis is ~0.04 volts; whereas for the AlBeMet 162 alloy the difference is ~0.07 volts. These results indicate that the Al-Be alloys may be susceptible to localized corrosion in solutions containing chlorides. The larger hysteresis exhibited for AlBeMet 162 suggest it may be more susceptible to localized corrosion than Beralcast 363. However, the actual degree of susceptibility to localized, or pitting corrosion, can not be accurately predicted from a cyclic polarization scan. This is because it does not factor in the kinetic factors governing pit growth. Cyclic polarization scan only tells you if an alloy has the potential for localized attack.

Corrosion Product and Substrate Characterization

Specimens of the two alloys were placed in separate 3.5% NaCl solutions for various lengths of time at room temperature and 50C, and then examined via optical microscopy and SEM analysis. The specimens were prepared with two different surface conditions; a one micron polish and a 600 grit SiC finish. The objective of the polished surface was to expose both phases of the alloy to the solution. This was deemed important because SEM analysis indicated the 600 grit finish has aluminum smeared locally over the surface. The polished surfaces would help determine if preferential attack of one of the two phases occurs. The specimens were cleaned with isopropanol and D.I. water prior to the exposures.

Inspection of the specimens during the exposures revealed the significant presence of a corrosion product suspended in the NaCl solutions after a few days of exposure. Chemical analysis (ICP) of the corrosion products that formed after 285 hours indicated that they contained the same approximate Be and Al concentration ratios as the respective alloys. For the Beralcast 363 alloy the corrosion product's metal content was 65 wt.% Be. Whereas, the AlBeMet 162 corrosion product's metal content was 62 wt.% Be. The chemical analyses revealed that Be is

being released into the NaCl solutions, and that the Al and Be phases are being attacked at similar rates for the given exposures.

Examination of the specimens after 285 hours in the 3.5% NaCl solutions indicated that there was localized corrosion starting to occur. The AlBeMet 162 alloy contained localized pits that grew into a canyon morphology as shown in Figures 10 - note the crystallographic etching of the pitted areas. This form of localized corrosion was apparent in both the polished and 600 grit SiC finish specimens at both room temperature and at 50C.

The Beralcast 363 alloy also contained pits after 285 hours in the 3.5% NaCl solutions. The pits appear to be related to casting porosity that experienced localized corrosive attack.

The significance and causes of the observed localized attack, as well as the effects of longer exposure times, are currently being investigated. Those results will be presented in a future publication.

DISCUSSION

The oxide layer that forms on Al-Be alloys is thin and protective in air environments as expected based upon the behavior of the two metals separately. The observation that the oxide layer over the Al phase contains both Be and Al oxide is not surprising based upon the fact that the phase diagram for the two oxides exhibits mixed oxide phases containing both BeO and Al_2O_3[7]. Another contributing factor to the observation that the oxide film contains both Be and Al only over the Al phase, is that Be generally has a higher diffusion coefficient than Al. An understanding of the passivating oxide films that form on Al-Be alloys will help explain the basic mechanisms controlling their corrosion behavior.

Potentiodynamic polarization curves for the two alloys indicate that they corrode in aerated 3.5 % NaCl at rates of 0.03 to 0.14 mm per year. In light of the toxic nature of the BeO in the corrosion product, the observed corrosion rates are considered too rapid for using these alloys in a wet salt containing environment without a protective coating. The alloys also exhibited a tendency to form corrosion pits in NaCl solutions.

The manufacturers of Al-Be alloys realize that Al-Be alloys are susceptible to corrosion in aqueous solutions. Therefore, when Al-Be alloys are used in areas that might encounter salt spray from the ocean, or significant condensation, such as is the case for many military aircraft, protective coatings are specified and the component has a warning label indicating the material contains Be.

Various types of protective coatings have been successfully utilized for Al-Be alloys. Examples of some of the protective treatments include: chromate conversion coatings, anodizing, Ni plating, Al plating, as well as epoxy primers. With proper surface treatments, Al-Be alloys reportedly exhibit good corrosion behavior for several hundred hours in ASTM B117 salt spray tests[8].

Work is continuing to further understand the corrosion behavior of these alloys and additional results will be reported at a future date.

CONCLUSIONS

Al-Be alloys have very high modulus to density ratios and good thermal conductivity. This makes them attractive for many aerospace applications. Unprotected Al-Be alloys are susceptible to corrosion in aqueous environments. In addition, the corrosion product that forms on Al-Be alloys contains BeO, which presents a health hazard if inhaled. Al-Be alloys therefore require protective coatings for most applications. Al-Be alloys are on the active end of the galvanic series, being slightly more active than Al alloys. It is therefore important to avoid galvanic couples that can drive the corrosion of an Al-Be alloy in a wet environment. With proper corrosion protection strategies, this class of alloys offers significant potential for applications that require high stiffness and low density, as well as for applications requiring high thermal conductivity.

ACKNOWLEDGEMENTS

The support of this work by the Office of Naval Research and the Naval Air Warfare Center under Contract N00014-94-C-0098 is gratefully acknowledged. The program is jointly monitored by Dr. Steve Fishman and Dr. Gil London and their technical guidance is appreciated. The assistance of Dr. Bruce Laube for the SAM analysis, and Dr. Michael Kryzman for the potentiodynamic polarization analysis is also appreciated.

REFERENCES

1. V. C. Nardone, "Beryllium Reinforced Metals for Aerospace Applications", Interim Report #R96-5.903.0002-1, ONR Contract #N00014-94-C-0098, 1996, p. 65.

2. Metals Handbook, "Corrosion", Vol. 13 Ninth Edition, ASM Publications, 1987, p.809

3 V. C. Nardone & T. J. Garosshen, "Evaluation of the Tensile and Fatigue Behavior of a Powder Metallurgy Beryllium/Aluminum Alloy", J. of Materials Science, **32,** 1997, p. 2549.

4. V. C. Nardone & T. J. Garosshen, "Evaluation of the Tensile and Fatigue Behavior of a Ingot Metallurgy Beryllium/Aluminum Alloys", J. of Materials Science, **36,** 1997, p. 3975.

5. Corrosion Tests and Standards, Editor: R. Baboian, ASTM Publication, 1995, p.187.

6. Corrosion Tests and Standards, Editor: R. Baboian, ASTM Publication, 1995, p.82.

7. Phase Diagrams for Ceramist; Editor: M. Reser, The American Ceramic Society; 1964, p. 99.

8. Technical information supplied by Brush Wellman and Nuclear Metals Inc.

Figure 1. Optical Micrographs of Beralcast 363 and AlBeMet 162.

(A) Beralcast 363

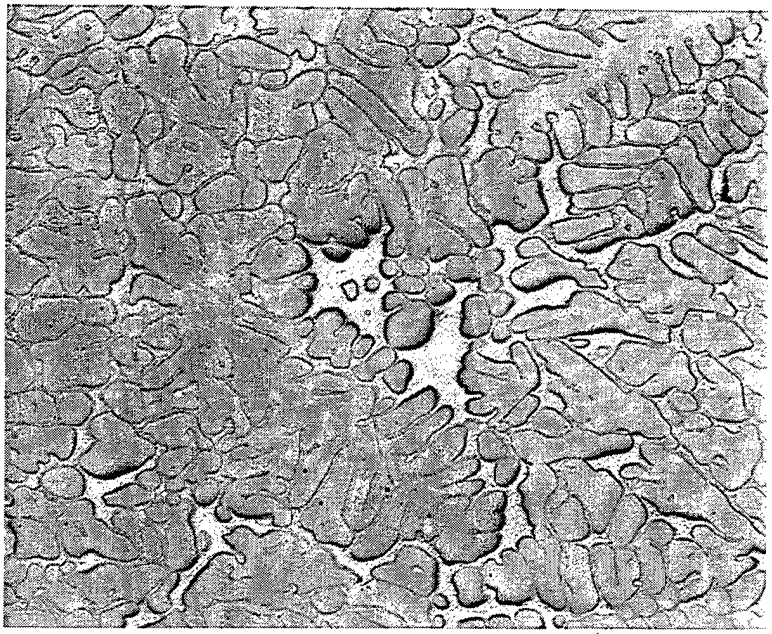

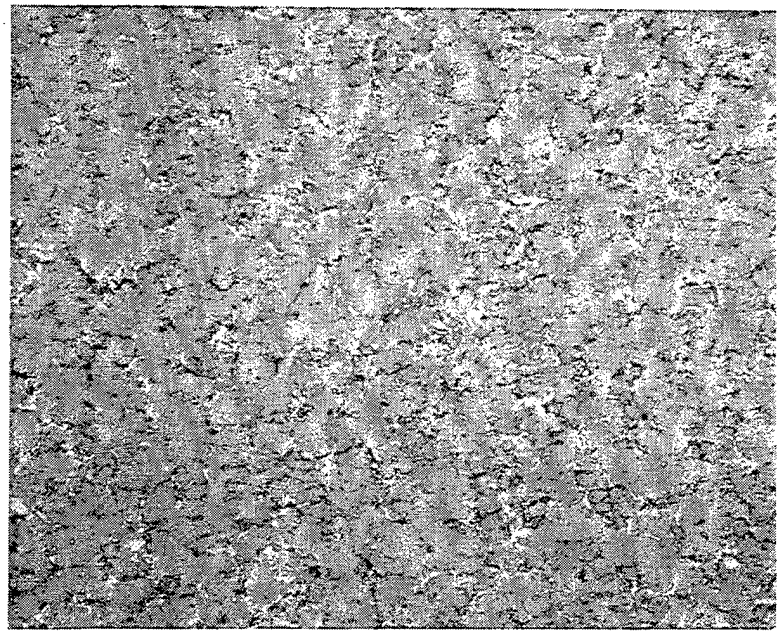

(B) AlBeMet 162

Figure 2. SEM Images of (A) Beralcast 363 and (B) AlBeMet 162 Areas Subject to SAM Analysis.

Beralcast 363

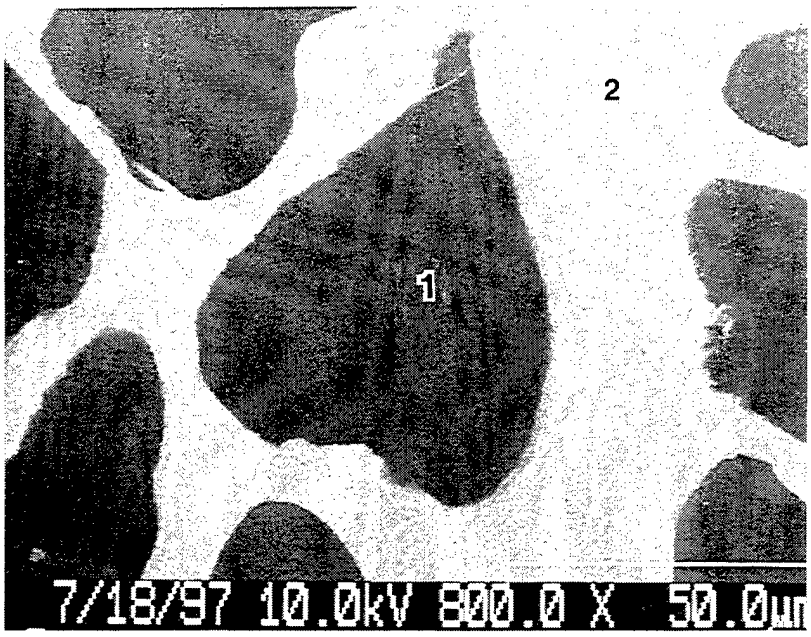

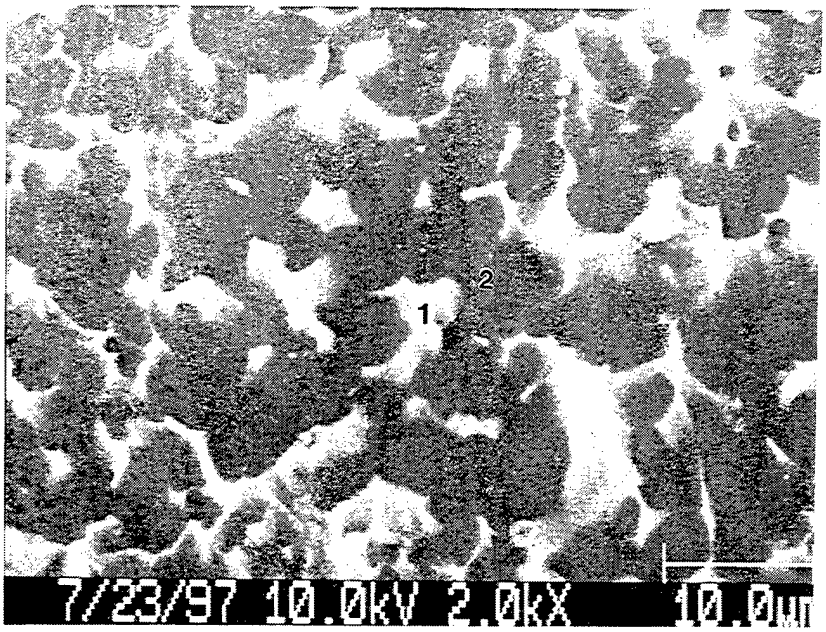

AlBeMet 162

Figure 3. AES Spectrums of Beralcast 363 Surface After 31 Days.

Be Phase

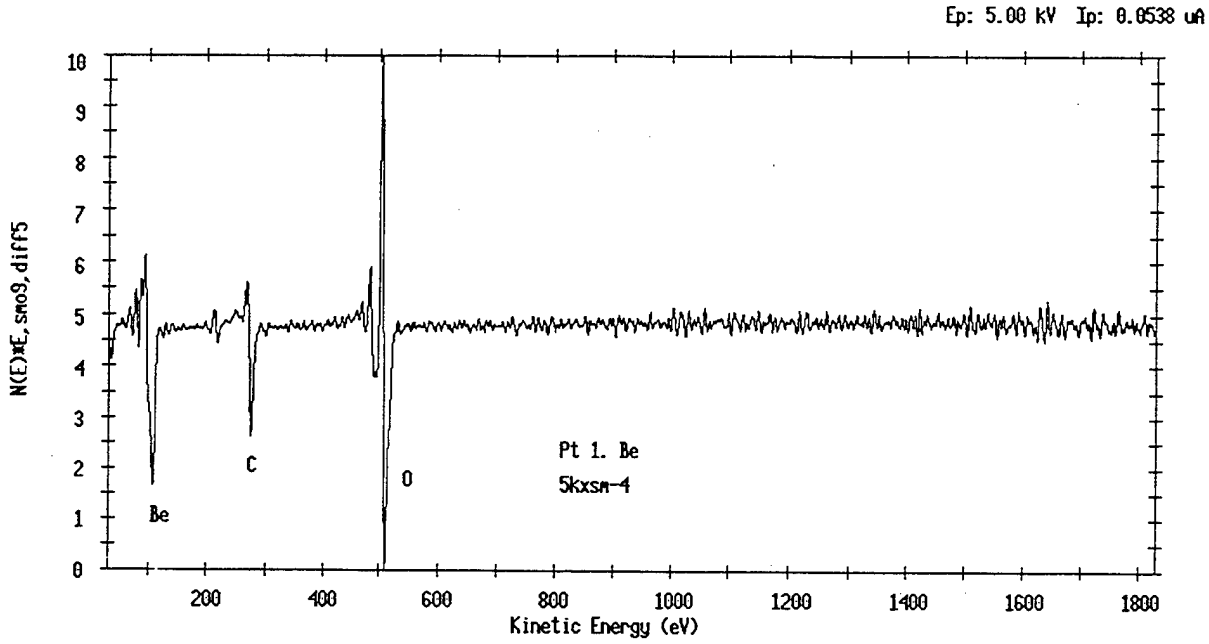

Al Phase

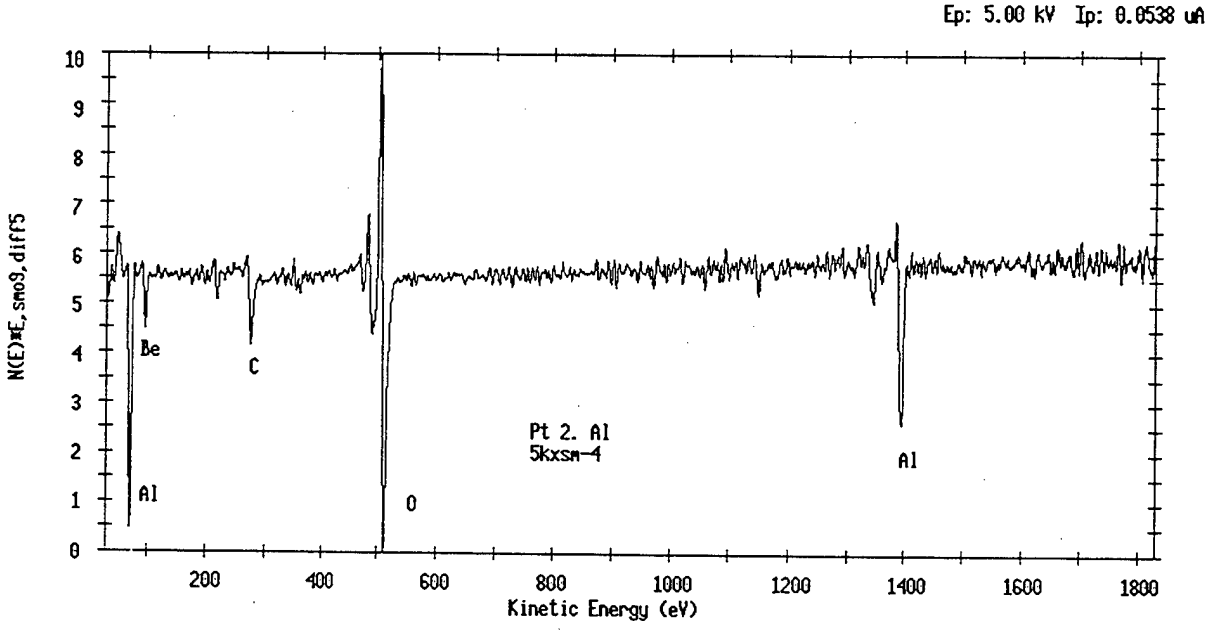

Figure 4. AES Depth Profile Analyses for Beralcast 363 Surface After 31 Days.

Be Phase Depth Profile

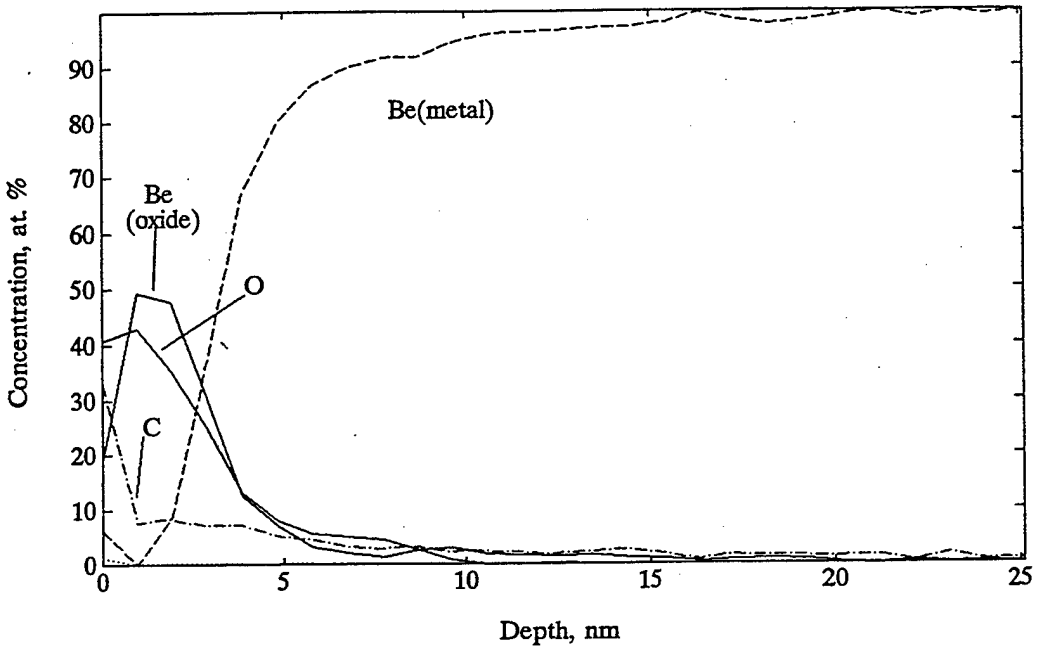

Al Phase Depth Profile

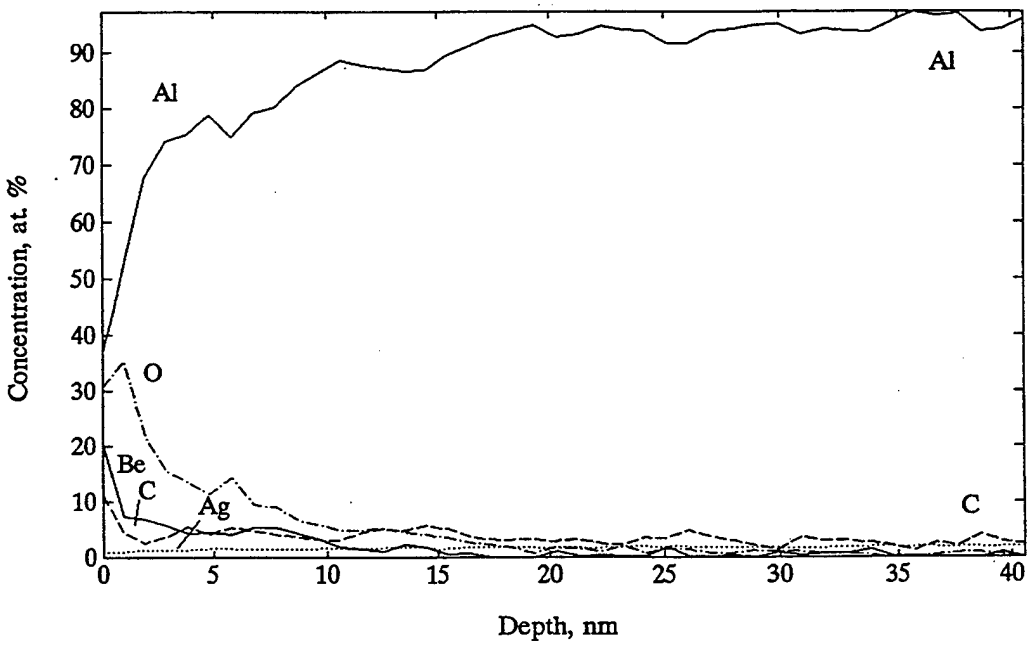

Figure 5. AES Spectrums of AlBeMet 162 Surface After 36 Days.

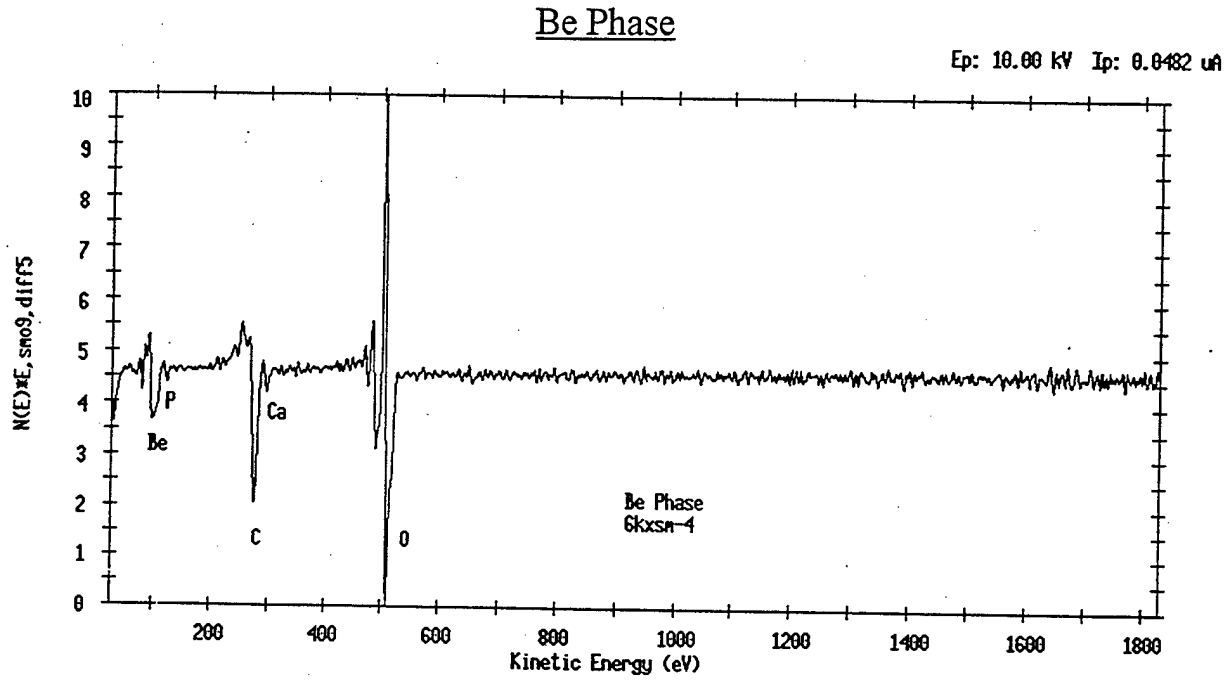

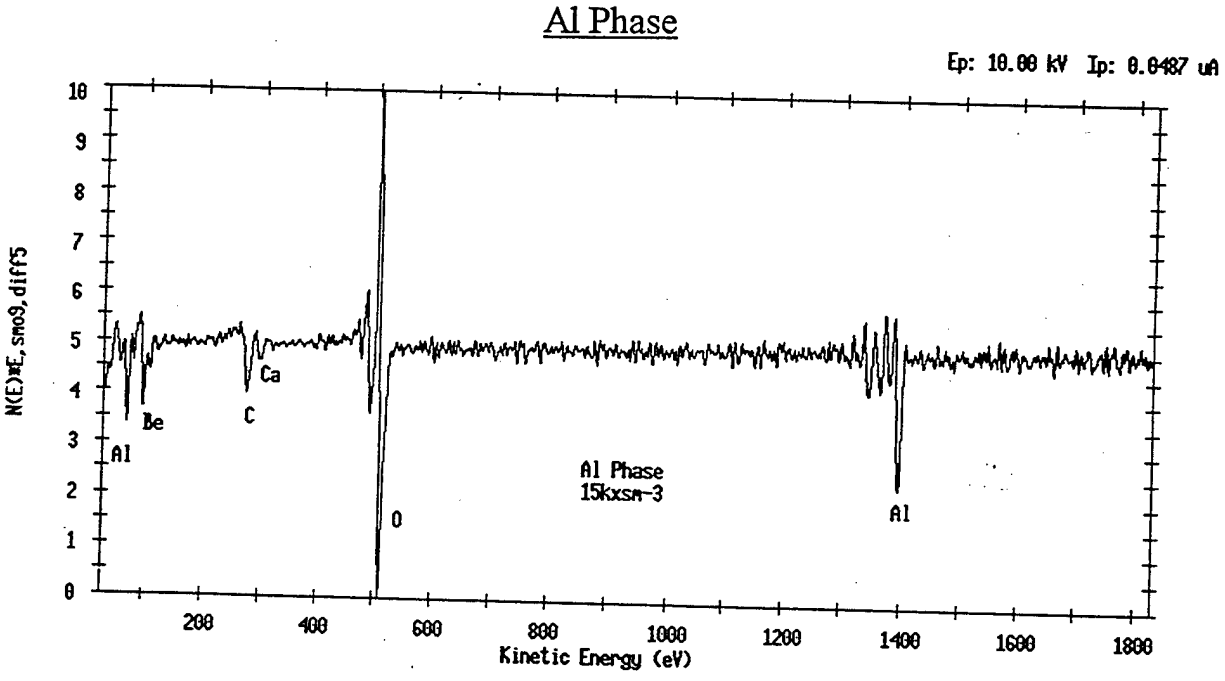

Figure 6. AES Depth Profile Analyses for AlBeMet Surface After 36 Days.

Be Phase Depth Profile

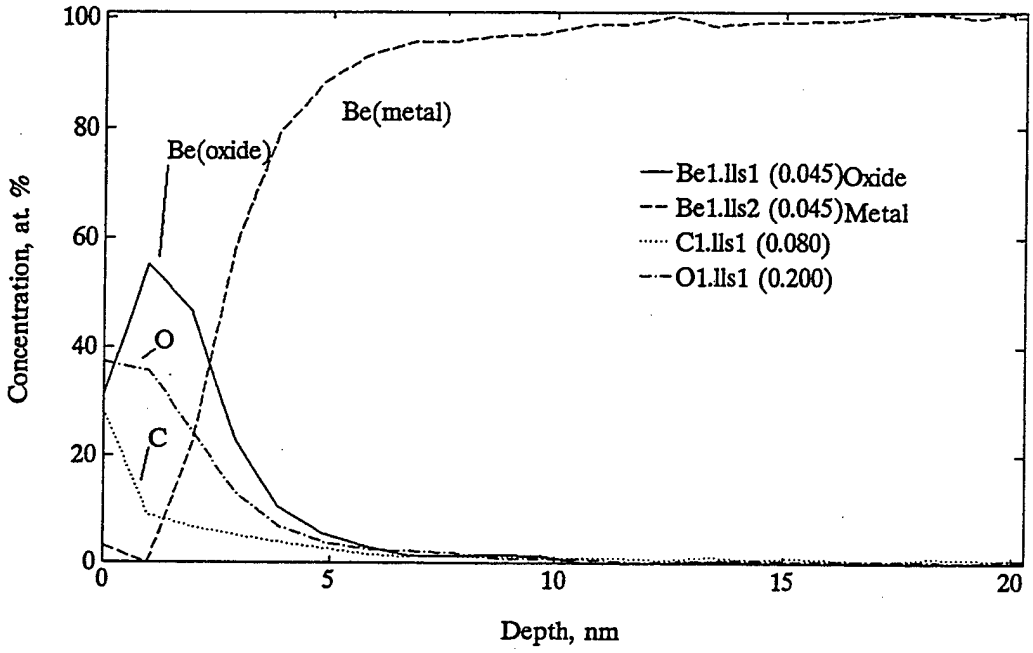

Al Phase Depth Profile

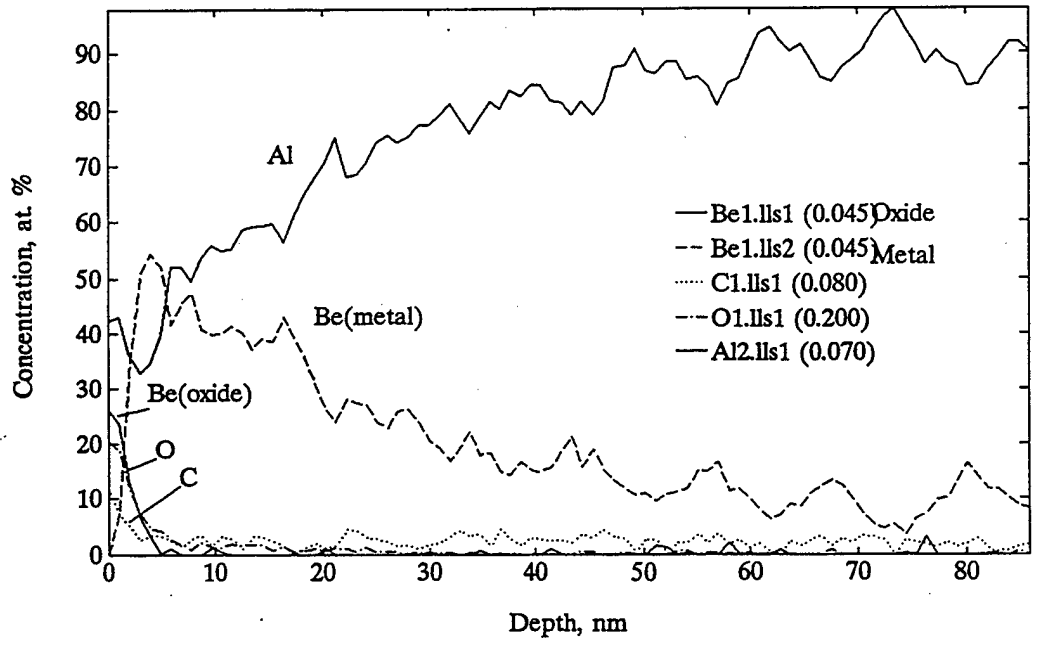

Figure 7. Potentiodynamic Polarization Scans for Beralcast 363.
(Ag/AgCl Reference Electrode)

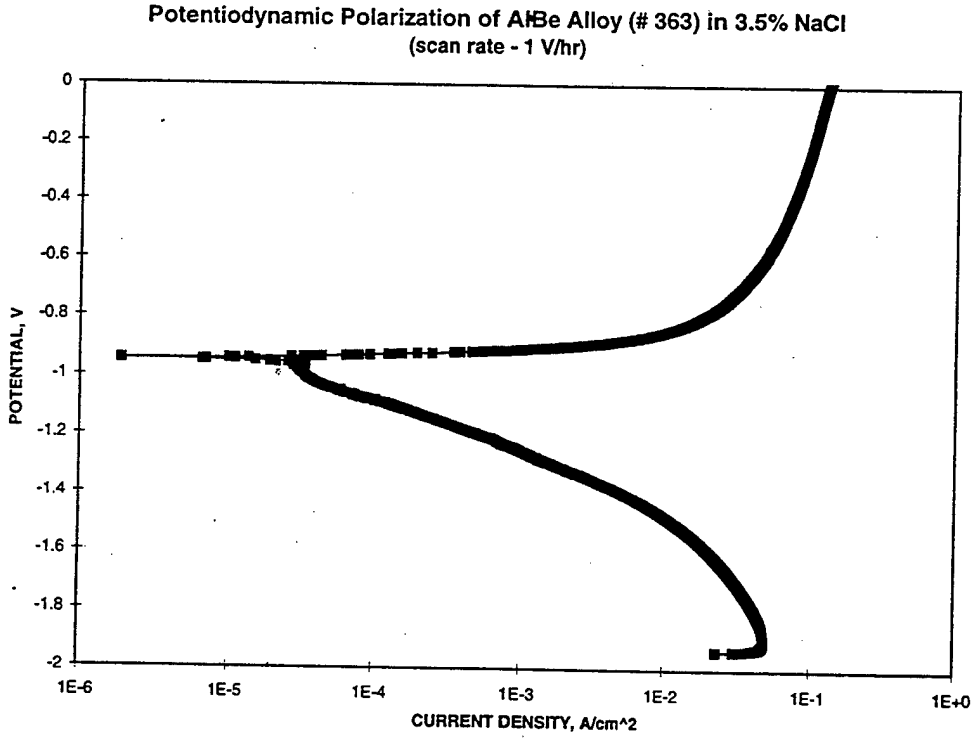

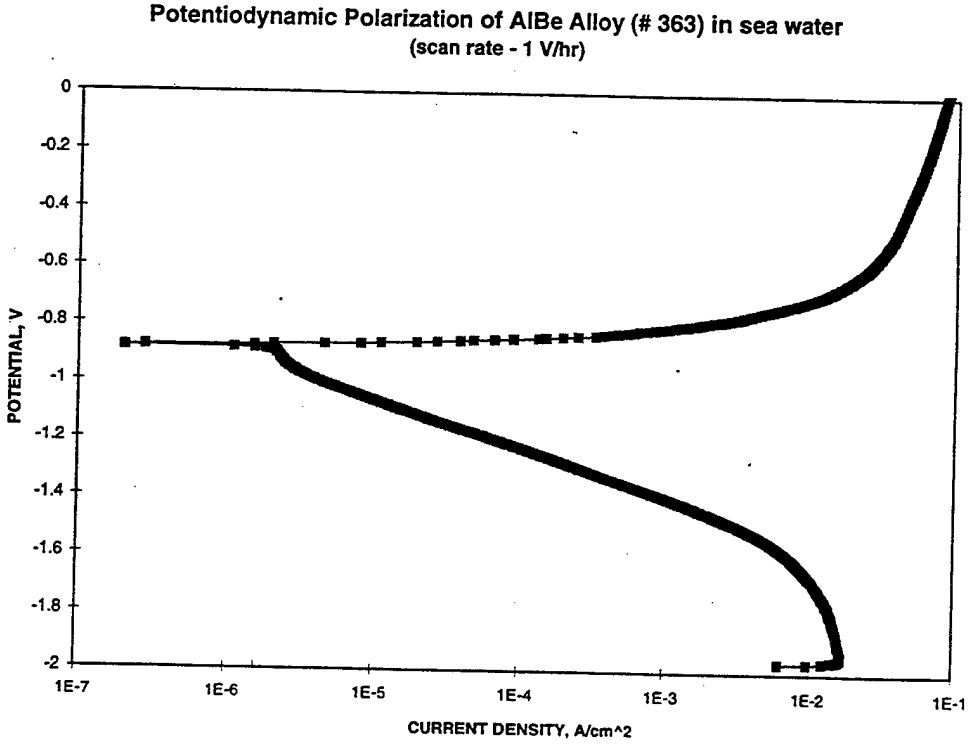

Figure 8. Potentiodynamic Polarization Scans for AlBeMet 162.
(Ag/AgCl Reference Electrode)

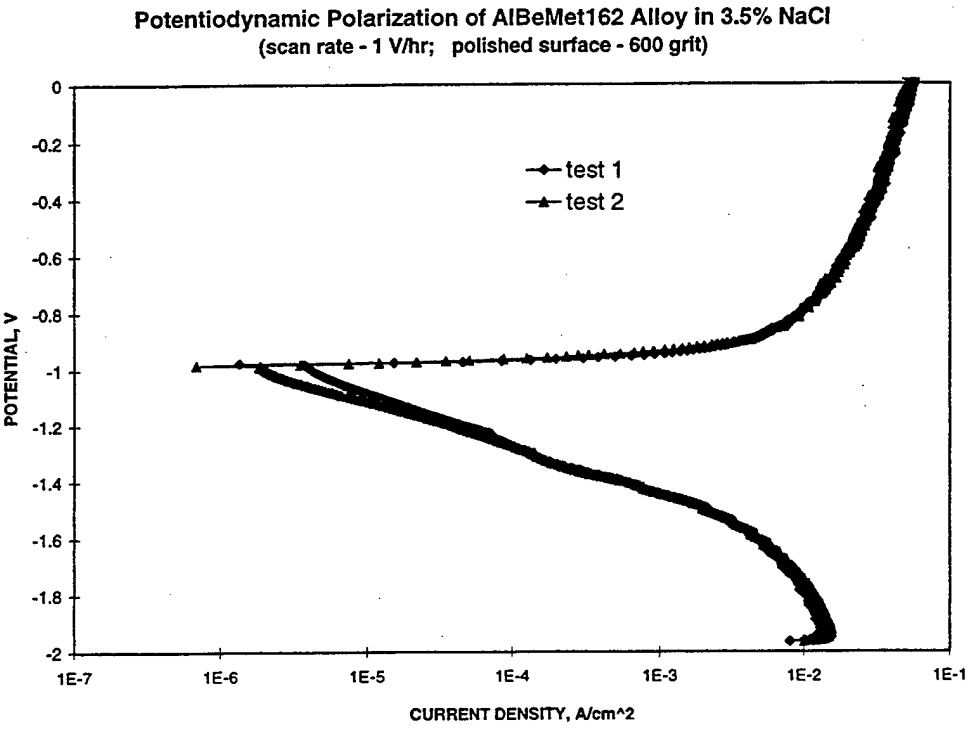

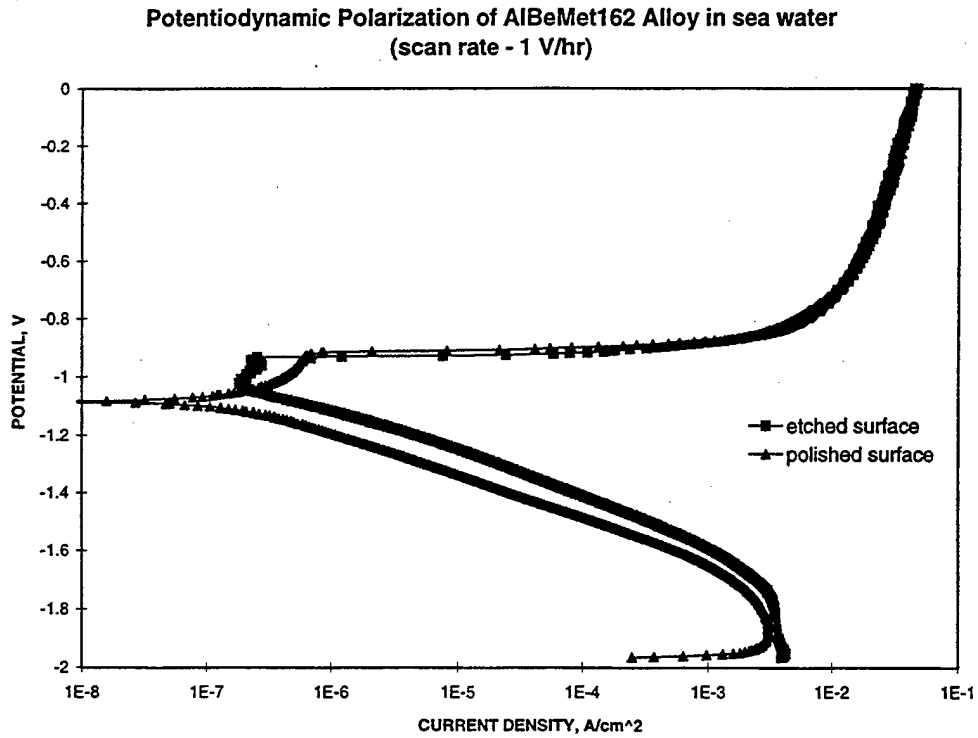

Figure 9. Cyclic Polarization Curves for Beralcast 363 and AlBeMet 162.

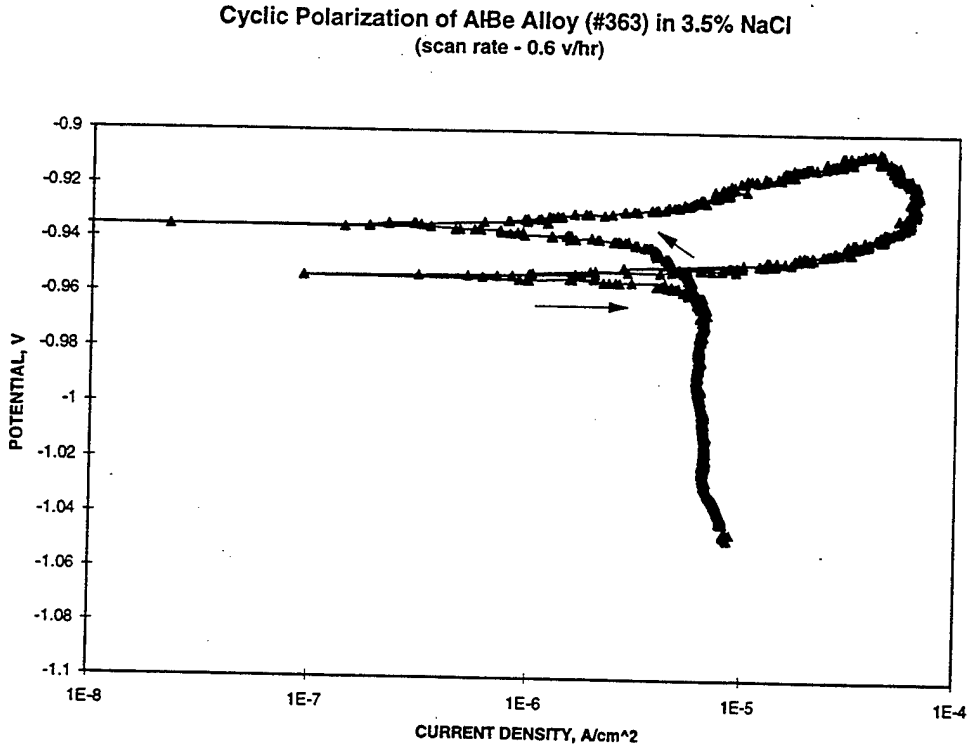

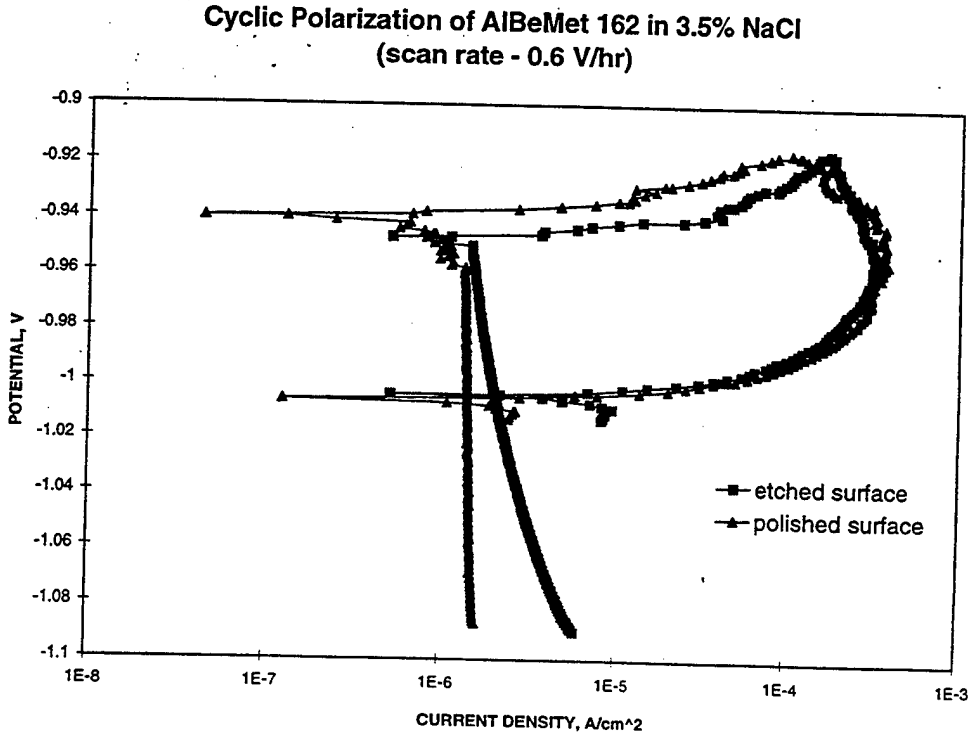

Figure 10. SEM Micrographs of Localized Corrosion on AlBeMet 162 Specimen that was Exposed to a 3.5% NaCl Solution for 285 Hours at 50C.

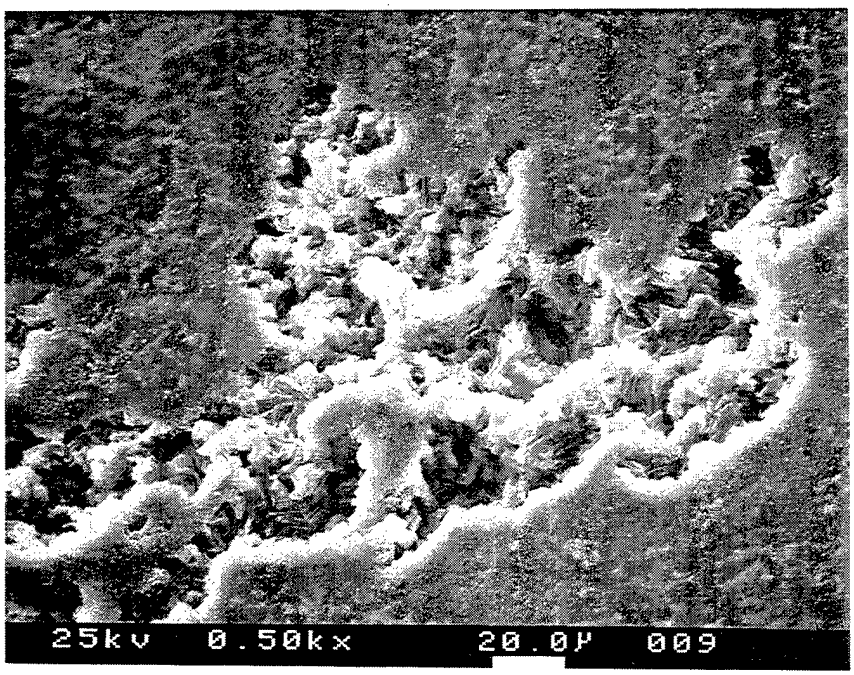

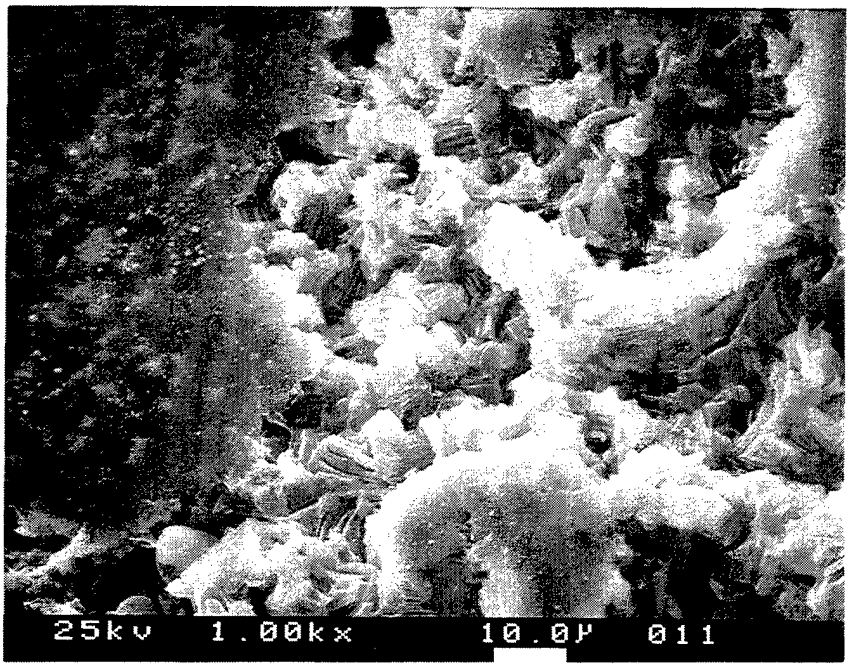

Combination use of Dehumidification (DH) and VCI (Vapor Corrosion Inhibitor) for Corrosion Protection

1997 TRI SERVICE CONFERENCE ON CORROSION

Leo (Chip) Crotty, Jr.
Larry Gelner
Protec, Inc.
216 Lafayette Road
N. Hampton, NH 03862

ABSTRACT

Dehumidification (DH) and VCI (vapor corrosion inhibitor) technology has been used extensively and successfully by the military for equipment and material protection with excellent results. Inhibitor usage was limited for several reasons, including toxicity and lack of multi-metal protection.

This paper discusses improved DH procedures using liquid membrane sealing systems and modern VCI non-hazardous, environmentally safe multi-metal protective materials and systems .

INTRODUCTION

Corrosion protection of structures, ships, equipment and spare parts is necessary when they are not being used, but future use is anticipated. Ideally the system should be moderate in cost, easy to maintain, and allow fast, inexpensive reactivation. Fortunately there are several methods which allow achievement of this goal. This paper discusses both DH and VCI. The methods are combined to preserve complex machinery, or even complete ships. Commercial structures such as offshore oil platforms have benefited from this marriage for years.

Dehumidification (DH)

DH is a very effective corrosion control technology. Corrosion virtually stops when the RH (Relative Humidity) is less than 35%. This is independent of temperature. DH has been used on ships since WWII with excellent results. Brass fittings show no signs of corrosion after 40 years!

There are several ways to remove humidity from air. In all cases, the energy cost is substantial. The goal is to find the optimum combination of low initial cost and low operational cost. Since there is no need for temperature control (normally), refrigeration is not necessary. The simplest way to remove moisture is to use desiccant technology. Refrigeration technology uses compressors, expansion valves, piping, and cooling coils, adding maintenance

intensive requirements. AC is not very good at removing moisture when temperatures are low.

There are many designs of desiccant equipment—spray, rotating horizontal fixed bed, bed, but desiccant wheel dehumidifier designs minimize space requirements and offer proven high reliability. The initial cost is slightly higher than other types, but is offset by minimal maintenance requirements. DH is energy intensive in high humidity conditions. In warm coastal and marine environments, this becomes significant. Both the sealing procedure and geometry of equipment to be protected are major considerations.

While dry air is extremely effective in controlling corrosion (elimination of mold, mildew, and insect infestation is a tremendous side benefit), energy costs are unacceptable if the enclosure is not well sealed. Ships contain thousands of penetrations and openings where air leakage is possible. A key part of the success of DH is the use of a liquid applied polymer system installed by trained crews, which result in dramatically lower energy costs. Installation costs are substantially lower than trying to seal all these gaps and holes with sheet metal and caulking systems. Just as importantly, the success in making airtight seals is much higher. This polymer system yields a 30-40 mil (750-1000 nm) high strength, tear resistant, seamless membrane. This system has the ability to span or bridge over large openings and gaps, as well as minor crevices. Exterior durability is excellent. The system offers a very low perm rating, high tensile and mechanical strengths, good adhesion to substrates, and high UV resistance. It is extremely tough, yet easily removed without damage to painted surfaces when necessary for partial or complete operational requirements. Resealing after opening is relatively easy. Where a very high adhesion factor is necessary, a simple brush or spray applied primer assures high adhesion values .

MARAD and other organizations require a pressure test of vessels, where the volume is pressurized slightly, then held for several hours. This system can meets the specifications, assuring low utility costs.

In the recent past larger use has been made of PVC clad steel framed relocatable buildings. These are erected on the top deck of ships, withstanding ice, rain and storms. They are also placed in cargo holds for specific area containment. Others have been erected inside warehouses for limited space DH. These clad structures offer fast, simple covered space with emphasis on quality and durability. Spans range from 10 feet (3.3 meters) to over 200' (*** meters). If a total structure is not needed, custom fit bags or drop shrouds can be tailored to the application. The membrane can be very effectively sealed to prevent moisture entering, and ground sheets can easily be welded into the sidewalls to prevent rising moisture. They offer excellent reuse capability, making them even more economical.

This DH/PSS system is currently being used on many of the pre position ships now in service. It is widely used in other marine, military and commercial preservation projects.

VCI Technology

VCI's take up where DH is difficult to use or not practical. While DH is an excellent technology, there are many situations where it may not be the best or most economical choice. Typical examples are isolated pumps, motors, and other equipment which need protection, but are not close to the main DH area, or where power is not available. Long runs of ductwork to isolated locations are not cost efficient. In the past smaller motors and pumps have not been protected, as providing DH was not practical. VCI technology can protect even fractional HP motors at nominal cost. Isolated piping runs now can have VCI protection. With increasing concerns on cost, these options must be investigated. In the case of these small pieces of equipment, or small diameter pipe, the material cost is not substantial, but when removal and replacement labor is included, the cost is a major consideration. A $50 pump now is a $500 replacement expense!

The original VCI technology was introduced by Shell Chemical during WWII as VPI—Vapor Phase Inhibitor. VCI protection is simple—a corrosion inhibitor with moderate vapor pressure is introduced to an environment which needs corrosion protection. The vapors deposit on the metal surfaces at 1-2 molecules thick, penetrating even the smallest crevices and orifices. Protection remains as long as the concentration of inhibitor is sufficient. This protection occurs even in the presence of high levels of moisture or other corrosive gases such as sulfur dioxide, carbon dioxide, and even in chlorine environments. Early uses of VPI powder included placing the powder in equipment, saturating paper with VPI and using it as wrapping, and treating cardboard tubes with VPI for placement in gun barrels. Protection was excellent—as long as the metal was carbon steel. However, brass, copper and other non-ferrous metals were not protected, or even worse, were sometimes damaged by contact with VPI.

In the last 20 years, a lot of time, money, and energy was expended investigating and refining this technology, with the goal of eliminating the negatives. This work resulted in the discovery of a new class of modern VCI's. These materials are effective on most metals, ferrous and non-ferrous. More importantly, they are environmentally friendly, and of low toxicity—about the same as table salt. Modern VCI technology does not use nitrite, phosphate, chromate or other toxic inhibitors which were used frequently in the past.

		Oral ld-50*
TOXICITY:	Older "Nitrite" VPI/VCI:	284
	Newer VCI	2500
	Table salt	3000
	Sodium Chromate	150

*Milligrams of chemical/Kilogram of body weight, fed to a population of rats, which will kill 50% of the population.

Basic VCI powders solved some corrosion problems, but uses were limited. In many applications, freely dusting powder in the environment was not desirable. A variety of delivery systems were developed to address other specific requirements and to expand the "envelop" of effective uses.

VCI DEVICES AND POUCHES:

Corrosion protection of electronics and electrical equipment is extremely difficult with normal technology. Plating, metallurgy, and protective enclosures are used with varying degrees of success. VCI's provide protection simply and inexpensively. VCI's are impregnated in foam or packaged as a powder in plastic cups or packets (commercially called "devices, emitters, vaporizers") with a permeable membrane. After removing from the sealed package, the unit is placed in control panels, junction boxes, and equipment where the inhibitor vapors saturate the atmosphere (at very low concentrations—there is no fire, explosion, or health hazard). Vaporizers for electrical panels are often called "stick ups", because they have an adhesive film used for mounting. On initial opening of equipment a slight odor may be noticed, but it is not obnoxious or hazardous. The inhibitor deposits on the surface at 1-2 molecules thick, forming a protective chem-adsorbed layer which stops or slows corrosion substantially. Surface electrical functions are not affected. The inhibitor is effective on iron, steel, copper, brass, silver, cadmium, aluminum, and other metals used in modern electronic and electrical equipment. Active protection is for at least a year, even in harsh marine and chemical environments.

Service life is greatly extended for electrical and electronic equipment. Dr. Vasanth of NSWC ran an evaluation several years ago on radar diode assemblies, and found a substantial reduction of corrosion compared to unprotected assemblies. The test was terminated early, and specifications written to start protecting working equipment immediately, rather than suffer more corrosion damage.

Packets are added to packaging for protection of the MK19 Grenade Machine Gun by the Saco Defense. They also use these packets for protection of expensive Weatherby rifles in the other portion of this facility.

Commercially these products are used for protection of computers, all types of electronics, electric control panels, ATM machines, switch gear,

machinery packaging and void protection. Protection is for both during storage as well as active use, depending on the application.

Solvent Based VCI Spray

VCI protection of electronics and electrical gear has proven to be extremely effective, both in performance and cost, especially when used in conjunction with the "stick-up's". A very light mist coat of an electrical grade VCI liquid is applied. The spray does not affect any of the electrical properties. This spray gives an initial boost of VCI concentration, resulting in even better protection. Electric winch brakes with VCI spray last years longer in marine environments. Treated power cord connectors withstand months of harsh oil rig use. Telephone company electronic circuit boards in the Venezuelan jungle last years longer when protected with the electrical spray and a VCI device. Tarnish (corrosion) of Copper and brass in marine and chemical is substantially reduced.

VCI POWDERS

VCI powders useful but limited in applications. They must be enclosed to contain the volatile inhibitors. Commercially VCI powders are used in voids in ships, structural steel box beams, straight run and fabricated pipe assemblies such as boiler tubes and heat exchanger tube bundles, and in containerized packaging. They are "fogged" into boilers, tanks, and vessels for short or long term storage. The amount used is dependent on the volume to be protected.

VCI's are now incorporated in plastic films, oil and water based inhibitor solutions, and in greases and other film forming materials. The carriers bind the inhibitor, allowing very slow release, yet help keep them at the metal surface as well. Some very interesting and very effective inhibitor corrosion protection systems are now being used commercially with excellent results.

VCI Plastic film

VCI is added during the blowing or extrusion process of plastic film manufacture. A VCI masterbatch is blended with polyethylene or polypropylene resin, and "blown" or extruded to the gauge and width desired. The film is used as packaging around sensitive equipment. VCI's slowly release from the film, saturating the interior. If the volume is large, additional VCI protection is incorporated using foam, packets, or sprays. Export packers use these methods with excellent results. Packaged cost is much less compared to vacuum or desiccant methods.

Easy to use Zip-Lock® or heat seal bags are commonly used to protect spare parts, nuts, bolts, fasteners, small assemblies, tools, and even complete small arms. There is no messy and time consuming cleaning required—parts are ready to use; oil, grease and corrosion free!

The primary advantage (besides lower cost) over vacuum packaging or desiccant pouches use is that if the barrier film is punctured, protection still exists. Desiccants absorb only so much moisture, then release the excess. Chlorides may be present. Corrosion can result.

Water and oil based VCI's

Water and oil based carriers are used for short to medium term protection where products being stored are sheltered from direct rain and sun. The part is dipped in the liquid, or sprayed with the VCI solution. High humidity, marine salts, and chemicals may be present. Higher molecular weight inhibitors are used which do not volatilize so readily.

One product, water based, is used by Avondale shipyards on steel pipe. The inhibitor protects against corrosion during fabrication, which may last for months. Welds are treated for rust protection. Removal after fabrication, if necessary, is by water wash or abrasive blasting

Oil based VCI's are used either for surface protection; or for interiors of crankcases, gear boxes, and hydraulics. Both the liquid immersed phase and vapor phase are protected. It is important to confirm that the carrier oil is compatible with the lubricant system in use. Removal often is not necessary prior to start up of the equipment.

VCI films, liquid applied (TPC-Temporary Protective Coatings)

Liquid VCI films are classed as soft, hard; temporary and permanent. Soft films leave a thick oily surface. Hard films range from firm, waxy to very hard. Permanent films have more paint like properties, yet incorporate the extreme effectiveness of VCI inhibitor technology. These are similar to MIL C 16173 temporary coatings, except the VCI component increases protective abilities.

A newer water based film similar to MIL 16173, Grade 1 (temporary, removable) was evaluated by Dr. Vasanth and found to be very effective in marine usage. A time proven product is a solvent based version, meeting the requirements this grade. In addition to protecting bare steel, TPC's are effective as an overcoat for painted surfaces when additional protection during shipping and storage is desired. A number of automotive and farm implement companies find this reduces corrosion damage is reduced during storage and export shipping. The small nicks, sharp edges with only a thin paint coat, hinges, and unprotected metal overlap areas often fail and start rusting during storage and shipping. The area involved is small, but the rust stained appearance when received is unacceptable. This overcoat virtually eliminates the problem. (If used, a check must be made to assure that the temporary film does not discolor the paint—this happened on a trial shipment with a Grade 2 type product).

Other successful uses are on winches, wire rope (saturate the wire rope—life is extended several-fold), chains, flanged pipe joints, nuts, bolts, and spare parts. Protection of flanged, bolted connections is almost impossible. With this VCI soft, waxy film product, protection is obtained as it even penetrates substantial amounts of pack rust. New bolts, nuts and flanges should be coated prior to bolting the system together, or while repairs are made. Offshore oil rigs protected with these products have been reactivated after 5 years or longer with minimal observed corrosion damage.

A very effective VCI-epoxy combination solves one serious problem—protection of salt contaminated, rusty steel. Most paint systems, even high cost epoxies, do not perform well on salt contaminated steel. This VCI-epoxy has performed extremely well when applied over damp, salty, corroded steel in warm marine environments. One or two coats gives years of service. Most coatings fail within weeks when applied under these conditions. One valuable feature is that the coating remains flexible for years—it does not embrittle with age. The aluminum version takes years of UV weathering with minimal effect. This product has been successfully used for ballast tanks as a 3-5 mil (75-125 nm) one coat, 3-5 year protection system over pressure washed rusted steel. VCI epoxy coated pumps, pipe and structural steel immersed in salt or waste water last far longer compared to those protected with standard epoxy systems. The VCI epoxy is tolerant of moisture, and is ideal for tidal zone applications.

CONCLUSION

Protection of modern complex equipment and machinery under storage conditions is difficult, but by using a combination of dry air and environmentally friendly VCI's, safe, long term protection can be achieved under field conditions at reasonable cost. Long term industrial use confirms the effectiveness of these systems. The technology is here.

A Recent Innovation in Corrosion Control for Electronics

Barry L. Rudman
Cortec Corporation
4119 White Bear Parkway
St. Paul, MN 55110
e-mail: info@Cortecvci.com

Christophe Chandler
Cortec Corporation
4119 White Bear Parkway
St. Paul, MN 55110
e-mail: info@Cortecvci.com

Bill Westerfield
NAVSEADET PERA-CV
1305 Ironsides
Bremerton, WA 98310-4924
e-mail:Westerfield@perasmtp.navy.mil

INTRODUCTION

Packaging materials for the electronics industry have become very specialized. There are static dissipative materials, static shielding materials and conductive materials to name a few. The choice amongst materials typically involves balancing several factors, such as the cost of materials, the cost of the components, and the sensitivity of the components to be packaged.

Typically corrosion protection is sacrificed in favor of protection from electrostatic discharge (ESD). If corrosion and ESD protection was desired the choice has been to use a metallizded static dissipative barrier bag with a desiccant. This option was usually very expensive and had several drawbacks. A main disadvantage was that these types of films are not transparent.

It was therefore desired to develop a new packaging material that was transparent and offered both corrosion and ESD protection. This new material was not to be a compromise between the two types of protection, but rather a combination of the best of both materials.

BACKGROUND

The principle of electrostatic dissipative films is quite well known. It is desired to increase the surface conductivity of the film. This can be accomplished by one of two means: bulk treatment or surface treatment. For bulk treatment an additive is mixed with the resin used to make the film. This additive increases the conductivity of the surface of the film. In surface treatment the

film is made first, and then the surface is treated in a manner that increases the conductivity of the films surface. Increasing the conductivity allows localized charges to be dissipated.

Electrostatic dissipative packaging is not new to the electronics industry. There have long been demands for packaging materials with increased conductivities. The use of these materials proved to be of great advantage over plain packaging materials. Rejection rates were decreased. These materials, however, leave their precious contents susceptible to damage from corrosion.

There are also packaging materials that are designed to control corrosion. One group of materials employ the use of volatile corrosion inhibitors (VCIs). VCIs can be added to plastic to make films, coated on paper or corrugated to make a variety of packaging materials.

To better understand the concept of VCIs, a of review the concepts of corrosion and the means of controlling it is useful.

Corrosion is caused by an electrochemical reaction. Just as some species such as sulfur dioxide, hydrogen sulfide or chlorides can accelerate the rate of corrosion, there are also species that can slow the rate of corrosion.

The corrosion reaction requires four components , an anode, a cathode, an electrolyte and an electrical connection between the anode and the cathode.

For any given piece of metal these components are all present. Unless the metal is comprised of a single crystal, the metal serves as the anode and the cathode. Ambient moisture often plays the role of the electrolyte. Finally, there is an electrical connection because the crystals that comprise the metal are in contact and are conductive.

Corrosion inhibitors control the rate of the electrochemical reaction. A corrosion inhibitor forms a layer on the metal surface. This layer acts as a barrier to the electrolyte. This shifts the electrochemical potential of the metal in a way that makes the corrosion reaction unfavorable. This state of shifted electrochemical potential is known as passivation. In this way corrosion inhibitors slow down or stop the electrochemical reaction known as corrosion.

The principles of VCIs are rather unique. VCIs function similar to conventional inhibitors. The difference is that the inhibitor is volatile. Because the inhibitor is volatile it diffuses through the air to the metal surface. Components, therefore do not need to be in direct contact with the packaging material. This allows parts with large internal surface areas and void spaces to be protected. Making VCIs well suited for use with most packaging substrates.

To make a corrosion inhibiting film, VCIs are loaded into the resin used to make the film. This resin is then extruded to form a film.

This film can now be used to protect metal from corrosion. The process is quite simple: The VCI in the film volatilizes, filling the enclosed space with VCIs. When a metal part is placed within this package the VCIs condense onto all metal surfaces forming a thin layer. This layer

passivates the metal. This passivation protects the metal from a variety of corrosive agents such as moisture, H_2S, SO_2 and other contaminants. The VCI mechanism is illustrated in figure 1.

Conventional corrosion inhibiting packaging does not fully meet the demands of the electronics industry either. VCI materials provide excellent protection from corrosion, however, these materials do not provide the static dissipative properties required by the electronics industry.

The solution to this problem is a hybrid technology. A material that combines electrostatic dissipation properties with corrosion inhibition would be of great advantage for packaging of electronic components. The result would be a film that provides total protection to electronic components.

METHODOLOGY

To provide an objective evaluation of the performance of these materials it was desired to use established standards. It was necessary to choose test methods that would characterize the static dissipative properties as well as the corrosion inhibiting ability of the films.

The performance standards used for this study are those of the U.S. military. The static dissipative requirements were taken from military specification MIL-B-81705. The standard for VCI performance comes from military specification MIL-B-22019.

For this undertaking the effectiveness of electrostatic dissipative materials were evaluated using two requirements of MIL-B-81705. This is the U.S. military's specification for static dissipative materials.

The first test of static dissipative ability is the surface resistivity. A measurement of the surface resistivity verifies the effectiveness of the additive in increasing the conductivity of the films' surface.

The second static dissipation test is the static decay rate. This is a measure of how quickly a localized charge is dissipated. A charge is placed on a film. The time it takes for the film to dissipate this charge is then measured.

Therefore, an accurate assessment of the films' static dissipative qualities is obtained by use of these two tests.

There are very few established methods for testing the effectiveness of VCI materials. The test used in MIL-B-22019 is called the Vapor Inhibiting Ability (VIA) test.

The concept of this test is fairly straightforward. The VCI material (film, paper, etc.) is suspended inside a jar that serves as a test chamber. In this jar there is a water-glycerin solution that results in a relative humidity of 90%. There is also a metal surface inside the jar. This surface is not allowed to contact the VCI material. After a conditioning period the metal is

chilled in a manner that causes condensation to occur on the surface. For non VCI materials this condensation causes corrosion. For materials that contain an adequate amount of the VCI, the metal surface will be passivated by the VCI, preventing corrosion. This procedure is depicted in Figure 2 . Thus it is possible to evaluate the VCI properties of packaging material by use of the VIA test method.

EXPERIMENTAL

Static Decay Rate

The static decay rate was tested in accordance with Federal Standard 101C method 4046.

The specimens to be tested were conditioned for twenty four hours in a chamber at 72 °F and 15% relative humidity.

The specimens were mounted between the electrodes using wing nuts to secure intimate contact.

The voltage output was set a 5000 volts. The switch was closed, applying 5000 volts to the sample.

The time for the charge to be reduced to 99% of the original charge was recorded.

This was performed for both positive and negative charges.

Surface Resistivity

The specimens to be tested were conditioned for twenty four hours in a chamber at 72 °F and 15% relative humidity.

The surface resistivity was measured and recorded.

VIA Test

The VCI properties were tested in accordance with Federal Standard 101 C method 4031 procedure B. This is also known as the VIA Test.

Ten milliliters of a water glycerin solution with a specific gravity of 1.076 was added to clean quart glass jars.

Plugs made using QQ-S-698 low carbon steel were polished using 240 grit silicone-carbide abrasive. The plugs were then cleaned using methanol.

The plugs were fitted into the bottom of a tube that runs through the lid for the one quart glass jar. Two one inch by six inch strips of the material to be tested were suspended from the jar lids.

The jars containing the water-glycerin solution were then sealed using these lids.

The jars were allowed to condition for a period of twenty hours.

After twenty hours water at 12 °C was poured into the tubes causing condensation on the test surface.

After three hours the lids were removed and the test surface on the steel plugs were inspected for signs of corrosion.

In addition, a control must be used. For the control, the test was run identically, except no material was suspended from the lid.

For the test to be valid there must be signs of corrosion on the control.

RESULTS

Three low density polyethylene films were tested for static dissipation and VCI performance. The first film used was a standard static dissipative film using an amide based "antistat" agent. The second film was a VCI film based on amine salts. The final film tested was a hybrid film containing the same static dissipative and VCI additives that each of the first two films contained.

The electrostatic dissipation requirements of MIL-B-81705 are simple. The surface resistivity is to be greater than or equal to $1x\ 10^5$ ohms per square but less than $1x10^{12}$ ohms per square. The static decay rate is to be less than 2 seconds.

The requirements from MIL-B-22019 is that the material must pass the VIA test. A material is considered to pass the VIA test if there is no visible sign of corrosion.

Table 1 shows the results of the static dissipative and VIA testing. The values given for the surface resistivity and static decay rates are the maximum values obtained.

The static dissipative material was found to meet the surface conductivity and the static decay rate requirements. The VCI film did not meet either requirement. The hybrid film met the requirements for the surface resistivity and static decay rate. Therefore, only the static dissipative film and the hybrid film met the static dissipation requirements of MIL-B-81705.

These same materials were also tested for VCI properties using the VIA test method. The static dissipative film was found to provide no corrosion protection. The VCI film passed the VIA test. The hybrid film also passed the VIA test and it was determined that it provides vapor phase corrosion protection. Thus the VCI and hybrid films pass the VIA test while the static dissipative film fails the VIA test.

In summary, the static dissipative film provides static dissipative qualities but no corrosion control properties. The VCI film has no static dissipative properties but provides corrosion protection. Finally the hybrid film provides both static dissipation and corrosion control.

CONCLUSIONS

Each material is limited only by its design. Each film provides the type of protection that it was intended to provide.

Static dissipative films provide only electrostatic discharge (ESD) protection. These materials are suitable for packaging applications in which ESD is a concern and corrosion is not. In applications that involve metals susceptible to corrosion, these materials are a poor choice as they offer no corrosion protection.

VCI films have been successfully used in a wide variety of industries to solve various corrosion problems, but they are not recommended for packaging of ESD sensitive materials.

The VCI/static dissipative film provides total protection. If ESD damage is a concern, the static dissipative properties accommodate this need, while the corrosion protection is not compromised. This allows sensitive components that may be damaged by ESD to be stored in an area that would otherwise not be possible due to corrosion. The VCI in the hybrid protects parts from corrosion caused by moisture and industrial pollutants. Since the VCIs in the hybrid are formulated for multimetal protection, copper, aluminum, solder, nickel, and silver are protected as well. Thus making it an ideal choice for the protection of electronic components.

References

EIA-541 June 1988,"Packaging Material Standards for ESD Sensitive Items", Electronic Industries Association, p. 2

Miksic B.A.,"Use of Vapor Phase Inhibitors for Corrosion Protection of Metal Products", April 1983

MIL-B-22019 C Amendment 2,"Barrier Materials, Transparent, Flexible, Sealable, Volatile Corrosion Inhibitor Treated", Military Specification November 1986

MIL-B-81705 C ,"Barrier Materials, Flexible, Electrostatic Protective, Heat Sealable", Military Specification January 1989

FED STD 101C,"Test Procedures for Packaging Materials", Federal Test Method Standard Method 4031, Procedure B, March 1980

Table 1. Testing Results

Material	Surface Conductivity	Static Decay Rate	VIA
Statis dissipative film	1×10^{19}	0.6	Fail
VCI Film	$>1 \times 10^{12}$	> 2	Pass
Hybrid Film	1×10^{9}	0.6	Pass

Figure 1. The VCI Mechanism

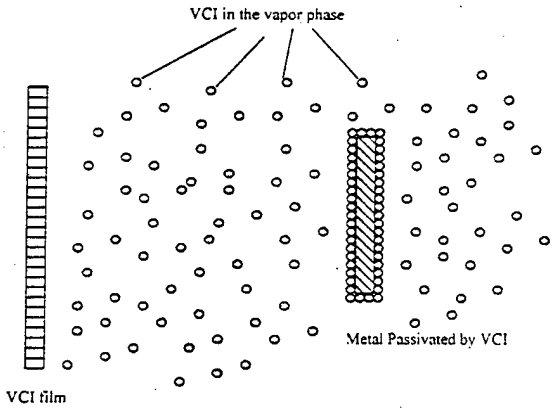

Figure 2. The VIA Test Method

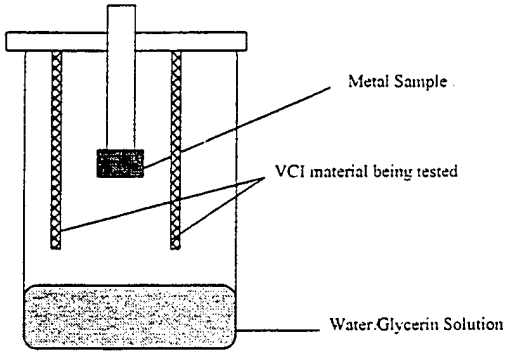

A Post-Design Corrosion Inhibition Technique for Marine Corps Light Vehicles

P.P. Trzaskoma-Paulette[1], S. G. Lambrakos[2], and H. N. Jones[2]
[1]Code 6310.2 [2]Code 6320
Materials Science and Technology Division
Naval Research Laboratory
Washington, DC 20375

ABSTRACT

Marine Corps HMMWV's (High Mobility Multipurpose Wheeled Vehicles) used in landing operations are exposed to periods of partial sea water immersion. The frame rails used in this vehicle are of a rectangular box section design and have holes on the sides which can allow entry of sea water. As originally designed no drain holes were incorporated to allow an exit point for entrapped sea water. Due in part to this design feature the frame rails are corroding on the interior surfaces at a rapid rate and the operational lifetime of this component is falling about 75% short of that originally anticipated. This is of great concern since the frame rails form the principle load bearing structure of the HMMWV. This paper discusses a proposed corrosion control method in which a closed cell polyurethane foam is injected into the frame rail interior cavity to form a barrier to sea water entry. The experiments being conducted at NRL (Naval Research Laboratory) to evaluate this and other corrosion control methods are described.

INTRODUCTION

Extensive corrosion has been observed on HMMWV's used by the Marine Corps[1]. Unlike the HMMWV's used by the Army, to whose requirements this vehicle was originally designed, those in Marine Corps service have been operated and stored in marine environments which involve exposure to sea water and high humidity with the consequent accelerated corrosion attack. The corrosion problem has been found to be particularly severe on the frame of the vehicle which consists of two parallel rectangular box section rails joined together by bolted-on crossmembers. While the use of box section frame rails is an excellent design feature for increased torsional rigidity of the vehicle it is not particularly desirable from a corrosion control standpoint. Because of the limited access to the interior surfaces the application of corrosion control methods such as some commercially available rust preventive compounds is difficult and of doubtful utility, particularly when the interior surfaces have already suffered some corrosion[2]. At the present time the only available solution involves removal and replacement of corrosion damaged frame rails. Frame rail replacement costs, however, are between $5000 and $7000 per vehicle. The I MEF (First Marine Expeditionary Force, Camp Pendleton, California) estimates corrosion related repairs for this and other components of HMMWV's are between $700-$900 thousand dollars per year for their vehicles[3].

The use of hot dip zinc galvanizing could significantly extend frame rail service life and is the corrosion control method of choice for boat trailers and other vehicles that are exposed to periodic salt water immersion. This approach is presently being evaluated by the Carderock Division of the Naval Surface Warfare Center and would be suitable for application during new vehicle manufacture, or for replacement of corrosion damaged frame rails during major overhauls, but is not an option for existing frame rails which already have suffered some limited degree of corrosion damage[2,4]. Corrosion control measures for existing frame rails such as the drilling of drain holes, coating the interior surfaces with commercial "rustproofing" compounds, and fresh water wash downs after sea water exposure have been only partially effective. One possible solution to the problem, at least for some of the over 17,000 vehicles now in Marine Corps service, is to provide an effective and economical means of preventing entry of water and dirt into the internal cavity of the frame rail.

Our proposal, when the condition of existing frame rails, the problem of field application, and cost are considered, is to fill the frame rails that have not been severely damaged by corrosion with a closed cell polyurethane foam. The basic corrosion control strategy, therefore, is to block entry of the corrosive media rather than to try and protect the entire interior surface with some coating or other treatment. This corrosion control technique is very commonly used in marine architecture and steel sailboat construction where hollow spaces that would otherwise be difficult or impossible to maintain are filled with a closed cell polyurethane foam[5,6]. This approach was explored at one time during the early 1960's as a corrosion control method for automotive body applications but was abandoned because of void and shrinkage problems with the foam formulations then available[7]. In this paper we discuss the frame rail construction, the type of corrosion damage observed, the corrosion test specimens developed to emulate the observed corrosion mechanism, and the test procedures that are being used to evaluate the effectiveness of foam filling and other corrosion control methods.

FRAME RAIL MATERIAL, DESIGN, CONSTRUCTION AND CORROSION BEHAVIOR

The basic material used in the HMMWV frame rail is a 0.125 inch (3.175 mm) thick high-strength, low-alloy steel manufactured to the requirements of SAE (Society of Automotive Engineers) Recommended Practice J410, "Selection and Use of Steels". The specific grade used within this general specification, based on a metallographic and hardness tests on material sampled from a frame rail, is thought to be 950A which has a combination of good weldability and formability at a yield strength of 42-50 ksi (289-345 MPa). This yield strength is achieved by creating a fine grain size during the final pass during hot rolling using carefully controlled temperatures sometimes in combination with small alloy additions such as niobium or vanadium[8]. The rectangular frame rail box section is fabricated from two cold formed channel sections welded together as shown in Fig. 1.

The frame rail has a total of 63 holes of which 55 normally have a bolt inserted for attachment of other parts of the vehicle chassis such as the crossmembers. Each of the

holes that are bolted have tubes associated with them welded on one end inside the frame rail cavity to support the clamping loads resulting from tightening the bolts as is also shown on Fig. 1. The remaining 8 holes are not associated with a bolt and do not have any interior tubes, an example of which is shown on Fig. 2. It is these holes which can allow entry of sea water during immersion of the frame rail such as might occur when a HMMWV exits a landing craft in the surf. Because of the box section geometry there is a tendency for the entrapment of sea water and other debris inside the frame rail.

As originally designed and constructed, however, there are no drain holes on the bottom to allow the sea water to drain out. This is a rather curious design feature since the production contract for these vehicles specified sufficient corrosion control to ensure a vehicle service life of 15 years in "a corrosive military environment involving high humidity, salt spray, etc., with no perforation or corrosion damage requiring repair or replacement"[9]. An example of a corroded section from a frame rail is shown on Fig. 3 where it clearly evident that almost all the corrosion has occurred on the interior surfaces with the final perforation occurring on the bottom where the entrapped water had collected. This sample was removed from a vehicle that had been in service for a period of less than ten years. Several layers of rust debris are present and the "E-coat" paint originally applied to the frame rail when manufactured is completely gone.

A metallographic section of the overlap associated with one of the welds used to join the two channel sections that make up the box section is shown on Fig. 4. The crevice between the two pieces shows only a slight corrosive attack whereas the interior surface pointed out shows a much greater loss of thickness. In fact, on the bottom of the frame rail the only intact area is that part associated with the overlap between the two channel sections. This suggests that the presence of the crevice is not relevant to the corrosion perforation of the frame rail.

As is usually the case with carbon steels exposed to salt water, where passivating films cannot form, the crevice is the point of first attack simply because it tends to stay wetter for longer periods of time, but only temporarily[10]. The crevice soon fills with rust which serves to block further entry of the corrosive solution and attack will then proceed elsewhere. This is in contrast to stainless steels and aluminum which form a protective and tenacious oxide layer that, however, can fail under crevice corrosion conditions[11,12]. It is concluded, based on these observations, that "crevice corrosion" in the sense that it is normally used is not the corrosion mechanism responsible for perforation of the frame rails. Rather, it is caused by gross interior surface corrosion induced by the entrapment of salt water.

CORROSION TEST SPECIMEN DESIGN AND EXPERIMENTAL TECHNIQUES

Corrosion Test Specimen Design and Fabrication

One of the first objectives in corrosion engineering is the duplication of the corrosive environment in a manner which can hopefully provide an accelerated rate of attack but still remain relevant to the service conditions causing damage. Once this is accomplished the various proposed or prototype corrosion control methods can then be subjected to the duplicated environment for an evaluation of their effectiveness within a reasonable period of time. The requirement of both accelerated attack and duplication of the corrosion mechanism were the primary considerations in the development of the corrosion test specimens discussed here.

Based on the examination of the failed frame rail described above and other reports it was determined that entrapped sea water was the most probable cause of the severe interior corrosion observed. There are several potential solutions to this problem which needed to be evaluated in parallel. One of the possible corrosion control methods is to simply drill drain holes to provide an exit point for any water accumulation that might occur. In combination with drain holes one might also use one of the commercial paraffin based "rustproofing" compounds sprayed into the interior to coat the surfaces. Or, as proposed here, the interior cavity could be filled with a closed cell foam to simply prevent entry of sea water.

To design a corrosion test specimen that would be useful for evaluating the effectiveness of the various corrosion control methods available required that both the intrinsic corrosion behavior of the steel and those aspects of the frame rail geometry germane to the corrosion problem be duplicated. Based on the metallographic examination of a weld and the associated overlap region from a failed frame rail it was determined that this aspect of its construction was not important as far as corrosion was concerned since there was no evidence of accelerated attack in this area. ASTM A500-93 Grade B low carbon steel structural tubing having an electric resistance weld on one side was selected for fabrication of the corrosion test specimens since this material would have an intrinsic corrosion behavior very similar to that used in the frame rail. The largest available section with a 0.125 in. (3.175 mm) wall thickness was 4 in. (101.6 mm) square structural tubing and this was cut into 2 ft. (0.61 m) lengths for the corrosion test specimens. This structural tubing is cold formed from hot rolled strip and as such is very similar to the frame rail material. The primary difference between the material used in the frame rail and that used in the corrosion test specimens is the grain size which does not affect the intrinsic corrosion behavior of the two materials.

The majority of the test specimens were painted on the outside with a metal primer and a urethane alkyd enamel to focus corrosion on the interior surfaces as is observed to be the case with the actual frame rails. Half of these were precorroded by a two week exposure inside a salt spray chamber (ASTM B-117). The specimens were rotated at intervals to insure a fairly consistent corrosion layer on all the interior surfaces.

These samples were used to evaluate the effectiveness of corrosion control measures on frame rails that have already been partially corroded in service. For some of the corrosion test specimens a 0.5 in. (12.7 mm) hole was drilled into the bottom to allow drainage. This was done to emulate frame rails using this corrosion control technique. The ends of the specimens were covered with duct tape to prevent a rapid dry out and to allow a condition of high humidity to persist since a shallow layer of salt water would be retained for some time after draining. A small hole was cut into the top of the taped over end to allow visual inspection of the interior surfaces. Test specimens for duplicating the entrapped water condition were similarly constructed using duct tape to cover the ends with a small hole on top to allow inspection and some ventilation.

Ten of the corrosion test specimens were taken to a commercial rust proofing firm for application of their corrosion control materials. Five of these specimens had the as manufactured surface which has a thin layer of mill scale. These were given an interior coating of a paraffin base material and is typical of the materials that would be used if the Marine Corps rustproofing procedures were followed[13]. The other five had been precorroded in a salt spray chamber and were given a two step treatment. The first part of the treatment was to stabilize the existing corrosion with a proprietary "rust eliminator" compound that reacted with the iron oxide to form a more stable compound. This was then given a coating of the paraffin based material.

As an initial evaluation of the foam fill corrosion control method a one part polymeric diisocyanate, polyol resin mixture was chosen as the filler. The primary advantage of this product was its low cost and ready availability. Additionally, since it was already packaged in a pressurized container with a plastic tube extension for application it could be injected into hollow cavities with ease. This foam formulation has excellent expansion characteristics and exhibits a strong adhesion to metal surfaces. On the surfaces exposed to air a dense "skin over" effect was observed to form. Depending on the amount of foam injected into the tube there would in some cases be an extrusion of material out of the ends. Sections cut from this extruded material and other samples of the single part foam showed that the interior cell structure was not uniform and would sometimes have large voids as shown on Fig. 5. Since this was a curing characteristic of the single part polyurethane foam that might affect the corrosion performance some specimens were prepared to evaluate this.

Foam was applied to tubes having interior surface conditions in the as-received state, the as-received with a paraffin coating, the salt spray corroded state, and the salt spray corroded state treated with the "rust eliminator" and the paraffin coating. Since a crucial aspect of the foam filling technique is the adherence of the foam to the interior surfaces these conditions needed to be evaluated. As was found in earlier investigations using this method if the foam pulled away from the interior surfaces it would not provide any protection. Trials with a two part foam formulation have also been conducted as this material has better curing characteristics inside closed spaces exhibiting a more uniform cell structure.

Four 15 inch (0.38 m) sections were cut from a new frame rail obtained from the HMMWV manufacturer, A. M. General. The location in the frame rail these specimens were removed from is the same area where the corrosion perforation is occurring in service. One of these sections was prepared by drilling a hole in the bottom and taping over the ends to evaluate the effectiveness of drain holes. Another was prepared to duplicate the entrapped sea water condition. The other two had the single part foam injected into their interiors.

Experimental Methods

Three basic exposure conditions were chosen for evaluation of the corrosion behavior of the steel tubes used to emulate the frame rail. These were periodic immersion in sea water, continuous immersion in sea water, and entrapped sea water. Of these three corrosive environments only two, the periodic immersion and the entrapped water conditions, were directly relevant to the service conditions encountered by the HMMWV. The continuous immersion condition was chosen to create a very adverse environment for some of the foam filled tubes in order to accelerate water penetration into the foam and the foam/metal interface. Artificial sea water was prepared by mixing a sea salt substitute with tap water to the required specific gravity. Polyethylene plastic tubs were used as containers for the saltwater and the test specimens. An example of a test is shown on Fig. 6 where the corrosion test specimens are supported above the tub to collect the sea water draining from them.

The periodic immersion test is used to evaluate the test specimens that have some provision for draining the sea water. These are immersed approximately every three days. During the three day interval inspection of the interior showed that it remained wet at the bottom for most of the time.

CURRENT EXPERIMENTAL RESULTS

The conditions of the test specimens as of 28 July 1997 are reported below. The interior surface condition of some of the foam filled specimens is not yet known since evaluation of this will require cutting open the specimens and removal of the foam which will be done upon completion of the test program.

Periodic Immersion Tests

Results of the periodic sea water immersion tests are shown in Table I. In these tests generalized corrosion of all unprotected surfaces of the test specimen interiors has progressed to the point of flaking layers of rust. An example of the interior condition of a test specimen with no interior coatings after 57 immersion cycles is shown on Fig. 7. The area of greatest attack is the bottom surface of the interior which tends to remain wet longer than the top and sides. This is very similar to the damage observed in the frame rails and is an important observation since it suggests that the presence of drain holes might not be an effective corrosion control method in the absence of good protective coatings on the interior surfaces.

Continuous Immersion Tests

The results of the continuous immersion tests in salt water are shown in Table II. Some of the foam filled specimens show that the there is some water penetration through the skinned over surface. Two of the foam filled specimens that initially displaced sufficient water to float have now, after about five months, sunk. The rate of water pickup, however, is extremely slow and should not be a problem with the relatively short immersion periods involved in landing operations. For the specimens with the foam cut to expose the cells it is observed that water is eventually transported through the larger cavities. Whether the water will reach the foam/steel interface and cause either debonding or corrosion will be determined by cutting the specimens open to allow inspection of the surfaces after about seven months of immersion. While the exposed steel rusts on the partially filled test specimens, there is very little evidence of water penetration at the interface once again demonstrating strong foam/metal bonding.

For specimens coated on the interior surfaces with a paraffin based corrosion prevention material the foam has pulled away from the walls as shown on Fig. 8. This observation indicates that the presence of rustproofing compounds prevents adhesion of the foam to the interior surfaces. Despite this lack of adhesion, the paraffin coating still provides some protection.

Entrapped Sea Water Tests

The status of the entrapped water tests, used to simulate conditions encountered with frame rails in existing HMMWV's that have not been provided with drain holes, are shown in Table III. Inspection of test specimens having untreated (as manufactured) interior surfaces shows extensive red flaking corrosion product on the sides and top surfaces with a black corrosion product on the sea water covered bottom surface. In general, the black corrosion product forms when oxygen access is limited. The fact that the top and side surfaces of this specimen show greater deterioration than that of the bottom indicates that corrosion rates are highest in areas that remain moist but have a shorter diffusion path for oxygen. Entrapped water actually acts to retard corrosion rates on the submerged surface by limiting oxygen access but also provides moisture to support higher corrosion rates just above the water line where there is more available oxygen. This is in contrast to the damage observed in frame rail where it is the bottom surface that shows the greatest attack. In service, the entrapped sea water is aerated during vehicle movement whereas for these corrosion test specimens the environment is more stagnant.

After a five month exposure, samples with the commercial rust-treatment coating show little apparent corrosion in the entrapped sea water tests. The precorroded sample that had been subjected to the two step rustproofing process has started to show some corrosion, however. These observation indicate that commercial rust-proofing does provide some protection from sea water in the short term, but only if it is applied before any interior corrosion has occurred.

Field tests

As a further evaluation of the feasibility of this corrosion control method a field test was initiated on 18 July 1997 with the I MEF at Camp Pendleton, California. Two HMMWV's had foam injected into their frame rails to prevent entry of sea water. This trial also evaluated the difficulty of applying this material to existing vehicles with the facilities that would normally be available to the Marine Corps. Based on this test it has been determined that the one part polymeric diisocyanate, polyol resin mixture is the most appropriate form for field installation outside of major maintenance depots despite the less than optimum curing characteristics. The two part systems, with their more uniform cell morphology, would be more appropriate for application during vehicle manufacture, or during a major rebuild at a maintenance depot.

CONCLUSIONS

The test results so far indicate that the foam filling technique has shown some promise in controlling the interior corrosion problem in the HMMWV frame rails. It has been determined, however, that the presence of any rustproofing materials on the interior surfaces will prevent adherence of the foam, and hence it would not be an effective corrosion control method for frame rails that had already been rustproofed according to the procedures in USMC TM 3080-34[13]. Surprisingly, it was observed that the presence of drain holes did not prevent extensive interior corrosion when there was frequent salt water immersion. Additionally, the use of a paraffin based coating on the interior surfaces of uncorroded frame rails also appears to be effective, at least for the exposure times involved with the tests reported here. However, our tests also indicate that rustproofing of frame rails that have already suffered some corrosion is not likely to be effective.

ACKNOWLEDGMENTS

This work was supported by the Office of Naval Research NSAP program. The authors would like to thank the I MEF science advisor, Chuck Francis and maintenance personnel for their technical guidance and Ms. Julie Jacks, Marine Corps Syscom, and Mr. Brad Bieberich, NSWC Carderock Division for their helpful discussions during the course of this investigation.

REFERENCES

1. E. B. Bierberich, T. J. Jackovic and R. M. Janeczko, "Corrosion of combat and Tactical Equipment on US Marine Corps Bases: Survey Results, Logistics and R&D", CARDIVNSWC-TR-61-94/19, pp. 7-8, October 1994.

2. E. B. Bierberich, T. J. Jackovic and R. M. Janeczko, "Corrosion of US Marine Corps Combat and Tactical Equipment: Evaluation of New Materials, Corrosion Prevention and Design", CARDIVNSWC-TR-61-95/24, p. 33, December 1995.

3. Private Communication, Letter from Commanding General, I MEF To Director, Naval Science Assistance Program, 30 Jan 1996.

4. E. B. Bieberich, R. M. Janeczko, and A. D. Sheetz, "Corrosion of US Marine Corps Combat and Tactical Equipment: Status of FY96 R&D Tasks", CARDIVNSWC-TR-61-96-14, pp. 68-70, March 1997.

5. "Handbook of Foamed Plastics", R. J. Bender, ed., Lake Publiushing Corp., p. 165, 1965.

6. Crusing World, pp. 78-80, November 1996.

7. "Environmental Effects on Polymeric Materials", D. V. Rosato and R. T. Schwartz, ed., Interscience Publishers, p. 738, 1968.

8. Metals Handbook, Ninth Edition, Vol. 1, American Society for Metals, Metals Park, Ohio, pp. 403-420, 1978.

9. Marine Corps Order 11240.102, "Advanced Logistics Order on Truck, Utility, TOW Carrier, w/Supplemental Armor, 1 1/4 -Ton, 4x4, High Mobility Multipurpose Wheeled Vehicle, M1045/M1046", p. 6, 4 Jun 1985.

10. Seawater Corrosion Handbook, M. Scumacher, ed., Noyes Data Corporation. Park Ridge, NJ, p. 14, 1979.

11. L .L. Shreir, "Corrosion", Vol. 1, Newness-Butterworths, Boston, MA, p.145-148, 1976.

12. R. Baboian, "Corrosion Tests and Standards, Application and Interpretation", American Society for Testing and Materials, W. Conshohocken, PA, pp. 175-176, 1995.

13. USMC TM 3080-34, "Corrosion Prevention and Control, Including Rustproofing Procedures for Tactical Vehicles and Trailers", Chapter 16, Sept. 1992.

Table I. Periodic Sea Water Immersion Tests

SPECIMEN DESCRIPTION	IMMERSION CYCLES	OBSERVATIONS
As manufactured exterior and interior surfaces, taped over ends, one 0.5 in. (12.7 mm) drain hole.	71	General corrosion with flaking reddish brown rust on exterior and interior surfaces.
Painted exterior surfaces, as manufactured interior surfaces, tape over ends, one 0.5 in. (12.7 mm) drain hole.	71	General corrosion with flaking reddish brown rust on interior surfaces.
Painted exterior surfaces, as manufactured interior surfaces coated with a paraffin based compound, taped over ends, one 0.5 in. (12.7 mm) drain hole.	57	Some corrosion around the drain hole, no evidence of interior surface corrosion.
Painted exterior surfaces, as manufactured interior surfaces coated with a paraffin based compound, partially filled with foam, taped over ends with drain holes cut in.	57	Some corrosion around drain holes cut in taped over ends.
Painted exterior surfaces, precorroded interior surfaces treated with stabilization compound and coated with paraffin material, partially filled with foam, taped over ends with drain holes cut in.	57	Rust has started to penetrate the paraffin based coating.
Painted exterior surfaces, as manufactured interior surfaces, tape over ends, one 0.5 in. (12.7 mm) drain hole.	57	Extensive interior surface corrosion is occurring, this is a control specimen.
15 in. (0.38 m) section of new frame rail, partially filled with foam, taped over ends with drain holes cut in.	33	Some corrosion is observed at the drain holes.
15 in. (0.38 m) section of new frame rail, taped over ends, one 0.5 in. (12.7 mm) drain hole.	49	Some corrosion near interior overlap or crevice. The corrosion is starting to migrate out from this location under the "E-coat" along the bottom.

TABLE II. Continuous Immersion Tests

SPECIMEN DESCRIPTION	EXPOSURE TIME	OBSERVATIONS
Painted exterior surfaces, as manufactured interior surface, filled with foam. The foam that extruded from the tube during curing has an intact "skin" .	started 1/27/97, 182 days	Specimen remains afloat but there is now some evidence of water pickup. To what extent the surfaces are corroded will be determined when the specimen is cut open at the end of the test program.
Painted exterior surfaces, precorroded interior surfaces, foam filled, exposed foam cells (skin cut).	started 2/10/97, 169 days	This specimen illustrates some of the undesirable curing characteristics of the single part foam as water has penetrated some of the cavities in the foam. Whether there is additional corrosion on the interior surfaces will be determined when it is cut open.
Painted exterior surfaces, as manufactured interior surface, partially filled with foam, intact skin.	started 2/13/97, 166 days	Interior surfaces exposed to sea water have corroded. Whether there is a rust migration along the foam/metal interface will be determined when it is cut open.
Painted exterior surfaces, precorroded interior surfaces, foam filled, exposed foam cells (skin cut).	started 2/14/97, 165 days	This specimen, despite the exposed cells at the end, had sufficient water displacement to float intially. After 55 days, however, sufficient water pick up had occurred for it to sink.
Painted exterior surfaces, as manufactured interior surfaces coated with paraffin, partially filled with foam.	started 3/4/97, 145 days	The foam has pulled away from the interior surfaces indicating that the presence of rustproofing compounds prevent adhesion of the foam.
Painted exterior surfaces, precorroded interior surfaces treated with rust stabilization compound and coated with paraffin, partially filled with foam.	started 3/4/97, 145 days	As observed above, the foam has pulled away from the interior surfaces again indicating that the presence of rustproofing compounds prevent adhesion of the foam.
Painted exterior surfaces, as manufactured interior surfaces, partially filled with foam.	started 3/4/97, 145 days	Corrosion on exposed interior surfaces, foam still adheres to steel. Control specimen for two above tests.
15 in. (0.38 m) section of new frame rail, partially filled with foam.	started 5/7/97, 82 days	Corrosion has started at the crevice

Table III. Entrapped Water Tests

SPECIMEN DESCRIPTION	EXPOSURE TIME	OBSERVATIONS
Painted exterior surfaces, precorroded interior surfaces, taped over ends, approximately 0.5 in. (12.7 mm) of sea water maintained.	started 1/23/97, 186 days	Generalized corrosion on all interior surfaces which is most intense above and at the water line. Black corrosion product in water immersed area indicates oxygen limited access.
Painted exterior surfaces, paraffin coated interior surfaces, approximately 0.5 in. (12.7 mm) of sea water maintained.	started 3/4/97, 145 days	No visible corrosion on interior surfaces
Painted exterior surfaces, as manufactured interior surfaces, approximately 0.5 in. (12.7 mm) of sea water maintained.	started 3/4/97, 145 days	Extensive corrosion on interior surfaces which is most intense at and just above the water line. Control specimen for above test.
Painted exterior surfaces, precorroded interior surfaces treated with stabilization compound and coated with paraffin, approximately 0.5 in. (12.7 mm) of sea water maintained.	started 3/4/97, 145 days	The paraffin coating is starting to be penetrated by corrosion.
Painted exterior surfaces, precorroded interior surfaces, taped over ends, approximately 0.5 in. (12.7 mm) of sea water maintained.	started 3/4/97, 145 days	Extensive corrosion on interior surfaces which is most intense at and above the water line
15 in. (0.38 m) section of new frame rail, taped over ends, approximately 0.5 in. (12.7 mm) of sea water maintained.	started 3/26/97, 123 days	Samples of the entrapped water show that interior surface corrosion has started, probably at the crevice.

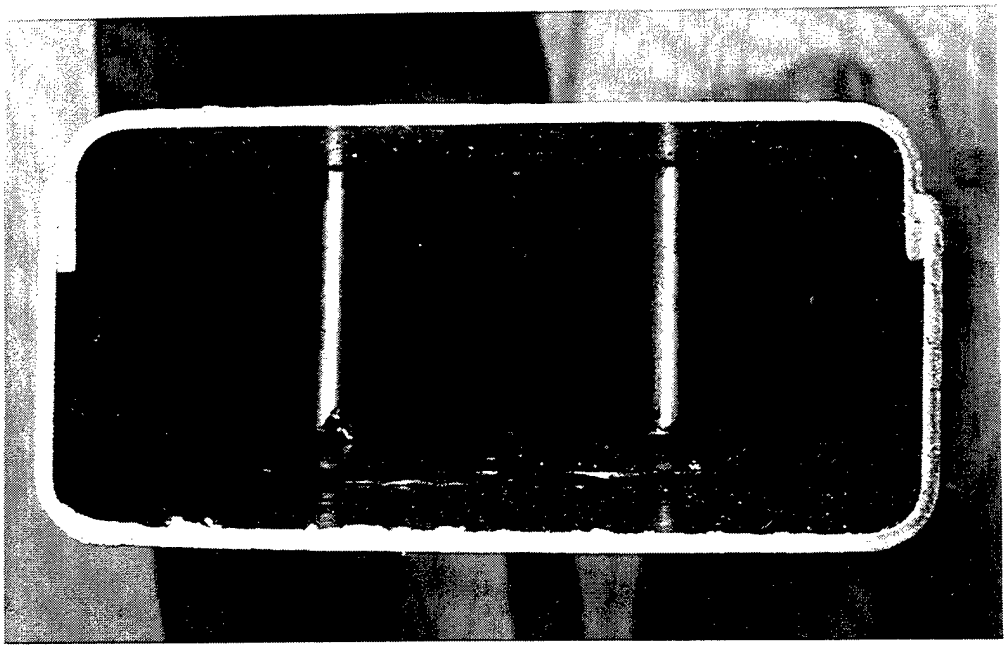

Figure 1. Photograph showing the construction of the frame rail which consists of two cold formed channels welded together with internal tubes to support the clamping loads from bolts.

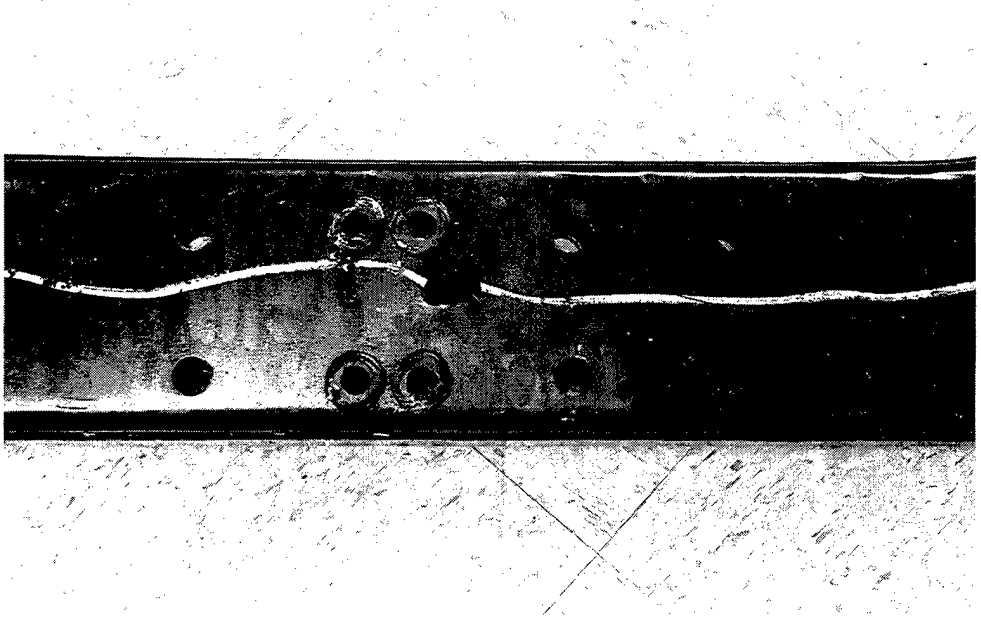

Figure 2. Photograph showing a section of the frame rail with some of the holes that allow entry of sea water.

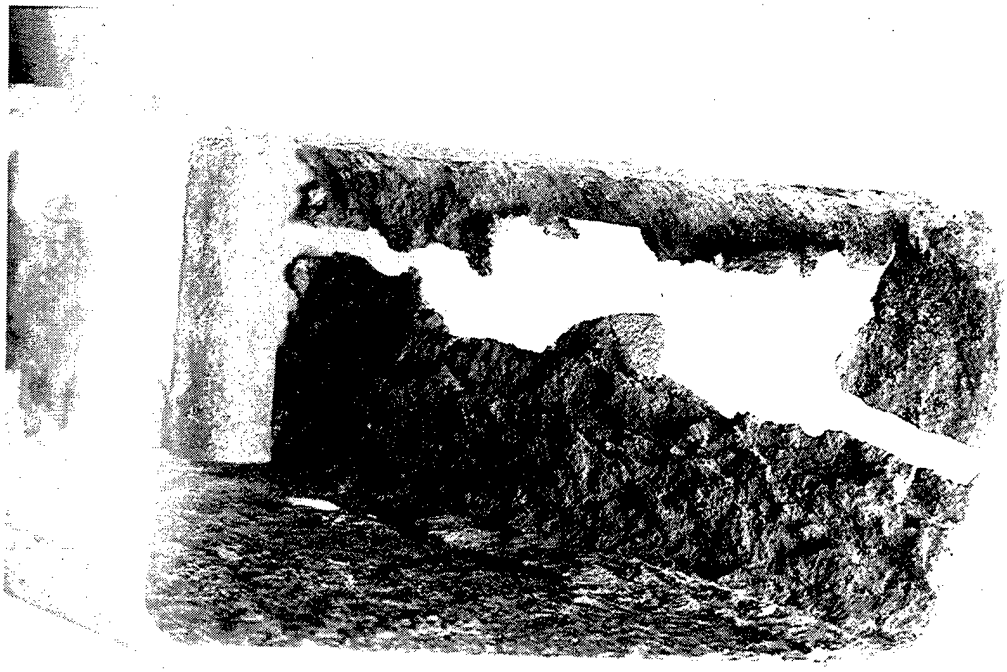

Figure 3. Photograph showing a corroded section from a frame rail. Note that the only intact area of the bottom is associated with the overlap or "crevice" region.

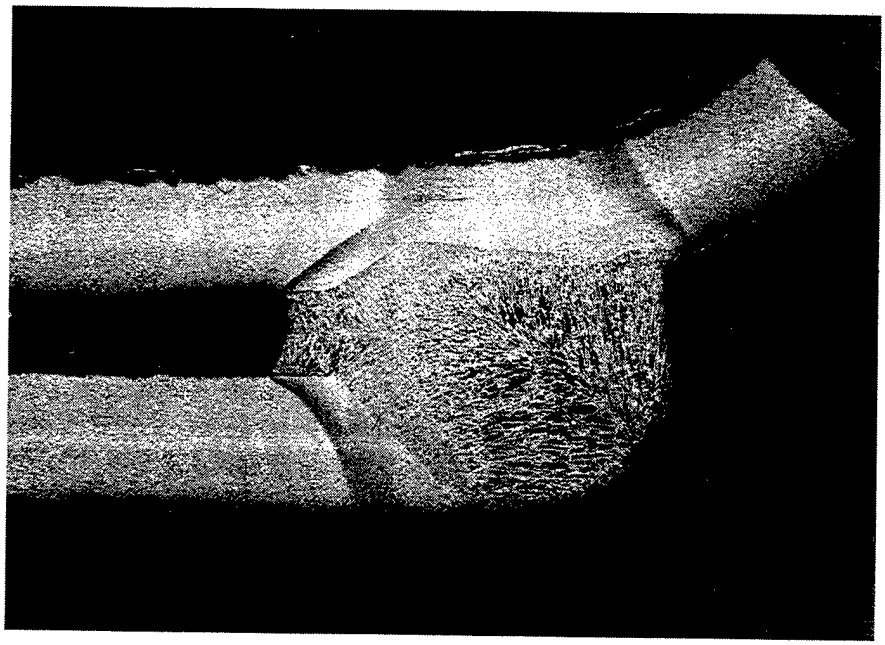

Figure 4. Photograph showing a metallographic section through the overlap area at the weld. Note that there is little corrosion inside the crevice and that most of the corrosion is on the inside surface.

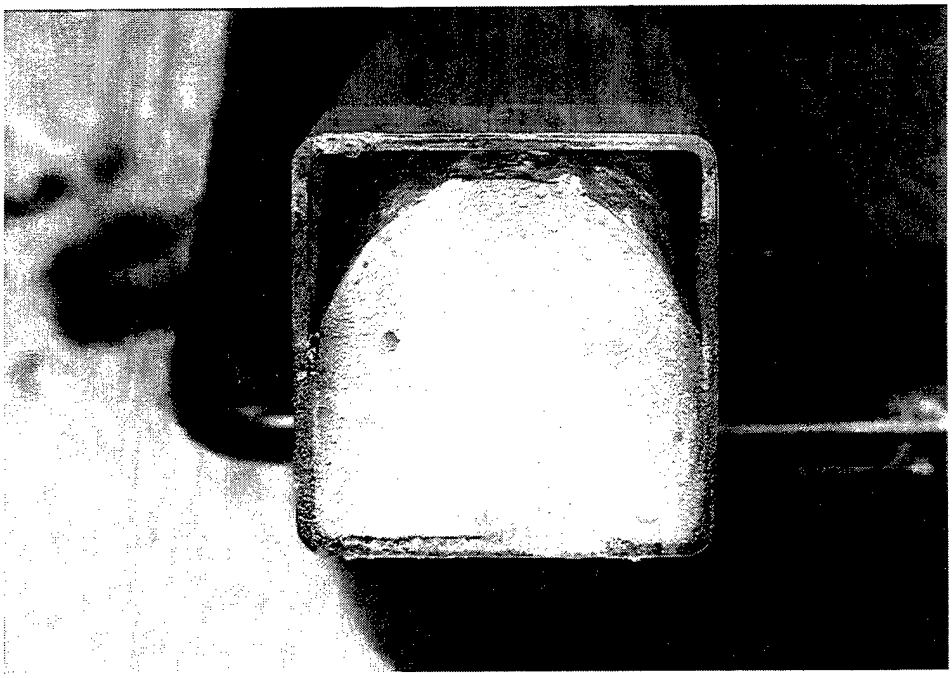

Figure 5. Photograph showing the nonuniform cell structure observed with the single part foam formulation used in most of the test specimens.

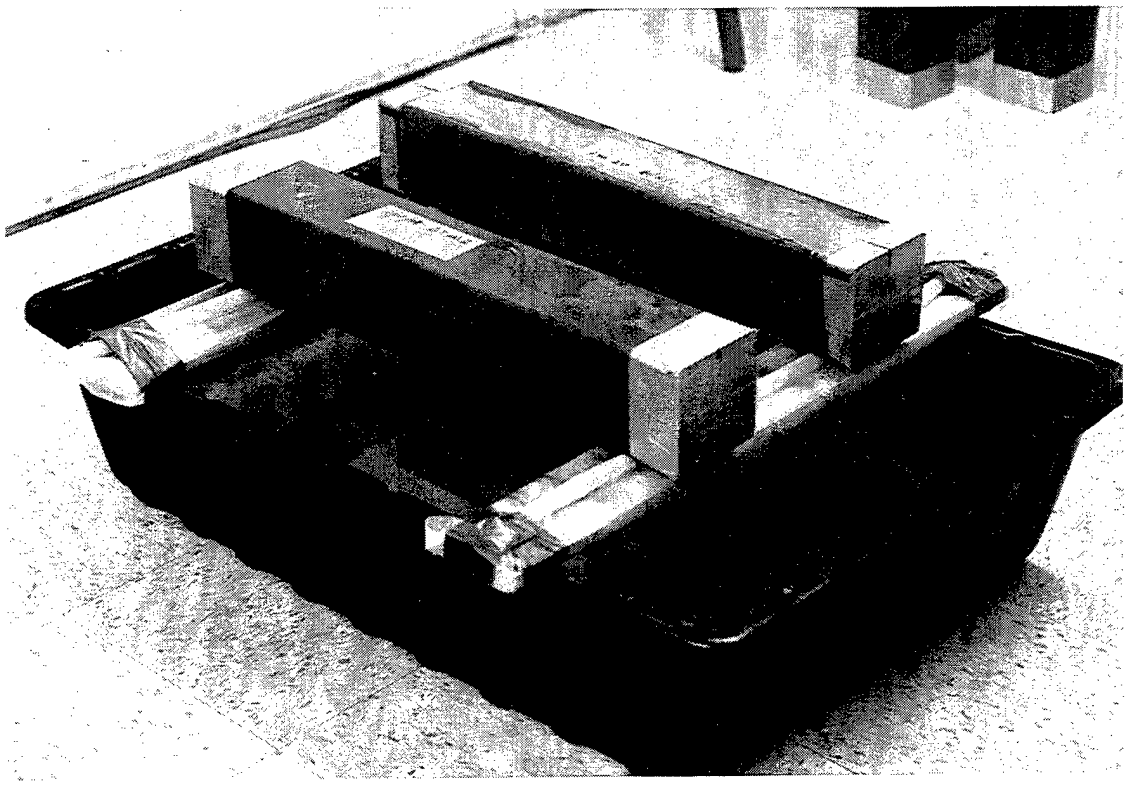

Figure 6. Photograph showing typical corrosion test specimens suspended above the tub containing the sea water.

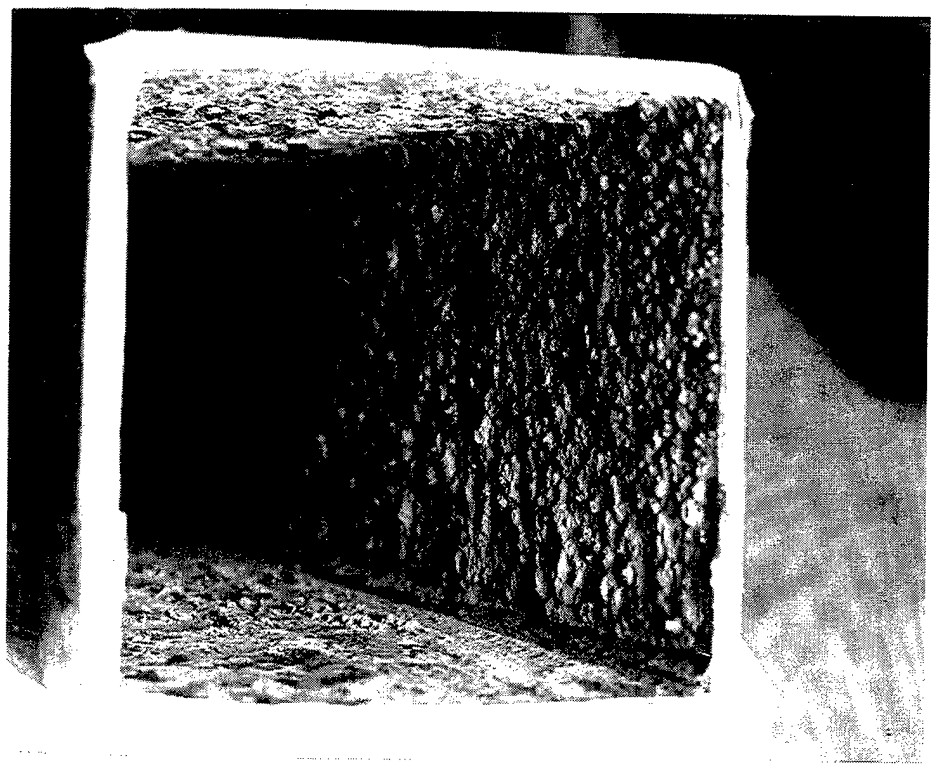

Figure 7. Photograph showing the interior surface condition of a test specimen subjected to 47 immersion cycles. Extensive corrosion is observed on all the surfaces, particularly the bottom.

Figure 8. Photograph showing the interior surfaces of a test specimen that had entrapped sea water for 140 days.

Corrosion of Mk19 Grenade Launchers in Storage

Mara Mortman and Jules F. Senske

ABSTRACT

In January 1996, approximately 35 of 150 Mk19 grenade launchers delivered to Ft. Hood, TX were determined to have corrosion problems when unpacked from their barrier bags. The majority of these weapons were stored for an extended period at depot facilities before shipment to Ft. Hood. The corrosion experienced on most of the weapons was generic in nature, except a high frequency of buffer receiver springs were cracked in one or several places upon tear down. Based on the investigation that followed, the source of chloride leading to the stress corrosion cracking of the buffer retaining springs has not been pinpointed.

INTRODUCTION

In January 1996, 35 of 150 MK19 weapons delivered to Ft. Hood, TX were determined to have corrosion-related problems upon unpacking. The majority of these weapons were manufactured between August 1992 and September 1993 and were subsequently stored for an extended period of time at Anniston Army Depot, AL before shipment to Ft. Hood. Each weapon was wrapped in volatile corrosion inhibitor (VCI) paper, placed in a cardboard box, sealed in a metalized barrier bag and stored in a wooden box. The MK19 was wrapped in VCI paper conforming to Mil-P-3420F, Class 1, Style C, Form a. The Mk19 feed throat was stored in a separate clear sealed plastic bag and wrapped in VCI paper, this paper was manufactured in accordance to Mil-P-3420F, Class 1, Style A, Form b.

Upon disassembly of the weapons at their initial production facility for refurbishment in June 1996, corrosion was observed on the following components: belleville washers, barrels, firing pin mechanisms, muzzle protectors, buffer receiver assemblies and feed throats. The corrosion on these components appeared to be general in nature, however, upon tear down of the buffer receiver assemblies, at least four of the buffer receiver springs were broken into two or more pieces.

Three of the spring fragments, shown in Figure 1, were submitted for a failure analysis and material characterization investigation to determine the mode of failure and verify that all

metallurgical properties were consistent with specifications. It was also of interest to verify whether the corrosion was traceable to the use of the two VCI papers.

PROCEDURE

The spring fragments were analyzed using several metallurgical techniques. First, each spring was visually examined and photographed. Next, an elemental analysis was performed on the residue covering the exterior surface of the springs. After this was completed, the residue was stripped from the spring using a solution consisting of hydrochloric acid, water and hexamethylene tetramine. The underlying fracture surfaces were then analyzed using a Scanning Electron Microscope (SEM). After this was completed, specimens were sectioned from each of the spring fragments. These specimens were mounted, prepared and examined to analyze the composition, hardness and microstructure of the spring material. Lastly, a silver nitrate precipitation test was conducted to determine the presence of halides in the VCI paper.

RESULTS

Representative results from the visual analysis are presented in Figures 1 and 2. These images show the as-received condition of the spring fragments. All fragments were covered with a residue, which was black/brown in color. It was not possible to discern any other features due to the thickness of the residue.

The fracture surfaces of the spring fragments were examined in both the as-received and cleaned condition using the SEM. Representative results from the as-received SEM analysis are presented in Figure 3 and indicate that the fracture surfaces were completely obscured by the black/brown residue. No features were visible in this condition. Representative results from the SEM analysis of the fracture surface in the cleaned condition are presented in Figure 4. These images show the intergranular fracture mode observed on the spring fragments. No precise initiation site was observed.

Representative results from the Energy Dispersive X-ray Spectroscopy (EDS) analysis of the as-received spring fragments are shown in Figure 5. The data contained in this spectrum confirms that the elemental breakdown of the spring residue was as follows: Fe, Mn, Cr, Si, and Cl. With the exception of chlorine, all the elements were attributed to the underlying steel used in the manufacture of the spring and were not considered unusual. In contrast, the presence of chlorine was considered unusual in that chlorine in the form of chlorides has been associated with stress corrosion cracking (SCC) in higher strength steels, should all the proper conditions occur. Although EDS cannot detect exact elemental compounds, the detection of chlorine frequently signifies the presence of chlorides.

Representative results from the semi-quantitative chemical analysis of the spring material are presented in Figure 6. This analysis was performed using the SEM in conjunction with EDS and the Leco carbon-sulfur analyzer. Results indicate that the spring material was consistent with a 9254 grade steel as specified per ASTM A401.

Diamond pyramid microhardness (DPH) measurements were also taken on the spring samples. Results indicated that the average hardness of the spring material was 610.5 DPH, which is approximately 55.5 Rockwell C scale (Rc). These data are provided for informational purposes only since no hardness requirement exists on the spring technical drawing or the associated specifications (Mil-S-13572, ASTM A401, and Mil-C-16173). Note that the hardness of the spring material is well above the 38 Rc minimum often considered to define high strength steel.

Representative results from the microstructural analysis of the spring material are presented in Figure 7. The microstructures were examined after etching with a nital solution. These images show a microstructure consisting of a very fine martensite, which was considered normal.

It was also of interest to determine whether the VCI paper was the source of the chlorine containing corrosive agent. Thus a test with silver nitrate was conducted to determine whether chlorides and other halides were present in the VCI papers used on both the MK19 and feed throat. For this test, a specimen of each of the two different VCI papers was dipped in 200 ml of deionized water for 28 hours. At the end of the 28-hour time period the paper was removed from each water solution, and a small amount of crystalline silver nitrate was added to the deionized water solution. The solutions were then observed for the development of any precipitates. The solution from the VCI paper which had been used to wrap the feed throat immediately became cloudy and in a short period of time white precipitates were present. The solution from the VCI paper used to wrap the MK19 weapon showed no evidence of any precipitates over time. Based on this qualitative test, and in conjunction with the EDS analysis it appears that chlorides were present in one of the two VCI papers used in the packaging of the MK19, however not in the VCI paper in the immediate vicinity of the MK19 weapon or it buffer receiver springs.

For stress corrosion cracking (SCC) to occur, a certain set of conditions must be present. These criteria include a susceptible material, a corrosive agent, and a component under a constant applied stress and time. All of these conditions were present in this particular situation. The susceptible material was the high strength steel, a chlorine containing corrosive agent was present in the residue found on the fractured springs, and the springs were stored in a stressed condition within the weapon for approximately three years. Note that SCC will normally have an intergranular fracture surface associated with it as occurred in this instance on the springs, and usually an applied tensile stress, which did not appear to be the case in this instance.

The exact source of the chlorine on the buffer receiver springs is still unclear, in that the silver nitrate test was not positive for both samples tested. Since the VCI paper which did have positive

results in the silver nitrate test was enclosed in a sealed plastic bag, it is unlikely that the chlorides passed through the bag, through the other VCI paper and to the buffer receiver springs.

CONCLUSION

Based on the data generated in this analysis, failure of the MK19 buffer receiver springs was due to stress corrosion cracking. This conclusion is supported by the intergranular fracture mode and chlorine containing residue present on the fracture surfaces of the springs. It is additionally supported by the presence of all the necessary criteria for stress corrosion cracking which include a susceptible material (9254 high strength steel), a corrosive agent (chlorides), a constant applied stress, and time under these conditions (approximately three years in storage at Anniston Army Depot). The result of the silver nitrate test indicated that the source of the corrosive agent (chloride) was not halides present in the VCI paper used to wrap the weapon containing the springs. Lastly, since all metallurgical properties of the spring material were consistent with specifications and were considered normal, a deficiency in the spring material does not account for the failure of these items.

ACKNOWLEDGEMENT

The authors wish to thank Mr. R. Rocha for his assistance with the preparation of all metallographic specimens required for this work.

Figure 1. Image representative of as-received condition of MK19 receiver buffer spring fragments.

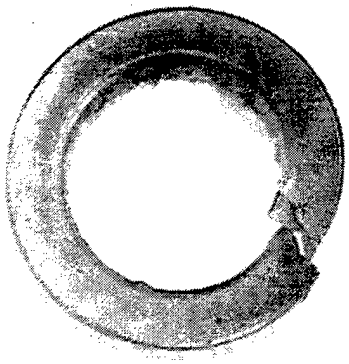

a

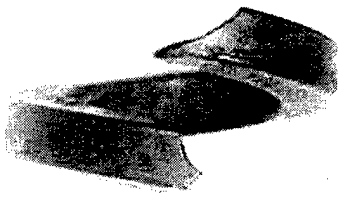

b

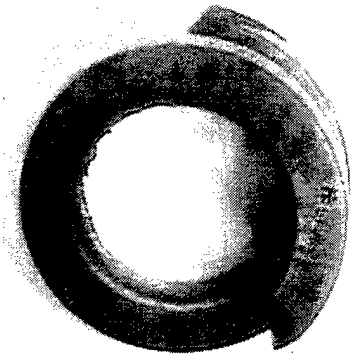

c

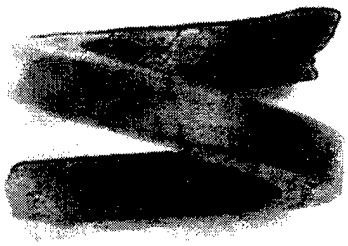

d

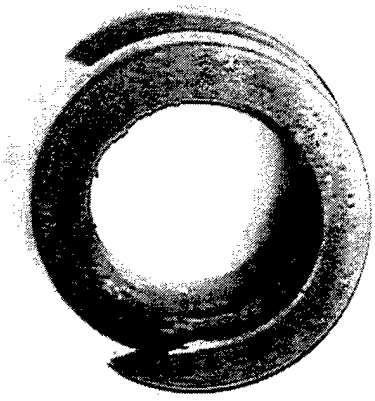

e

f

Figures 2a-f. Images showing higher magnification views of spring fragments.

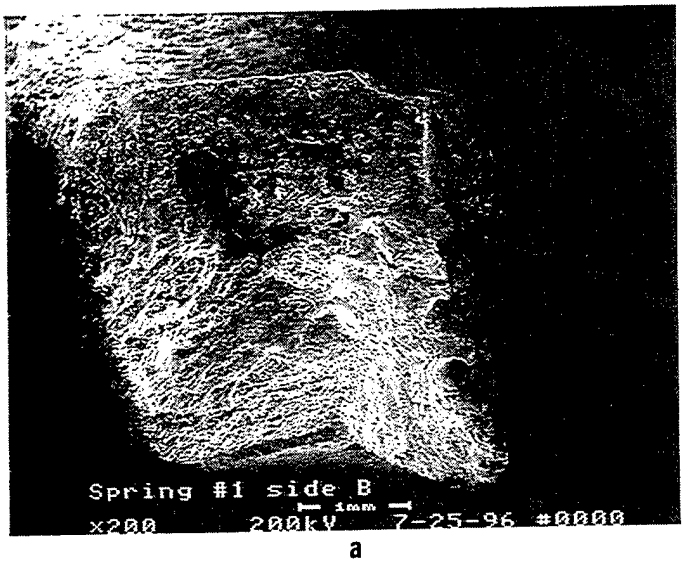

a

b

Figures 3a&b. SEM images representative of as-received condition of spring fragments. Note that surface is covered with residue which has completely obliterated the true fracture features. 15x, 75x.

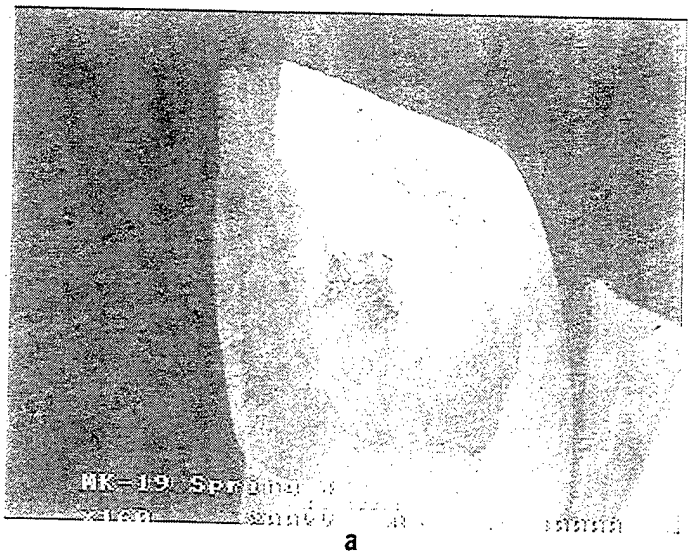

a

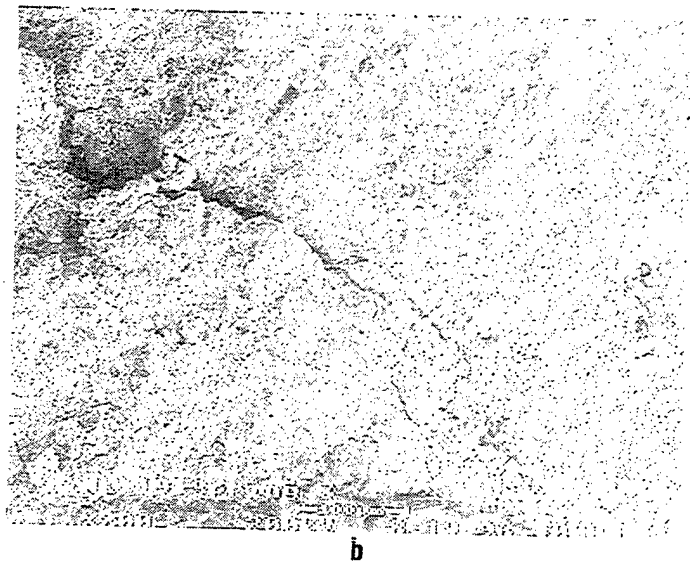

b

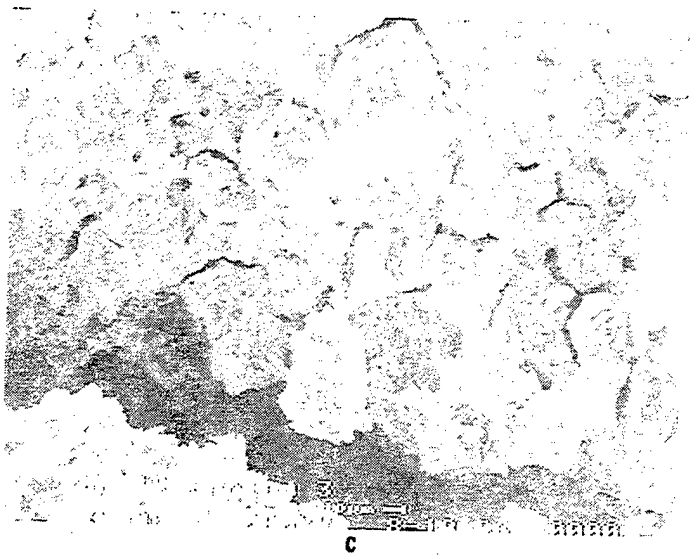

c

Figures 4a-c. SEM images representative of cleaned condition of spring fragments. Fracture mode is intergranular. 12x, 150x, 1500x.

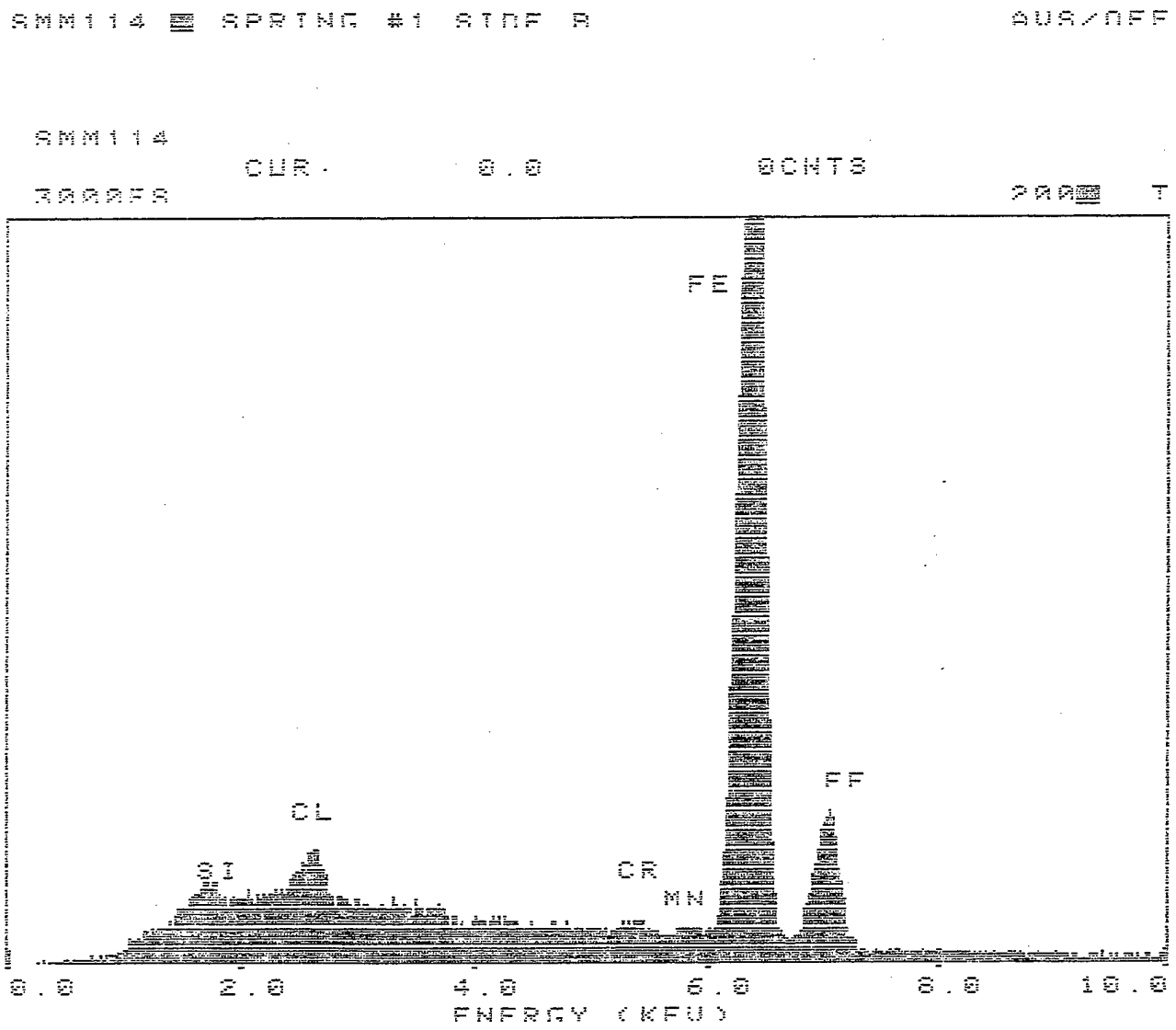

Figure 5. EDS spectrum representative of spring residue.

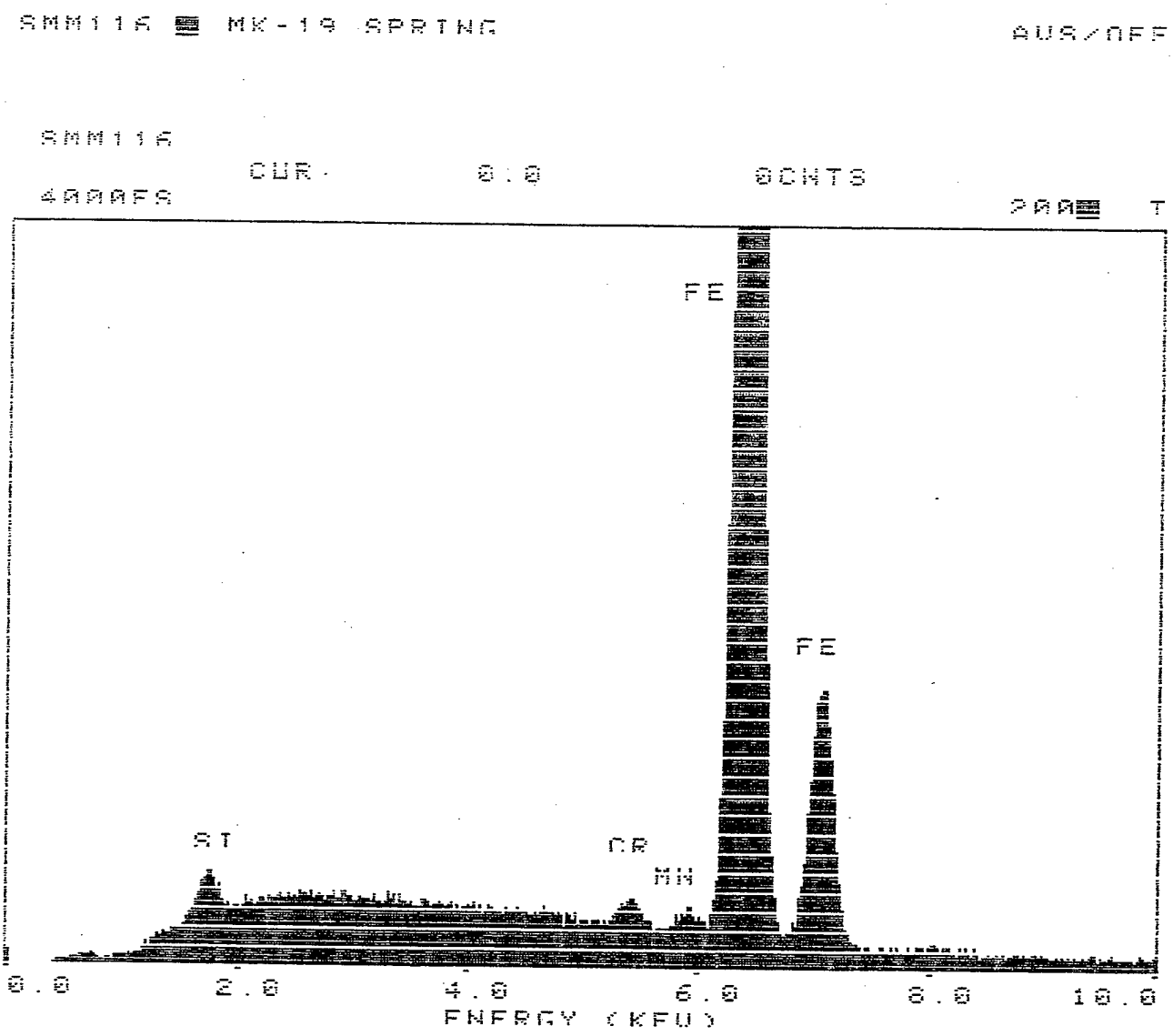

NUSIU: STANDARDLESS ANALYSIS OF BULK SAMPLE
SPECTRUM: MM116 MK-IV SPRING

ELEMENT	RELATIVE K	WT %	9254 Steel
FE	0.9673	97.08	BAL
C	LECO	0.55	.51/.59
SI	0.0036	0.78	1.20/1.6
S	LECO	0.02	.02 MAX
CR	0.0076	0.75	.6/.8
MN	0.0080	0.82	.6/.8
TOTAL		100.00	

Figure 6. EDS spectrum and analysis representative of spring material.

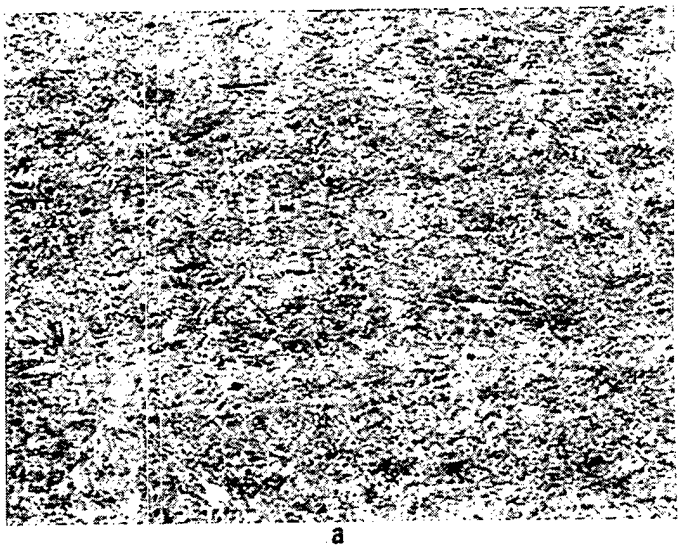

a

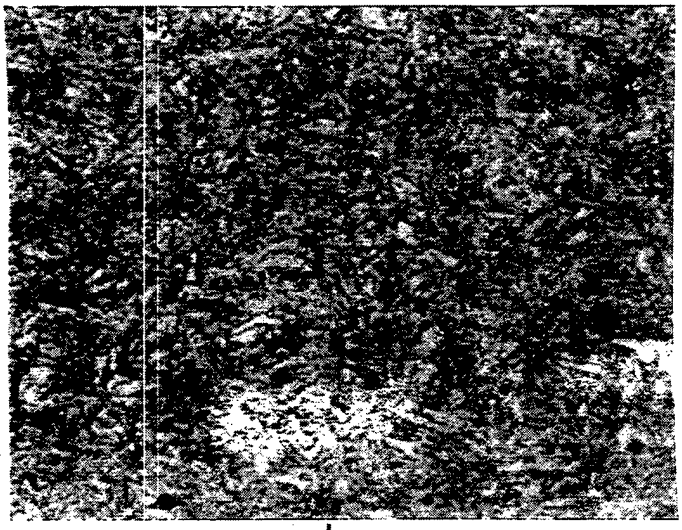

b

Figures 7a&b. Images showing fine martensitic microstructure present in spring material. 750x, 1500x.

Design and Construction of Electronic Systems for Military Environments

Edward Taylor
Northrop Grumman Corporation, Military Aircraft Systems Division,
One Hornet Way, 9B64/62 El Segundo, CA 90245-2804

ABSTRACT

Electronic systems failures resulting from corrosion have been prevented by implementing a design and manufacturing plan with suppliers and customers. This paper addresses the basic steps which have been found to provide reliable equipment. The cost of implementing these steps far outweighs the expense of redesigning and rebuilding state-of-the-art electronic systems.

Introduction

Corrosion prevention will probably never be a primary consideration for military electronic system manufacturers, but it should be near the top of the list. The economic losses to manufacturers and customers from natural and induced corrosion are overwhelming and the personal danger associated with malfunctioning electronic equipment, as a result of corrosion, is proven. Even so, electronic systems are being designed and manufactured by a younger generation of engineers without the extensive experience and training of their predecessors. Concurrently, numerous government specifications and standards, formerly used in contracts as rigid requirements, have been canceled or are being superseded by guidance documents. This situation is confusing and even chaotic to the inexperienced engineer, who is dependent on self explanatory contractual documents for developing a product.

Contractual documents, including government specifications and standards, do not thoroughly address electronic system corrosion prevention. Corrosion is the natural or induced degradation of metal, which is irreversible but controllable in intensity by means of engineering design. However, electronic system corrosion prevention can be achieved by employing the same basic principles recommended for aircraft structural corrosion.

To prevent electronic system corrosion at the source, a change in manufacturer mentality is needed to conduct a technically adequate program so that state-of-the-art corrosion resistant electronic hardware can be produced by suppliers with a lower level of technical expertise. The manufacturer's efforts to prevent electronic system corrosion should be structured and synchronized with customers and suppliers. This paper does not address the elements of electronic system corrosion, but identifies the key areas of concern and provides ten proven steps in terms familiar to the corrosion illiterate.

The First Step

Electronic system corrosion prevention begins with the ultimate military user, be it the Army, Navy, Marine Corps or Air Force. Every agency has product specific mission requirements which may depend on storage, handling, maintenance, repair or service conditions where diurnal cycles result in moisture condensation primarily at night. In order to generate these contractual requirements, the agencies conduct periodic inspections of their hardware and prepare internal reports for eventual use by the specific programs. These internal reports are not shared with the manufacturing community and actually, may not be used as guides when setting the requirements for a new but similar product. Thus, invaluable "lessons learned" may not be passed on to the manufacturer in the form of performance requirements. "Lessons learned" should be demanded to help the manufacturer negotiate with the "customer" before the contract is signed. Some lessons may not apply to the new hardware and may inhibit the designer if they remain in the contract. Eventually, the technical issues perceived by the manufacturer should be resolved by "tailoring" the contract to include the specific language necessary to satisfy system requirements. This contract document should be the "Bible" for the design engineer because every drawing he creates has to implement or meet the system requirements.

The Second Step

The manufacturer's next effort in preventing electronic system corrosion is to identify or develop one or more engineering designers who have some experience in material and process selection. Preferably, these designers should have participated in similar efforts where corrosion prevention was implemented and validated. A key attribute of the "corrosion smart" designer should be the ability to mentally store bits and pieces of information which can be retrieved later and combined with other data to form a story or supporting documentation. Even better is to have "corrosion smart" designers exposed to training from more authoritative sources. Training material is available in libraries, videotapes, government handbooks and professional courses. However, training without adequate guidance and purpose is useless. Because so much information is available on corrosion subjects, the student can be easily overcome by bewilderment, the notion that one will never finish reviewing the material, or that no reference exists which addresses the corrosion issue at hand. One of the best ways to obtain guidance on a specific subject is by networking with experienced corrosion scientists. However, in order to network, one has to learn who they are, what they do and where they work. This is accomplished by reading professional publications, attending symposia, getting referrals and learning their language. When all else fails, a consultant who is usually associated with a university, professional society or government agency, may be able to provide the necessary services.

The Third Step

The design engineering organization should have standard solutions for a family of products, similar to selecting standard hardware or material. Combinations of materials and finishes for fasteners, pins, pulleys, bearings, gaskets, springs and structures should be listed in a

design manual as "preferred" for benign and severe environments. Thus, a benign environment will not affect untreated aluminum alloy, whereas a severe environment requires anodizing, painting or, at least a chemical film. Similarly, stainless steel fasteners can be used without protection in aluminum structure in a benign environment, but must be wet installed with chromated primer or sealant in a severe environment. An example of a list of "preferred" materials, finishes and designs is shown in Table 1.

Design features known to prevent or resist corrosion should be alphabetically categorized for easy retrieval. An example is shown in Table 2. A checklist of "Do's and Don'ts" can be used to review a drawing prior to release. Examples are shown in Tables 3 and 4.

The Fourth Step

The ideal situation for the manufacturer is to have a corrosion control plan in place. This plan describes in detail how various aspects of design, fabrication and inspection will be administered. The detail should extend to who does what and when these things happen. An example of a Table of Contents for a Corrosion Control Plan is shown in Table 5.

The Fifth Step

Supplementing the corrosion control plan is a "Finish Specification," which specifies standardized treatments for standardized parts. Thus, one does not get a mixture of thick and thin coatings, different platings or inconsistencies from item to item. An example of listings from a Finish Specification is shown in Table 6.

The Sixth Step

Reviews and checklist assessments of detail drawings, next higher assemblies and systems are used to identify discrepancies by exposing selections and preferences to peers and experienced advisors. Discussions of key features and supporting rationale capture problems for action item listing and eventual resolution. The best design review team is composed of critics who offer constructive comments based on an extensive knowledge of the subject. No design review team is too large, although the logistics of organizing a group and the attendant cost are significant factors. An example of the composition of a design review team is shown in Table 7.

Detailed reviews of drawings and parts lists should be completed by engineering, manufacturing and quality staff members who are familiar with the design and the customer's requirements. There is no greater disconnect than to design without an intimate knowledge of the contractual requirements. A review of an assembly should encompass all of the individual detail drawings for that assembly and an exploded view, if possible. The designer should be consulted to explain how parts fit together. Issues of liquid entrapment, galvanic compatibility of materials, orientation and sealing methods should be discussed thoroughly to arrive at a complete

understanding. The corrosion prevention drawing notes should be self explanatory and consistent for each part. An example of adequate corrosion prevention drawing notes is shown in Table 8.

Drawings should reference materials using specifications with inspectable property requirements so that multiple sources are available. An example of brand names and generic specifications for materials is shown in Table 9.

The Seventh Step

Testing of parts, assemblies and systems to verify compliance to drawing and contractual requirements should be a normal way of doing business. Parts, rather than coupons, provide the actual configuration with crevices, holes, mating surfaces and accessory hardware. Orientation in an environmental test chamber should be the same as in service so that moisture drip patterns are established. Tests should be industry standards so that comparisons can be made with other configurations or products. After the test, the part should be cleaned, including the removal of surface contaminants and corrosion products. Analysis of the affected surface(s) should be thoroughly descriptive and preferably photographed so that diagnoses and prescriptions for corrective action are accurate. A detailed analysis using high tech tools may be warranted in order to quantitatively assess results. Design changes to correct inadequacies should be tested to verify technical adequacy and contractual compliance.

The Eighth Step

Manufacturing of parts at different suppliers invites the possibility of corrosion. Different people, procedures, process materials and storage conditions at the different suppliers sometimes cause anomalies which require addressing, resolution and corrective action. Personnel hygiene has been found to be a contributing factor when gloves are not worn or are reused, sneeze guards and whisker guards are not used, and training to minimize introduction of contaminants is not provided. The manufacturer and attendant subcontractors should periodically monitor their suppliers with personnel who are trained to recognize corrosion sources and provide useful commendations. Three basic questions should be asked:

1. Does a procedure exist?
2. Is the procedure valid?
3. Is the procedure being followed?

A review of the processes by the manufacturer should identify those for which no procedures exist. Where a procedure does exist, the manufacturer should assess its technical adequacy. Finally, the operator(s) should be observed to determine whether the procedures are being followed.

The Ninth Step

Inspection of hardware should identify all areas which are suspected of being corroded or are inconsistent with the appearance of similar hardware. If the inspector has an appreciation of the processes affecting the part, the critical areas will be known. These may be welds, faying surfaces, crevices, seals, bonds, fasteners or paint. Retained process fluid, flux, overspray, grease, exposed base metal, powder, spots and lumps are all suspected sources of corrosion. The inspector should be trained to recognize corrosion and to know where to look for it. Very often, surface contamination and corrosion are confused. Simply put, surface contamination is an obvious presence of a material, which is easily removed without affecting the surface finish. Corrosion, however, is usually under a deposit which is tenaciously adherent and covers a defect such as a hole, pore, crack, crevice, tear, seam or chip. Casual observations may not identify metal loss which is hidden or diminutive. A detailed examination with magnification, if necessary, should provide the level of confidence needed to accept or reject hardware.

The Tenth Step

Packaging and storage of hardware is in itself a science because of the wide assortment of packing materials. Every packing material is made from one or more chemical compounds and some emit vapors which cause degradation. Thus, a packing material not known to cause corrosion could affect a specific part with a sensitivity for the outgassed vapors. One packing material is known to emit chlorides, which are uncontrolled by the military specification governing it, thus permitting a potential extremely corrosive condition. Over a period of weeks and months, residual chloride and moisture form a strong electrolyte, which has been known to attack many metals. Some packing materials outgas organic compounds, which may or may not be flammable or explosive. The inexperienced engineer may not recognize these potential hazards to the electronic system or to personnel. A study of the applicable Material Safety Data Sheet(s) may identify the chemical compounds within the product, but only a detailed knowledge of the reactions between chemicals and metals will predict whether corrosion is a threat. This is another manufacturer task which often has a low priority but may have a huge effect on product integrity. Packing material compatibility awareness is insurance that a small preventive cost up front will save the cost of a large rework, repair or scrapout later.

Conclusion

Adherence to the ten steps described in this paper has resulted in designing and manufacturing electronic systems which are reliable and resistant to corrosion in the workplace and the operating military environment.

TABLE 1

Materials, Finishes and Designs in Benign and Severe Environments

Benign	Severe
Untreated aluminum alloy	Anodized aluminum alloy
Stainless steel fasteners	Cadmium plated fasteners
No sealing	Hermetic sealing
Dissimilar metals OK	No dissimilar metals
Gold over copper	Gold over nickel
Fungus nutrient	Fungus inert
Hygroscopic materials	Non-hygroscopic materials
Nickel plated aluminum	Cadmium plated aluminum
Outgassing materials	Non-outgassing materials
Crevices OK	No crevices

TABLE 2

Design Features Known to Prevent or Resist Corrosion

Bonding
Use adhesives without volatile chemicals
Use noncorrosive adhesives
Castings
Impregnate to eliminate porosity
Connectors
Use anodized aluminum or nickel plated steel
Use environmental seals
Dissimilar metals
Select metals which form similar couples
Seal joints
Electrical bonding
Obtain 2.5 millivolt maximum between surfaces
Seal bonded joints
Fasteners
Wet install
Use corrosion resistant alloys or coatings
Finishes
Passivate stainless steel alloys
Complete fabrication before surface finishing

TABLE 3

Checklist of Do's for Reviewing Drawings

Are dissimilar metals sealed?
Are printed wiring boards conformal coated?
Is aluminum anodized or conversion coated?
Does gold plating have a nickel underplate?
Are "O" rings made of fluorocarbon or fluorosilicone?
Are conductive and electromagnetic interference gaskets sealed from moisture?
Is a drain at the lowest point?
Are connectors mounted horizontally?

TABLE 4

Checklist of Don'ts for Reviewing Drawings

Don't use nickel plated aluminum connectors
Don't use hygroscopic materials
Don't mount connectors vertically
Don't use gold directly over silver or copper
Don't permit moisture traps
Don't use outgassing materials
Don't mount circuit cards horizontally
Don't permit dissimilar metals

TABLE 5

Corrosion Control Plan's Contents

Introduction
Applicable Documents
Organization
Corrosion Program
Support to Design
Concurrent Engineering
Subcontractor Evaluation
Test Program
Design Development Tests
Accelerated Life Cycle Tests
Manufacturing Support
Process Control
Design Guide

TABLE 6

Listings From a Finish Specification

Surface	Part Function	Finish
Aluminum	Electrically conductive	Chemical film
Aluminum	Solderability and low contact resistance	Electroless nickel under electroplated tin-lead
Aluminum	Very low contact resistance	Electroplated nickel under electroplated gold
Copper	Solderability	Electroplated tin-lead
Copper	Contact	Electroplated nickel under electroplated gold
Stainless steel	Corrosion protection	Passivate
Stainless steel	Hybrid cover	Electroplated nickel under electroplated gold

TABLE 7

Design Review Team Composition

Designer(s)
Design Manager
Manufacturing Engineer
Corrosion/ Materials Engineer
Stress Engineer
Thermal Engineer
System Engineer
Quality Engineer
Purchasing Agent
Customer

TABLE 8

Adequate Corrosion Prevention Drawing Notes

Passivate per QQ-P-35
Nickel plate per QQ-N-290, Class 1, Grade D
Conversion coat per MIL-C-5541, Class 1A
Anodize per MIL-A 8625, Type II, Class 2, Black, per Color No. 37038 per FED-STD-595
Impregnate per MIL-STD-276
Tin-lead plate per MIL-P-81728 and reflow
Gold plate per MIL-G-45204, Type III, Grade A, Class1

TABLE 9

Brand Name vs. Generic Specification for Materials

Brand Name	Generic Specification
Conformal coating A	MIL-I-46058, Type AR
Polysulfide sealant B	MIL-S-81733, Type I
Silicone sealant C	MIL-A-46146
Threadlocking sealant D	MIL-S-46163, Type II, Grade M

Corrosion Control Hardware Allowance Parts List (APLs): Logistics Support for Naval Surface Ship Corrosion Control Programs

Norm Clayton
Naval Surface Warfare Center, Carderock Division
Code 624, Marine Coatings and Corrosion Engineering Branch
Philadelphia Naval Business Center
Philadelphia, PA 19112-5083

William Steiner
Naval Surface Warfare Center, Carderock Division
Code 624, Marine Coatings and Corrosion Engineering Branch
Philadelphia Naval Business Center
Philadelphia, PA 19112-5083

ABSTRACT

All Navy ship acquisitions have had specifications for corrosion control requirements that a shipbuilder must follow. These requirements are especially well defined for weather-exposed equipment. One of the most common corrosion control methods called for is the use of corrosion resistant fastener materials. Due to the lack of logistics support for these "interface" fasteners and other corrosion control consumable materials, Allowance Parts Lists (APLs) are being developed for many ship classes to provide the necessary support. This paper will expand on the background for the need for these APLs, and will describe the approach used to create them and the accompanying guide that instructs ship's force on their use. It will also discuss the logistics support link between the APL and the Navy's Planned Maintenance System (PMS).

INTRODUCTION

The world's oceans are among the most corrosive natural environments to which human-made structures and equipment are exposed. Therefore, corrosion protection and prevention is a significant factor in the design, construction, and maintenance of U. S. Navy ships. Since the most economical and effective way to prevent shipboard corrosion is to build corrosion resistant features into the design, for many years each new class of Navy ship has had sections of the shipbuilding specifications dedicated to corrosion control. The specifications for each new ship class continue to be revised to update the corrosion control and other requirements as new technology reaches the production stage, and to incorporate lessons learned from previous experience.

There are many ways to prevent or control corrosion in the original design of a ship or structure. The methods include the use of corrosion resistant materials of construction, the use of different types of coatings for different types of service, the use of cathodic protection systems for areas immersed in sea water, and specific design features such as providing drainage, isolating dissimilar metals, and preparing welds and edges for optimum coating performance. The acquisition costs to use corrosion resistant materials, high technology coatings, and more detailed fabrication methods can be high. Therefore, these types of corrosion control requirements are only specified for areas of the ship that experience has shown will be most prone to corrosion attack, or have high life cycle maintenance and repair costs. These areas are generally the sea water wetted areas of the ship, such as the underwater hull, tanks and voids, machinery bilges, fan rooms, and, of course, weather-exposed equipment and structures.

The requirements specifications for the acquisition of each new class of Navy ship are arranged according to a hierarchical structure known as the Ship Work Breakdown Structure (SWBS). While each section dealing with a given machinery or weapon system may have specific materials, coatings, or other corrosion control requirements applicable to that equipment, for the most part, these requirements are contained in a couple of key sections listed below.

Section 075: Threaded Fasteners
Section 078: Materials Requirements
Section 630: Corrosion Prevention and Control
Section 631: Painting
Section 632: Metallic Coatings
Section 633: Cathodic Protection

Section 078, and more recently, Section 630 of the shipbuilding specifications contain the primary corrosion control requirements that a shipbuilder must follow when building a Navy ship. Section 630 generally contains a table that crosses standard Navy corrosion control measures to various types of equipment. Most of the equipment listed in the table is located in the weather, or in a weather-exposed area of the ship. One of the most common corrosion control methods called for is the use of "improved materials" for fasteners. These materials are stainless steel (CRES) grade 316, nickel-copper alloys 400 or K-500, or other specialty materials. Other corrosion control measures called for in Section 630 include the use of antiseize compounds, sealants, electrical connector weatherproofing, and vapor-phase corrosion inhibitors (VCI's).

Sections 078 and 630 may also require that the shipbuilder prepare various types of documentation to support the corrosion control effort, such as a "Corrosion Control Plan", a corrosion control drawing, or a class Corrosion Control Manual (CCM). However, until the recent LPD-17 ship specifications, there was generally no requirement for the shipbuilder to provide the logistics support documentation needed for the corrosion resistant hardware installed during new construction, particularly for routine, low to normal strength "interface" fasteners and hardware used to attach a piece of equipment to a bulkhead or deck bracket. In general, fasteners and this type of hardware were considered to be "not APL worthy" in the philosophy of the logistics and provisioning community. Proper logistics support documentation would have

included identifying each fastener on the applicable drawings, technical manuals, and APLs by part identifying numbers, or by the vendor's Commercial and Government Entity (CAGE) code number and that vendor's part number. Key to the ability of ship's force (S/F) to maintain a piece of equipment is also the identification of a National Stock Number (NSN) that can used to order the correct item in the event that the original was lost or broken.

Before proceeding further, just what an APL is should be defined. As its name implies, an Allowance Parts List is simply a listing of individual parts of an assembly that are considered to be replaceable or repairable. The great majority of APLs are tied to a specific piece of equipment, such as a specific style, size, and model number of valve, motor, or pump. The listing includes the part nomenclature, the NSN, codes that indicate the level of repairability, the quantity of the item present in one piece of the equipment, and an on-board allowance table based on the total shipboard population of that piece of equipment. The "corrosion control hardware" APL's discussed in this paper are different, in that the parts listed on them apply to a wide variety of weather exposed equipment on a given ship class.

The corrosion control plans, manuals, and drawings that have been developed for previous ship classes have not contained the information that S/F would need to replace a missing or broken fastener. For example, if Section 630 required CRES 316 fasteners and hardware to be used in all lifeline installations, then lifelines would have their own page in the CCM, which would simply state that all fasteners are to be CRES 316. However, there is usually no distinction made between different sizes or uses of the fasteners (lifeline stanchion fasteners vs. terminations vs. support hooks, etc.), and no NSNs, part numbers, or other specifications are given. S/F and other waterfront activities may have access to the ship class corrosion control drawing, if one was developed, which would contain a "work note" for lifelines stating that all fasteners are to be CRES 316. Unfortunately, these drawings also did not contain part number information for the CRES fasteners, but instead referred to several detail drawings. If the equipment did not have its own Technical Manual (TM) or Allowance Parts List (APL), then S/F would be left without the means to obtain the correct replacement corrosion resistant hardware. Even if the equipment involved had its own APL, as indicated above, fasteners have historically been omitted from APL's since they were not considered to be "maintenance significant". This often resulted in the use of anything that fits, such as a zinc or cadmium plated steel fastener, which would begin to rust after about three to six months of exposure.

The situation described above has contributed to the fact that corrosion of fasteners has been identified by the Fleet and waterfront activities as one of the surface Navy's "Top Ten" corrosion problems. Even when good-intentioned personnel attempted to obtain stainless steel replacement hardware from the stock system or open purchase sources, they would encounter another problem: Grade 316 CRES often could not be procured due to a lack of NSNs or part numbers for this specific grade. The materials associated with existing part numbers were generally listed in generic ways such as "300-series CRES", or "18-8 stainless". This resulted in Grade 303 CRES being provided, since it is less expensive and easier to machine than Grade 316. Unfortunately, it is also much less corrosion resistant in a topside marine environment.

All of the above factors produced the need for a means of logistics support for the Grade 316 CRES fasteners that were installed in topside areas of the ship during new construction. The "miscellaneous parts" APLs that were created as a part of the effort described herein are intended to fill that need in a relatively quick and economical manner. It is intended for this hardware to be used by the ship to replace missing, broken, or rusted steel hardware that has been used on specific types of equipment installed topside or otherwise exposed to the weather. The types of hardware on the APLs are generally fasteners (nuts, screws, washers, etc.), cotter pins, grease fittings, and other replaceable items that do not require special high strength materials. The majority of the types of equipment affected includes lights, speakers, miscellaneous electrical boxes, piping clamps, liferails, and other topside-mounted outfitting equipment. Furthermore, once the decision was made to create these APLs for fasteners and other routine outfitting hardware, it was also logical to include various types of consumable corrosion control materials on the APLs. These materials include antiseizes and other thread treatments, sealants, VCI emitting devices, and electrical connector weatherproofing materials.

PROCEDURE

The main approach taken to creating these APLs was to conduct an on-board survey of the topside and weather-exposed areas of one ship of each class, determining the types and population of each piece of equipment, and directly counting, identifying, and measuring each fastener type or other hardware item on each type of equipment. During the survey, each hardware item was specifically identified as to where it was used in the equipment assembly. This approach was deemed to be more economical than retrieving and reviewing all of the detail, installation, and interface drawings for each type of equipment. In order to ensure that there was coverage of each type of equipment that had CRES hardware requirements for new construction, the applicable ship class corrosion control manual, corrosion control drawing, or corrosion control plan, as appropriate was reviewed prior to the survey, and a candidate list of topside equipment was compiled.

The single shipcheck was used as a notional baseline taken to represent the topside configuration of the entire class. Since the main goal of this effort was to make corrosion control material readily available to the ship, it was not critical that the resulting APL exactly reflected the configuration and total quantities of each type of fastener. Equipment on other ships of the class that differed from the ship surveyed could be added later as directed by the sponsoring platform office.

The resulting data was then compiled into a relational database system, using three linked databases: one for the given ship class configuration, one for the equipment-unique background data, and one for the individual part-unique data. Not only did this allow on-demand sorting according to either the equipment or the hardware nomenclature, but it made each subsequent ship class APL creation effort more efficient and economical, since the basic equipment and individual part data (such as nomenclatures, specification designations, and NSNs) did not change from ship class to ship class. This database system also permitted flexible report formatting options, which proved useful in preparing the supplemental guide documents described below.

Concurrent with the data compilation, the applicable military and federal specifications and standard drawings had to be identified for each fastener style and material combination. In most cases, Military Standard (MS) drawings were identified for the necessary parts, except that they had the problem described above of allowing generic 300-series CRES to be used. With the Department of Defense (DOD) effort to move away from military specifications and standards and toward commercial standards, this phase also involved researching the applicable commercial equivalent specifications, if any. In general, American Society for Testing and Materials (ASTM) specifications and American National Standards Institute/American Society of Mechanical Engineers (ANSI/ASME) standards were the most common ones to be cited.

Upon approval by the sponsoring ship platform manager, the data were properly formatted and sent through the provisioning and supply process for creation of the APL. At this time, determinations were made regarding items that required new NSNs. New NSNs were required for either items that were completely new to the system, or for those fasteners where the existing NSN crossed to a generic 300-series CRES fastener. In the latter case, the new NSNs were created for Grade 316 CRES exclusively. In the last stage of this process, the APLs are electronically sent to the Configuration Design Manager (CDM) for the given ship class, and are "loaded" against the ship and provisioned accordingly.

RESULTS

The APLs that have been created to date as a result of these efforts are listed below.

990990588, "Corrosion Control Hardware CG-47 Class"
990990673, "Corrosion Control Hardware DDG-51 Class"
990990674, "Corrosion Control Hardware DD-963 Class"
990990701, "Corrosion Control Hardware LSD-41 Class", Deck Department
990990702, "Corrosion Control Hardware LSD-41 Class", Engineering Department
990990703, "Corrosion Control Hardware LSD-41 Class", Operations Department
990990704, "Corrosion Control Hardware LSD-41 Class", Navigation Department

To the eyes of the Sailor, these APLs were simply lists of hardware and consumables by their nomenclature. Therefore, a "tie-in" was needed to tell the ship where this material was supposed to be used. To accomplish this, supplemental "APL Guides" have been created and issued to the ship's and various waterfront support offices. Guides for the CG-47 and DDG-51 classes have been issued[1,2], and similar guides for the other ship classes are in preparation. These guides include tables that cross-reference the hardware types and sizes to the equipment that it is to be used in, and lists the NSNs for each item on the corresponding APL. In addition to this basic usage information, these guides provide background information on other reference sources, a description of typical fastener materials and their associated head markings, descriptions and

[1] NSWC Carderock Division letter "CG-47 CLASS CORROSION CONTROL HARDWARE APL GUIDE", 9630, Ser 624/254, 16 January 1997
[2] NSWC Carderock Division letter "DDG-51 CLASS CORROSION CONTROL HARDWARE ALLOWANCE PARTS LIST (APL) GUIDE", 9630, Ser 624/315, 20 May 1997

illustrations of various fastener styles, and the descriptions of the uses of the other consumable corrosion control materials contained in the APLs.

Another link in the logistics and documentation chain being forged to help S/F in their corrosion control efforts is the Navy's Planned Maintenance System (PMS). This system consists of Maintenance Index Pages (MIPs) assigned to one or more ship classes that lists periodic maintenance actions that should be taken to either prevent or detect a problem. Each of the maintenance actions is given a code that indicates the periodicity, and is more fully described in a stepwise procedure on a Maintenance Requirements Card (MRC).

Similar to most conventional APLs, most MIPs are specific to a given ship system or piece of equipment. However, a special "corrosion control" MIP has been developed for the Naval surface Fleet[3], which is not tied to any specific type of equipment. This MIP and its MRCs call for a periodic corrosion inspection by S/F, and provides very basic descriptions of the appearance of corrosion on common materials of construction, and of several corrosion prone areas on a typical ship. The main part of the MIP is a number of generic maintenance procedures for using various corrosion control materials that are well within the capability of S/F, such as antiseizes, sealants, coatings, VCIs, and electrical connector weatherproofing methods. While the detailed MRCs for each of these treatments list the consumable materials needed for each method, the corrosion control APLs described herein help to ensure that the materials needed will be properly provisioned and on-board to support the Sailor.

As lessons have been learned from the past, it is not likely that new Navy ship classes will require these types of APLs in the future. This is because the ship specifications have been changed to require better documentation and logistics support for fasteners. While these changes were made to help address fastener standardization issues and the use of commercial specifications within the DOD, the end result is that they will help preclude the need for these APLs. An example of these changes is provided below, which is an excerpt from the recent ship specifications for the new amphibious ship LPD-17 class.

Section 075 Threaded Fasteners[4]

075a. General

This section defines threaded fastener requirements applicable to assembled joints and attachment of machinery and components to their foundation or to hull structure. This section also applies to systems and components where definitive fastener requirements are not specified in the applicable system and component specification.

Fastener hardware, including washers and other unthreaded items, shall be identified on drawings, technical manuals and logistic support documentation by part identifying numbers in accordance with the requirements of SAE J2280[5]*, including Appendix A.*

---

[3] Maintenance Index Page (MIP) 6300/001, "Preservatives and Coverings (Corrosion Control)"
[4] LPD-17 Ship Specifications, 17 December 1996
[5] SAE J2280, "Ship Systems and Equipment - Fasteners - Selection and Identification Requirements", 1 April 1996

075d. Technical documentation

The following documentation shall be prepared:

a. *Drawings for all fasteners which are not identified by standard industry or military part identifying numbers. Drawings need not be submitted for fasteners identified by CAGE Code and drawing numbers in accordance with SAE J2280, including Appendix A for which logistic support has already been established.*

b. *A list or individual submittals for all fasteners with part or identifying numbers to industry or military standards for which approval for use is required in accordance with SAE J2280, including Appendix A.*

CONCLUSIONS

The corrosion control hardware APLs described herein are another tool that S/F and waterfront activities can use in their corrosion control efforts. In particular, these APLs help provide the logistics and supply pieces of the overall corrosion control puzzle, by making sure that the specified materials are readily available to the ships. The APLs complement the Navy PMS maintenance requirements in this regard. The supplemental guides for the APLs also help with the training piece of the puzzle, by raising the overall awareness of corrosion control issues and measures that can be taken on the waterfront.

While the next generation of Navy ships, such as the LPD-17 class, may not need equivalent corrosion control APLs due to improved logistics documentation requirements for fasteners in the ship specifications, these APLs still are valuable for existing ships. Interest has been expressed in expanding the coverage of these APLs to include the FFG-7, aircraft carriers, and other amphibious ship classes.

ACKNOWLEDGEMENTS

The work on the APLs for the CG-47, DDG-51, and DD-963 classes was sponsored by the Program Executive Office, Surface Combatants/AEGIS Program (PEO-SC/AP), PMS-400F5 and the former PMS-335. The APL effort for the LSD-41 class was sponsored by the LSD-49 and follow Integrated Logistics Support (ILS) manager, NAVSEA PMS-3771. Other contributors to this effort include Mr. Frank Vapniarek, Code 624, Ms. Christine Socha, Code 622, and Mr. William Dowd, Code 1361 of the Naval Surface Warfare Center, Carderock Division, and Mr. Ron Kimmel of the Naval Inventory Control Point (NAVICP), Mechanicsburg, PA.

Corrosion Control Systematic Approach and Trends

Jeff M. Sakai and Brian Gilp
Naval Air Systems Command
Patuxent River, Maryland

Abstract

The following paper will discuss the trends and operations of the NAVAL AIR SYSTEMS COMMAND Corrosion Control Program. Current procedures/requirements for combating corrosion in the Naval Aviation environment will be emphasized. Paper discussion will include a brief overview of organizational elements required to support the corrosion control efforts, required corrosion control training, recent areas of emphasis, field implementation of newly developed materials and processes, and technical field representative support system available to all Naval Aviation Fleet Activities.

Introduction

Corrosion Control efforts of the NAVAL AIR SYSTEMS COMMAND are an on going task that will continue through-out the entire service life of aircraft that are operating in and exposed to harsh marine environments. The total cost of corrosion control efforts has been estimated to be in excess of $1 Billion. This corrosion control effort included both preventative maintenance and repair/overhaul operations that are incurred at the various levels of Naval Aviation Maintenance, e.g., Organizational (O), Intermediate (I) and Depot (D). An overview of the corrosion control capabilities and responsibilities for each level of maintenance will be one of the topics of discussion in this paper .

Recent advancements in the Corrosion Control materials and processes, have resulted in the fielding of new products and equipment used for combating corrosion on Naval Aircraft. Thorough test and evaluations, i.e., in both laboratory and field environments, were conducted or coordinated by the Naval Warfare Center, Aircraft Division, Patuxent River, Maryland. Brief discussion of some of these tests and evaluations of new corrosion control materials and processes will also be covered in this paper.

The remainder of the paper will pertain to the technical corrosion control field assistance system available to all Naval Aviation Fleet Activities.

DISCUSSION

Organizational, Intermediate and Depot Corrosion Control

Corrosion prevention and control are applicable to all Naval Aviation aircraft and associated hardware. Commands within the Naval Aviation community are responsible for ensuring that corrosion prevention and control receives a priority for timely accomplishment, along with other required maintenance. The overall objective of the corrosion prevention and control program is to detect corrosion and correct it in its earliest stages of development. Detection and prevention will prevent aircraft flight mishaps, flight related mishaps, excessive out-of-service time, serious damage to aircraft and equipment, and an increased maintenance cost.

The extent of corrosion prevention and control for each level of Naval Aviation Maintenance are dependent upon the Maintenance Level capabilities and are accomplished in accordance with the specific aircraft Maintenance Instruction Manual (MIM) and/or Structural Repair Manual.

The following will basically summarize the corrosion control capabilities of the O, I and D Level of Naval Aviation Maintenance:

Organizational

The level of effort provided at the organizational level is limited to aircraft surface washing , cleaning and treatment without extensive materials removal, e.g., without the use of power assisted equipment. This will include hand blending/surface finishing, followed up with paint touch -up and sealant application. Major corrosion damage is usually corrected by the remove and replace action or sent to the next higher level of maintenance for repairs.

Intermediate

This level includes the organizational level capabilities plus the use of some power assisted equipment used for aircraft washing, cleaning, blending and removal of surface corrosion and corrosion damage. Power assisted equipment may include the use of glovebox plastic media blasting, glassbead glove box, portable vacuum abrasive and wet abrasive blasting equipment, surface blending and grinding equipment, hot tank chemical paint stripping, and high pressure aqueous part washers.

Depot

Corrosion control capabilities at the Depot Level can be more extensive and will definitely include capabilities that are currently being done by the organizational and intermediate level of maintenance.

Corrosion Control Training

In order to achieve an effective Corrosion Prevention and Control Program, the Naval Aviation community has developed in-service and formal schools. These schools provide instruction in the detection, identification and treatment of the various forms of corrosion found on aircraft, engines, components, support equipment and provides direction for emergency reclamation.

Personnel assigned to both the organizational and intermediate level maintenance activities are required to complete corrosion control training in accordance with the Naval Aviation Maintenance Program (NAMP) requirements in the Office of the Chief of Naval Operations Instruction (OPNAVINST) 4790.2, Volume I. Volume II of OPNAVIST 4790.2 pertains to DEPOT level Maintenance requirements.

O and I Level Maintenance Activities: In accordance with OPNAVINST 4790.2, Vol I, all personnel in aircraft, engine, component or equipment maintenance shall complete one of the mandatory minimum corrosion control courses administered by one of the following facilities:

a. Naval Air Maintenance Training Group (NAMTRAGRU), Course C-600-3180 or C-100-4176.
b. Aviation rating specific "A" School (After 1 April 1992)
c. Naval Aviation Engineering Service Unit (NAESU), equivalent training

Corrosion Control Work center, Intermediate Maintenance Activity (IMA) Airframes, and Support Equipment corrosion control work center supervisors must complete the Naval Aviation Depot (NAVAVNDEPOT) Course N-701-0013 (Corrosion Control). Completion of one of the courses above is a prerequisite to attending the NAVAVNDEPOT course.
To be qualified to perform aircraft or support equipment painting, O and I level maintenance personnel must complete both the Basic Corrosion Control Course and the NAVAVNDEPOT course N-701-0014 (Aircraft Paint and Touch-up and Marking). These qualifications are valid for an unlimited period.

Depot Level: The following training for the qualification in corrosion control is required for Depot personnel performing corrosion inspections, prevention, arrestment, and removal:

a. Completion of the NAVANDEPOT corrosion control course, N-701-0013.
b. Completion of the NAVAVNDEPOT aircraft painting course for aircraft painters, N-701-0014.

Key references utilized by both training and maintenance activities for conducting corrosion prevention and controls are the following:
NAVAIR 01-1A-509, Aircraft Weapons Systems Cleaning and Corrosion Control
NAVAIR 15-01-500, Preservation of Naval Aircraft
NAVAIR 16-1-540, Avionics Cleaning and Corrosion Prevention/Control
NAVAIR 17-1-125, Support Equipment Cleaning, Preservation, and Corrosion Control
OPNAVINST 4790.2, Volume 5, Naval Aviation Maintenance Program Standard Operating Procedures, Chapter 14
Maintenance Publications Peculiar to Aircraft Models and Related Equipment.

Recent Advancements

Current developments in environmental compliance have resulted in changes to various materials and processes utilized in the aircraft corrosion control program. The Naval Aviation community has a continuing effort to incorporate new materials and processes into both field and depot corrosion control activities. While there currently are many promising new materials, processes or technologies being investigated, most have not had sufficient field testing for widespread utilization. The following will discuss some of the recent materials and processes that are currently being utilized by both field and depot corrosion control activities.

Glove box Plastic Media Blasting: Plastic media blasting (PMB) is a dry media blasting process that uses angular plastic particles to remove paint and other similar coatings without generating hazardous liquid chemical waste, and when properly applied, without damaging the substrate. PMB will not effectively remove corrosion products. Recently, the use of plastic media blasting as an alternative to chemical paint removal on aircraft components has been authorized for intermediate maintenance level activities. PMB of aircraft component surfaces is authorized for use only in a blast cabinet (glove box) specifically designed for plastic media. Furthermore, all operators of the PMB glove box must complete a specialized PMB operator training prior to the use/operation of the PMB glove box. Plastic media used in the PMB glove box shall conform to MIL-P-85891, Plastic Media for Removal of Organic Coatings, Type V (Acrylic, Thermoplastic), size 20/30 mesh materials. Type V plastic blast media was selected as the predominant materials used for aircraft PMB process because it was considered to have the best all around blasting characteristics. Operating PMB nozzle blasting pressure shall be 30 psi maximum.
Other limitations: PMB of aircraft component surfaces is restricted to metallic surfaces 0.032 inch thick or greater. Nonmetal surfaces, such as composites or fiberglass, and metal bonded structures are not authorized for PMB. Because there is a potential for PMB to peen or smear soft metals, it shall NOT be used to remove paint from aluminum or magnesium components requiring subsequent fluorescent penetrant inspection, unless specifically directed by engineering authority for that component.

Aqueous Parts washers and MIL-C-29602: Alternative processes are used to replace the solvent vapor degreasers and immersion tanks for removing oils and surface contaminants from air craft components. The use of the aqueous parts washers has reduced the use of Ozone Depleting Substances (ODS) and other materials and their accompanying hazardous wastes. Parts washers currently being delivered and used by Intermediate Maintenance Activities are industrial power washers that are comprised of an enclosed cleaning cabinet with a system of spray impingement nozzles, cleaning solution heater, fluid pump, skimmer for oil and its residues, and separate reservoirs for cleaning solution and effluents. The cleaning cabinet's spray nozzles blast a bio-degradable water based detergent, MIL-C-29602, on to dirty parts. The combination of high temperature (up to 200 degrees Fahrenheit) and high blasting pressure (up to 300 psi) enables the washers to remove dirt, grime, oils, grease, fluorescent penetrant, plating waxes and tape residue from parts. Due to the entrapment of water based detergent, the Naval Aviation community has a restriction of the parts washers on bearing components.

MIL-C-29602, Cleaning Compound for Parts Washers and Spray Cabinets: The cleaning compound supplied under this specification shall have no-ODS, no-(Hazardous Air Pollutants (HAPs) and No-Volatile Organic Compounds (VOCs) with biodegradable surfactants. This cleaning compound is supplied under two Types: Type I, Water Soluble Liquid Concentrate and Type II, Water Soluble Powder. The pH of the cleaning compound shall be no less than 10 and no more than 13.5 when run at the manufacturer's recommended cleaning concentration.

P-W-2891, ODS, No- HAPs, and Low vapor pressure (<7mm Hg) Wipe Solvent. This intent of P-W-2891 is for critical cleaning applications. Critical cleaning is defined as those applications that require a follow-up application of sealing, non-structural bonding, priming, painting, nondestructive inspection and dry film lubrication.

TT-R-2819: No HAPs Paint Remover. This paint remover was developed for stripping paint from metal surfaces of aircraft exteriors. There are three types available for this specification. Type I paint removers are used to strip epoxy primer coating/polyurethane topcoat systems and flexible polyurethane primer/polyurethane topcoat systems and may be useful for removing self-priming polyurethane coating (TT-P-2756) systems. Type II paint removers are used to remove polysulfide-based systems by digestion of the polysulfide polymer.

Coating Touch-up Pens, SEMPEN™: This is a touch-up coating applicator that was designed for the convenient storage, mixing and application of pre-proportioned coating materials. Each touch-up pen is supplied with two or more precisely metered materials that are barrier-separated during storage. Each applicator contains 10 ml (10cc) of material.
The coating systems packaged in the touch-up pens are:
MIL-P-23377, High Solids Epoxy Primer, Type I (Standard Pigments) and Type II (Low Infrared Reflective Pigments), Low Volatile Organic Compound (VOC) content of 340 g/l. Materials covered by this specification are low VOC, corrosion-inhibitive, chemical resistant, strippable primer coatings. Type I is for general use. Type II is for use where low infared reflectance is required.
MIL-P-85528, Epoxy Waterborne Primer, Type I (Standard Pigments) and Type II (Low infrared Reflective Pigments). Materials covered by this specification are waterborne, low VOC (340 g/l or less) epoxy type, corrosion inhibiting, chemical and solvent resistant primers.
MIL-C-85285, High Solids Polyurethane, Type I, Aircraft application (420 g/l VOC). Exterior use on aircraft, weapons systems. Type II is intended for use on ground support equipment (VOC 340 g/l).

Polytetrafluoroethylene (PTFE) Aircraft Sealant, SKYFLEX™ : SKYFLEX™ sealant is a modified Teflon™ (Expanded Polytetraflouroethylene) designed for aircraft sealing applications. This particular sealant provides improved weather sealing, avoids excessive handling of hazardous chemicals, and saves time as no curing is required. The properties of the sealing material allow it to easily conform to irregularities and complex shapes. The sealing material is a tape which comes in three different widths, 0.25" , 1.1" , 1.65" and has an acrylic pressure sensitive adhesive on the back of each tape. Current application of the SKYFLEX™ sealant is on the S-3 Aircraft. It has been field tested on non-pressurized panels over the past 2 years, and on seven pressurized panel areas for 15 months. With additional successful field trials on other aircraft models and long term S-3 test data, future applications can be considered.

Technical Corrosion Control Assist System

Communication and networking between various commands and field activities are vital to the success of any major program. The Naval Aviation Community has attempted to increase corrosion control awareness and up-dates to new materials and processes by establishing a strong communication/support network system. The following information will provide key points of contacts for the Naval Aviation Corrosion Control Activities.

Lead Maintenance Technology Center for Corrosion Prevention and Control

A Lead Maintenance Technology Center (LMTC) is a Naval Aviation Depot (NADEP) or Naval Air Warfare Center (NAWC) or Naval Surface Warfare Center (NSWC) activity responsible for developing maintenance processes and supportability requirements within a particular Maintenance Technology (MT) area. LMTCs will provide support to fleet activities, Program Management Teams, and Product Support Teams. Their primary purpose is to enhance mission and readiness capabilities, for both fielded and emerging aviation systems, by developing and pursuing technologies that will improve maintenance and repair abilities and lower operating costs. Rapid evolution of new materials, equipment, and increasingly stringent environmental regulations makes it essential to incorporate maintenance experience into developmental programs to assure effective implementation of technology improvements into the maintenance operations.

The Lead Maintenance Technology Center for Corrosion Prevention and Control (LMTC-C) is Naval Aviation Depot, North Island. It is responsible for actively developing maintenance processes and supportability requirements within the Corrosion Control Maintenance Technology (MT) area. The LMTC-C's MT encompasses the protection of operational aircraft and support equipment systems from material corrosion through corrective and preventative maintenance actions. The protection of the systems is provided by, but not limited to, the following areas: Cleaning, Inspections, Sealants, Surface Coatings, Materials and Processes (M&P) Selection, and Emergency Reclamation.

LMTC capabilities for corrosion prevention and control support are provided out of the 27,060 square foot Materials Engineering Laboratory Facility, located at the Naval Aviation Depot, North Island. This facility houses 10 of the 29 LMTC activities. The other nine LMTC activities are Aircraft Preservation, Non-Destructive Inspection, Bearings, Adhesives, Tires, Heat Damage Evaluation, Heat Treatment, Welding/Brazing and Canopies/Transparencies

Additional support for LMTC-C coordination is supplied by Naval Aviation Depots at Cherry Point, North Carolina and Jacksonville, Florida, the Naval Air Warfare Center Weapons Division, China Lake, California and the Naval Air Warfare Center Aircraft Division, Lakehurst, New Jersey.

Naval Air Warfare Center - Aircraft Division, Aerospace Materials Division, Materials Protection Branch

Primary materials science and technology for corrosion control materials and processes are provided by the Materials Protection Branch of NAWC. The Aerospace Materials Division located is a 44,000 square foot new laboratory building at Patuxent River, Maryland. Within the Materials Protection Branch, there exist three primary Teams: Protective Coatings, Operational Chemicals and Surface Interactions, which provide the following support in the area of corrosion prevention and control:

Protective Coating Team: Develop and analyze advanced coatings for the protection of aircraft from corrosive environments and detection/weapon threats.

Operational Chemicals team: Responsible for the research, development, testing and evaluation of operational and maintenance chemicals used in cleaning technology and corrosion prevention.

Surface Interactions Team: Provide solutions for corrosion and wear control problems unique to Naval aircraft and anticipate future needs by establishing fundamental principles related to surface interactions under a wide range of conditions and developing the necessary products and processes.

TYPE COMMANDER Aviation Maintenance Management Teams

Under the TYPE COMMANDERs (TYCOMs) Aviation Maintenance Management Team (AMMT), there exist Corrosion Control Inspection Teams for the O and I level of Naval Aviation Maintenance. One of the primary responsibilities for the Corrosion Control Inspection Teams is to conduct on-site inspection at the O and I level Maintenance Activities and assist fleet personnel in resolving their corrosion control issues and concerns.

NAVAL AVIATION ENGINEERING SUPPORT UNIT

Naval Aviation Engineering Support Unit, NAESU, is a field activity of the Naval Air Systems Command and reports directly to the Assistant Commander for Logistics and Fleet Support. NAESU Headquarters is currently located at the Philadelphia Naval Business Center, Philadelphia, Pennsylvania. Primary support to the Naval Aviation Corrosion Control efforts is provided by the NAESU Corrosion Control Materials technologist. The NAESU Corrosion Control Materials technologists are responsible for providing on-site field engineering technical assistance and instruction to naval aviation activities in the corrosion control of aviation systems and equipment.

REFERENCE DOCUMENTS

1. NA 01-1A-509/T.O. 1-1-691/TM 1-1500-344-23, Aircraft Weapons Systems Cleaning and Corrosion Control, NAVAL AIR SYSTEMS COMMAND, 1 May 1996.

2. OPNAVINST 4790.2F, The Naval Aviation Maintenance Program (NAMP), Department of the Navy, Office of the Chief of Naval Operations, Washington D.C., 1 June 1995.

3. Lead Maintenance Technology Center Directory, Naval Air Systems Command, 26 May 1996

Approaches to Corrosion Control on the USMC Riverine Assault Craft (RAC)

William Steiner
Naval Surface Warfare Center, Carderock Division
Code 624, Marine Coatings and Corrosion Engineering Branch
Philadelphia Naval Business Center, Philadelphia, PA 19112-5083

Norm Clayton
Naval Surface Warfare Center, Carderock Division
Code 624, Marine Coatings and Corrosion Engineering Branch
Philadelphia Naval Business Center, Philadelphia, PA 19112-5083

ABSTRACT

The Riverine Assault Craft (RAC) is a 35 ft. long aluminum craft that is operated by the United States Marine Corps (USMC). In their three years of operation, a number of significant corrosion-related problems have developed as a result of poor designs or material choices. These included: poor reliability of the original engine starters and solenoids; a raw water cooling system (RWCS) that used plain steel sensor fittings in stainless steel piping; use of plated steel electrical system components; and potential future hull corrosion in the bilges due to water traps and the use of intermittently welded stiffeners. While the Naval Ordnance Center, Fallbrook Detachment (NOC Fallbrook) has been tasked to develop Engineering Change Proposals (ECPs) to address various electrical system and RWCS deficiencies, NSWCCD has been tasked to look at overall life cycle corrosion control improvements. Work completed or ongoing includes alternate material recommendations, revising the Technical Manual and training materials, and development of a corrosion control course for maintenance personnel.

INTRODUCTION

The Riverine Assault Craft (RAC) is a 35 ft. long, light, highly maneuverable craft that is operated by the United States Marine Corps (USMC). See Figure 1 for an illustration. It is used primarily in drug interdiction operations. Propulsion is provided by two Hamilton waterjets powered by a pair of Cummins diesel engines. The RAC currently operates mainly in brackish waters, but may also be used in fresh water or sea water. Between 1993 and 1995 25 RACs were built by Swiftships, Inc. The RAC was designed for a 4-person crew: the boat captain, the coxswain, and the forward and aft gunners.

BACKGROUND

In 1990, a Statement of Urgency (SOU) was issued by the Commandant of the Marine Corps to develop a highly maneuverable craft to support drug interdiction operations conducted by the federal government. To meet this requirement in a minimal amount of time, an acquisition plan (AP) which included a Non-Developmental Item (NDI) strategy was employed. This resulted in the awarding of a sole source contract for construction of seven (7) craft for initial evaluation. The craft performed adequately, and plans to submit a contract to competitive bidding were initiated. These plans also used an NDI strategy. The Department of the Navy (DoN) Office of Acquisition Reform has written a detailed discussion of the RAC acquisition process[1].

The request for proposal (RFP) for the contract specified procurement of a commercial/NDI RAC that met the requirements of the approved Performance Description (PD) and Statement of Work (SOW). The proposals of the contractors who responded were subjected to a rating system that evaluated technical compliance and cost. The proposals were further evaluated using the following criteria:

1. Go/No Go. The contractors were required to meet or exceed specific performance and operational criteria, such as top speed, endurance, etc.

2. Performance. The contractors were judged in their ability to meet the requirements of the PD and SOW.

Ultimately, a vendor was selected and a contract awarded for construction of the 25 RACs. The crafts have been in service for approximately four years. During this time, a number of significant corrosion-related problems have developed, which were the result of a number of events that occurred prior to construction. These included:

- Failure of the PD and SOW to sufficiently describe the environment that the craft would be operated in;
- No requirements for the contractor to operationally and developmentally test the design;
- Use of Best Commercial Practices (BCP) that proved to be unsuitable for a military application;
- Design inconsistencies between individual craft, i.e. each RAC has fundamentally different designs such as electrical wiring, routing of piping, cabling, engine configuration, and the like;
- Use of parts that were not designed for a marine environment, resulting in rapid corrosion and failure;
- Lack of Integrated Logistics Support (ILS) and support for parts;
- Lack of adequate technical documentation.

Additional problems have occurred in the structural, electrical, raw water cooling, and propulsion systems. Often these problems were exacerbated when it was revealed that there were a number of inconsistencies in parts used among the crafts, as well as in their relative locations.

To help resolve these issues, the USMC tasked the Naval Surface Warfare Center, Carderock Division (NSWCCD) to participate in the development of a Corrosion Prevention and Control Program (CPAC) for the RACs. In the initial kickoff meeting between NSWCCD and USMC personnel, many of the prominent design and material issues were discussed. These included the following:

1) The original starters and solenoids were non-marinized and therefore highly susceptible to corrosion. This condition was worsened during periods of extreme maneuvers when large quantities of water entered the bilges, resulting in the uncovered engine flywheels spraying the bilge water directly onto the starters.

2) The extensive use of non-marinized, plain steel electrical and other system componentry as terminal strips, couplings, tubing, and fasteners that easily corrode and fail.

In order to corroborate this information, NSWCCD conducted an initial survey of the RAC during July of 1996. NSWCCD discussed the observations made during this survey[1] . During the course of the evaluation, a number of both existing and potential corrosion problems were revealed. These are divided by system, and are discussed below.

FINDINGS

Structural

The bilge and internal stiffeners are unpainted aluminum. Although the transverse frames were fully welded to the hull, the majority of the longitudinal stiffeners were attached using intermittent welds, thereby introducing crevices between the stiffeners and the bilge plating. Although no signs of corrosion were visible, these areas were considered to be potential sites of future crevice corrosion. This concern was magnified when it was found that the bilge pockets forward of the craft examined did not drain back to the engine compartment bilge where the two bilge pumps were located. Each bilge section examined was found to be full of water. Although no evidence of corrosion was apparent, it nevertheless presents a corrosion risk. However, it was uncertain if this problem was common to all 25 RACs, for as noted earlier configurational differences exist between craft. Another potential site for crevice corrosion was found in the anchor compartment. This compartment is located in the bow, with an access hatch in the deck. It appeared to have been filled with floatation foam from the keel to within about 20" from the overhead. At this level, there were horizontal stiffeners intermittently welded to the hull to provide support for removable gratings that support the anchor. Overboard drain pipes were present from the port and starboard aft corners of the compartment just below the stiffeners. Due to the way in which the foam was installed (having been sprayed), it had a very uneven surface contour. While some foam had been removed from the area of the drain pipes to facilitate

---

[1] NSWCCD Ltr 9630 Ser 624/237 of 27 Nov 96, Riverine Assault Craft (RAC) Corrosion Control Program Trip Reports

drainage, most of the remaining foam provides many pockets where water collects. Again, while no corrosion was observed, it did present a corrosion risk.

Propulsion

Corrosion problems in this system were a combination of poor material choices and ill-conceived designs. Examples of dissimilar metal corrosion were observed throughout. During the survey a cooling water temperature sensor broke off on its own accord; it failed due to severe corrosion of the threaded steel fitting used to mount the sensor line in a boss on the stainless steel (CRES) piping. Corrosion was accelerated by a large cathodic area (the CRES piping) coupled to a small anodic area (the sensor's steel fitting).

More serious problems were observed with regards to the engine driveshaft and universal joint, which are fabricated from bare steel, and were heavily rusted. RAC maintenance personnel reported to NSWCCD during the survey that whenever engine replacement was necessary, severe seizing of the mating splines due to corrosion was encountered.

The steel V-belt covers on the forward sides of the engines were rusting badly due to paint failure. Although the problem is mostly cosmetic, with no impact on either craft performance or reliability, the recommended powder coating solution to this problem discussed in the Results section may be applied to additional areas of the craft.

Another corrosion problem in the propulsion system involved the waterjet rake actuating cable. This rake is used to help clear debris from the waterjet intakes. It is actuated manually via an armored, plastic-jacketed control cable from a handle in the troop compartment. It was reported by RAC maintenance personnel that this assembly seizes frequently, and that the problem could be resolved only be replacing the cables. A section of cable was analyzed subsequent to the survey and examined (see Figure 2). The armor windings and the inner and outer cable strands are all steel and subject to rusting if water enters the cable. As the corrosion products accumulate and expand, they can exert considerable pressure on the inner cable, causing it to seize. Plausible entry routes for the water are at the cable terminations, as well as at any sites of damage to the plastic jacketing.

Electrical/Communications/Navigation

The coxswain instrument panels and the boat captain's communications station are both open at the rear and bottom. Attempts were made by the RAC crew to prevent entry of water via extensive use of silicone Room-Temperature Vulcanizing (RTV) sealant. Figure 3 shows corrosion of the components on the panel underside. The control and instrument panels are located directly over the bilge, with the coxswain's station being the more openly exposed of the two. As previously mentioned, this bilge pocket was filled with water, thereby increasing the exposure to humidity experienced by the individual components and terminal boards. Further aggravating the situation is the protective tarp used to shield the RAC from the elements when stored on land. Use of this cover results in the containment of moisture and humidity, resulting in

alternating cycles of condensation and evaporation inside the craft (and especially on these panels) day and night.

One relatively minor corrosion problem that was observed entailed the electrical cable loop clamps that are used throughout the craft. According to their reference drawing (MS21919) and procurement specification (MIL-C-8603), these clamps employ a strip of either aluminum alloy, low carbon steel, or CRES to provide support, within a cushion of either ethylene propylene, nitrile, chloroprene, silicone, or fluorosilicone that protects the cable. They have either a chemical conversion, cadmium plated, or passivated finish. These clamps are used within the Navy and USMC in a variety of applications. Those on the RAC use the aluminum alloy within a chloroprene cushion, with a chemical conversion finish. The clamps fasten to the structure via a single CRES screw. This particular aluminum alloy is not suitable for marine environments and is prone to exfoliation, causing the clamps to disintegrate and ultimately fail.

Auxiliary/Outfitting

There were a few miscellaneous items that were revealed during the survey. The snaps used on the craft's seat covers were CRES, but they were fastened to the aluminum seat frames with aluminum screws; many of the screws had corroded and broken off on the craft surveyed. Another item was the swage fitting on the wire rope support for the swimmer's platform (located aft). The wire rope used is CRES, but the swage fitting is aluminum; galvanic and crevice corrosion causes the fitting to split and eventually fall off.

RESULTS

Following the initial RAC survey, NSWCCD conducted a follow-up visit to the Naval Ordnance Center, Pacific Division, Fallbrook (NOC Fallbrook). NOC Fallbrook was tasked with developing Engineering Change Proposals (ECPs) for the RAC's electrical and raw water cooling systems. During this visit, NSWCCD discussed its and Fallbrook's findings with the craft, and examined a RAC in Fallbrook's possession which was serving as the prototype platform for the electrical system ECP changes. NSWCCD's original recommendations and references to the Fallbrook visit, in addition to the results of exchanging information with Fallbrook personnel are presented below.

Structural

To address the problem of lack of bilge drainage in the area forward of the engine compartment, a procedure for providing a drainage path was drafted. However, after attempting to follow the procedure on some of the affected craft, the RAC maintainers reported that configurational differences between craft required custom procedures for each craft.

With regards to the potential for crevice corrosion in the forward anchor compartment, it may be minimized by periodically flushing the compartment with fresh water, to remove any salt or brackish water that may be present.

Propulsion

The first item of concern in this system involved the cooling water temperature sensors, which was an example of galvanic corrosion. As previously stated, the problem occurred from use of a CRES pipe coupled to a plain steel fitting. This problem is currently being addressed by the RAC maintainers by replacing the steel fittings with CRES units as they fail.

The initial recommendation for the rusting engine driveshaft and universal joint issue was to use a marine-grade grease that is resistant to water wash-out. Concurrently, NOC Fallbrook had applied zinc metal sprayed coating to these components, and has included this change as a part of an ECP. No sealer coat was applied over this coating. The procedure was performed according to American Welding Society (AWS) specification ANSI/AWS C2.18-93. Discussed during the visit was the actual procedure used, degree of surface preparation, and thickness of the applied coating. This procedure follows the AWS specification, detailing the degree of surface cleanliness (near white metal, as per Steel Structures Painting Council standard SSPC-SP-10), minimum anchor tooth blast profile (0.002" - 0.004"), and required coating thickness range (0.005" - 0.012"). NSWCCD will track the performance of this coating in concert with NOC Fallbrook. A photograph of the coated assembly is shown in Figure 4.

As previously discussed, the steel V-belt covers were rusting badly due to paint failure. One possible means of solving this problem would be to apply polyester powder coating to the covers. This coating would effectively control corrosion, due to its toughness and ability to cover edges well. Another advantage is that it contains no Volatile Organic Compounds (VOCs). Currently, Camp Lejuene, North Carolina (CLNC), the primary RAC operating facility, does not have the capability to apply this coating, and would have to use local commercial applicators. However, as a part of NSWCCD's overall corrosion control support to the USMC, the feasibility of setting up powder coating facilities for multi-platform use at major USMC bases will be explored in the future.

Regarding the waterjet rake cable, a new, more corrosion-resistant cable assembly has been approved to replace the previous setup. The use of cold shrink tubing at the cable terminations was recommended, which would help prevent entry of water into the cable. It was also recommended to use heat shrink tubing for repairing cuts or tears in the cable's outer jacketing. For RACs that still have the original cable assembly, it was recommended that in addition to the above measures, the actuating lever be cycled periodically to ensure that the cable does not seize.

Electrical/Communications/Navigation

The ECPs prepared by NOC Fallbrook thoroughly addressed much of the RAC's electrical system corrosion problems. The major features of the ECPs are as follows:

- Extensive use of 300-series CRES fasteners. Type 316 was desired for all fasteners, but when unavailable generic 300-series CRES was deemed acceptable. When new, marinized

replacement components contained bare or plated steel fasteners; these also were replaced with 300-CRES and documented accordingly.

- Terminal blocks changed to 300-series CRES, with CRES or nickel-plated brass screws.
- Coxswain instrument panel gages changed to marinized styles.
- Copper vacuum tubing changed to U.S. Coast Guard-approved rubber tubing.
- One-part polysulfide sealant used on CRES fasteners in aluminum panels and raceway covers, to prevent dissimilar metal corrosion.
- Clear, RTV adhesive/sealant used on all panel edges and seams, and on top of mechanically fastened electrical connections after the connection was made. This sealant was used extensively in other areas as well. The use of a clear sealant will permit early signs of corrosion and disbonding to be detected.
- Electrical connectors under coxswain's panel changed to cadmium-plated aluminum.
- Cable run stand-offs added to prevent jacket/insulation cutting by sharp edges of structures.
- Bilge pump electrical connections moved up out of bilge to side of battery support tray.

In addition to the above ECP measures, two corrosion preventive treatments were recommended for use in conjunction with the above upgrades: cold-shrink tubing for weatherproofing electrical connectors, and a polytetrafluoroethylene (PTFE)- based thread treatment for dissimilar metal fastener installations. The cold-shrink tubing was recommended for those connectors that the RAC operators would not routinely need to disassemble, since disassembly would require cutting and destroying the costly tubing sleeves. This is especially recommended for the cadmium-plated aluminum connectors, since experience on Naval surface ships has shown that these connectors are prone to corrosion after a relatively short period of time in marine exposure. The thread treatment was recommended for those fasteners which the RAC crews and maintainers would have to remove and reinstall periodically.

Finally, the issue of corroding electrical cable loop clamps was resolved by locating CRES-style loop clamps (Grade 321) having weather-resistant chloroprene cushions. Since these replacement clamps still use CRES screws to mount the clamp to the aluminum structure, use of either zinc dust antiseize compound or PTFE thread treatment compound must be used on the screws to prevent dissimilar metal corrosion.

Auxiliary/Outfitting

Several options are being considered for solving the problem of containment of moisture and humidity due to the RAC's protective cover used during land-based storage. Testing and

monitoring would be required to quantify the extent of the problem, but this type of effort is beyond the scope of this program. A summary of the options that have been considered is provided below. Factors that will affect the decision include cost, logistics support required, and the impact on the time needed to put a RAC into or out of storage.

1. **Replace current tarp with new design.** Fabricate a new tarp, using materials that are waterproof yet can "breathe" to permit adequate ventilation, while meeting the strength and other requirements of the previous design.

2. **Place desiccant bags inside the craft.** Desiccant bags of different sizes would be placed in the craft. This could aid in "drying out" the craft. This could be present problems, in that the bags may become saturated rather quickly, and drying ovens would be required for spent desiccant.

3. **Seal current cover and dehumidify.** The existing cover would be retained, and a method of sealing it to the craft gunwales would be devised. The tarp would also be modified to allow a hose connection to a portable dehumidifier. The end result is that a dehumidification "tent" would be created. This option would also require appropriate facilities support, and maintenance of the dehumidification units themselves.

4. **Install solar powered exhaust fan on current tarp.** This proposal would involve an exhaust fan, powered by a solar cell, that would fit over a section cut out of the existing tarp. During the day, the sunlight would power the fan. At night, the fan would be powered by a battery charged by the stored solar energy. The fan would serve to exhaust the moist air trapped underneath the tarp. This solution would be relatively inexpensive and easy to implement; however, the durability of the system, fan effectiveness, and logistics support issues would need to be assessed.

5. **Add ventilation flaps to existing tarp.** Using the existing tarps, reinforced vent openings would be added in a number of places. This solution would be relatively inexpensive and easy to do, but it is not known how effective it would be. The size, number, and locations of the vents would need to be resolved, as well as creating a design that will still shed rainwater.

Resolution of this issue is still under investigation.

Technical Documentation And Training

In order to effectively execute the corrosion control measures recommended and also to prevent future corrosion issues from arising, it is necessary for RAC maintainers to have a working knowledge of corrosion principles, prevention, and control, and to have readily available reference material specific to their craft. To achieve this goal, a thorough review of the RAC Technical Manual (TM)[2] was conducted. Corrosion control information and procedures were added to the existing maintenance procedures, and a new Appendix dedicated to corrosion control was added[1][2].

---

[1] NSWCCD Ltr 9630 Ser 624/278 of 21 Mar 97, Recommended Changes to the Riverine Assault Craft (RAC) Technical Manual, TM 09557A/14-1

A summary of the changes made are provided below:

- Inclusion of various "Corrosion Control Notes," interspersed throughout the text. These notes offer "tips" for better controlling and preventing corrosion in the particular system or component in question. A beneficial side effect is that they help increase the corrosion awareness of RAC maintainers and remind them that corrosion prevention and control procedures are applicable to the entire craft, not simply to isolated components;

- Updating the consumable parts list to include such items as electrical connector sealants and weatherproofing tubing, marine-grade greases, zinc antiseize compounds, corrosion preventive compounds, and polysulfide sealants;

- Updating scheduled maintenance procedures for the structural, propulsion, and electrical systems;

- Revising the symptoms, probable causes, and corrective actions needed to better troubleshoot problems that arise, and inspections for specific component corrosion problems;

- The new Appendix to the TM, which provides an introduction to corrosion principles, prevention, and control. It includes a summary of the most corrosion-prone areas on the RAC, as well as a description of and instructions for using the various corrosion control compounds, sealants, etc. referred to in the body of the text.

Use of the various types of water-displacing, sprayable, short to intermediate term corrosion preventive compounds (CPCs) was also discussed. There are generally three types of CPCs currently available in the stock system, covered by specifications MIL-C-85054 and MIL-C-81309 Types II and III. Although MIL-C-85054 CPC provides the most corrosion protection of the three choices, it has the drawbacks of forming an excessive film buildup after repeated application. Consequently, it is typically only recommended for non-moving parts. However, it would be suitable for use in static applications, such as with terminal boards. For temporary preservation of RAC electrical components at the first and second maintenance levels (or "echelons") MIL-C-81309 Type II is recommended. This CPC remains soft (unlike MIL-C-85054, which dries to form a hard film about 1 mil thick) and typically forms a film 0.5 mil thick. Note that since it is a very thin film product, it only provides short term corrosion protection, depending upon the actual severity of the environment. In the case of the RAC, it would have to be reapplied every six months.

The USMC Engineering School, which trains RAC operators and maintainers, is using the new appendix to modify their course curriculum to include corrosion control information. In

---

[2] NSWCCD Ltr 9630 Ser 624/317 of 5 Jun 97, Changes to Riverine Assault Craft (RAC) Technical Manual, TM 09557A-14/1

addition, a one and a half-day corrosion control course is being developed. This course will use the above TM appendix as the student guide.

CONCLUSIONS

The Riverine Assault Craft (RAC) is a necessary, high-visibility USMC asset used in drug interdiction operations. Unfortunately, it has experienced a number of significant corrosion-related problems in its short existence. These problems have not been isolated to any one component or system, instead pervading nearly every system on the craft. To help solve these problems, the USMC tasked both the Naval Surface Warfare Center, Carderock Division (NSWCCD), and the Naval Ordnance Center, Pacific Division, Fallbrook Detachment (NOC Fallbrook). NOC Fallbrook's task was specific- development of Engineering Change Proposals (ECPs) for the RAC's electrical and cooling water systems. However, the role played by NSWCCD was more of a consultant, where the RACs were surveyed, problems were documented, and subsequent recommendations were made. To help ensure that these recommendations were fully implemented, NSWCCD also revised the craft's Technical Manual maintenance documentation and training materials, and began the process of setting up a course for RAC maintainers. The changes made by both NOC Fallbrook and NSWCCD were designed to be effective from both a cost- and time standpoint, to improve the reliability and maintainability of the RAC, and to ensure that it will continue to be able to successfully fulfill its mission.

ACKNOWLEDGMENTS

The authors wish to express their thanks to the following activities that helped develop the CPAC Program for the RAC and assist it in the two on-site surveys performed during CY96: Marine Corps System Command (MARCORSYSCOM) Code PSE, for sponsoring the work and providing general support; to the USMC 2nd Small Craft Company, Camp Lejuene, North Carolina; to the RAC Program Manager; to NOC Fallbrook; and to Naval Surface Warfare Center, Carderock Division, Code 613.

REFERENCES

1. Riverine Assault Craft (RAC) Program: A Case Study in Commercial Item/NDI Procurement Strategies, DoN Office of Acquisition Reform, Oct 96

2. Riverine Assault Craft (RAC) Technical Manual, USMC TM 0557A-14/1, Sept 95

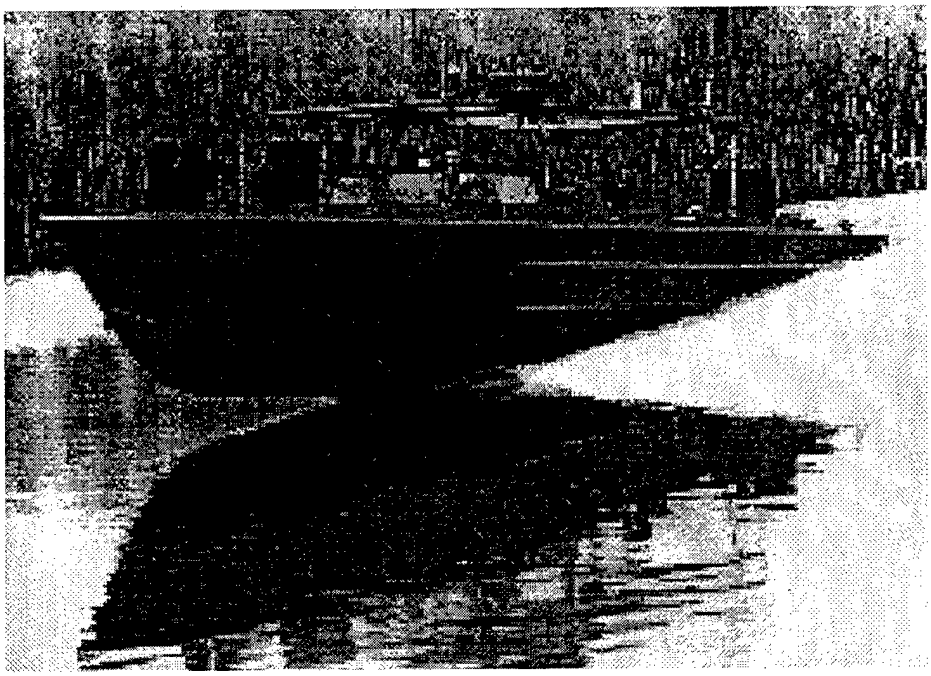

Figure 1. Riverine Assault Craft.

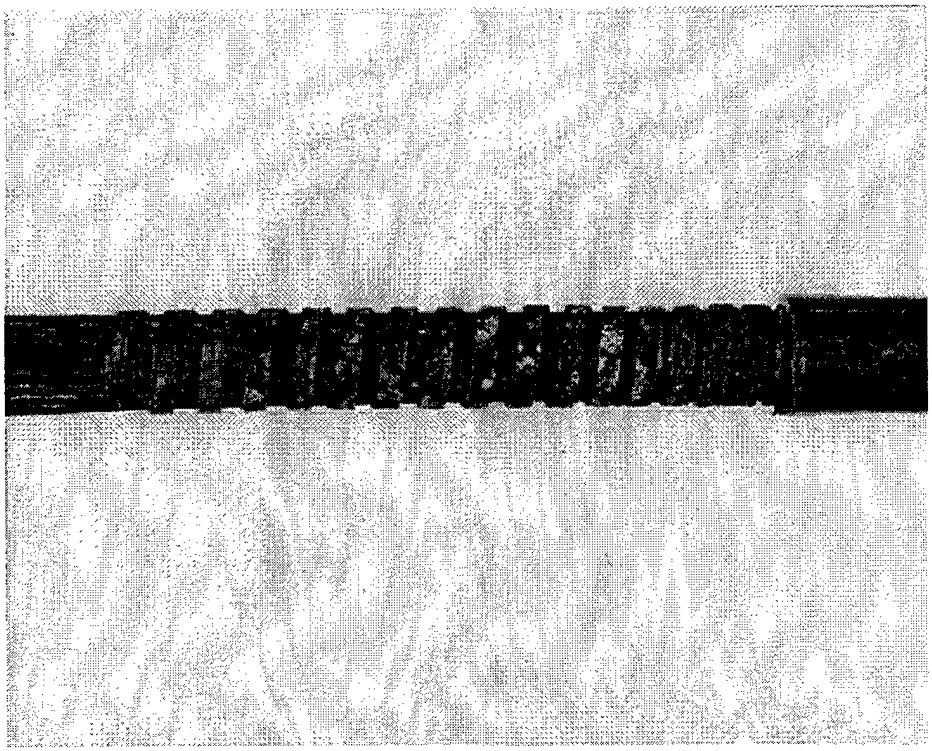

Figure 2. Waterjet Rake Cable (dissected).

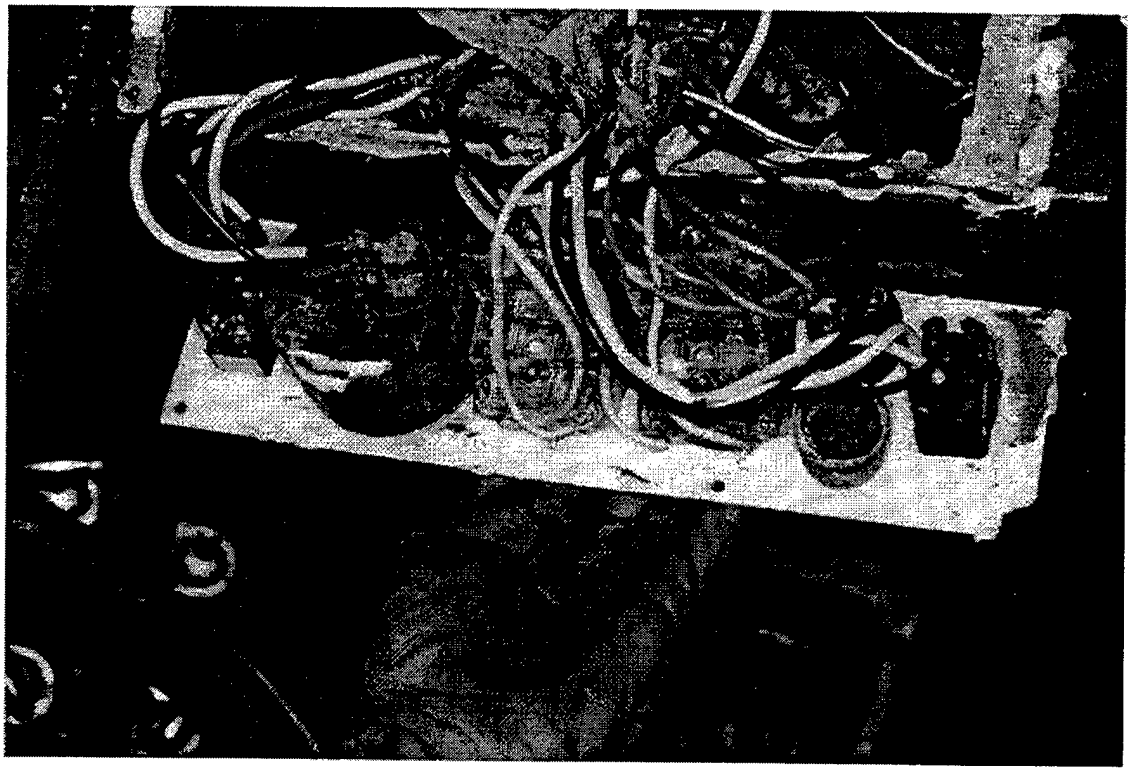

Figure 3. Underside of Coxswain Control Panel.

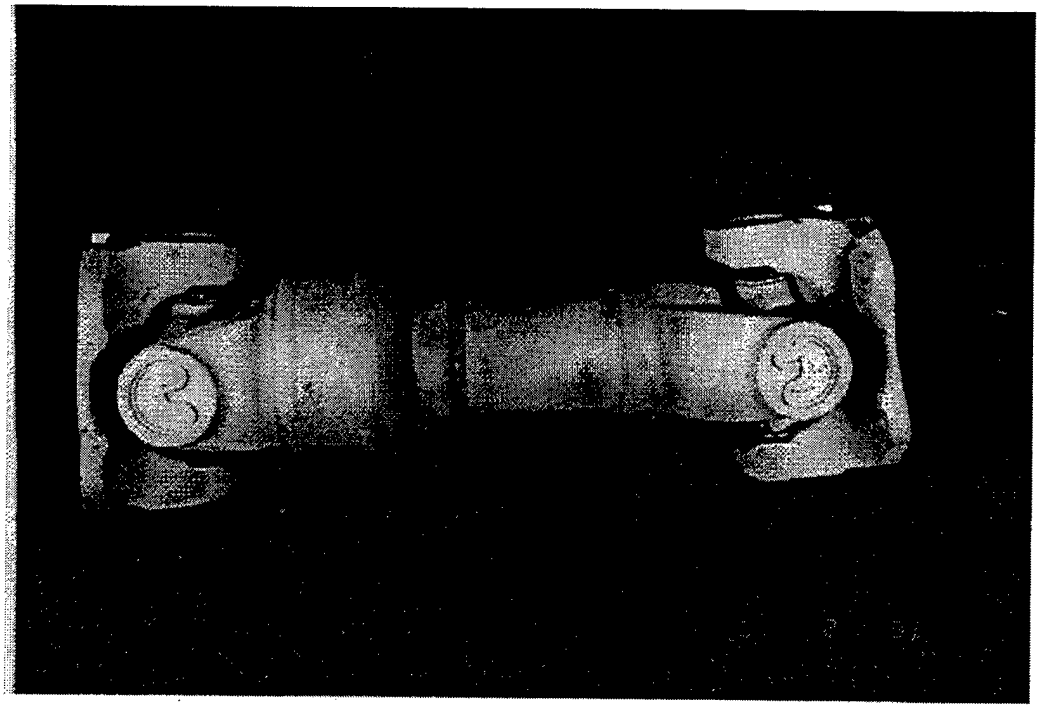

Figure 4. Zinc-sprayed Driveshaft Assembly.

AEGIS Corrosion Control Web Page

Commander Randy Hickman
Commander Ken Spiro
Program Executive Office Surface Combatant/Aegis Program
2531 Jefferson Davis Highway
Arlington, VA 22242-5165

ABSTRACT

The Naval Reserve unit of the AEGIS Fleet Introduction Office (PMS-400F) is developing a project to improve access to corrosion control information aboard Naval ships. The intent of this effort is to reduce manpower expenditure and material consumption, make efficient use of manpower, extend the life of ships and prevent premature failure of systems/components. Information about corrosion control products and procedures is not widely distributed, nor is it organized for ease of use by the fleet and engineering activities. Therefore, we are conducting market and literature research to assemble an electronic library of information on corrosion control. We formulated a world wide web page with summary information about material and operational methods for controlling corrosion. We are creating sublevels and links to more detailed information on each topic. We are coordinating with Naval organizations to capture information and ensure that the Web page is accessible by ships on the waterfront.

INTRODUCTION

The Fleet Support section (PMS-400F5) of Program Executive Office, Surface Combatant/Aegis Program (PEO SC/AP) is concerned with corrosion of Aegis ships. The impact of corrosion is a significant drain on maintenance resources and results in premature failure of metallic systems. The Naval Sea Systems Command and ship Type Commanders have devised numerous approved solutions to these problems, yet there is an inconsistent level of knowledge at the "deckplate" onboard ships, and the solutions are not easily accessible. The PMS Aegis 106 Naval Reserve Unit has embarked on a task to close the gap in knowledge by collecting and disseminating proven shipboard corrosion solutions so that they reach the ultimate users in the fleet. The vehicle for dissemination of the solutions is a World Wide Web page as shown in figure 1.

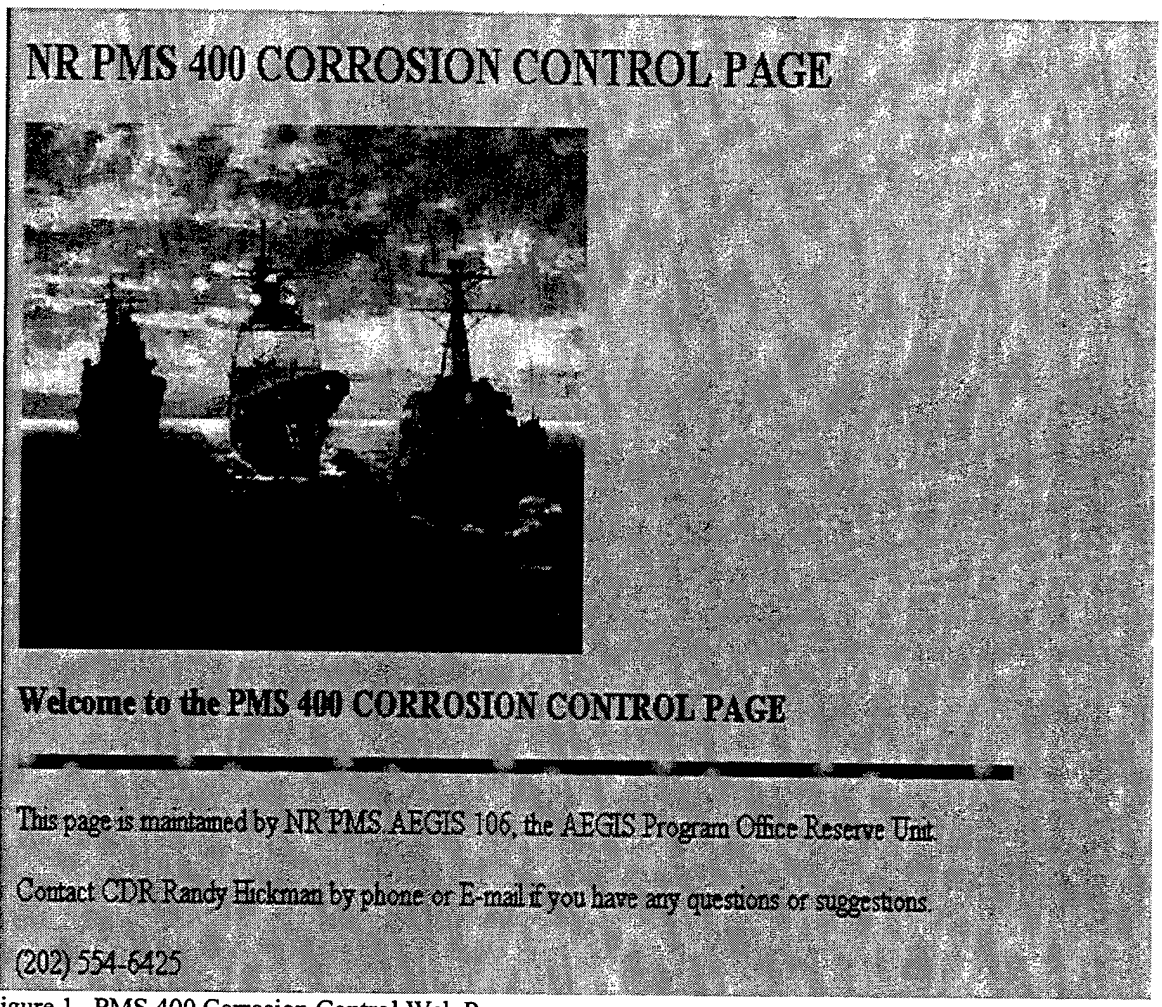

Figure 1. PMS 400 Corrosion Control Web Page

Access to the page is accomplished through the following address:

HTTP://WWW.WAM.UMD.EDU/~RGUBA/NAVY.HTM

PROCEDURE

The team collected data on shipboard corrosion through ship inspections, industry conferences, technical papers, Naval messages from NAVSEA, Type Commanders, and ships. The data were organized into common categories and the team determined the appropriate user groups for each topic on corrosion control. Once the users were defined (their roles and how they would use the data), we placed the information into three categories: (see figure (2))

1) Shipboard Corrosion Control Manager
2) Program Office Engineer
3) Maintenance and Overhaul Planning

The resulting front page to the web site allows specific user groups to focus on their needs for solving corrosion problems by clicking on the appropriate button.

Subsequent pages describe types of corrosion and explain proven solutions. (see figures 3 - 6)

RESULT

The result is an easy-to-use source of information on shipboard corrosion, available through the Internet. It provides solutions to three categories of corrosion managers in the Navy: those at the organizational (shipboard) level, those at the system engineering level, and those responsible for planning major ship renovations.

Shipboard Corrosion Control Manager

For the shipboard corrosion manager, a listing (see sample index, figure 3) is provided of approved shipboard corrosion solutions including reference to National Stock Numbered material, Allowance Parts Lists, part numbers, technical manuals, tools, and points of contact to solve specific problems. Other selections include a highlight for Navy ships in the Atlantic Fleet which lists Type Commander (COMNAVSURFLANT) funded corrosion control material such as cold shrink tubing, stainless steel fasteners, gasket material, coatings and greases. The web page provides further promotion of SURFLANT's innovative concept to use a waterfront van to issue corrosion prevention material at no cost to its ships. Other topics for the shipboard corrosion control manager include an index of helpful solutions for ship's force, issues and responses from In Service Engineering Agent (ISEA), and a summary of VHS tapes available for training on corrosion.

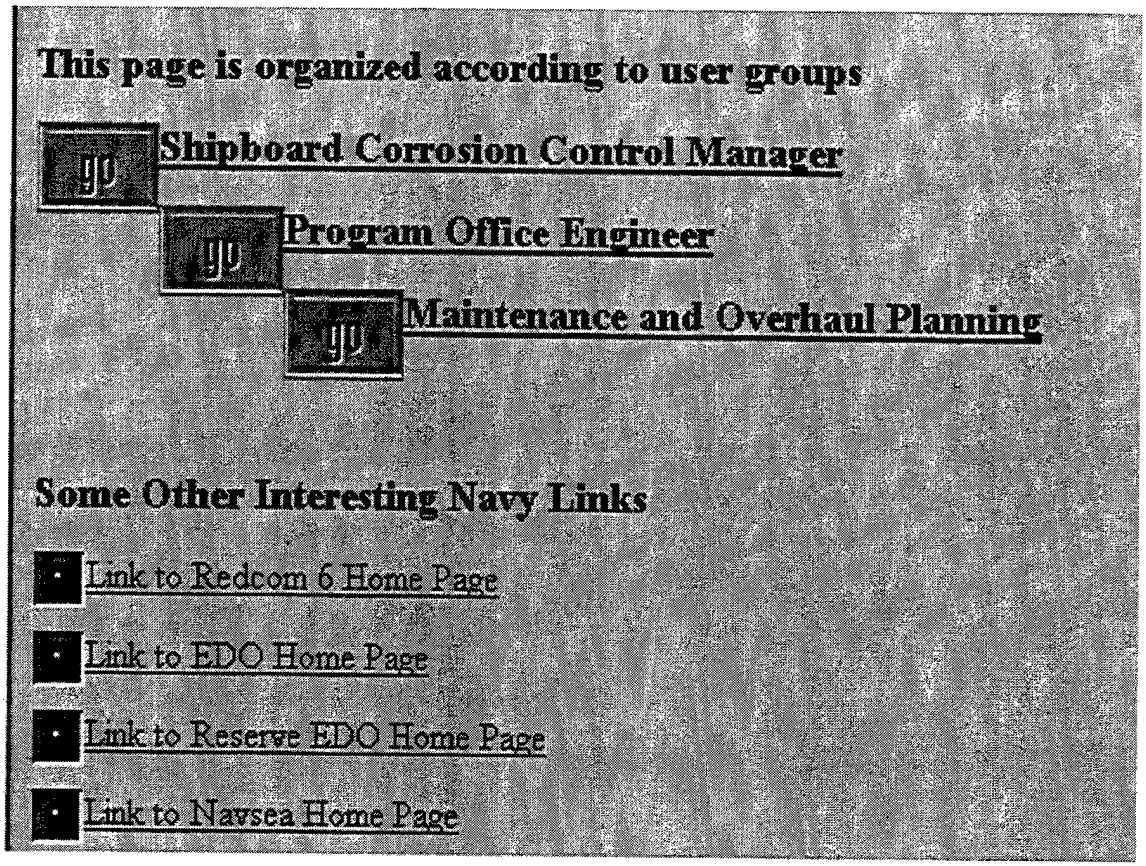

Figure 2. User Groups

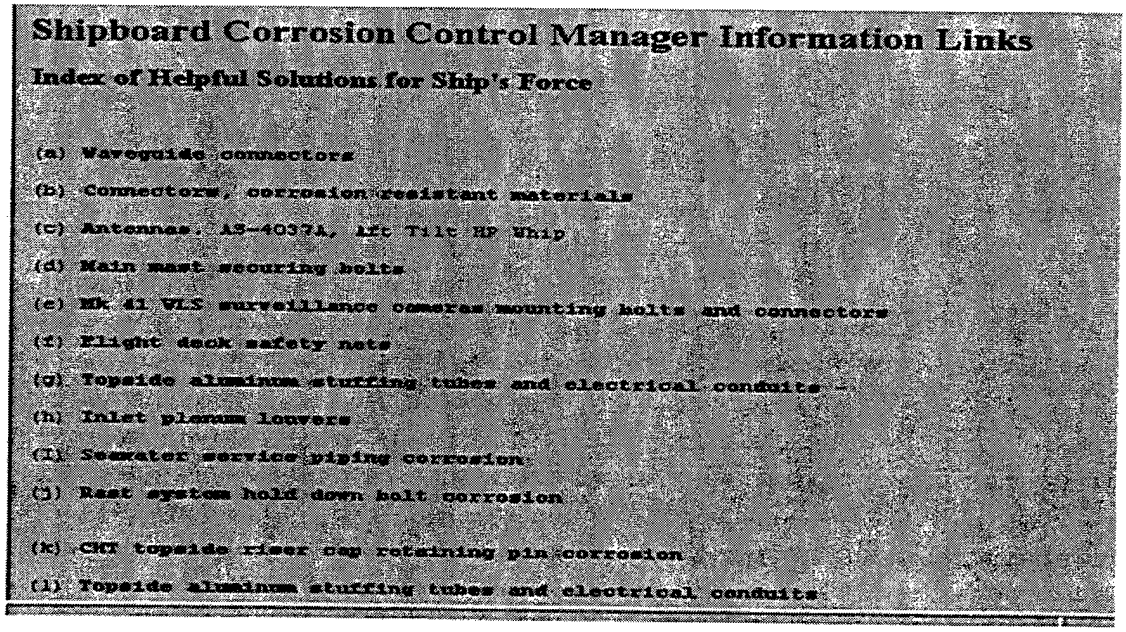

Figure 3. Shipboard Corrosion Control Manager Information Links

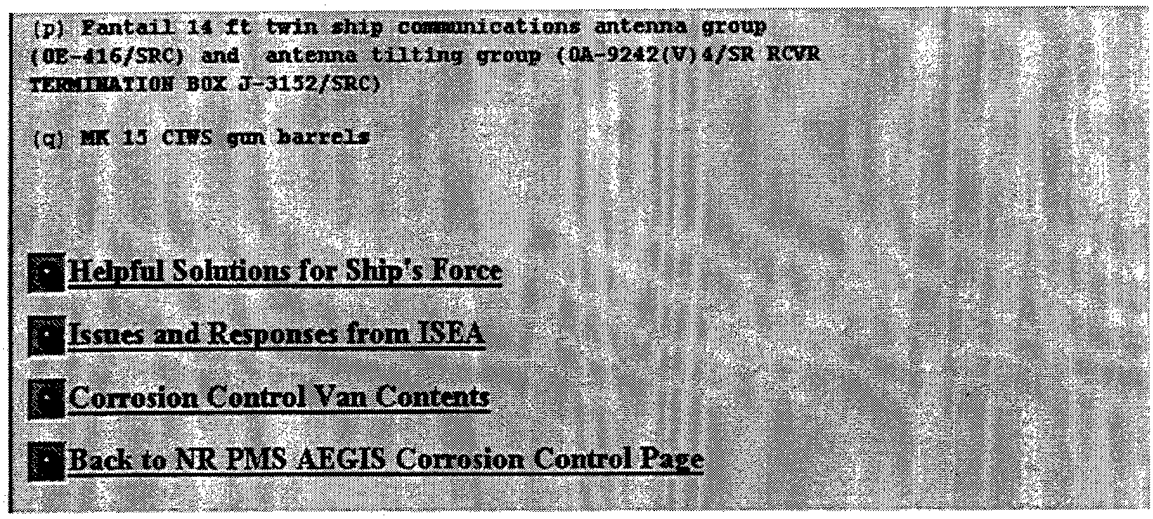

Figure 4. Other Links for the Shipboard Corrosion Manager

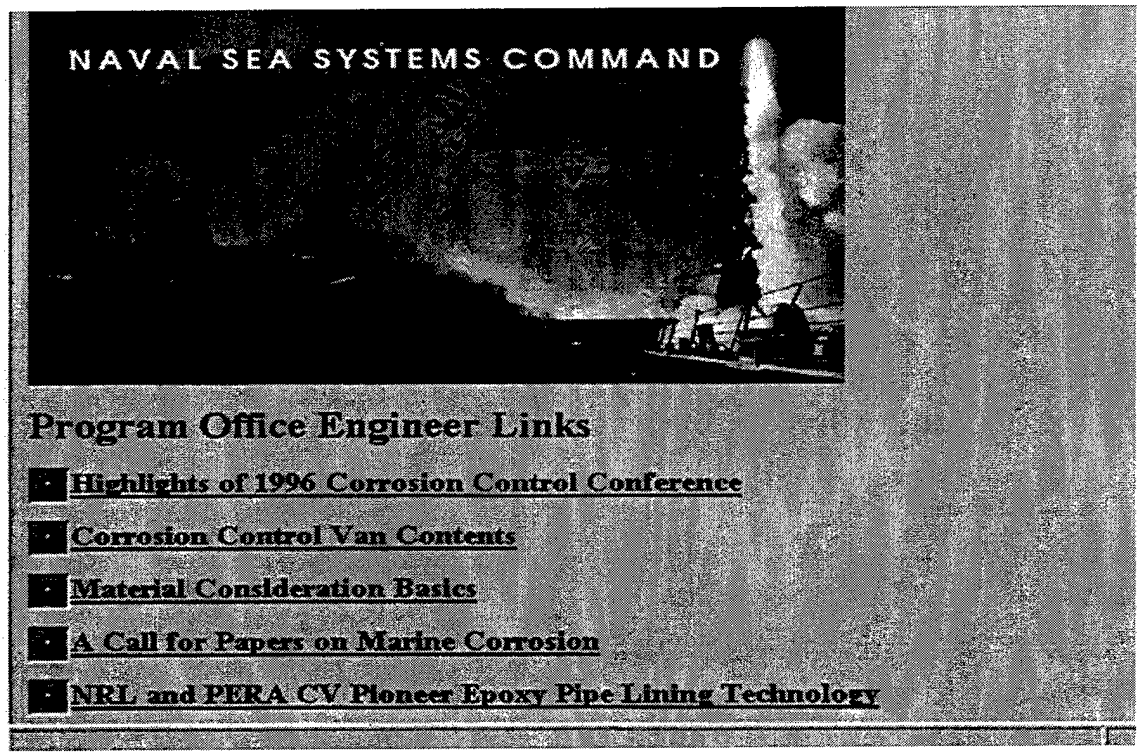

Figure 5. Program Office Engineer Links

Program Office Engineer.

The links to information for the Program Office (NAVSEA) Engineer include a mixture of theoretical material and practical information for designing solutions to improve ship production and implementation of systems on operational platforms. Topics include a primer on corrosion basics, calls for technical papers, and links to laboratory sites where corrosion research is being conducted. (See Figure 5)

Maintenance and Overhaul Planner.

The Maintenance and Overhaul Planner is interested in approved corrosion solutions from the System Command, Type Commanders, ISEA, and industry that can be applied during a ship's repair and upkeep availabilities. The links to maintenance and overhaul planning information include issues addressed by the in service engineering agent, approved shipboard solutions, and some leading edge technology being demonstrated by the Naval Research Laboratory (see figure 6).

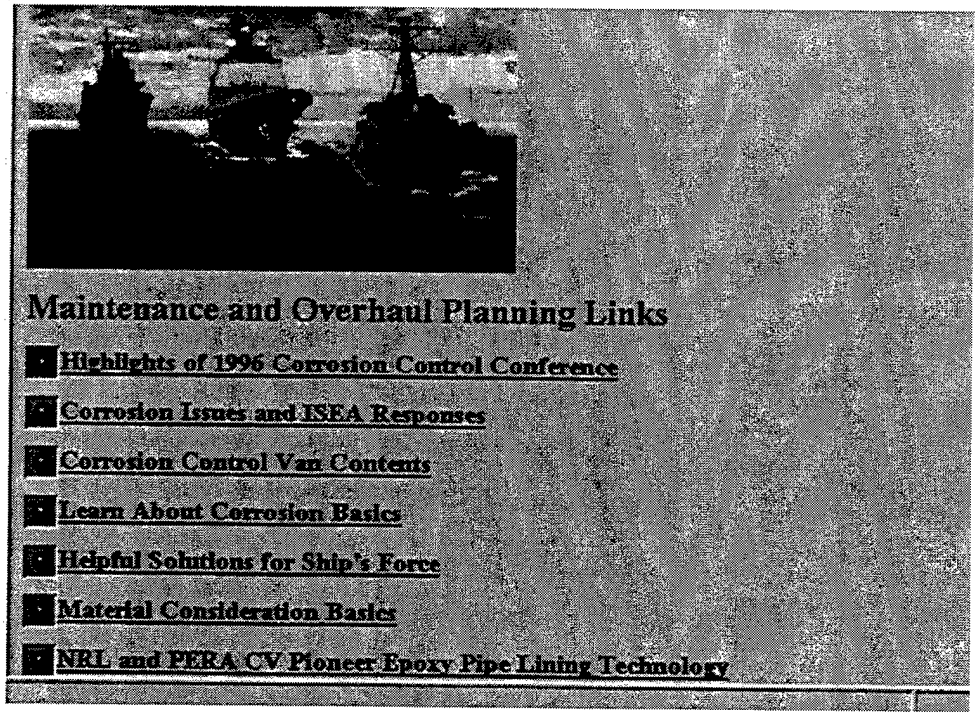

Figure 6. Maintenance and Overhaul Planning Links

CONCLUSION

The page will be a dynamic source of information on shipboard corrosion control with periodic updates to reflect new approved shipboard solutions, areas of research and points of contact for further details. The information is presented hierarchically to allow easy access in logical groupings.

ACKNOWLEDGMENTS

The Aegis Corrosion Control Web Page was designed by the PMS Aegis 106 Naval Reserve Unit. Research and data collection for the page was done by CDR Randy Hickman, LCDR Rich Guba, LT Rob Uhlig, LCDR Greg Miller, and LTJG Paul Kim. Development of the web page was done by LCDR Rich Guba.

1997 TRI-SERVICE CONFERENCE ON CORROSION
November 17-21, 1997
Wrightsville Beach, NC

ATTENDANCE LIST

Dr. Vinod S. Agarwala
Senior Scientist
NAWC-AD
Code 4.3.4, 48110 Shaw Road, Building 2187, Rm. 3356
Patuxent River, MD 20670-1906
ph: 301/342-8002; fax: 301/342-8062
email: Agarwala_Vinod%PAX5@ MR.NAWCAD.
NAVY.MIL

Dr. William P. Allen
Manager, Surface Engineering
United Technologies Research Center
411 Silver Lane, M/S 129-22
East Hartford, CT 06108
ph: 860/610-1698; fax: 860-610-1697
email: allenwp@utrc.utc.com

Clifford Anderson
Head, Materials Evaluation Branch
Carderock Division
Naval Surface Warfare Center, Code 684
Bethesda, MD 20817-5700
ph: 301-227-5390; fax: 301/227-4732
email: anderscw@oasys.dt.navy.mil

William F. Anspach
Senior Program Manager
Universal Technology Corporation
1270 N. Fairfield Road
Dayton, OH 45432-2600
ph: 937/255-9039; fax: 937/255-2176
email: anspacwf@ml.wpafb.af.mil

Chris G. Athanasopoulos
Marketing Director
DEFT Inc.
1304 Devon Avenue
Park Ridge, IL 60068
ph: 847/698-7535; fax: 847/698-7536

Mrs. Denise Aylor
Materials Engineer
Carderock Div., Naval Surface Warfare Center
9500 MacArthur Blvd., Code 613
West Bethesda, MD 20817-5700
ph: 301/227-5136; fax: 301/227-5548
email: aylor@metals.dt.navy.mil

William G. Balcom
Vice President, Operations
CarWell Products, Inc.
275 Cooper Avenue, #105
Tonawanda, NY 14150
ph: 1/800/856-6798; fax: 716/877-2364
email: bill@carwell.com

Bob Battaglia
U.S. Paint
1115 Timberlea Drive
Bel Air, MD 21014
ph: 4410/893-6111; fax: 410/893-8111

Dr. John H. Beatty
U.S. Army Research Laboratory
Weapons & Materials Directorate, AMSRL-WM-ME
Aberdeen Proving Ground, MD 21005
ph: 410/306-0869; fax: 410/306-0829
email: jbeatty@arl.mil

Ms. Jenny Been
Senior Corrosion Engineer
Titanium Metals Corporation (TIMET)
P. O. Box 2128
Henderson, NV 89009
ph: 702/566-4413; fax: 702/564-9038
email: jbeen@concentric.net

John M. Bell
Senior Engineer
Techmatics Inc. (AEGIS Weapons System)
2231 Crystal Drive, Suite 1000
Arlington, VA 22202
ph: 703/769-6508; fax: 703/521-1027
email: BELL_John_M@Techmatics.com

John A. Benavides
General Engineer
Marine Corps Systems Command
2033 Barnett Ave., Suite 315, ATTN PSE
Quantico, VA 22134-5010
ph: 703/784-4554; fax: 703/784-3432
email: benavidesj@quantico.usmc.mil

Phil Bevilacqua
Naval Air Warfare Center
Building 2188, M/S 5
Patuxent River, MD 20670
ph: 301/757-2325; fax: 301/342-8062
email: Bevilacqua_Philip%PAX5@MR.NAWCAD.
Navy.Mil

Brad Bieberich
Materials Engineer
Carderock Division
Naval Surface Warfare Center
9500 MacArthur Blvd., Code 613
West Bethesda, MD 20817-5700
ph: 301/227-4971; fax: 301/227-5548
email: brad@metals.dt.navy.mil

Dr. Gordon Bierwagen
Professor
North Dakota State University
Dept. of Polymers & Coatings. Dunbar Hall, Rm 64
Fargo, ND 58105
ph: 701/231-8294; fax: 701/231-8439
email: bierwage@plains.nodak.edu

Ms. Christine Bowles
Materials Engineer
Carderock Division, Naval Surface Warfare Center
9500 MacArthur Blvd., Code 613
West Bethesda, MD 20817
ph: 301/227-5034; fax: 301/227-5548
email: bowlesc@metals.dt.navy.mil

Ms. Barbara Brown
Graduate Student
Rensselaer Polytechnic Institute
Materials Science & Engineering Dept.
Troy, NY 12180
ph: 518/276-8061; fax: 518/276-8554
email: brownb@rpi.edu

Dr. Richard Brown
Professor
The University of Rhode Island
Chemical Engineering Dept., 205 Crawford Hall
Kingston, RI 02881
ph: 401/874-2707; fax: 401/874-4689
email: brown@egr.uri.edu

Paul F. Buckley
Materials Engineer
Army Research Laboratory
Weapons & Materials Res. Directorate,
Rodman Materials Research Bldg., AMSRL-WM-ME
Aberdeen Proving Ground, MD 21005
ph: 410/306-0848; fax: 410/306-0829
email: pbuckley@arl.mil

Dr. William B. Campbell
Chief Scientist/Research Director
Parallax, Inc.
795 West Main Street (2nd Floor)
Oak Ridge, TN 37931
ph: 423/481-8285; fax: 423/481-3234
email: Parallax@usit.net

Lewis H. Carbaugh, Jr.
Port Engineer
Commander Naval Surface Forces Atlantic
5205 Bennetts Pasture Road
Suffolk, VA 23435
ph: 757/484-1232; fax: 757-444-1017
email: carbaugh_lou_AMSEC@hq.navsea.navy.mil
or lcarbaugh@force.cnsl.spear.navy.mil

Steven F. Carr
Materials Engineer, Missile RDEC
Aviation and Missile Command
AMSAM-RD-ST-CM, Bldg. 7103
Redstone Arsenal, AL 35898-5247
ph: 205/876-7472; fax: 205/842/1359
email: scarr@redstone.army.mil

Joseph L. Cavallaro
Carderock Division, Naval Surface Warfare Center
9500 MacArthur Blvd.
West Bethesda, MD 20817-5700
ph: 301/227-4803; fax: 301/227-4813
email: cavallar@orsys.dt.navy.mil

Dr. Frank Chang
U.S. Army Research Lab
ATTN: AMSRL-WM-ME
Aberdeen Proving Ground, MD 21005
ph: 410/306-0865; fax: 410/306-0829
email: fchang@arl.mil

David Chase
Materials Engineer
U.S. Air Force
OO-ALC/TIELM, 7278 4th Street
Hill AFB, UT 84056
ph: 801/777-9403; fax: 801/775-2628

Donald L. Chilton
Quality Sr. Specialist - Coating Systems
Stewart & Stevenson
Tactical Vehical Systems, P. O. Box 330
Sealy, TX 77474
ph: 713/867-1700; fax: 713/867-1415

Norm Clayton
Materials Engineer
Carderock Division, Naval Surface Warfare Center
Phila. Naval Business Center, Code 624
Philadelphia, PA 19112
ph: 215/897-8435; fax: 215/897-8450
email: nclayton@mailgate.navsses.navy.mil

Dr. Stuart F. Cogan
Head, Materials Science
EIC Laboratories, Inc.
111 Downey Street
Norwood, MA 02062
ph: 781/769-9450; fax: 781/551-0283
email: scogan@eiclabs.com

Shawn Colson
Sr. Project Engineer
Bath Iron Works
700 Washington St, M/S 2390
Bath, ME 04530
ph: 207/442-1217; fax: 207/442-1845
email: scolson@biw.com

Doug Connor
Engineer Officer
U.S. Coast Guard
Aircraft Repair & Supply Center, Building 78
Elizabeth City, NC 27909-5001
ph: 919/3335-6240; fax: 919/335-6463

Regis K. Conrad
Materials Engineer
Carderock Division, Naval Surface Warfare Center
9500 MacArthur Blvd., Code 683
West Bethesda, MD 20817-5700
ph: 301/227-1659; fax: 301/227-5698
email: conradr@oasys.dt.navy.mil

Ernie Czyryca
Senior Scientist
Carderock Division, Naval Surface Warfare Center
9500 MacArthur Blvd., Code 614
West Bethesda, MD 20817-5700
ph: 301/227-5073; fax: 301/227-5548
email: czyryca@metals.dt.navy.mil

Gary Daniels
Chemist
U. S. Paint Corporation
831 S. 21st Street
Saint Louis, MD 63103
ph: 314/342-0290; fax: 314/621-0722
email: techgld@stlsct.com

James Dante
University of Dayton Research Institute
300 College Park, 0137
Dayton, OH 45469
ph: 937/255-4191; fax: 937/656-7129

Dan A. Davis
Metallurgist
Carderock Division, Naval Surface Warfare Center
9500 MacArthur Blvd., Code 613
West Bethesda, MD 20817-5700
ph: 301/227-5036; fax: 301/227-5548
email: davis@metals.dt.navy.mil

Jon Davis
Chemist
Hill Air Force Base (OO-ALC/TIELC)
7278 - 4th Street, Building 100E
Hill AFB, UT 84056-5205
ph: 801/777-2302; fax: 801/775-2628
email: davisjon@hillwpos.hill.af.mil

Paul A. Decker
Materials Engineer
U.S. Army TACOM
AMSTA-TR-E/MATL/267
Warren, MI 483797-5000
ph: 810/574-8771; fax: 810/574-5413
email: deckepau@cc.tacom.army.mil

Dr. Hugh C. DeLong
Program Manager
Air Force Office of Scientist Research
110 Duncan Avenue, Suite B115
Bolling AFB, DC 20785
ph: 202/767-7761; fax: 202/404-7475
email: hugh.delong@afosr.af.mil

Dr. Stephen C. Dexter
Professor
University of Delaware
College of Marine Studies
Lewes, DE 19958
ph: 302/645-4261; fax: 302/645-4007
email: dexter@udel.edu

David Dixon
Head, Engineering Division
Naval Undersea Warfare Center
1176 Howell St., Bldg. 1319/1, Code 343
Newport, RI 02841
ph: 401/841-3400 x35543; fax: 401/841-7347
email: dave_dixon@code34.npt.nuwc.navy.mil

Ross D. Dotson
Materials Engineer
Naval Aviation Depot
PSC Box 8021, Code 4.3.4.1
Cherry Point, NC 28533-0021
ph: 919/464-7159; fax: 919/464-8108

Dr. Dennis L. Dull
Principal Engineer
Boeing Info., Space & Defense Systems
P. O. Box 3999, M/S 82-32
Seattle, WA 98124-2499
ph: 253/773-8855; fax: 253/773-5941
email: dennis.l.dull@boeing.com

Michael Evans
Materials Research Engineer
Naval Research Laboratory
P. O. Box 1739
Key West, FL 33040
ph: 305/293-4372; fax: 305/293-4213
email: mevans@anvil.nrl.navy.mil

Robert J. Ferrara
Branch Head
Carderock Division, Naval Surface Warfare Center
9500 MacArthur Blvd., Code 613
West Bethesda, MD 20817-5700
ph: 301/227-4973; fax: 301/227-5548
email: ferrara@metals.dt.navy.mil

Richard E. Franke
Associate Director
U.S. Army TARDEC
Warren, MI 48397
ph: 810/574-5246; fax: 810/574-6897
email: franker@cc.tacom.army.mil

Dr. Gerald S. Frankel
Professor, Fontana Corrosion Center
Materials Science & Engineering
The Ohio State University
477 Watts Hall, 2041 College Road
Columbus, OH 43210
ph: 614-688-4128; fax: 614/292-9857
email: frankel.10@osu.edu

Steven Frerichmann
Engineering Technician
Naval Aviation Engineering Service Unit
Director, NAESU Detachment New Orleans
Aircraft Maint. System, Naval Air Station
New Orleans, LA 70143-4000
ph: 504/678-3154; fax: 504/678-3892

Dr. Richard P. Gangloff
Professor
University of Virginia
Department of Materials Science, Thornton Hall
Charlottesville, VA 22903
ph: 804/982-5782; fax: 804/982-5799
email: rpg7y@Virginia.edu

Dr. Thomas J. Garosshen
Senior Research Scientist
United Technologies Research Center
411 Silver Lane, M/S-26
East Hartford, CT 06108
ph: 860/610-7916; fax: 860/610-1697
email: GAROSTJ@UTRC.UTC.COM

Larry Gelner
Client Services
Protec, Inc.
216 Lafayette Road
N. Hampton, NH 03862
ph: 603/964-9421; fax: 603/964-2271
email: lgelner@protec-inc.com

Ms. Jacqueline Grant
Chemist
Naval Aviation Depot
PSC Box 8021, Code 4.3.4.2
Cherry Point, NC 28533-0021
ph: 919/464-7164; fax: 919/464-8101

Robert E. Gremp
NAVSSES/Corrosion Control
USN-Combatant Homeport Engineering, Team/PRC
5840 Decatur Avenue, Suite 100
Norfolk, VA 23511-3288
ph: 757/444-1999; fax: 757/444-1017
email: GREMP_BOB@hq.navsea.navy.mil

Dr. Harvey Hack
Senior Engineer
Northrop Grumman Corp.
P. O. Box 1488, M/S 9105
Annapolis, MD 21401
ph: 410/260-5349; fax: 410/260-5454
email: hack.n.p@postal.essd.northgrum.com

Fred Hammond
Coordinator, Technical Services
LaQue Corrosion Services
P. O. Box 656
Wrightsville Beach, NC 28480
ph: 910/256-2271; fax: 910/256-9816
email: fred@laque.com

I. Carl Handsy
Materials Engineer
U.S. Army TACOM
AMSTA-TR-E/MATL/267
Warren, MI 483797-5000
ph: 810/574-7738; fax: 810/574-5413
email: handsyi@cc.tacom.army.mil

LCDR John T. Hardin
U.S. Coast Guard Air Station
SFO InH Airport, Bldg. 1020
San Francisco, CA 94128
ph: 650/876-2950; fax: 650/876-2709

Christopher Hartline
Staff Engineer
Ocean City Research Corporation
Tennessee Avenue & Beach Thorofare
Ocean City, NJ 08226
ph: 609/399-2417; fax: 609/399-5233
email: ocrclab@aol.com

Richard Hawkins
Engineering Technician
Naval Aviation Engineering Service Unit, Det. El Toro
Officer in Charge, NAESU MCAS El Toro
P. O. Box 99016
Santa Ana, CA 92709-9016
ph: 714/726-3194; fax: 714/726-2890

Richard Hays
Senior Engineer
Proteus Engineering
301 Pier One Road, Suite 200
Stevensville, MD 21666
ph: 410/643-7496; fax: 410/643-7535
email: rhays@atinc.com

E. L. Hibner
Inco Alloy International, Inc.
3200 Riverside Drive
Huntington, WV 25705
ph: 304/526-5742; fax: 304/526-5973

CMDR Randy Hickman
AEGIS PROGRAM - U.S. Navy
12204 Meadowstream Ct.
Herndon, VA 20170
ph: 703/709-9772
email: Randy_Hickman@mail.hq.faa.gov

Don Hileman
CACI
160 Rochester Dr.
Louisville, KY 40214
ph: 502/364-5231; fax: 502/364-5354
email: Don_Hi@SMTP.NOSL.SEA06.NAVY.MIL

Vincent F. Hock
Metallurgist
U.S. Army CERL
P. O. Box 9005
Champaign, IL 61826
ph: 217/373-6753; fax: 217/373-6732
email: v-hock@cecer.army.mil

Dr. Gordon R. Holcomb
Materials Research Engineer
Albany Research Center, U. S. Dept. of Energy
1450 Queen Avenue, SW
Albany, OR 97321
ph: 541/967-5874; fax: 541/967-5914
email: holcomb@alrc.doe.gov

Albert Holder
Chemist
Carderock Division, Naval Surface Warfare Center
9500 MacArthur Blvd., Code 641
West Bethesda, MD 20817-5700
ph: 301/227-4787; fax: 301/227-4789
email: holder@oasys.dt.navy.mil

Paul W. Holsberg
Head, Metals Department
Carderock Division, Naval Surface Warfare Center
9500 MacArthur Blvd., Code 61
West Bethesda, MD 20817-5700
ph: 301/227-4401; fax: 301/227-5576
email: 281divhd@oasys.dt.mil.navy

Jacob Huffman
Materials Engineer
U. S. Coast Guard
Aircraft Repair & Supply Center, Building 78
Elizabeth City, NC 27909
ph: 919/335-6123; fax: 919/335-6463
email: aveng!@jacob@uunet.uu.net

Joe Hunter
Associate Research Engineer
University of Dayton Research Institute
300 College Park, M/S 0137
Dayton, OH 45469
ph: 937/255-4191; fax: 937/656-7129
email: hunterjt@ml.wpafb.af.mil

Dr. Maria Inman
Project Engineer
Faraday Technology, Inc.
315 Huls Drive
Clayton, OH 45315-8983
ph: 937/836-7749; fax: 937/836-9498
email: faratech@erinet.com

Ms. Julie A. Jacks
General Engineer
Marine Corps Systems Command
2033 Barnett Avenue, Suite 315, ATTN PSE
Quantico, VA 22134-5010
ph: 703/784-4551; fax: 703/784-3432
email: jacksj@quantico.usmc.mil

Dr. Kumar Jata
Wright-Patterson AFB
WL/MLLM, 2230 Tenth Street
Wright-Patterson AFB, OH 45437
ph: 937/255-1304; fax: 937/255-3007
email: jatakv@ml.wpaft.af.mil

Dr. Carol Jeffcoate
Visiting Scientist
Systran Corporation
4126 Linden Avenue
Dayton, OH 45432
ph: 937/255-2235; fax: 513/255-2176
email: jeffcoat@erinet.com

John J. Jusko
Materials Engineer
Hill Air Force Base (OO-ALC/TIELM)
7278 - 4th Street
Hill AFB, UT 84056-5205
ph: 801/777-9409; fax: 801/775-2628
email: JuskoJ@hillwpos.hill.af.mil

Robert M. Kain
Senior Corrosion Scientist
LaQue Corrosion Services
P. O. Box 656
Wrightsville Beach, NC 28480
ph: 910/256-2271; fax: 910/256-9816
email: bob@laque.com

Dr. Michael J. Kane
Chemical Engineer
NAWCAD, Unit 5
48066 Shaw Road, Bldg. 2188
Patuxent River, MD 20670
ph: 301/342-0986; fax: 301/342-8062
email: kane_michae%pax5@mr.mawcad.navy.mil

John V. Kelley
Materials Engineer
Army Research Laboratory
AMSRL-WM-ME, Bldg. 4600
Aberdeen Proving Ground, MD 21005
ph: 410/306-0837; fax: 410/306-0829
email: jkelley@arl.mil

Alan Kerr
Advanced Repair Technology International
One Ridgmar Place, 6500 West Freeway
Fort Worth, TX 76116
ph: 817/737-1656; fax: 817/737-1605
email: kerra@dyncorp.com

Robert E. Kestler
Materials Engineer
Naval Aviation Depot
PSC Box 8021, Code 4.3.4.1
Cherry Point, NC 28533-0021
ph: 919/464-9888; fax: 919/464-8108

Stephen Keys
NSWC-SSES
Carderock Division, Naval Surface Warfare Center
Phila. Naval Business Center, Code 9131
Philadelphia, PA 19112-5083
ph: 215/897-1443; fax: 215/897-1450
email: keyss@mailgate.navsses.navy.mil

Dr. Mohammad Khobaib
Research Engineer
University of Dayton
300 College Park Dr.
Dayton, OH 45469
ph: 937/255-9050; fax: 937/255-1363
email: khobaim@ml.wpafb.af.mil

Richard Kinzie
Materials Engineer
U. S. Air Force
325 2nd Street
Robins AFB, GA 31098
ph: 912/926-3284; fax: 912/926-6619
email: rkinzie@wrdiss1.robins.af.mil

F. D. Kisor
Wright Labs
5270 Starlight Dr., S.
Ft. Worth, TX 76126
ph: 817/249-1602; fax: 817/249-6408
email: fkisor@flash.net

Dr. Edward Knobbe
Professor
Oklahoma State University
Department of Chemistry, 201 CITD
Stillwater, OK 74078-3011
ph: 405/744-9994; fax: 405/744-7673
email: knobbe@okway.okstate.edu

Dr. Kevin J. Kovaleski
Chemist
Naval Air Warfare Center, Aircraft Div.
48066 Shaw Road, Unit 5
Patuxent River, MD 20670-1908
ph: 301/342-8049; fax: 301/342-8119
email: kovaleski_kevin%PAX5@MR.NAWCAD.
NAVY.MIL

Dr. W. Kevin Kuhn
Director, Coatings Technology Integration Office
Wright-Patterson AFB
WL/MLSS, 2179 12th Street, Suite 1
Wright-Patterson AFB, OH 45433-7718
ph: 937/255-0943; fax: 937/255-0945
email: kuhnwk@ml.wpafb.af.mil

A. K. Kuruvilla
AMPTIAC/ IIT Research Institute
7501 S. Mem. Parkway, Suite 104
Huntsville, AL 35802
ph: 205/880-0884,x238; fax: 205/880-0886
email: akuruvilla@iitri.com

Thomas M. Landy
Materials Engineer
U.S. Army TACOM
AMSTA-TR-E/MATL/267
Warren, MI 48397-5000
ph: 810/574-5954; fax: 810/574-5413
email: landyt@cc.tacom.army.mil

Ms. Tania Lantz
PMS400D4 Representative
Tracor Systems Engineering, PMS400D4
2611 Jefferson Davis Highway, 5000
Arlington, VA 22202
ph: 703/413-4063; fax: 703/413-9276
email: lantzt@vitro.com

Dr. Ron Latanision
Professor
Massachusetts Institute of Technology
Rm 8-202, 77 Massachusetts Ave.
Cambridge, MA 02139
ph: 617/253-4697; fax: 617/2535-8745
email: lats@mit.edu

Dr. Eun U. Lee
Materials Engineer
Naval Air Warfare Center
Aircraft Division, Bldg. 2188, M/S 5
Patuxent River, MD 20670
ph: 301/342-8069; fax: 301/342-8062
email: eun_lee%pax5@mr.nawcad.navy.mil

Anthony Leofsky
Materials Engineer
NAVSEA PMS 450
NSWCCD, Bldg. 619, Code 622
Philadelphia, PA 19112
ph: 703/602-0330, x201; fax: 703/602-5354
email: leofsky_anthony@hq.navsea.navy.mil

Kenneth Lerner
Materials Engineer
Navmar Applied Sciences Corp.
65 W. Street Road, B-104
Warminster, PA 18974
ph: 215/675-4900; fax: 215/672-0597
email: navmar1@bellatlantic.net

Les Leutwiler
Chemist
U. S. Paint Corporation
831 S. 21st
St. Louis, MO 63103
ph: 314/342-0244; fax: 314/621-0722

Dr. Norris Lindsey
Research Chemist
Carderock Division, Naval Surface Warfare Center
9500 MacArthur Blvd., Code 683
West Bethesda, MD 20084
ph: 301/227-3976; fax: 301/227-5698
email: lindsey@oasys.dt.navy.mil

Dr. Brenda J. Little
Senior Scientist
Naval Research Laboratory
Bldg. 1105, Code 7303
Stennis Space Center, MS 39529
ph: 601/688-5494; fax: 601/688-5379
email: blittle@nrlssc.navy.mil

Raymond Luken
Materials Engineer
Naval Aviation Depot
PSC Box 8021, Code 4.3.4.1
Cherry Point, NC 28533-0021
ph: 919/464-7168; fax: 919/464-8108

Dr. Digby D. Macdonald
Professor
The Pennsylvania State University
517 Deike Building
University Park, PA 16802
ph: 814/863-7772; fax: 814/863-4718
email: digby@essc.psu.edu

Dr. Florian B. Mansfeld
Professor
University of Southern California
Materials Science Department
Los Angeles, CA 90089-0241
ph: 213/740-3016; fax: 213/740-7797
email: mansfeld@usc.edu

L. Scott Marshall
Senior Corrosion Engineer
LaQue Corrosion Services
P. O. Box 656
Wrightsville Beach, NC 28480
ph: 910/256-2271; fax: 910/256-9816
email: scott@laque.com

Joe Martinez, Jr.
DTI Associates, Inc.
2920 S. Glebe Rd.
Arlington, VA 22206
ph: 703/299-1650; fax: 703/706-0476
email: jmartinez@dtihq.com

Kevin M. Mawhinney
U.S. Coast Guard Air Station
SFO, Bldg. 1020
San Francisco, CA 94128
ph: 650/876-2964; fax: 650/876-2706
email: k.mawhinney/assanfran@uscg.mil

Thomas R. McCammon
Electrical Engineering Technician
NSWCCD
Code 9770
Philadelphia, PA 19112-5083
ph: 215/897-1083; fax: 215/897-8451
email: mccammon@mailgate.navsses.navy.mil

Ms. Laurie S. McDowell
Materials Engineer
Naval Aviation Depot
PSC Box 8021, Code 4.3.4.1
Cherry Point, NC 28533-0021
ph: 919/464-7155; fax: 919/464-8108

Terrence McGrath
General Manager
Northwest Anti-Corrosion, Inc.
1910 St. Joe Center Road, Ste. 11
Ft. Wayne, IN 46825
ph: 219/471-8674; fax: 219/471-7769
email: www.norust.com

Charles McIntire
Engineering Technician
Naval Aviation Engineering Service Unit
Detachment Brunswick
Officer in Charge, NAESU Det. Brunswick
1251 Orion St., S., Room 286A
Brunswick, ME 04011-5000
ph: 207/921-2426; fax: 207/921-2668

Dr. Jack McIntyre
Director of Technical Services
Man-Gill Chemical
23000 St. Clair Ave.
Cleveland, OH 44117
ph: 216/486-5300; fax: 216/486-1214

James R. Meeker
C, Logistics System Support Branch
AFRL/MLSS
2179 12th Street, Room 122, Bldg. 652
Wright-Patterson AFB, OH 45433-7718
ph: 937/255-3206; fax: 937/656-7844
email: MEEKERJR@ml.af

Dr. Gerald H. Meier
Professor
University of Pittsburgh
Dept. of Materials Science & Engineering
848 Benedum Hall
Pittsburgh, PA 15261
ph: 412/624-9741; fax: 412/624-8069
email: ghmeier@engrng.pitt.edu

Dennis G. Melton
Corrosion Engineer
LaQue Corrosion Services
P. O. Box 656
Wrightsville Beach, NC 28480
ph: 910/256-2271; fax: 910/256-9816
email: dennis@laque.com

Joseph Menke
Chemist
U.S. Army ARDEC
AMSTA-AR-ESM
Rock Island, IL 61299
ph: 309/782-3065; fax: 309/782-6339
email: jmenke@RIA.emh2.army.mil

Dr. William T. Messick
Materials Technology Manager
Carderock Division, Naval Surface Warfare Center
9500 MacArthur Blvd., Code 0115
West Bethesda, MD 20817
ph: 301/227-4811; fax: 301/227-4813
email: messick@oasys.dt.navy.mil

Stephen M. Michetti
Mechanical Engineer
NSWCCD
Code 9770
Philadelphia, PA 19112-5083
ph: 215/897-7369; fax: 215/897-8451
email: michetti@mailgate.navsses.navy.mil

Christopher Miller
Materials Engineer
Army Research Laboratory
Bldg. 4600, Deer Creek Loop
AMSRL-WM-ME
Aberdeen Proving Ground, MD 21005
ph: 410/306-0849; fax: 410/306-0829
email: cemiller@arl.mil

Dr. Merrill L. Minges
Consultant
A.F. Aging Aircraft Offices
WL/XPZ, Bldg. 45, 2130 Eighth St., Suite 1
Wright-Patterson AFB, OH 45433-7541
ph: 937/255-4269; fax: 937/656-4646
email: Merrill.Minges@wl.wpafb.af.mil

Ms. Barbara R. Moore
USARPAC Science Advisor
U.S. Army, Pacific (Science Advisor's Office)
ATTN: APSA (Science Advisor), Bldg. T-115, RM 118
Fort Shafter, HI 96858-5100
ph: 808/438-1480; fax: 808/438-6242
email: fastpac@nemo.nosc.mil

Dr. Patrick J. Moran
Professor
U.S. Naval Academy
Mechanical Engineering Dept., Rickover Hall
Annapolis, MD 21402-5042
ph: 410/293-6526; fax: 410/293-2591
email: moran@nadn.navy.mil

Joseph R. Mosher
Acquisition Management Specialist
ASC/SMA (SY)
2145 Monahan Way
Wright-Patterson AFB, OH 45433-7017
ph: 937/255-6053; fax:

Edwin G. Mullin
Aero Engineer
Naval Aviation Depot North Island
P. O. Box 357058, S3FST.6
San Diego, CA 92135-7058
ph: 619/545-0745; fax: 619/545-0763
email: Mullin_E@a1.nadepni.navy.mil

Dr. Paul Natishan
Naval Research Laboratory
Code 6314
Washington, DC 20375
ph: 202/767-9255; fax: 202/767-4642
email: natishan@anvil.nrl.navy.mil

Dr. Douglas H. Neale
Chief Scientist
SAIC
2220 Northwest Parkway, Suite 200
Marietta, GA 30067
ph: 770/612-2107; fax: 770-952-6223
email: DOUG_NEALE@cpqm.saic.com

Ms. Louise Nicoloff
Preservation Program Manager
Naval Aviation Depot
P. O. Box 357058, Code 43460, Bldg. 469
San Diego, CA 92135
ph: 619/545-9759; fax: 619/545-7810
email: nicoloff_l@a1.nadepni.navy.mil

Barry O'Halloran
President
CarWell Products, Inc.
275 Cooper Ave., U105
Tonawanda, NY 14150
ph: 716/877-2363; fax: 716/877-2364
email: barry@carwell.com

Dr. Mark E. Orazem
Professor
University of Florida
Dept. of Chemical Engineering
Gainesville, FL 32611
ph: 352/392-6207; fax: 352/392-9513
email: meo@electro.che.ufl.edu

Youngun Pae
Graduate Student
North Dakota State University
Department of Polymers and Coatings
Fargo, ND 58105
ph: 701/231-8385; fax: 701/231-8439
email: Pae@prairie.nodak.edu

Dr. Peter S. Pao
Engineer
Naval Research Laboratory
Code 6312
Washington, DC 20375
ph: 202/767-0224; fax: 202/767-54642
email: pao@anvil.nrl.navy.mil

Robert Parkhill
Graduate Student
Oklahoma State University
Department of Chemistry, 201 CITD
Stillwater, OK 74078-3011
ph: 405/744-9994; fax: 405/744-7673
email: chnlrob@oksate.edu

Hugh Patrick
H&M Marine
Lear Chemical, P. O. Box 16468
Surfside Beach, SC 29587-6468
ph: 803/238-1585; fax: 803/357-0633

Dr. Patricia Paulette
Chemist
Naval Research Laboratory
Washington, DC 20375
ph: 202/767-1344; fax: 202/767-4642
email: paulette@anvil.nrl.navy.mil

Dr. Sharad Pednekar
Army Research Lab
AMSRL-WM-MD
Aberdeen Proving Ground, MD 21005
ph: 410/306-0808; fax: 410/306-0806
email: Sharad@arl.mil

Dr. Deb Peeler
University of Dayton Research Institute
Coatings, Corrosion, Control and Analysis
300 College Park, P. O. Box 0137
Dayton, OH 45469
ph: 937/255-4191; fax: 937/656-7129

Bopinder S. Phull
Principal Corrosion Scientist
LaQue Corrosion Services
P. O. Box 656
Wrightsville Beach, NC 28480
ph: 910/256-2271; fax: 910/256-9816
email: bop@laque.com

Dr. Robert S. Piascik
Senior Scientist
NASA Langley Research Center
M/S 188E
Hampton, VA 23681-0001
ph; 757/864-3483; fax: 757/864-8911
email: r.s.piascik@larc.nasa.gov

Brian E. Placzankis
Materials Engineer
U.S. Army Research Laboratory
Weapons & Materials Research Directorate
AMSRL-WM-ME
Aberdeen Proving Ground, MD 21005
ph: 410/306-0841; fax: 410/306-0829
email: plaz@arl.mil

Mrs. Karen Poole
Carderock Division, Naval Surface Warfare Center
9500 MacArthur Blvd., Code 641
West Bethesda, MD 20817
ph: 301/227-4783; fax: 301/227-4814
email: poolek@oasys.dt.navy.mil

Dr. Bruce Pound
Department Director
SRI International
333 Ravenswood Avenue
Menlo Park, CA 94025
ph: 650/859-5527; fax: 950/859-3678
email: bruce_pound@qm.sri.com

Maroof Qurashi
Chemist
Dept. of Navy, Naval Surface Warfare Center
Naval Surfwarcendiv-300, Highway 361
Crane, IN 47522-5001
ph: 812/854-4230; fax: 812/854-5054

W. T. Raines
Vice President, Finance & Administration
LaQue Corrosion Services
P. O. Box 656
Wrightsville Beach, NC 28480
ph: 910/256-2271; fax: 910/256-9816
email: tim@laque.com

Dr. Krishna S. Rajan
Science Advisor
IIT Research Institute
10 West 35th Street
Chicago, IL 60616
ph: 312/567-4262; fax: 312/567-4286
email: mhaberichter@hq.iitri.com

Ms. Susan Reilly
Research Specialist
University of Dayton Research Institute
300 College Park Dr.
Dayton, OH 45469-0102
ph: 937/229-3515; fax: 937/229-3873
email: reilly@udri.udayton.edu

Captain Lance B. Reynolds
USAF (WPAFB)
WL/MLBT, Bldg. 654, 2941 P. Street, Ste. 1
Wright-Patterson AFB, OH 45433-7750
ph: 937/255-8097; fax: 937/255-2176
email: reynollb@ml.wpafb.af.mil

Michael Roach
Engineer
CAE Aviation Ltd.
P.O. Box 9864
Edmonton, Alberta, Canada T5J-2T2
ph: 403/890-6600; fax: 403/890-6543
email: roachm@cae-aviation.ab.ca

James M Roberts
Materials Engineer
Naval Aviation Depot
PSC Box 8021, Code 4.3.4.1
Cherry Point, NC 28533-0021
ph: 919/464-7159; fax: 919/464-8108

Major David Robertson
Chief, AF Corrosion Program Office
Air Force Corrosion Program Office
329 2nd Street
Robins AFB, GA 31098-1639
ph: 912/926-3284; fax: 912/926-6619
email: darobert@wrdiss1.robins.af.mil

James Paul Robinson
AmDyne Corporation
600 Blvd. South, Suite 301
Huntsville, AL 35802
ph: 205/880-5080; fax: 205/880-5086
email: robinson@amdyne.com

Steven J. Rogovich
Port Engineer
U.S. Navy COMNAVSURFLANT
N43EM, 1612 Lake Christopher Drive
Virginia Beach, VA 23464-7802
ph: 757/464-8885; fax: 757/464-8673
email: srogovich@force.cnsl.spear.navy.mil

Ms. Celeste Roper
Chemist
Naval Air Warfare Center
Code 4B2100D, 1 Administration Circle
China Lake, CA 93555
ph: 760/939-1946; fax: 760/939-1617
email: roper@scf.chinalake.navy.mil

Robert Rubolin
Sales Executive
Dynamic Materials Corporation
3 Meadow Wood Lane
West Grove, PA 19390
ph: 610/869-5707; fax: 610/869-5714

Barry L. Rudman
Polymer Additive Specialist
Cortec Corporation
4119 White Bear Parkway
White Bear Lake, MN 55110
ph: 612/407-2747; fax: 612/429-1122
email: info@Cortecvci.com

James Rudroff
Engineer
NAVSEA 03M
2531 Jefferson Davis Highway
Arlington, VA 22242
ph: 703/602-0214, x226
fax: 703/602-0247
email: RUDROFF_JAMES@HQ.NAVSEA.NAVY.MIL

David T. Ruppel
Student
University of Delaware
College of Marine Studies
Lewes, DE 19958
ph: 302/645-4284; fax: 302/645-4007
email: druppel@udel.edu

Dr. K. Sadananda
Metallurgist
Naval Research Lab
Code 6323
Washington, DC 20375
ph: 202/767-2117; fax: 202/767-2623
email: Seda@anul.nrl.navy.mil

Col. Gustave A. Sague, PE (Ret)
Marketing Director
Global Corrosion Technologies, Inc.
10655 Richmond Ave., Suite 180
Houston, TX 77042
ph: 713/785-4141; fax: 713/361-0470
email: colgssague@hotmail.com

Jeff M. Sakai
Metallurgical Engineer
Naval Aviation Systems Team
North Island, Code 4.3.4.6.0, B469
San Diego, CA 921335-7058
ph: 619/545-0857; fax: 619/545-7810
email: sakai_j@a1.nadepni.navy.mil

Dr. Krishnan Sankaran
Engineering Manager
The Boeing Company
P. O. Box 516, M/S S11 1041
St. Louis, MO 63166-0516
ph: 314/233-8680; fax: 314/2332-0888
email: krishnan.k.sankaran@boeing.com

Carl Schmitt
RCM
U. S. Coast Guard
Aircraft Repair & Supply Center, Bldg. 78
Elizabeth City, NC 27909
ph: 919/335-6966

Dr. A. John Sedriks
Program Officer
Office of Naval Research
800 N. Quincy St., ONR 332
Arlington, VA 22217
ph: 703/696-4402; fax: 703/696-0934
email: sedrikj@onrhq.onr.navy.mil

Jules F. Senske
Materials Engineer
U.S. Army, ARDEC
Bldg. 355, AMSTA-AR-WEA
Picatinny Arsenal, NJ 07806-5000
ph: 937/724-42225; fax: 973/724-7378
email: jsenske@pica.army.mil

Dr. Barbara A. Shaw
Associate Professor
The Pennsylvania State University
Dept. of Engrg. Services and Mechanics
211 Hallowell Building
University Park, PA 16802
ph: 814/865-7828; fax: 814/863-0490
email: bas13@psu.edu

Andrew Sheetz
Materials Engineer
Carderock Division, Naval Surface Warfare Center
9500 MacArthur Blvd., Code 613
West Bethesda, MD 20817
ph: 301/227-5037; fax: 301/227-5548
email: sheetz@metals.dt.navy.mil

Dr. David A. Shifler
Materials Engineer
Carderock Division, Naval Surface Warfare Center
9500 MacArthur Boulevard, Code 613
West Bethesda, MD 20817-5700
ph: 301/227-5128; fax: 301/227-5548
email: shifler@metals.dt.navy.mil

Phil C. Simon
Mechanical Engineer
PHD NSWC
4363 Missile Way, Code 1H20, Bldg. 445
Port Hueneme, CA 93043-4307
ph: 805/982-0336; fax: 805/982-8770

Stephen J. Spadafora
Head, Materials Protection
Naval Air Systems Command
48066 Shaw Road, M/S 5
Patuxent River, MD 20670
ph: 301/342-8007; fax: 301/342-8062
email: Spadafora_Stephen%PAX5@MR.NAWCAD.
NAVY.MIL

William Steiner
Mechanical Engineer
Carderock Division, Naval Surface Warfare Center
Naval Business Center, Code 624, Bldg. 619
Philadelphia, PA 19112-5083
ph: 215/897-7183; fax: 215/897-8450
email: steiner@oasys.dt.navy.mil

John Stevens
Graduate Student
Rensselaer Polytechnic Institute
MRC 235, RPI
Troy, NY 12180
ph: 518/276-8061; fax: 518/276-8554
email: stevej4@rpi.edu

Dr. Todd Steyer
Senior Engineer
Northrop Grumman Military Aircraft Systems Div.,
Materials & Processes R&D
8900 E. Washington Blvd., M/S 9B61/GK
Pico Rivera, CA 90660-3737
ph: 562/948-9641; fax: 562/948-0100
email: tsteyer@world.northgrum.com

Donald C. Stuart
611 CES (PACAF)
21885 2nd Street; CEOF
Elmendorf AFB, AK 99506-4420
ph: 907/552-5518; fax: 907/552-7565

Dr. Toshi Sugama
Chemist
Brookhaven National Laboratory
P. O. Box 5000, Bldg. 526
Upton, NY 11973-5000
ph: 516/344-4029; fax: 516/344-2359
email: sugama@bnl.gov

Dr. E. Jennings Taylor
President
Faraday Technology, Inc.
315 Huls Drive
Clayton, OH 45315-8983
ph: 937/836-7749; fax: 937/836-9498
email: faratech@erinet.com

Edward Taylor
Sr. Technical Specialist
Northrop Grumman Corp.
One Hornet Way, 9B20/W10
El Segundo, CA 90245
ph: 310/332-0016; fax: 310/332-1074

E. Dail Thomas, II
Branch Head
Naval Research Laboratory
4555 Overlook Avenue, SW, Code 6310
Washington, DC 20375
ph: 202/767-0833; fax: 202/767-4642
email: thomas@anvil.nrl.navy.mil

Ms. Rebecca Twite
Graduate Student
North Dakota State University
Dept. of Polymers & Coatings, 54 Dunbar Hall
Fargo, ND 58105
ph: 701/231-8385; fax: 701/231-8439
email: twite@plains.nodak.edu

Craig Valentine
611 CES/CEVC
6900 9th St., Ste. 360
Elmendorf AFB, AK 99506-2270
ph: 907/552-4498; fax: 907/552-9563
email: ValentiC@611lsspo.topcover.af.mil

Ms. Vicki VanBlaricum
General Engineer
U.S. Army CERL
P. O. Box 9005, CECER-FL-M
Champaign, IL 61826-9005
ph: 217/373-6771; fax: 217/373-6732
email: v-vanblaricum@cecer.army.mil

Dr. K. L. Vasanth
Research Chemist
Carderock Division, Naval Surface Warfare Center
9500 MacArthur Blvd., Code 683
West Bethesda, MD 20817-5700
ph: 301/227-1698; fax: 301/227-1230
email: vasanth@oasys.dt.navy.mil

Ms. Natasha Voevodin
Visiting Scientist
Systran Corporation
4126 Linden Avenue
Dayton, OH 45432
ph: 937/255-5161; fax: 513/255-2176
email: VOEVODNN@ml.wpafb.af.mil

William Westerfield
Combat Systems
NAVSEA DET PERA-CV
1305 Ironsides Ave., Code 1815
Bremerton, WA 98310-4924
ph: 360/476-1030; fax: 360/476-3078
email: westerfield@perasmtp.navy.mil

James A. Whitfield
Chemist
Naval Aviation Depot
PSC Box 8021, Code 4.3.4.2
Cherry Point, NC 28533-0021
ph: 919/464-7342; fax: 919/464-8108

Sam Winters
Supervisor MDS
Allison Engine Co.
Box 420, 5-52
Indianspolis, IN 46206
ph: 317/230-5117; fax: 317/230-3356

Randy D. Wood
Chemist
NAWCAD
Bldg. 2188 M/S 5, 48066 Shaw Road
Patuxent River, MD 20653
ph: 301/342-8076; fax: 301/342-8062
email: Wood_Randy%PAX5@MR.NAWCAD.
NAVY.MIL

Gene Wyman
RCM
U. S. Coast Guard
Aircraft Repair & Supply Center
Building 78
Elizabeth City, NC 27909
ph: 919/335-6953

Dr. Peter Zarras
Research Chemist
Naval Air Warfare Center, Weapons Div./Research and
Technology Division
1 Administration Circle, Code 4B2200D
China Lake, CA 93555
ph: 760/939-1396; fax: 760/939-1617
email: Peter_Zarras@imdgw.chinalake.navy.mil

INDEX - AUTHORS

LastName	FirstName	Session	*Title*
Agarwala	Vinod S.	2	*"Fluorescence-Based Corrosion Indicators: Exploration of Schiff-Base Compounds"*
		2	*"Corrosivity Monitoring on Operational Aircraft Using Thin Film Galvanic Sensors"*
		8	*"Trivalent Chromium Conversion Coating for Aluminum - A Replacement for Hexavalent Chromium Pretrreatment"*
Allen	William P.	1	*"Effect of Minor Impurities on the Oxidation Resistance of Alumina-Forming Alloys"*
Arvanites	A. C.	8	*Novel Chromium-Free Surface Pretreatment Process for Corrosion Inhibitors"*
Aylor	Denise M.	5	*"Stress Corrosion Cracking of Naval Structural Alloys"*
		6	*"High Strength Fasteners for Seawater Immersion Service"*
		9	*"Post-Processing of Thermal Sprayed Coatings Using Hot Isotatic Pressing"*
Baldwin	Kevin	4	*"An Acoustic Emission Method for the Evaluation of Environmentally Assisted Cracking"*
Bayles	Robert A.	5	*"Ripple-Load Cracking Sensitivity in Engineering Alloys"*
Beard	M.	10	*"Inhibition of Microbiologically Influenced Corrosion"*
Beatty	John H.	6	*"Noble Metal Additions to Mitigate Hydrogen Embrittlement of Ultra High Strength Steels: Research In Progress"*
		6	*"Galvanic Corrosion of Tungsten Coupled with Several Metals/Alloys"*
		7	*"Extending Use of Ion Vapor Deposited (IVD) Aluminum as a Replacement for Electroplated Cadmium"*
Beck	J.	6	*"Galvanic Corrosion of Tungsten Coupled with Several Metals/Alloys"*
Bieberich	E. Bradley	3	*"Corrosion Testing in the U.S. Marine Corps"*
Bierwagen	Gordon P.	3	*"Initial Studies of Electrochemical Comparison of Coating Performance in a Flowing vs Stationary Electrolyte"*
		4	*"Investigation of Corrosion Protection of Steel by Electrically Conductive Polyaniline Coating"*
Bornstein	N. S.	1	*"Effect of Minor Impurities on the Oxidation Resistance of Alumina-Forming Alloys"*

INDEX - AUTHORS

LastName	FirstName	Session	*Title*
Bowles	Christene A.	3	*"Evaluating Anti-Galling Thread Treatment for Beta-C Titanium Fasteners Exposed to Marine Environments"*
		4	*"Evaluation of Vapor Phase Corrosion Inhibitors and Dehumidification as Corrosion Control Methods for Advanced Double Hull Navy Ships"*
		6	*"High Strength Fasteners for Seawater Immersion Service"*
Brent	R. J.	8	*"A Chromate-Free Chemical Conversion Coating for Aluminum and Steel Alloys"*
Brown	B. E.	1	*"The Effects of Dissolved Ozone on the Corrosion Behavior of Nickel, Stainless Steel and Aluminum-Based Alloys in Seawater"*
Brown	Richard	1	*"Corrosion Protection of Aluminum Alloys by Conductive Organic and Inorganic Polymers"*
Buckley	Paul F.	4	*"An Acoustic Emission Method for the Evaluation of Environmentally Assisted Cracking"*
		6	*"Noble Metal Additions to Mitigate Hydrogen Embrittlement of Ultra High Strength Steels: Research in Progress"*
Bullard	Sophie J.	7A	*"Thermal-Spray Coatings for Coastal Infrastructure"*
Caputy	N.	1	*"Corrosion Mechanisms in Supercritical Water Oxidation Systems for Hazardous Waste Disposal"*
Carmody	T. A.	11	*"The Determination of the Corrosion Behavior of a Developmental Al-Mg-Li-Ag Alloy"*
Cerchiara	R.	11	*"Oxidation and Embrittlement of Titanium Aluminides"*
Chandler	C.	12	*"A Recent Innovation in Corrosion Control for Electronics"*
Chang	Frank	6	*"Galvanic Corrosion of Tungsten Coupled with Several Metals/Alloys"*
Chen	Guoling	4	*"Investigation of Corrosion Protection of Steel by Electrically Conductive Polyaniline Coating"*
Charrier	Eric	1	*"Experimental Study of the Erosion-Corrosion of Copper and Copper-Nickel Alloys at the Corrosion Potential and at Anodic Potentials"*

INDEX - AUTHORS

LastName	FirstName	Session	*Title*
Claffey	W. J.	8	*"A Chromate-Free Chemical Conversion Coating for Aluminum and Steel Alloys"*
Clark	R.	1	*"Corrosion Protection of Aluminum Alloys by Conductive Organic and Inorganic Polymers"*
Clayton	Norman	13	*"Approaches to Corrosion Control on the USMC Riverine Assault Craft (RAC)"*
		13	*"Corrosion Control Hardware Allowance Parts List (APLs): Logistics Support for Naval Surface Ship Corrosion Control Programs"*
Cline	J. A.	1	*"Corrosion Mechanisms in Supercritical Water Oxidation Systems for Hazardous Waste Disposal"*
Conrad	Regis R.	3	*"Evaluating Anti-Galling Thread Treatment of Beta-C Titanium Fasteners Exposed to Marine Environments"*
		8	*"A Chromate-Free Chemical Conversion Coating for Aluminum and Steel Alloys"*
Covino	Bernard S.	7A	*"Thermal-Spray Coatings for Coastal Infrastructure"*
Cramer	Keith	9	*"Development of an Alternative Material Selection System for Cadmium Electroplating"*
Cramer	Stephen D.	7A	*"Thermal-Spray Coatings for Coastal Infrastructure"*
Crotty	Chip	12	*"Combination Use of Dehumidification (DH) and VCI (Vapor Corrosion Inhibitor) for Corrosion Protection"*
Czyryca	Ernest J.	5	*"The Fatigue and Corrosion Fatigue Properties of Alloy 625 and 70/30 Copper-Nickel Alloy Electroslag Surfacing"*
Daniel	Fred	2	*"Fluorescence-Based Corrosion Indicators: Exploration of Schiff-Base Compounds"*
Dante	Jim F..	11	*"Localized Corrosion Behavior of Aluminum-Lithium Alloy, 2097"*
Davis	Daniel A.	5	*"Stress Corrosion Cracking of Naval Structural Alloys"*
		9	*"Post-Processing of Thermal Sprayed Coatings Using Hot Isostatic Pressing"*

INDEX - AUTHORS

LastName	FirstName	Session	*Title*
Davis	N.	3	*"Initial Studies of Electrochemical Comparison of Coating Performance in a Flowing vs Stationary Electrolyte"*
Decker	P.	9	*"Development of an Alternative Material Selection System for Cadmium Electroplating"*
Dexter	Stephen C.	6	*"Effect of Marine Biofilms on Galvanic Corrosion"*
Dixon	David S.	11	*"Development of a Nano-Particle Composite Material with Corrosion Resistant EMI Shielding Properties"*
Dorogy, Jr.	William E.	7A	*"Functionalized Sol-Gel Conversion Coatings"*
Donley	Mike S.	7A	*"Corrosion Resistant Evaluation of High Performance Aircraft Coating Systems (HPACS)"*
Duquette	David J.	1	*"The Effects of Dissolved Ozone on the Corrosion Behavior of Nickel, Stainless Steel and Aluminum-Based Alloys in Seawater"*
Ehrlich	Michael J.	4	*"An Accoustic Emission Method for the Evaluation of Environmentally Assisted Cracking"*
Evans	M. J.	9	*"Design of Seawater Ballast Tank Impressed Current Cathodic Protection (ICCP) Systems"*
Frankel	Gerald S.	2	*"Paint as a Corrosion Sensor: A Comparison of the Sensitivity of Different Coating Systems"*
Frazier	William E.	5	*"Environment Assisted Fatigue Cracking of AerMet 100 Steel"*
Gangloff	Richard P.	1	*"Environmental Cracking Limitations to the Application of High Strength Beta-Titanium Alloys in the Marine Environment"*
Garosshen	Thomas J.	11	*"Corrosion Behavior of Aluminum-Beryllium Alloys"*
Gelner	Larry	12	*"Combination Use of Dehumidification (DH) and VCI (Vapor Corrosion Inhibitor) for Corrosion Protection"*
George	K.	5	*"Environment Assisted Fatigue Cracking of AerMet 100 Steel"*

INDEX - AUTHORS

LastName	FirstName	Session	*Title*
Gerena	Maria	2	*"Oxidized Dextrine Coatings for Preventing Corrosion of Aluminum"*
Gill	S. J.	5	*"Ripple-Load Cracking Sensitivity in Engineering Alloys"*
Gilp	Brian	13	*"Corrosion Control Systematic Approach and Trends"*
Gray	N.	10	*"Inhibition of Microbiologically Influenced Corrosion"*
Hack	Harvey P.	4	*"Evaluation of Vapor Phase Corrosion Inhibitors and Dehumidification as Corrosion Control Methods for Advanced Double Hull Naval Ships"*
		6	*"New Techniques for Galvanic Corrosion Prevention in Piping Systems"*
		10	*"Corrosion Control for the AN/BQG-5A(V)1 Wide Aperture Array"*
Han	L. T.	3	*"Electrochemical Impedance and Noise Data for Polymer Coated Steel Exposed at Remote Marine Test Sites"*
Handsy	I. Carl	8	*"Advanced Zinc Phosphate Conversion Coatings"*
Hays	Richard A.	5	*"Stress Corrosion Cracking of Naval Structural Alloys"*
		9	*"Post-Processing of Thermal Sprayed Coatings Using Hot Isostatic Pressing"*
Hess	R.	9	*"Demonstration of Ozone Treatment System for Cooling Towers at Thayer Hall, U.S. Military Academy at West Point, NY"*
Hickman	Randy	13	*"AEGIS Corrosion Control Web Page"*
Hock	Vincent F.	3	*"Laboratory Evaluation of an In-Situ Coating Process for Mitigation of Lead and Copper in Drinking Water"*
		3	*"Lessons Learned: Leak Detection Sensors for Water, Fuel and Energy Pipe Systems"*
		9	*"Demonstration of Ozone Treatment System for Cooling Towers at Thayer Hall, U.S. Military Academy at West Point, NY"*
		9	*"Demonstration of Electro-Osmotic Pulse Technology for Groundwater Intrusion Control in Concrete"*
Hogan	Elizabeth A.	9	*"Design of Seawater Ballast Tank Impressed Current Cathodic Protection (ICCP) Systems"*

INDEX - AUTHORS

LastName	FirstName	Session	*Title*
Holcomb	Gordon R.	7A	*"Thermal-Spray Coatings for Coastal Infrastructure"*
Holder	Albert G.	3	*"Marine Coatings"*
Hunter	Joe T.	11	*"Localized Corrosion Behavior of Alunimum-Lithium Alloy, 2097"*
Inman	Marie E.	2	*"Detection and Monitoring of Crevice Corrosion Inside Pipe Flanges"*
Janakiraman	R.	10	*"The Effect of Water Vapor on the Oxidation of Alloys that Develop Alumina Scales for Protection"*
Jata	Kumar V.	6	*"Kinetics of Pitting Corrosion and Effects on Fatigue Behavior of Aluminum Alloy 7075-T6"*
Jayaraj	K.	7A	*"Functionalized Sol-Gel Conversion Coatings"*
Jeffcoate	Carol S.	3	*"Initial Studies of Electrochemical Comparison of Coating Performance in a Flowing vs Stationary Electrolyte"*
		7A	*"Corrosion Resistant Evaluation of High Performance Aircraft Coatings Systems (HPACS)"*
Johnson	B.	6	*"Kinetics of Pitting Corrosion and Effects on Fatigue Behavior of Aluminum Alloy 7075-T6*
Johnson	Richard E.	2	*"Fluorescence-Based Corrosion Indicators: Exploration of Schiff-Base Compounds"*
Jones	H. N.	12	*"A Post-Design Corrosion Inhibition Technique for Marine Corps Light Vehicles"*
Jones-Meehan	J.	10	*"Inhibition of Microbiologically Influenced Corrosion"*
Kain	Robert M.	2	*"Detection and Monitoring of Crevice Corrosion Inside Pipe Flanges"*
Kane	M. J.	6	*"Galvanic Corrosion of Tungsten Coupled with Several Metals/Alloys"*
Keohan	F. L.	8	*"Novel Chromium-Free Surface Pretreatment Process for Corrosion Inhibitors"*

INDEX - AUTHORS

LastName	FirstName	Session	*Title*
Kerr	Alan P.	7B	*"Bonded Repairs for Corrosion Damage"*
Khobaib	Mohammad	7A	*"Corrosion Resistant Evaluation of High Performance Aircraft Coating Systems (HPACS)"*
Kirstein	E.	3	*"Laboratory Evaluation of an In-Situ Coating Processing for Mitigation of Lead and Copper in Drinking Water"*
		9	*"Demonstration of Electro-Osmotic Pulse Technology for Groundwater Intrusion Control in Concrete Structures"*
Kuhn	W. Kevin	7B	*"Air Force Coatings Technology Integration Office: Operations and Objectives"*
Labbe	N.	9	*"Demonstration of Ozone Treatment System for Cooling Towers at Thayer Hall, U.S. Military Academy at West Point, NY*
LaFontaine	J. P.	6	*"Effect of Marine Biofilms on Galvanic Corrosion"*
Lambrokos	S. G.	12	*"A Post-Design Corrosion Inhibition Technique for Marine Corps Light Vehicles"*
Landy	T. M.	8	*"Novel Chromium-Free Surface Pretreatment Process for Corrosion Inhibitors"*
Latanison	Ronald M.	1	*"Corrosion Mechanisms in Supercritical Water Oxidation Systems for Hazardous Waste Disposal"*
Lavoie	D.	10	*"Fungal Degradation of Military Assets"*
Lee	C. C.	3	*"Electrochemical Impedance and Noise Data for Polymer Coated Steel Exposed at Remote Marine Test Sites"*
Lee	Eun U.	5	*"Environment Assisted Fatigue Cracking of AerMet 100 Steel"*
Lerner	K. B.	2	*"Corrosivity Monitoring on Operational Aircraft Using Thin Film Galvanic Sensors"*
Lincoln	Mike	7A	*"US Navy Coating Alternatives Utilizing Portable Systems"*
Little	Brenda	10	*"Inhibition of Microbiologically Influenced Corrosion"*
		10	*"Fungal Degradation of Military Assets"*

INDEX - AUTHORS

LastName	FirstName	Session	*Title*
Lizarralde	H. J.	8	*"Novel Chromium-Free Surface Pretreatment Process for Corrosion Inhibitors"*
Loeb	G. I.	10	*"Inhibition of Microbiologically Influenced Corrosion"*
Lucas	Keith E.	9	*"Design of Seawater Ballast Tank Impressed Current Cathodic Protection (ICCP) Systems"*
Macdonald	Digby D.	1	*"Defining the Corrosion Chemistry of Supercritical Water Oxidation Systems"*
Mansfeld	Florian	3	*"Electrochemical Impedance and Noise Data for Polymer Coated Steel Exposed at Remote Marine Test Sites"*
Masai	James	11	*"Development of a Nano-Particle Composite Material with Corrosion Resistance EMI Shielding Properties"*
McCammon	Thomas R.	4	*"Preservation Testing of Cargo/Weapons Elevators"*
McCaw	R. L.	9	*"Post-Processing of Thermal Sprayed Coatings Using Hot Isostatic Pressing"*
McGill	Galen E.	7A	*"Thermal-Spray Coatings for Coastal Infrastructure"*
McInerney	Michael	9	*"Demonstration of Electro-Osmotic Pulse Technology for Groundwater Intrusion Control in Concrete Structures"*
McIntyre	Jack F.	8	*"A Chromate-Free Chemical Conversion Coating for Aluminum and Steel Alloys"*
Meier	Gerald H.	10	*"The Effect of Water Vapor on the Oxidation of Alloys that Develop Alumina Scales for Protection"*
		11	*"Oxidation and Embrittlement of Titanium Aluminides"*
Melton	Dennis G.	6	*"New Techniques for Galvanic Corrosion Prevention in Piping Systems"*
Menke	Joseph T.	8	*"Failure Analysis of ASTM F519 Specimens"*
Mitton	D. B.	1	*"Corrosion Mechanisms in Supercritical Water Oxidation Systems for Hazardous Waste Disposal"*
Montemarano	Jean A.	3	*"Marine Coatings"*

INDEX - AUTHORS

LastName	FirstName	Session	*Title*
Mortman	Mara	12	*"Corrosion of Mk19 Grenade Launchers in Storage"*
Moran	Patrick J.	2	*"Detection and Monitoring of Crevice Corrosion Inside Pipe Flanges"*
Myers	D. L.	2	*"Detection and Monitoring of Crevice Corrosion Inside Pipe Flanges"*
Nardone	Vincent C.	11	*"Corrosion Behavior of Aluminum-Beryllium Alloys"*
Natishan	Paul M.	10	*"Inhibition of Microbiologically Influenced Corrosion"*
Nazeri	Azar	11	*"Preparation and Properties of Corrosion-Resistant Thin Ceramic Coatings on Metallic Substrates by Sol-Gel Processing"*
Neale	Douglas H.	9	*"Integration of Wire Arc Spray Technology for Corrosion Protection of General Purpose Bombs at the Kadena AB Bomb Renovation"*
Nelly	J.	1	*"Corrosion Protection of Aluminum Alloys by Conductive Organic and Inorganic Polymers"*
Orazem	Mark E.	1	*"Experimental Study of the Erosion-Corrosion of Copper and Copper-Nickel Alloys at the Corrosion Potential and at Anodic Potentials"*
Overmann	Jeremy L.	3	*"Laboratory Evaluation of an In-Situ Coating Process for Mitigation of Lead and Copper in Drinking Water"*
Pae	Youngun	4	*"Investigation of Corrosion Protection of Steel by Electrically Conductive Polyaniline Coating"*
Pan	M-L	7A	*"Functionalized Sol-Gel Conversion Coatings"*
Pao	Peter S.	5	*"Ripple-Load Cracking Sensitivity in Engineering Alloys"*
Paulette	Paulette	12	*see author Trzaskoma-Paulette*
Pearlstein	Fred	8	*"Trivalent Chromium Conversion Coating for Aluminum - A Replacement for Hexavalent Chromium Pretreatment"*
Pednekar	Sharad P.	4	*"The Salt-Spray Test as an Alternative to Long-Term Marine Exposure"*

INDEX - AUTHORS

LastName	FirstName	Session	*Title*
Perez	R.	6	*"Kinetics of Pitting Corrosion and Effects on Fatigue Behavior of Aluminum Alloy 7075-T6"*
Pettit	Fred S.	10	*"The Effect of Water Vapor on the Oxidation of Alloys that Develop Alumina Scales for Protection"*
		11	*"Oxidation and Embrittlement of Titanium Aluminides"*
Phillips	Peter	8	*"Novel Chromium-Free Surface Pretreatment Process for Corrosion Inhibitors"*
Pinkham	J.	10	*"Corrosion Control for the AN/BQG-5A(V)1 Wide Aperture Array"*
Piskin	D.	9	*"Demonstration of Ozone Treatment System for Cooling Towers at Thayer Hall, U.S. Military Academy at West Point, NY"*
Placzankis	Brian E.	7A	*"Extending Use of Ion Vapor Deposited (IVD) Aluminum as a Replacement for Electroplated Cadmium"*
Pound	Bruce G.	5	*"The Effect of Heat Treatment on Hydrogen Trapping in AerMet 100 and Alloy K-500"*
Quintana	M. S.	1	*"Corrosion Mechanisms in Supercritical Water Oxidation Systems for Hazardous Waste Disposal"*
Racicot	R.	1	*"Corrosion Protection of Aluminum Alloys by Conductive Organic and Inorganic Polymers"*
Rakowski	J.	11	*"Oxidation and Embrittlement of Titanium Aluminides"*
Rajan	Krishna S.	2	*"Fluorescence-Based Corrosion Indicators: Exploration of Schiff-Base Compounds"*
Ray	R.	10	*"Inhibition of Microbiologically Influenced Corrosion"*
		10	*"Fungal Degradation of Military Assets"*
Reynolds	Lance B.	7A	*"Corrosion Resistant Evaluation of High Performance Aircraft Coating Systems (HPACS)"*
Rudman	Barry L.	12	*"A Recent Innovation in Corrosion Control for Electronics"*
Sadananda	K.	5	*"Role of Aqueous Environment on the Growth of Long Fatigue Cracks"*

INDEX - AUTHORS

LastName	FirstName	Session	*Title*
Sakai	Jeff	13	*"Corrosion Control Systematic Approach and Trends"*
Sankaran	K. K.	6	*"Kinetics of Pitting Corrosion and Effects on Fatigue Behavior of Aluminum Alloy 7075-T6"*
Searson	Peter	6	*"Noble Metal Additions to Mitigate Hydrogen Embrittlement of Ultra High Strength Steels: Research in Progress"*
Senske	Jules A.	12	*"Corrosion of Mk19 Grenade Launchers in Storage"*
Shaffer	Irv S.	2	*"Corrosivity Monitoring of Operational Aircraft Using Thin Film Galvanic Sensors"*
Shaw	Barbara A.	11	*"The Determination of the Corrosion Behavior of a Developmental Al-Mg-Li-Ag Alloy"*
Sheetz	Andrew D.	3	*"Evaluating Anti-Galling Thread Treatment for Beta-C Titanium Fasteners Exposed to Marine Environments"*
		3	*"Corrosion Testing in the U.S. Marine Corps"*
		4	*"Evaluation of Vapor Phase Corrosion Inhibitors and Dehumidification as Corrosion Control Methods for Advanced Double Hull Naval Ships"*
Shifler	David A.	6	*"New Techniques for Galvanic Corrosion Prevention in Piping Systems"*
		10	*"Material Considerations for the Navy Shipboard Waste Destruction System"*
Simmons	R.	3	*"Evaluating Anti-Galling Thread Treatment for Beta-C Titanium Fasteners Exposed to Marine Environments"*
		4	*"Evaluation of Vapor Phase Corrosion Inhibitors and Dehumidification as Corrosion Control Methods for Advanced Double Hull Naval Ships"*
Slebodnick	P. F.	9	*"Design of Seawater Ballast Tank Impressed Current Cathodic Protection (ICCP) Systems"*
		11	*"Preparation and Properties of Corrosion-Resistant Thin Ceramic Coatings on Metallic Substrates by Sol-Gel Processing"*
Smothers	Kent W.	3	*"Laboratory Evaluation of an In-Situ Coating Process for Mitigation of Lead and Copper in Drinking Water"*

INDEX - AUTHORS

LastName	FirstName	Session	*Title*
Somerday	B. P.	1	*"Environmental Cracking Limitations to the Application of High Strength Beta-Titanium Alloys in the Marine Environment"*
Spiro	Ken	13	*"AEGIS Corrosion Control Web Page"*
Steiner	William	13	*"Approaches to Corrosion Control on the USMC Riverine Assault Craft (RAC)"*
		13	*"Corrosion Control Hardware Allowance Parts List (APLs): Logistics Support for Naval Surface Corrosion Control Programs"*
Stevens	J. H.	1	*"The Effect of Dissolved Ozone on the Corrosion Behavior of Nickel, Stainless Steel and Aluminum-Based Alloys in Seawater"*
Sugama	Toshi	2	*"Oxidized Dextrine Coatings for Preventing Corrosion of Aluminum"*
		8	*"Advanced Zinc Phosphate Conversion Coating"*
Tallman	Dennis E.	4	*"Investigation of Corrosion Protection of Steel by Electrically Conductive Polyaniline Coating"*
Taylor	E. Jennings	2	*"Detection and Monitoring of Crevice Corrosion Inside Pipe Flanges"*
Taylor	Edward	12	*"Design and Construction of Electronic Systems for Military Environments"*
Thomas	E. Dail	9	*"Design of Seawater Ballast Tank Impressed Current Cathodic Protection (ICCP) Systems"*
Tiano	T.	7A	*"Functionalized Sol-Gel Conversion Coatings"*
Timmins	Jeff	3	*"Lessons Learned: Leak Detection Sensors for Water, Fuel, and Energy Pipe Systems"*
Tipton	David G.	10	*"Corrosion Control for the AN/BQG-5A(V)1 Wide Aperture Array"*
Touzain	Sebastien	3	*"Initial Studies of Electrochemical Comparison of Coating Performance in a Flowing vs Stationary Electrolyte"*

INDEX - AUTHORS

LastName	FirstName	Session	*Title*
Tregoning	R. L.	6	*"High Strength Fasteners for Seawater Immersion Service"*
Trzaskoma-Paulette	Patricia P.	12	*"A Post-Design Corrosion Inhibition Technique for Marine Corps Light Vehicles"*
Turpin	R. J.	5	*"The Fatigue and Corrosion Fatigue Properties of Alloy 625 and 70/30 Copper-Nickel Alloy Electroslag Surfacing"*
Twite	Rebecca L.	7A	*"Corrosion Resistant Evaluation of High Performance Aircraft Coating Systems (HPACS)"*
Van Blaricum	Vicki	2	*"Demonstration of Cathodic Protection Remote Monitoring Systems"*
		7B	*"Utilities Engineered Management Systems: Maximizing the Impact of Limited Maintenance and Repair Resources"*
Vasudevan	A. K.	5	*"Role of Aqueous Environment on the Growth of Long Fatigue Cracks"*
Voevodin	Natasha N.	7A	*"Corrosion Resistant Evaluation of High Performance Aircraft Coating Systems (HPACS)"*
Wagner	James W.	4	*"An Acoustic Emission Evaluation of Environmentally Assisted Cracking"*
Wagner	P.	10	*"Fungal Degradation of Military Assets"*
Weber	R. A.	3	*"Lessons Learned: Leak Detection Sensors for Water, Fuel, and Energy Pipe Systems"*
Westerfield	Bill	12	*"A Recent Innovation in Corrosion Control for Electronics"*
Wojcik	P. O.	1	*"Experimental Study of the Erosion-Corrosion of Copper and Copper-Nickel Alloys at the Corrosion Potential and at Anodic Potentials"*
Wong	C.	14	*"Material Considerations for the Navy Shipboard Waste Destruction System"*
Wyllie	W. E.	1	*"The Effects of Dissolved Ozone on the Corrosion Behavior of Nickel, Stainless Steel and Aluminum-Based Alloys in Seawater"*

INDEX - AUTHORS

LastName	FirstName	Session	*Title*
Yang	S.	1	*"Corrosion Protection of Aluminum Alloys by Conductive Organic and Inorganic Polymers"*
Yoder	George R.	5	*"Ripple-Load Cracking Sensitivity in Engineering Alloys"*
Zhang	G.	3	*"Electrochemical Impedance and Noise Data for Polymer Coated Steel Exposed at Remote Marine Test Sites"*
Zhang	J.	2	*"Paint as a Corrosion Sensor; A Comparison of the Sensitivity of Different Coating Systems"*
Zhang	S-H.	1	*"Corrosion Mechanisms in Supercritical Water Oxidation Systems for Hazardous Waste Disposal"*